Pincer-Ruthenium Catalyzed (De)Hydrofunctionalization of Alcohols and Related Value-Added Transformations

A Dissertation

Submitted in Partial Fulfillment for the Degree of

Doctor of Philosophy

by

Kanu Das
(Roll No: 166122006)

Thesis Supervisor: Dr. Akshai Kumar A. S.

Department of Chemistry
Indian Institute of Technology Guwahati
Guwahati – 781039, Assam, INDIA

September 2022

Dedicated

To

To my parents and Friends

We are what our thoughts have made us; so take care about what you think.

Words are secondary. Thoughts live; they travel far

- Swami Vivekananda

Acknowledgments

I would like to express my wholehearted gratitude to all the imparts with the association of the scientific elite of the Indian Institute of Technology Guwahati, India. I would like to sincerely acknowledge all who have put an endless support and assistance during my research journey and made it possible to submitting this thesis.

- First, I express my earnest gratitude to my Ph.D. thesis supervisor **Dr. Akshai Kumar A. S**. for his continuous support, motivation and efficient advises throughout my entire research work. His precious suggestions and discussions helped me in achieving this feat of submitting my research work in the form of this thesis. I am also thankful for his intellectual guidance and motivation to assure me to explore challenging research fields that includes organometallics and catalysis.
- I am highly indebted to **Late Dr. Hemanth K. Srivastava** and **Dr. Farhan Ahmad Pasha** for their invaluable suggestion with DFT calculation.
- I am very much grateful to the collaborator **Prof. Biman Mondal** during the research work and discussion.
- I am very thankful to my doctoral committee chairman **Prof. Biplab Mondal**, and the doctoral committee members **Dr. Tapas Kumar Mondal**, and **Dr. Pavan Kumar Kanchrala** for their valuable suggestions, encouragement, and evaluation during my entire research period.
- I am also expressing my opportunity to thank my lab mates **Dr. Moumita Dutta**, **Mr. Khadimul Islam**, **Mr. Pran Gobinda Nandi**, **Mr. Vinay Arora, Ms. Himani Narjinari, Ms. Eileen Yasmin, Ms. Akshara Bisarya, Ms. Niharika Tanwar, Dr. Lakshay Kathuria, Mr. Vikas** and **Mr. Bedabara Nag** for their support and valuable time during my Ph.D. time. I sincerely thank them for their contribution to my research work.
- I am also thankful to **IIT Guwahati** for providing me with the doctoral fellowship. I am highly grateful to the **Department of Chemistry**, IIT Guwahati and **Central Instruments Facilities** (CIF, NECBH, IIT Guwahati) for utilizing the instrument facilities in my research work.

- Thanks to **Dr. Babulal Das**, **Dr. Prasenjit Sarkar** and **Dr**. **Prathapa S Jagannatha** for their support and elegant work with X-ray crystallography.

- My honest regards to **Prof. B. Kumar Patel** (IIT Guwahati), **Prof. Chandan Mukherjee** (IIT Guwahati), **Prof. Debapratim Das** (IIT Guwahati), **Dr. Sunanda Chatterjee** (IIT Guwahati) and **Prof. Abu Taleb Khan** (IIT Guwahati), for their inspiration in my research work.

- I would like to express my gratitude to my seniors **Dr. Manas K. Mandal, Dr. Ganesh Chandra Paul, Dr. Prasenjit Sarkar, Dr. Bedika Phukan, Dr. Mahmuda Khannam, Dr. Rajat Subhra Giri, Dr. Subhra Kanti Roy, Dr. Keshab Mondal, Dr. Nilotpal Singha, Dr. Buddhadeb Mondal, Dr. Utpal Nath, Dr. Sahnawaz Ahmed, Dr. Bapan Pramanik, Dr. Satyapriya Bhandari, Dr. Sabyasachi Pramanik, Dr. Shilaj Roy, Dr. Uday Narayan Pan, Dr. Ayan Pal, Dr. Raghunath Bag, Dr. Shubhadip Das, Dr. Srijita Paul, Dr. Saikat Pal, Dr. Krishna Gopal Chattaraj, Dr. Pinaki Bhusan De, Dr. Dinabandhu Sar, Dr. Sourav Pradhan, Dr. Prasenjit Barman, Dr. Gourab Mukherjee, Dr. Sayanta Sekhar Nag, Dr. Surajit Haldar, Dr. Utsab Manna, Dr. Santanu Ghosh, Dr. Subhankar Panda, Dr. Soumi Das, Dr. Rana Dalapati, Dr. Soumendra Nath Mukhopadhyay, Dr. Rajendra Maity, Dr. Mostakim SK, Dr. Aniruddha Das, Dr. Subas Chandra Sahoo, Dr. Soutick Nandi, Dr. Maimur Hossain, Dr. Niranjan Meher, Dr. Arvin Sain Tanwar, Dr. Sayan Roy Chowdhury, Dr. Debasish Kundu, Dr. Kalicharan Das, Mr. Malay Das, Dr. Sounak Bhattacharya, Dr. Tanmay Dutta, Dr. Sumana Mandal, Dr. Anisha Purkait, Mr. Gopal Pandit, Dr. Soumita Dwari, Dr. Soumen Saha, Dr. Baishakhi Mondal, Dr. Tanmay Mondal, Dr. Srinivasa Rao Manne, Dr. Avishek Banik, Dr. Nirmalya Pradhan, Dr. Arup Tarai** and **Dr. Chandan Gharui** for their encouragement in research during my entire PhD program.

- I would like to show appreciation to **Assam State Disaster Management Authority** (ASDMA) and **IIT Guwahati** (CRT) during the lockdown & unlocking of COVID-19 pandemic situation for helping in maintaining the research work unhampered.

- I am very much thankful to the **Academic Section**, **Student Affairs** and **R&D Section** of IIT Guwahati for their help whenever I required.

- My heartiest thanks always go above and beyond its limit to the compassionate **Doctors** of **IIT Guwahati** hospital, who treat me like a son when I fell in sick.

- I am grateful to the **Student Activity Center** (SAC, IIT Guwahati) for providing me with various facilities (Gym, Sports, ..) during my Research duration.

- Undoubtedly, I am very much thankful to every Security person (IIT Guwahati), as they make me feel so safe in campus. I am also grateful to all the **Cleaners** of IIT Guwahati as they maintain the whole campus so neat and clean, very glad that I have spent my research life in such a clean and beautiful campus.

- I desire to manifest my thankfulness to **Saraswati Puja Committee** (IIT Guwahati) making me part of this group during my entire research period.

- I would like to thank **Ganesh Da**, **Surjya Da**, and **Susil Da** as they are so kind-hearted when we are going for tea or snack break. Also, to the **mess** and **mess workers** of Kameng Hostel (IIT Guwahati) for providing me proper food without interruption.

- I express my gratitude to the annual cultural festival event organizers of IIT Guwahati (Alcheringa, Techniche), which spread over three to four days and diverted the conventional research day life to a new world.

- Thank to my dearest friends **Mr. Sandip Mondal**, **Mr. Bhim Majhi**, **Mr. Ramprosad Nandi, Dr. Amitava Rakshit, Mr. Pritam Dey, Mr. Srikanta Dey, Mr. Chirantan Jash, Mr. Swapan K. Mazumder, Dr. Nirmal Roy, Mr. Avijit Nayak, Mr. Krishnakanta Ghosh, Mr. Sushovan Hens, Mr. Sthitadhi Maiti, Dr. Debayan Chakraborty, Mr. Rajarshi Panigrahi, Dr. Avisek Dutta, Dr. Swapno Mondal, Dr. Surojit Bhunia, Mr. Tanmay Sarkar, Dr. Shamik Das, Mr. Rupam Roy, Dr. Basab Kanti Das, Mr. Subhajit Bal, Mr. Aksha Pal, Mr. Soumen Acharyya, Mr. Subhendu Halder, Mr. Subhajit Saha, Dr. Tanumay Sarkar, Dr. Bijay Ketan Das, Dr. Rohit Chaudhuri, Dr. Dipanjan Bhattacharyya, Mr. Laxmikanta Khamari, Dr. Tanumay Sarkar, Mr. Gobinda Dolai**, **Dr. Ashes Das, Mr. Debasis Barman**, **Mr. Suprakash Medda, Dr. Mihir Manna, Mr. Khadimul Islam, Dr. Nasim Akhtar, Dr. Sumit Goswami, Mr. Retwik Parui**, **Mr. Arghyajit Datta, Mr. Shyam Swarup Mondal, Mr. Mrinmoy Basak, Dr. Ankan Mukhopadhyay, Dr. Chiranjib Gogoi, Dr. Rabindranath Garai, Dr.**

Rabindranath Paul, Mr. Subhendu Ghosh, Ms. Samnam Khanam, Ms. Aindrila Ghosal, Ms. Riya Mallik, Dr. Senjuti Halder, Ms. Kaustari Ganguli, Ms. Rinku Dutta, Dr. Nandita Biswas, Dr. Laxmikanta Khamari, Dr. Payel Dowari and **Ms. Swapna Debnath** for their constant support and for making my journey at Indian Institute of Technology Guwahati as smooth as it can be.

- I would like to thank all my Ph.D. batchmates, seniors and juniors who helped directly or indirectly during my research.

Last but not least, I am gratified to my **Parents, Sister** and **Relatives** for their constant support, inspiration and encouragement throughout my life.

Indian Institute of Technology Guwahati

Department of Chemistry

Declaration

I do hereby declare that the research work embodied in this thesis entitled "***Pincer-Ruthenium Catalyzed (De)Hydrofunctionalization of Alcohols and Related Value-Added Transformations***" has been carried out by me in the Department of Chemistry, Indian Institute of Technology Guwahati, Assam-781039, India, under the supervision of Dr. Akshai Kumar A. S. for the award of the degree of doctor of philosophy and it has not been submitted elsewhere for the award of any degree or diploma.

In keeping with the general practice of reporting scientific observation, due acknowledgments have been made wherever the work described is based on the findings of other investigators

Kanu Das

Guwahati

September, 2022

Kanu Das

Roll No– 166122006

Department of Chemistry,

IIT Guwahati, Guwahati,

Assam, INDIA-781039

भारतीय प्रौद्योगिकी संस्थान गुवाहाटी
Indian Institute of Technology Guwahati

Dr. Akshai Kuamr Alape Seetharam
Associate Professor, Department of Chemistry, Guwahati – 781039, Assam, INDIA
Tel: +91 3612583479 (O), Mobile: +918133036890, Fax: +913612582349
Email: akshaikumar@iitg.ac.in, akshaikumara@gmail.com

@iit-g
Centre for Nanotechnology

CERTIFICATE

I hereby certify that the entire work embodied in this thesis entitled ***"Pincer-Ruthenium Catalyzed (De)Hydrofunctionalization of Alcohols and Related Value-Added Transformations"*** is the result of investigations carried out by **Mr. Kanu Das** (Roll No. 166122006) at the Department of Chemistry, Indian Institute of Technology Guwahati, India under my guidance and the same has not been submitted elsewhere for the awarded of any degree or diploma.

Guwahati
September, 2022

Dr. Akshai Kumar A. S.
(Thesis Supervisor)

Abbreviation

T	Temperature	equiv.	Equivalent(s)
°C	Degree Celsius	rt	Room temperature
K	Kelvin	IR	Infrared
δ	Chemical shifts	*m/z*	Mass to charge ratio
g	Grams	*e.g.*	For example
mg	milligram	ca.	around
mmol	millimole	*et al.*	and coworkers
μmol	micromole	*i.e.*	namely
mL	milliliter	vs.	versus
ppm	parts per million	*via*	through
kcal	Kilocalories	Me	Methyl
h	Hours	Et	Ethyl
EPR	Electron Paramagnetic Resonance	^{i}Pr	*iso*-propyl
MS	Mass spectrometry	^{t}Bu	*tert*-butyl
HRMS	High-resolution mass spectrometry	Cy	Cyclohexyl
XPS	X-ray photoelectron spectroscopy	Ph	Phenyl
Hz	Hertz	py	Pyridine
MHz	Megahertz	Ar	Aromatic
NMR	Nuclear Magnetic Resonance	THF	Tetrahydrofuran
J	Spin – spin coupling constant	DFT	Density functional theory
s	Singlet	TS	Transition State
d	Doublet	RDS	rate determining step
dd	Doublet of Doublet	RDTS	rate determining transition state
ddd	Doublet of Doublet of Doublet	TON	Turnover number
t	Triplet	TOF	Turnover frequency
q	Quartet	TO/h	Turnover per hour
m	Multiplate	2-MeTHF	2-Methyltetrahydrofuran
bs	Broad singlet	Bim	*Bis*(benzimidazole)
ORTEP	Oak Ridge Thermal Ellipsoid Plot	EWG	Electron withdrawing group
CCDC	Cambridge Crystallographic Data Center		

Abstract

The contents of the present thesis entitled ***"Pincer-Ruthenium Catalyzed (De)Hydrofunctionalization of Alcohols and Related Value-Added Transformation"*** have been divided into five chapters based on the results achieved from the experimental and computational work carried out during the entire course of the PhD research program.

Chapter I provides about a brief literature survey on organic transformations catalyzed by organometallic complexes. The use of various type of pincer-metal complexes having versatile activity towards organic transformations is also discussed. The chapter ends by identifying and defining the scope of the thesis.

Chapter II describes the synthesis of a series of new (*bis*)imino pincer-ruthenium complexes of type (^{R2}NNN)RuCl$_2$(PPh$_3$) (R = Cy, R = Ph, R = ^{i}Pr and R = ^{t}Bu). The use of sodium results in the formation of sodium alkoxide as a base which is generated *in-situ* from the substrate alcohol, and also acts as a water scavenger for the *N*-alkylation of amines. The use of these new pincer-Ru complexes have provided high reactivity towards *N*-alkylation reaction of amines with alcohols and excellent turnovers (ca. 29000 TON) were obtained. The detailed mechanistic and computational studies provide a better understanding of the reaction. Apparently, the *β*-hydride elimination is the overall RDS. This protocol has also been used to transform benzene-1,2-diamines to benzimidazoles with high productivity (ca. 12000 TON).

Chapter III discusses about the synthesis of a series of a phosphine free (*bis*)imino pincer-ruthenium carbonyl complexes of the type (^{R2}NNN)RuCl$_2$(CO) (R = Cy, R = Ph, R = ^{i}Pr and R = ^{t}Bu). The *β*-alkylation of 1-phenyl ethanol with benzyl alcohol at 140 °C under solvent-free conditions catalyzed by (^{Cy2}NNN)RuCl$_2$(CO) in the presence of catalytic amount of NaOH provides very high turnover number (ca. 93 % yield, 372000 TONs at 12000 TO/h). DFT studies are complementary to mechanistic studies and indicate the insertion of *α*-alkylated ketone into the Ru-H bond to be the overall RDS.

Chapter IV investigates the upgrading of bio-ethanol to *n*-butanol which has been accomplished *via* the pincer-ruthenium catalyzed Guerbet reaction under thermal conditions as well as under microwave irradiation. Under the microwave irradiation, high efficiency has been achieved after only 2 h in the presence of 10 mol% sodium ethoxide (NaOEt). Among all the NNN pincer-ruthenium complexes that have been utilized, ruthenium catalysts based

on 2,6-*bis*(benzimidazole-2-yl)pyridine ligands showed higher activity towards the Guerbet reaction. The highest rate (8534 TO/h, ca. 18 % yield of *n*-butanol at 90 % selectivity) was obtained and up to 72 % ethanol (42 % *n*-butanol yield) conversion was achieved under the microwave irradiation. The DFT calculations indicate the generation of hydrogen to be the rate-determining step (RDS). The catalytic system comprising of (*p*-OH^{Bim2}NNN)RuCl$_2$(CO) immobilized over neutral alumina resulted in best productivity of 15510 TON.

Chapter V describes a dehydration strategy that has been formulated for the selective etherification of secondary alcohols catalyzed by the pincer-ruthenium catalyst (^{Ph2}NNN)RuCl$_2$(CO) in the presence of molecular oxygen under solvent-free and base-free conditions at 140 °C. Up to 92 % yield (ca. 6133 TON) of the corresponding ethers are obtained at a very low catalyst loading. The detailed mechanistic studies provide the role of oxygen as a co-catalyst, non-labile nature of the ancillary CO ligand and the hemi-labile nature of the pincer-ligand arm. Ru(III) species formed *via* single electron transfer (SET) from O_2 is detected as the resting-state of the etherification. This work has been extended not only to the etherification of various aromatic secondary alcohols but also to the cross etherification and/or *o*-alkylation of 1-phenyl ethanols with a variety of phenols.

The current thesis demonstrates a synthetic protocol for a new series of pincer-ruthenium complexes. These complexes have been utilized for various organic transformations with a systematic understanding of the reaction mechanism.

Contents

Contents

Contents

Chapter I

Pincer Catalytic Systems in Organic Transformations

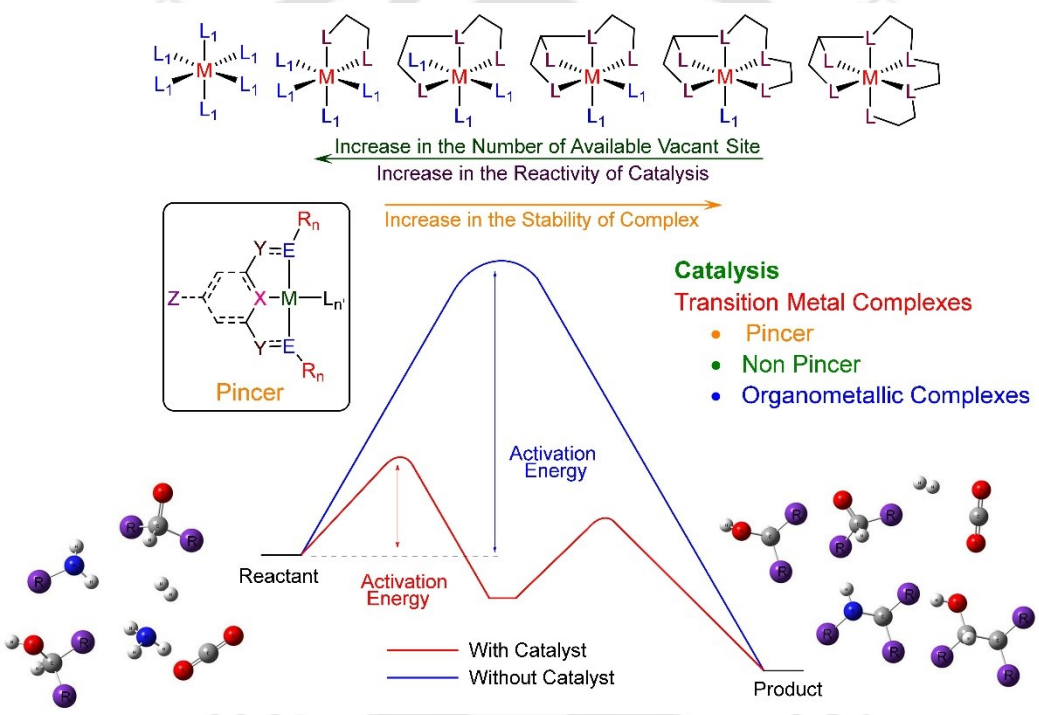

1.1 Organometallic chemistry: Organometallic chemistry has become a fundamental part of catalysis, with broad applications in organic synthesis. By definition, organometallic compounds should contain at least one direct carbon-metal bond or at least one metal-hydrogen/phosphorous bond. In 1827, William Zeise synthesized the first organometallic compound, which is a platinum(II) based compound named *Zeise's salt* $K[(\eta^2\text{-}C_2H_4)PtCl_3]$.[1] This development in the field of chemistry has led to the discovery of large number of organometallic compounds. Typically, organometallic compounds reflect a common chemical property (due to the presence of same number of valence electrons). For instance, the carbonyl complexes of transition metals typically exhibits a count of 18 valance electrons. The earliest transition metal based carbonyl complex was reported in 1890 by Mond, who synthesized the $Ni(CO)_4$ complex.[2] This was followed by Mond and Langer who reported a viscous straw yellow color liquid $Fe(CO)_5$.[3] In 1899, Victor Grignard introduced a groundbreaking organometallic compound for the various organic transformations named "Grignard reagent."[4-5] Over the decades, several organometallic compounds have been employed in a plethora of industrial-level applications in synthesis of valuable chemicals. However, since the organometallic chemistry has come to the fore, the improvement of catalysts has been one of the primary focus. Karl Zieglar[6] and Giulio Natta[7] introduced a bimetallic organometallic complex based on Ti or Zr with organoaluminium, which provided selective olefin polymerization[6-7] eventually leading to a 'Nobel Prize'. The transition metal catalyzed functionalization of active substrates or X–H (X = B, C, N, O, and Si)[8] bonds in organic reactions has led to valuable fine chemicals and fuel production.[9] The catalysis based on precious metals such as Ru,[10] Ir,[11] Pt,[12] and Pd[13] has greatly succeeded in accomplishing the C–X (X = Cl, Br and I) activation reactions.[14] However, in the last decade, it has been observed that the emphasis on development of efficient catalytic systems has shifted towards inexpensive and readily available transition metals such as Mn,[15] Cr,[16] Cu,[17] Fe,[12] Co,[12] and Ni.[10, 12]

1.1.1 Hydrofunctionalization reactions

The hydrofunctionalization reactions involve the addition of X–H (X = H, C, O, N, B and Si) bonds across C–C/C–N or C–O multiple bonds, which has a tremendous synthetic utility (Scheme **1.1**). Organometallic systems have been reported to efficiently catalyze (de)hydrofunctionalization reactions such as (de)hydrogenation,[18-19] hydroamination,[20] hydroetherification,[21-23] hydrosilylation,[24] hydroboration,[25] hydroformylation[26] and hydrocarboxylation.[27] Ideally, the catalytic transformation involving organometallic systems

often mitigate the stoichiometric amount of waste formation leading to an atom-economic transformation involving a minimum number of steps.

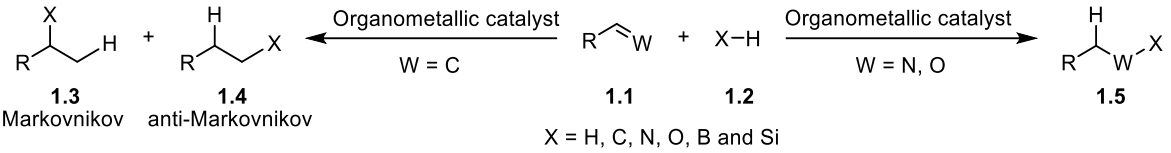

Scheme 1.1: Representative functionalization reaction.

For example, Williamson's[28] ether synthesis is known to be the best method[29] among various industrial methods[30-31] known to synthesize ethers. However, this process involves the formation of stoichiometric amounts of metal waste (Scheme **1.2**).

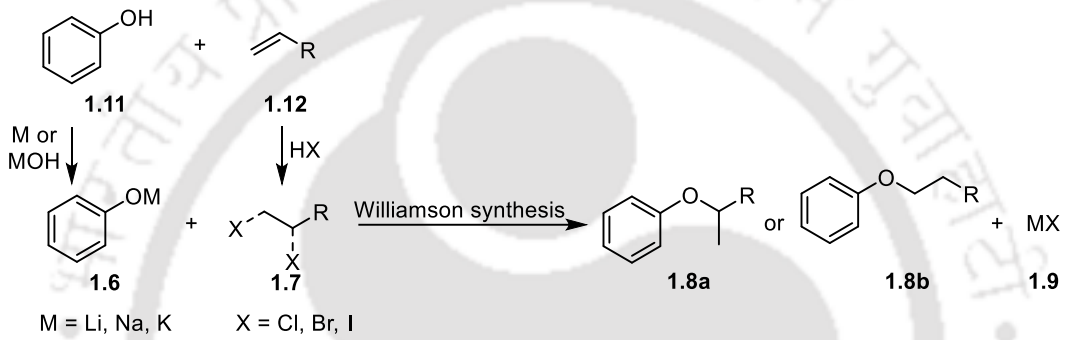

Scheme 1.2: Williamson's ether synthesis.[28]

Recently, Hartwig and co-workers have reported iridium catalyzed hydroetherification reaction, which directly transforms phenol and olefin into an ether (Scheme **1.3**).[21] Similarly, a plethora of organometallic-based catalysts have been reported to accomplish a variety of hydrofunctionalization not only in an atom-economical fashion but also in many instances with high regio-,[32] chemo-[33] and stereo-selectivity.[32]

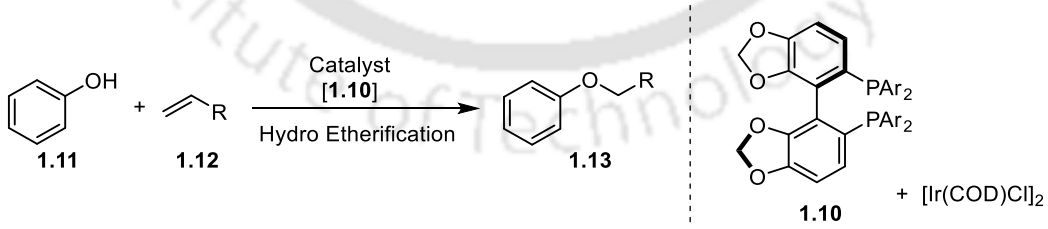

Scheme 1.3: Ir-catalyzed hydroetherification reaction.[21]

The general mechanism of organometallic catalyzed hydrofunctionalization reactions towards olefins/alkynes is given in Scheme **1.4**. Initially, heteromolecular (H–X) (X = C, O, N, B and Si) species undergoes oxidative addition at the metal center, which leads to an increase in the oxidation state of the metal. Then, the olefin/alkyne interacts with the metal center and is followed by the olefin insertion into the M–H/X bond. However, insertions could take place

via two possible pathways; insertion of olefin/alkyne either into the M–H bond (Path **A**) or into the M–X bond (Path **B**). In both cases, the insertion mode determines the regioselectivity in the final products, leading to the Markovnikov (branched) or the *anti*-Markovnikov (linear) products.

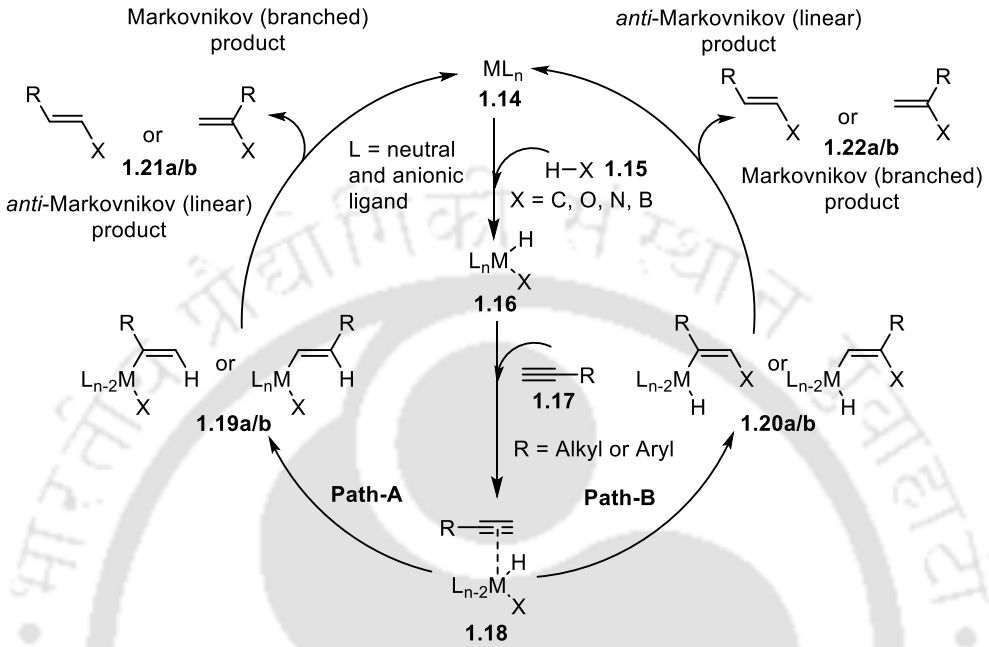

Scheme 1.4: Plausible catalytic cycle involved in hydrofunctionalization reaction.

1.1.2 Hydrogenation and dehydrogenation

(De)hydrogenation is a widely studied hydrofunctionalization, where hydrogenation[34-37] refers to the addition of hydrogen molecule(s) across multiple bonds. On the other hand, dehydrogenation[38-39] is the reverse of hydrogenation (Scheme **1.5**). Typically, it is widely accepted that the conditions of the reaction controls these microscopically reversible reactivity between hydrogenation and dehydrogenation.[40]

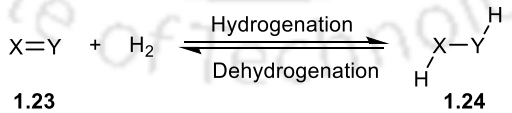

Scheme 1.5: Equilibrium between hydrogenation and dehydrogenation.

Hydrogenation is an exothermic process (thermodynamically favorable) and it often requires a stoichiometric or catalytic amount of transition metal (homogeneous[41] or heterogeneous[42-44]) complex. The hydrogenation reaction's efficiency depends not only on temperature[40] but also on catalyst loading, substrate purity, choice of solvent, and operating reaction condition. A large number of hydrogenation of unsaturated groups are well explored by using a variety of systems (stoichiometric or catalytic) based on pure metals,[45] frustrated Lewis acid-base

adducts,[46] metal-oxides,[47] metal hydrides,[48] metal-organic frameworks,[49] zeolites[50] and organometallic complexes.[51] Typically, carbon dioxide,[52] aldehydes,[53] ketones,[54] esters,[55] amides,[56] acid,[56] alkynes,[57] alkenes,[58] nitro groups,[59] nitriles moieties[60] and aromatic rings[61] (Scheme **1.6**) are primarily utilized as unsaturated substrates for hydrogenation. Notably, organometallic catalysts have enjoyed remarkable success under both under homogeneous[62] and heterogeneous[63] conditions for the hydrogenation reactions.

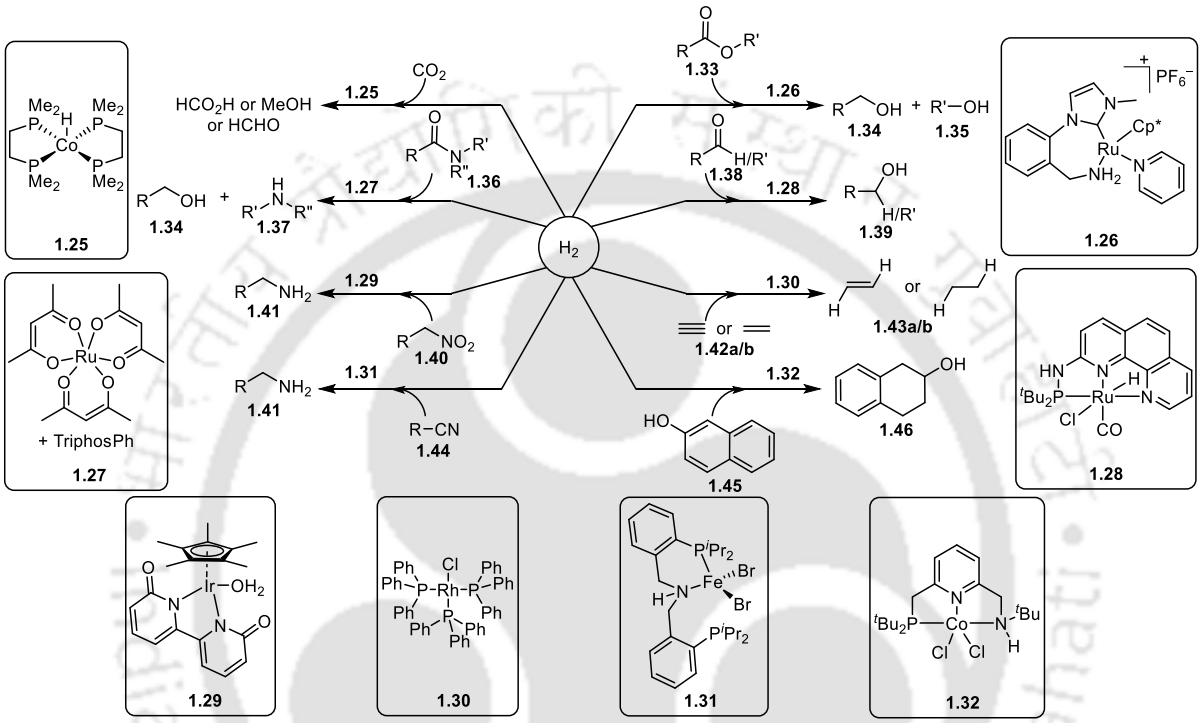

Scheme 1.6: Schematic representation of organometallic complex catalyzed hydrogenation of various unsaturated substrates.

On the other hand, the dehydrogenation reaction is a generally endothermic (driven by temperature (TΔS) or acceptor) process that converts saturated to unsaturated substrates. Dehydrogenation of highly abundant, unreactive alkanes to olefins[64] has been considered a valuable transformation in organic synthesis. In addition, organometallic systems have been known to accomplish the dehydrogenation of other substrates such as alcohols[65] and amines with a vast substrate scope.[66]

From the catalytic point of view, multiple factors are involved in the efficiency of a catalytic cycle, such as catalyst stability, number of vacant sites available on the metal and oxidation states. As in the case of complexes, multidentate ligand systems provides higher stability compared to monodentate ones however at the cost of the catalytic reactivity. Ligands can be systematically tuned from monodentate system to polydentate, to obtain a optimal balance between the stability and the reactivity of organometallic systems. In general, monodentate

ligand based complexes are less stable than bidentate, which are again less stable than tri-dentate systems and so on (Figure **1.1**).[67]

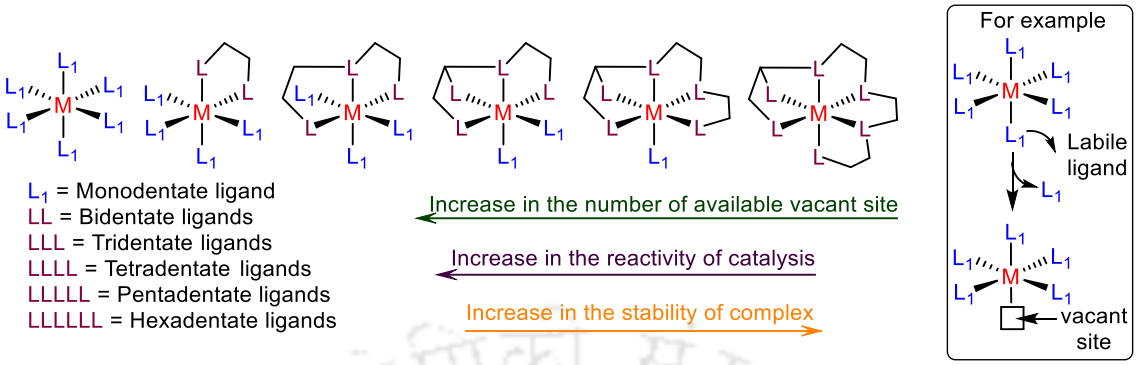

Figure 1.1: Type of complexes, along with the typical trend in their reactivity and stability.

1.2 Pincer complexes

In particular, tridentate ligands binds to the metal center creating a good balance between stability and reactivity. The tridentate ligand that binds in a meridional fashion have the ability to tune the various steric and electronic control around the metal center. While the rigid framework provides robustness to the complex, thereby enhancing its thermal stability, the catalytic versatility is provided by the ease of ligand tailoring to suit one's steric and electronic requirements as depicted in Figure **1.2**.[68-70]

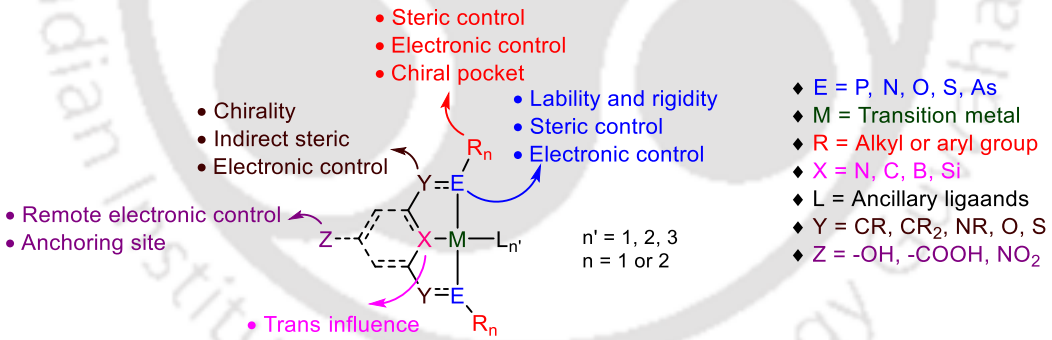

Figure 1.2: Schematic representation of a pincer metal complex depicting the variable parameters.

Such type of ligand systems were first reported by Shaw and co-workers[69, 71] in 1976, but van-Koten[72] first designated this as a "Pincer" where the three ligating atoms of the ligand clasp on the metal tightly. Shaw and co-workers also proved that the complexes of aromatic pincers backbone have high thermal stability compared to aliphatic pincers backbone.[69, 71] Over the years, a variety of ligating atom combinations (soft/hard) have provided the versatility to pincer ligand platform. In the initial reports, the treatment of *bis*phosphines ligand of the type (^{t}Bu4PCP)H (**1.47**) in combination with metal salts resulted in a spontaneous C–H activation at the *ipso*-carbon of the ligand (Scheme **1.7**).[73-74] Typical synthesis of the pincer-metal complex

depends on the nature of the ligand backbone, hybridization (*ipso*-atom), nature of the donor atoms' and the reaction solvent's polarity (polar to non-polar). While group **IX** metals tend to give corresponding hydrido-chloride complexes (**1.48** and **1.49**), the group **VIII** and group **X** analogs result in the formation of dichloride and chloride complexes (**1.50**-**1.52**) respectively (Scheme **1.7**).

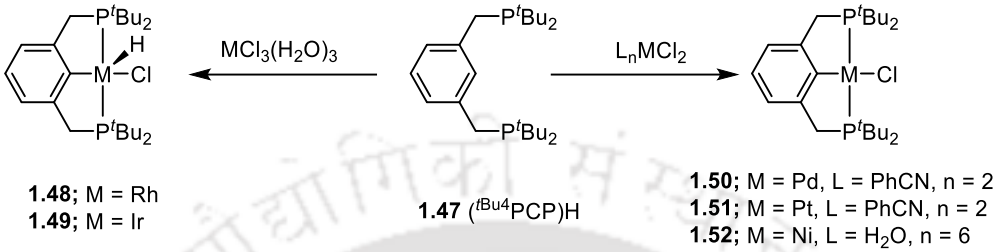

Scheme 1.7: Original synthesis of Shaw's metallo-PCP pincer complexes.[69, 71]

1.2.1 Types of pincer complexes

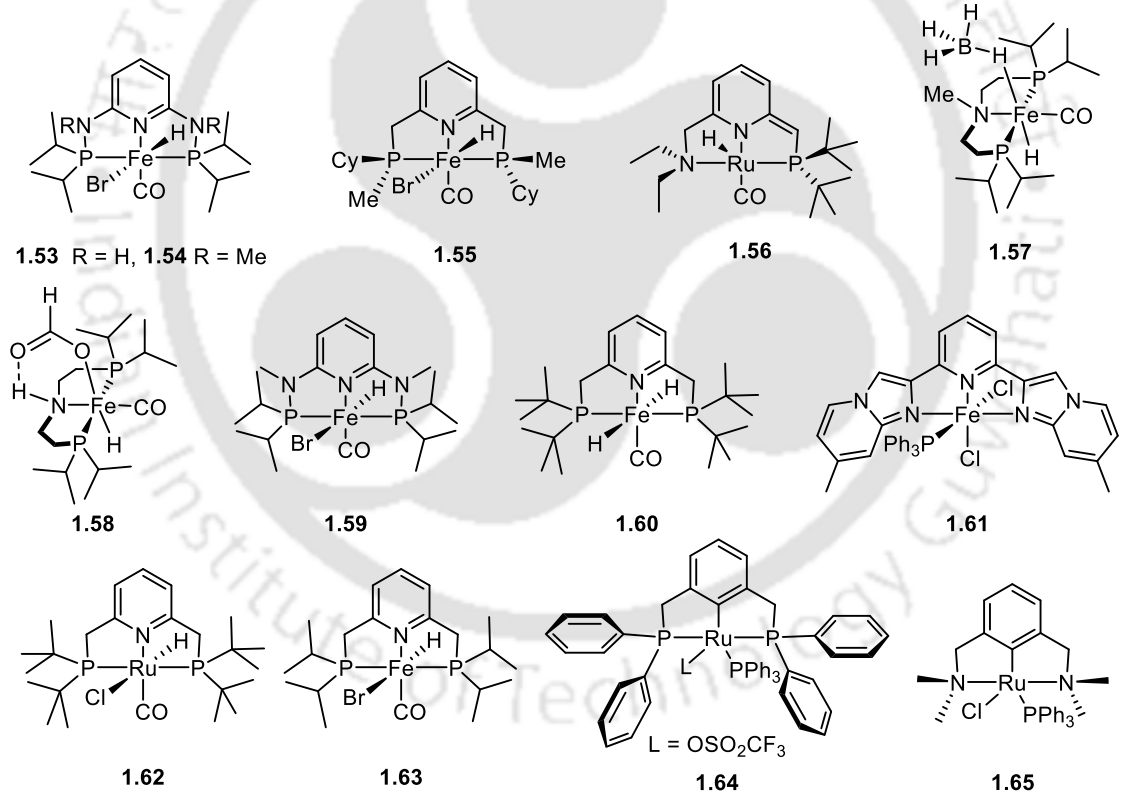

Figure 1.3: Various types of pincer-metal complexes reported in literature.

Over the years, several modifications of the pincer motif have been reported owing to the easily tailorable ligand backbone. Pincer complexes with desired catalytic properties have been obtained by varying the ligating groups[71-72] or changing the linker atoms.[75] Furthermore, an aryl backbone offers the possibility of introducing several polar functionalities on the carbon *para* to the *ipso* carbon, which helps in controlling the electronics remotely[72] and facilitates the

heterogenization of the molecular catalysts on many solid supports.[76] The chemistry of pincer complexes is vast and has been reviewed partially in various contexts.[31, 42] The pincer complexes were generalized in multiple types, such as PNP,[77-79] PCP,[80] NNN,[81-83] NCN,[80, 84] PNN,[79, 85-86] PCN[87] and CNC.[88-89] A detailed survey of the literature is beyond the scope of the current thesis; hence, only the literature relevant to the present thesis is provided (Figure **1.3**).

1.2.2 Synthesis protocol of several forms of pincer complexes

In the development of pincer ligand based transition metal complexes, the Milstein group demonstrated the synthetic protocol of PNP pincer-iron complex (Scheme **1.8**).[90] In the initial step, an equivalent amount of PNP pincer ligand and $FeBr_2$ in the presence of four equivalent of $NaBH_4$ were stirred in acetonitrile/ethanol medium which resulted in a monohydride cationic complex **1.67** having one molecule of solvent (acetonitrile) coordinated to the metal center. Treating the equivalent amount of PNP pincer ligand and $FeBr_2$ in the presence of CO provided PNP pincer-iron dibromo complex **1.70**.[35] The complex **1.67**, upon applying vacuum loses the coordinated solvent molecule and resulted into a *tri*-hydrido borohydride iron (II) complex **1.68**. On the other hand, the complex **1.67,** when subjected to a CO atmosphere yields a *trans* CO complex **1.69** (with respect to hydride), where acetonitrile remained coordinated to the metal center. This result also proved the strong *trans* effect of the hydride ligand, where acetonitrile gets substituted by carbon monoxide. Similarly, treating the complex **1.69** under the vacuum, the solvent molecule is lost resulting in a *trans* dihydride carbon monoxide iron PNP pincer complex **1.60**.

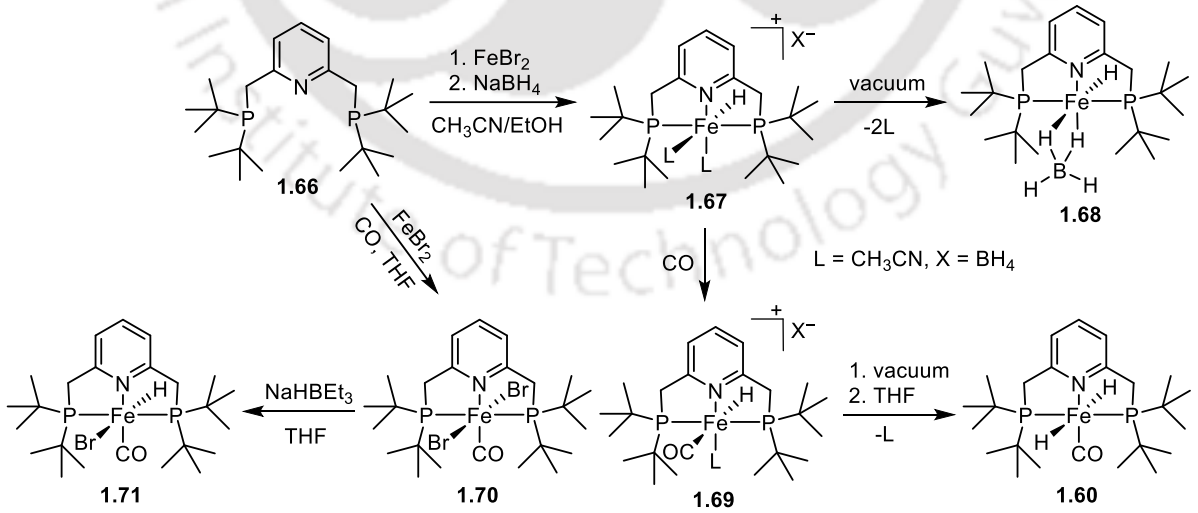

Scheme 1.8: Synthetic routes to different forms of the PNP pincer-iron complexes.[35, 90]

The PNP pincer-iron dihydride complex **1.60** showed remarkably very good reactivity towards CO_2 activation to generate formate salt ($HCOO^-Na^+$) under very low pressure and obtained 788 TON.[90] The pincer-iron dibromo complex **1.70** in the presence of one equivalent of $NaHBEt_3$

provided mono hydrido iron complex **1.71** (Scheme **1.8**), which showed good hydrogenation activity. In addition, hydrogenation of ketone derivative at low pressure of H_2 (4.1 atm) was achieved at 1880 TON.[35]

The *trans* pincer dihydride complex is uncommon mainly as it has *trans* influence by the hydride ligand. These electronic factors are slightly different from the *cis* isomer, which is stabilized by the bulky ligands.[91-92] Milstein group designed a synthetic protocol for the various type of PONOP pincer-ruthenium complexes and demonstrated its stability towards various additives.[93]

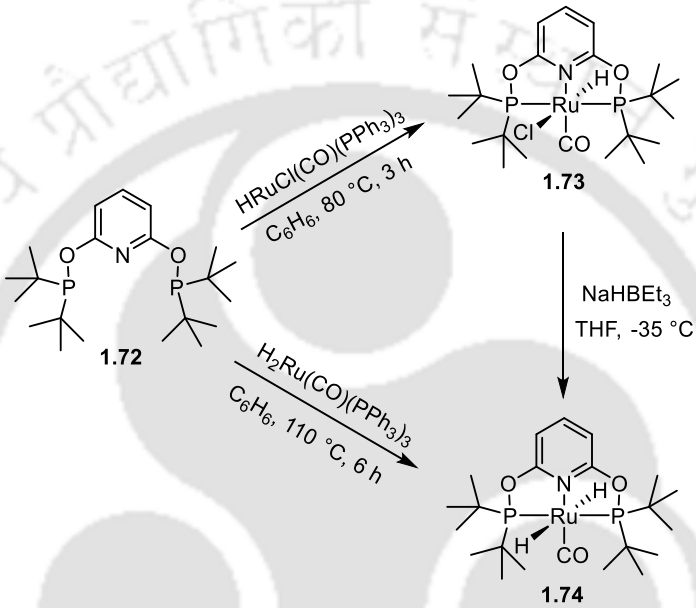

Scheme 1.9: Synthetic protocol of PONOP pincer-Ru mono/di-hydride complex.[93]

The treatment of ^{t}Bu4PONOP ligand with $HRuCl(CO)(PPh_3)_3$ afforded the mono hydride complex **1.73** (Scheme **1.9**).[94] The IR stretching frequency of the C≡O bond in complex **1.73** appears at 1932 cm^{-1} whereas CO group of the analogous PNP-ruthenium system stretches at 1906 cm^{-1}.[94] The IR analysis of both ^{t}Bu4PONOPRuHCl(CO) (**1.73**) and ^{t}Bu4PNPRuHCl(CO) (**1.62**) demonstrated that the replacement of methylene group by oxygen atoms increased the electron density at the metal center, which thereby increased the π back bonding to π* of the CO group, lowering the stretching frequency by $\Delta\nu = 26$ cm^{-1}.[93] Interestingly, the treatment of one equivalent of $NaHBEt_3$ resulted in dihydrido complex **1.74**. Alternatively, the complex **1.74** could also be synthesized by treating ligand **1.72** with $H_2Ru(CO)(PPh_3)_3$ (Scheme **1.9**).

The active pincer-Ru dihydrido complex **1.74** in the presence of CO atmosphere in THF solution resulted in a 5-coordinated 18-electron *bis*-carbonyl pincer-Ru(0) complex **1.75** (Scheme **1.10**), where the elimination of H_2 was confirmed by GC analysis. Alternatively, the complex **1.75** could be obtained either by treating one equivalent of KO^{t}Bu under CO

atmosphere with monohydrido complex **1.73** or by adding one equivalent of CO with complex **1.77** (Scheme **1.10**).[93] They demonstrated that the unstable complex **1.77** could be synthesized by reacting **1.73** with one equivalent of KO^{t}Bu in benzene or THF. The presence of 4-coordinated complex **1.77** (16-electron) was confirmed by the absence of hydride signal in ^{1}H NMR, ^{31}P NMR (a singlet at δ = 233.45 ppm), and appearance of a carbonyl group at 1928 cm^{-1} in the IR spectra. The 5-coordinated *bis*-carbonyl Ru(0) complex **1.75** could react with water *via* the cleavage of one of the P–O bond (scheme **1.10**). The zwitterionic complex **1.76** exhibits a doublet of doublet (δ = 214.01 and 154.59 ppm) in the ^{31}P NMR and two hydride signals as a doublet (δ = -5.9 ppm) in the ^{1}H NMR. The IR spectra (ν_{CO} = 1992, 1948 cm^{-1} and ν_{Ru-H} = 2061cm^{-1}) suggested strong *trans* influence nature of the CO ligand in complex **1.76**.

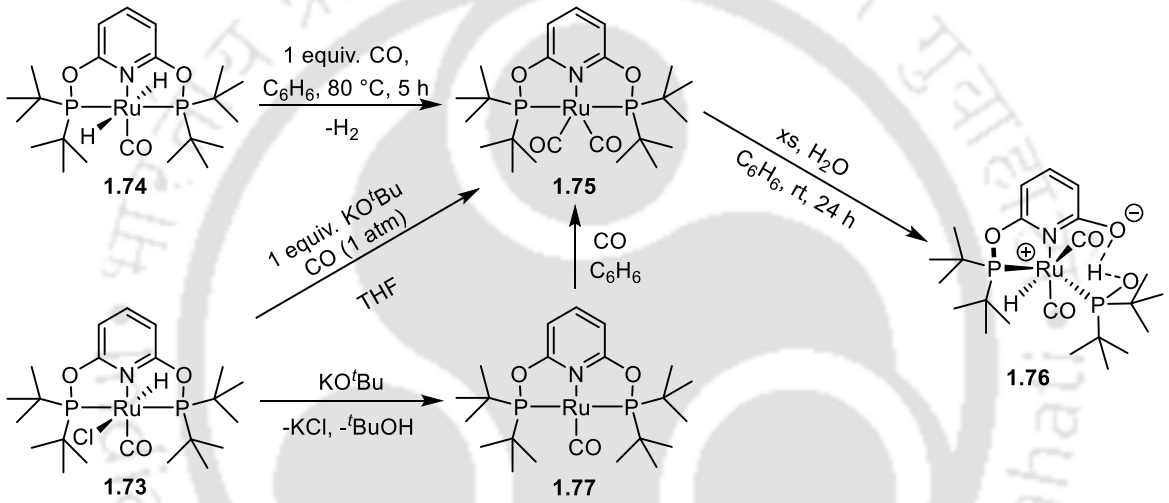

Scheme 1.10: Synthetic route to various PONOP pincer-Ru arbonyl complexes.[93]

The 4-coordinated complex **1.77** (16-electron) in the presence of H_2 atmosphere has two broad singlets δ = -6.41 and -11.46 ppm in ^{1}H NMR with a ratio 1:1, which proves the presence of *cis*-dihydrido complex **1.74′**. Furthermore, the complex **1.74′** gets converted into the thermodynamically more stable isomer *trans*-dihydrido complex **1.74** (Scheme **1.11**).

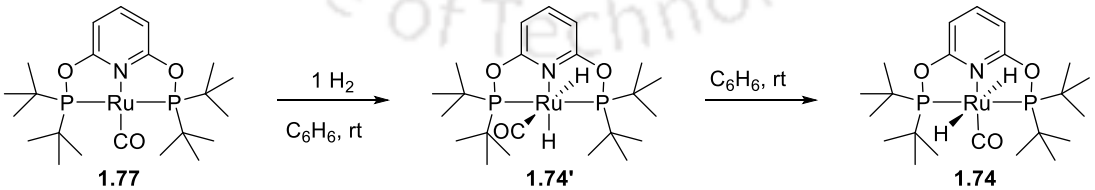

Scheme 1.11: The 16*e* to18*e* *cis-trans* isomerization of PONOP-Ru dihydride complex.[93]

The mono hydrido-chloro complex of both **1.73** and **1.78** leads to chloride ligand abstraction on treatment with MeOTf and MeI (Scheme **1.12**).[93] Interestingly, they observed that the presence of hydride signal in ^{1}H NMR reflects that MeX is not attacking as a electrophile to the metal center. In contrast to the reactivity exhibited by **1.78**, the treatment of MeI with

complex **1.73** resulted in a prolonged reaction even at a high loading of MeI compared to the corresponding reaction with MeOTf. This result indicates both the electrophilicity of MeI and the steric effect of the ^{t}Bu group (compared with the ^{i}Pr group) on the pincer-Ru complex have a pivotal role to play.

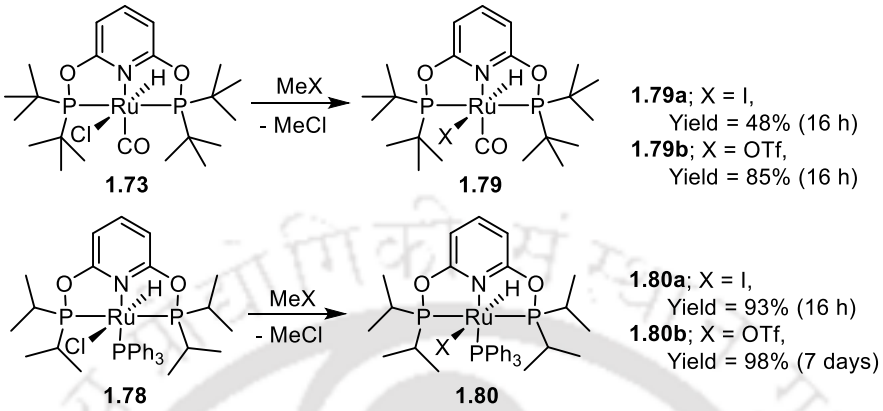

Scheme 1.12: Reaction of hydrido chloride complex with reactive methyl species.[93]

The treatment of ligand **1.81** with $RuCl_2(PPh_3)_3$ at 80 °C resulted in a *trans* dichloro pincer-Ru complex **1.82** where PPh_3 is coordinated to the metal center (Scheme **1.13**). The PPh_3 complex **1.82** formation was confirmed by ^{31}P NMR, which has two phosphorus signals observed as a triplet (δ = 194.30 ppm) and doublet (δ = 3.95 ppm). On the other hand, treating **1.72** with $RuCl_2(PPh_3)_3$ at room temperature resulted in a 5-coordinated complex **1.83** (Scheme **1.13**).[93]

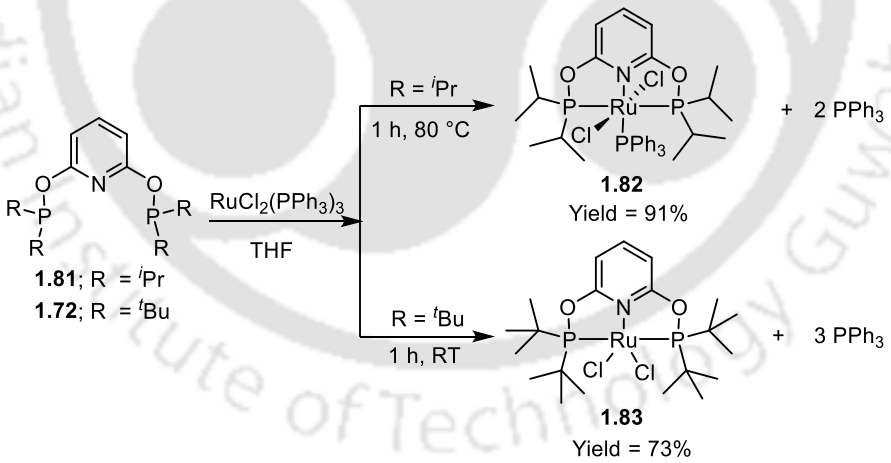

Scheme 1.13: Synthesis of the dichloro pincer-ruthenium complex.[93]

1.2.3 Synthesis of pincer-iron(0) complex from its dichloride precursor

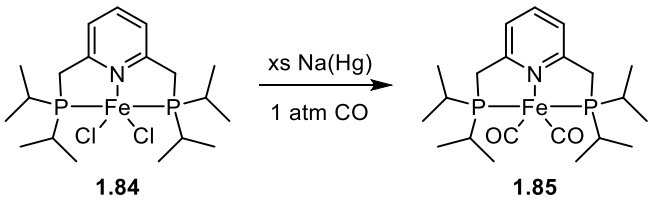

Scheme 1.14: Synthesis of pincer-iron (0) complex.[95]

Chirik and co-workers reported that in the presence of 4 atm of carbon monoxide with an excess of sodium amalgam (0.5%), the complex **1.84** affords an iron (0) dicarbonyl complex **1.85** (Scheme **1.14**).[95]

1.2.4 Synthesis of pincer-iron dihydride complex from its dihalocomplex

Chirik and co-workers reported that the treatment of **1.87a** with 2 equivalent of $NaBEt_3H$ under nitrogen leads to an iron(0) complex **1.86**, in which the dihydride complex presumably undergoes reductive elimination of H_2 molecule. On the other hand, complex **1.87b** under the same reaction condition provides a dihydride nitrogen complex **1.88** (Scheme **1.15**).[95]

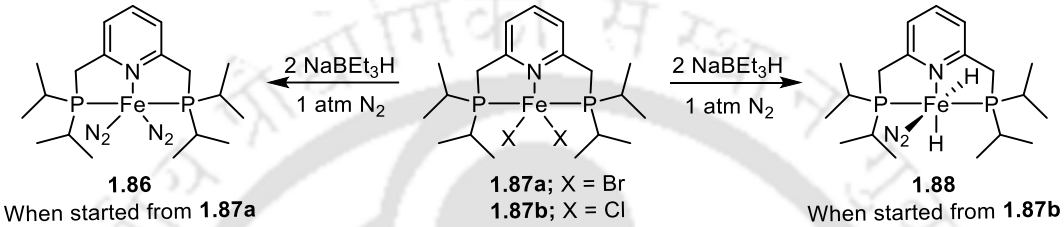

Scheme 1.15: Synthesis of pincer-iron dihydride complex.[95]

1.2.5 Synthesis of pincer-ruthenium dinitrogen complex

Choice of inert environment (nitrogen vs. argon) in the synthesis of transition metal (especially Ru) pincer complexes, has been found to be important. Typically in Ru(II) phosphine complexes, the PPh_3 ligand is easily being substituted by an external ligand. Milstein and coworkers reported that $RuCl_2(PPh_3)_3$ in the presence of ^{t}BuPNP (2,6-Bis[[bis(1,1-dimethylethyl)phosphino]methyl]pyridine) ligand under nitrogen atmosphere resulted in the formation of a nitrogen coordinate complex **1.90** (Scheme **1.16**).[96] They found that the solution of complex **1.90**, when bubbled with argon gas, resulted in a dimeric N_2 complex **1.91** (Scheme **1.16**).[96]

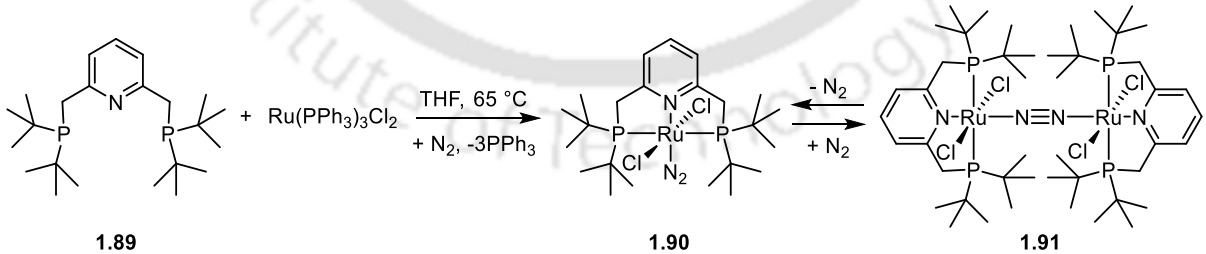

Scheme 1.16: Synthesis of dinitrogen pincer-ruthenium complex.[96]

1.3 Catalytic applications of pincer complexes

1.3.1 Dehydrogenation of alcohols

Acceptorless dehydrogenation of alcohols to esters is one of the areas of recent interest in organic synthesis.[97] This method bears an oxidant-free, atom-efficient environment friendly process with simultaneous production of hydrogen gas. Milstein and co-workers reported that

the PNN-ruthenium catalyst resulted in extraordinary acceptorless dehydrogenation of alcohols to esters under mild conditions (Scheme **1.17**). They achieved 995 TON[98] in case of **1.95** catalyzed conversion of primary alcohols to ester, while in case of **1.94**, 99 TON[99] were obtained for esterification of secondary alcohols. Beller and co-workers reported the pincer-ruthenium **1.97** catalyzed esterification of ethanol to ethyl acetate via dehydrogenative coupling, which resulted in high yields and 15400 TON (Scheme **1.17**).[100] Later, Gusev reported PNN pincer-ruthenium **1.96** catalyzed esterification of ethanol with 8200 TON (Scheme **1.17**).[101] Yu and co-workers reported that flexible and unsymmetrical CNP based pincer-ruthenium **1.98** provided good to excellent yields (95 TON) in the catalytic esterification of alcohols(Scheme **1.17**).[102]

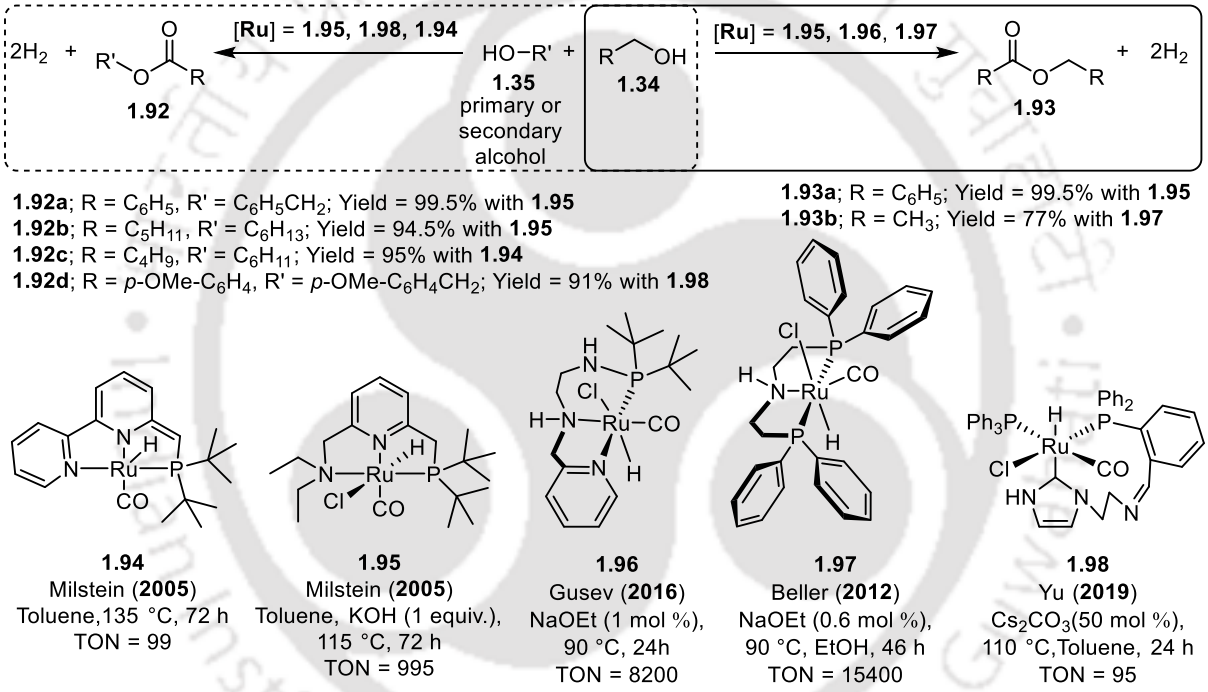

Scheme1.17: Pincer-ruthenium catalyzed esterification of alcohols.[98-102]

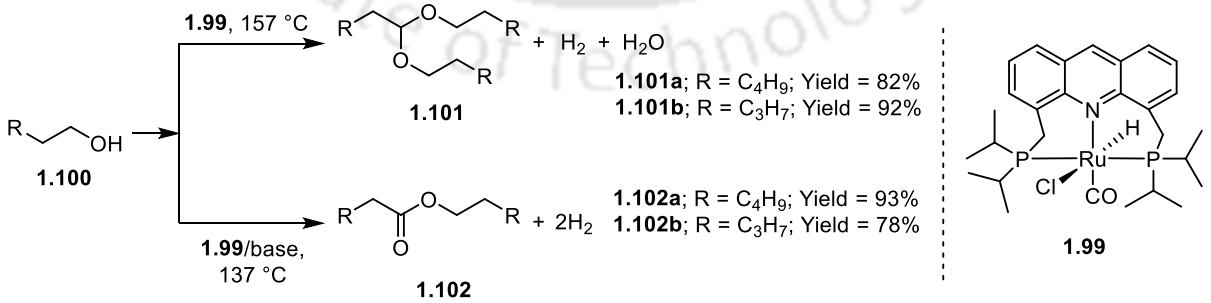

Scheme 1.18: PNP pincer-ruthenium catalyzed alcohol to ester and acetal conversion.[103]

Acetals, esters, and amines are important in polymers, dyestuffs, emulsifiers, pigments, chemicals, and pharmaceutics.[104-105] The acetal synthesis is mainly done with aldehyde or ketone by acid-catalyzed reactions, which requires toxic and corrosive reagents to accomplish

the reaction. The Milstein group reported primary alcohols to acetal without any additives (Scheme **1.18**).[103]

1.3.2 Dehydrogenative coupling (*N*/*C*-alkylation) reaction

Amides are vital chemicals in organic synthesis, pharmaceuticals, and biochemistry.[106] Generally, amide synthesis requires carboxylic acid, acid chloride, acid anhydride and inorganic additives.[107] A few reports are present in literature with ruthenium catalysts for coupling of secondary amines with alcohols under base-free and hydrogen accepter free conditions.[108] Milstein group reported the most noticeable result for amide synthesis *via* dehydrogenative coupling of primary amines with alcohols.[109] Various other groups have also reported the acceptorless amide synthesis from alcohols and amines and obtained up to 990 TON with **1.56**,[86] 600 TON with **1.104**,[110] 89 TON with **1.105**,[111] and 495 TON with **1.94**[112] based on pincer-iron catalysts and pincer-ruthenium catalysts (Scheme **1.19**).[110]

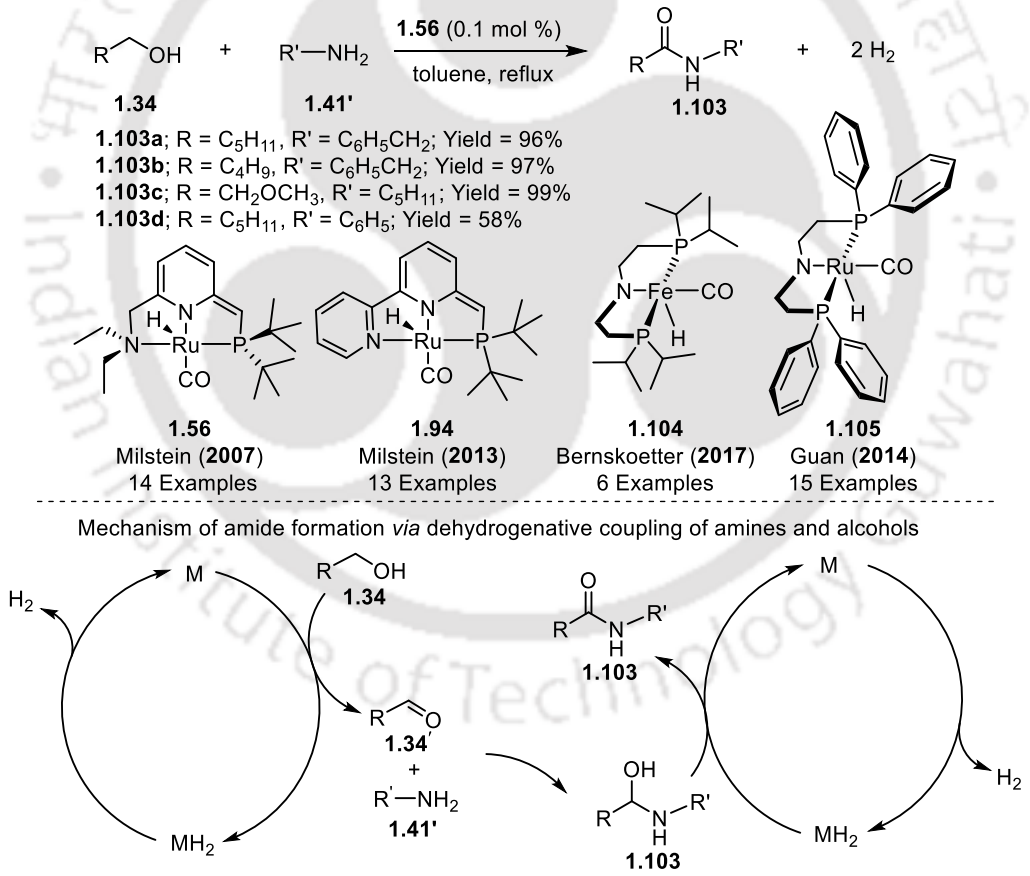

Scheme 1.19: Amide synthesis catalyzed by pincer complexes starting from alcohols and amines.[112]

N-alkylated amines are versatile intermediates that find wide utility in the synthesis of fine chemicals, polymers, dyes and pharmaceutical products.[113] Classical synthetic approaches towards *N*-alkylated amines involve treatment of environmentally toxic alkyl halide with

amines.[114] As alkyl halides are obtained either from alcohols or from olefins, it would be less hazardous and more atom economical if one transforms either of these precursors directly to the *N*-alkylated products. Accordingly, the development of efficient synthetic routes to *N*-alkylated amines in a "greener and atom economical" fashion remains a field of immense interest.[115] One of the most studied routes to *N*-alkylated amines involves the use of alcohols as the alkyl precursor in transition metal-catalyzed reactions. The use of stoichiometric amounts of base or use of molecular sieves is required to scavenge the by-product water formed in catalysis.[116] Use of base, however, is likely to result in the formation of additional by-products. Using this approach Krishner[117] Meilstein[118] and Kundu[119] reported amine alkylation via "hydrogen borrowing" strategy (Scheme **1.20**).

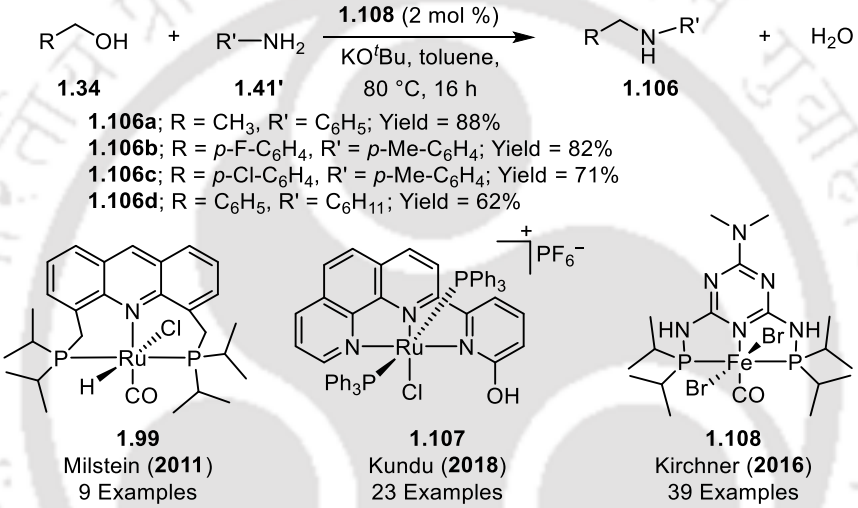

Scheme 1.20: Pincer-ruthenium and pincer-iron catalyzed *N*-alkylation of alcohols with amine.[117-119]

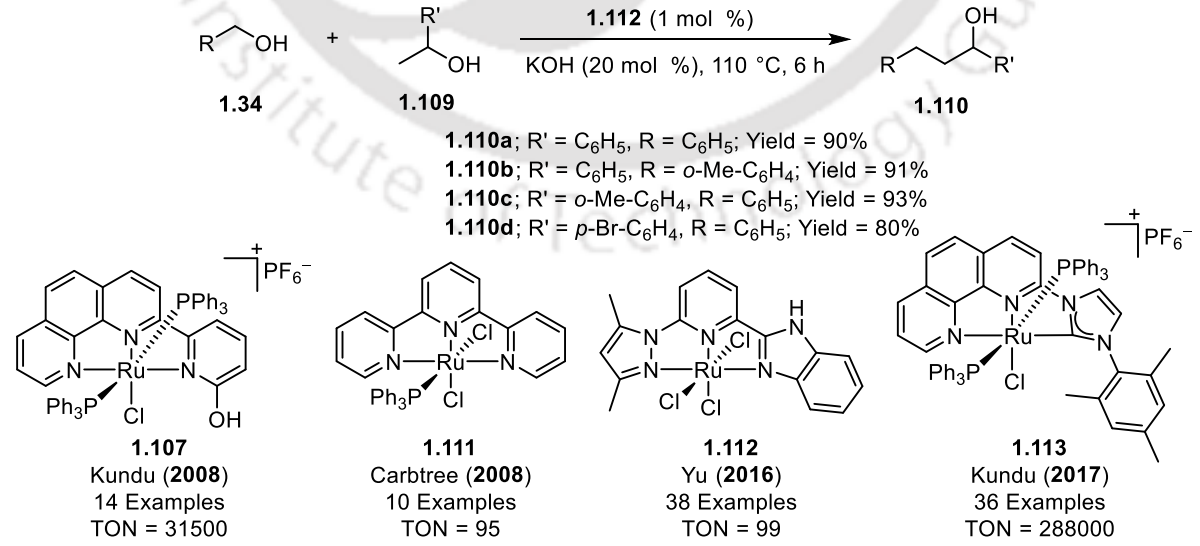

Scheme 1.21: Pincer-Ru catalyzed C-alkylation of primary alcohols with secondary alcohols.[120]

The dehydrogenation of alcohols in the anaerobic condition is widely explored by employing various transition metals. In comparison, the hydrogen borrowing strategy is much more efficient in aerobic conditions than in anaerobic conditions. However, in aerobic conditions, the dehydrogenation of alcohol holds some drawbacks as metal hydride species are involved and it is air-sensitive. The hydrogen borrowing methodology with a greener process under mild reaction conditions is the focus of *C*-alkylation. In general, transition metal-catalyzed *C*–alkylation reaction involves an inert condition with a pre-coordinated ligand to the metal center. Inspired by this work, Carbtree,[121] Yu,[122] and Kundu[120] reported *β*–alkylation of secondary alcohols with primary and higher alcohols. Despite reports from several groups, there has been no significant achievement in this transformation and the efficiency of the reported catalysts are very low. Till now, a highest of 288000 TON (TOF 12000 h^{-1}) has been reported by Kundu and co-workers (Scheme **1.21**).[120]

1.3.3 Imine synthesis from alcohols and/or amines

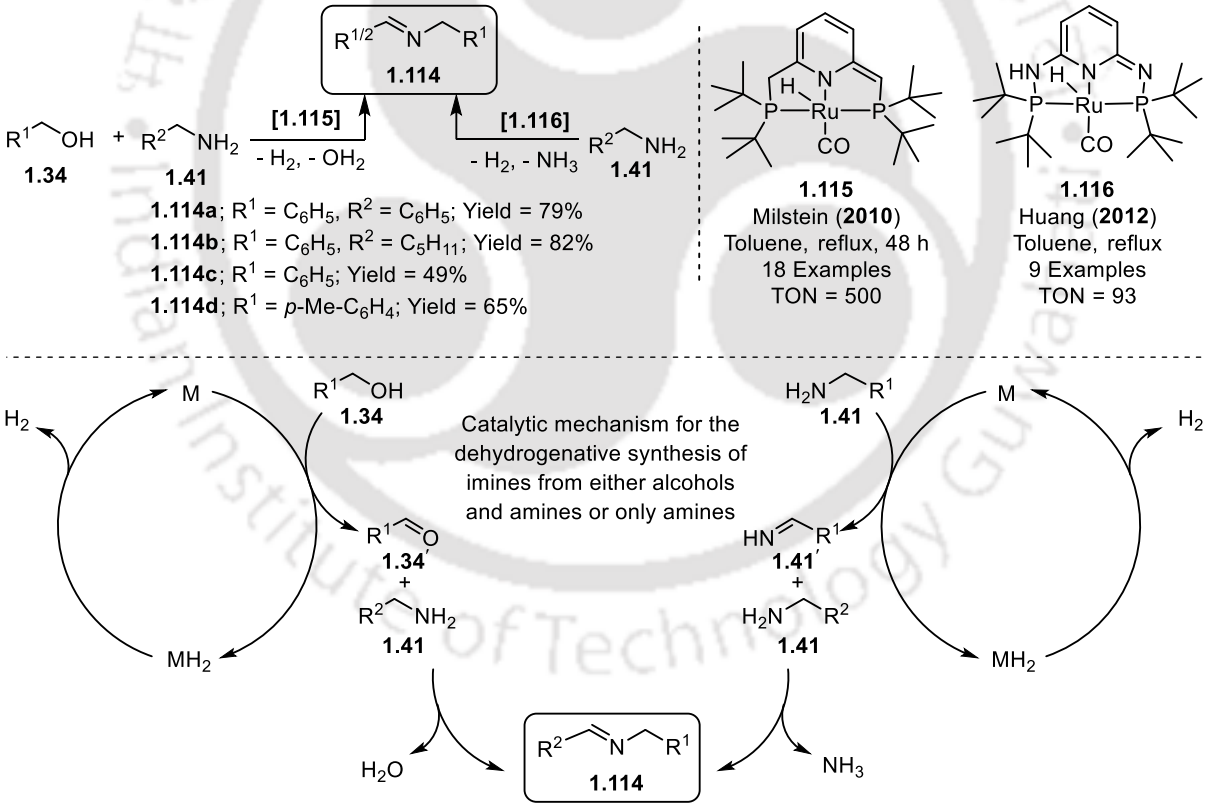

Scheme 1.22: Catalytic imine synthesis via dehydrogenative coupling reaction.[94]

Dehydrogenative coupling of alcohols to imines is an essential synthetic protocol that leads to a useful building block, and finds biological importance in the pharmaceutical industry.[123] Imine is mainly synthesized by condensing aldehyde or ketones with amines.[124-125] Alternatively, catalytic dehydrogenation of amines to prepare imine is a more significant and

more effective transformation as there is no requirement for additional alcohols. In this regard, Huang and co-workers reported a dehydrogenative coupling of primary amines to imines in the presence of pincer-Ru **1.116** with the release of ammonia (Scheme **1.22**).[126] On the other hand, Milstein and co-workers reported an environmentally benign imine synthesis with the liberation of molecular hydrogen from alcohols and amines by pincer-Ru **1.115**. This reaction also tolerates a variety of alcohols and amines for the synthesis of imines with high turnover numbers (Scheme **1.22**).[94]

1.3.4 Heterocyclic derivative synthesis from amino alcohols with alcohols

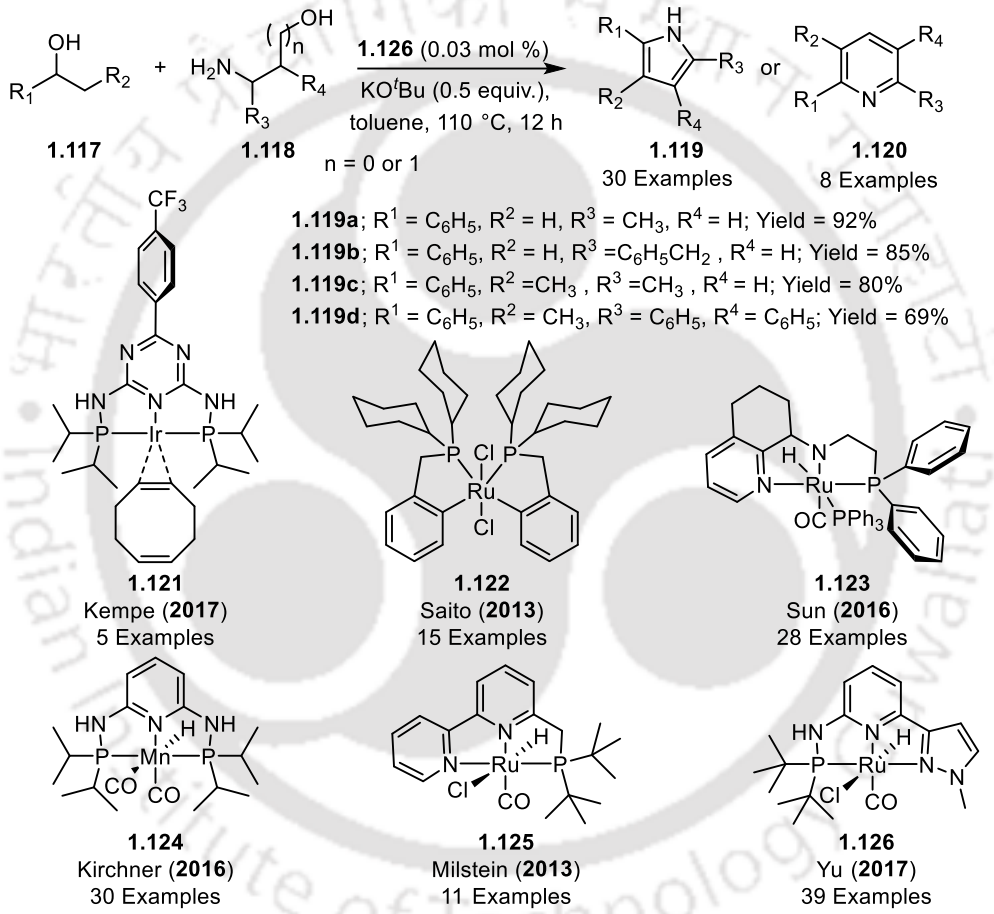

Scheme 1.23: Catalytic dehydrogenative coupling of secondary alcohol with amino alcohol by pincer complexes.[127-132]

Nitrogen-containing heterocyclic compounds such as pyridines and pyrroles are omnipresent in pharmaceuticals and natural products.[133] A large number of synthetic protocols reported by Knorr, Pall-Knorr, Hantzsch, Chichibabin and Kröhnke have been established for synthesis of *N*-heterocyclic compounds.[134] Though, these methods are widely applicable for heterocyclic compound synthesis, there are some drawbacks (harsh reaction conditions, long reaction time and lack of availability of starting material) of this process. Therefore, the synthesis of *N*-

heterocyclic compounds using secondary alcohols with amino alcohols is of great interest.[135] The acceptorless dehydrogenative coupling for the synthesis of pyrrole and pyridine derivatives have been developed using pincer-metal catalysts. *N*-heterocyclic compound synthesis using pincer catalysts have been studied by the groups of Kempe,[127] Yu,[128] Milstein,[129] Saito,[130] Sun[131] and Kirchner[132] with high reactivity and selectivity (Figure **1.23**).

1.3.5 Azines synthesis from alcohols with hydrazine

Azines (RHC=N−N=CHR) are a class of important chemicals required to synthesize *N*-heterocyclic compounds and various polymers.[136] Milstein and co-workers reported PNP pincer-ruthenium **1.62** catalyzed dehydrogenative coupling of alcohol and hydrazine affords azine, which is an atom economical and environmentally benign process (Scheme **1.24**).[137]

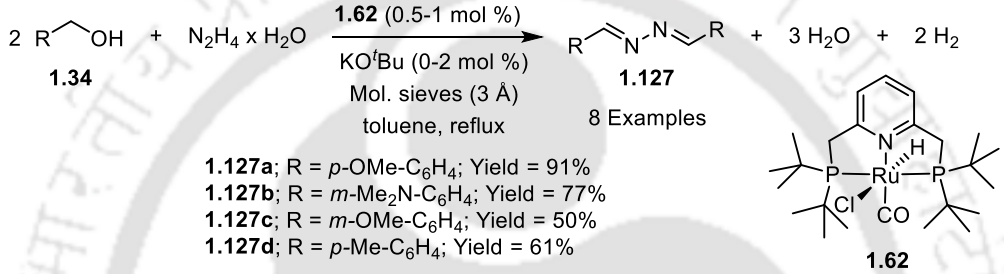

Scheme 1.24: PNP pincer-ruthenium catalyzed synthesis of azines.[137]

1.3.6 Amines synthesis from alcohols with ammonia

Primary amines are synthetically useful, and their synthesis is more challenging than the other amines. The conventional methods typically involve the synthesis of primary amines utilizing toxic agents and often suffer from atom economy.[138-139] Only a few classical techniques are reported for one-pot synthesis of primary amines from alcohols.[140] Alternatively, iridium and rhodium-catalyzed amine synthesis from its corresponding aldehyde have been studied in the presence of hydrogen.[141] However, iridium catalyzed alkylation of alcohol to amines require the presence of ammonium salt.[141] Recently, Milstein and co-workers in an attractive organic transformation, demonstrated the direct catalytic synthesis of primary amines from ammonia using alcohols as an alkylating agent (Scheme **1.25**)[142]. The elimination of water as an only by-product leads to an economically and environmentally highly desirable reaction.

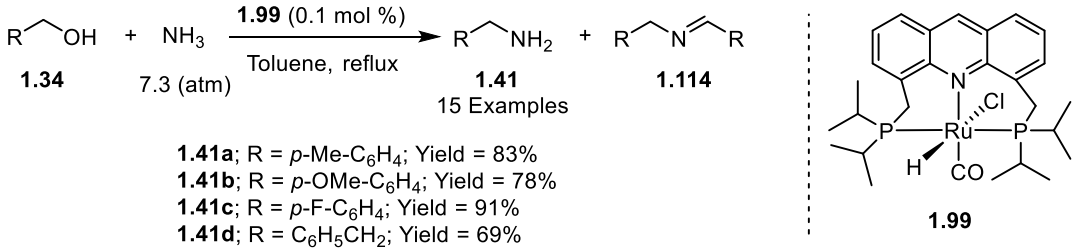

Scheme 1.25: Pincer-ruthenium catalyzed primary amine synthesis starting from ammonia and alcohol.[142]

1.3.7 Pincer-iridium catalyzed alkane dehydrogenation

The catalytic transfer dehydrogenation of alkenes by homogenous pincer complexes has been well developed.[143-145] However, scaling up these catalytic processes on an industrial level has been challenging due to expensive catalysts, poor recyclability, and sensitivity. The current focus is to develop earth-abundant pincer catalysts for dehydrogenation reactions in industrial applications.[146] While the first catalytic alkane dehydrogenation was reported by Crabtree in 1979 in the presence of an acceptor, in 1997, Kaska[147] and Jensen[148] reported the use of a pincer-iridium complex **1.128** for the dehydrogenation of cycloalkanes (equation 1, Scheme **1.26**).[149] Later on, Goldman group reported several PCP pincer-Ir complexes, which demonstrated exceptional activity for the alkane dehydrogenation either in the presence or absence of an acceptor (equation 2, Scheme **1.26**).[42]

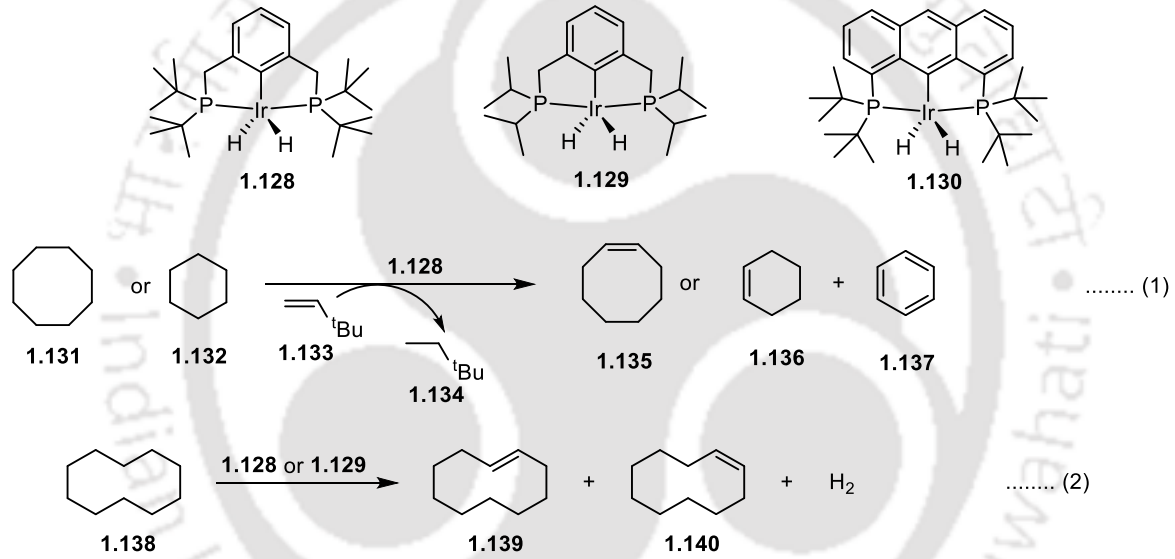

Scheme 1.26: Dehydrogenation of alkane to alkene by pincer-iridium complex.[42, 149]

1.3.8 Pincer-metal catalyzed dehydrogenation of formic acid

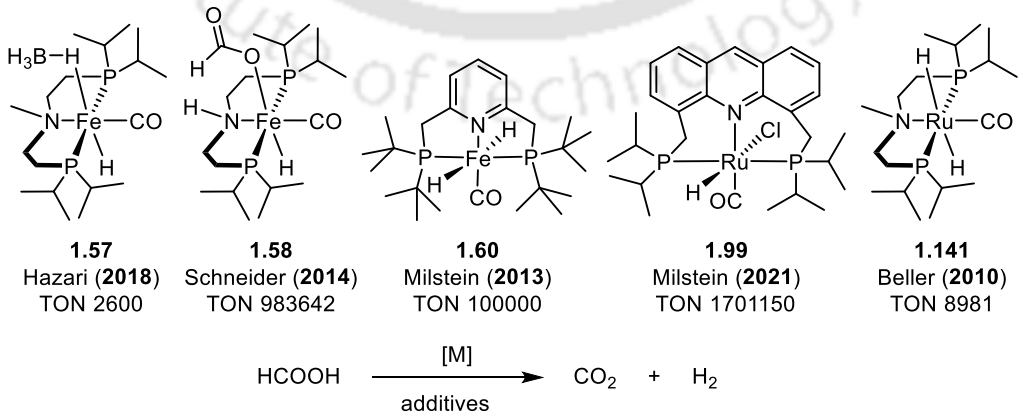

Scheme 1.27: Formic acid dehydrogenation to CO_2 and H_2 catalyzed by pincer complexes.[150-154]

Recently, there has been a surge in the requirement of highly sustainable energy sources, and molecular hydrogen is one of the best options. Formic acid, which is a non-toxic liquid and is easily dehydrogenated in the presence of a catalyst contains 4.4 wt. % hydrogen. In the last decade, pincer complexes have shown remarkable catalytic reactivity towards formic acid dehydrogenation.[155] Milstein and co-workers reported the formic acid dehydrogenation to hydrogen in the presence of pincer-iron catalyst **1.60**. The full conversion of formic acid was observed and up to 100000 TON were obtained in the presence of 50 mol % NEt_3.[154] The same group reported additive-free acridine-based complex **1.99** for the formic acid dehydrogenation to CO_2 and H_2 and observed up to 1701150 TON after a long reaction time (50 days).[153] On the other hand, Beller and co-workers reported pincer-ruthenium **1.141** catalyzed dehydrogenation of formic acid at 4.5 pH to obtain 8981 TON.[152] Schneider group reported pincer-iron **1.58** catalyzed Lewis acid assisted dehydrogenation of formic acid to hydrogen and got up to 983642 TON.[151] Hazari and co-workers reported $PN^{Me}P$ pincer-iron **1.57** catalyzed dehydrogenation of formic acid to CO_2 in the presence of 50 mol % NEt_3 to and achieved up to 2600 TON (Scheme **1.27**).[150]

1.3.9 Hydrogenation of alkenes and alkynes

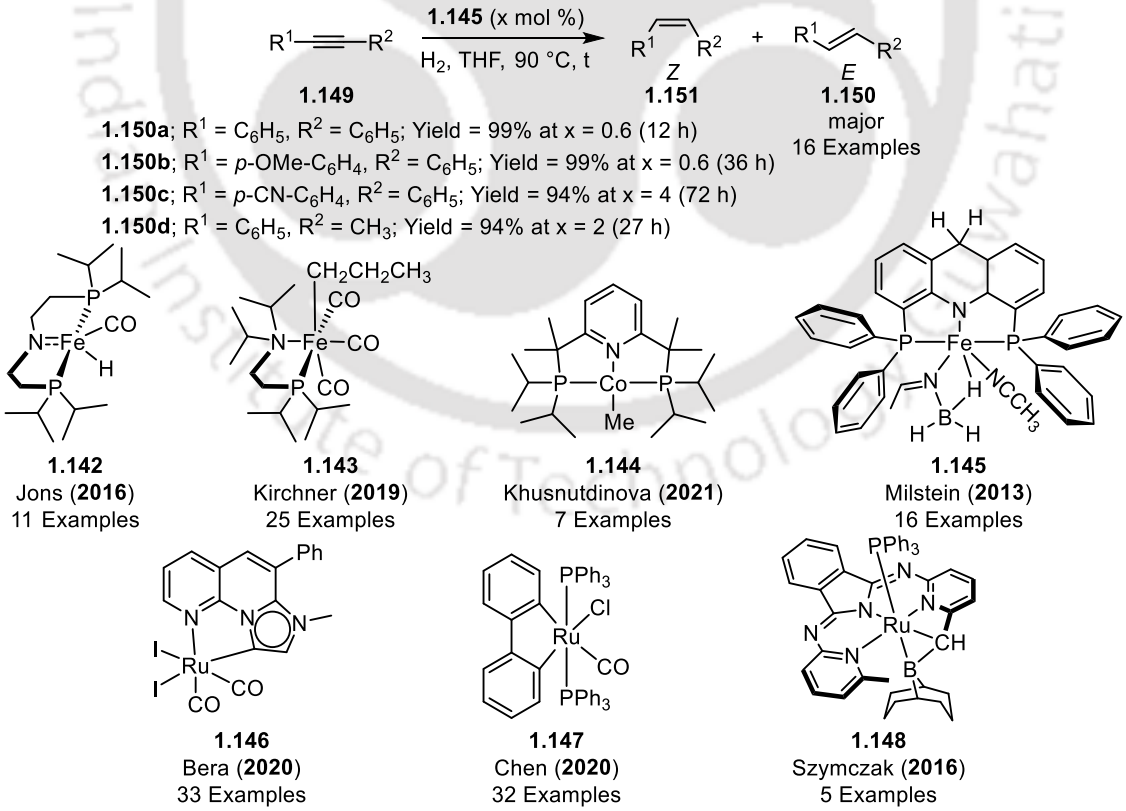

Figure 1.28: Transition metal-catalyzed hydrogenation of alkynes and alkenes.[58, 156-162]

Alkenes are versatile precursors to organic compounds and pharmaceuticals.[163] The design of catalyst for the controlled semi-hydrogenation of alkynes to alkenes remains challenging. The major issue arises due to lack of selectivity and over reduction to alkanes, which has lead to a search for a suitable catalyst.[164] However, obtaining the stereospecific *E*-isomer is more difficult and requires the mode of reduction path in a *syn* fashion. A typical example is the Birch reduction, which lacks functional group tolerance.[165] Therefore, transition metal-catalyzed hydrogenation of alkynes or transfer hydrogenation of alkynes are alternative pathways (Scheme **1.28**).[159] Utilizing molecular hydrogen in hydrogenation reaction is attractive and advantageous in modern technology. In this context, Milstein[158] and Bera[157] group reported the hydrogenation of alkyne by molecular hydrogen to *E*-alkenes using **1.145** and **1.146** as catalyst. Also, the complex **1.146** reported by Bera and co-workers could tolerate the various functional group and provide *E*-alkene in the presence of water. Though utilizing molecular hydrogen is one of the best methods for hydrogenation of alkyne, Chen[156] and co-workers reported ethanol as a hydrogenating source and obtained *E*-isomer selectively in the transfer hydrogenation of several alkynes.

The hydrogenation of olefin with molecular hydrogen is a prominent reaction and several precious metals have been used to hydrogenate alkene or alkyne systems. Particularly base metals like Fe, Co, and Mn are more promising for hydrogenation as a catalyst. They are highly abundant in the earth's crust. Jones[58] group reported 5-coordinated PNP pincer-iron catalyzed hydrogenation of olefin under solvent-free conditions. The reaction has been extended to the reducible functional groups under base-free conditions.

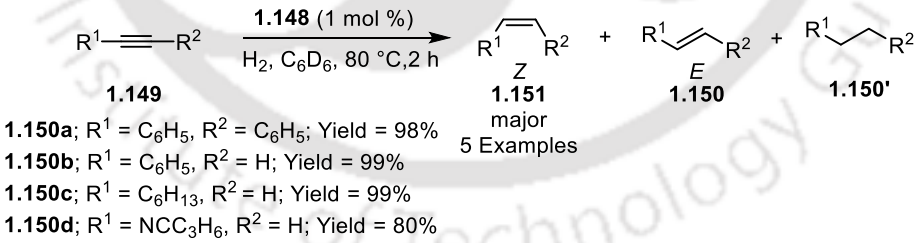

Scheme 1.29: Ruthenium catalyzed selective alkyne hydrogenation.[161]

Similarly, Kirchner and co-workers reported the first example of Mn(I) based catalyst, which hydrogenates olefin to alkane.[160] Khusnutdinova and co-workers reported PNP pincer-cobalt catalyzed hydrogenation of terminal and internal alkynes/alkenes by using molecular hydrogen.[162] Szymczak group reported bifunctional ruthenium-catalyzed alkyne hydrogenation, in which metal-ligand cooperativity plays an important role in catalysis (Scheme **1.29**).[161]

1.3.10 Hydrosilyltion reaction

Hydrosilylation of alkene is one of the pivotal organic transformation reactions and has wide applications in the production of molding products, silicon rubber and pressure-sensitive adhesives.[166] In this process, catalysts obtained from the precious metal complex (mainly Pt and Rh)[167] are involved and an annual 5.6 tons of Pt loss occurs in the hydrosilylation process.[168] Among the other catalytic transformation, hydrosilylation is safer and works under mild reaction conditions.[169] Chirik and co-workers reported the iron(0) complex **1.153** towards the catalytic *anti*-Markovnikov hydrosilylation of olefins (equation 1, Scheme **1.30**).[170] Though the inexpensive and readily available iron complex is environmentally accessible, handling iron (0) complexes requires complete air and moisture-free conditions. However, iron(II) complexes are also active in the hydrosilylation reaction of olefins. Thomas and co-workers reported pincer-iron (II) **1.154** catalyzed hydrosilylation of the olefin at room temperature (equation 1, Scheme **1.30**).[171] Guan and co-workers reported pincer-iron **1.152** catalyzed hydrogenation of ketone derivative in the presence of silane (1.1 equivalent).[172] In particular, PNP or PONOP based pincer-iridium or pincer-ruthenium complexes have emerged as successful catalysts towards this valuable catalytic transformations. The pincer-iron **1.155-156** catalyzed hydrosilylation reactions of carbonyl compounds to alcohols proceeds at room temperature. Thus, PNP and PONOP ligand systems have proved to be versatile for the inexpensive hydrosilylation of carbonyl compounds (equation 2, Scheme **1.30**).[173]

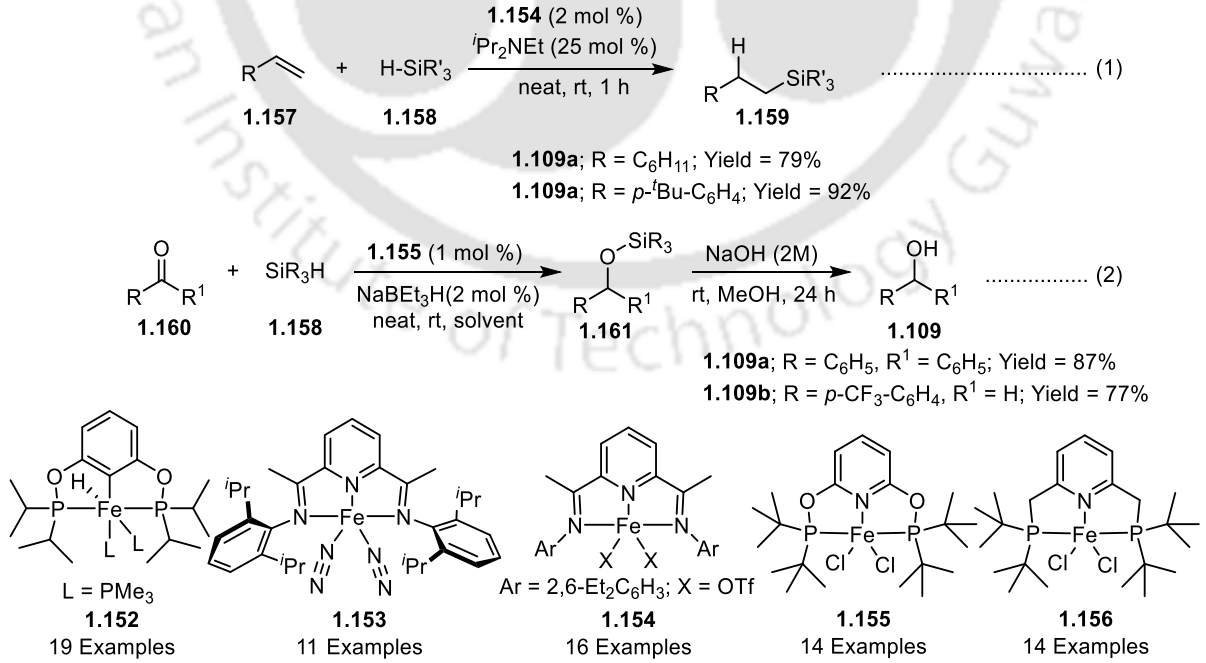

Scheme 1.30: Few examples of pincer-iron catalysts for the hydrosilylation of alkenes and carbonyl compounds.[173]

1.3.11 Transfer hydrogenation of alcohols

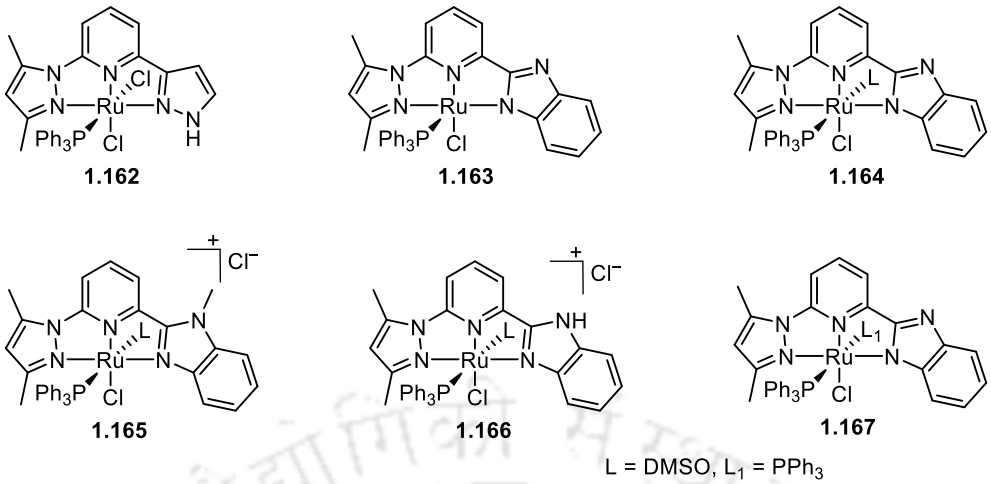

Figure 1.4: Few examples of pincer-ruthenium catalysts reported for transfer (de)hydrogenation.[174-175]

The catalytic transfer hydrogenation of carbonyl compounds to alcohols has been extensively studied.[176] In general, ruthenium complexes (pincer-ruthenium, in particular) have demonstrated exceptional activity towards transfer hydrogenation reaction (TH) of alcohols. Among pincer-Ru catalysts, the unsymmetrical pyridine-pyrazole ligand in combination with ruthenium(II) complexes show an exceptionally high alcohol transfer hydrogenation activity (Figure **1.4**). These NNN ligands have tunable coordination and inherent property that shows hydrogen auto-transfer reactivity of ketones from alcohols, reaching up to 99% conversion. Yu and co-workers reported a series of unsymmetrical pyrazolyl-imidazolyl pyridyl backbone based pincer-ruthenium complexes for the transfer hydrogenation (TH) of ketones and got very high TO/h.[174-175] The 5-coordinated complex **1.163** led to 720000 TO/h within 10 seconds of TH of ketones at 82 °C.[186-175] Similarly, 720000 TO/h was achieved for 6-coordinated complex **1.162** at room temperature (Scheme **1.31**). On the other hand, coordinately saturated complexes **1.164** and **1.167** resulted in 232800 TO/h and 11760 TO/h respectively.[175] These results reflect that the 5-coordinated complex is a more active species and active catalytic precursor. However, 6-coordinated cationic complexes **1.165** and **1.166** demonstrated better activity than the neutral complex and resulted in 240000 TO/h and 29100 TO/h respectively.[175]

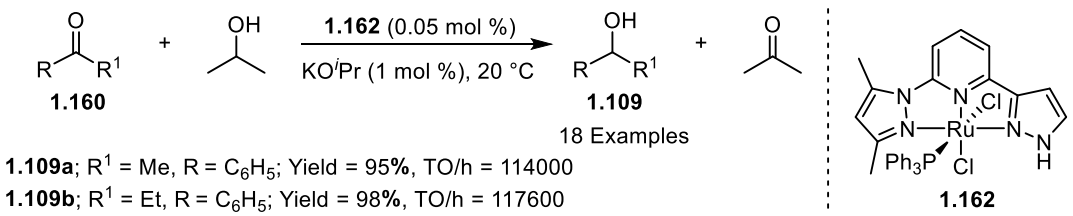

1.109a; R^1 = Me, R = C_6H_5; Yield = 95%, TO/h = 114000
1.109b; R^1 = Et, R = C_6H_5; Yield = 98%, TO/h = 117600
1.109c; R^1 = Me, R = *o*-Br-C_6H_4; Yield = 100%, TO/h = 720000
1.109d; R^1 = Me, R = *o*-Me-C_6H_4; Yield = 96%, TO/h = 691200

Scheme 1.31: Pincer-ruthenium catalyzed transfer hydrogenation reactions.[177]

The replacement of precious metals (like ruthenium) with an inexpensive and readily available base metals such as iron in the transformation of carbonyl compounds using molecular hydrogen are more attractive. Milstein and co-workers reported the hydrogenation of ketone in the presence of molecular hydrogen by hydrido tetrahydridoborate pincer-iron complex **1.168** and obtained up to 330 TO/h. [178] On the other hand, analogous mono hydride complex **1.63** in the presence of the catalytic amount of base gave up to 116 TO/h.[35] This indicates that the dihydrido (hydrido tetrahydridoborate) complex is the active catalyst for hydrogenation of the ketone (Scheme **1.32**).

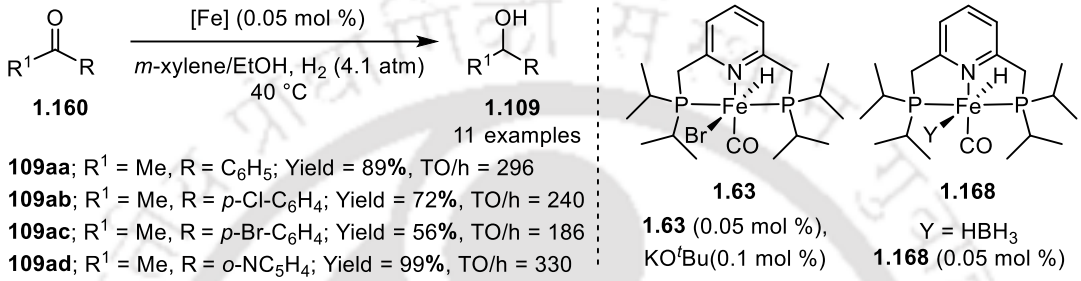

Scheme 1.32: Pincer-iron-catalyzed transfer hydrogenation of ketones.[178]

Pincer complexes have been routinely used to catalytically hydrogenate a wide range of substrates. Owing to their easy tunability, many times the hydrogenation has been shown to be accomplished with a remarkable (regio-, chemo- and stereo-) selectivity. For instance, Xile's group synthesized (^{i}Pr4PONOP)Fe(Br)(H)(CO) **1.169**, which is highly active and selective for hydrogenation of aldehyde moiety (Scheme **1.33**).[179] Use of sodium formate resulted in very high turnover numbers for this chemoselective transformation and is attributed to the involvement of an iron dihydride species.

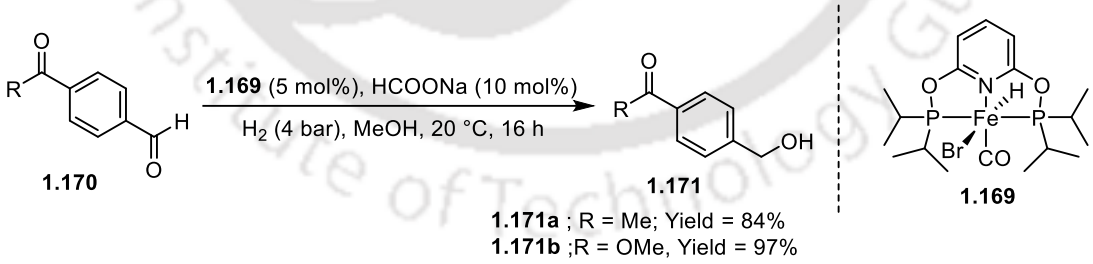

Scheme1.33: Selective hydrogenation of the aldehyde group by a pincer-iron complex.[179]

The hydrogenation of polar double bond by iron (II) catalysts has been widely studied, but achieving the enantioselectivity is one of the essential requirements in the pharmaceuticals.[180] For this purpose, asymmetric transfer hydrogenation (ATH) or direct asymmetric hydrogenation (AH) by using a pincer catalyst is an excellent option.[181] Though, the corresponding chemistry with the pincer ligand is relatively unexplored,[182] Mezzetti group has demonstrated the use of pincer-iron catalyst having C2-symmetry for the direct asymmetric

hydrogenation of ketones. The *S*-isomer of the alcohol was obtained in high yield and good enantiomeric excess (*ee* 49%) (Scheme **1.34**).[183]

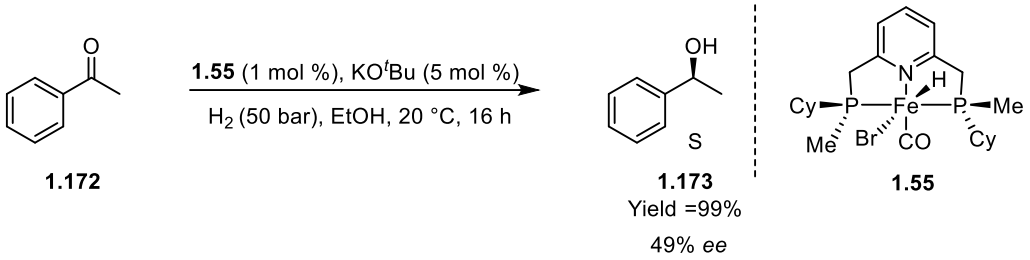

1.172 **1.173** Yield =99% 49% *ee* **1.55**

Scheme 1.34: Asymmetric hydrogenation of acetophenone catalyzed by a pincer-iron complex.[183]

1.3.12 Hydrogenation of carbon dioxide and its derivatives

The last century has seen an unacceptable accumulation of greenhouse gas CO_2 in the earth's environment, which may be attributed to multiple reasons such as excessive use of fossil fuels and [184] fine chemicals. On an optimistic note, one could consider CO_2 as a fundamental, cheap, and readily available C1 feedstock in the natural carbon cycle, whose abundance could be conveniently used to synthesize precious precursors such as formic acid, formaldehyde, and methanol ultimately leading to fine and commodity chemicals. However, it is challenging to activate a highly kinetically inert and thermodynamically stable molecule like CO_2.[40, 185-187]

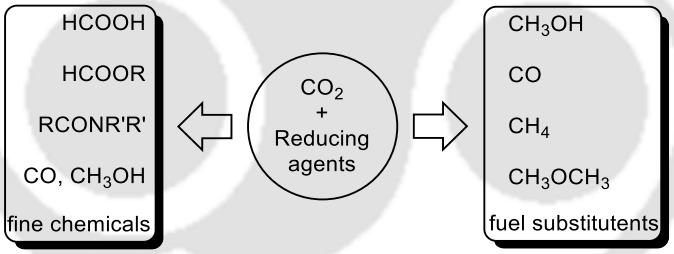

Figure 1.5: Various possible sources of C_1 as a feedstock for fine chemicals and fuels from CO_2.[185]

Being a linear nonpolar molecule with two different reactive sites, high energy is required to overcome the thermodynamic and kinetic barrier.[186] However, in this era of rapidly dwindling fossil fuels and an ever-increasing energy demand associated with steep accumulation of atmospheric CO_2 levels, attempts are being continuously made to positively impact the ecological system via recycling CO_2 as a precursor to fuels and/or fine chemicals.[40, 187] Hydrogenation of CO_2 leads to several useful building blocks that are versatile starting points (Figure **1.5**), mainly via the formation of new C–O, C–N and C–C bonds.[185] Recently, there has been a surge in the industrial use of less reactive CO_2 as a masked source of CO.[186] Milstein and co-workers reported PNP pincer-iron complex **1.60** catalyzed the conversion of $NaHCO_3$ to sodium formate in the presence of molecular hydrogen (8.3 bar) and achieved 320 TON. On

the other hand, the use of molecular carbon dioxide in the presence of hydrogen atmosphere under 10 bar (CO_2: H_2 = 2:1) hydrogenates to formate with 788 TON (Scheme **1.35**).[188] Employing the pincer-iridium complex **1.174,** Nozaki and co-workers reported the hydrogenation of CO_2 at 60 bar (CO_2 : H_2 = 1:1) to formate salts while achieving 3,500,000 TON.[189] However, introducing formate ligand in pincer-iridium complex showed slightly lower reactivity where Hazari and co-workers observed that **1.175** catalyzed CO_2 hydrogenation to formate salt gave 348000 TON at 55 bar (CO_2 : H_2 = 1:1) .[190] Gonsalvi and co-workers demonstrated 10275 TON under 8.5 bar of (CO_2 : H_2 = 1:1) by using **1.59** as a catalyst.[191] Pidko and co-workers observed 1100000 TON at 40 bar (CO_2 : H_2 = 1:1) for the **1.62** catalyzed CO_2 hydrogenation to formate salt (Scheme **1.35**).[192]

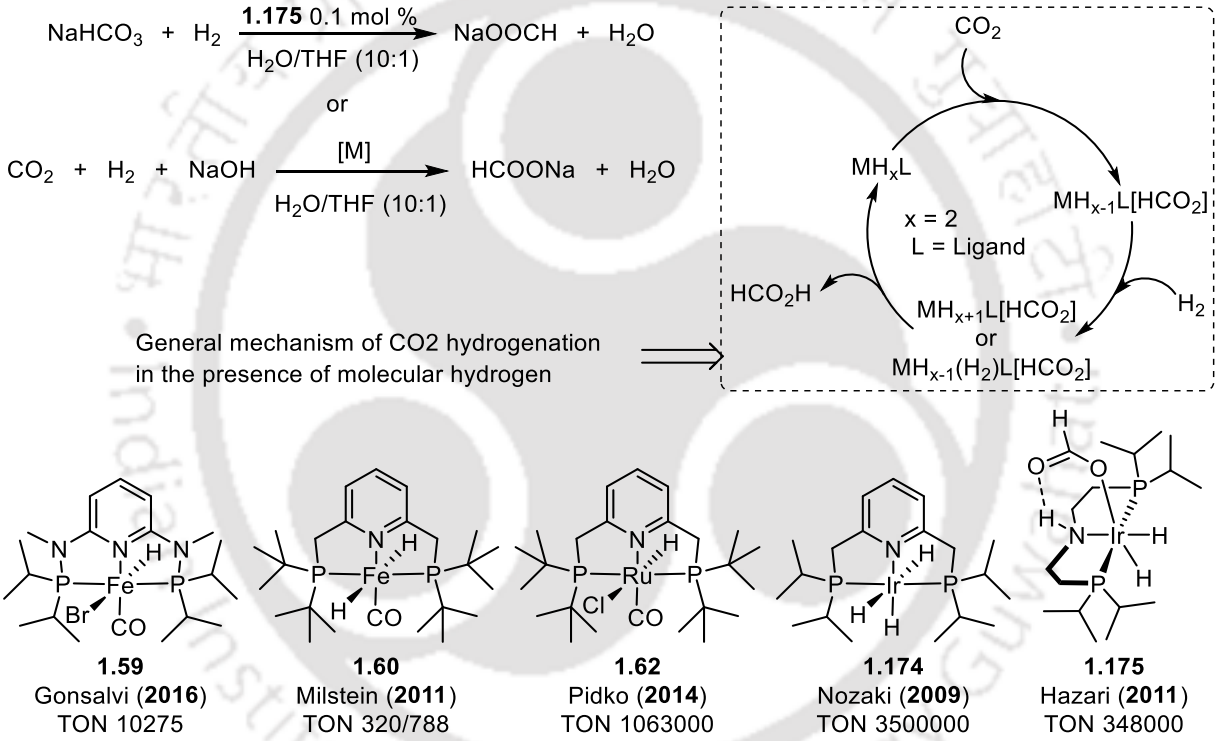

Scheme 1.35: Pincer-metal catalysts screened for the formic acid production from CO_2.[188-192]

The direct hydrogenation of CO_2 to formate is challenging and catalytic efficiency is less under homogenous conditions. The first transition metal catalyzed CO_2 hydrogenation to formic acid and its derivatives was reported by Hashimoto and co-workers in 1976.[193] After this seminal discovery, there has been a flurry of activity, and many organometallic catalytic systems for reduction of carbon dioxide were reported by Periana,[194] Beller,[195] and Sanford.[196] In addition to catalysts based on precious metals such as Ru,[196] Rh,[197] Ir,[195] Pt,[198] Pd[199], complexes based on first-row transition metals have also been reported. For instance, the Beller group has done pioneering work on the catalytic reduction of CO_2 using Co and Fe complexes.[52] The reaction was performed in an alcohol (MeOH and EtOH) medium, which was found to give a formate

ester arising due to condensation between alcohol and formic acid. On the other hand, formic acid underwent a condensation reaction to yield a formamide when amine was used (Scheme **1.36**).

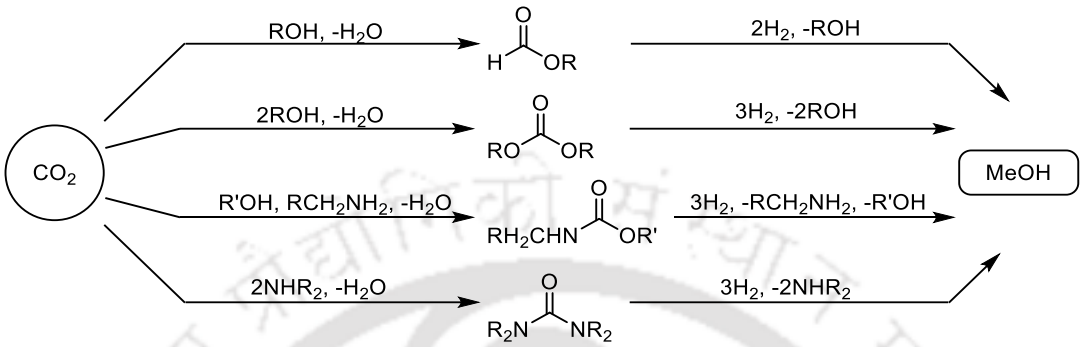

Scheme 1.36: Reported protocols for indirect methanol synthesis from CO_2 using various additives.

1.3.13 Hydrogenation of carbonate and carbamate derivatives

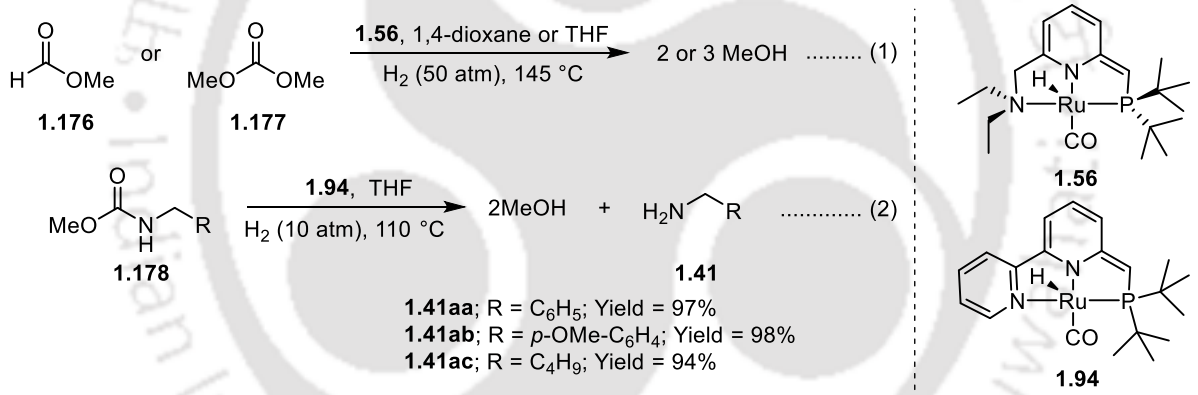

Scheme 1.37: Pincer-Ru catalyzed hydrogenation of carbonate and carbamate derivatives.[200,201-202]

One such example, in the context of indirect methanol formation, is the transformation of CO_2 derivatives as demonstrated by the Milstein's group.[200] For the first time, they used (^{tBu2}PNN^{Et2})Ru(CO)(H) **1.56** to catalytically hydrogenate dimethyl carbonate (DMC) and methyl formate to three and two equivalents of methanol respectively with high turnovers (equation 1, Scheme **1.37**).[200,201] Similarly, carbamates were also transformed into two equivalents of methanol and one equivalent of amine at 100-110 °C under H_2 atmosphere (equation 2, Scheme **1.37**).[203] The methyl formate and methylcarbamate can be readily generated from CO_2+MeOH and CO_2+MeOH+amine, respectively.

1.3.14 Ester hydrogenation to alcohols

Milstein and co-workers demonstrated the (PNN) ruthenium hydride **1.56** catalyzed hydrogenation of non-activated aromatic and aliphatic esters to alcohols under relatively mild and neutral conditions. This reaction proceeds *via* the unusual aromatization/dearomatization sequence of the complex and points to the hemilability of the pincer ligand during catalysis (Scheme **1.38**).[204] Chianese and co-workers reported a CNN pincer-ruthenium precatalyst, which exhibited high reactivity for the ester hydrogenation. In addition, the precatalyst in the presence of NaO^{t}Bu and phosphine ligands undergoes unusual transformation to the rearranged CC version **1.180**, which is a highly active for ester hydrogenation and achieves 990 TON (Scheme **1.38**).[205] Vries and co-workers showed that NNS pincer-ruthenium **1.181** is highly active for ester hydrogenation.[206] This hetero ligand pincer system also tolerates various functional groups towards ester hydrogenation and gives up to 1820 TON (Scheme **1.38**). Guan and co-workers reported the first example of PNP pincer-iron **1.182** catalyzed hydrogenation of unactivated ester to alcohols (Scheme **1.38**).[207]

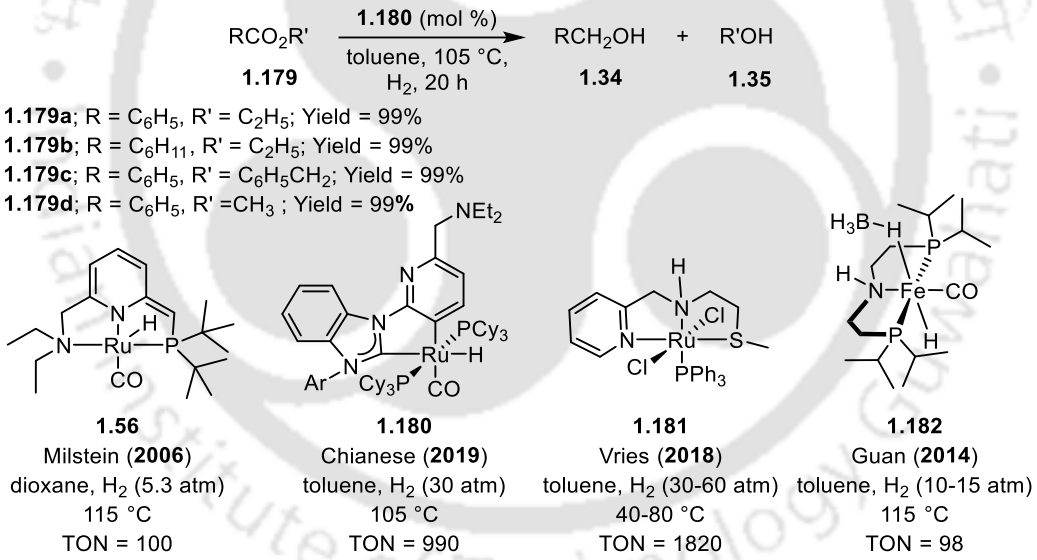

Scheme 1.38: Pincer-metal catalyzed hydrogenation of esters to alcohols.[204-207]

1.3.15 Transfer hydrogenation and oxidation of olefines

Carbene ligands are known as an alternative replacement of phosphine-ligands in homogenous catalysis as it has a higher *trans* effect compared to *N* or *P*.[208] The *mono* carbene requires harsh reaction conditions to get coordinated to the metal center than the *bis* carbene. The chelating pincer carbene complex provides extra thermal stability compared to lower dentate ligands. Peris and co-workers reported a CNC pincer-ruthenium complex for the catalytic transfer hydrogenation of ketone in the presence of 0.1 M of KOH in isopropanol (Scheme **1.39**).[88] In

case of the complex **1.183,** the highest TON (up to 126000) were observed with cyclohexanone as a substrate and $NaIO_4$ as co-catalyst. The olefin oxidation to corresponding carbonyl species were also catalyzed by the complex **1.183** (12 examples, Scheme **1.39**).

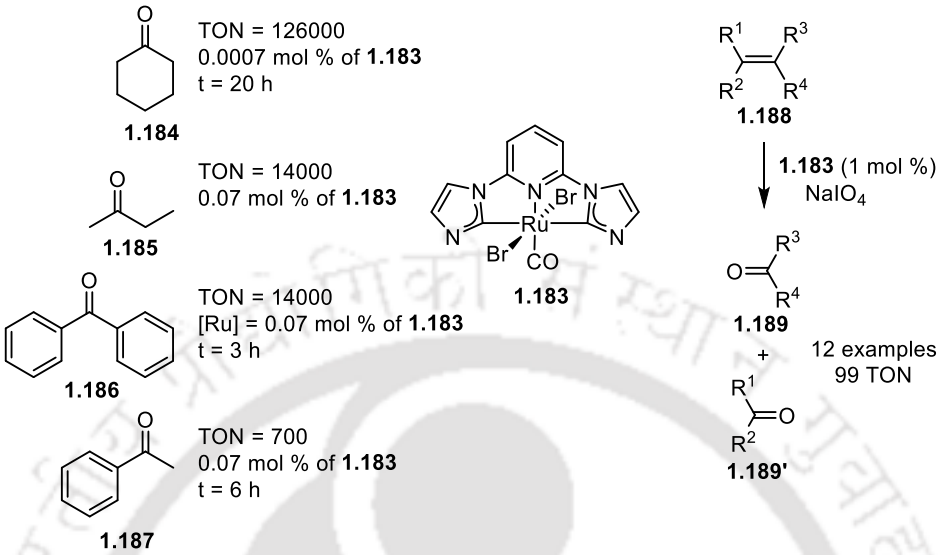

Scheme 1.39: Pincer-ruthenium carbene catalyzed transfer hydrogenation and oxidation reactions.[88]

1.3.16 Pincer-iron catalyzed 3-hydroxyacrylates production from aldehydes

Aromatic aldehydes react with ethyldiazoacetate (EDA) in the presence of Lewis acids (BF_3, $AlCl_3$, $ZnCl_2$, $SnCl_2$, etc.) to give mainly 3-oxo-3-arylpropanoic acid ethyl esters (**1.193**) as major products (Scheme **1.40**).[209-211] Some reports indicate that 3-hydroxy-2-arylacrylic acid ethyl esters **1.194** is formed as a primary product.[212-213] The Kirchner group demonstrated that the PNNNP pincer-iron catalyst **1.190** selectively affords 3-hydroxyacrylates (Scheme **1.40**).

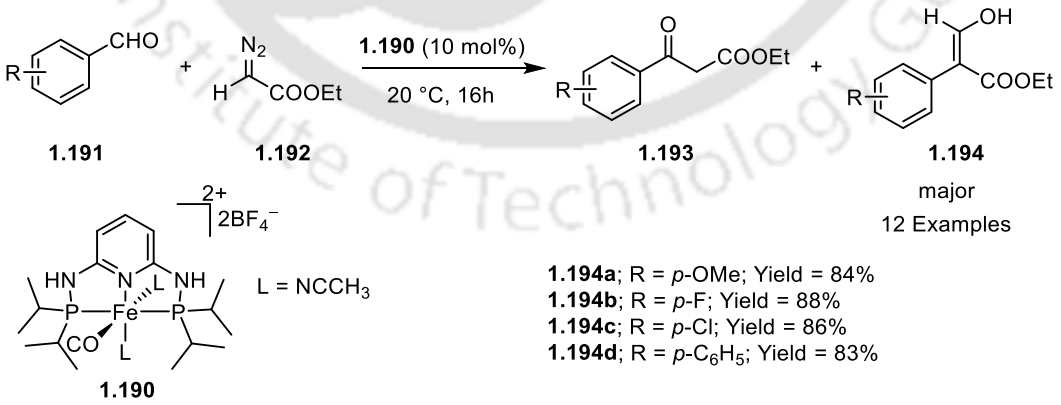

Scheme 1.40: PNNNP pincer-iron catalyzed chemoselective 3-Hydroxyacrylates formation.[209]

1.3.17 Pincer catalyzed deuteration and tritiation of pharmaceuticals

Deuterium or tritium labeling of drug molecules is widely applicable in the pharmaceutical industry as they have altered metabolism and kinetic isotope effect.[214-215] In most of the cases

^{3}H radiolabeled drug molecule is obtained by functional group reduction with stoichiometric reagents or by directly involving the catalytic exchange of hydrogen isotope. Transition metal-catalyzed hydrogen exchange with $^3H_2$ and ^3H_2O has been applied in drug discovery and ADME (Absorption, Distribution, Metabolism and Excretion) studies[216]. Chirik and co-workers reported the hydrogen isotope exchange (HIE)[216] of pharmaceutically relevant drug molecule like Paroxetine, known as a selective serotonin reuptake inhibitor and Cinacalcet which is used alone or with other medications to treat secondary hyperparathyroidism (Scheme **1.41**).[217]

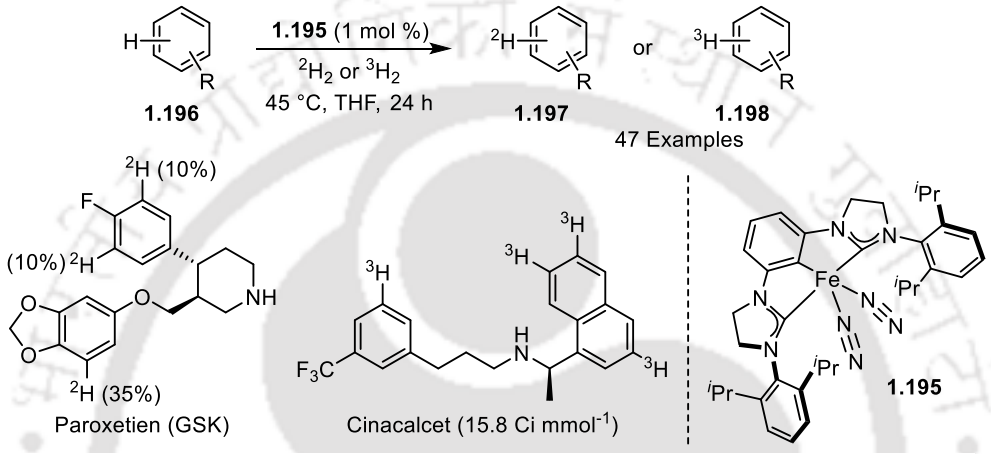

Scheme 1.41: Iron catalyzed deuterium and tritium labeling of the drug molecule.[217]

1.3.18 Olefin polymerizations by (*bis*)imino pincer-complexes

Organometallic complex catalyzed C–C bond forming reaction has been widely used in the laboratory and also in industry.[218] In particular, organometallic catalysts have revolutionized the catalytic olefin polymerization and olefin metathesis reaction.[83] The co-ordination of the ligand is an important point and the spin state of the metal atom plays unique chemistry in these catalysis.[218] Brookhart,[219] Bennett,[220] and Gibson[221] have made pioneering contributions using (*bis*)imino pincer-iron or pincer-cobalt complexes as catalysts for highly active ethylene polymerization (Figure **1.7**)[83] leading to a wide molecular weight range of the ethylene polymer.[222]

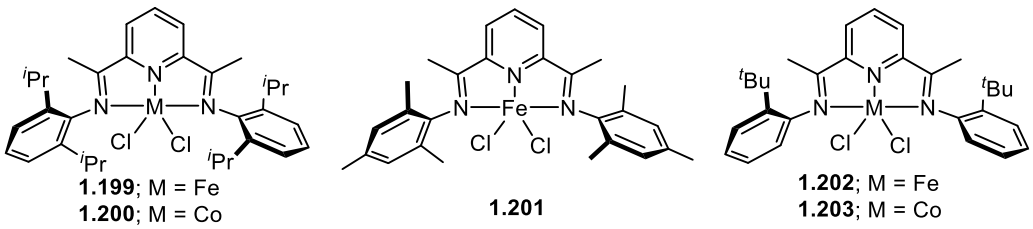

Figure 1.7: Few examples of (*bis*)imino complexes reported for olefin polymerizations.[219-221]

1.3.19 2+2 cycloadditions reaction

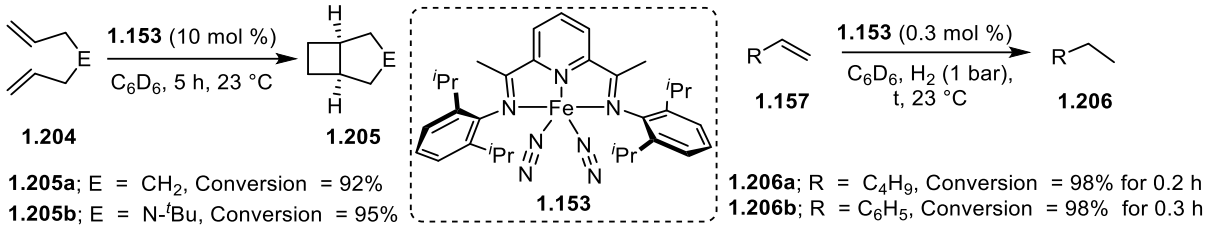

Scheme 1.42: A few valuable transformations of olefins catalyzed by (*bis*)imino based pincer-iron complex.[223]

The metal-catalyzed (2π + 2π) cycloaddition of olefin to cycloalkane is an attractive transformation.[224-225] Transition metal complexes facilitate interaction among the π-systems in the olefins which has restricted orbital symmetry via thermal or photochemical cycloaddition.[224] There has been a large number of literature featuring *bis*(imino)-pyridine, an active redox ligand that have achieved reasonable success in olefin polymerization reactions.[226] Chirik and co-workers reported that the complex **1.153** is a highly efficient catalyst for the hydrogenation of the olefins (Scheme **1.42**).[227] The iron(0) species is also highly efficient for the olefin cycloaddition (Scheme **1.42**).[223]

Enyne cyclization is important in organic synthesis which often requires silanes or weak acids.[228] With the advancement of synthetic methods, there have been significant efforts to replace catalysts based on the expensive metals with earth-abundant metals.[229] Echavarren and co-workers have reported that metal iron precursors like $FeCl_3$ can catalyze the enyne cyclomerization reaction.[230] Though simple metal precursors have limited scope, Fürstnera and co-workers reported a well-defined [(η^5-C_5H_5)Fe(C_2H_4)$_2$][Li(TMEDA)] catalyzed cyclization of enyne having a wide range of scope.[231] Similarly, Chirik and co-workers reported cyclization of enyne and diyne catalyzed by a pincer-iron complex **1.153**, which demostrated comparable turnover frequencies compared to catalyst based on precious metals (Scheme **1.43**).[232-233]

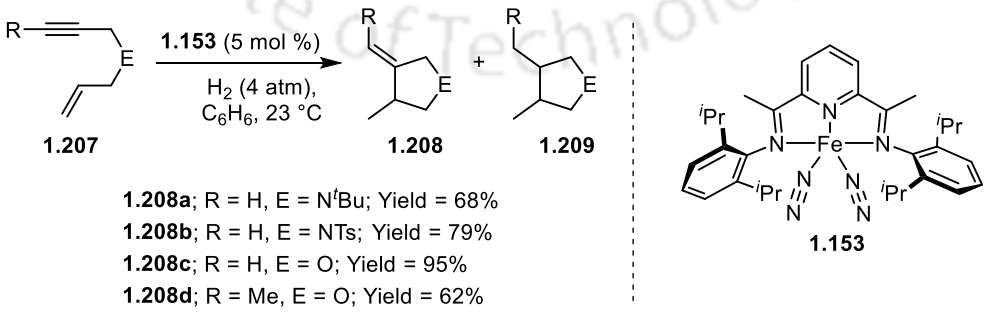

Scheme 1.43: Pincer-iron catalyzed enyen to cyclic product.[232-233]

1.3.20 Heterogenization of molecular-pincer catalysts

In the chemical industry, catalysis is essential to the sector's economic growth and environmental sustainability.[234] In fields as diverse as polymers, pharmaceuticals, agrochemicals, and petrochemicals, catalysts are used in more than 75% of all industrial chemical transformations. In fact, 90% of newly developed processes involve the use of heterogenous catalysts. In addition, these catalysts have wide applicability and their separation is simple which is crucial to the environmental preservation.[234]

Thus, heterogeneous catalysts are frequently used in industrial settings which however operates with typical lack of selectivity under harsh conditions. Homogeneous catalysis, however selective, lacks in the recovery, separation of the catalyst and are expensive compared to heterogenous catalyst. Synthesis of homogenous catalyst not only require expensive starting material but also process through a multistep synthetic pathway. An ideal situation would be to immobilize a homogenous catalyst, so that the resulting system would be recyclable like a heterogenous catalyst while retaining the selectivity that is signature of the homogenous catalyst.[235]

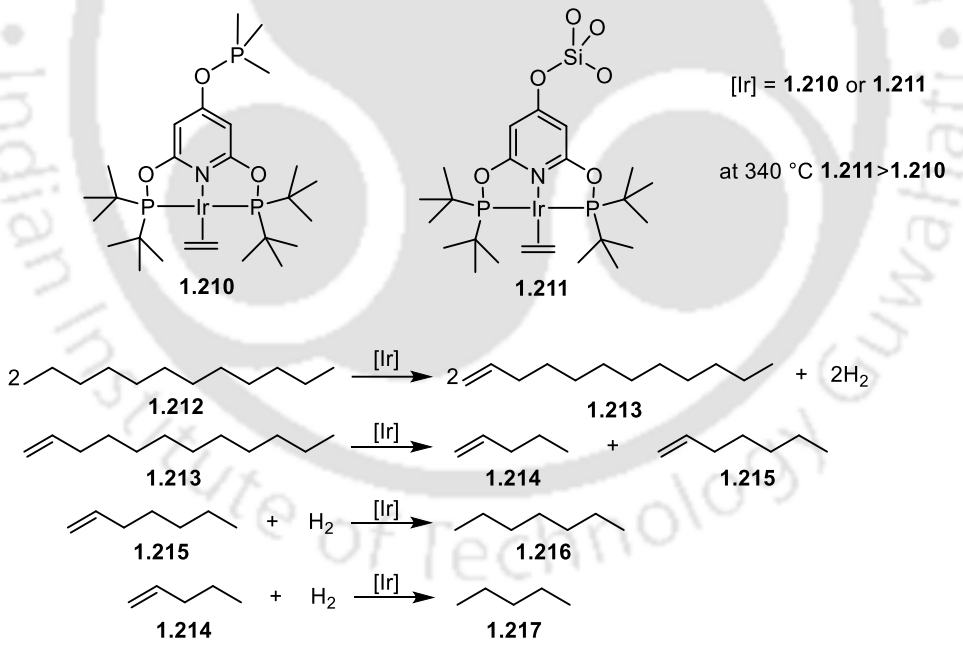

Scheme 1.44: Illustration of iridium catalyzed distribution of dodecane dehydrogenation and cracking-hydrogenation.[235-237]

In this regard, one such example is the dehydrogenation of alkane or cracking-hydrogenation of the alkane which is thermodynamically unfavorable and often requires very high temperature. As, heterogenous catalysts are thermally stable as compared to homogenous counterparts at higher temperature,[235] they will be able to achieve this transformation over the

latter albeit with lack of selectivity. In this context, Celik[235, 237] and Goldman[235-237] have demonstrated that the dehydrogenation of alkane to alkene is more favorable with heterogenous molecular catalyst (solid support on silica) over its analogous homogenous system (Scheme **1.44**).[235] They demonstrated that, the thermal cracking of dodecene at 340 °C provided two lighter olefins, which hydrogenates to give rise to lighter alkane *via* transfer hydrogenation. The overall reaction involves the transformation of 2 equiv. of dodecane to 1 equiv. of dodecene and 2 equiv of lighter alkanes (Scheme **1.44**).[237] However, the rate of cracking is slow relative to dehydrogenation and is independent of catalyst, leading to similar results regardless of which catalyst is employed. On the other hand, dehydrogenation of alkanes to olefin is more efficient, selective and has lower cost as compared to steam cracking. Goldman and Celik have thus described the use of pincer-iridium complexes supported on silica for the effective acceptorless dehydrogenation of alkane and this immobilized molecular catalyst is also stable even at higher temperature.[235]

1.4 Objectives

The extensive literature survey in this chapter discusses metal and pincer-metal complexes in various organic transformations. Energy self-sufficiency is pivotal for a healthy global economy. It is important to generate fuels and fine chemicals from abundant and cheap raw materials in an economical and environmentally-friendly fashion. From an organometallic chemist's perspective, many complexes with a variety of pincer-ligand-metals combinations have been fairly successful in accomplishing this task. There have been a lot of efforts to heterogenize molecular pincer-metal systems. This has helped to circumvent the selectivity issues posed by typical, heterogenous catalysts. However, sensitive reaction conditions, expensive catalysts and poor recyclability are challenges that need to be addressed in the near future. In general, improving the methods to transform organic molecules into value-added chemicals and fuels are desirable. It would be an advantage if one could accomplish this by using a catalyst with reduced toxicity. This thesis as a part of doctoral studies attempts to address the following questions,

- Is it possible to retain and/or enhance the catalytic activity (if any) of pincer-Ru by switching from phosphine-based to nitrogen-based complexes?
- What will be the similarities and/or differences in the mechanistic path followed in the reactions catalyzed by these new class of pincer-Ru?

- Can one generate stable (air and moisture) pincer-Ru complexes based on environmentally friendly amines and imines?
- Will the new pincer-Ru complexes have good thermal stability?
- Do these new pincer-Ru complexes show good activities towards hydrofunctionalization or its microscopic reverse dehydrofunctionalization?
- Can a (de)hydrofunctionilazation of alcohol be coupled with a secondary reaction to attain value-addition?
- Is it possible to accomplish catalytic reactions that are tolerant to water and oxygen?

1.5 References

1. Zeise, W. C., *Ann. Phys. Chem.* **1831**, *97*, 497-541.
2. Mond, L.; Langer, C.; Quincke, F., *J. Chem. Soc., Trans.* **1890**, *57*, 749-753.
3. Mond, L.; Langer, C., *J. Chem. Soc., Trans.* **1891**, *59*, 1090-1093.
4. Grignard, V., Dissertation, Theses sur les combinaisons organomagnesienes mixtes et leur application ades syntheses. University of Lyon, France: Lyon: 1901.
5. Seyferth, D., *Organometallics* **2009**, *28*, 1598-1605.
6. Ziegler, K.; Holzkamp, E.; Breil, H.; Martin, H., *Angew. Chem.* **1955**, *67*, 426-426.
7. Natta, G., *J. Polym. Sci. A Polym. Chem.* **1996**, *34*, 321-332.
8. Kubas, G. J., HETEROLYTIC SPLITTING OF H□H, Si□H, AND OTHER σ BONDS ON ELECTROPHILIC METAL CENTERS. In *Adv. Inorg. Chem.*, Academic Press: **2004**; Vol. 56, pp 127-177.
9. Alonso, F.; Beletskaya, I. P.; Yus, M., *Chem. Rev.* **2004**, *104*, 3079-3160.
10. Ojima, I.; Tzamarioudaki, M.; Li, Z.; Donovan, R. J., *Chem. Rev.* **1996**, *96*, 635-662.
11. Merola Joseph, S., *Iridium: Organometallic Chemistry*. **2006**.
12. Chen, J. T., *Platinum: Organometallic Chemistry Based in part on the article Platinum: Organometallic Chemistry by Charles M. Lukehart which appeared in the Encyclopedia of Inorganic Chemistry, First Edition*. **2006**.
13. Sperger, T.; Sanhueza, I. A.; Kalvet, I.; Schoenebeck, F., *Chem. Rev.* **2015**, *115*, 9532-9586.
14. Luh, T.-Y.; Leung, M.-k.; Wong, K.-T., *Chem. Rev.* **2000**, *100*, 3187-3204.
15. Paradine, S. M.; Griffin, J. R.; Zhao, J.; Petronico, A. L.; Miller, S. M.; Christina White, M., *Nat. Chem.* **2015**, *7*, 987-994.
16. Zhang, W.; Sun, W.-H.; Zhang, S.; Hou, J.; Wedeking, K.; Schultz, S.; Fröhlich, R.; Song, H., *Organometallics* **2006**, *25*, 1961-1969.
17. Altenhoff, G.; Glorius, F., *Adv. Synth. Catal.* **2004**, *346*, 1661-1664.
18. Witcoff, H.; Reuben, B.; Plotkin, J., **1996**, *Industrial Organic Chemistry*.
19. Sanfilippo, D.; Rylander, P. N., *Ullmann's encycl. ind. chem.* **2000**, *Hydrogenation and dehydrogenation*.
20. Togni, A.; Grützmacher, H., *Catalytic Heterofunctionalization: From Hydroamination to Hydrozirconization*. Wiley-VCH: **2001**.
21. Sevov, C. S.; Hartwig, J. F., *J. Am. Chem. Soc.* **2013**, *135*, 9303-9306.
22. Haibach, M. C.; Guan, C.; Wang, D. Y.; Li, B.; Lease, N.; Steffens, A. M.; Krogh-Jespersen, K.; Goldman, A. S., *J. Am. Chem. Soc.* **2013**, *135*, 15062-15070.
23. Sevov, C. S.; Hartwig, J. F., *J. Am. Chem. Soc.* **2013**, *135*, 9303-9306.

24. Marciniec, B., *Hydrosilylation: a comprehensive review on recent advances*. Springer Science & Business Media: **2008**; Vol. 1.
25. Brown, H. C., *Tetrahedron* **1961**, *12*, 117-138.
26. Franke, R.; Selent, D.; Börner, A., *Chem. Rev.* **2012**, *112*, 5675-5732.
27. Takaya, J.; Iwasawa, N., *J. Am. Chem. Soc.* **2008**, *130*, 15254-15255.
28. Williamson, A., *Lond. Edinb. Dublin philos. mag. j. sci.* **1850**, *37*, 350-356.
29. Williamson, A., *Philos. Mag. Lett.* **1850**, *37*, 350-356.
30. Crabtree, R. H., *Chem. Rev.* **2017**, *117*, 9228-9246.
31. Gunanathan, C.; Milstein, D., *Chem. Rev.* **2014**, *114*, 12024-12087.
32. Xi, Y.; Hartwig, J. F., *J. Am. Chem. Soc.* **2016**, *138*, 6703-6706.
33. Jung, M. S.; Kim, W. S.; Shin, Y. H.; Jin, H. J.; Kim, Y. S.; Kang, E. J., *Org. Lett.* **2012**, *14*, 6262-6265.
34. Gorgas, N.; Stöger, B.; Veiros, L. F.; Kirchner, K., *ACS Catal.* **2016**, *6*, 2664-2672.
35. Langer, R.; Leitus, G.; Ben-David, Y.; Milstein, D., *Angew. Chem. Int. Ed.* **2011**, *50*, 2120-2124.
36. Elangovan, S.; Topf, C.; Fischer, S.; Jiao, H.; Spannenberg, A.; Baumann, W.; Ludwig, R.; Junge, K.; Beller, M., *J. Am. Chem. Soc.* **2016**, *138*, 8809-8814.
37. Jessop, P. G.; Ikariya, T.; Noyori, R., *Chem. Rev.* **1995**, *95*, 259-272.
38. Bielinski, E. A.; Förster, M.; Zhang, Y.; Bernskoetter, W. H.; Hazari, N.; Holthausen, M. C., *ACS Catal.* **2015**, *5*, 2404-2415.
39. Heim, L. E.; Schlörer, N. E.; Choi, J.-H.; Prechtl, M. H. G., *Nat. Commun.* **2014**, *5*, 3621.
40. Rylander, P. N., Hydrogenation and Dehydrogenation. In *Ullmann's Encyclopedia of Industrial Chemistry*, Wiley-VCH Verlag GmbH & Co. KGaA: **2000**.
41. Birch, A.; Williamson, D., *Org. React.* **2004**, *24*, 1-186.
42. Kumar, A.; Bhatti, T. M.; Goldman, A. S., *Chem. Rev.* **2017**, *117*, 12357-12384.
43. Jia, W.-G.; Ling, S.; Zhang, H.-N.; Sheng, E.-H.; Lee, R., *Organometallics* **2017**.
44. Chakraborty, S.; Milstein, D., *ACS Catal.* **2017**, 3968-3972.
45. Yang, T. K.; Lee, D. S.; Haas, J., *Raney Nickel* **2006**, https://doi.org/10.1002/047084289X.rr001.pub2.
46. Heiden, Z. M.; Gorecki, B. J.; Rauchfuss, T. B., *Organometallics* **2008**, *27*, 1542-1549.
47. Komarewsky, V. I.; Miller, D., 71 Hydrogenation with Metal Oxide Catalysts. In *Advances in Catalysis*, Farkas, A., Ed. Academic Press: 1957; Vol. 9, pp 707-715.
48. Slaugh, L. H., *J. Org. Chem.* **1967**, *32*, 108-113.
49. Chen, Z.; Chen, J.; Li, Y., *Chinese J. Catal.* **2017**, *38*, 1108-1126.
50. Senger, S.; Radom, L., *J. Am. Chem. Soc.* **2000**, *122*, 2613-2620.
51. Axenov, K. V.; Kehr, G.; Fröhlich, R.; Erker, G., *J. Am. Chem. Soc.* **2009**, *131*, 3454-3455.
52. Bernskoetter, W. H.; Hazari, N., *Acc. Chem. Res.* **2017**, *50*, 1049-1058.
53. Tan, X.; Wang, G.; Zhu, Z.; Ren, C.; Zhou, J.; Lv, H.; Zhang, X.; Chung, L. W.; Zhang, L.; Zhang, X., *Org. Lett.* **2016**, *18*, 1518-1521.
54. Wang, R.; Tang, Y.; Xu, M.; Meng, C.; Li, F., *J. Org. Chem.* **2018**, *83*, 2274-2281.
55. O, W. W. N.; Morris, R. H., *ACS Catal.* **2013**, *3*, 32-40.
56. Werkmeister, S.; Junge, K.; Beller, M., *Org. Process Res. Dev.* **2014**, *18*, 289-302.
57. Konnerth, H.; Prechtl, M. H. G., *Chem. Commun.* **2016**, *52*, 9129-9132.
58. Xu, R.; Chakraborty, S.; Bellows, S. M.; Yuan, H.; Cundari, T. R.; Jones, W. D., *ACS Catal.* **2016**, *6*, 2127-2135.
59. Deshpande, R. M.; Mahajan, A. N.; Diwakar, M. M.; Ozarde, P. S.; Chaudhari, R. V., *J. Org. Chem.* **2004**, *69*, 4835-4838.
60. Chakraborty, S.; Leitus, G.; Milstein, D., *Chem. Commun.* **2016**, *52*, 1812-1815.

61. Li, H.; Wang, Y.; Lai, Z.; Huang, K.-W., *ACS Catal.* **2017**, *7*, 4446-4450.
62. Harmon, R. E.; Gupta, S. K.; Brown, D. J., *Chem. Rev.* **1973**, *73*, 21-52.
63. Heutz Frank, J. L.; Erken, C.; Aguila Mae Joanne, B.; Lefort, L.; Kamer Paul, C. J., *ChemCatChem* **2016**, *8*, 1896-1900.
64. Yamamoto, T.; Hasegawa, H.; Hakogi, T.; Katsumura, S., *Org. Lett.* **2006**, *8*, 5569-5572.
65. Kim, W.-H.; Park, I. S.; Park, J., *Org. Lett.* **2006**, *8*, 2543-2545.
66. Tseng, K.-N. T.; Rizzi, A. M.; Szymczak, N. K., *J. Am. Chem. Soc.* **2013**, *135*, 16352-16355.
67. Das, K.; Kumar, A., Chapter One - Alkane dehydrogenation reactions catalyzed by pincer-metal complexes. In *Adv. Organomet. Chem.*, Pérez, P. J., Ed. Academic Press: **2019**; Vol. 72, pp 1-57.
68. van der Boom, M. E.; Milstein, D., *Chem. Rev.* **2003**, *103*, 1759-1792.
69. Moulton, C. J.; Shaw, B. L., *J. Chem. Soc., Dalton Trans.* **1976**, 1020-1024.
70. Wang, W.; Gu, P.; Wang, Y.; Wei, H., *Organometallics* **2014**, *33*, 847-857.
71. Empsall, H. D.; Hyde, E. M.; Markham, R.; McDonald, W. S.; Norton, M. C.; Shaw, B. L.; Weeks, B., *J. Chem. Soc., Chem. Commun.* **1977**, 589-590.
72. van Koten, G., Tuning the reactivity of metals held in a rigid ligand environment. In *Pure Appl. Chem.*, 1989; Vol. 61, p 1681.
73. Miller, E. M.; Shaw, B. L., *J. Chem. Soc., Dalton Trans.* **1974**, 480-485.
74. Jones, C. E.; Shaw, B. L.; Turtle, B. L., *J. Chem. Soc., Dalton Trans.* **1974**, 992-999.
75. Younus, H. A.; Su, W.; Ahmad, N.; Chen, S.; Verpoort, F., *Adv. Synth. Catal.* **2015**, *357*, 283-330.
76. Weissberg, A.; Portnoy, M., *Chem. Commun.* **2003**, 1538-1539.
77. Krishnakumar, V.; Chatterjee, B.; Gunanathan, C., *Inorg. Chem* **2017**, *56*, 7278-7284.
78. Pelczar, E. M.; Emge, T. J.; Krogh-Jespersen, K.; Goldman, A. S., *Organometallics* **2008**, *27*, 5759-5767.
79. Zhang, J.; Gandelman, M.; Herrman, D.; Leitus, G.; Shimon, L. J. W.; Ben-David, Y.; Milstein, D., *Inorg. Chim. Acta* **2006**, *359*, 1955-1960.
80. Dani, P.; Karlen, T.; Gossage Robert, A.; Gladiali, S.; van Koten, G., *Angew. Chem. Int. Ed.* **2000**, *39*, 743-745.
81. Cao, X.-N.; Wan, X.-M.; Yang, F.-L.; Li, K.; Hao, X.-Q.; Shao, T.; Zhu, X.; Song, M.-P., *J. Org. Chem.* **2018**, *83*, 3657-3668.
82. Kiernicki, J. J.; Zeller, M.; Szymczak, N. K., *J. Am. Chem. Soc.* **2017**, *139*, 18194-18197.
83. Chirik, P. J., *Angew. Chem. Int. Ed.* **2017**, *56*, 5170-5181.
84. Sutter, J.-P.; James, S. L.; Steenwinkel, P.; Karlen, T.; Grove, D. M.; Veldman, N.; Smeets, W. J. J.; Spek, A. L.; van Koten, G., *Organometallics* **1996**, *15*, 941-948.
85. Feichtner, K.-S.; Scherpf, T.; Gessner, V. H., *Organometallics* **2017**, *37*, 645–654.
86. Gunanathan, C.; Ben-David, Y.; Milstein, D., *Science* **2007**, *317*, 790.
87. Poverenov, E.; Gandelman, M.; Shimon, L. J. W.; Rozenberg, H.; Ben-David, Y.; Milstein, D., *Organometallics* **2005**, *24*, 1082-1090.
88. Poyatos, M.; Mata, J. A.; Falomir, E.; Crabtree, R. H.; Peris, E., *Organometallics* **2003**, *22*, 1110-1114.
89. Danopoulos, A. A.; Winston, S.; Motherwell, W. B., *Chem. Commun.* **2002**, 1376-1377.
90. Langer, R.; Diskin-Posner, Y.; Leitus, G.; Shimon Linda, J. W.; Ben-David, Y.; Milstein, D., *Angew. Chem. Int. Ed.* **2011**, *50*, 9948-9952.
91. Yoshida, T.; Otsuka, S., *J. Am. Chem. Soc.* **1977**, *99*, 2134-2140.
92. Paonessa, R. S.; Trogler, W. C., *J. Am. Chem. Soc.* **1982**, *104*, 1138-1140.

93. Salem, H.; Shimon, L. J. W.; Diskin-Posner, Y.; Leitus, G.; Ben-David, Y.; Milstein, D., *Organometallics* **2009**, *28*, 4791-4806.
94. Gnanaprakasam, B.; Zhang, J.; Milstein, D., *Angew. Chem. Int. Ed.* **2010**, *49*, 1468-1471.
95. Trovitch, R. J.; Lobkovsky, E.; Chirik, P. J., *Inorg. Chem* **2006**, *45*, 7252-7260.
96. Zhang, J.; Gandelman, M.; Shimon, L. J. W.; Rozenberg, H.; Milstein, D., *Organometallics* **2004**, *23*, 4026-4033.
97. Alabau, R. G.; Esteruelas, M. A.; Martínez, A.; Oliván, M.; Oñate, E., *Organometallics* **2018**, *37*, 2732-2740.
98. Zhang, J.; Leitus, G.; Ben-David, Y.; Milstein, D., *J. Am. Chem. Soc.* **2005**, *127*, 10840-10841.
99. Srimani, D.; Balaraman, E.; Gnanaprakasam, B.; Ben-David, Y.; Milstein, D., *Adv. Syn. Catal* **2012**, *354*, 2403-2406.
100. Nielsen, M.; Junge, H.; Kammer, A.; Beller, M., *Angew. Chem. Int. Ed.* **2012**, *51*, 5711-5713.
101. Gusev, D. G., *ACS Catal.* **2016**, *6*, 6967-6981.
102. He, X.; Li, Y.; Fu, H.; Zheng, X.; Chen, H.; Li, R.; Yu, X., *Organometallics* **2019**, *38*, 1750-1760.
103. Gunanathan, C.; Shimon, L. J. W.; Milstein, D., *J. Am. Chem. Soc.* **2009**, *131*, 3146-3147.
104. Lawrence, S. A., *Amines: synthesis, properties and applications*. Cambridge University Press: **2004**.
105. Tojo, G.; Fernandez, M. I., *Oxidation of alcohols to aldehydes and ketones: a guide to current common practice*. Springer Science & Business Media: **2006**.
106. Pattabiraman, V. R.; Bode, J. W., *Nature* **2011**, *480*, 471-479.
107. Kolakowski, R. V.; Shangguan, N.; Sauers, R. R.; Williams, L. J., *J. Am. Chem. Soc.* **2006**, *128*, 5695-5702.
108. Schley, N. D.; Dobereiner, G. E.; Crabtree, R. H., *Organometallics* **2011**, *30*, 4174-4179.
109. Gunanathan, C.; Ben-David, Y.; Milstein, D., *Science* **2007**, *317*, 790-792.
110. Lane, E. M.; Uttley, K. B.; Hazari, N.; Bernskoetter, W., *Organometallics* **2017**, *36*, 2020–2025.
111. Oldenhuis, N. J.; Dong, V. M.; Guan, Z., *Tetrahedron* **2014**, *70*, 4213-4218.
112. Srimani, D.; Balaraman, E.; Hu, P.; Ben-David, Y.; Milstein, D., *Adv. Synth. Catal.* **2013**, *355*, 2525-2530.
113. Kobayashi, S.; Ishitani, H., *Chem. Rev.* **1999**, *99*, 1069-1094.
114. Salvatore, R. N.; Yoon, C. H.; Jung, K. W., *Tetrahedron* **2001**, *57*, 7785-7811.
115. Gunanathan, C.; Milstein, D., *Science* **2013**, *341*, 1229712.
116. Filonenko, G. A.; van Putten, R.; Hensen, E. J. M.; Pidko, E. A., *Chem. Soc. Rev.* **2018**, *47*, 1459-1483.
117. Mastalir, M.; Stöger, B.; Pittenauer, E.; Puchberger, M.; Allmaier, G.; Kirchner, K., *Adv. Synth. Catal.* **2016**, *358*, 3824-3831.
118. Gunanathan, C.; Milstein, D., *Acc. Chem. Res.* **2011**, *44*, 588-602.
119. Maji, M.; Chakrabarti, K.; Paul, B.; Roy, B. C.; Kundu, S., *Adv. Synth. Catal.* **2017**, *360*, 722-729.
120. Shee, S.; Paul, B.; Panja, D.; Roy, B. C.; Chakrabarti, K.; Ganguli, K.; Das, A.; Das, G. K.; Kundu, S., *Adv. Synth. Catal.* **2017**, *359*, 3888-3893.
121. Gnanamgari, D.; Leung, C. H.; Schley, N. D.; Hilton, S. T.; Crabtree, R. H., *Org. Biomol. Chem.* **2008**, *6*, 4442-4445.
122. Wang, Q.; Wu, K.; Yu, Z., *Organometallics* **2016**, *35*, 1251-1256.

123. Bloch, R., *Chem. Rev.* **1998**, *98*, 1407-1438.
124. Su, F.; Mathew, S. C.; Möhlmann, L.; Antonietti, M.; Wang, X.; Blechert, S., *Angew. Chem. Int. Ed.* **2011**, *50*, 657-660.
125. Liu, L.; Zhang, S.; Fu, X.; Yan, C.-H., *Chem. Commun.* **2011**, *47*, 10148-10150.
126. He, L.-P.; Chen, T.; Gong, D.; Lai, Z.; Huang, K.-W., *Organometallics* **2012**, *31*, 5208-5211.
127. Hille, T.; Irrgang, T.; Kempe, R., *Angew. Chem. Int. Ed.* **2017**, *56*, 371-374.
128. Chai, H.; Wang, L.; Liu, T.; Yu, Z., *Organometallics* **2017**, *36*, 4936–4942.
129. Srimani, D.; Ben-David, Y.; Milstein, D., *Angew. Chem. Int. Ed.* **2013**, *52*, 4012-4015.
130. Iida, K.; Miura, T.; Ando, J.; Saito, S., *Org. Lett.* **2013**, *15*, 1436-1439.
131. Pan, B.; Liu, B.; Yue, E.; Liu, Q.; Yang, X.; Wang, Z.; Sun, W.-H., *ACS Catal.* **2016**, *6*, 1247-1253.
132. Mastalir, M.; Glatz, M.; Pittenauer, E.; Allmaier, G.; Kirchner, K., *J. Am. Chem. Soc.* **2016**, *138*, 15543-15546.
133. Estévez, V.; Villacampa, M.; Menéndez, J. C., *Chem. Soc. Rev.* **2010**, *39*, 4402-4421.
134. Allais, C.; Grassot, J.-M.; Rodriguez, J.; Constantieux, T., *Chem. Rev.* **2014**, *114*, 10829-10868.
135. Chelucci, G., *Coord. Chem. Rev.* **2017**, *331*, 37-53.
136. Goodall, G. W.; Hayes, W., *Chem. Soc. Rev.* **2006**, *35*, 280-312.
137. Bauer, J. O.; Leitus, G.; Ben-David, Y.; Milstein, D., *ACS Catal.* **2016**, *6*, 8415-8419.
138. White, E. H.; Elliger, C. A., *J. Am. Chem. Soc.* **1965**, *87*, 5261-5262.
139. Bartoli, G.; Di Antonio, G.; Giovannini, R.; Giuli, S.; Lanari, S.; Paoletti, M.; Marcantoni, E., *J. Org. Chem.* **2008**, *73*, 1919-1924.
140. Kitamura, M.; Suga, T.; Chiba, S.; Narasaka, K., *Org. Lett.* **2004**, *6*, 4619-4621.
141. Gross, T.; Seayad, A. M.; Ahmad, M.; Beller, M., *Org. Lett.* **2002**, *4*, 2055-2058.
142. Gunanathan, C.; Milstein, D., *Angew. Chem. Int. Ed.* **2008**, *47*, 8661-8664.
143. Dobereiner, G. E.; Crabtree, R. H., *Chem. Rev.* **2010**, *110*, 681-703.
144. Wang, D.; Astruc, D., *Chem. Rev.* **2015**, *115*, 6621-6686.
145. Choi, J.; MacArthur, A. H. R.; Brookhart, M.; Goldman, A. S., *Chem. Rev.* **2011**, *111*, 1761-1779.
146. Zell, T.; Milstein, D., *Acc. Chem. Res.* **2015**, *48*, 1979-1994.
147. Gupta, M.; Hagen, C.; Flesher, R. J.; Kaska, W. C.; Jensen, C. M., *Chem. Commun.* **1996**, 2083-2084.
148. Gupta, M.; C. Kaska, W.; M. Jensen, C., *Chem. Commun.* **1997**, 461-462.
149. Gupta, M.; Hagen, C.; Kaska, W. C.; Cramer, R. E.; Jensen, C. M., *J. Am. Chem. Soc.* **1997**, *119*, 840-841.
150. Curley, J. B.; Smith, N. E.; Bernskoetter, W. H.; Hazari, N.; Mercado, B. Q., *Organometallics* **2018**, *37*, 3846-3853.
151. Bielinski, E. A.; Lagaditis, P. O.; Zhang, Y.; Mercado, B. Q.; Würtele, C.; Bernskoetter, W. H.; Hazari, N.; Schneider, S., *J. Am. Chem. Soc.* **2014**, *136*, 10234-10237.
152. Boddien, A.; Loges, B.; Gärtner, F.; Torborg, C.; Fumino, K.; Junge, H.; Ludwig, R.; Beller, M., *J. Am. Chem. Soc.* **2010**, *132*, 8924-8934.
153. Kar, S.; Rauch, M.; Leitus, G.; Ben-David, Y.; Milstein, D., *Nat. Catal.* **2021**, *4*, 193-201.
154. Zell, T.; Butschke, B.; Ben-David, Y.; Milstein, D., *Chem. Eur. J.* **2013**, *19*, 8068-8072.
155. Nielsen, M.; Alberico, E.; Baumann, W.; Drexler, H.-J.; Junge, H.; Gladiali, S.; Beller, M., *Nature* **2013**, *495*, 85.
156. Gong, D.; Hu, B.; Yang, W.; Kong, D.; Xia, H.; Chen, D., *Organometallics* **2020**, *39*, 862-869.

157. Yadav, S.; Dutta, I.; Saha, S.; Das, S.; Pati, S. K.; Choudhury, J.; Bera, J. K., *Organometallics* **2020**, *39*, 3212-3223.
158. Srimani, D.; Diskin-Posner, Y.; Ben-David, Y.; Milstein, D., *Angew. Chem. Int. Ed.* **2013**, *52*, 14131-14134.
159. Swamy, K. C. K.; Reddy, A. S.; Sandeep, K.; Kalyani, A., *Tetrahedron Lett.* **2018**, *59*, 419-429.
160. Weber, S.; Stöger, B.; Veiros, L. F.; Kirchner, K., *ACS Catal.* **2019**, *9*, 9715-9720.
161. Tseng, K.-N. T.; Kampf, J. W.; Szymczak, N. K., *J. Am. Chem. Soc.* **2016**, *138*, 10378-10381.
162. Lapointe, S.; Pandey, D. K.; Gallagher, J. M.; Osborne, J.; Fayzullin, R. R.; Khaskin, E.; Khusnutdinova, J. R., *Organometallics* **2021**, *40*, 3617-3626.
163. Mabeta, P.; McGaw, L. J., Chapter 2 - Combretastatins: Plant Anticancer Phenolics. In *Stud. Nat. Prod. Chem.*, Atta ur, R., Ed. Elsevier: **2018**; Vol. 56, pp 53-67.
164. Mitsudome, T.; Takahashi, Y.; Ichikawa, S.; Mizugaki, T.; Jitsukawa, K.; Kaneda, K., *Angew. Chem. Int. Ed.* **2013**, *52*, 1481-1485.
165. Benkeser, R. A.; Schroll, G.; Sauve, D. M., *J. Am. Chem. Soc.* **1955**, *77*, 3378-3379.
166. Hydrosilylation, A., *Advances In Silicon Science, Springer, Dordrecht* **2009**.
167. Marciniec, B.; Guliński, J., *J. Org. Chem.* **1993**, *446*, 15-23.
168. Tondreau Aaron, M.; Atienza Crisita Carmen, H.; Weller Keith, J.; Nye Susan, A.; Lewis Kenrick, M.; Delis Johannes, G. P.; Chirik Paul, J., *Science* **2012**, *335*, 567-570.
169. Raya-Barón, Á.; Oña-Burgos, P.; Fernández, I., *ACS Catal.* **2019**, *9*, 5400-5417.
170. Bart, S. C.; Chłopek, K.; Bill, E.; Bouwkamp, M. W.; Lobkovsky, E.; Neese, F.; Wieghardt, K.; Chirik, P. J., *J. Am. Chem. Soc.* **2006**, *128*, 13901-13912.
171. Challinor, A. J.; Calin, M.; Nichol, G. S.; Carter, N. B.; Thomas, S. P., *Adv. Synth. Catal.* **2016**, *358*, 2404-2409.
172. Bhattacharya, P.; Krause, J. A.; Guan, H., *Organometallics* **2011**, *30*, 4720-4729.
173. Smith, A. D.; Saini, A.; Singer, L. M.; Phadke, N.; Findlater, M., *Polyhedron* **2016**, *114*, 286-291.
174. Zeng, F.; Yu, Z., *Organometallics* **2009**, *28*, 1855-1862.
175. Zeng, F.; Yu, Z., *Organometallics* **2008**, *27*, 2898-2901.
176. Samec, J. S. M.; Bäckvall, J.-E.; Andersson, P. G.; Brandt, P., *Chem. Soc. Rev.* **2006**, *35*, 237-248.
177. Jin, W.; Wang, L.; Yu, Z., *Organometallics* **2012**, *31*, 5664-5667.
178. Langer, R.; Iron, M. A.; Konstantinovski, L.; Diskin-Posner, Y.; Leitus, G.; Ben-David, Y.; Milstein, D., *Chem. Eur. J.* **2012**, *18*, 7196-7209.
179. Mazza, S.; Scopelliti, R.; Hu, X., *Organometallics* **2015**, *34*, 1538-1545.
180. Magano, J.; Dunetz, J. R., *Org. Process Res. Dev.* **2012**, *16*, 1156-1184.
181. Morris, R. H., *Chem. Soc. Rev.* **2009**, *38*, 2282-2291.
182. Arenas, I.; Boutureira, O.; Matheu, M. I.; Díaz, Y.; Castillón, S., *Eur. J. Org. Chem.* **2015**, *2015*, 3666-3669.
183. Huber, R.; Passera, A.; Mezzetti, A., *Organometallics* **2018**, *37*, 396–405.
184. Lewis, N. S.; Nocera, D. G., *Proc. Natl. Acad. Sci.* **2006**, *103*, 15729.
185. Sakakura, T.; Choi, J.-C.; Yasuda, H., *Chem. Rev.* **2007**, *107*, 2365-2387.
186. Li, Y.-N.; Ma, R.; He, L.-N.; Diao, Z.-F., *Catal. Sci. Technol.* **2014**, *4*, 1498-1512.
187. Riduan, S. N.; Zhang, Y., *Dalton Trans.* **2010**, *39*, 3347-3357.
188. Langer, R.; Diskin-Posner, Y.; Leitus, G.; Shimon, L. J. W.; Ben-David, Y.; Milstein, D., *Angew. Chem.* **2011**, *123*, 10122-10126.
189. Tanaka, R.; Yamashita, M.; Nozaki, K., *J. Am. Chem. Soc.* **2009**, *131*, 14168-14169.
190. Schmeier, T. J.; Dobereiner, G. E.; Crabtree, R. H.; Hazari, N., *J. Am. Chem. Soc.* **2011**, *133*, 9274-9277.

191. Bertini, F.; Gorgas, N.; Stöger, B.; Peruzzini, M.; Veiros, L. F.; Kirchner, K.; Gonsalvi, L., *ACS Catal.* **2016**, *6*, 2889-2893.
192. Filonenko, G. A.; van Putten, R.; Schulpen, E. N.; Hensen, E. J. M.; Pidko, E. A., *ChemCatChem* **2014**, 1526-1530.
193. Inoue, Y.; Izumida, H.; Sasaki, Y.; Hashimoto, H., *Chem. Lett.* **1976**, *5*, 863-864.
194. Hull, J. F.; Himeda, Y.; Wang, W.-H.; Hashiguchi, B.; Periana, R.; Szalda, D. J.; Muckerman, J. T.; Fujita, E., *Nat. Chem.* **2012**, *4*, 383.
195. Federsel, C.; Jackstell, R.; Beller, M., *Angew. Chem. Int. Ed.* **2010**, *49*, 6254-6257.
196. Huff, C. A.; Sanford, M. S., *ACS Catal.* **2013**, *3*, 2412-2416.
197. Musashi, Y.; Sakaki, S., *J. Am. Chem. Soc.* **2002**, *124*, 7588-7603.
198. Therrien, J. A.; Wolf, M. O.; Patrick, B. O., *Dalton Trans.* **2018**, *47*, 1827-1840.
199. Denise, B.; Sneeden, R. P. A., *J. Organomet. Chem.* **1981**, *221*, 111-116.
200. Aresta, M.; Dibenedetto, A., *Dalton Trans.* **2007**, 2975-2992.
201. Balaraman, E.; Gunanathan, C.; Zhang, J.; Shimon, L. J. W.; Milstein, D., *Nat. Chem.* **2011**, *3*, 609.
202. Balaraman, E.; Gnanaprakasam, B.; Shimon, L. J. W.; Milstein, D., *J. Am. Chem. Soc.* **2010**, *132*, 16756-16758.
203. Balaraman, E.; Gunanathan, C.; Zhang, J.; Shimon, L. J. W.; Milstein, D., *Nat. Chem.* **2011**, *3*, 609-614.
204. Zhang, J.; Leitus, G.; Ben-David, Y.; Milstein, D., *Angew. Chem., Int. Ed.* **2006**, *45*, 1113-1115.
205. Le, L.; Liu, J.; He, T.; Malek, J. C.; Cervarich, T. N.; Buttner, J. C.; Pham, J.; Keith, J. M.; Chianese, A. R., *Organometallics* **2019**, *38*, 3311-3321.
206. Stadler, B. M.; Puylaert, P.; Diekamp, J.; van Heck, R.; Fan, Y.; Spannenberg, A.; Hinze, S.; de Vries, J. G., *Adv. Synt. Catal.* **2018**, *360*, 1151-1158.
207. Chakraborty, S.; Dai, H.; Bhattacharya, P.; Fairweather, N. T.; Gibson, M. S.; Krause, J. A.; Guan, H., *J. Am. Chem. Soc.* **2014**, *136*, 7869-7872.
208. Bourissou, D.; Guerret, O.; Gabbaï, F. P.; Bertrand, G., *Chem. Rev.* **2000**, *100*, 39-92.
209. Benito-Garagorri, D.; Wiedermann, J.; Pollak, M.; Mereiter, K.; Kirchner, K., *Organometallics* **2007**, *26*, 217-222.
210. Padwa, A.; Hornbuckle, S. F.; Zhang, Z.; Zhi, L., *J. Org. Chem.* **1990**, *55*, 5297-5299.
211. Holmquist, C. R.; Roskamp, E. J., *Tetrahedron Lett.* **1992**, *33*, 1131-1134.
212. Mahmood, S. J.; Hossain, M. M., *J. Org. Chem.* **1998**, *63*, 3333-3336.
213. Dudley, M. E.; Morshed, M. M.; Brennan, C. L.; Islam, M. S.; Ahmad, M. S.; Atuu, M.-R.; Branstetter, B.; Hossain, M. M., *J. Org. Chem.* **2004**, *69*, 7599-7608.
214. Jarman, M.; Poon, G. K.; Rowlands, M. G.; Grimshaw, R. M.; Horton, M. N.; Potter, G. A.; McCague, R., *Carcinogenesis* **1995**, *16*, 683-688.
215. Katsnelson, A., *Nature Med.* **2013**, *19*, 656-656.
216. Voges, R.; Heys, J. R.; Moenius, T., *Preparation of compounds labeled with tritium and carbon-14*. John Wiley & Sons: **2009**.
217. Pony Yu, R.; Hesk, D.; Rivera, N.; Pelczer, I.; Chirik, P. J., *Nature* **2016**, *529*, 195.
218. Brintzinger, H. H.; Fischer, D.; Mülhaupt, R.; Rieger, B.; Waymouth, R. M., *Angew. Chem. Int. Ed. Engl.* **1995**, *34*, 1143-1170.
219. Small, B. L.; Brookhart, M.; Bennett, A. M. A., *J. Am. Chem. Soc.* **1998**, *120*, 4049-4050.
220. Bennett, A. M. A., Iron catalyst for the polymerization of olefins. Google Patents: **2001**; p US6214761B1.
221. J. P. Britovsek, G.; C. Gibson, V.; J. McTavish, S.; A. Solan, G.; J. P. White, A.; J. Williams, D.; J. P. Britovsek, G.; S. Kimberley, B.; J. Maddox, P., *Chem. Commun.* **1998**, 849-850.

222. Britovsek, G. J. P.; Bruce, M.; Gibson, V. C.; Kimberley, B. S.; Maddox, P. J.; Mastroianni, S.; McTavish, S. J.; Redshaw, C.; Solan, G. A.; Strömberg, S.; White, A. J. P.; Williams, D. J., *J. Am. Chem. Soc.* **1999**, *121*, 8728-8740.
223. Bouwkamp, M. W.; Bowman, A. C.; Lobkovsky, E.; Chirik, P. J., *J. Am. Chem. Soc.* **2006**, *128*, 13340-13341.
224. Lautens, M.; Klute, W.; Tam, W., *Chem. Rev.* **1996**, *96*, 49-92.
225. Hoyt, J. M.; Schmidt, V. A.; Tondreau, A. M.; Chirik, P. J., *Science* **2015**, *349*, 960.
226. Zhao, M.; Chen, C., *ACS Catal.* **2017**, *7*, 7490-7494.
227. Bart, S. C.; Lobkovsky, E.; Chirik, P. J., *J. Am. Chem. Soc.* **2004**, *126*, 13794-13807.
228. Yamada, H.; Aoyagi, S.; Kibayashi*, C., *Tetrahedron Lett.* **1997**, *38*, 3027-3030.
229. Enthaler, S.; Junge, K.; Beller, M., *Angew. Chem. Int. Ed.* **2008**, *47*, 3317-3321.
230. Nieto-Oberhuber, C.; Muñoz, M. P.; López, S.; Jiménez-Núñez, E.; Nevado, C.; Herrero-Gómez, E.; Raducan, M.; Echavarren, A. M., *Chem. Eur. J.* **2006**, *12*, 1677-1693.
231. Fürstner, A.; Majima, K.; Martín, R.; Krause, H.; Kattnig, E.; Goddard, R.; Lehmann, C. W., *J. Am. Chem. Soc.* **2008**, *130*, 1992-2004.
232. Sylvester, K. T.; Chirik, P. J., *J. Am. Chem. Soc.* **2009**, *131*, 8772-8774.
233. Bouwkamp, M. W.; Bowman, A. C.; Lobkovsky, E.; Chirik, P. J., *J. Am. Chem. Soc.* **2006**, *128*, 13340-13341.
234. Fadhel, A. Z. A. U. P. P. L. C. L. A. U. E. C. A. T. I. C. t. B. o. H.; Heterogeneous Catalysis with Tunable, S.; Nearcritical, W.*Molecules* [Online], **2010**, p. 8400-8424. https://mdpi-res.com/d_attachment/molecules/molecules-15-08400/article_deploy/molecules-15-08400.pdf?version=1403112926.
235. Sheludko, B.; Castro, C. F.; Khalap, C. A.; Emge, T. J.; Goldman, A. S.; Celik, F. E., *ChemCatChem* **2021**, *13*, 407-415.
236. Huang, Z.; Brookhart, M.; Goldman, A. S.; Kundu, S.; Ray, A.; Scott, S. L.; Vicente, B. C., *Adv. Syn. Catal.* **2009**, *351*, 188-206.
237. Sheludko, B.; Cunningham, M. T.; Goldman, A. S.; Celik, F. E., *ACS Catal.* **2018**, *8*, 7828-7841.

Chapter II

Pincer-Ruthenium Catalyzed N-Alkylation of Amines Using Alcohols

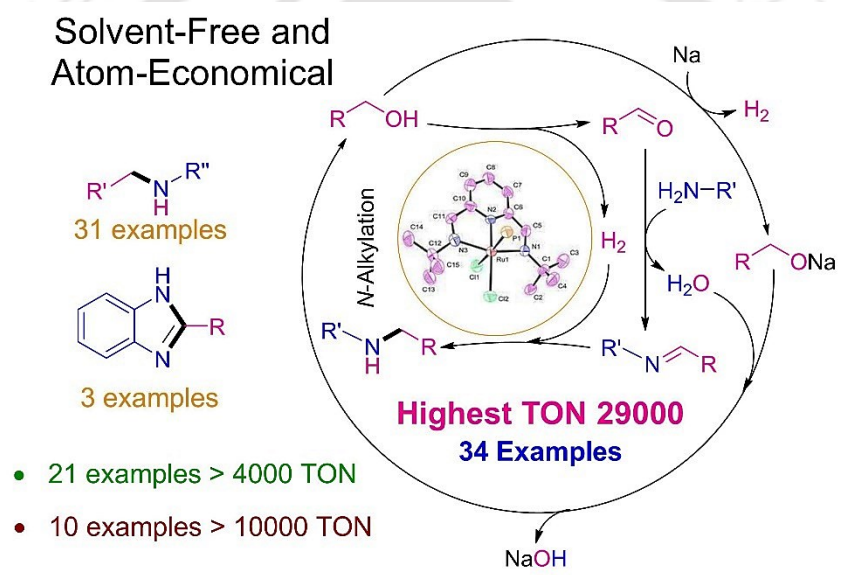

- **K. Das**, M. Dutta, B. Das, H. K. Srivastava, A. Kumar, *Adv. Synth. Catal*. **2019**, *361*, 2965.
- **K. Das**, P. G. Nandi, K. Islam, H. K. Srivastava, A. Kumar, *Eur. J. Org. Chem.* **2019**, *2019*, 6855.

2.1 Introduction

Nitrogen containing compounds play an important role in synthetic applications involving fine chemicals, polymers, pharmaceutical products and dyes.[1-2] Importantly, the nitrogen atom in these compounds is associated with a variety of physical properties (*e.g.* hydrogen bonding) that control numerous biological interactions. Figure **2.1** provides representative examples of pharmaceutical amines that are globally accepted as preclinical compounds and small molecule biological probes.[3] From this perspective, efforts are being made towards achieving highly selective pathways with minimum number of synthetic steps to obtain nitrogen containing compounds which can play a key role in pharmaceutical and medicinal chemistry. Few examples of such compounds are represented as follows: Pramipexole an agonist dopamine receptor is effective for Parkinson disease, Sertraline is an effective antidepressant of various etiologies, Escitalopram is a serotonin reuptake inhibitor, Sumatriptan is used to arrest migraine attacks, Retigabine is used to normalize the potassium channel in neurons of the brain and Donepezil is a cholinesterase inhibitor (Figure **2.1**).[3]

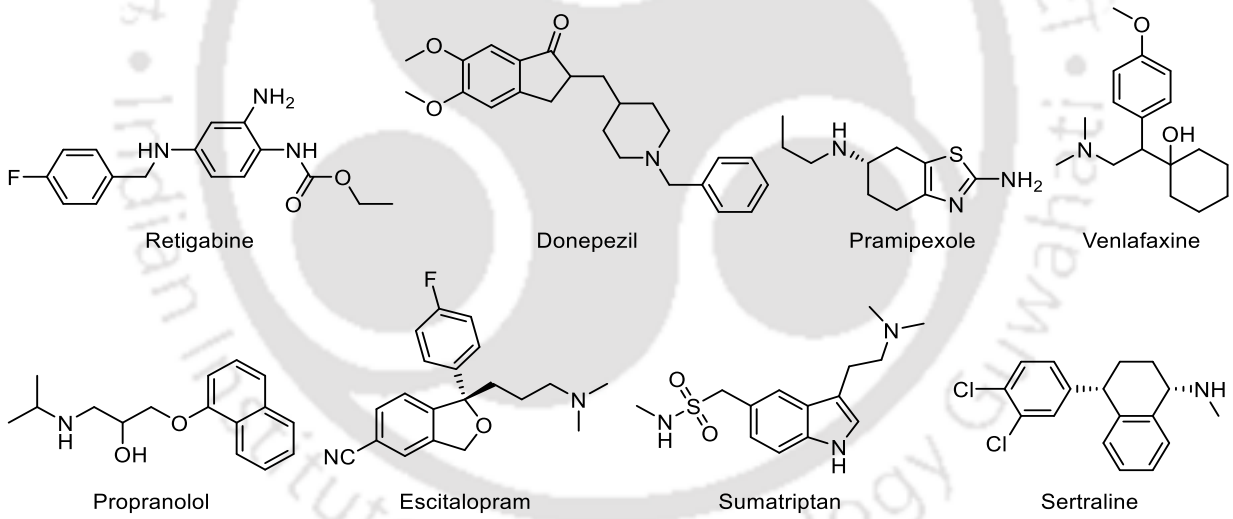

Figure 2.1: A few representative examples of biologically active pharmaceutical *N*-alkylated products.

Synthesis of secondary or tertiary amines has been carried out in various ways (Scheme **2.1**). Traditional approaches are devoted either to multi-step pathways or directing groups involving substitution reactions for the synthesis of higher-order amines. One such approach is the nucleophilic addition or reduction reaction of the imine bond that requires stoichiometric amounts of substrates, which generates equivalent amount of waste products. Milder approaches have been reported in recent years such as the Chan-Evans-Lam[4] coupling and the Ullman[5] coupling that reduces the reaction temperature as well as the catalyst loading.[6] Another

convenient route involves the palladium-catalyzed Buchwald-Hartwig amination for the C–N bond formation reactions.[6] Classical approaches involving environmentally toxic alkyl/aryl halides often suffer from the formation of an equivalent amount of side or waste product (Scheme **2.1**).[7]

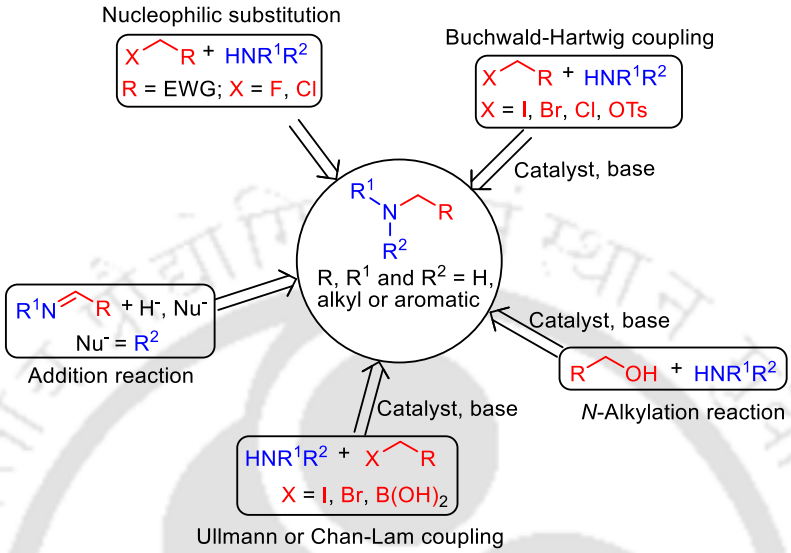

Scheme 2.1: General strategies for the synthesis of *N*-alkyl amines.[6]

Chusov and co-workers reported a unique reaction pathway for the synthesis of higher-order amines using carbonyls, amines and carbon monoxide as starting materials (Scheme **2.2**).[8] With this methodology, they demonstrated the synthesis of higher-order amines in good to excellent yields with turnovers as high as 2465 TON *via* a deoxygenative route using ruthenium trichloride as a catalyst precursor. Importantly, CO plays a key role as deoxygenative agent in this transformation in the absence of hydrogen or a hydride source. They have reported the gram-scale synthesis of Ladasten which is an anti-anxiety agent and following this strategy lowers the cost-effectiveness of this reaction.

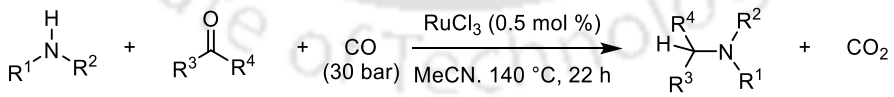

2.3a; R^1 = H, R^2 = *p*-OMe-C_6H_4, R^3 = H and R^4 = *p*-OMe-C_6H_4; Yield = 90%
2.3b; R^1 = H, R^2 = *p*-OMe-C_6H_4, R^3 = H and R^4 = *o*-F-C_6H_4; Yield = 80%
2.3c; R^1 = H, R^2 = *p*-OMe-C_6H_4, R^3 = H and R^4 = $C_{10}H_7$; Yield = 95%
2.3d; R^1 = H, R^2 = *p*-OMe-C_6H_4, R^3 = H and R^4 = C_6H_{11}; Yield = 70%

Scheme 2.2: Ru-catalyzed reductive amination of carbonyl compounds in the presence of high pressure of carbon monoxide.[8]

Substituted alkylated amines have also been synthesized starting from amines and carboxylic acids followed by reductive amination rather than using aldehydes or ketones (Scheme **2.3**).[9]

Beller and co-workers demonstrated a straightforward reaction by applying commercially available Karstedt's catalyst **2.7** with the combination of dppe ligand **2.6** under mild reaction conditions. The synthetic protocol gives a wide range of alkylated amines with high productivity where phenylsilane has been used as a reducing agent. Though high TON (up to 760) were achieved, usage of excess amount of reducing agent (phenylsilane) is the main drawback of this reaction.

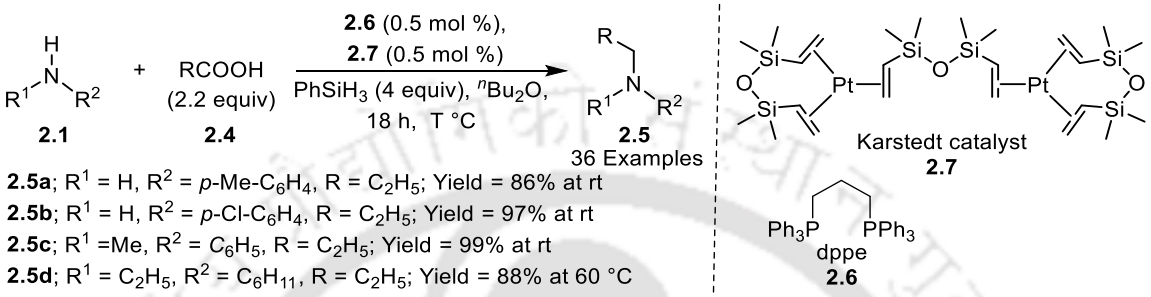

Scheme 2.3: Reductive alkylation of amine with carboxylic acid.[9]

Hence, with the development of various methods, the symbolic attention could be towards "greener and atom economical" process involving the usage of alcohols as a source of alkylating agent. Not surprisingly, this has become one of the favorite routes to accomplish the *N*-alkylation (Scheme **2.1**)[6] as alcohols are readily available, less hazardous and the reaction involves water as the sole by-product with hardly any waste generation (Scheme **2.4**).[10-14] The first step involves the metal-catalyzed dehydrogenation of alcohol to give metal-dihydride complex and the corresponding aldehyde or ketone, which progresses to an uncatalyzed condensation reaction with the amine to give the corresponding imine. Finally, in a metal-dihydride catalyzed process, the imine acts as a hydrogen acceptor to yield the *N*-alkylated product along with the regeneration of catalyst (Scheme **2.4**).[10-14] In 2004, Willams[15] first coined the term "hydrogen borrowing" for these types of reactions. This process is fully green and atom economical where water is the sole by-product. This reaction often requires a stoichiometric amount of base or use of molecular sieves to scavenge the by-product water, which ensures that the catalyst remains active in the reaction medium.

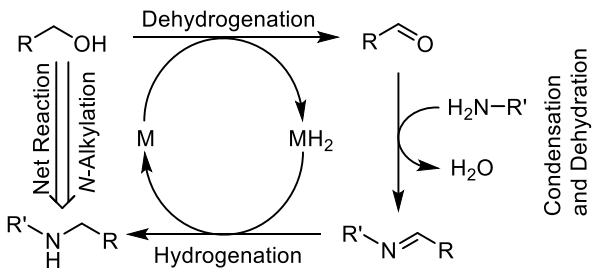

Scheme 2.4: Hydrogen-borrowing strategy for *N*-Alkylation.

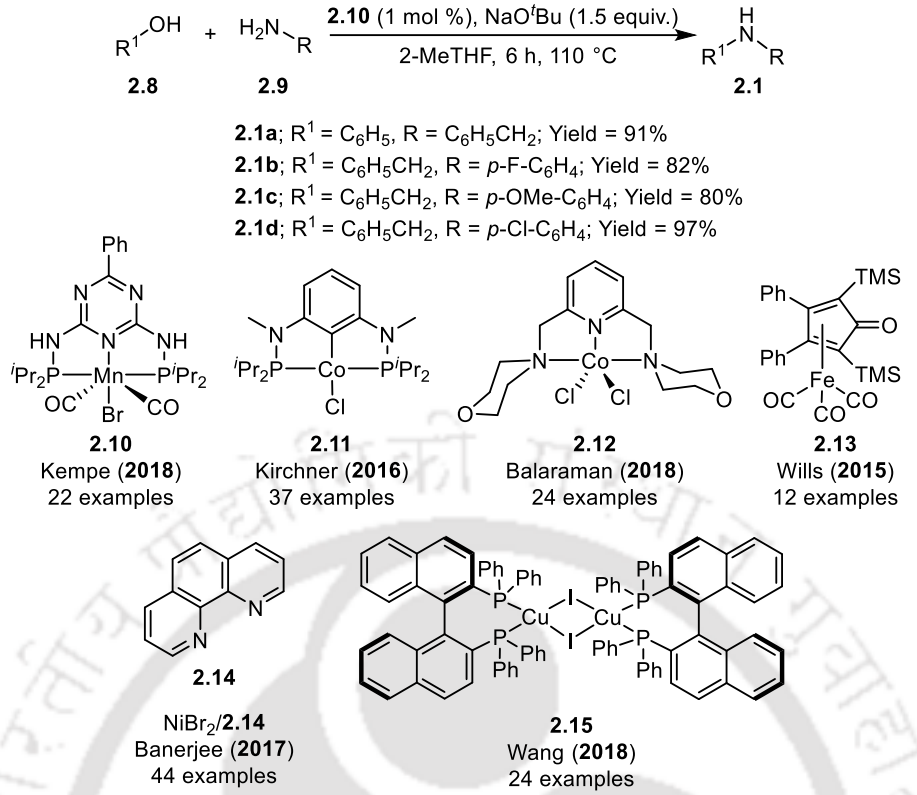

Scheme 2.5: Transition metal catalyzed *N*-alkylation of amines with alcohols.[16-23]

The concept of "hydrogen borrowing" for catalytic alkylation of amine was first implemented independently by Grigg[24] and Watanabe[25] in 1981. Subsequently, over the years, catalytic *N*-alkylation has been reported with complexes based on precious metals such as Pd,[26-27] Ru,[25, 28-48] Rh,[24] and Ir.[49-66] However, in recent years, the studies on the development of the catalytic systems have led to the replacement of expensive noble-metal based complexes by inexpensive metal based complexes such as PNNNP pincer-Mn,[19-23, 67-70] and PNCNP/NNN pincer-Co[16-18] along with complexes based on Fe,[9, 71-79] Ni[80-81] and Cu[27, 82] (Scheme **2.5**). Notably, several heterogeneous catalytic systems derived from Pd,[26, 83] Ag,[84-85] W,[86] Cu[82] and Ni[87-88] have also enjoyed great success in catalytic *N*-alkylation.

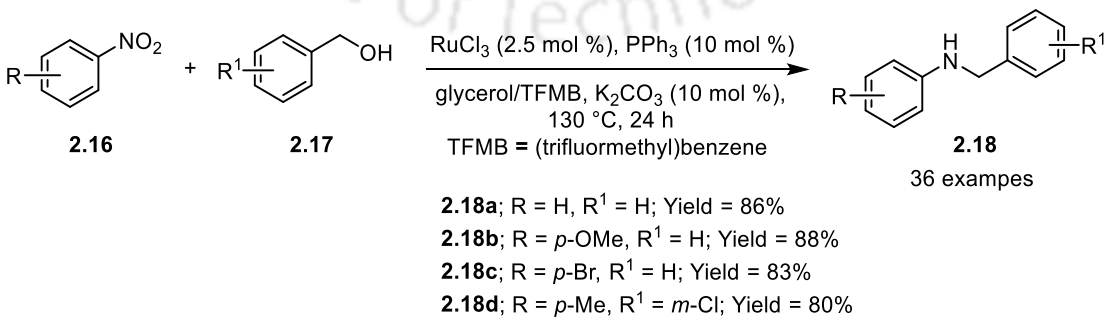

Scheme 2.6: Alkylation of nitroarene catalyzed by ruthenium trichloride.[89]

N-alkylated amines could be synthesized using nitrenes as an amine precursor with alcohols as alkylating agents (Scheme **2.6**).[89] In many cases, a large excess of alcohol was used not only as alkylating agents but also as a hydrogen source to reduce the nitrenes.[90-91] Usually, an excess amount of alcohol is required in a ratio of 6:1 to 8:1 with respect to nitrenes.[90-91] Shi and co-workers reported a clean synthetic pathway with feedstock glycerol as a hydrogen source. In this way, they demonstrated a one-pot ruthenium catalyzed *N*-alkylation without using a large amount of alcohol, which gave very high productivity (up to 40 TON).

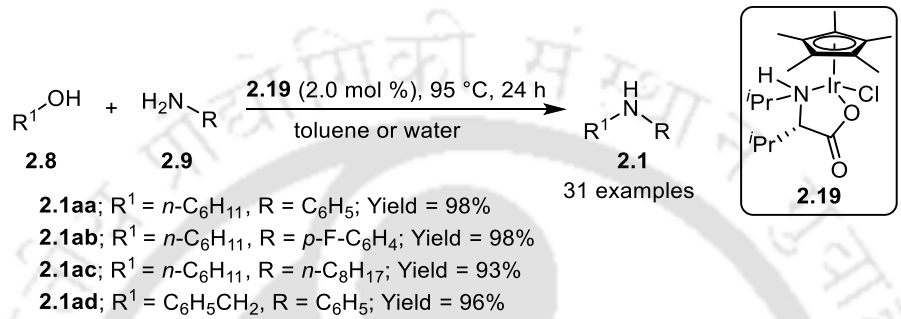

Scheme 2.7: Alkylation of amines catalyzed by an iridium half-sandwich complex.[61]

Efficient *N*-alkylation was demonstrated by Limbach using the iridium half-sandwich complex (Scheme **2.7**).[61] Notably, this condition shows high reactivity not only under base-free condition but also at lower temperature (95 °C). The reaction occurred both in organic medium as well as in water with high activity.

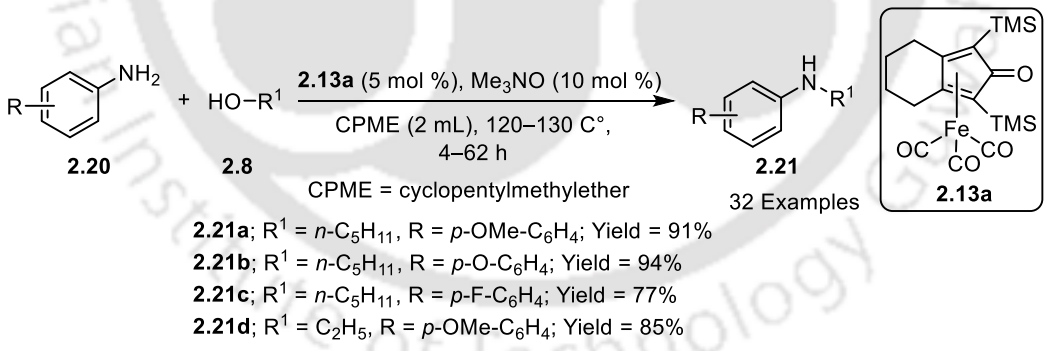

Scheme 2.8: Iron catalyzed *N*-alkylation of amines.[71]

A large number of transition metal complexes, particularly iridium and ruthenium have been studied for catalytic C–N bond formation.[71] A better alternate for ruthenium was reported by the Barta group, who investigated an inexpensive and sustainable iron complex for the direct alkylation of amines with alcohol *via* "hydrogen-borrowing" strategy (Scheme **2.8**).[71]

Beller and co-workers demonstrated that the scope of *N*-alkylation was not limited to simple amines,[71] but also could be extended to alkylation of amides and sulfonamides with alcohols.[92] A hydrogen-borrowing strategy was employed in these copper catalyzed alkylation of

sulfonamides with primary alcohols in the presence of K_2CO_3 and air (Scheme **2.9**).[92] Excellent yields (up to 99 TON) are obtained in this reaction where active species appears to be a *bis*sulfonylated amidine intermediate with the $Cu(OAc)_2/K_2CO_3$/air system.

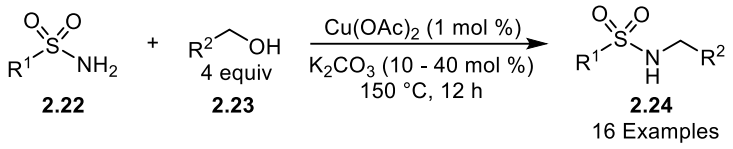

2.24a; R^1 = *p*-Me-C_6H_4, R^2 = C_6H_5; Yield = 96%
2.24b; R^1 = *p*-Br-C_6H_4, R^2 = C_6H_5; Yield = 96%
2.24c; R^1 = *p*-Me-C_6H_4, R^2 = C_4H_4S; Yield = 93%
2.24d; R^1 = CH_3, R^2 = C_6H_5; Yield = 95%

Scheme 2.9: *N*-alkylation of sulfonamides with alcohol using a copper catalyst.[92]

Chiral amines, which have great value in the pharmaceutical industry can be conveniently obtained *via* asymmetric hydrogenation of ketimines,[93-94] which in turn can be easily synthesized by the above discussed atom economical 'hydrogen borrowing' methodology.[62] Zhao group was the first to report the synthesis of chiral amines *via* the *N*-alkylation of amines with alcohols (Scheme **2.10**). The chiral iridium catalyst (*S*,*S*-**2.26**) in the presence of chiral phosphoric acid **2.25** catalyzed the synthesis of a large number of chiral enantioselective amines with good to excellent yields.

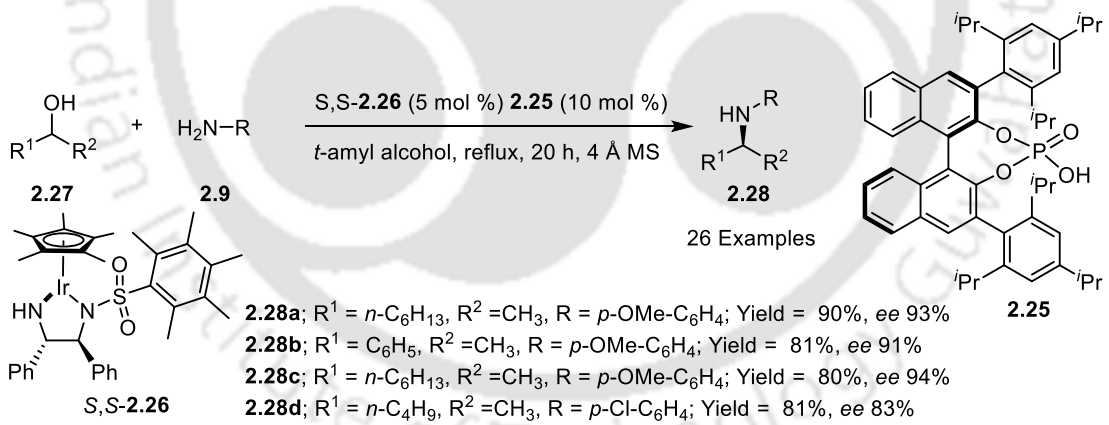

2.28a; R^1 = *n*-C_6H_{13}, R^2 =CH_3, R = *p*-OMe-C_6H_4; Yield = 90%, *ee* 93%
2.28b; R^1 = C_6H_5, R^2 =CH_3, R = *p*-OMe-C_6H_4; Yield = 81%, *ee* 91%
2.28c; R^1 = *n*-C_6H_{13}, R^2 =CH_3, R = *p*-OMe-C_6H_4; Yield = 80%, *ee* 94%
2.28d; R^1 = *n*-C_4H_9, R^2 =CH_3, R = *p*-Cl-C_6H_4; Yield = 81%, *ee* 83%

Scheme 2.10: Synthesis of chiral amines using hydrogen-borrowing strategy.[62]

It is notable that *N*-alkylation reactions have also been catalyzed by ruthenium-based complexes. Watanabe and co-workers reported several ruthenium based complexes such as $[RuX_2(PPh_3)_3]$ (X = Cl,[25, 30] Br[48]), $[RuH_2(PPh_3)_4]$,[25] $[RuHCl(PPh_3)_3]$[48] for the *N*-alkylation of amines using alcohols. The *N*-alkylation of amines with alcohols have also been successfully demonstrated by using a variety of other ruthenium-phosphine containing complexes.[32, 38, 48, 95-96] The use of ruthenium precursors in the presence of amino/amide ligands resulted in one-pot *N*-alkylation of primary and secondary amines with alcohols along with a vast substrate

scope.[34, 43] The *N*-heterocyclic carbene (NHC) ligand **2.30** based ruthenium system catalyzed *N*-alkylation of amines with alcohols exhibiting high activity and selectivity under low catalyst loading (Scheme **2.11**).[97]

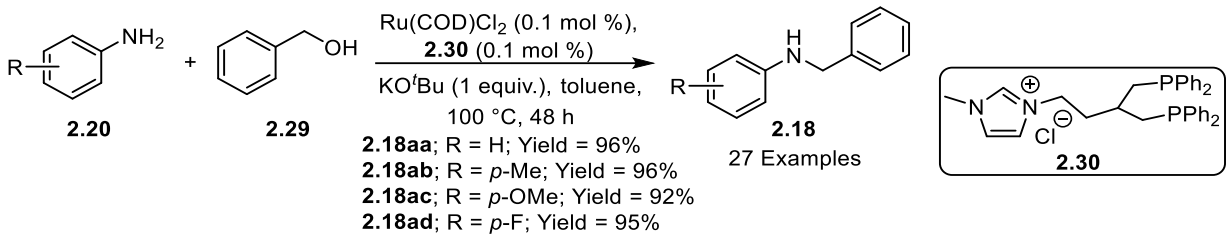

Scheme 2.11: *N*-alkylation of amines with alcohols catalyzed by $Ru(COD)Cl_2$ in the presence of NHC ligand **2.30**.[97]

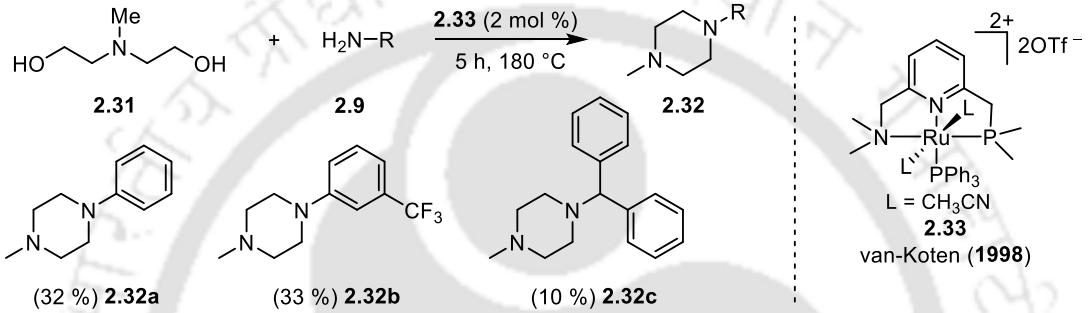

Scheme 2.12: Pincer-ruthenium catalyzed *N*-alkylation of amines with alcohols.[35]

In their pioneering work, van-Koten and co-workers reported *N*-(cyclo)alkylation reactions of amines with diols by well-defined dicationic pincer-ruthenium(II) complex **2.33** (Scheme **2.12**).[35] The ^{Me2}NNN pincer-ruthenium complex system gave up to 33 % yield of *N*-phenylpiperidine derivative.

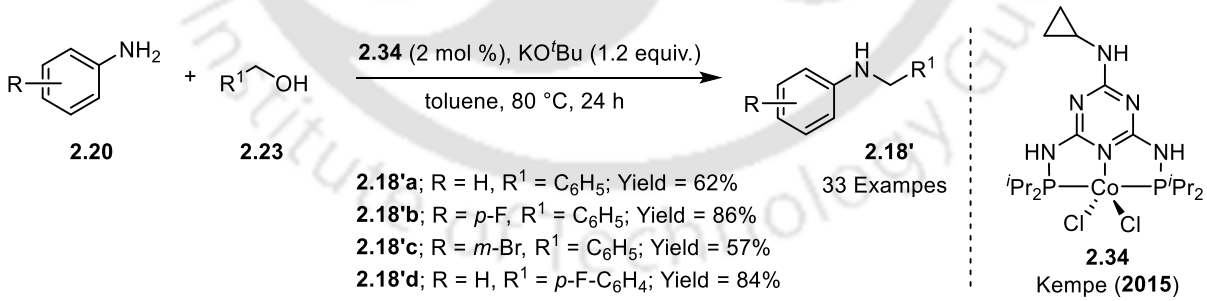

Scheme 2.13: Pincer-cobalt catalyzed *N*-alkylation reaction of amines with alcohols.[50, 98]

Kempe and co-workers reported the first PNP pincer-cobalt **2.34** catalyzed *N*-alkylation of amines with alcohols under relatively mild conditions.[50, 98] They also demonstrated the selective synthesis of unsymmetrically substituted diamines (Scheme **2.13**).

Beller and co-workers reported highly stable pincer-manganese **2.35** catalyzed inter- and intramolecular *N*-alkylation of amines with alcohols. The catalytic system under mild

conditions provided excellent chemoselectivity and tolerates various functional groups (Scheme **2.14**).[21, 99]

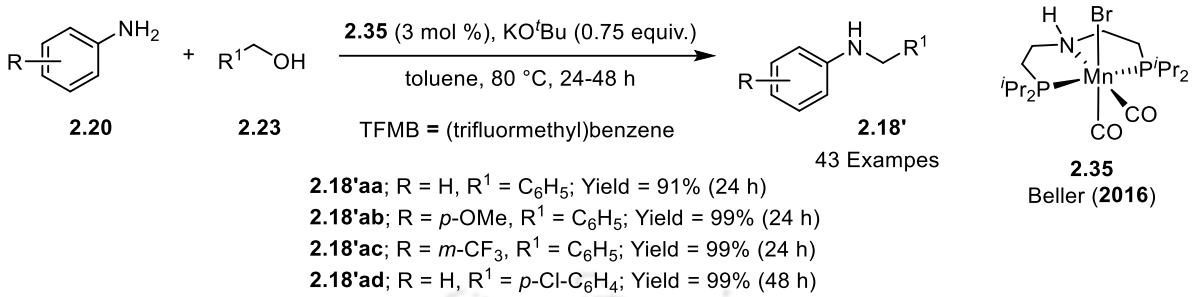

Scheme 2.14: Pincer-manganese catalyzed *N*-alkylation of amines with alcohols.[21, 99]

Milstein group has demonstrated higher order amine synthesis following the similar procedure when amines were reacted with alcohols in the presence of pincer catalyst **2.36**. Similarly, reacting ammonia with alcohols provided access to direct synthesis of secondary amines (*via* *N*-alkylation reaction catalyzed by PNN pincer-ruthenium complex **2.36** (Scheme **2.15**).[100-101]

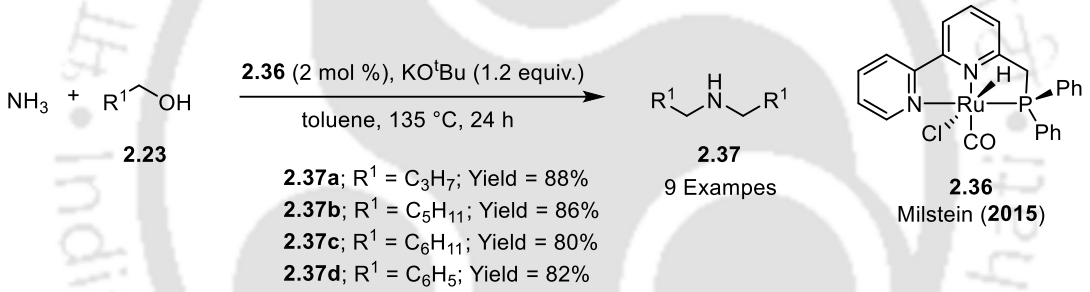

Scheme 2.15: Pincer-ruthenium catalyzed *N*-alkylation of alcohols with ammonia.[101]

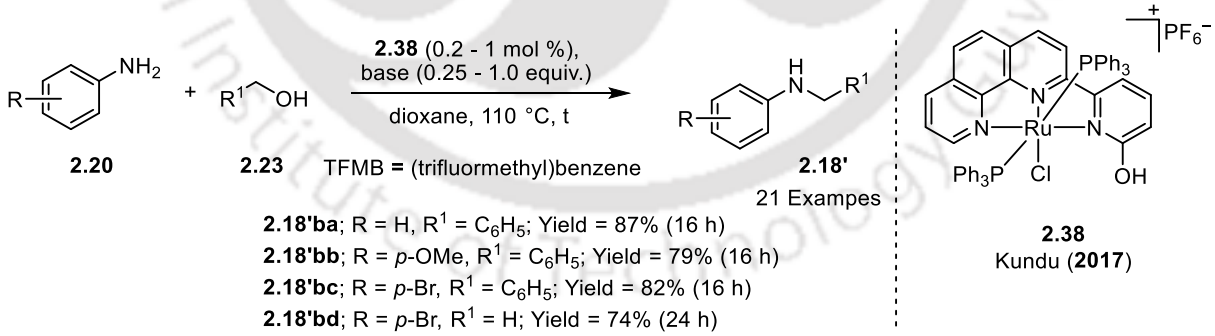

Scheme 2.16: Pincer-ruthenium catalyzed *N*-alkylation of amines with alcohols.[46]

Kundu and co-workers demonstrated the excellent catalytic activity of bifunctional 2-hydroxypyridine based NNN pincer-ruthenium(II) complex **2.38** towards *N*-alkylation reaction. Notably, they also studied the mono *N*-methylation of amines under the same catalytic conditions. In addition, a wide substrate scope with various functional groups are tolerated for *N*-alkylation to achieve remarkably high turnovers (42840 TON, Scheme **2.16**).[46] Including

these examples many other groups have demonstrated a significant progress on pincer-metal catalyzed *N*-alkylation reaction.[102]

Thus, among the various complexes tested for *N*-alkylation, pincer complexes based on a variety of metals (Ru in particular have enjoyed) great success. Generally, either for *N*-alkylation or for dehydrogenative coupling, stoichiometric amounts of base such as KO^{t}Bu[43, 50] or NaO^{t}Bu[19, 81] are required as water scavengers. This results in the generation of equivalent amount of metal hydroxide and *t*-butanol. While the use of molecular seives[62] would be more atom economical for this reaction, it would be advantageous even if one avoids the formation of one of the possible by-products.

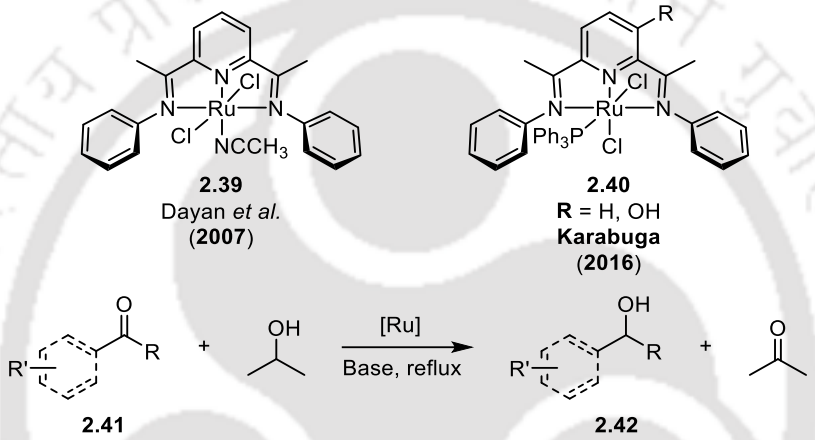

Scheme 2.17: Transfer hydrogenation by *bis*(ketimino) pincer-ruthenium complexes.[103-104]

A comprehensive literature survey reveals that pincer complexes are more effective than others in catalyzing *N*-alkylation reactions and that there are no reports on *N*-alkylation that are catalyzed by pincer based on *bis*(imino) pyridine ligands. However, there are only two reports on transfer hydrogenation reaction by imine-based pincer-Ru complexes. Çetinkaya group demonstrated a ketimine-based pincer-ruthenium complex **2.39** for transfer hydrogenation of acetophenone (Scheme **2.17**). In the presence of 1 mol % of KOH, ruthenium-ketimine catalyst **2.39** (0.1 mol%) gave 990 TON of 1-phenylethanol upon transfer hydrogenation (Scheme **2.17**).[104] Karabuga and co-workers explored *bis*(ketimino) pyridine-based pincer-ruthenium complex **2.40** catalyzed transfer hydrogenation of secondary alcohols using isopropanol as a hydrogen source and obtained a maximum of 198 TON (Scheme **2.17**).[103-104]

2.2 Objectives

Considering the vast literature that is available on the Ru-catalyzed *N*-alkylation and the fact that the studies with environmentally benign 'nitrogen' based ligand systems are very sparse, the studies on the chemistry of ruthenium catalyzed *N*-alkylation is still relevant. Furthermore,

while use of molecular sieves would be the best way to make the *N*-alkylation reaction atom economical, it would be a win-win situation even if one accomplishes the reaction with the minimal by-products. These formed the basis of the current chapter that attempts to address the following questions.

- Can one utilize pincer-Ru complexes based on air stable NNN *bis*(imino) pyridine ligands for *N*-alkylation?
- Could Na be used effectively to generate the required base *in-situ* for the pincer-ruthenium catalyzed *N*-alkylation reaction (Scheme **2.18**)?
- What is the operative mechanism in these NNN-Ru catalyzed *N*-alkylation?

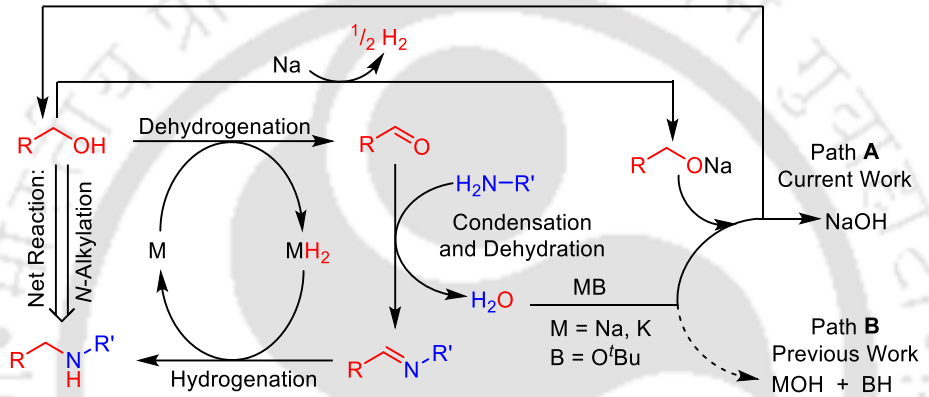

Scheme 2.18: Transition metal catalyzed *N*-alkylation using hydrogen-borrowing strategy.

2.3 Result and Discussions

2.3.1 Synthesis of pincer *bis*(imino) ligands and their complexes

The synthetic strategy for the new NNN *bis*(imino) pyridine based pincer-Ru complexes of the type (^{R2}NNN)RuCl$_2$(PPh$_3$) (**2.48a**; R = Cy, **2.48b**; R = Ph, **2.48c**; R = ^{i}Pr and **2.48d**; R = ^{t}Bu) is shown in Scheme **2.19**. The compound dimethyl pyridine-2,6-dicarboxylate (**2.44**) was obtained in 90% yield by refluxing pyridine-2,6-dicarboxylic acid (**2.43**) with $SOCl_2$ in methanol. The ^{13}C NMR spectroscopy of compound **2.44** shows a signal at 165.18 ppm, which is indicative of the carbonyl carbon of an ester group and the corresponding protons of methylate ester group were observed at δ = 4.03 ppm in the ^{1}H NMR spectroscopy. The reduction of **2.44** with $NaBH_4$ resulted in pyridine-2,6-diyldimethanol (**2.45**) as a white solid in 86% yield. Subsequently, the oxidation of **2.45** with SeO_2 in 1,4-dioxane gave pyridine-2,6-dicarbaldehyde (**2.46**) in 82% yield. The formation of *bis*-aldehyde was confirmed by ^{1}H and ^{13}C NMR spectroscopy analysis which exhibited peaks at δ = 10.17 ppm (for the aldehydic proton) and at δ = 192.44 ppm (for the carbonyl carbon) respectively. Finally, a series of pincer

diimine based NNN ligands (**2.47a**; R = Cy, **2.47b**; R = Ph, **2.47c**; R = ^{i}Pr and **2.47d**; R = ^{t}Bu) were synthesized by condensation reaction between pyridine-2,6-dicarbaldehyde (**2.46**) with the corresponding amines. While in the ^{1}H NMR spectroscopy, the imine protons of all the considered pincer ligands (**2.47a-d**) resonate in the range of δ = 8.69-8.42 ppm, the corresponding aza-carbonyl carbons appears at δ = 160.29-156.39 ppm in the ^{13}C NMR spectroscopy.

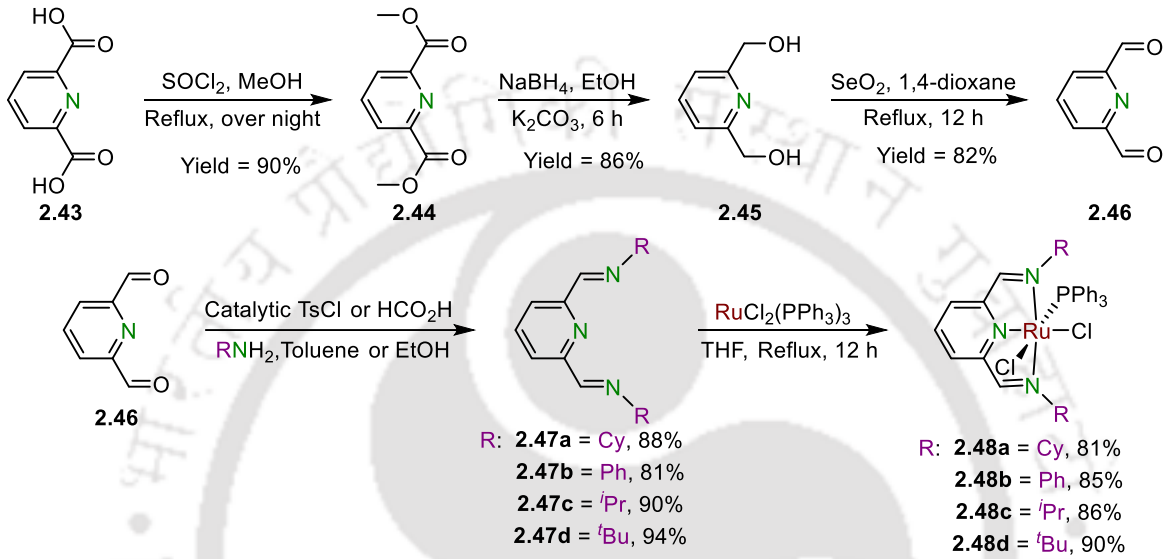

Scheme 2.19: General synthetic route to pincer-ruthenium complexes (^{R2}NNN)RuCl$_2$(PPh$_3$) (**2.48a**; R = Cy, **2.48b**; R = Ph, **2.48c**; R = ^{i}Pr and **2.48d**; R = ^{t}Bu).

The corresponding pincer-ruthenium complexes (**2.48a**; R = Cy, **2.48b**; R = Ph, **2.48c**; R = ^{i}Pr and **2.48d**; R = ^{t}Bu) were obtained in good yields by heating to reflux a solution of the NNN ligands (**2.47a**; R = Cy, **2.47b**; R = Ph, **2.47c**; R = ^{i}Pr and **2.47d**; R = ^{t}Bu) and RuCl$_2$(PPh$_3$)$_3$ in THF. The newly synthesized complex (**2.48b**) showed high thermal stability (up to 334 °C) (Appendix I, Figure **2.104**). The pincer-Ru complexes (**2.48a**; R = Cy, **2.48b**; R = Ph, **2.48c**; R = ^{i}Pr and **2.48d**; R = ^{t}Bu) were fully characterized by NMR spectroscopy, HRMS spectroscopy and single crystal X-ray analysis. The crystals were obtained by slow diffusion of pentane (1 mL) into dichloromethane (1 mL) solution of the ruthenium complexes (10 mg). The structure with ORTEP drawn at 50% probability is provided in Figure **2.2**. The Ph groups on P, all the hydrogen atoms and the solvent molecules are omitted for the sake of clarity.

The crystallographic data is provided in Table **2.10**. Selected bond distances and bond angles are given in Table **2.1**. In all the complexes, the Ru center adopted a distorted octahedral geometry with the ligand (**2.47**) coordinated in a meridional fashion. The other three coordination sites are satisfied by two chlorides and one PPh$_3$ moiety. Notably, the PPh$_3$ moiety

is *trans* to one of the chlorides and both the coordinated chlorides are *cis* to each other. In the solid-state, all the complexes are stabilized mainly by C–H···Cl–Ru interactions either with the solvent molecules or the ligand itself. The complex (**2.48a**) crystallizes in the triclinic crystal system having *P-1* space group with two symmetry non-equivalent molecules being present in the asymmetric unit.

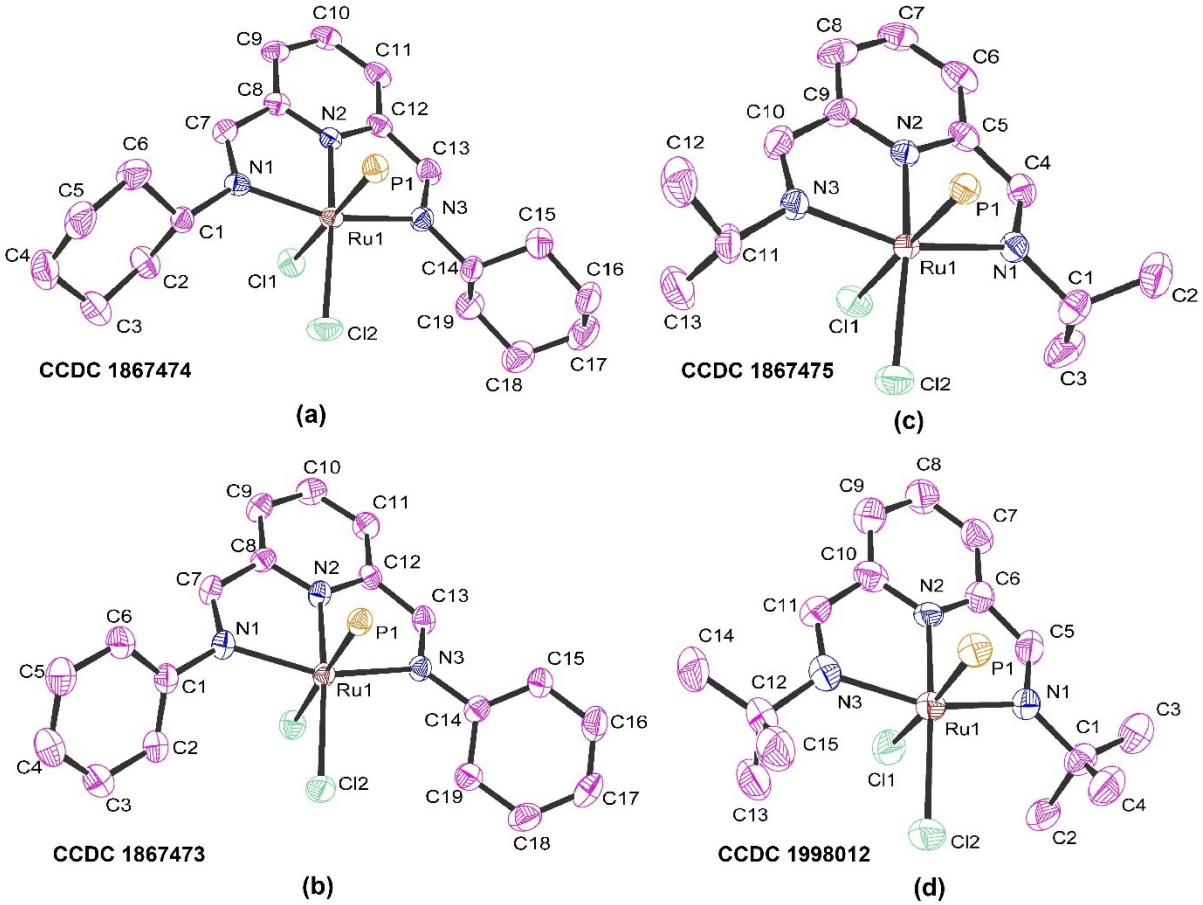

Figure 2.2: ORTEP diagram of (**a**) (^{Cy2}NNN)RuCl$_2$(PPh$_3$) (**2.48a**); (**b**) (^{Ph2}NNN)RuCl$_2$(PPh$_3$) (**2.48b**); (**c**) (^{iPr2}NNN)RuCl$_2$(PPh$_3$) (**2.48c**) and (**d**) (^{tBu2}NNN)RuCl$_2$(PPh$_3$) (**2.48d**) with the ellipsoids drawn at the 50% probability level. The Ph groups on P, all the H atoms and the solvent molecules were omitted for the sake of clarity.

The complex **2.48a** also has of one molecule of dichloromethane in the crystal lattice. In one of the non-equivalent units of complex **2.48a**, the chloride *trans* to pyridyl–*N* exhibits C–H···Cl–Ru interactions with C–H of both the cyclohexyl groups (2.942 Å & 3.040 Å) and with C–H of the phenyl groups in PPh$_3$ (2.665 Å & 2.628 Å) respectively. Similarly, the chloride that is *trans* to PPh$_3$ exhibits C–H···Cl–Ru interactions with C–H cyclohexyl group (2.996 Å & 3.015 Å). The second non-equivalent unit of **2.48a** also shows similar type of C–H···Cl–Ru interactions. Additionally, the chloride *trans* to pyridyl–*N* in one of the non-equivalent unit of **2.48a**, shows C–H···Cl–Ru interaction with the imine C–H (2.657 Å),

cyclohexyl C–H (3.260 Å) and pyridyl C–H (3.014 Å) of the other non-equivalent unit in **2.48a**. Surprisingly, the solvent molecules do not show any kind of interaction with both the units in **2.48a** and is likely to act as a space-filler.[105]

Table 2.1: Selected crystallographic bond distances (Å) and bond angles (°) of complexes **2.48a-d**

	2.48a	**2.48b**	**2.48c**	**2.48d**
Ru–N(imine)	2.103 (4) (unit I) 2.081 (4) (unit I) 2.079 (4) (unit II) 2.095 (4) (unit II)	2.128 (3) 2.111 (3)	2.103 (3) 2.071 (3)	2.151 (9) 2.154 (10)
Ru–N(pyridine)	1.943 (3) (unit I) 1.938 (3) (unit II)	1.939 (3)	1.936 (3)	1.930 (8)
Ru–Cl	2.4419 (12) (unit I) 2.4480 (11) (unit I) 2.4513 (12) (unit II) 2.4298 (11) (unit II)	2.449 (13) 2.461 (12)	2.461 (11) 2.453 (12)	2.463 (3) 2.455 (3)
Ru–P	2.3093 (12) (unit I) 2.3157 (12) (unit II)	2.322 (13)	2.315 (11)	2.366 (3)
C=N(imine)	1.295 (5) (unit I) 1.293 (5) (unit I) 1.287 (5) (unit II) 1.297 (5) (unit II)	1.296 (5) 1.287 (5)	1.293 (6) 1.283 (6)	1.297 (14) 1.293 (13)
(imine)N–Ru–N(imine)	156.44 (14) (unit I) 157.58 (13) (unit II)	155.64 (14)	156.54 (14)	155.6 (4)

Both the complexes **2.48b** and **2.48c** crystallizes in a monoclinic crystal system ($P2_1/n$ and $P2_1/c$ space group respectively). The complex **2.48b** contains one molecule each of dichloromethane and water but complex **2.48c** contains only one molecule of dichloromethane in the crystal lattice. The chloride which is *trans* to the pyridyl *N* of complex **2.48b** exhibits C–H···Cl–Ru interaction with phenyl C–H of the imine group (2.667 Å & 2.898 Å) and with C–H of phenyl group in PPh_3 molecule (2.668 Å & 2.685 Å) respectively. On the other hand, the chloride which is *trans* to the PPh_3 group exhibits C–H···Cl–Ru interaction only with the phenyl C–H of the imine group (3.145 Å & 3.482 Å). Similarly, while the chloride (*trans* to pyridyl *N*) in complex **2.48c** shows C–H···Cl–Ru interaction with isopropyl C–H of the imine group (2.900 Å, 3.226 Å and 3.528 Å) and with C–H of phenyl group in PPh_3 (2.615 Å & 2.739 Å) respectively, the chloride which is *trans* to PPh_3 shows C–H···Cl–Ru interactions with isopropyl C–H of the imine group (3.024 Å & 3.193 Å).[105]

Interestingly, the solvent molecules in the crystal shows strong Ru–Cl···H–C interaction in both the complexes **2.48b** and **2.48c**. In complex **2.48b**, the dichloromethane interacts with the chloride atom that is *trans* to PPh_3 (2.606 Å) and with the chloride atom which is *trans* to pyridyl–*N* (3.091 Å). Similarly, in **2.48c**, dichloromethane demonstrates Ru–Cl···H–C interaction with the chloride atom (*trans* to pyridyl *N*, ca. 2.654 Å) and a C–H···Cl–C interactions with the isopropyl of the imine group (3.109 Å & 3.504 Å). The complex **2.48d** crystallizes in orthorhombic crystal system. In the resulting *Pbca* space group of **2.48d** two molecules of dichloromethane are present in the crystal lattice. The chloride, which is *trans* to pyridyl–*N* exhibit interactions with C–H of the phenyl group in PPh_3 (2.549 Å) and C–H of both the tert-butyl groups (2.734 Å, 2.761 Å, 2.733 Å and 2.705 Å). Similarly, the chloride (*trans* to PPh_3) shows C–H···Cl–Ru interactions with C–H of the *tert*-butyl groups (3.055 Å, 3.077 Å, 3.117 Å and 2.940 Å). Both the dichloromethane molecules present in the crystal lattice shows C–H···Cl–Ru interaction with chloride atom that is *trans* to PPh_3 group (2.303 Å & 2.612 Å).[105]

2.3.2 *N*-alkylation catalyzed by the pincer-ruthenium complexes of the type (^{R2}NNN)RuCl$_2$(PPh$_3$) (2.48a; R = Cy, 2.48b; R = Ph, 2.48c; R = ^{i}Pr and 2.48d; R = ^{t}Bu)

To arrive at the optimal reaction conditions (Scheme **2.20**), the **2.48d** (0.02 mol %) catalyzed reactions were carried out at 120 °C in a sealed vessel using benzyl alcohol (**2.29**) and aniline (**2.49**) as model substrates in the presence of varying amounts of KO^{t}Bu (entries 1-4, Table **2.2**) for 20 h. For this variation, the best results (26% yield, 1300 TON) (TON = [Product]/[Catalyst]) were obtained with use of 0.75 equivalent KO^{t}Bu (entry 3, Table **2.2**). Operating at a catalyst loading of 0.05 mol % resulted in a higher yield albeit with lower turnover (entry 5, Table **2.2**). Further increment in catalyst loading hardly improved the yields (entries 6 and 7, Table **2.2**).

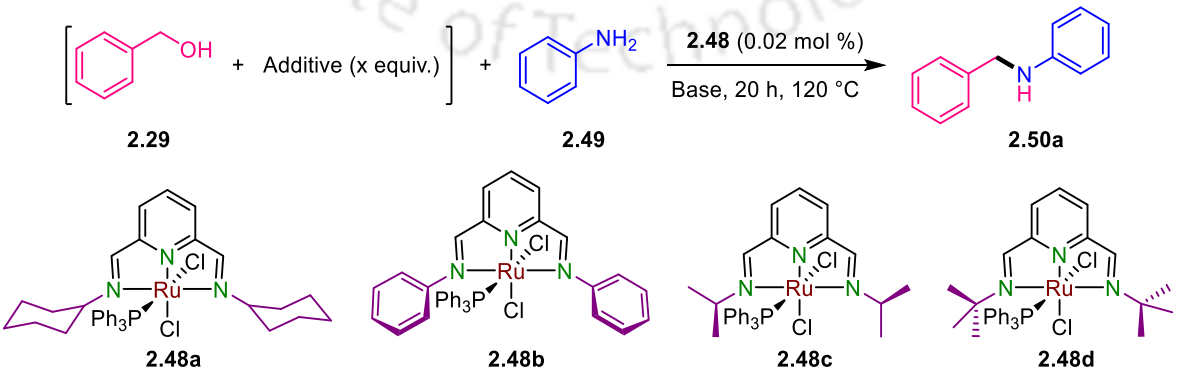

Scheme 2.20: *N*-alkylation reaction catalyzed by the pincer-ruthenium complexes of the type (^{R2}NNN)RuCl$_2$(PPh$_3$) (**2.48a**; R = Cy, **2.48b**; R = Ph, **2.48c**; R = ^{i}Pr and **2.48d**; R = ^{t}Bu).

Table 2.2: *N*-Alkylation of aniline with benzyl alcohol under varying loading of the base and catalyst **2.48d**

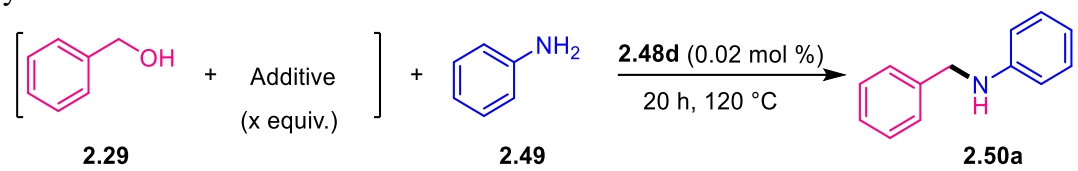

2.29 **2.49** **2.50a**

Entry	Additive (x equiv.)	**2.48d** (mol %)	Yield (%)[a]	TON
1	KO^{t}Bu (0.25)	0.02	7	350
2	KO^{t}Bu (0.50)	0.02	15	750
3	KO^{t}Bu (0.75)	0.02	26	1300
4	KO^{t}Bu (1.00)	0.02	16	800
5	KO^{t}Bu (0.75)	0.05	46±1[b]	920
6[b]	KO^{t}Bu (0.75)	0.10	45	450
7	KO^{t}Bu (0.75)	0.20	52	260
8	Et_3N (0.75)	0.02	0	0
9	KOH (0.75)	0.02	9	450
10	K_2CO_3 (0.75)	0.02	0	0
11	Na (0.75)	0.02	53	2650
12	NaO^{t}Bu (0.75)	0.02	53	2650
13	NaOH (0.75)	0.02	12 (6)[c]	600

Reaction conditions: benzyl alcohol (0.53 mL, 5.1 mmol), additive (x equiv.), aniline (0.47 mL, 5.14 mmol) and **2.48d** (0.02 mol %) at 120 °C. [a]Yield determined from ^{1}H NMR spectroscopy using toluene as an internal standard. [b]Reported as an average of NMR spectroscopy and isolated yield. [c]Yield of the corresponding imine is given in parenthesis.

Use of 0.75 equivalents of either K_2CO_3 or Et_3N as the base in the (^{t}Bu^{2}NNN)RuCl$_2$(PPh$_3$) (**2.48d**) (0.02 mol %) catalyzed reactions did not yield any products (entries 8 and 10, Table **2.2**). On the other hand, presence of 0.75 equivalents of KOH resulted in very poor yield (entry 9, Table **2.2**). To test the hypothesis of generating the base *in-situ* (*vide-supra*), 0.75 equivalents of sodium was treated with benzyl alcohol **2.29** at 120 °C. To the resulting slurry (likely to be **2.29** and sodium benzyloxide in the ratio 0.25:0.75) at room temperature, equivalent amounts of aniline (**2.49**) containing 0.02 mol % of **2.48d** was added and stirred at 120 °C in a sealed vessel. This reaction resulted in 53% yields and better turnovers (2650) (entry 11, Table **2.2**). Notably, under these conditions, the use of an additional base such as KO^{t}Bu is completely mitigated. In addition, there is no possibility of the formation of one of the by-products (Path **B**, Scheme **2.18**). These features make the current reaction (entry 11, Table **2.2**) more atom-economical in comparison with other reactions (entries 1-10, Table **2.2**) and earlier reports.[19, 75] Interestingly, the water formed in the reaction promotes the conversion of sodium benzyloxide back to **2.29**, thus maintaining its continuous supply in the catalytic cycle (Path **A**, Scheme **2.18**).

Under these optimized conditions, the introduction of solvent gave reduced yields (entries 2-5, Table **2.3**) of *N*-alkylated product. Under solvent-free conditions, the yield of **2.48d** catalyzed *N*-alkylation could be improved (ca. 73%) at higher catalyst loading (entry 9, Table **2.3**) however at the cost of TON. The catalytic activity of other complexes **2.48a**, **2.48b** and **2.48c** were not on par when compared to that of **2.48d** (compare entries 10, 11 and 12 with entry 1, Table **2.3**).

Table 2.3: *N*-Alkylation catalyzed by (**2.48a-d**) in different solvents.

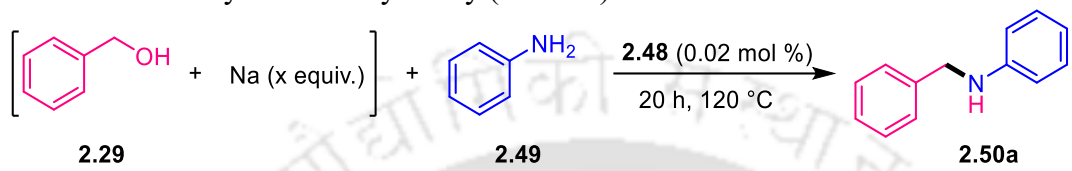

2.29 **2.49** **2.50a**

Entry	Na (x equiv.)	(**2.48d**) (mol %)	Solvent	Yield (%)[a]	TON
1	0.75	0.02	--	53	2650
2	0.75	0.02	Benzene	17 (8)[c]	850
3	0.75	0.02	Dioxane	28 (7)[c]	1400
4	0.75	0.02	THF	26 (2)[c]	1300
5[b]	0.75	0.02	Toluene	21±1 (10)[c]	1050
6[d]	0.75	0.02	--	57	2850
7[e]	0.75	0.02	--	16	800
8	1.00	0.10	--	47	470
9	0.75	0.10	--	73	730
10	0.75	(**2.48a**) 0.02	--	44	2200
11	0.75	(**2.48b**) 0.02	--	37	1850
12	0.75	(**2.48c**) 0.02	--	44	2200

Reaction conditions: benzyl alcohol (0.53 mL, 5.1 mmol), Na (x equiv.), aniline (0.47 mL, 5.14 mmol) and **2.48** (0.02 mol %) at 120 °C. [a]Yield determined from ^{1}H NMR by using toluene as an internal standard. [b]Reported as an average of NMR spectra and GC yield. [c]Yield of the corresponding imine given in parenthesis. [d]Reaction was performed at 140 °C. [e]Reaction was performed at 100 °C.

2.3.3 Scope of the pincer-ruthenium catalyzed *N*-Alkylation reaction

As the catalytic system comprising of 0.02 mol % **2.48d** in combination with 0.75 equivalents of sodium at 140 °C provided the best turnovers (ca. 2850) (entry 6, Table **2.3**), similar conditions were used to check the reactivity towards a variety of alcohols and amines (Table **2.4**). In the (^{t}Bu2NNN)RuCl$_2$(PPh$_3$) (**2.48d**) (0.02 mol %) catalyzed *N*-alkylation using benzyl alcohol, amines with electron-withdrawing groups provided good but slightly lower TON when compared to the use of aniline (compare TON of product **2.50a** with **2.50b** and with **2.50d**, Table **2.4**).

Table 2.4: *N*-Alkylation of various primary amines with several alcohols catalyzed by **2.48d**.[a]

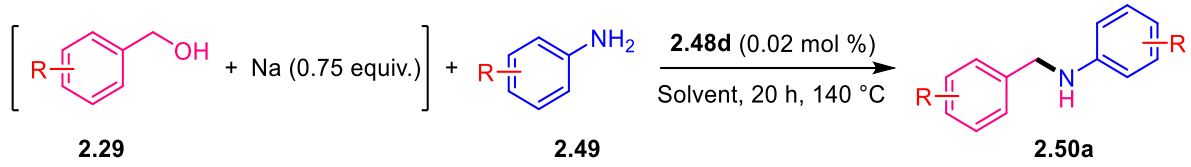

2.29 **2.49** **2.50a**

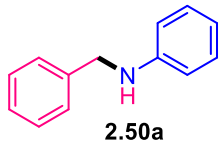

2.50a
57%, 2850 TON[a]
25%, 12500 TON[a,d]

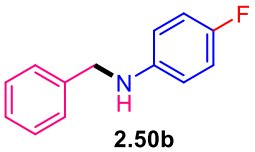

2.50b
47%, 2350 TON[a]
18%, 9000 TON[a,d]
80%, 400 TON[a,f]

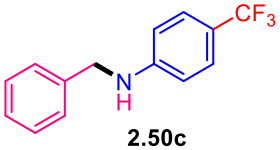

2.50c
0%, 0 TON[a]

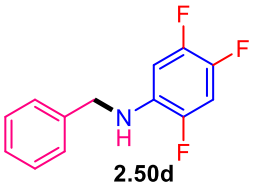

2.50d
35%, 1750 TON[a]
21%, 10500 TON[a,d]

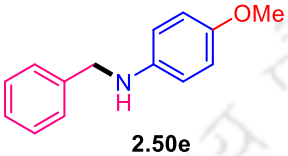

2.50e
17±0.2%, 850 TON[b]
34%, 17000 TON[a,d]

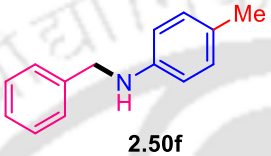

2.50f
25%, 1250 TON[a]
24%, 12000 TON[a,d]
60%, 300 TON[a,f]

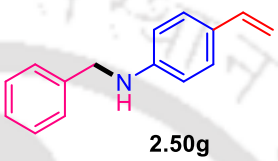

2.50g
0%, 0 TON[a]

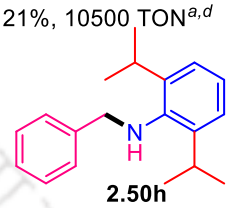

2.50h
0%, 0 TON[a]

2.50i
17%, 850 TON[a]
16%, 8000 TON[a,d]
32%, 160 TON[a,f]

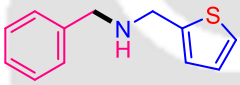

2.50j
13%, 650 TON[a]

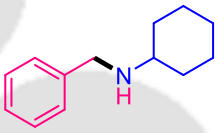

2.50k
0%, 0 TON[a]
34%, 1700 TON[a,c]

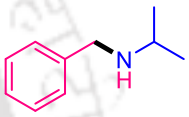

2.50l
0%, 0 TON[a]
7%, 350 TON[a,c]

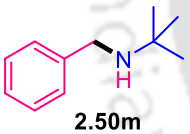

2.50m
0%, 0 TON[a]
3%, 150 TON[a,c]

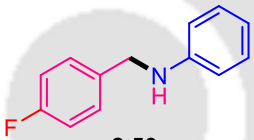

2.50n
28±2%, 1400 TON[b]
8%, 4000 TON[a,d]
40%, 400 TON[a,f]

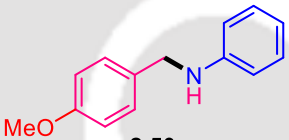

2.50o
62±2%, 3100 TON[b]
35±1%, 17500 TON[a,d]
90%, 450 TON[a,f]

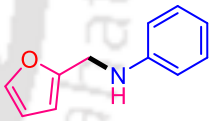

2.50p
20%, 1000 TON[a]
9%, 4500 TON[a,d]

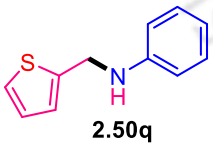

2.50q
20%, 1000 TON[a]
14%, 7000 TON[a,d]
40%, 200 TON[a,f]

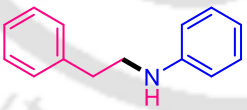

2.50r
23%, 1150 TON[a]
9%, 4500 TON[a,d]

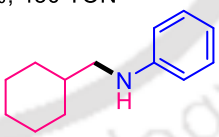

2.50s
30±1%, 1500 TON[b]
37%, 18500 TON[a,d]
58%, 29000 TON[a,g]
70%, 350 TON[a,f]

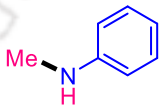

2.51a
12%, 600 TON[a]

Reaction condition: benzyl alcohol (0.53 mL, 5.1 mmol), Na (0.75 equiv.), aniline (0.47 mL, 5.14 mmol) and **2.48d** (0.02 mol %) at 140 °C. [a]Yield determined from ^{1}H NMR spectroscopy by using toluene as internal standard. [b]Average of NMR spectroscopy and isolated yield. [c]Yield of the corresponding imine. [d]Reaction performed for 48 h with 0.002 mol % **2.48d**. [e]Average of NMR spectra and isolated yield of two runs. [f]Reaction performed for 20 h with 0.2 mol % **2.48d**. [g]Reaction performed for 96 h with 0.002 mol % **2.48d**.

On the other hand, amines with electron-donating groups resulted in moderate turnovers (compare TON of product **2.50a** with **2.50e** and with **2.50f**, Table **2.4**). The turnovers of **2.50a** and **2.50b-f** could be greatly enhanced by operating at lower loading (0.002 mol %) of **2.48d**.

Amines with terminal double bonds and those with sterically demanding substituents were unreactive towards *N*-alkylation (**2.50g** and **2.50h**, Table **2.4**). Aliphatic amines showed poor reactivity in general and mainly lead to formation of corresponding imines (**2.50k**, **2.50l**, and **2.50m**, Table **2.4**). Amines based on heterocyclic compounds gave moderate turnovers (products **2.50i** and **2.50j**, Table **2.4**) with 0.02 mol % **2.48d** which however improved upon lowering the catalyst loading to 0.002 mol %. For the (^{t}Bu2NNN)RuCl$_2$(PPh$_3$) (**2.48d**) (0.02 mol %) catalyzed *N*-alkylation of aniline, while electron-withdrawing groups on benzyl alcohol (product **2.50n**, Table **2.4**) lowered the turnovers, presence of electron-donating groups (product **2.50o**, Table **2.4**) gave very high TON. In particular, in the *N*-alkylation of aniline with 4-methoxy benzyl alcohol, very high turnovers (ca. 17500) could be obtained by operating at a very low (0.002 mol %) loading of (^{t}Bu2NNN)RuCl$_2$(PPh$_3$) (**2.48d**). Moderate turnovers (products **2.50p** and **2.50q**, Table **2.4**) were obtained when alcohols containing heterocyclic substituents were used as an alkyl precursor.

Under the reaction conditions, cyclohexyl methanol provided excellent turnovers (29000 TON for **2.50s**, Table **2.4**) among the aliphatic alcohols used for the *N*-alkylation of aniline. The alkylation of representative substrates with higher loading (0.2 mol %) of **2.48d** showed an increase in yields (Table **2.4**, footnote f, **2.50b**, **2.50f**, **2.50i**, **2.50n**, **2.50o**, **2.50q**, and **2.50s**).

2.3.4 *N*-methylation reaction

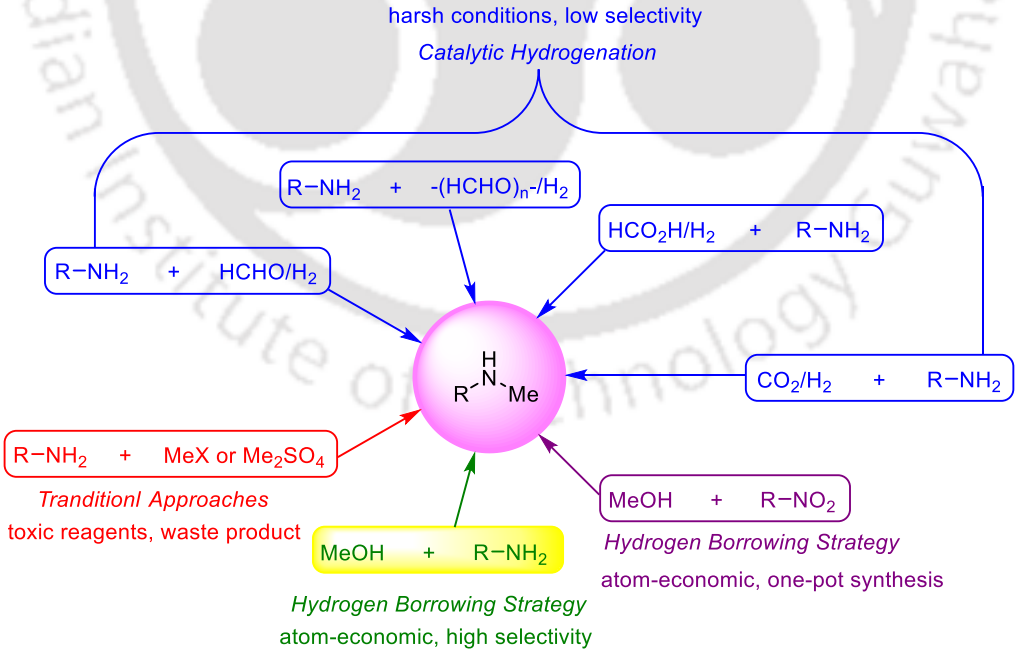

Scheme 2.21: Schematic diagram of *N*-methylation of amine *via* various methodologies.

N-methylated amines have important uses in the pharmaceutical industry (Figure **2.1**). Among the various methods that are available for methylations of amines, most of the cases lead to an

equivalent amount of waste products (Scheme **2.21**). The use of methanol as a methylating agent[21, 28, 31, 59, 64, 72, 83-84, 106-110] presents an attractive strategy to generate valuable *N*-methylated amines.

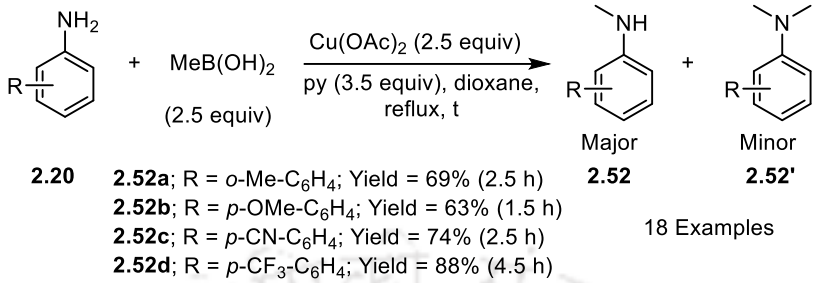

Scheme 2.22: Copper catalyzed coupling reaction that lead to methylation of amines.[108]

Methodologies involving the palladium-catalyzed[111] and copper-catalyzed[112] coupling reactions have been explored for the C–N bond formation. The formation of mono/di methylated products usually requires the controlled addition of reagents. So, copper-mediated C–N bond formation *via* the cross-coupling of amine with aryl boronic acids have been a powerful method in this respect. A plethora of boronic acids have been used in the presence of an excess nitrogenous base and a stoichiometric amount of copper salt (Scheme **2.22**). Gonzalez an co-workers have studied the monomethylation of various aniline derivatives including heterocycle amines in a single step with good to excellent yield.[108]

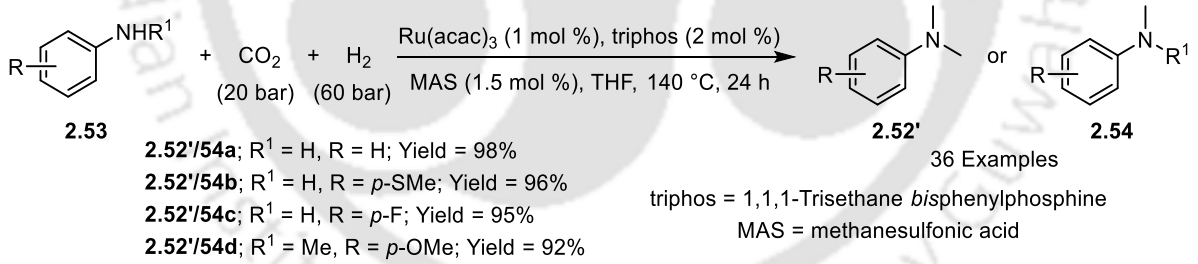

Scheme 2.23: Ruthenium catalyzed methylation of amine with carbon dioxide.[109]

In general, classical methods for mono/di methylation have been well explored (Scheme **2.21**). However, using CO_2 as a C_1 source remains a highly attractive route. Using a renewable source of thermodynamically stable CO_2 for the application of methylation with high selectivity requires a different strategy. In a representative process, Beller used the ruthenium-complexes in the presence of phosphine ligand to obtain good chemoselectivity and good productivity towards *N*-methylation (Scheme **2.23**). Interestingly, Beller demonstrated that the ruthenium complex initially hydrogenates CO_2 to methanol and formic acid in the presence of H_2. From the mechanistic pathway, it is understood that formamide was formed during the reaction,

which reduces to the corresponding methylated product. Thus, by applying this method they have screened a wide range of substrates that demonstrate good to excellent yield.[109]

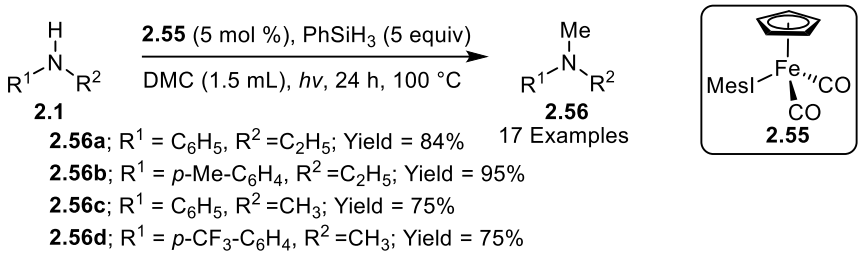

Scheme 2.24: Iron catalyzed methylation of amines using DMC as a C_1 source.[72]

Another alternative methodology for the methylation of primary/secondary amines that have attracted attention is the use of dimethyl carbonate (DMC) or diethyl carbonate (DEC) as a C_1 source while using silane or hydrogen as reducing agents. Notably, due to the electrophilic nature of DMC, it can easily be attacked by a nucleophile (*e.g.* alcohols, amines) at high temperature at the methyl carbon, which leads to the formation of CO_2 and methanol. The advantages of using DMC are its non-toxicity, biodegradable in nature, and easy handling. Using iron carbene complex Darcel and co-workers reported the methylation of secondary amines under mild reaction conditions (Scheme **2.24**).

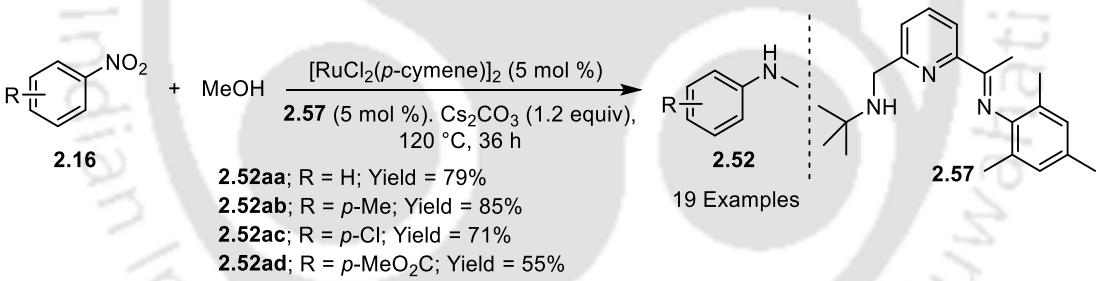

Scheme 2.25: One-pot methylation of nitro compounds through hydrogen-borrowing approach.[113]

Yang and co-workers reported ruthenium-catalyzed one-pot methylation of nitroarenes using methanol as a methylating agent (Scheme **2.25**). Using this method, without involving amines they successfully demonstrated the desired methylation of the corresponding nitroarenes by combining dichloro(*p*-cymene)ruthenium(II) dimer with pincer ligand *in-situ*. This process initially reduced the nitro group to amine, which further participates in the *N*-methylation reaction.

The versatile and environmentally benign *N*-methylation starting from methanol is the most accepted route. Following the pioneering work of Grigg *et al*., many groups developed their methodologies using iridium,[114-115] ruthenium[31, 116-117] and other transition metals.[22, 118-119] Though the hydrogen-borrowing method provides alternative greener approaches for

methylation, there are some restrictions in the substrate scope due to lack of selectivity. However, Chen and co-workers reported iridium catalyzed methylation reaction with a broad substrate scope, high selectivity and lower catalyst loading (Scheme **2.26**).

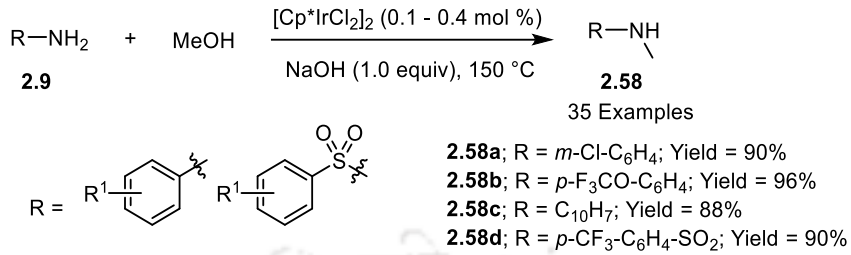

Scheme 2.26: Iridium catalyzed methylation of amines.[59]

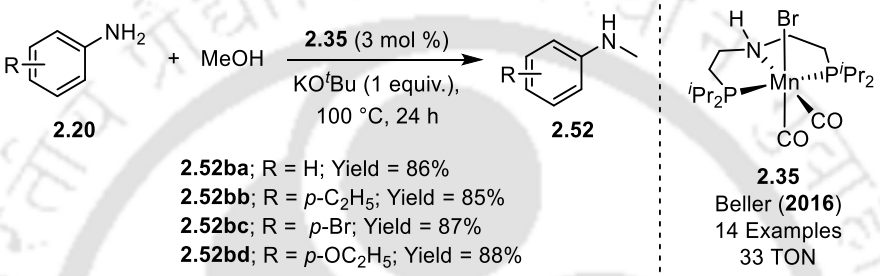

Scheme 2.27: *N*-methylation of amines with methanol catalyzed by a pincer-manganese complex.[21, 99]

The direct transformation of *N*-methylated amines using methanol with amines are highly advantageous.[120] There are few examples of methylated amines reported using methanol as a source of alkylating agents, such as Ru,[28, 31, 37, 46, 117] Ir,[59] and Mn.[21] Beller and co-workers demonstrated the first example of non-noble metal catalyzed *N*–methylations of various amines with methanol under mild conditions (Scheme **2.27**) using a pincer-manganese complex **2.35**.[21, 99]

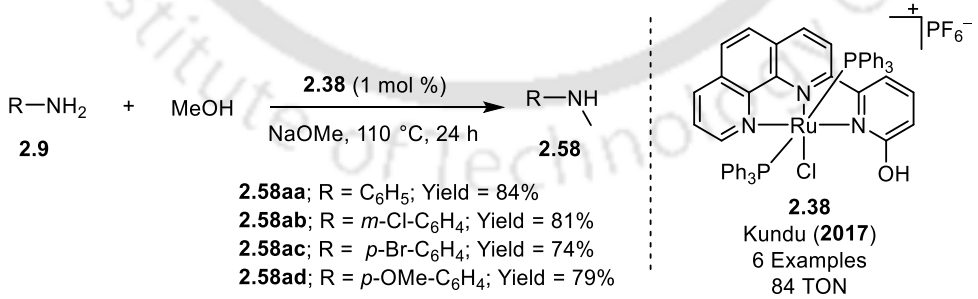

Scheme 2.28: *N*-methylation of amines with methanol catalyzed by pincer-ruthenium complex.[46]

Similarly, Kundu and co-workers demonstrated NNN pincer-ruthenium **2.38** catalyzed selective mono *N*-methylation of amines using methanol as an alkylating precursor with a greener synthetic route (Scheme **2.28**).[46] Considering these facts, the imine-based ruthenium

pincer catalytic system is still relevant in the methylation of amine using methanol as an alkylating agent.

2.3.5 *N*-methylation catalyzed by pincer-ruthenium complex (^{t}Bu2NNN)RuCl$_2$(PPh$_3$) (2.48d)

As the optimized conditions given in Table **2.3** (entry 6) gave poor yield of methylated aniline (**2.51a**, Table **2.4**) the reaction parameters were further optimized for the use of methanol as the alkylating agent (Table **2.5**). While high turnovers (ca. 1750, entries 5 and 6, Table **2.5**) were observed for a combination of aniline and methanol in the ratio of 1:4.8 using 0.02 mol % (^{t}Bu2NNN)RuCl$_2$(PPh$_3$) (**2.48d**), the yields could be further improved (81%, entry 9, Table **2.5**) upon increasing the catalyst loading. The optimized condition (entry 6, Table **2.5**) that provided the best turnover was employed for the (^{t}Bu2NNN)RuCl$_2$(PPh$_3$) (**2.48d**) catalyzed *N*-methylation of various amines (Table **2.6**).

Table 2.5. Optimization of *N*-methylation of aniline catalyzed by **2.48d**.

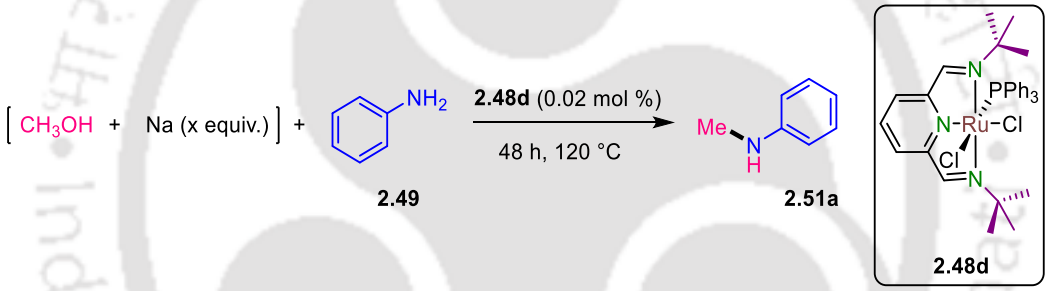

Entry	Sodium (x equiv.)[a]	**(2.48d)** (mol %)	**(2.49)**: MeOH	Yield (%)[b]	TON
1	0.75	0.02	1.0:1.0	12	600
2	1.00	0.02	1.0:1.0	3	150
3	0.75	0.02	1.0:2.5	18	900
4[c]	1.00	0.02	1.0:4.8	22±2	1100±80
5	1.00	0.02	1.0:4.8	30	1500
6[d]	1.00	0.02	1.0:4.8	35	1750
7[d]	1.00	0.05	1.0:4.8	52	1040
8[d]	1.00	0.10	1.0:4.8	66	660
9[d,e]	1.00	0.20	1.0:4.8	81±2.6	405±12

Reaction conditions: Methanol (0.5 mL, 12.35 mmol), Na (x equiv.), aniline (0.23 mL, 2.4 mmol) and **2.48d** (0.02 mol %) at 120 °C. [a]Equivalent calculated with respect to aniline. [b]Yield was determined from ^{1}H NMR spectroscopy by using toluene as an internal standard. [c]Reported as an average of NMR spectra and GC yield. [d]Reaction was performed at 140 °C. [e]Reported as an average of NMR spectra and isolated yield.

2.3.6. Scope of the pincer-ruthenium catalyzed *N*-methylation reaction

The TON obtained in the **2.48d** (0.02 mol %) catalyzed *N*-methylation of amines with electron-withdrawing groups were comparable to those obtained with aniline (compare TON of product **2.51a** with **2.51b** and with **2.51d**, Table **2.6**). The *N*-methylation reactions of amines with electron-donating groups, proceeded with higher TON (compare TON of product **2.51a** with **2.51e** and with **2.51f**, Table **2.6**). Furthermore, the turnovers obtained in the *N*-methylation of *p*-anisidine could be improved (12000 TON of product **2.51e**, Table **2.6**) by operating at very low loading (0.002 mol %) of **2.48d**. While the *N*-methylated products **2.51g** and **2.51h** (Table **2.6**) did not form, moderate TON were obtained in the **2.48d** (0.02 mol %) catalyzed *N*-alkylation of aniline with ethanol and 2-propanol (products **2.51i-l**, Table **2.6**). Upon lowering the loading of **2.48d** (0.002 mol %), excellent turnovers were observed for the catalytic *N*-alkylation of aniline with *n*-butanol and *n*-hexanol (products **2.51k** and **2.51l**, Table **2.6**).

Table 2.6: Scope of *N*-Methylation and *N*-alkylation of aniline catalyzed by (**2.48d**)[a]

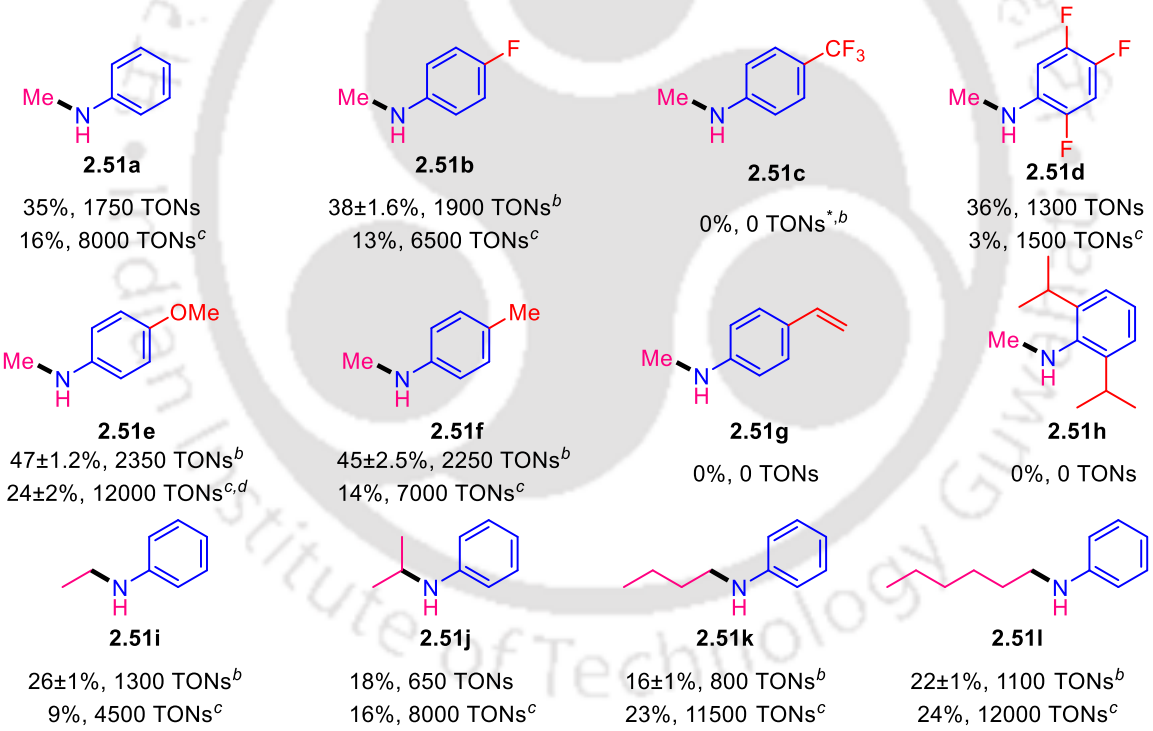

Reaction conditions: Methanol (0.5 mL, 12.35 mmol), Na (1 equiv.), aniline (0.23 mL, 2.4 mmol) and **2.48d** (0.02 mol %) at 140 °C. [a]Yield was determined from ^{1}H NMR spectroscopy by using toluene as an internal standard. [b]Reported as an average of NMR spectroscopy and isolated yield. [c]Reaction was performed 48h with 0.002 mol % **2.48d**. [d]Average of NMR spectra and isolated yield of two runs. [*]Side product was obtained.

However, when methylation of 4-(trifluoromethyl) aniline was attempted, instead of the expected product **2.51c**, 1700 turnovers of methyl-4-(dimethylamino) benzoate (**2.51cc**) were obtained along with trace amounts of **2.51ca** and **2.51cb**. Accordingly, one could anticipate the involvement of hydrolysis and subsequent esterification reactions leading to the formation of

2.51ca (Scheme **2.29**). Subsequent methylation of **2.51ca** could lead to product **2.51cc** *via* **2.51cb**. Grinter[121] and Jones[122] have independently demonstrated the hydrolysis of hydroxy-substituted and amino-substituted benzotrifluorides to the corresponding benzoic acids.

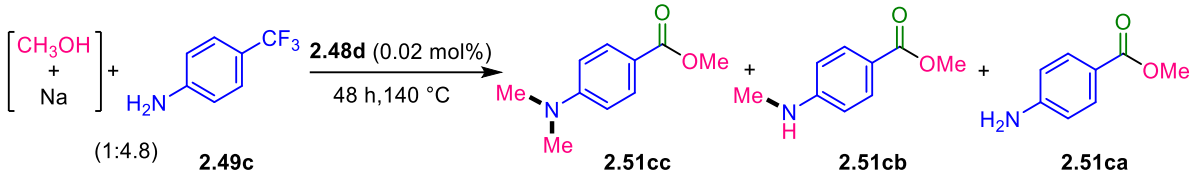

Scheme 2.29: Unexpected products obtained in *N*-methylation of 4-(trifluoromethyl)aniline.

2.3.7 Control experiment

In order to justify the plausible mechanism of the *N*-alkylation reaction, where sodium alkoxide reacts with water (by-product) to regenerate the alcohol *in-situ*, several control experiments were performed.

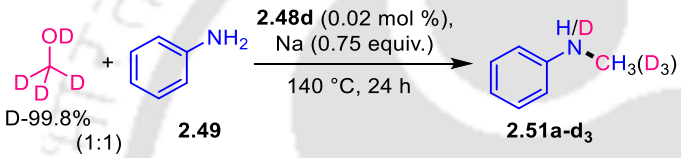

To validate the hypothesis that the base generated *in-situ* (Scheme **2.13**), reacts with the by-product water while regenerating the alcohol, deuterium labeling experiments were performed. For this purpose, the reaction of CD_3OD with aniline catalyzed by (^{t}Bu2NNN)$RuCl_2(PPh_3)$ (**2.48d**) was carried out in the presence of 0.75 equivalents of sodium. If Path **A** (Scheme **2.18**) was not involved, then complete deuterium incorporation is expected in product **2.51**. However, if Path **A** (Scheme **2.18**) is operative, then in addition to the dehydrogenation of CD_3OD to DCDO and D_2, one would expect the formation of CD_3ONa and its subsequent reaction with H_2O (formed by reaction of DCDO with **2.49**) to generate CD_3OH (Scheme **2.18**). Further CD_3OH upon dehydrogenation would give HD and DCDO. The hydrogenation of imine **2.51′** with HD is likely to result in partial deuterium loss in the methyl group of **2.51**. Alternatively, considering the fact that dehydrogenation of alcohol is endothermic with the equilibrium more towards the left (see computational studies, *vide-infra*), the possibility of reverse reaction of HD with DCDO to give CD_3OH and CHD_2OD cannot be ruled out. Similarly, reversible dehydrogenation of CHD_2OD could further lead to stochastic mixtures of HCDO, DCDO, HD, D_2, CHD_2OD, CD_3OD, CH_2DOD, and CHD_2OH. Over several cycles, due to the combined effect of both forward and reverse reaction of hydrogen (labeled and unlabelled) with imine **2.51′** and formaldehyde (labeled and unlabelled) respectively, the deuterium content on the methyl group on **2.51** is expected to be lowered. Significantly using

methanol-D_4 in this experiment resulted in 75% loss of deuterium on the methyl group of the product **2.51a** (equation 1).

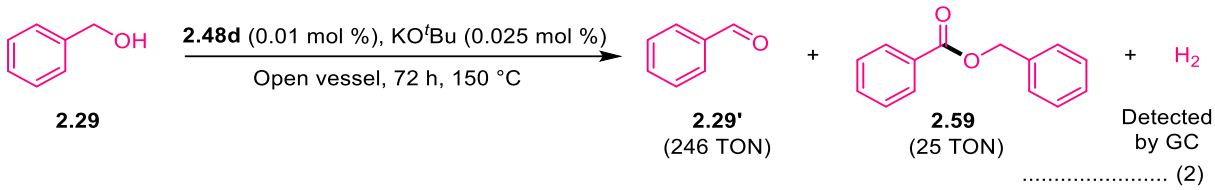

..... (2)

The complex **2.48d** (0.01 mol %) was found to catalyze the dehydrogenation of benzyl alcohol (**2.29**) at 150 °C under solvent-free conditions in an open vessel (equation 2). In this reaction, about 245 turnovers of benzaldehyde (**2.29′**) and 25 turnovers of benzyl benzoate (**2.59**)[123-124] were observed. Following a recent literature procedure,[125] it was also possible to detect hydrogen using GC by withdrawing an aliquot of gas from the headspace of this reaction mixture (Figure **2.3**).

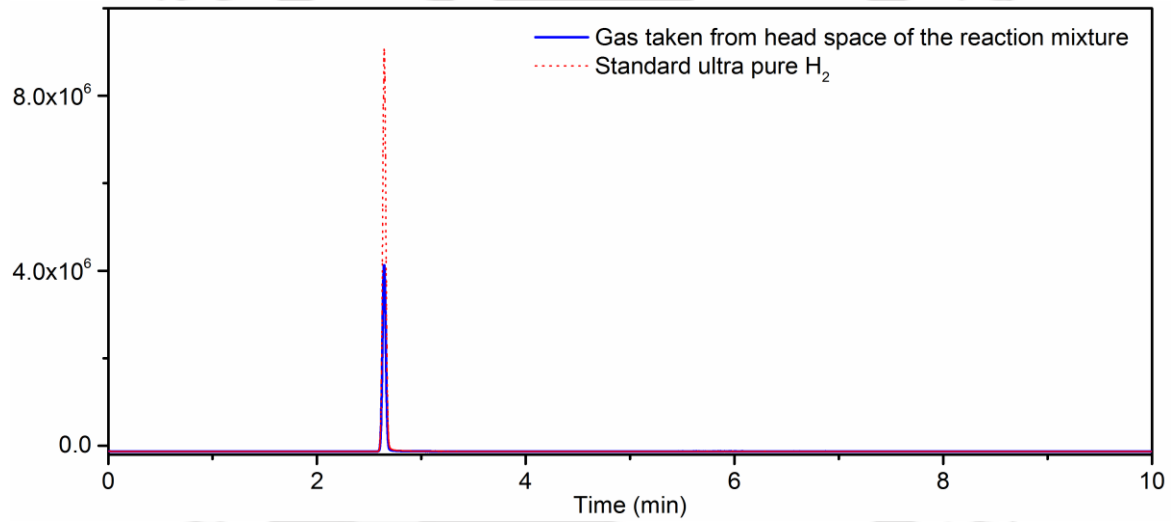

Figure 2.3: H_2 evolution in the dehydrogenation reaction of **2.29** catalyzed by **2.48d** at 150 °C *via* GC analysis.

While carrying out the same experiment, upon heating **2.29** with **2.49** in the presence of **2.48d** (0.02 mol %) and NaO^{t}Bu (0.1 mol %) at 140 °C under solvent-free conditions in an open vessel, 250 turnovers of imine **2.50′** was obtained (equation 3). On the other hand, it has been already demonstrated that under sealed-vessel conditions exclusive formation of **2.50** is observed (Table **2.2-3**).

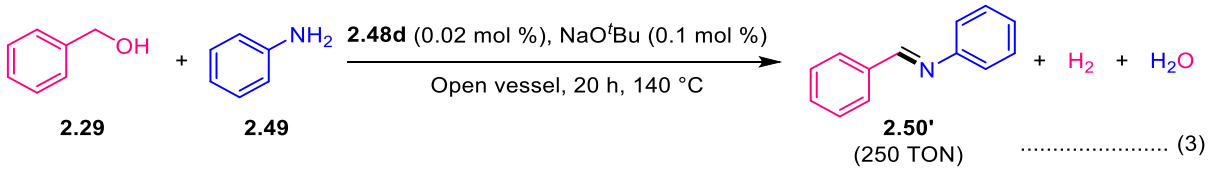

..... (3)

Furthermore, reaction of **2.50′** with H_2 (4 atm) in the presence of **2.48d** (0.2 mol %) and NaO^{t}Bu (1 mol %) at 140 °C gave **2.50** in quantitative yield (equation 4). The kinetic studies

were also performed though were inconclusive as obtaining meaningful and reproducible data was challenging owing to the highly viscous nature of the reaction mixture. However, plots depicting the changes in concentration (as determined by ^{1}H NMR spectroscopy using toluene as internal standard) of **2.29**, **2.29′**, **2.50′** and **2.50** with time for a variety of reaction conditions in the **2.48d** catalyzed alkylation of **2.49** have been provided (Figures **2.95-2.102**, Appendix **I**). Figure **2.103** (Appendix **I**) demonstrates the increase in yield of **2.50** with catalyst loading.

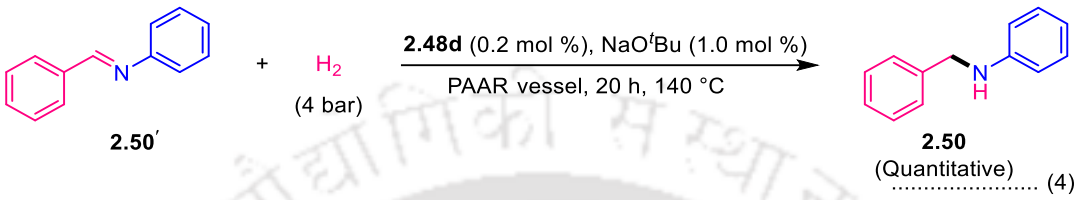

(4)

HRMS (ESI) analysis of a **2.48d** (10 mol %) catalyzed the reaction of **2.29** with **2.49** in the presence of 0.75 equivalents of NaOtBu at 140 °C after 3 hours indicated the major peak (*m/z* = 730.2165) to correspond to an adduct of **2.50a** with **2.48d** (Figure **2.4**). Rest to minor peaks could also be assigned to several derivatives of **2.48d** that presumably are involved in the catalytic cycle (Scheme **2.29-2.30**). These observations form the basis of our mechanistic studies.

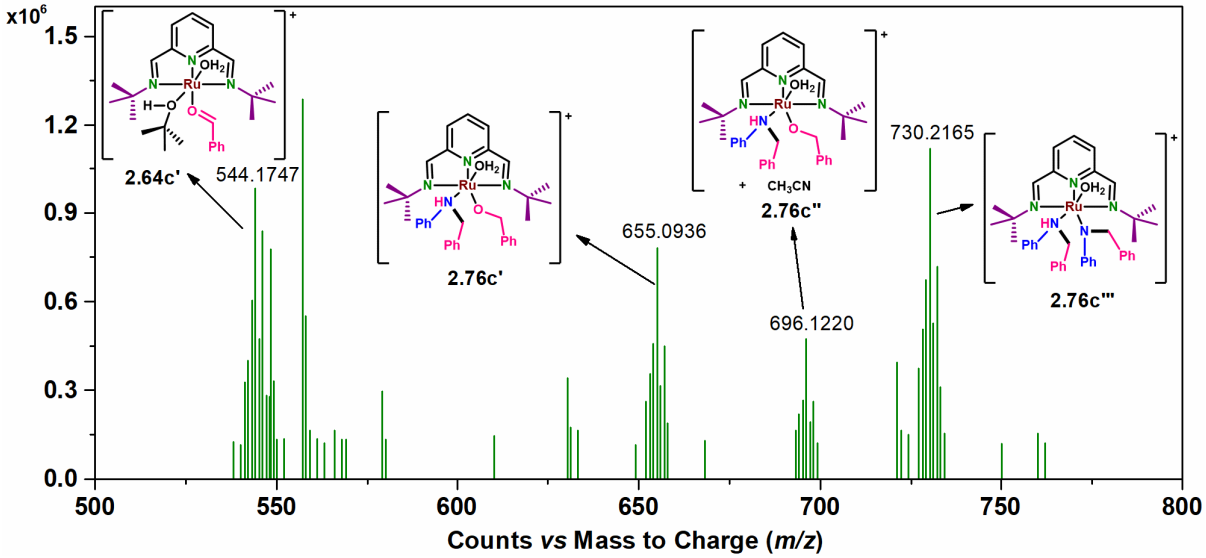

Figure 2.4: HRMS (ESI) analysis of reaction mixture obtained from a **2.48d** catalyzed (10 mol %) *N*-alkylation of aniline with benzyl alcohol at 140 °C after 3 hours.

2.3.8 Plausible mechanism

The plausible mechanism involved in the (^{R2}NNN)RuCl$_2$(PPh$_3$) (**2.48a**; R = Cy, **2.48b**; R = Ph, **2.48c**; R = ^{i}Pr, and **2.48d**; R = ^{t}Bu) catalyzed *N*-alkylation is depicted in Scheme **2.30-31** for aniline with benzyl alcohol using **2.48c** as a model catalyst. As shown in Scheme **2.30**, the precursor **2.66c** is readily generated from salt metathesis of **2.48c** with the *in-situ* generated

base $NaOCH_2Ph$. Loss of phosphine from **2.60c** would lead to the 16-electron complex **2.61c** (Figure **2.5**). The 16-electron complex **2.61c** is presumably the catalytically active species. A similar 16-electron NNN–Ru species was shown to be active for methanol dehydrogenation by Kundu and co-workers.[120] Very recently, Yu and Li have also proposed the release of phosphine and generation of CNP–Ru(II) species as the first step in the dehydrogenation of benzyl alcohol.[126]

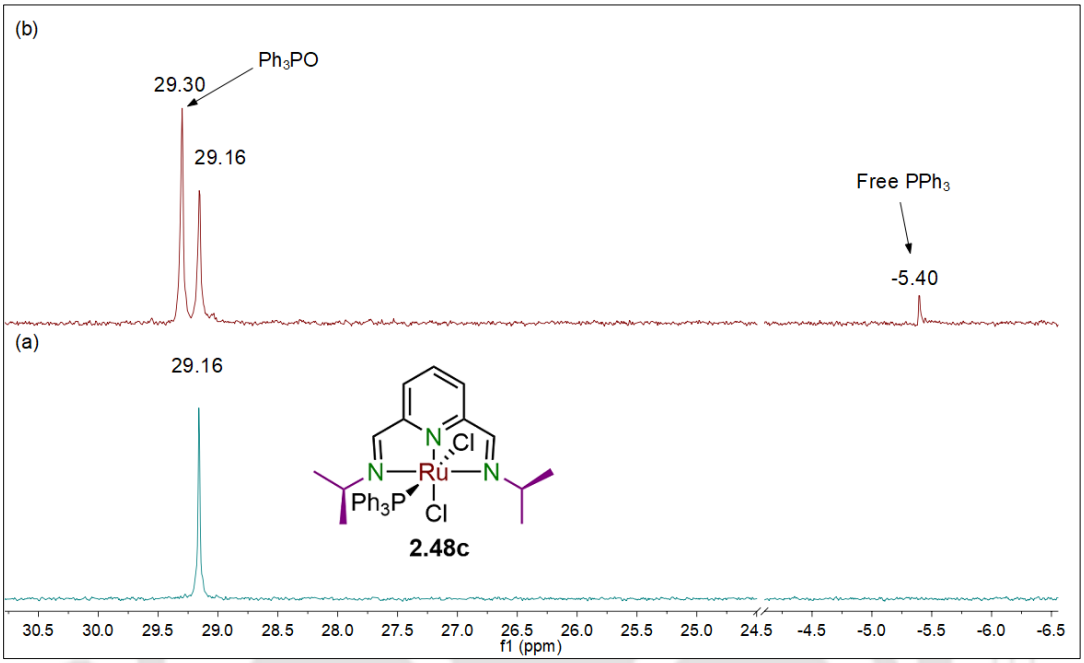

Figure 2.5: (a) ^{31}P NMR spectra of the complex **2.48c** in $CDCl_3$. (b) ^{31}P NMR spectra of **2.48c** (10 mol %), NaO^{t}Bu (10 mol %) in $CDCl_3$ containing aniline and benzyl alcohol (1:1, 0.13 mmol) after heating for (140 °C) 30 minutes.

The *β*-hydride elimination from the benzyloxide in complex **2.61c** through **TS-2.62c** could lead directly to the formation of **2.66c** along with benzaldehyde (**2.29′**) (purple dotted arrows, Scheme **2.30**). Alternatively, a *β*-hydride elimination *via* **TS-2.63c** could result in **2.64c** where the benzaldehyde remains coordinated to the Ru center. Dissociation of benzaldehyde from **2.64c** can occur *via* **TS-2.65c** giving rise to **2.66c**. Benzaldehyde (**2.29′**) undergoes an uncatalyzed condensation with aniline **2.49** giving imine **2.50′ (**Scheme **2.31)**. Complex **2.66c** could either react *via* Path **C** (purple colored arrows, Scheme **2.30**) or *via* Path **D** (magenta colored arrows, Scheme **2.31**). Along Path **C**, coordination of benzyl alcohol (**2.29**) to **2.66c** results in formation of **2.68c** *via* **TS-2.67c**. Subsequent *σ*-bond metathesis in **2.68c** between O–H and Ru–H going through **TS-2.69c** could give rise to η^2–H_2 complex **2.70c**. Dissociation of coordinated dihydrogen from **2.70c** *via* **TS-2.71c** would regenerate the active complex **2.61c.** GC experiments (*vide-supra*) provide conclusive evidence for the liberation of H_2 (Figure **2.3**).

Under open-vessel conditions, only Path **C** is likely to be operative with imine **2.50′** being the sole product.

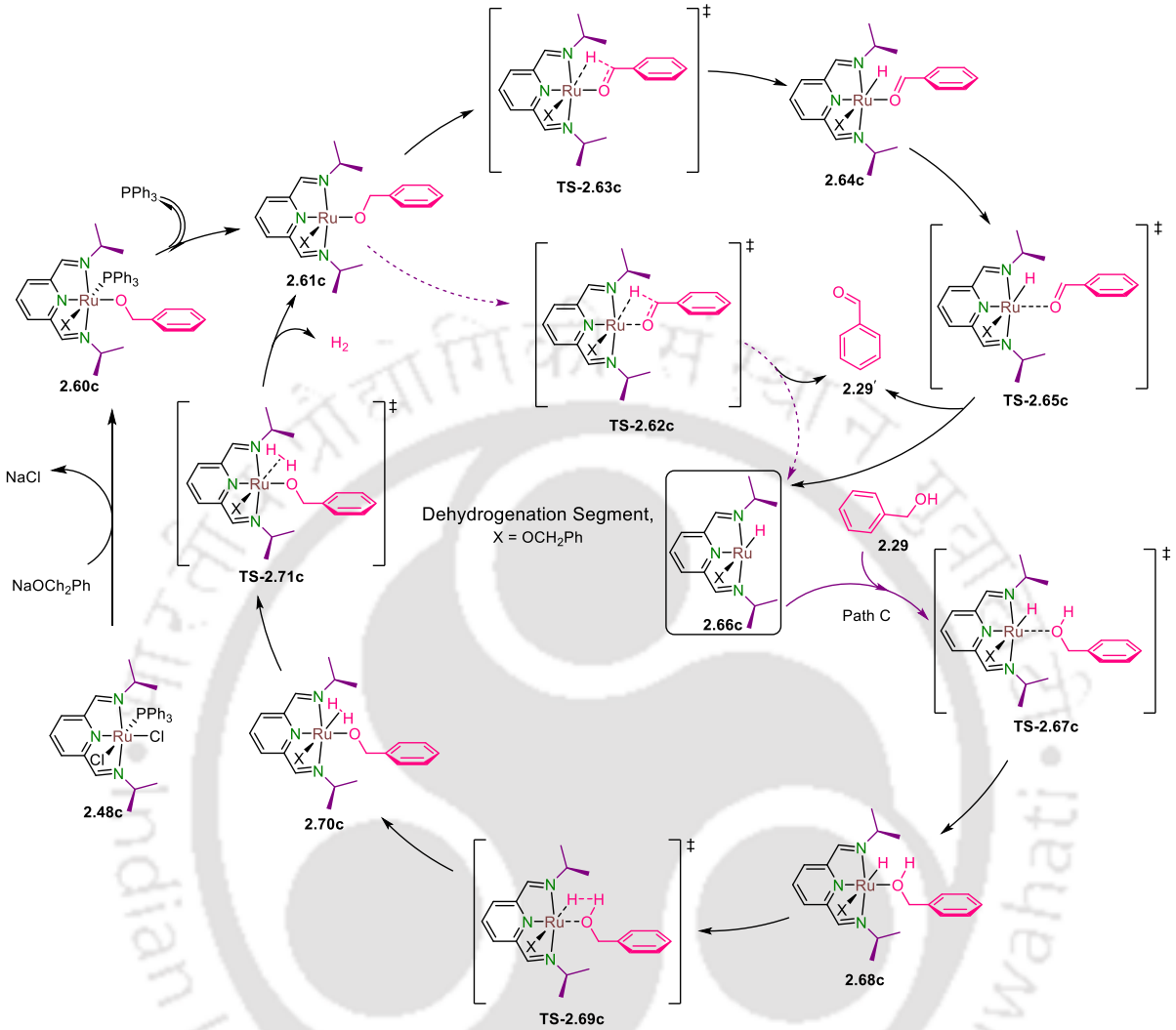

Scheme 2.30: Plausible mechanism involved in the dehydrogenation of alcohols during *N*-alkylation of amines.

Accordingly, reaction of **2.29** and **2.49** catalyzed by **2.48d** (0.02 mol %) in the presence of NaO^{t}Bu (0.1 mol %) at 140 °C in an open-vessel provided 250 TON of **2.50′** (equation 3). Closed vessel conditions would result in the accumulation of hydrogen which opens the possibility of Path **D** which involves the reaction with H_2. Independent experiments (*vide-supra*) have been carried out to show the ability of **2.48d** to hydrogenate **2.50′** using H_2 (equation 5). Along this path, the imine **2.50′** could insert directly into the Ru–H bond in **2.66c** *via* **TS-2.72c** resulting in the formation of **2.76c**. Another possibility would involve the coordination of imine **2.50′** to Ru in **2.66c** to give **2.74c** *via* **TS-2.73c** (magenta dotted arrows, Scheme **2.31**). Migratory insertion of the coordinated imine in **2.74c**[127] results in the formation of **2.76c** while going through **TS-2.75c**. A σ-bond metathesis reaction of H_2 and Ru–N in **2.74c** *via* **TS-2.77c** regenerates **2.66c** along with the formation of *N*-alkylated product **2.50**.

Interestingly, derivative of species **2.64c** (*m/z* = 544.1747) and various derivatives of species **2.76c** (*m/z* = 655.0936, 696.1220, 730.2165) are observed in the HRMS (ESI) analysis (*vide-supra*).

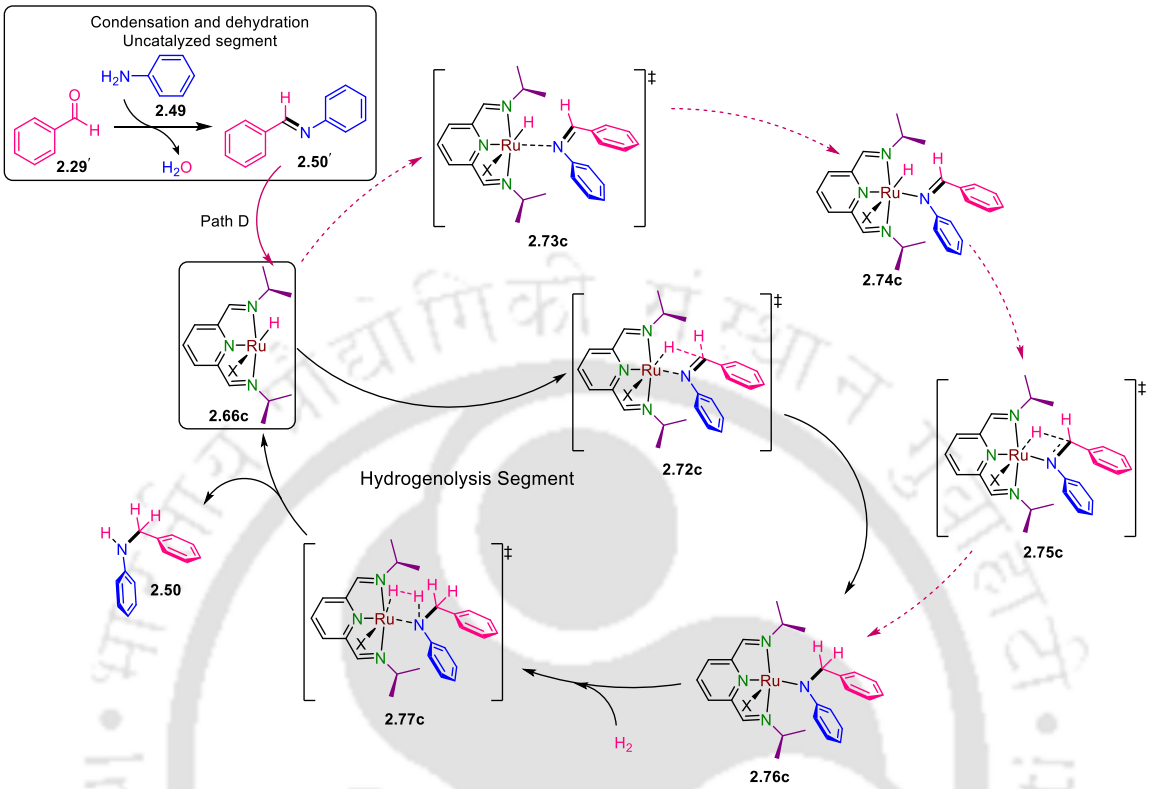

Scheme 2.31: Plausible mechanism involved in the hydrogenolysis of imine during *N*-alkylation.

2.3.9 Computational study

From the quantum mechanical calculation, it was observed that the Ru–PPh_3 binding energy follows the order **2.48b >2.48c >2.48a >2.48d**. Considering the fact that the reactivity is highest for **2.48d** and least for **2.4b** (Table **2.7**), one may infer the involvement of the dissociation of PPh_3 during the reaction (Scheme **2.30**), in line with the observation by ^{31}P NMR spectroscopy studies (Figure **2.5**)

Table 2.7: Binding energies and ^{31}P NMR Spectra shifts for complexes (**2.48a-d**).

Entry	Complex	Binding energy of Ru–PPh_3 (kcal/mol)	^{31}P shift	Yield (%) of **4.50**	TON
1	**2.48a**	20.86	29.42	44	2200
2	**2.48b**	25.21	32.27	37	1850
3	**2.48c**	23.86	29.16	44	2200
4	**2.48d**	08.90	--	57	2850

In order to attain insight into the energetics of the **2.48c** catalyzed *N*-alkylation, the various intermediates and transition states (TSs) involved in the dehydrogenation segment (Figure **2.6**)

and hydrogenation segment (Figure **2.7**) were modeled by DFT studies. Concerted β-hydride elimination and release of benzaldehyde from **2.61c** to generate **2.66c** along **TS-2.62c** (purple dotted arrows, Scheme **2.30** and blue dotted lines, Figure **2.6**) is endothermic (ca. 9.32 kcal/mol) and requires high activation (ca. 34.19 kcal/mol).

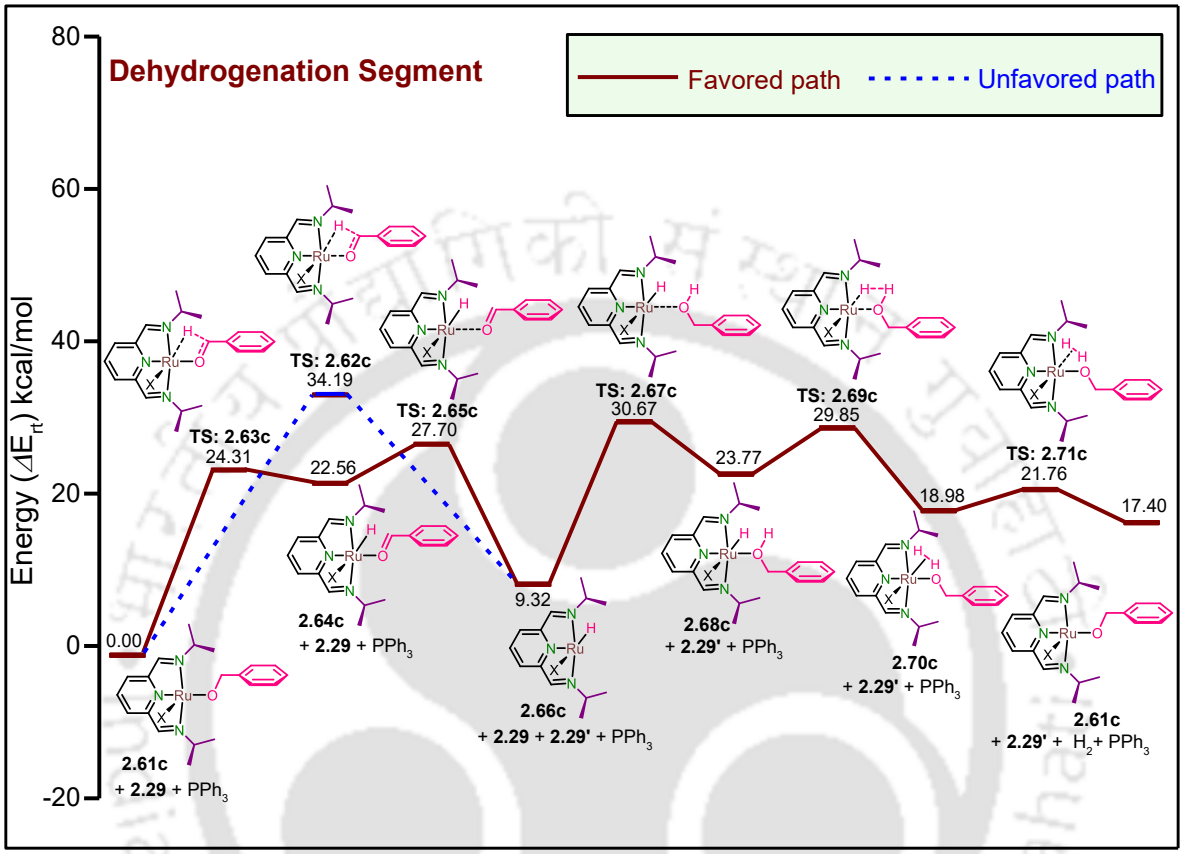

Figure 2.6: Energy profile of various intermediates involved in the dehydrogenation segment of **2.48c** catalyzed *N*-alkylation of aniline with benzyl alcohol.

On the other hand, in a sequential reaction, the initial β-hydride elimination step (**2.61c→2.64c**) is endothermic (ca. 22.56 kcal/mol) and has a lower barrier (**TS-2.63c**; ca. 24.31 kcal/mol). The subsequent step involving the dissociation of benzaldehyde from **2.64c** leading to **2.66c** is exothermic (-13.24 kcal/mol) and has a low energy of activation (**TS-2.65c**; ca. 5.14 kcal/mol). Thus, the sequential β-hydride elimination and benzaldehyde dissociation is clearly the favorable pathway (Figure **2.6**). Furthermore, it is evident that the β-hydride elimination (**2.61c→2.64c**) is the rate-determining step (RDS) (Figure **2.6**). The next step (**2.66c→2.68c**) involving the coordination of benzyl alcohol to the Ru in **2.66c** is more endothermic (ca. 14.45 kcal/ mol) with a relatively lower barrier of 21.35 kcal/mol (**TS-2.67c**). Subsequent σ-bond metathesis in **2.68c** between O–H and Ru–H to generate η^2–H_2 complex **2.70c** is exothermic (-4.79 kcal/mol) and proceeds with a lower activation energy (**TS-2.69c** ca. 6.08 kcal/mol). The release of hydrogen from **2.70c** to regenerate **2.61c** is also exothermic (-1.58 kcal/mol) with a

very low barrier (**TS-2.71c** ca. 2.78 kcal/mol). The overall cycle catalyzed by **2.61c** for the transformation of benzyl alcohol (**2.29**) to give benzaldehyde (**2.29′**) with the liberation of hydrogen is endothermic by 17.40 kcal/ mol.

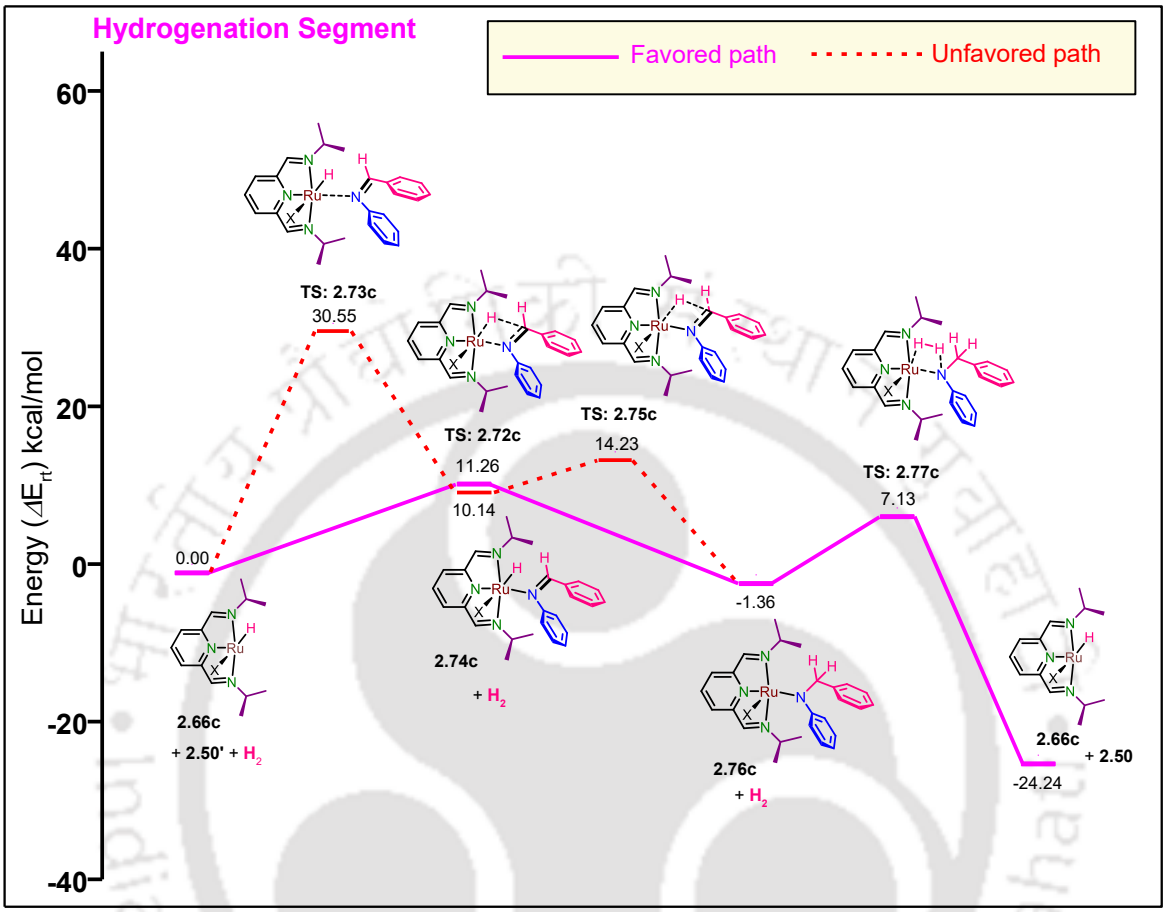

Figure 2.7: Energy profile of various intermediates involved in the hydrogenation segment of **2.48c** catalyzed *N*-alkylation of aniline with benzyl alcohol.

In the hydrogenolysis segment, the step (**2.66c→2.76c**) involving the concerted insertion of imine (**2.50′**) into the Ru–H appears to be RDS (**TS-2.72c** ca. 11.26 kcal/mol) and is exothermic (ca. -1.36 kcal/mol) (Figure **2.7**). The alternate path that involves the initial coordination of the imine (**2.50′**) to **2.66c** leading to **2.74c** is endothermic (ca. 10.14 kcal/mol) with a very high barrier (**TS-2.73c**; ca. 30.55 kcal/mol). Thus, it is highly unlikely that this path (magenta dotted arrows, Scheme **2.31** and red dotted lines, Figure **2.7**) will be followed although the subsequent migratory insertion in **2.74c** to generate **2.76c** is exothermic (ca. 11.50 kcal/mol) with a very low barrier (**TS-2.75c**; 4.09 kcal/mol). The regeneration of **2.66c** and release of the *N*-alkylated product (**2.50**) which involves the σ-bond metathesis reaction of H_2 and Ru–N is exothermic (-22.88 kcal/mol) with a relatively low barrier (**TS-2.77c** ca. 8.49 kcal/mol). The overall **2.66c** catalyzed hydrogenolysis of **2.50′** to **2.50** is exothermic (-24.24 kcal/mol).

2.3.10 Bisimidazole synthesis

The development of an efficient method for the synthesis of benzimidazole in a greener fashion has great significance due to the importance of benzimidazole in biological activity and being a medicinally important compound.[128] Several pharmaceutical important derivatives like Xa (FXa) inhibitors,[129] antiallergics,[130] antivirals,[131] antihypertensives,[132] anti-cancer agents NSC-693638[133] and HIV reverse transcriptase inhibitors are known to contain a benzimidazole moiety.[134] In addition, the use of benzimidazoles are also accepted as a frame in many fluorescent probes.[135]

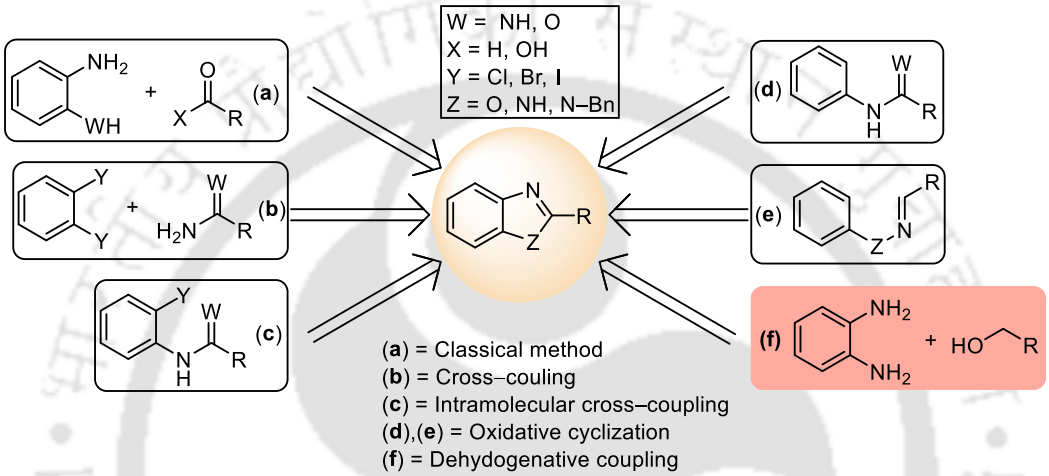

Scheme 2.32: Synthetic path for the formation of 2-substituted benzimidazoles.

There are distinct approaches adopted for the synthesis of benzimidazoles which involve: (**a**) direct one-pot cyclo-condensation reaction of *o*-phenylenediamine with an aldehyde or carboxylic acid,[136-137] (**b**) cross-coupling intermolecular C–N cyclization reactions,[138] (**c**) cross-coupling intramolecular C–N cyclization reactions,[139-142] (**d**) or (**e**) the cyclization to C–N bond formation *via* intramolecular cross-coupling reaction or C–H (activation) functionalization[143-144] and (**f**) dehydrogenative coupling of a primary alcohol with benzene-1,2-diamine[145-152] (Scheme **2.32**). Several other approaches are reported,[153] but many of them suffer from the use of stoichiometric amounts of oxidizing agents[154-155] or from the generation of excessive waste products[153] (Scheme **2.32**). However, the synthesis of benzimidazole faces major problem in selectivity as it may lead to 2-substituted benzimidazoles along with 1,2-disubstituted benzimidazoles.

In recent times, acceptorless dehydrogenative strategies for synthesizing benzimidazole from alcohols have gained interest, as alcohols are readily available. The synthesis of benzimidazole from the reaction of *o*-penylenediamine with alcohol was first reported by Watanbe group using the dichlorotris(*tri*phenylphosphine)ruthenium(II) catalyst (at 215 °C).[156] Over the years, there

have been several reports by Kemp,[70] Milstein,[157] Kirchner,[67] Wang,[158] Kundu[65] and Srimani[159] group. Beller and co-workers reported the synthesis of several heterocyclic compounds such as pyrroles, pyrimidines, quinolones and benzimidazoles using this approach (Scheme **2.33**).[21, 160] In the current study, the good *N*-alkylation activity of NNN pincer-Ru complexes were extended to synthesize valuable benzimidazoles.

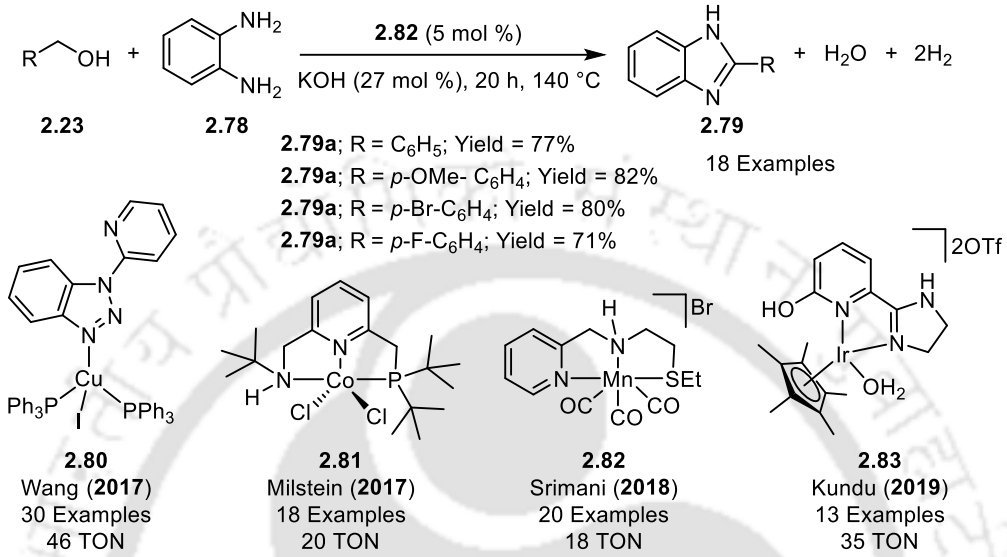

Scheme 2.33: Effective metal-catalyzed synthesis of benzimidazoles using alcohol as a precursor.[157-158, 161-164]

Table 2.8. Optimization of 2-substituted benzimidazoles *via* dehydrogenative coupling of *o*-phenylene diamine with benzyl alcohol catalyzed by (^{t}Bu2NNN)RuCl$_2$(PPh$_3$) (**2.48d**).

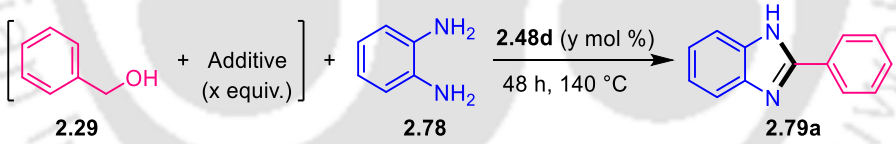

Entry	Additives (x equiv.)	(**2.48d**) (y mol %)	Solvent	Yield (%)[a]	TON
1	NaO^{t}Bu (0.001)	0.02	--	10±1	500
2	NaO^{t}Bu (0.75)	0.02	THF	Trace	--
3	NaO^{t}Bu (0.75)	0.02	Toluene	Trace	--
4	Na (0.001)	0.02	--	32±2	1600
5[c]	Na (0.25)	0.02	--	28	1400
6	Na (0.005)	0.10	--	15	750

Reaction conditions: Benzyl alcohol (0.53 mL, 5.1 mmol), Na (x equiv.), *o*-phenyleneaimine (0.55 g, 5.14 mmol) and **2.48d** (y mol %) at 140 °C. [a]Yield was determined from ^{1}H NMR spectroscopy by using toluene as an internal standard. [b]Report as an average of NMR spectra and isolated yield. [c]Reaction performed at 200 °C.

As discussed earlier, exclusion of the hydrogenation segment in Scheme **2.18** would result in a net dehydrogenative coupling reaction. Accordingly, the reactivity of the catalytic systems

was probed towards dehydrogenative coupling of benzene-1,2-diamine with various primary alcohols (Table **2.8**). The best results (ca. 1700 TON, entry 4, Table **2.8**) towards the formation of benzimidazoles were obtained with 0.02 mol % **2.48d** in the presence of only 0.1 mol % of Na.

Table 2.9. Synthesis of 2-substituted benzimidazoles using **2.48d** as a catalyst.[a]

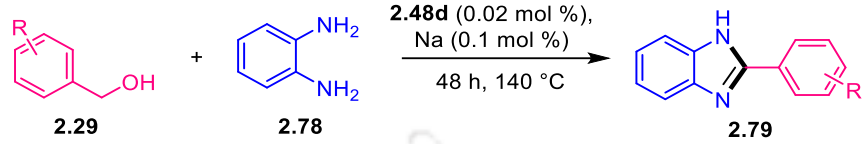

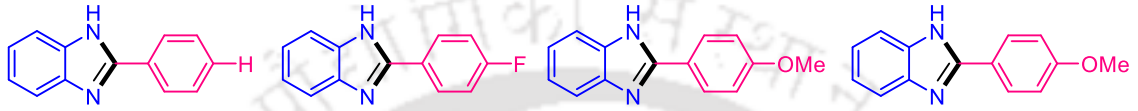

32±2, 1600 TONs[b] | 34, 1700 TONs | 46±2, 2300 TONs[b] | 24±1, 12000 TONs[b,c]

Reaction condition: Benzyl alcohol (0.53 mL, 5.1 mmol), Na (0.1 mol %), *o*-phenyleneaimine (0.55 g, 5.14 mmol) and **2.48d** (0.02 mol %) at 140 °C. [a]Yield was determined from ^{1}H NMR spectroscopy by using toluene as an internal standard. [b]Report as an average of NMR spectra and isolated yield. [c]Reaction performed using 0.002 mol % catalyst.

As the reaction is performed at 140 °C under open-vessel condition, water is effectively siphoned out making the need for stoichiometric amounts of base unnecessary. While the turnover numbers of dehydrogenative coupling of benzene-1,2-diamine with benzyl alcohols with electron-withdrawing group was comparable, higher turnovers were obtained upon using benzyl alcohols with electron-donating group (Table **2.9**). The turnovers could be further enhanced (Table **2.9**) at lower loading (0.002 mol %) of **2.48d**.

2.4 Conclusion

Pincer-ruthenium complexes of the type (^{R2}NNN)RuCl$_2$(PPh$_3$) (**2.48a**; R = Cy, **2.48b**; R = Ph, **2.48c**; R = ^{i}Pr, and **2.48d**; R = ^{t}Bu) have been utilized to accomplish the *N*-alkylation of primary amines. For the first time, sodium is used in these reactions to generate the required base *in-situ* thus making the reaction more atom-economical. Interestingly, water that is formed in the reaction promotes the catalytic cycle by regenerating the alcohol precursor from sodium alkoxide. Among the catalysts used, ($^{t\text{Bu}2}$NNN)RuCl$_2$(PPh$_3$) demonstrates the best activity towards the solvent-free *N*-alkylation of various amines with a variety of alcohols. In this study, while highest turnovers (29000) is obtained for alkylation of aniline with cyclohexyl methanol, very good results (12000 TON) are also obtained for *N*-methylation of *p*-anisidine. The work has been extended to the synthesis of benzimidazoles with excellent turnovers (12000 TON)

under solvent-free and open-vessel conditions *via* dehydrogenative coupling of benzene-1,2-diamine with benzyl alcohols.

Quantum mechanical calculations performed to understand the plausible reaction pathway indicates the dehydrogenation of benzyl alcohol to be endothermic (ca. 17.40 kcal/mol) with β-hydride elimination as the RDTS (ca. 24.31 kcal/mol). Notably, sequential β-hydride elimination and benzaldehyde dissociation are favored over a concerted pathway. On the other hand, the imine hydrogenation is exothermic (ca. -24.24 kcal/mol) with insertion of the imine **2.50′** into the Ru–H bond as the RDTS (ca. 11.26 kcal/mol). In case of hydrogenation, direct insertion of imine into the Ru–H bond is preferred over sequential imine coordination and subsequent migratory insertion.

2.5 Experimental Section

2.5.1 General methods and material

All manipulations were carried out under purified argon using a standard double manifold. Tetrahydrofuran (THF), 1,4-dioxane, p-xylene were dried *via* double distillation over Na/Benzophenone prior to the experiment,[165-166] methanol & ethanol were dried and distilled under argon according to literature procedure.[165-166] The $CDCl_3$ and DMSO-d_6 were purchased either from MERCK or Sigma-Aldrich and used as such.

^{1}H, ^{13}C, ^{19}F and ^{31}P NMR spectra were recorded either on Bruker ASCEND 600 operating at 600 MHz for ^{1}H, 150 MHz for ^{13}C, 565 MHz for ^{19}F & 242 MHz for ^{31}P or on Bruker AVANCE 400 operating at 400 MHz for ^{1}H, 100 MHz for ^{13}C, 376 MHz for ^{19}F & 162 MHz for ^{31}P. HRMS measurements were done using an Agilent Accurate-Mass Q-TOF ESI–MS 6520. GC measurements were performed on an Agilent 7820-GC instrument fitted with Agilent Front SS7 inlet N2 HP5 column (30 m length x 0.32 mm ID). X–ray crystallographic data were collected either on a Bruker Nonius Smart Apex II X–ray diffractometer or on an Oxford SuperNova microfocus X–ray diffractometer with graphite–monochromatized Mo–Kα radiation. The data refinement and cell reductions were carried out either by Bruker SAINT[167] program or by CrysAlisPro.[168] Structures were solved by direct methods using SHELXS–14.[169] The solved structures were further refined by the full matrix least–squares method using SHELXL–14.[169] GC analyses (TCD detection) were performed on a Agilent 7820-GC instrument fitted with Agilent Front SS7 inlet N2 HP5 column (30 m length ´ 0.32 mm ID) using the following method: Agilent 7820-GC Detector, Oven temperature 70 °C, Time at

starting temp: 0 min, Hold time = 10 min, Flow rate (carrier): 5 mL/min (N_2), Split ration: 50, Inlet temperature: 70 °C, Detector temperature: 250 °C.

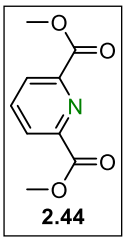
2.44

Synthesis of dimethyl pyridine-2,6-dicarboxylate (2.44): To a single neck round bottom flask containing pyridine-2,6-dicarboxylic acid (**2.43**) (4.08 g, 24.41 mmol), $SOCl_2$ (30 mL, 413.72 mmol) was added dropwise at 0 °C. The reaction mixture was refluxed for 6 h followed by slow addition of methanol (30 mL) at 0 °C. The resulting mixture was refluxed for an additional 12 h. Subsequently, excess $SOCl_2$ and MeOH were distilled off. Saturated $NaHCO_3$ solution was added to the residue and stirred for 30 minutes. The product was extracted from the aqueous phase using dichloromethane. The organic fraction was dried over anhydrous Na_2SO_4 and the solvent was evacuated from the organic portion to yield 4.2 g (90%) of pyridine-2,6-dicarboxylate (**2.44**) as a white solid. ^{1}H NMR (600 MHz, $CDCl_3$): δ = 8.32 (d, J = 7.8 Hz, 2H, Ar), 8.03 (t, J = 7.8 Hz, 1H, Ar), 4.03 (s, 6H, CO_2CH_3). ^{13}C NMR (150 MHz, $CDCl_3$): δ = 165.18 (CO_2CH_3), 148.29, 138.55, 128.21 (Ar), 53.38 (CO_2CH_3). HRMS (ESI): m/z calculated for $[C_9H_9NO_4+H]^+$: 196.0610, found: 196.0612.

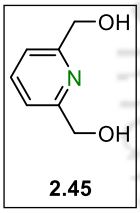
2.45

Synthesis of pyridine-2,6-diyldimethanol (2.45): Pyridine-2,6-dicarboxylate (**2.44**) (1.00 g, 5.15 mmol) was dissolved in absolute ethanol (20 mL) under an argon atmosphere. Subsequently, $NaBH_4$ (1.21 g, 31.98 mmol) was slowly added into the above solution at 0 °C. The reaction mixture was then stirred for 2 h at room temperature followed by reflux for 6 h. The reaction mixture was concentrated under vacuum followed by addition of saturated solution of K_2CO_3 (40 mL). The mixture was stirred for additional 2 h at 60 °C. The product was extracted into dichloromethane (20 mL x 3) and the organic fraction was dried over anhydrous Na_2SO_4. Removal of volatiles under reduced pressure resulted in pyridine-2,6-diyldimethanol (**2.45**) as a white solid. Yield: 0.626 g (87%). ^{1}H NMR (600 MHz, $CDCl_3$): δ = 7.70 (t, J = 7.7 Hz, 1H, Ar), 7.19 (d, J = 7.7 Hz, 2H, Ar), 4.78 (s, 4H, CH_2), 3.32 (bs, 2H, CH_2OH). ^{13}C NMR (150 MHz, $CDCl_3$): δ = 158.51, 137.62, 119.32 (Ar), 64.51 (CH_2OH). HRMS (ESI): m/z calculated for $[C_7H_9NO_2+H]^+$: 140.0712, found: 140.0701.

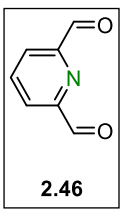
2.46

Synthesis of pyridine-2,6-dicarbaldehyde (2.46): A mixture of pyridine-2,6-diyldimethanol (**2.45**) (0.25 g, 1.79 mmol) and SeO2 (0.19 g 1.79 mmol) in 1,4-dioxane (10 mL) was refluxed for 12 h and then passed through a celite pad. The solvent was evaporated under vacuum to obtain a reddish type solid. Pyridine-2,6-

dicarbaldehyde (**2.46**) was obtained as a white solid after purification by silica column chromatography using hexane and ethyl acetate (80:20) as eluent. Yield 0.201 g (82%). ^{1}H NMR (600 MHz, $CDCl_3$): δ = 10.17 (s, 2H, C*H*=O), 8.19 (d, *J* = 7.5 Hz, 2H, Ar), 8.15 – 8.03 (m, 1H, Ar). ^{13}C NMR (150 MHz, $CDCl_3$): δ = 192.44 (*C*H=O), 153.06, 138.51, 125.44 (Ar). HRMS (ESI): m/z calculated for $[C_7H_5NO_2+H]^+$: 136.0399 , found: 136.0392.

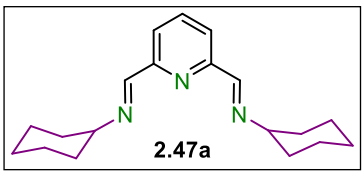

Synthesis of (1*E*,1′*E*)-1,1′-(pyridine-2,6-diyl)*bis*(*N*-cyclohexylmethanimine) (2.47a): To 10 mL of toluene, containing pyridine-2,6-dicarbaldehyde (**2.46**) (0.21 g, 1.55 mmol) and cyclohexyl amine (0.32 mL, 3.31 mmol), catalytic amounts of *p*-toluenesulfonyl chloride (1 mg, 5 μmol) was added and refluxed for 30 minutes. The solution was filtered, solvent was evaporated from filtrate and the resulting residue was extracted with hexane. The product (1*E*,1′*E*)-1,1′-(pyridine-2,6-diyl)*bis*(*N*-cyclohexylmethanimine) (**2.47a**) was obtained as a yellow gel (0.41 g, 88%) after removal of hexane. ^{1}H NMR (600 MHz, $CDCl_3$): δ = 8.43 (s, 2H, N=C*H*), 8.00 (d, *J* = 7.7 Hz, 2H, Ar), 7.76 (t, *J* = 7.8 Hz, 1H, Ar), 3.30 (ddd, *J* = 10.7, 6.5, 4.1 Hz, 2H, NC*H*$(CH_2)_5$), 1.83 (dt, *J* = 13.2, 3.7 Hz, 4H, NCH(C*H*$_2)_5$), 1.76 (dd, *J* = 12.5, 3.8 Hz, 4H), 1.72 – 1.64 (m, 2H, NCH(C*H*$_2)_5$), 1.59 (tdd, *J* = 12.9, 10.8, 3.7 Hz, 4H, NCH(C*H*$_2)_5$), 1.44 – 1.31 (m, 4H, NCH(C*H*$_2)_5$), 1.31 – 1.18 (m, 2H, NCH(C*H*$_2)_5$). ^{13}C NMR (150 MHz, $CDCl_3$): δ = 159.51 (N=*C*H), 154.71, 137.13, 122.25 (Ar), 69.78 (N*C*H$(CH_2)_5$), 34.26, 25.71, 24.82 (NCH(*C*H$_2)_5$). HRMS (ESI): m/z calculated for $[C_{19}H_{27}N_3+H]^+$: 298.2283, found: 298.2304

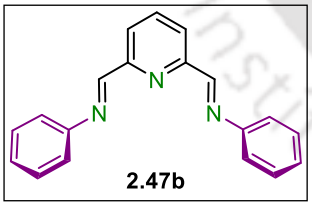

Synthesis of (1*E*,1′*E*)-1,1′-(pyridine-2,6-diyl)*bis*(*N*-phenylmethanimine) (2.47b): To 25 mL of toluene, containing pyridine-2,6-dicarbaldehyde (**2.46**) (1.0 g, 7.4 mmol) and aniline (1.5 mL, 16.4 mmol) catalytic amounts of *p*-toluenesulfonyl chloride (5 mg, 25 μmol) was added and refluxed for 30 minutes. The solution was filtered, solvent was evaporated from filtrate and the resulting residue was extracted with hexane. The product (1*E*,1′*E*)-1,1′-(pyridine-2,6-diyl)*bis*(*N*-phenylmethanimine) (**2.47b**) was obtained as a reddish yellow solid (1.71 g, 81%) after removal of hexane. ^{1}H NMR (600 MHz, $CDCl_3$): δ = 8.69 (s, 2H, N=C*H*), 8.30 (d, *J* = 7.7 Hz, 2H, Ar), 7.95 (t, *J* = 7.7 Hz, 1H, Ar), 7.47 – 7.41 (m, 4H, Ar), 7.37 – 7.28 (m, 6H, Ar). ^{13}C NMR (150 MHz, $CDCl_3$): δ = 160.29 (N=*C*H), 154.76, 150.94, 137.49, 129.41, 127.07, 123.42, 121.33 (Ar). HRMS (ESI): m/z calculated for $[C_{19}H_{15}N_3+H]^+$: 286.1344, Found 286.1407.

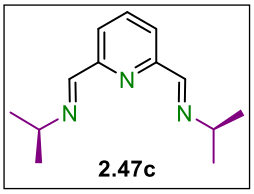

Synthesis of (1*E*,1′*E*)-1,1′-(pyridine-2,6-diyl)*bis*(*N*-isopropylmethanimine) (2.47c): To 10 mL of ethanol, containing pyridine-2,6-dicarbaldehyde (**2.46**) (0.21 g, 1.55 mmol) and isopropyl amine (0.32 mL, 3.91 mmol) catalytic amounts of *p*-toluenesulfonyl chloride (1 mg, 5 μmol) was added and refluxed for 30 minutes. The solution was filtered, solvent was evaporated from filtrate and the resulting residue was extracted with hexane. The product (1*E*,1′*E*)-1,1′-(pyridine-2,6-diyl)*bis*(*N*-isopropylmethanimine) (**2.47c**) was obtained as a reddish yellow oil (0.30 g, 90%) after removal of hexane. ^{1}H NMR (400 MHz, $CDCl_3$): δ = 8.42 (s, 2H, N=C*H*), 8.02 (d, J = 7.8 Hz, 2H, Ar), 7.77 (t, J = 7.7 Hz, 1H, Ar), 3.65 (septet, J = 6.4 Hz, 2H, NC*H*(CH_3)$_2$), 1.28 (d, J = 6.4 Hz, 12H, NCH(C*H*$_3$)$_2$). ^{13}C NMR (100 MHz, $CDCl_3$): δ = 159.23 (N=*C*H), 154.72, 137.17, 122.29 (Ar), 61.51 (N*C*H(CH_3)$_2$), 24.08 (NCH(*C*H$_3$)$_2$). HRMS (ESI): m/z calculated for $[C_{13}H_{19}N_3+H]^+$ 246.1970 , found: 246.1954.

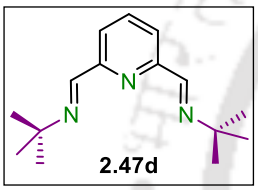

Synthesis of (1*E*,1′*E*)-1,1′-(pyridine-2,6-diyl)*bis*(*N*-tertbutylmethanimine) (2.47d): To 10 mL of ethanol, containing pyridine-2,6-dicarbaldehyde (**2.46**) (0.23 g, 1.70 mmol) and tert-butyl amine (0.5 mL, 4.7 mmol), catalytic amounts of *p*-toluenesulfonyl chloride (1 mg, 5 μmol) was added and refluxed for 30 minutes. The solution was filtered, solvent was evaporated from filtrate and the resulting residue was extracted with hexane. The product (1*E*,1′*E*)-1,1′-(pyridine-2,6-diyl)*bis*(*N*-tertbutylmethanimine) (**2.47d**) was obtained as a reddish yellow oil (0.32 g, 94%) after removal of hexane. ^{1}H NMR (600 MHz, $CDCl_3$): δ = 8.40 (s, 2H, N=C*H*), 8.05 (d, J = 7.7 Hz, 2H, Ar), 7.77 (t, J = 7.5 Hz 1H, Ar), 1.32 (s, 18H, NC(C*H*$_3$)$_3$). ^{13}C NMR (150 MHz, $CDCl_3$): δ = 156.39 (N=*C*H), 155.25, 137.22, 121.82 (Ar), 58.10 (N*C*(CH_3)$_3$), 29.75 (NC(*C*H$_3$)$_3$). HRMS (ESI): m/z calculated for $[C_{15}H_{23}N_3+H]^+$: 246.1970 , found: 246.1954.

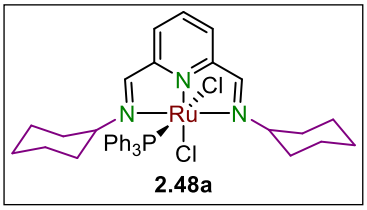

Synthesis of dichloro[*N*,*N*-(2,6-pyridinediyl-κ*N*)dimethylidyne]*bis*[cyclohexanamine-κ*N*](triphenylphosphine)ruthenium (2.48a): A mixture of (1*E*,1′*E*)-1,1′-(pyridine-2,6-diyl)*bis*(*N*-cyclohexylmethanimine) (**2.47a**) (0.043 g, 0.15 mmol) and $RuCl_2(PPh_3)_3$ (0.143 g, 0.15 mmol) were dissolved in dry tetrahydrofuran (5 mL) under an argon atmosphere and refluxed for 12 h. During the course of the reaction the colour changed from violet to reddish brown. The solvent was evacuated and the residue was washed with diethyl ether (3 x 5 mL) followed by pentane (2 x 5mL). Upon

vacuum drying of the washed residue, 0.085 g (81%) of **2.48a** was obtained as a reddish-brown solid. Crystals suitable for X–ray analysis were obtained by a slow diffusion of pentane (1 mL) into a dichloromethane solution (1 mL) of **2.48a** (10 mg). ^{1}H NMR (400 MHz, $CDCl_3$): δ = 7.94 (s, 2H, N=C*H*), 7.71 – 7.61 (m, 6H, Ar), 7.25 – 7.07 (m, 12H, Ar), 4.41 – 4.35 (m, 2H, NC*H*$(CH_2)_5$), 3.11 – 3.08 (m, 2H, NCH(CH_2)$_5$), 1.81 – 1.77 (m, 2H, NCH(CH_2)$_5$), 1.68 – 1.36 (m, 8H, NCH(CH_2)$_5$), 1.26 – 0.97 (m, 6H, NCH(CH_2)$_5$), 0.85 – 0.83 (m, 2H, NCH(CH_2)$_5$). ^{13}C NMR (100 MHz, $CDCl_3$): δ = 162.41, 160.81 (N=*C*H), 132.75, 132.66, 132.59, 132.17, 129.20, 129.18, 128.18, 128.06, 127.97, 122.91, 67.47 (N*C*H$(CH_2)_5$), 36.64, 32.07, 25.99, 25.97, 25.66 (NCH(*C*H_2)$_5$). ^{31}P NMR (162 MHz, $CDCl_3$): δ = 29.42. HRMS (ESI): m/z calculated for $[C_{37}H_{42}ClN_3PRu]^+$: 696.1848, found: 696.1835.

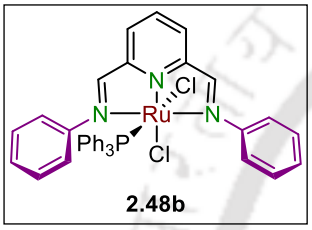

2.48b

Synthesis of dichloro[*N*,*N*-(2,6-pyridinediyl-*κN*)dimethylidyne]*bis*[benzenamine-*κN*](triphenylphosphine)ruthenium (2.48b): A mixture of (1*E*,1′*E*)-1,1′-(pyridine-2,6-diyl)*bis*(*N*-phenylmethanimine) (**2.47b**) (0.030 g, 0.10 mmol) and $RuCl_2(PPh_3)_3$ (0.096 g, 0.10 mmol) were dissolved in dry tetrahydrofuran (5 mL) under an argon atmosphere and refluxed for 12 h. During the course of the reaction the colour changed from violet to reddish brown. The solvent was evacuated and the residue was washed with diethyl ether (3 x 5 mL) followed by pentane (2 x 5mL). Upon vacuum drying of the washed residue, **2.48b** was obtained as a reddish-brown solid in quantitative yield. Crystals suitable for X–ray analysis were obtained by a slow diffusion of pentane (1 mL) into a dichloromethane solution (1 mL) of **2.48b** (10 mg). ^{1}H NMR (400 MHz, $CDCl_3$): δ = 7.97 (s, 2H, N=C*H*), 7.58 (d, 4H, *J* = 7.2 Hz, Ar), 7.36 – 7.26 (m, 8H, Ar), 7.18 – 7.03 (m, 10H, Ar), 6.84 – 6.76 (m, 6H, Ar). ^{13}C NMR (100 MHz, $CDCl_3$): δ = 164.34, 161.86, 150.98, 133.00, 132.91, 130.99, 130.54, 129.08, 129.06, 128.54, 128.46, 128.13, 127.68, 127.58, 125.21, 125.06 (Ar). ^{31}P NMR (162 MHz, $CDCl_3$): δ = 32.27. HRMS (ESI): m/z calculated for $[C_{37}H_{30}ClN_3PRu]^+$: 684.0909, found: 684.0908.

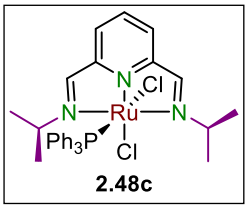

2.48c

Synthesis of drichloro[*N*,*N*-(2,6-pyridinediyl-*κN*)dimethylidyne]*bis*[2-propanamine-*κN*](triphenylphosphine)ruthenium (2.48c): A mixture of (1*E*,1′*E*)-1,1′-(pyridine-2,6-diyl)*bis*(*N*-isopropylmethanimine) (**2.47c**) (0.036 g, 0.16 mmol) and $RuCl_2(PPh_3)_3$ (0.152 g, 0.16 mmol) were dissolved in dry tetrahydrofuran (5 mL) under an argon atmosphere and refluxed for 12 h. During the course of the reaction the

colour changed from violet to reddish brown. The solvent was evacuated and the residue was washed with diethyl ether (3 x 5 mL) followed by pentane (2 x 5mL). Upon vacuum drying of the washed residue, 0.098 g (85%) of **2.48c** was obtained as a reddish-brown solid. Crystals suitable for X–ray analysis were obtained by a slow diffusion of pentane (1 mL) into a dichloromethane solution (1 mL) of **2.48c** (10 mg). ^{1}H NMR (400 MHz, $CDCl_3$): δ = 7.98 (s, 2H, N=C*H*), 7.71 – 7.47 (m, 6H, Ar), 7.25 – 7.10 (m, 12H, Ar), 4.81 (septet, J =6.4 Hz, 2H, NC*H*$(CH_3)_2$), 1.57 (d, J = 6.5 Hz, 6H, NCH(C*H*$_3)_2$), 0.86 (d, J = 6.6 Hz, 6H, NCH(C*H*$_3)_2$). ^{13}C NMR (100 MHz, $CDCl_3$): δ= 162.37, 160.63 (N=*C*H), 132.73, 132.64, 132.56, 132.14, 129.34, 129.32, 128.34, 128.17, 128.07, 123.09 (Ar), 59.33 (N*C*H$(CH_3)_2$), 25.56, 21.67 (NCH(*C*H$_3)_2$). ^{31}P NMR (162 MHz, $CDCl_3$): δ= 29.16. HRMS (ESI): m/z calculated for $[C_{31}H_{34}ClN_3PRu]^+$: 616.1222, found: 616.1204.

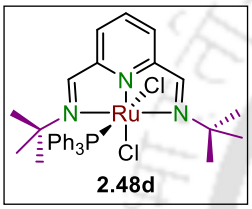

2.48d

Synthesis of dichloro[*N*,*N*-(2,6-pyridinediyl-*κN*)dimethylidyne]*bis*[2-methyl-2-propanamine-*κN*](triphenylphosphine)ruthenium (1.48d): A mixture of (1*E*,1′*E*)-1,1′-(pyridine-2,6-diyl)*bis*(*N*-tertbutylmethanimine) (**2.47d**) (0.050 g, 0.20 mmol) and $RuCl_2(PPh_3)_3$ (0.196 g, 0.20 mmol) were dissolved in dry tetrahydrofuran (5 mL) under an argon atmosphere and refluxed for 12 h. During the course of the reaction the colour changed from violet to reddish brown. The solvent was evacuated and the residue was washed with diethyl ether (3 x 5 mL) followed by pentane (2 x 5mL). Upon vacuum drying of the washed residue, 0.119 g (86%) of **2.48d** was obtained as a reddish-brown solid. Crystals suitable for X–ray analysis were obtained by a slow diffusion of pentane (1 mL) into a dichloromethane solution (1 mL) of **2.48d** (10 mg). HRMS (ESI): m/z calculated for $[C_{33}H_{38}ClN_3PRu]^+$: 644.1535, found: 644.1531.

2.5.2 General synthesis procedure for *N*-alkylation

To a Schlenk flask (5 mL) containing benzyl alcohol (**2.29**) (0.53 mL, 5.09 mmol), 0.75 equivalents of sodium (0.087 g, 3.6 mmol) were added under an argon atmosphere. Under closed conditions the mixture was stirred at 140 °C for about 2 hours with periodic venting of the hydrogen gas which builds up during the process. The mixture was then cooled to room temperature resulting in a white slurry, followed by addition of aniline (**2.49**) (0.47 mL, 5.14 mmol) and ($^{t\text{Bu2}}$NNN)Ru(Cl_2)(PPh_3)(**2.48d**) (0.7 mg, 1 μmol). Then the reaction mixture was heated at 140 °C for 20 hours. After that the reaction was cooled to room temperature followed by the addition of toluene (0.1 mL) as an internal standard. An aliquot (30 mg) was withdrawn

from the reaction mixture and the yield was determined from ^{1}H NMR using $CDCl_3$ (0.5 mL) as a solvent. The rest of the reaction mixture was quenched by water and the mixture was extracted with dichloromethane. The organic phase dried with anhydrous $MgSO_4$ and the solvent was removed under reduced pressure. Silica gel column chromatography was performed with hexane/ethyl acetate mixture (0% – 5%) as eluent to give the product (**2.50**) in the pure form. The isolated product was characterized by NMR spectroscopy.

2.5.3 Computational Details

All the calculations were performed using the Gaussian-16 (revision C.01) program package.[170] PBEPBE level of DFT functional, along with LANL2DZ basis set for Ruthenium atom and 6-311G(d,p) basis set for all other atoms, was selected on the basis of previous reports for geometry optimization of all considered complexes.[171-174] Frequency calculations were performed at the same level of theory to confirm the minimum energy and transition state structures. Inclusion of higher basis set usually increases the barrier and inclusion of dispersion corrections decreases the overall energetics.

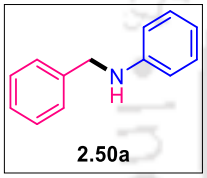

2.50a

***N*-benzylaniline (2.50a):**[46] Yellow oil; ^{1}H NMR (400 MHz, $CDCl_3$): δ = 7.41 – 7.32 (m, 4H, Ar) 7.31 – 7.26 (m, 1H, Ar), 7.18 (td, J = 7.4, 1.9 Hz, 2H, Ar), 6.72 (t, J = 7.3 Hz, 1H, Ar), 6.68 – 6.62 (m, 2H, Ar), 4.34 (s, 2H, NHCH_2), 4.03 (bs, 1H, NHCH$_2$). ^{13}C NMR (100 MHz, $CDCl_3$): δ = 148.31, 139.59, 129.40, 128.77, 127.66, 127.37, 117.72, 113.00 (Ar), 48.50 (NHCH$_2$). HRMS (ESI): $[M+H]^+$, Calculated 184.1126, Found 184.1170.

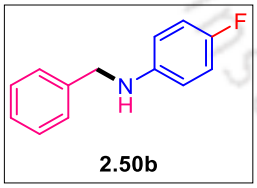

2.50b

***N*-benzyl-4-fluoroaniline (2.50b):**[175] Yellow liquid; ^{1}H NMR (400 MHz, $CDCl_3$): δ = 7.43 – 7.26 (m, 5H, Ar), 6.88 (t, J = 8.7 Hz, 2H, Ar), 6.61 – 6.53 (m, 2H, Ar), 4.30 (s, 2H, NHCH_2), 3.93 (bs, 1H, NHCH$_2$). ^{13}C NMR (151 MHz, $CDCl_3$): δ = 156.00 (d, J_1 *C-F* = 234.9 Hz), 144.61, 139.35, 128.80, 127.62, 127.44, 115.80 (d, J_2 *C-F* = 22.3 Hz), 113.63 (d, J_3 *C-F* = 7.4 Hz) (Ar), 49.06 (NHCH$_2$). ^{19}F NMR (377 MHz, $CDCl_3$): δ = -127.96. HRMS (ESI): $[M+H]^+$, Calculated 202.1032, Found 202.1048.

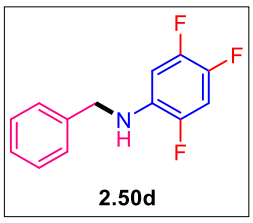

2.50d

***N*-benzyl-2,4,5-trifluoroaniline (2.50d):**[176] Yellow solid; ^{1}H NMR (400 MHz, $CDCl_3$): δ = 7.40 – 7.29 (m, 5H, Ar), 6.92 – 6.83 (m, 1H, Ar), 6.44 (dt, J = 12.1, 7.9 Hz, 1H, Ar), 4.31 (d, J = 5.5 Hz, 2H, (NHCH_2), 4.24 (bs, 1H, NHCH$_2$). ^{13}C NMR (100 MHz, $CDCl_3$): δ = 138.18, 128.99, 128.56, 127.94, 127.80, 127.47, 104.84 (t, J_2 *C-F* = 22.4 Hz), 100.77 (dd, J_2 *C-F* = 23.6, 4.4 Hz) (Ar),

48.21 ($NHCH_2$). ^{19}F NMR (377 MHz, $CDCl_3$): δ = -138.71 (dd, J = 13.4, 2.6 Hz), -142.53 (dd, J = 22.1, 13.4 Hz), -151.15 (dd, J = 22.2, 2.6 Hz). ESI-MS:$[M+H]^+$, Calculated 238.0844, Found 238.0865.

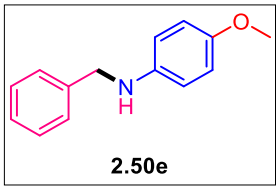

2.50e

***N*-benzyl-4-methoxyaniline (2.50e):**[46] Yellow solid; ^1H NMR (600 MHz, $CDCl_3$): δ = 7.41 – 7.33 (m, 4H), 7.28 (t, J = 7.2 Hz, 1H), 6.79 (d, J = 8.9 Hz, 2H), 6.62 (d, J = 8.9 Hz, 2H), 4.30 (s, 2H), 3.75 (s, 3H, $ArOCH_3$). ^{13}C NMR (151 MHz, $CDCl_3$): δ = 152.29, 142.53, 139.77, 128.72, 127.68, 127.30, 115.01, 114.23, 55.92 ($ArOCH_3$), 49.37 ($NHCH_2$). HRMS (ESI): $[M+H]^+$, Calculated 214.1232, Found 214.1252.

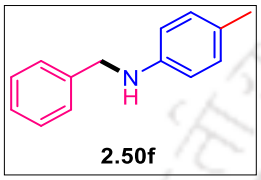

2.50f

***N*-benzyl-4-methylaniline (2.50f+2.50f′):**[46] Yellow liquid; ^1H NMR (400 MHz, $CDCl_3$): δ = δ 8.48 (s, 1H, Ar), 7.90 (dd, J = 6.6, 3.0 Hz, 2H, Ar), 7.50 – 7.46 (m, 3H, Ar), 7.18 (dd, J = 23.8, 8.2 Hz, 4H, Ar) 2.38 (s, 3H, $ArCH_3$), 7.38 – 7.32 (m, 4H, Ar), 7.28 – 7.25 (m, 1H, Ar), 6.99 (d, J = 8.1 Hz, 2H, Ar), 6.57 (d, J = 8.4 Hz, 2H, Ar), 4.31 (s, 2H, $NHCH_2$), 3.91 (bs, 1H, $NHCH_2$), 2.24 (s, 3H, $ArCH_3$). ^{13}C NMR (151 MHz, $CDCl_3$): δ = 146.03, 139.76, 129.87, 128.73, 127.62, 127.28, 126.88, 113.10 (Ar), 48.75 ($NHCH_2$), 20.54 ($ArCH_3$). HRMS (ESI): $[M+H]^+$, Calculated 198.1283, Found 198.1298.

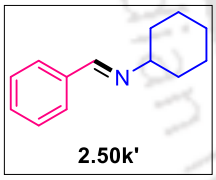

2.50k'

***N*-benzylcyclohexanimine (2.50k′):**[177] Yellow liquid; ^1H NMR (600 MHz, $CDCl_3$): δ = 8.32 (s, 1H, N=C*H*), 7.77 – 7.66 (m, 2H, Ar), 7.40 (dd, J = 4.0, 2.5 Hz, 3H, Ar), 3.19 (tt, J = 10.7, 4.2 Hz, 1H, $NCH(CH_2)_5$), 1.88 – 1.26 (m, 10H, $NCH(CH_2)_5$). ^{13}C NMR (151 MHz, $CDCl_3$): δ = 158.84, 136.69, 130.48, 128.67, 128.19 (Ar), 70.21 ($NCH(CH_2)_5$), 34.49, 25.77, 24.98 ($NCH(CH_2)_5$). HRMS (ESI): $[M+H]^+$, Calculated 188.1439, Found 188.1457.

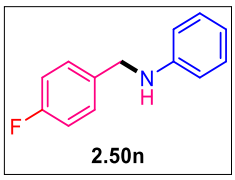

2.50n

***N*-(4-fluorobenzyl)aniline (2.50n):**[52] Yellow oil; ^1H NMR (600 MHz, $CDCl_3$): δ = 7.34 (dd, J = 8.3, 5.4 Hz, 2H, Ar), 7.22 – 7.15 (m, 2H, Ar), 7.03 (t, J = 8.7 Hz, 2H, Ar), 6.73 (t, J = 7.3 Hz, 1H, Ar), 6.66 – 6.60 (m, 2H, Ar), 4.30 (s, 2H, $NHCH_2$), 4.03 (bs, 1H, $NHCH_2$). ^{13}C NMR (151 MHz, $CDCl_3$): δ = 162.17 (d, J_1 *C-F* = 245.0 Hz), 148.05, 135.21 (d, J_4 *C-F* = 3.2 Hz), 129.42, 129.13 (d, J_3 *C-F* = 8.2 Hz), 117.87, 115.58 (d, J_2 *C-F*= 21.3 Hz), 112.99 (Ar), 47.85 ($NHCH_2$). ^{19}F NMR (565 MHz, $CDCl_3$): δ = -115.66. HRMS (ESI): $[M+H]^+$, Calculated 202.1032, Found 202.1040.

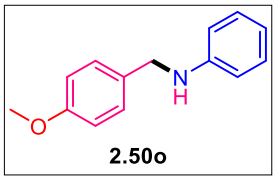

2.50o

***N*-(4-methoxybenzyl)aniline (2.50o):**[46] Yellow liquid; ^{1}H NMR (600 MHz, $CDCl_3$): δ = 7.36 (d, J = 8.6 Hz, 2H, Ar), 7.26 (t, J = 7.6 Hz, 2H, Ar), 7.00 – 6.92 (m, 2H, Ar), 6.83 – 6.77 (m, 1H, Ar), 6.75 – 6.67 (m, 2H, Ar), 4.31 (s, 2H, NHCH_2), 3.87 (s, 3H, ArOCH_3). ^{13}C NMR (151 MHz, $CDCl_3$): δ = 158.86, 148.25, 131.45, 129.31, 128.86, 117.52, 114.05, 112.88 (Ar), 55.33 (ArO*C*H_3), 47.80 (NH*C*H_2). HRMS (ESI): $[M+H]^+$, Calculated 214.1232, Found 214.1245.

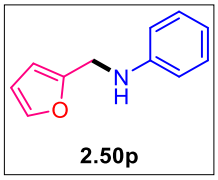

2.50p

***N*-(furan-2-ylmethyl)aniline (2.50p):**[46] Yellow oil; ^{1}H NMR (400 MHz, $CDCl_3$): δ = 7.37 (s, 1H, Ar), 7.19 (t, J = 7.9 Hz, 2H, Ar), 6.75 (t, J = 7.3 Hz, 1H, Ar), 6.68 (d, J = 7.8 Hz, 2H, Ar), 6.33 (dd, J = 3.0, 1.9 Hz, 1H, Ar), 6.24 (d, J = 2.9 Hz, 1H, Ar), 4.33 (s, 2H, NHCH_2), 4.01 (bs, 1H, N*H*CH$_2$). ^{13}C NMR (100 MHz, $CDCl_3$): δ = 152.86, 147.75, 142.06, 129.37, 118.16, 113.28, 110.46, 107.12 (Ar), 41.57 (NH*C*H$_2$). HRMS (ESI): $[M+H]^+$, Calculated 174.0919, Found 174.0934.

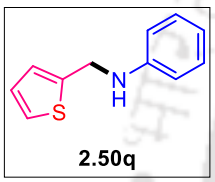

2.50q

***N*-(thiophen-2-ylmethyl)aniline (2.50q):**[46] Reddish yellow oil; ^{1}H NMR (400 MHz, $CDCl_3$): δ = 7.24 – 7.17 (m, 3H, Ar), 7.04 – 7.00 (m, 1H, Ar), 6.97 (dd, J = 5.0, 3.5 Hz, 1H, Ar), 6.75 (t, J = 7.3 Hz, 1H, Ar), 6.68 (d, J = 7.5 Hz, 2H, Ar), 4.52 (s, 2H, NHCH_2), 4.05 (bs, 1H, N*H*CH$_2$). ^{13}C NMR (151 MHz, $CDCl_3$): δ = 147.72, 143.04, 129.41, 126.99, 125.18, 124.73, 118.22, 113.28 (Ar), 43.63 (NH*C*H$_2$). HRMS (ESI):[M+H]$^+$, Calculated 190.0690, Found 190.0700.

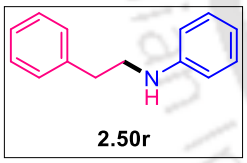

2.50r

***N*-phenethylaniline (2.50r):**[46] Yellow oil; ^{1}H NMR (600 MHz, $CDCl_3$): δ = 7.33 (t, J = 7.4 Hz, 2H, Ar), 7.27 – 7.22 (m, 3H, Ar), 7.19 (dd, J = 8.4, 7.5 Hz, 2H, Ar), 6.72 (t, J = 7.3 Hz, 1H, Ar), 6.63 (d, J = 7.7 Hz, 2H, Ar), 3.75 (bs, 1H N*H*CH$_2$), 3.41 (t, J = 7.1 Hz, 2H, NHCH_2 CH$_2$), 2.93 (t, J = 7.0 Hz, 2H, NHCH$_2$CH_2). ^{13}C NMR (151 MHz, $CDCl_3$): δ = 148.06, 139.41, 129.42, 128.93, 128.74, 126.56, 117.65, 113.16 (Ar), 45.19 (NH*C*H$_2$CH$_2$), 35.62 (NHCH$_2$*C*H$_2$). HRMS (ESI):[M+H]$^+$, Calculated 198.1283, Found 198.1304.

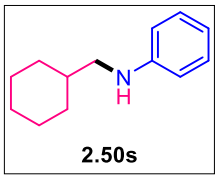

2.50s

***N*-(cyclohexylmethyl)aniline (2.50s):**[46] Yellow oil; ^{1}H NMR (600 MHz, $CDCl_3$): δ = 7.17 (t, J = 7.9 Hz, 2H, Ar), 6.68 (t, J = 7.3 Hz, 1H, Ar), 6.60 (d, J = 7.7 Hz, 2H, Ar), 3.71 (bs, 1H, N*H*CH$_2$), 2.95 (d, J = 6.7 Hz, 2H, NHCH_2), 1.86 – 1.52 (m, 6H, NHCH$_2$C*H*(CH_2)$_5$), 1.33 – 1.11 (m, 3H, NHCH$_2$C*H*(CH_2)$_5$), 0.99 (qd, J = 12.4, 2.9 Hz, 2H, NHCH_2CH(CH_2)$_5$). ^{13}C NMR (151 MHz, $CDCl_3$): δ = 148.76, 129.35, 116.99, 112.73 (Ar), 50.72 (NH*C*H$_2$CH(CH$_2$)$_5$), 37.68, 31.44,

26.72, 26.11 (NHCH$_2$*C*H(*C*H$_2$)$_5$). HRMS (ESI):[M+H]$^+$, Calculated 190.1596, Found 190.1611.

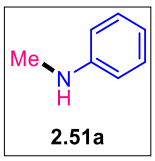

2.51a

***N*-methylaniline (2.51a):**[46] Yellow liquid; ^{1}H NMR (400 MHz, CDCl$_3$): δ = 7.23 - 7.17 (m, 2H, Ar), 6.72 (t, J =7.3 Hz, 1H, Ar), 6.67-6.58 (m, 2H, Ar), 2.85 (s, 3H, NHC*H*$_3$). ^{13}C NMR (100 MHz, CDCl$_3$): δ = 149.46, 129.33, 117.38, 112.55 (Ar), 30.86 (NH*C*H$_3$). HRMS (ESI):[M+H]$^+$, Calculated 108.0813, Found 108.0814.

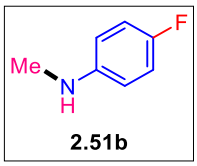

2.51b

4-fluoro-*N*-methylaniline (2.51b):[178] Yellow liquid; ^{1}H NMR (400 MHz, CDCl$_3$): δ = 6.90 (t, J = 8.8 Hz, 2H, Ar), 6.54 (dd, J = 9.0, 4.4 Hz, 2H, Ar), 2.81 (s, 3H, NHC*H*$_3$). ^{13}C NMR (151 MHz, CDCl$_3$): δ = 155.93 (d, J_1 *C-F* = 234.4 Hz), 145.81, 115.73 (d, J_2 *C-F* = 22.3 Hz), 113.26 (d, J_3 *C-F* = 7.3 Hz) (Ar), 31.48 (NH*C*H$_3$). ^{19}F NMR (377 MHz, CDCl$_3$): -128.49. HRMS (ESI): [M+H]$^+$, Calculated 126.0719, Found 126.0743.

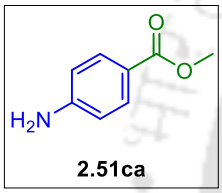

2.51ca

methyl-4-aminobenzoate (2.51ca):[179] White solid; ^{1}H NMR (400 MHz, CDCl$_3$) δ = 7.84 (d, J = 8.7 Hz, 2H, Ar), 6.63 (d, J = 8.7 Hz, 2H, Ar), 4.08 (bs, 2H, N*H*$_2$), 3.85 (s, 3H, CO$_2$C*H*$_3$). ^{13}C NMR (100 MHz, CDCl$_3$) δ = 167.30 (C=O), 150.97, 131.72, 119.83, 113.91 (Ar), 51.72 (CO$_2$*C*H$_3$).

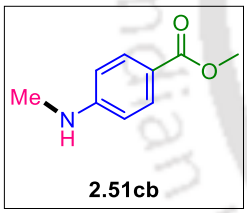

2.51cb

methyl 4-(*N*-methylamino)benzoate (2.51cb):[64] White solid; ^{1}H NMR (400 MHz, CDCl$_3$) δ = 7.87 (d, J = 8.8 Hz, 2H, Ar), 6.55 (d, J = 8.8 Hz, 2H, Ar), 4.20 (bs, 1H, N*H*), 3.85 (s, 3H, NHC*H*$_3$), 2.88 (s, 3H, CO$_2$C*H*$_3$). ^{13}C NMR (100 MHz, CDCl$_3$) δ = 167.52 (C=O), 153.02, 131.64, 118.36, 111.22 (Ar), 51.64 (CO$_2$*C*H$_3$), 30.27 (NH*C*H$_3$). HRMS (ESI): [M+H]$^+$, Calculated 166.0868, Found 166.0889.

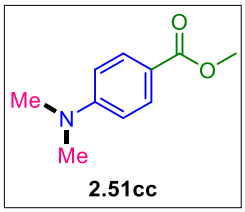

2.51cc

methyl 4-(*N*,*N*-dimethylamino)benzoate (2.51cc):[180] White solid; ^{1}H NMR (400 MHz, CDCl$_3$) δ = 7.91 (d, J = 9.1 Hz, 2H, Ar), 6.65 (d, J = 9.0 Hz, 2H, Ar), 3.85 (s, 3H, CO$_2$C*H*$_3$), 3.04 (s, 6H, N(C*H*$_3$)$_2$). ^{13}C NMR (100 MHz, CDCl$_3$) δ = 167.64 (C=O), 153.35, 131.41, 117.15, 110.99 (Ar), 51.65 (CO$_2$*C*H$_3$), 40.29 (N(*C*H$_3$)$_2$). HRMS (ESI): [M+H]$^+$, Calculated 180.1025, Found 180.1041.

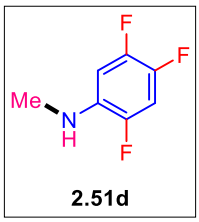

2.51d

2,4,5-trifluoro-*N*-methylaniline (2.51d): Colorless liquid; ^{1}H NMR (400 MHz, CDCl$_3$): δ = 6.86 (ddd, J = 11.1, 10.0, 7.2 Hz, 1H, Ar), 6.45 (dt, J = 12.1, 8.0 Hz, 1H, Ar), 3.84 (bs, 1H, N*H*CH$_3$), 2.83 (d, J = 3.9 Hz, 3H, NHC*H*$_3$). ^{13}C NMR (100 MHz, CDCl$_3$): δ = 104.91, 104.89, 104.69, 104.67,

104.65, 104.44, 104.43, 100.00, 99.95, 99.76, 99.72 (Ar), 30.55 (NH*C*H$_3$). ^{19}F NMR (377 MHz, CDCl$_3$): δ = -139.55 (dd, J = 13.6, 3.1 Hz), -142.84 (dd, J = 22.2, 13.4 Hz), -152.02 (dd, J = 22.3, 3.0 Hz).

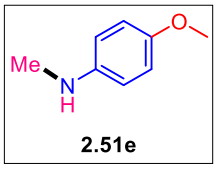

2.51e

4-methoxy-*N*-methylaniline (2.51e):[46] Yellow liquid; ^{1}H NMR (400 MHz, CDCl$_3$): δ = 6.80 (d, J = 8.9 Hz, 2H, Ar), 6.59 (d, J = 8.9 Hz, 2H, Ar), 3.75 (s, 3H, ArOC*H*$_3$), 2.81 (s, 3H, NHC*H*$_3$). ^{13}C NMR (100 MHz, CDCl$_3$): δ = 152.21, 143.81, 115.03, 113.79 (Ar), 56.00 (ArO*C*H$_3$), 31.78 (NH*C*H$_3$). HRMS (ESI): [M+H]$^+$, Calculated 138.0919, Found 138.0936.

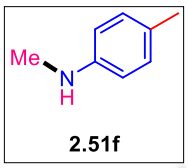

2.51f

4-methyl-*N*-methylaniline (2.51f):[108] Yellow oil; ^{1}H NMR (400 MHz, CDCl$_3$): δ = 7.00 (d, J = 8.1 Hz, 2H, Ar), 6.55 (d, J = 8.4 Hz, 2H, Ar), 2.82 (s, 3H, NHC*H*$_3$), 2.24 (s, 3H, ArC*H*$_3$). ^{13}C NMR (100 MHz, CDCl$_3$): δ = 147.28, 129.82, 126.63, 112.75 (Ar), 31.25 (NH*C*H$_3$), 20.52 (Ar*C*H$_3$). HRMS (ESI): [M+H]$^+$, Calculated 122.0970, Found 122.0994.

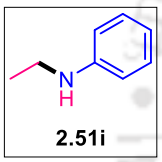

2.51i

***N*-ethylaniline (2.51i):**[181] Yellow oil; ^{1}H NMR (400 MHz, CDCl$_3$): δ = 7.18 (dd, J = 8.5, 7.4 Hz, 2H, Ar), 6.70 (t, J = 7.3 Hz, 1H, Ar), 6.62 (dd, J = 8.4, 0.8 Hz, 2H, Ar), 3.54 (bs, 1H, N*H*CH$_3$), 3.16 (q, J = 7.1 Hz, 2H, NHC*H*$_2$CH$_3$), 1.26 (t, J = 7.1 Hz, 3H, NHCH$_2$C*H*$_3$). ^{13}C NMR (100 MHz, CDCl$_3$): δ = 148.59, 129.36, 117.35, 112.88 (Ar), 38.60 (NH*C*H$_2$CH$_3$), 15.03 (NHCH$_2$*C*H$_3$). HRMS (ESI): [M+H]$^+$, Calculated 122.0970, Found 122.0992.

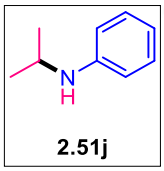

2.51j

***N*-isopropylaniline(2.51j):**[52] Yellow oil; ^{1}H NMR (400 MHz, CDCl$_3$) δ = 7.16 (dd, J = 8.5, 7.4 Hz, 2H, Ar), 6.68 (d, J = 7.3 Hz, 1H, Ar), 6.59 (dd, J = 8.5, 0.9 Hz, 2H, Ar), 3.62 (dq, J = 12.5, 6.3 Hz, 1H, NHC*H*(CH$_3$)$_2$), 3.44 (bs, 1H, N*H*CH(CH$_3$)$_2$), 1.21 (d, J = 6.3 Hz, 6H, NHCH(C*H*$_3$)$_2$). ^{13}C NMR (101 MHz, CDCl$_3$) δ = 147.65, 129.41, 117.09, 113.37 (Ar), 44.34 (NH*C*H(CH$_3$)$_2$), 23.17 (NHCH(*C*H$_3$)$_2$). HRMS (ESI): [M+H]$^+$, Calculated 136.2180, Found 136.1145

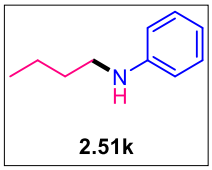

2.51k

***N*-butylaniline (2.51k):**[46] Pale yellow oil; ^{1}H NMR (400 MHz, CDCl$_3$): δ = 7.23 – 7.13 (m, 2H, Ar), 6.69 (t, J = 7.3 Hz, 1H, Ar), 6.61 (d, J = 7.7 Hz, 2H, Ar), 3.12 (t, J = 7.1 Hz, 2H, NHC*H*$_2$(CH$_2$)$_2$CH$_3$), 1.65 – 1.57 (m, 2H, NHCH$_2$(C*H*$_2$)$_2$CH$_3$), 1.44 (dq, J = 14.4, 7.3 Hz, 2H, NHCH$_2$(C*H*$_2$)$_2$CH$_3$), 0.97 (t, J = 7.3 Hz, 3H, NHCH$_2$(CH$_2$)$_2$C*H*$_3$). ^{13}C NMR (101 MHz, CDCl$_3$): δ = 148.70, 129.35, 117.21, 112.83 (Ar), 43.82 (NH*C*H$_2$(CH$_2$)$_2$CH$_3$), 31.83, 20.45 (NHCH$_2$(*C*H$_2$)$_2$CH$_3$), 14.05 (NHCH$_2$(CH$_2$)$_2$*C*H$_3$). HRMS (ESI): [M+H]$^+$, Calculated 150.1283, Found 150.1299.

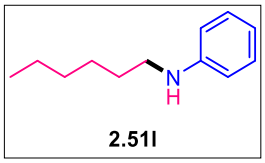

2.51l

N-hexylaniline (2.51l):[182] Pale yellow oil; ^{1}H NMR (600 MHz, $CDCl_3$): δ = 7.17 (t, J = 7.9 Hz, 2H, Ar), 6.68 (t, J = 7.3 Hz, 1H, Ar), 6.60 (d, J = 7.7 Hz, 2H, Ar), 3.60 (bs, 1H, N*H*$CH_2(CH_2)_4CH_3$), 3.10 (t, J = 7.1 Hz, 2H, NHC*H*$_2(CH_2)_4CH_3$), 1.65 – 1.59 (m, 2H, $NHCH_2(CH_2)_4CH_3$), 1.43 – 1.37 (m, 2H, $NHCH_2(CH_2)_2CH_3$), 1.36 – 1.29 (m, 4H, $NHCH_2(CH_2)_2CH_3$), 0.92 – 0.88 (m, 3H, $NHCH_2(CH_2)_4CH_3$). ^{13}C NMR (151 MHz, $CDCl_3$): δ = 148.67, 129.35, 117.20, 112.81 (Ar), 44.14 (NH*C*$H_2(CH_2)_4CH_3$), 31.80, 29.68, 27.01, 22.78 ($NHCH_2(CH_2)_2CH_3$), 14.20 ($NHCH_2(CH_2)_4CH_3$). HRMS (ESI): $[M+H]^+$, Calculated 178.1596, Found 178.1629.

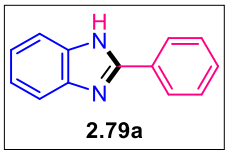

2.79a

2-Phenyl-1H-benzo[d]imidazole (2.79a):[159] Yellowish solid; ^{1}H NMR (400 MHz, DMSO-D_6) δ = 12.89 (bs, 1H, N*H*), 8.18 (d, J = 7.1 Hz, 2H), 7.74 – 7.42 (m, 5H, Ar), 7.20 (d, J = 3.8 Hz, 2H, Ar). ^{13}C NMR (101 MHz, DMSO-D_6) δ = 151.21 (N=*C*), 143.81, 135.00, 130.17, 129.83, 128.94, 126.43, 122.52, 121.66, 118.87, 111.31 (Ar). HRMS (ESI): $[M+H]^+$, Calculated 195.0922, Found 195.0956.

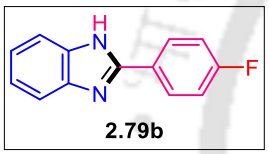

2.79b

2-(4-fluorophenyl)-1H-benzo[d]imidazole(2.79b):[163] Yellowish solid; ^{1}H NMR (600 MHz, DMSO-D_6): δ = 12.93 (bs, 1H, N*H*), 8.22 (dd, J = 9.9, 3.2 Hz, 2H, Ar), 7.66 (d, J = 7.5 Hz, 1H, Ar), 7.53 (d, J = 7.5 Hz, 1H, Ar), 7.41 (t, J = 8.7 Hz, 2H, Ar), 7.20 (dt, J = 14.5, 6.7 Hz, 2H, Ar). ^{13}C NMR (151 MHz, DMSO) δ = 163.07 (d, J_1 *C-F* = 247.3 Hz), 150.39 (N=*C*), 143.76, 135.03, 128.73 (d, J_3 *C-F* = 8.7 Hz), 126.81 (d, J_4 *C-F* = 2.9 Hz), 122.58, 121.74, 118.86, 116.05 (d, J_2 *C-F* = 21.9 Hz), 111.35 (Ar). ^{19}F NMR (565 MHz, DMSO-D_6) δ = -111.13 (qd, J = 8.5, 5.5 Hz). HRMS (ESI): $[M+H]^+$, Calculated 213.0828, Found 213.0833.

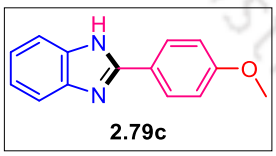

2.79c

2-(4-methoxyphenyl)-1H-benzo[d]imidazole(2.79c):[163] White solid; ^{1}H NMR (400 MHz, DMSO-D_6): δ = 12.74 (bs, 1H, N*H*), 8.12 (d, J = 8.8 Hz, 2H, Ar), 7.56 (bs, 2H, Ar), 7.23 – 7.07 (m, 4H, Ar), 3.84 (s, 3H, ArOC*H*$_3$). ^{13}C NMR (101 MHz, DMSO-D_6): δ = 160.63, 151.37 (N=*C*), 128.03, 122.70, 122.07, 114.39 (Ar), 55.35 (ArO*C*H_3). HRMS (ESI): $[M+H]^+$, Calculated 225.1028, Found 225.1045.

Table 2.10: Crystallography data of complexes **2.48a-d**

Name	(^{Cy}NNN)RuCl$_2$(PPh$_3$) **2.48a**	(^{Ph}NNN)RuCl$_2$(PPh$_3$) **2.48b**	(^{iPr}NNN)RuCl$_2$(PPh$_3$) **2.48c**	(^{tBu2}NNN)RuCl$_2$(PPh$_3$) **2.48d**
CCDC	1867474	1867473	1867475	1998012
Empirical formula	$C_{75}H_{86}Cl_6N_6P_2Ru_2$	$C_{38}H_{32}Cl_4N_3PRu$	$C_{32}H_{38}Cl_4N_3PRuO$	$C_{35}H_{42}Cl_6N_3PRu$
Formula weight	1548.28	804.51	752.48	849.45
Crystal size (mm^3)	0.32 x 0.29 x 0.25	0.33 x 0.30 x 0.28	0.33 x 0.29 x 0.23	0.31 x 0.26 x 0.22
Crystal system	triclinic	Monoclinic	Monoclinic	orthorhombic
Space group	P-1	P2$_1$/n	P2$_1$/c	Pbca
a (Å)	13.9237(7)	11.4960(19)	15.7870(3)	16.093(4)
b (Å)	15.1061(5)	21.270(3)	13.5245(3)	20.363(5)
c (Å)	19.8599(11)	14.909(3)	17.0597(4)	23.088(6)
α (°)	70.061(4)	90.00	90.00	90.00
β (°)	72.951(4)	105.848(17)	102.815(2)	90.00
γ (°)	84.319(3)	90.00	90.00	90.00
V (Å^3)	3754.2(3)	3506.9(10)	3551.71(13)	7566(3)
Z	2	4	4	8
ρ_{calc} (g cm^{-3})	1.370	1.524	1.411	1.491
μ (M$_0$ Kα) (mm^{-1})	0.703	0.830	0.816	0.910
F (000)	1596.0	1632.0	1544.0	3472.0
T(K)	293(2)	293(2)	293(2)	296(2)
Range of indices (h; k; l)	-16, 16; -17, 17; -23, 20	-12, 13; -25, 24; -17, 16	-18, 18; -16, 9; -19, 20	-20, 20; -26, 26; -29, 29
Number of reflections collected	29844	14763	15163	222123
Unique reflection	13209	6166	6235	8640
Completeness to 2θ	99.8	99.8	99.8	99.9
R$_{int}$	0.0359	0.0392	0.0273	0.5367
Data / restraints / parameters	13209/0/820	6166/0/424	6235/0/383	8640/108/449
goodness-of-fit	1.054	1.039	1.111	1.013
R$_1$[$I \geq 2\sigma(I)$]	0.0468	0.0469	0.0443	0.1091
wR$_2$[$I \geq 2\sigma(I)$]	0.1119	0.1102	0.1343	0.2416
R$_1$ (all data)	0.0678	0.0664	0.0549	0.2603
wR$_2$ (all data)	0.1288	0.1253	0.1438	0.3385
Δ_r (max, min) e Å^{-3}	1.74/-0.80	1.21/-0.83	0.99/-0.69	1.25/-0.97

Supporting information (containing NMR spectra of various compound, HRMS, Kinetics data and Cartesian coordinates of the computed complexes) for chapter **II** is available as appendix **I** and can be found at

https://drive.google.com/file/d/1X7JRlSmfIlof5NVGMfEf2g-zNxTkNJsc/view?usp=sharing

2.6 References

1. Kobayashi, S.; Ishitani, H., *Chem. Rev.* **1999**, *99*, 1069-1094.
2. Hall, D. G., *J. Am. Chem. Soc.* **2005**, *127*, 9655-9655.
3. Afanasyev, O. I.; Kuchuk, E.; Usanov, D. L.; Chusov, D., *Chem. Rev.* **2019**, *119*, 11857-11911.
4. Hardouin Duparc, V.; Bano, G. L.; Schaper, F., *ACS Catal.* **2018**, *8*, 7308-7325.
5. Beletskaya, I. P.; Cheprakov, A. V., *Coord. Chem. Rev.* **2004**, *248*, 2337-2364.
6. Salvatore, R. N.; Yoon, C. H.; Jung, K. W., *Tetrahedron* **2001**, *57*, 7785-7811.
7. Shafir, A.; Lichtor, P. A.; Buchwald, S. L., *J. Am. Chem. Soc.* **2007**, *129*, 3490-3491.
8. Kolesnikov, P. N.; Yagafarov, N. Z.; Usanov, D. L.; Maleev, V. I.; Chusov, D., *Org. Lett.* **2015**, *17*, 173-175.
9. Sorribes, I.; Junge, K.; Beller, M., *J. Am. Chem. Soc.* **2014**, *136*, 14314-14319.
10. Gunanathan, C.; Milstein, D., *Science* **2013**, *341*, 1229712.
11. Obora, Y., *ACS Catal.* **2014**, *4*, 3972-3981.
12. Dobereiner, G. E.; Crabtree, R. H., *Chem. Rev.* **2010**, *110*, 681-703.
13. Albrecht, M.; Lindner, M. M., *Dalton Trans.* **2011**, *40*, 8733-8744.
14. Guillena, G.; Ramón, D. J.; Yus, M., *Chem. Rev.* **2010**, *110*, 1611-1641.
15. Edwards, M. G.; Jazzar, R. F. R.; Paine, B. M.; Shermer, D. J.; Whittlesey, M. K.; Williams, J. M. J.; Edney, D. D., *Chem. Commun.* **2004**, 90-91.
16. Mastalir, M.; Tomsu, G.; Pittenauer, E.; Allmaier, G.; Kirchner, K., *Org. Lett.* **2016**, *18*, 3462-3465.
17. Zhang, G.; Yin, Z.; Zheng, S., *Org. Lett.* **2016**, *18*, 300-303.
18. Midya, S. P.; Pitchaimani, J.; Landge, V. G.; Madhu, V.; Balaraman, E., *Cat. Sci. Technol.* **2018**, *8*, 3469-3473.
19. Fertig, R.; Irrgang, T.; Freitag, F.; Zander, J.; Kempe, R., *ACS Catal.* **2018**, *8*, 8525-8530.
20. Mastalir, M.; Pittenauer, E.; Allmaier, G.; Kirchner, K., *J. Am. Chem. Soc.* **2017**, *139*, 8812-8815.
21. Elangovan, S.; Neumann, J.; Sortais, J.-B.; Junge, K.; Darcel, C.; Beller, M., *Nat. Commun.* **2016**, *7*, 12641.
22. Bruneau-Voisine, A.; Wang, D.; Dorcet, V.; Roisnel, T.; Darcel, C.; Sortais, J.-B., *J. Catal.* **2017**, *347*, 57-62.
23. Neumann, J.; Elangovan, S.; Spannenberg, A.; Junge, K.; Beller, M., *Chem. Eur. J.* **2017**, *23*, 5410-5413.
24. Grigg, R.; Mitchell, T. R. B.; Sutthivaiyakit, S.; Tongpenyai, N., *J. Chem. Soc., Chem. Commun.* **1981**, 611-612.
25. Watanabe, Y.; Tsuji, Y.; Ohsugi, Y., *Tetrahedron Lett.* **1981**, *22*, 2667-2670.
26. Reyes-Rios, G.; García, J. J., *Inorg. Chim. Acta* **2012**, *392*, 317-321.
27. Zhao, G.-m.; Liu, H.-l.; Zhang, D.-d.; Huang, X.-r.; Yang, X., *ACS Catal.* **2014**, *4*, 2231-2240.
28. Dang, T. T.; Ramalingam, B.; Seayad, A. M., *ACS Catal.* **2015**, *5*, 4082-4088.
29. Murahashi, S.-I.; Kondo, K.; Hakata, T., *Tetrahedron Lett.* **1982**, *23*, 229-232.
30. Watanabe, Y.; Tsuji, Y.; Ige, H.; Ohsugi, Y.; Ohta, T., *J. Org. Chem.* **1984**, *49*, 3359-3363.
31. Huh, K.-T.; Tsuji, Y.; Kobayashi, M.; Okuda, F.; Watanabe, Y., *Chem. Lett.* **1988**, *17*, 449-452.
32. Ganguly, S.; Roundhill, D. M., *Polyhedron* **1990**, *9*, 2517-2526.
33. Tominaga, K.-i.; Sasaki, Y.; Kawai, M.; Watanabe, T.; Saito, M., *J. Chem. Soc., Chem. Commun.* **1993**, 629-631.

34. Watanabe, Y.; Morisaki, Y.; Kondo, T.; Mitsudo, T.-a., *J. Org. Chem.* **1996**, *61*, 4214-4218.
35. Abbenhuis, R. A. T. M.; Boersma, J.; van Koten, G., *J. Org. Chem.* **1998**, *63*, 4282-4290.
36. Zhang, J.; Gandelman, M.; Shimon, L. J. W.; Rozenberg, H.; Milstein, D., *Organometallics* **2004**, *23*, 4026-4033.
37. Naskar, S.; Bhattacharjee, M., *Tetrahedron Lett.* **2007**, *48*, 3367-3370.
38. Hamid, M. H. S. A.; Allen, C. L.; Lamb, G. W.; Maxwell, A. C.; Maytum, H. C.; Watson, A. J. A.; Williams, J. M. J., *J. Am. Chem. Soc.* **2009**, *131*, 1766-1774.
39. Jensen, T.; Madsen, R., *J. Org. Chem.* **2009**, *74*, 3990-3992.
40. Zhang, Y.; Chen, C.; Ghosh, S. C.; Li, Y.; Hong, S. H., *Organometallics* **2010**, *29*, 1374-1378.
41. Esteruelas, M. A.; Honczek, N.; Oliván, M.; Oñate, E.; Valencia, M., *Organometallics* **2011**, *30*, 2468-2471.
42. Li, H.; Wang, X.; Wen, M.; Wang, Z. X., *Eur. J. Inorg. Chem.* **2012**, *2012*, 5011-5020.
43. Enyong, A. B.; Moasser, B., *J. Org. Chem.* **2014**, *79*, 7553-7563.
44. Sindhuja, E.; Ramesh, R., *Tetrahedron Lett.* **2014**, *55*, 5504-5507.
45. Marichev, K. O.; Takacs, J. M., *ACS Catal.* **2016**, *6*, 2205-2210.
46. Maji, M.; Chakrabarti, K.; Paul, B.; Roy, B. C.; Kundu, S., *Adv. Synth. Catal.* **2017**, *360*, 722-729.
47. Thiyagarajan, S.; Gunanathan, C., *ACS Catal.* **2017**, *7*, 5483-5490.
48. Tsuji, Y.; Huh, K. T.; Watanabe, Y., *J. Org. Chem.* **1987**, *52*, 1673-1680.
49. Ruch, S.; Irrgang, T.; Kempe, R., *Chem. Eur. J.* **2014**, *20*, 13279-13285.
50. Blank, B.; Madalska, M.; Kempe, R., *Adv. Synth. Catal.* **2008**, *350*, 749-758.
51. Campos, J.; Sharninghausen, L. S.; Manas, M. G.; Crabtree, R. H., *Inorg. Chem.* **2015**, *54*, 5079-5084.
52. Zou, Q.; Wang, C.; Smith, J.; Xue, D.; Xiao, J., *Chem. Eur. J.* **2015**, *21*, 9656-9661.
53. Chang, Y.-H.; Tanigawa, I.; Taguchi, H.-o.; Takeuchi, K.; Ozawa, F., *Eur. J. Inorg. Chem.* **2016**, *2016*, 754-760.
54. Lim, C. S.; Quach, T. T.; Zhao, Y., *Angew. Chem. Int. Ed.* **2017**, *56*, 7176-7180.
55. Cami-Kobeci, G.; Williams, J. M. J., *Chem. Commun.* **2004**, 1072-1073.
56. Fujita, K.-i.; Fujii, T.; Yamaguchi, R., *Org. Lett.* **2004**, *6*, 3525-3528.
57. Cami-Kobeci, G.; Slatford, P. A.; Whittlesey, M. K.; Williams, J. M. J., *Bioorg. Med. Chem. Lett.* **2005**, *15*, 535-537.
58. Prades, A.; Corberán, R.; Poyatos, M.; Peris, E., *Chem. Eur. J.* **2008**, *14*, 11474-11479.
59. Li, F.; Xie, J.; Shan, H.; Sun, C.; Chen, L., *RSC Adv.* **2012**, *2*, 8645-8652.
60. Li, J.-Q.; Andersson, P. G., *Chem. Commun.* **2013**, *49*, 6131-6133.
61. Wetzel, A.; Wöckel, S.; Schelwies, M.; Brinks, M. K.; Rominger, F.; Hofmann, P.; Limbach, M., *Org. Lett.* **2013**, *15*, 266-269.
62. Zhang, Y.; Lim, C.-S.; Sim, D. S. B.; Pan, H.-J.; Zhao, Y., *Angew. Chem. Int. Ed.* **2014**, *53*, 1399-1403.
63. Rong, Z.-Q.; Zhang, Y.; Chua, R. H. B.; Pan, H.-J.; Zhao, Y., *J. Am. Chem. Soc.* **2015**, *137*, 4944-4947.
64. Liang, R.; Li, S.; Wang, R.; Lu, L.; Li, F., *Org. Lett.* **2017**, *19*, 5790-5793.
65. Chakrabarti, K.; Maji, M.; Kundu, S., *Green Chem.* **2019**, *21*, 1999-2004.
66. Maji, M.; Chakrabarti, K.; Panja, D.; Kundu, S., *J. Catal.* **2019**, *373*, 93-102.
67. Mastalir, M.; Glatz, M.; Pittenauer, E.; Allmaier, G.; Kirchner, K., *J. Am. Chem. Soc.* **2016**, *138*, 15543-15546.
68. Das, K.; Mondal, A.; Pal, D.; Srivastava, H. K.; Srimani, D., *Organometallics* **2019**, *38*, 1815-1825.

69. Kallmeier, F.; Dudziec, B.; Irrgang, T.; Kempe, R., *Angew. Chem., Int. Ed.* **2017**, *56*, 7261-7265.
70. Deibl, N.; Kempe, R., *Angew. Chem. Int. Ed.* **2017**, *56*, 1663-1666.
71. Yan, T.; Feringa, B. L.; Barta, K., *Nat. Commun.* **2014**, *5*, 5602.
72. Zheng, J.; Darcel, C.; Sortais, J.-B., *Chem. Commun.* **2014**, *50*, 14229-14232.
73. Pan, H.-J.; Ng, T. W.; Zhao, Y., *Chem. Commun.* **2015**, *51*, 11907-11910.
74. Rawlings, A. J.; Diorazio, L. J.; Wills, M., *Org. Lett.* **2015**, *17*, 1086-1089.
75. Mastalir, M.; Stöger, B.; Pittenauer, E.; Puchberger, M.; Allmaier, G.; Kirchner, K., *Adv. Synth. Catal.* **2016**, *358*, 3824-3831.
76. Yan, T.; Feringa, B. L.; Barta, K., *ACS Catal.* **2016**, *6*, 381-388.
77. Zhao, Y.; Foo, S. W.; Saito, S., *Angew. Chem. Int. Ed.* **2011**, *50*, 3006-3009.
78. Bala, M.; Verma, P. K.; Sharma, U.; Kumar, N.; Singh, B., *Green Chem.* **2013**, *15*, 1687-1693.
79. Emayavaramban, B.; Roy, M.; Sundararaju, B., *Chem. Eur. J.* **2016**, *22*, 3952-3955.
80. Vellakkaran, M.; Singh, K.; Banerjee, D., *ACS Catal.* **2017**, *7*, 8152-8158.
81. Das, S.; Maiti, D.; De Sarkar, S., *J. Org. Chem.* **2018**, *83*, 2309-2316.
82. Xu, Z.; Yu, X.; Sang, X.; Wang, D., *Green Chem.* **2018**, *20*, 2571-2577.
83. Zhang, L.; Zhang, Y.; Deng, Y.; Shi, F., *RSC Adv.* **2015**, *5*, 14514-14521.
84. Tsarev, V. N.; Morioka, Y.; Caner, J.; Wang, Q.; Ushimaru, R.; Kudo, A.; Naka, H.; Saito, S., *Org. Lett.* **2015**, *17*, 2530-2533.
85. Liu, H.; Chuah, G.-K.; Jaenicke, S., *J. Catal.* **2012**, *292*, 130-137.
86. Kamiguchi, S.; Takahashi, I.; Nagashima, S.; Nakamura, A.; Chihara, T., *J. Clust. Sci.* **2007**, *18*, 935-945.
87. Shimizu, K.-i.; Kon, K.; Onodera, W.; Yamazaki, H.; Kondo, J. N., *ACS Catal.* **2013**, *3*, 112-117.
88. Shimizu, K.-i.; Imaiida, N.; Kon, K.; Hakim Siddiki, S. M. A.; Satsuma, A., *ACS Catal.* **2013**, *3*, 998-1005.
89. Cui, X.; Deng, Y.; Shi, F., *ACS Catal.* **2013**, *3*, 808-811.
90. Lee, C.-C.; Liu, S.-T., *Chem. Commun.* **2011**, *47*, 6981-6983.
91. Liu, Y.; Chen, W.; Feng, C.; Deng, G., *Chem. Asian J.* **2011**, *6*, 1142-1146.
92. Shi, F.; Tse, M. K.; Cui, X.; Gördes, D.; Michalik, D.; Thurow, K.; Deng, Y.; Beller, M., *Angew. Chem. Int. Ed.* **2009**, *48*, 5912-5915.
93. Han, Z.; Wang, Z.; Zhang, X.; Ding, K., *Angew. Chem. Int. Ed.* **2009**, *48*, 5345-5349.
94. Hoffmann, S.; Nicoletti, M.; List, B., *J. Am. Chem. Soc.* **2006**, *128*, 13074-13075.
95. Ma, W. M. J.; James, T. D.; Williams, J. M. J., *Org. Lett.* **2013**, *15*, 4850-4853.
96. Broomfield, L. M.; Wu, Y.; Martin, E.; Shafir, A., *Adv. Synth. Catal.* **2015**, *357*, 3538-3548.
97. Yu, X.-J.; He, H.-Y.; Yang, L.; Fu, H.-Y.; Zheng, X.-L.; Chen, H.; Li, R.-X., *Catalysis Commun.* **2017**, *95*, 54-57.
98. Rösler, S.; Ertl, M.; Irrgang, T.; Kempe, R., *Angew. Chem. Int. Ed.* **2015**, *54*, 15046-15050.
99. Schranck, J.; Tlili, A.; Beller, M., *Angew. Chem. Int. Ed.* **2013**, *52*, 7642-7644.
100. Gnanaprakasam, B.; Zhang, J.; Milstein, D., *Angew. Chem. Int. Ed.* **2010**, *49*, 1468-1471.
101. Balaraman, E.; Srimani, D.; Diskin-Posner, Y.; Milstein, D., *Catal. Lett.* **2015**, *145*, 139-144.
102. Gunanathan, C.; Milstein, D., *Acc. Chem. Res.* **2011**, *44*, 588-602.
103. Sahin, I.; Emir, S.; Ispir, E.; Karakaya, I.; Gumus, S.; Ulusoy, M.; Karabuga, S., *Catal. Commun.* **2016**, *85*, 30-33.
104. Dayan, O.; Çetinkaya, B., *J. Mol. Catal. A: Chem.* **2007**, *271*, 134-141.

105. Pansuriya, P. B.; Maguire, G. E. M.; Friedrich, H. B., *J. Therm. Anal. Calorim.* **2016**, *124*, 269-278.
106. Oku, T.; Ikariya, T., *Angew. Chem. Int. Ed.* **2002**, *41*, 3476-3479.
107. Selva, M.; Perosa, A.; Tundo, P.; Brunelli, D., *J. Org. Chem.* **2006**, *71*, 5770-5773.
108. González, I.; Mosquera, J.; Guerrero, C.; Rodríguez, R.; Cruces, J., *Org. Lett.* **2009**, *11*, 1677-1680.
109. Li, Y.; Sorribes, I.; Yan, T.; Junge, K.; Beller, M., *Angew. Chem. Int. Ed.* **2013**, *52*, 12156-12160.
110. Lebleu, T.; Ma, X.; Maddaluno, J.; Legros, J., *Chem. Commun.* **2014**, *50*, 1836-1838.
111. Rayadurgam, J.; Sana, S.; Sasikumar, M.; Gu, Q., *Org. Chem. Front.* **2021**, *8*, 384-414.
112. Yashwantrao, G.; Saha, S., *Tetrahedron* **2021**, *97*, 132406.
113. Zhang, S.; Ibrahim, J. J.; Yang, Y., *Org. Chem. Front* **2019**, *6*, 2726-2731.
114. Huang, S.; Hong, X.; Cui, H.-Z.; Zhou, Q.; Lin, Y.-J.; Hou, X.-F., *Dalton Trans.* **2019**, *48*, 5072-5082.
115. Toyooka, G.; Tuji, A.; Fujita, K.-i., *Synthesis* **2018**, *50*, 4617-4626.
116. Arcelli, A.; Bui The, K.; Porzi, G., *J. Organomet. Chem.* **1982**, *235*, 93-96.
117. Del Zotto, A.; Baratta, W.; Sandri, M.; Verardo, G.; Rigo, P., *Eur. J. Inorg. Chem.* **2004**, *2004*, 524-529.
118. Liu, Z.; Yang, Z.; Yu, X.; Zhang, H.; Yu, B.; Zhao, Y.; Liu, Z., *Adv. Synth. Catal.* **2017**, *359*, 4278-4283.
119. Polidano, K.; Allen, B. D. W.; Williams, J. M. J.; Morrill, L. C., *ACS Catal.* **2018**, *8*, 6440-6445.
120. Paul, B.; Shee, S.; Panja, D.; Chakrabarti, K.; Kundu, S., *ACS Catal.* **2018**, *8*, 2890-2896.
121. Grinter, R.; Heilbronner, E.; Petrzilka, T.; Seiler, P., *Tetrahedron Lett.* **1968**, *9*, 3845-3848.
122. Jones, R. G., *J. Am. Chem. Soc.* **1947**, *69*, 2346-2350.
123. Gunanathan, C.; Milstein, D., *Chem. Rev.* **2014**, *114*, 12024-12087.
124. Wang, Y.; Huang, Z.; Leng, X.; Zhu, H.; Liu, G.; Huang, Z., *J. Am. Chem. Soc.* **2018**, *140*, 4417-4429.
125. Landge, V. G.; Yadav, V.; Subaramanian, M.; Dangarh, P.; Balaraman, E., *Chem. Commun.* **2019**, *55*, 6130–6133.
126. He, X.; Li, Y.; Fu, H.; Zheng, X.; Chen, H.; Li, R.; Yu, X., *Organometallics* **2019**, *38*, 1750-1760.
127. Xie, X.; Huynh, H. V., *ACS Catal.* **2015**, *5*, 4143-4151.
128. Etsell, T. H.; Flengas, S. N., *Chem. Rev.* **1970**, *70*, 339-376.
129. Zhao, Z.; Arnaiz, D. O.; Griedel, B.; Sakata, S.; Dallas, J. L.; Whitlow, M.; Trinh, L.; Post, J.; Liang, A.; Morrissey, M. M.; Shaw, K. J., *Bioorg. Med. Chem. Lett.* **2000**, *10*, 963-966.
130. Nakano, H.; Inoue, T.; Kawasaki, N.; Miyataka, H.; Matsumoto, H.; Taguchi, T.; Inagaki, N.; Nagai, H.; Satoh, T., *Biorg. Med. Chem.* **2000**, *8*, 373-380.
131. Zhu, Z.; Lippa, B.; Drach, J. C.; Townsend, L. B., *J. Med. Chem.* **2000**, *43*, 2430-2437.
132. Vasiliou, S., *Drugs of today (Barcelona, Spain: 1998)* **2011**, *47*, 647-651.
133. Easmon, J.; Pürstinger, G.; Thies, K.-S.; Heinisch, G.; Hofmann, J., *J. Med. Chem.* **2006**, *49*, 6343-6350.
134. Grobler, J. A.; Dornadula, G.; Rice, M. R.; Simcoe, A. L.; Hazuda, D. J.; Miller, M. D., *J. Biol. Chem.* **2007**, *282*, 8005-8010.
135. Taki, M.; Wolford, J. L.; O'Halloran, T. V., *J. Am. Chem. Soc.* **2004**, *126*, 712-713.
136. Rostamizadeh, S.; Aryan, R.; Ghaieni, H. R.; Amani, A. M., *J. Heterocycl. Chem.* **2009**, *46*, 74-78.

137. Benincori, T.; Sannicolò, F., *J. Heterocycl. Chem.* **1988**, *25*, 1029-1033.
138. Altenhoff, G.; Glorius, F., *Adv. Synth. Catal.* **2004**, *346*, 1661-1664.
139. Evindar, G.; Batey, R. A., *J. Org. Chem.* **2006**, *71*, 1802-1808.
140. Bonnamour, J.; Bolm, C., *Org. Lett.* **2008**, *10*, 2665-2667.
141. Saha, P.; Ali, M. A.; Ghosh, P.; Punniyamurthy, T., *Org. Biomol. Chem.* **2010**, *8*, 5692-5699.
142. Saha, P.; Ramana, T.; Purkait, N.; Ali, M. A.; Paul, R.; Punniyamurthy, T., *J. Org. Chem.* **2009**, *74*, 8719-8725.
143. Brasche, G.; Buchwald, S. L., *Angew. Chem. Int. Ed.* **2008**, *47*, 1932-1934.
144. Guru, M. M.; Ali, M. A.; Punniyamurthy, T., *Org. Lett.* **2011**, *13*, 1194-1197.
145. Chen, Y.-X.; Qian, L.-F.; Zhang, W.; Han, B., *Angew. Chem. Int. Ed.* **2008**, *47*, 9330-9333.
146. Zali Boeini, H.; Hajibabaei Najafabadi, K., *Eur. J. Org. Chem.* **2009**, *2009*, 4926-4929.
147. Deng, X.; McAllister, H.; Mani, N. S., *J. Org. Chem.* **2009**, *74*, 5742-5745.
148. Kawashita, Y.; Nakamichi, N.; Kawabata, H.; Hayashi, M., *Org. Lett.* **2003**, *5*, 3713-3715.
149. Bougrin, K.; Loupy, A.; Soufiaoui, M., *Tetrahedron* **1998**, *54*, 8055-8064.
150. Sharghi, H.; Aberi, M.; Doroodmand, M. M., *Adv. Synth. Catal.* **2008**, *350*, 2380-2390.
151. Terashima, M.; Ishii, M.; Kanaoka, Y., *Synthesis* **1982**, *1982*, 484-485.
152. Saha, D.; Saha, A.; Ranu, B. C., *Green Chem.* **2009**, *11*, 733-737.
153. Faheem, M.; Rathaur, A.; Pandey, A.; Kumar Singh, V.; Tiwari, A. K., *ChemistrySelect* **2020**, *5*, 3981-3994.
154. Varma, R. S.; Saini, R. K.; Prakash, O., *Tetrahedron Lett.* **1997**, *38*, 2621-2622.
155. Chang, J.; Zhao, K.; Pan, S., *Tetrahedron Lett.* **2002**, *43*, 951-954.
156. Kondo, T.; Yang, S.; Huh, K.-T.; Kobayashi, M.; Kotachi, S.; Watanabe, Y., *Chem. Lett.* **1991**, *20*, 1275-1278.
157. Daw, P.; Ben-David, Y.; Milstein, D., *ACS Catal.* **2017**, 7456-7460.
158. Xu, Z.; Wang, D.-S.; Yu, X.; Yang, Y.; Wang, D., *Adv. Synth. Catal.* **2017**, *359*, 3332-3340.
159. Das, K.; Mondal, A.; Srimani, D., *J. Org. Chem.* **2018**, *83*, 9553-9560.
160. Elangovan, S.; Topf, C.; Fischer, S.; Jiao, H.; Spannenberg, A.; Baumann, W.; Ludwig, R.; Junge, K.; Beller, M., *J. Am. Chem. Soc.* **2016**, *138*, 8809-8814.
161. Zhang, M.; Fang, X.; Neumann, H.; Beller, M., *J. Am. Chem. Soc.* **2013**, *135*, 11384-11388.
162. Hille, T.; Irrgang, T.; Kempe, R., *Chem. Eur. J.* **2014**, *20*, 5569-5572.
163. Shi, X.; Guo, J.; Liu, J.; Ye, M.; Xu, Q., *Chem. Eur. J.* **2015**, *21*, 9988-9993.
164. Das, K.; Mondal, A.; Srimani, D., *Chem. Commun.* **2018**.
165. Armarego, W. L. F.; Chai, C., Chapter 4 - Purification of Organic Chemicals. In *Purification of Laboratory Chemicals (Seventh Edition)*, Armarego, W. L. F.; Chai, C., Eds. Butterworth-Heinemann: Boston, **2013**; pp 103-554.
166. Armarego, W. L. F.; Chai, C., Chapter 5 - Purification of Inorganic and Metal-Organic Chemicals. In *Purification of Laboratory Chemicals (Seventh Edition)*, Armarego, W. L. F.; Chai, C., Eds. Butterworth-Heinemann: Boston, **2013**; pp 555-661.
167. *APEX2, SAINT and SADABS.,* , Bruker (**2013**) Bruker AXS Inc., Madison, Wisconsin, USA Section C.
168. *CrysAlisPro* **2015**, *71* (version 1, 171; Oxford Diffraction Ltd., 133.134d [release 127-102-2009 CrysAlis 2171. NET]version 1, 171; Oxford Diffraction Ltd., 133.134d [release 127-102-2009 CrysAlis 2171. NET]).
169. Sheldrick, G., *Acta Crystallographica Section C* **2015**, *71*, 3-8.

170. Gaussian 16, R. C., M. J. Frisch, G. W. Trucks, H. B. Schlegel, G. E. Scuseria, M. A. Robb, J. R. Cheeseman, G. Scalmani, V. Barone, G. A. Petersson, H. Nakatsuji, X. Li, M. Caricato, A. V. Marenich, J. Bloino, B. G. Janesko, R. Gomperts, B. Mennucci, H. P. Hratchian, J. V. Ortiz, A. F. Izmaylov, J. L. Sonnenberg, D. Williams-Young, F. Ding, F. Lipparini, F. Egidi, J. Goings, B. Peng, A. Petrone, T. Henderson, D. Ranasinghe, V. G. Zakrzewski, J. Gao, N. Rega, G. Zheng, W. Liang, M. Hada, M. Ehara, K. Toyota, R. Fukuda, J. Hasegawa, M. Ishida, T. Nakajima, Y. Honda, O. Kitao, H. Nakai, T. Vreven, K. Throssell, J. A. Montgomery, Jr., J. E. Peralta, F. Ogliaro, M. J. Bearpark, J. J. Heyd, E. N. Brothers, K. N. Kudin, V. N. Staroverov, T. A. Keith, R. Kobayashi, J. Normand, K. Raghavachari, A. P. Rendell, J. C. Burant, S. S. Iyengar, J. Tomasi, M. Cossi, J. M. Millam, M. Klene, C. Adamo, R. Cammi, J. W. Ochterski, R. L. Martin, K. Morokuma, O. Farkas, J. B. Foresman, and D. J. Fox,, *Gaussian inc., Wallingford CT 2016* **2016**, *2*, 4.
171. Perdew, J. P.; Burke, K.; Ernzerhof, M., *Phys. Rev. Lett.* **1996**, *77*, 3865.
172. Wadt, W. R.; Hay, P. J., *J. Chem. Phy.* **1985**, *82*, 284-298.
173. Hay, P. J.; Wadt, W. R., *J.Chem. Phy.s* **1985**, *82*, 299-310.
174. Hay, P. J.; Wadt, W. R., *J. Chem. Phy.* **1985**, *82*, 270-283.
175. Du, Y.; Oishi, S.; Saito, S., *Chem. Eur. J.* **2011**, *17*, 12262-12267.
176. Iglesias, A. L.; García, J. J., *J. Mol. Catal. A: Chem.* **2009**, *298*, 51-59.
177. Wei, D.; Bruneau-Voisine, A.; Valyaev, D. A.; Lugan, N.; Sortais, J.-B., *Chem. Commun.* **2018**, *54*, 4302-4305.
178. Sun, N.; Wang, S.; Mo, W.; Hu, B.; Shen, Z.; Hu, X., *Tetrahedron* **2010**, *66*, 7142-7148.
179. Yang, H.; Li, Y.; Jiang, M.; Wang, J.; Fu, H., *Chem. Eur. J.* **2011**, 5652-5660.
180. Yamamoto, Y., *Adv. Synth. Catal.* **2010**, *352*, 478-492.
181. Hollmann, D.; Bähn, S.; Tillack, A.; Beller, M., *Chem. Commun.* **2008**, 3199-3201.
182. Wang, D.; Ding, K., *Chem. Commun.* **2009**, 1891-1893.

Chapter III

Pincer-Ruthenium Catalyzed β-Alkylation of Secondary Alcohols with Primary Alcohols

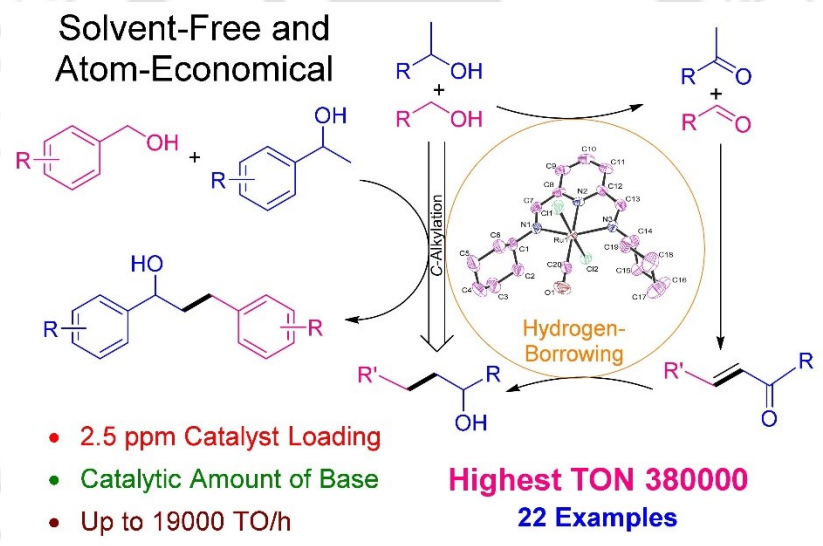

- **K. Das**, M. Dutta, B. Das, H. K. Srivastava, A. Kumar, *Adv. Synth. Catal*. **2019**, *361*, 2965.
- **K. Das**, E. Yasmin, B. Das, H. K. Srivastava, A. Kumar, *Catal. Sci. Technol*. **2020**, *10*, 8347.

3.1 Introduction

Alcohols are very versatile chemicals that have been commonly used in organic transformations and chemical industries.[1-2] The formation of new C–C bonds are not only important in organic chemistry but also acts as an alternative carbon source in petrochemical industry. The major concern is to synthesize alcohols through an alternative pathway. The traditional process used for the production of *β*-alkylated alcohols consist of a multistep synthetic pathway. This process led to the generation of a stoichiometric amount of waste product[3-5] along with the consumption of expensive and toxic reagents, and strong bases[3-5] (Scheme **3.1**).

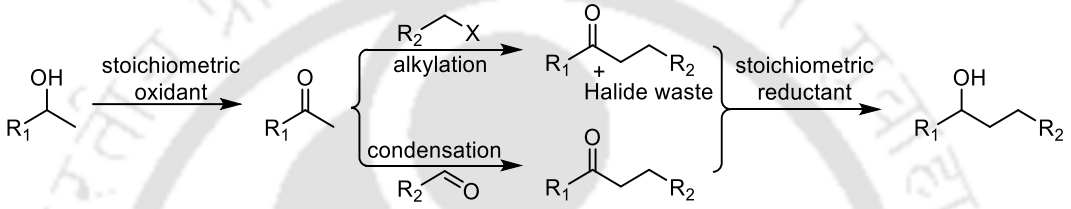

Scheme 3.1: Traditional approach to *C*-alkylation reaction.[6-7]

Among the various protocols, transition metal-catalyzed C–C bond formation *via β*-alkylation of alcohols has garnered a lot of attention. Accounting for an environment friendly process, the use of alcohols to form higher *β*-alkylated alcohols *via* an acceptorless dehydrogenative coupling proves to be an attractive approach. In this process: initial dehydrogenation of both (primary and secondary) alcohols to the corresponding carbonyl compounds is followed by aldol condensation to form corresponding unsaturated ketones which eventually gets hydrogenated to afford *β*-alkylated alcohols (Scheme **3.2**).

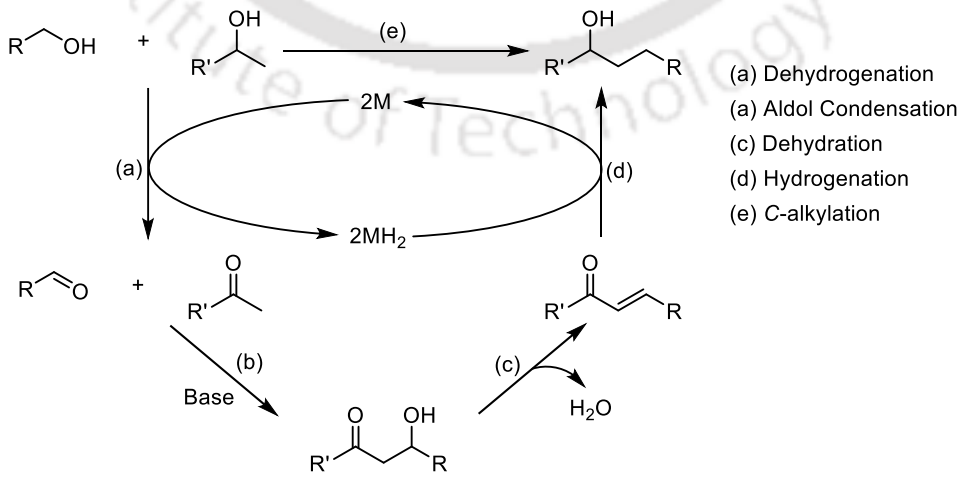

Scheme 3.2: A greener strategy towards *C*-alkylation.[7]

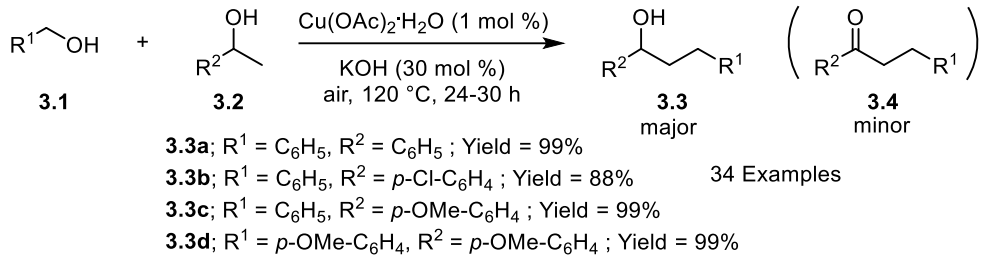

Scheme 3.3: *C*-alkylation reaction catalyzed by copper.[8]

The dehydrogenation of alcohols in anaerobic conditions is widely explored by employing various transition metals.[9-11] In aerobic condition, hydrogen-borrowing strategy for the dehydrogenation of alcohol holds some drawbacks involving a metal hydride species (*i.e* MH_2; Scheme **3.2**) as it seems to be air sensitive or not readily formed. In fact, *C*-alkylation *via* hydrogen-borrowing methodology under mild reaction conditions is more desirable in organic synthesis. In general, transition metal catalyzed *C*-alkylation reaction involves inert condition with a pre-coordinated ligand to the metal center. Xu and co-workers investigated the *β*-alkylation of secondary alcohols and *α*-alkylation of ketones using a ligand-free copper catalyst (Scheme **3.3**).[8] Their methodology involves an earth abundant transition metal (copper) that holds wide scope to provide an alternative route in synthetic chemistry.

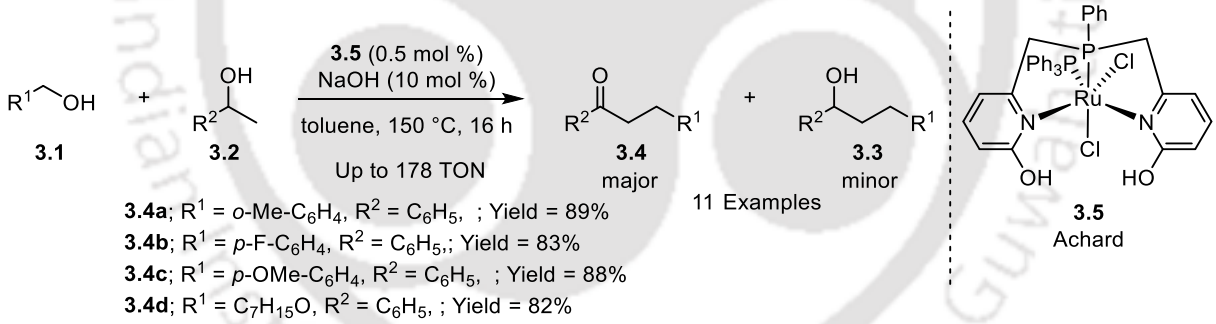

Scheme 3.4: Over oxidation of product during pincer-Ru catalyzed *C*-alkylation reaction.[12]

Achard and co-workers demonstrated the use of bi/tri-dentate phosphine pyridine ligand-based metal complexes to form ester through alcohol dehydrogenation. Interestingly, the use of complex **3.5** resulted in *α*-alkylated ketone *via* dehydrogenative cross-coupling of secondary alcohol with primary alcohol along with the formation of a trace amount of *β*-alkylated alcohol (Scheme **3.4**).[12] While, the *α*-alkylated ketones could be obtained either from primary alcohols with a ketone or secondary alcohols with an aldehyde in the presence of a base and catalyst, the sequential de/hydrogenation strategy utilized here to synthesize *α*-alkylated ketone directly is an effective alternative pathway. This implies that the alkylation of secondary alcohol with

primary alcohols directly produces either *β*-alkylated alcohol or takes part in further dehydrogenation of *β*-alkylated alcohol to form the *α*-alkylated ketone.

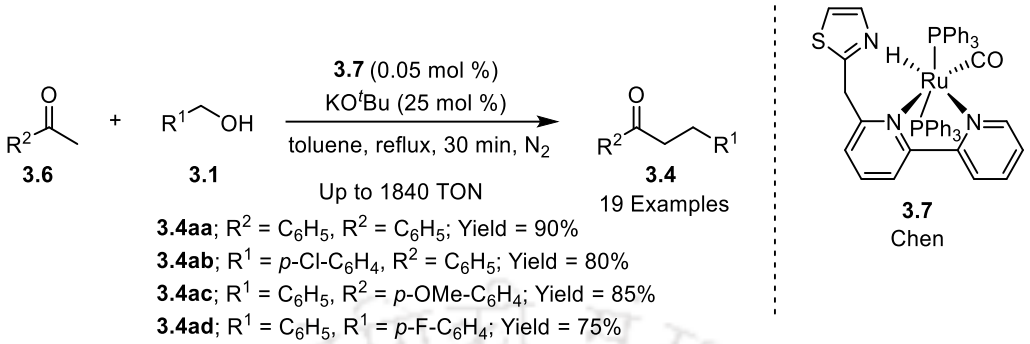

Scheme 3.5: Ruthenium catalyzed formation of *α*-alkylated ketones.[13]

Chen and co-workers demonstrated ruthenium catalyst based on NNN tridentate ligand, which involves bifunctional uncoordinated pyridyl group in catalytic system of *β*-alkylation of secondary alcohols with primary alcohols.[14] The reactivity mainly depends on the nucleophilicity of the 2-hydroxypryrdine group (one of the ligating arm), which reflects the systematic involvement of metal-ligand co-operativity in the alkylation reaction. Similarly, pyridines, quinolines and pyrroles have been synthesized by the same NNN-Ru catalyzed acceptorless dehydrogenation.[15] An analogous Ru-catalyzed thiazolium group-containing ligand system demonstrated *α*-alkylation of ketones with primary alcohols, giving up to 1840 TON with 3680 TO/h (Scheme **3.5**).[13]

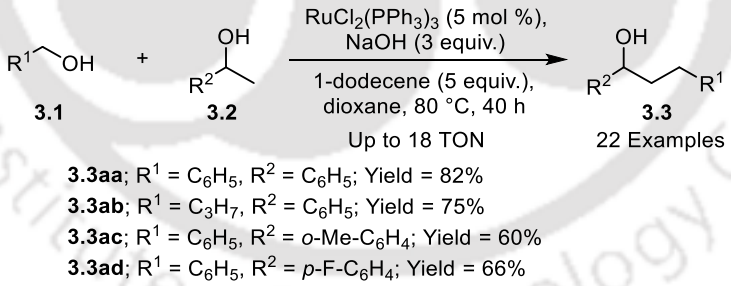

Scheme 3.6: Ruthenium catalyzed *β*-alkylation of alcohols.[16]

Cho first demonstrated the dichloro*tris*(triphenylphosphine)ruthenium(II) catalyzed *β*-alkylation of secondary alcohols with primary alcohols in the presence of 1-dodcene (Scheme **3.6**).[16] This protocol selectively afforded regioselective *β*-alkylation of secondary alcohols with primary alcohols with a variety of substrate scope (including aryl methyl, alkyl methyl, and cyclic carbinols, along with alkyl methyl carbinols).

In order to explore this process, several transition metal complexes based on Ir,[17-26] Rh,[27] Ru,[6, 13, 16, 28-32] Pd,[33] Mn,[34-35] Co,[36] Fe,[37] Ni,[38] and Cu[8] were used significantly (Figure **3.1**). Sun and

co-workers demonstrated the inexpensive, environmentally benign iron complex **3.10** catalyzed *β*-alkylation of secondary alcohols with primary alcohols using catalytic amount of NaOH without any hydrogen acceptors or phosphorus based ligands.[37] Later, Li and Lang described the versatility of the nickel-thiolate-based cluster (**3.11**) system in the *C*-alkylation reaction. The C–C cross-coupling of secondary and primary alcohols to *α,β*-unsaturated ketones, *α*-alkylated ketones or *β*-alkylated secondary alcohols under mild conditions has multiple chemoselectivities.[38] Xu and co-workers reported the ligand-free copper catalysis under aerobic condition which exhibited superior catalytic activity.[8] They deduced a new mechanism for *C*-alkylation reactions *via* the Meerwein-Pondorf-Verley type transition state rather than involvement of copper-hydride species.[39] Similarly, Kempe,[36] Pullarkat,[19] Saito[33] and Maheswaran[27] also reported the *C*-alkylation reaction of secondary alcohols with primary alcohols using the hydrogen-borrowing methodology. However, ruthenium and iridium-based complexes have shown higher reactivity and selectivity than other transition metals. Notably, several complexes have been used in *β*-alkylation of secondary alcohols using pincer-Ru complexes.

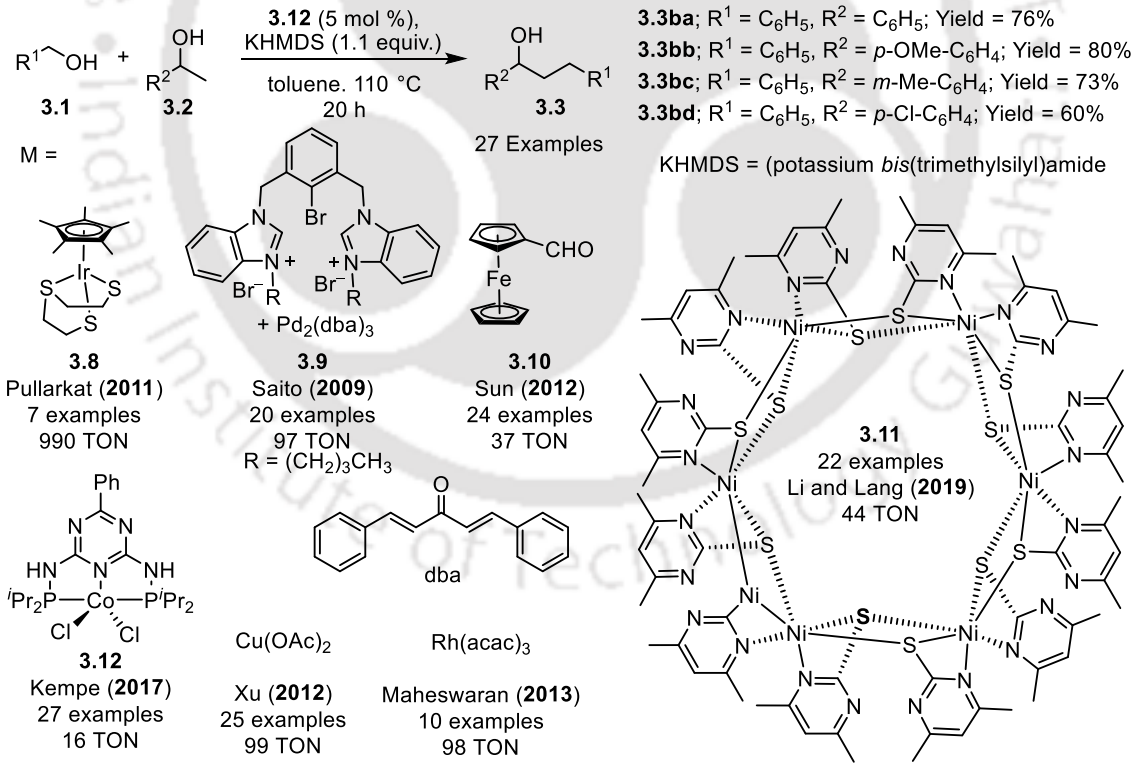

Figure 3.1: Reported catalytic systems for the *β*-alkylation of secondary alcohols with primary alcohols.

Gülcemal and co-workers reported the imidazol-2-ylidene ligand-based iridium(I) **3.13** catalyzed *β*-alkylation of secondary alcohols with primary alcohols. This simple catalytic

system provided the *β*-alkylated alcohols (including cholesterol derivatives) with good yields under a very low loading of the catalyst **3.13** (Scheme **3.7**).[40] The catalyst **3.13** achieved up to 940000 TON with a catalytic amount of NaOH or KOH under aerobic conditions *via* hydrogen-borrowing strategy.

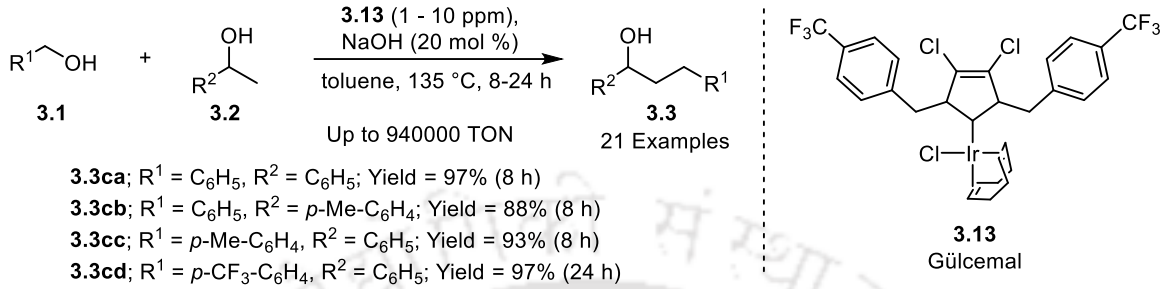

3.3ca; $R^1 = C_6H_5$, $R^2 = C_6H_5$; Yield = 97% (8 h)
3.3cb; $R^1 = C_6H_5$, $R^2 = p$-Me-C_6H_4; Yield = 88% (8 h)
3.3cc; $R^1 = p$-Me-C_6H_4, $R^2 = C_6H_5$; Yield = 93% (8 h)
3.3cd; $R^1 = p$-CF_3-C_6H_4, $R^2 = C_6H_5$; Yield = 97% (24 h)

Scheme 3.7: *β*-alkylation of secondary alcohols investigated using a Ir-catalyst.[40]

Bera and co-workers reported Ir-*N*-heterocyclic carbene **3.14** catalyzed *β*-alkylation of secondary alcohols with primary alcohols. The complex **3.14** demonstrated remarkable activity due to pyridyl(benzamide)-functionalized NHC backbone, which involves dearomatization/aromatization of pyridine backbone during catalysis. These catalytic systems demonstrated a wide range of substrate scope under low base and catalyst loading within a short reaction time (Scheme **3.8**).[41] The same methodology, was applied to the *α*-alkylation of ketones using primary alcohols in addition to the synthesis of quinoline and lactone derivatives.[41]

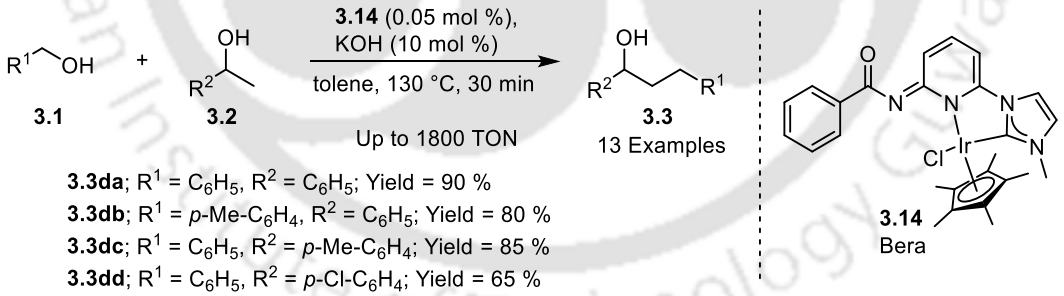

3.3da; $R^1 = C_6H_5$, $R^2 = C_6H_5$; Yield = 90 %
3.3db; $R^1 = p$-Me-C_6H_4, $R^2 = C_6H_5$; Yield = 80 %
3.3dc; $R^1 = C_6H_5$, $R^2 = p$-Me-C_6H_4; Yield = 85 %
3.3dd; $R^1 = C_6H_5$, $R^2 = p$-Cl-C_6H_4; Yield = 65 %

Scheme 3.8: *β*-alkylation of secondary alcohols with primary alcohols catalyzed by a Ir-complex.[41]

Thus, catalytic, one-pot acceptorless coupling of a mixture of alcohols (primary and secondary) gives rise to high carbon-containing alcohols and ketones. Following the same reaction methodology, Gelman and co-workers reported an efficient and selective synthesis of *β*-alkylated ketones *via* cross-coupling of secondary alcohols with primary/secondary alcohols. The ligand-metal cooperation is presumed to be involved in the catalytic cycle which operates *via* dehydrogenation and hydrogenation pathway to achieve a maximum of 48 turnovers (TON) (Scheme **3.9**).[42]

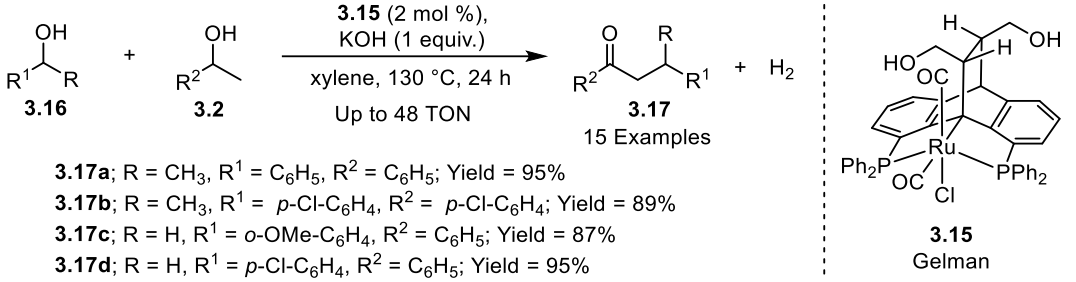

Scheme 3.9: Ruthenium catalyzed synthesis of *β*-alkylated ketones from secondary alcohols with primary/secondary alcohols.[42]

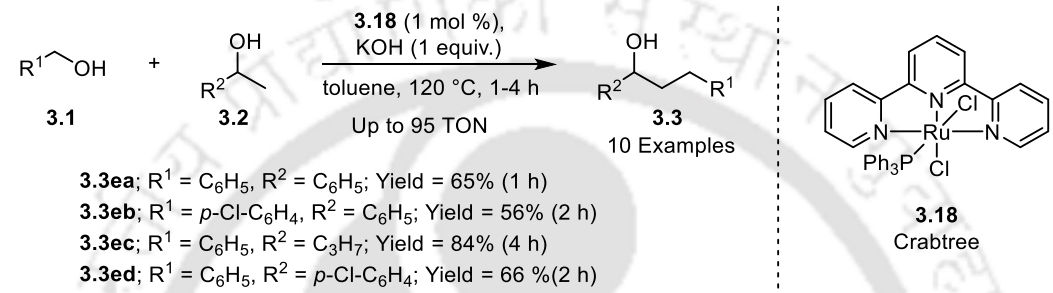

Scheme 3.10: Pincer-ruthenium catalyzed *β*-alkylation of secondary alcohols with primary alcohols.[25]

Though NNN 2,2′:6′,2″-terpyridine (terpy) ligand is considered as a strong π-acceptor relative to other *N*-donors ligands,[43] it also has oxidatively and thermally robust properties.[44] Despite the incompatible nature of terpy ligands in transition metal complex systems, it offers a variety of catalytic organic transformations.[45] In this regard, Crabtree and co-workers reported *β*-alkylation of secondary alcohols with primary alcohols based on terpy pincer-ruthenium catalyst (Scheme **3.10**).[25] The use of 20 mol % KOH resulted in the complete conversion to alkylated products with a maximum of 95 TON along with formation of H_2O as a byproduct.

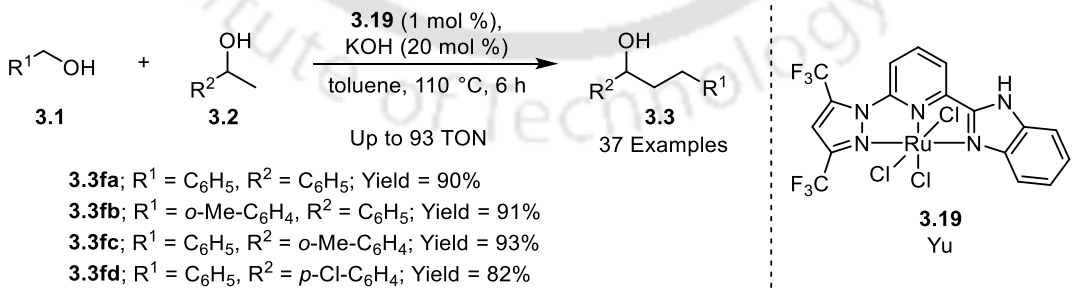

Scheme 3.11: Pincer-ruthenium catalyzed *β*-alkylation of secondary alcohols with primary alcohols.[6]

Similarly, introducing trifluoromethylated molecules to the ligand system has provided versatile applications in catalysis because of the innate qualities of the CF_3 group (like high electronegativity, lipophilicity and H-bond formation ability).[46] In this context, Yu and co-

workers reported the *β*-alkylation of secondary alcohols with primary alcohols through a hydrogen borrowing pathway and achieved up to 93 TON (Scheme **3.11**).[6] In mechanistic studies, they proved that the precatalyst Ru(III) initially gets converted to Ru(II) species in the presence of KOH.[47]

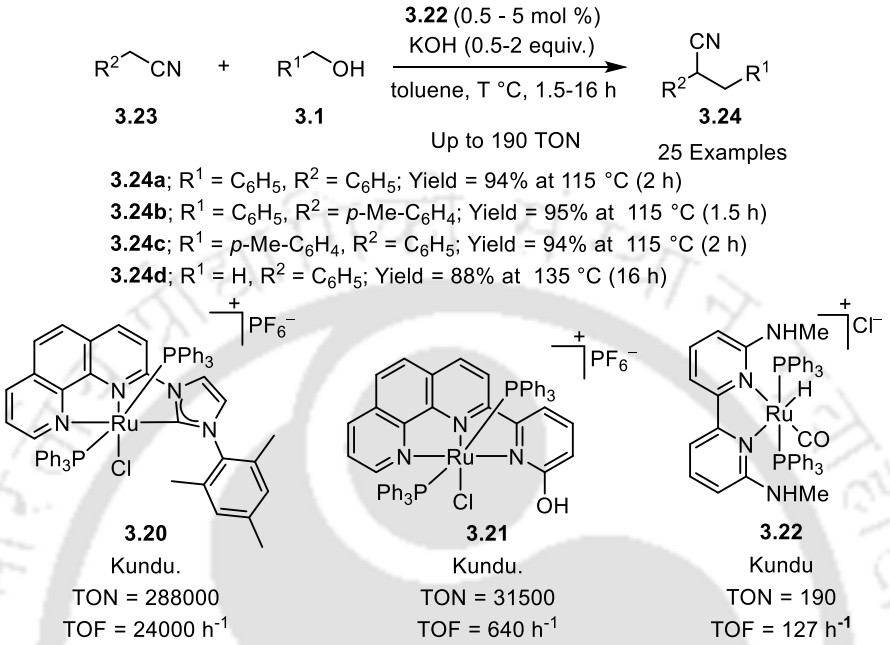

Scheme 3.12: Ruthenium catalyzed *C*-alkylation reaction.[28]

Kundu and co-workers reported a series of pincer-ruthenium catalysts for *β*-alkylation of secondary alcohols with primary alcohols. Upon significantly lowering the catalyst loading, the NHC ligand-based NNC pincer-ruthenium complex **3.20** provided a very high turnover of 288000 for the *β*-alkylation reaction.[30] They performed the reaction efficiently under solvent-free conditions with a large scope (towards aromatic, aliphatic and heterocyclic alcohols). Similarly, they demonstrated bifunctional metal-ligand cooperativity in complex **3.21** for the *β*-alkylation of secondary alcohols and primary alcohols with high selectivity while achieving 31500 TON.[31] They extended the above protocol to the direct synthesis of *α*-alkylated nitriles starting from nitrile and alcohols. Generally, a toxic alkyl halide, strong base and harmful cyanating (KCN or NaCN) agent is required for the synthesis of *α*-alkylated nitriles which leads to stoichiometric amounts of waste.[48-49] The complex **3.22** showed excellent reactivity in *α*-alkylation of acetonitrile and arylacetonitriles with alcohols which provided up to 190 TON (Scheme **3.12**).[28]

Ghosh and co-workers reported an amido-functionalized ruthenium carbene complex **3.25** catalyzed *β*-alkylation of secondary alcohols with primary alcohols.[50] They also demonstrated

that a similar cationic picolyl functionalized NHC ruthenium complex exhibited a comparable reactivity towards *C*-alkylation (Scheme **3.13**).[50] The catalyst **3.25** was detected as a hydride intermediate and it remained active till 120 h.

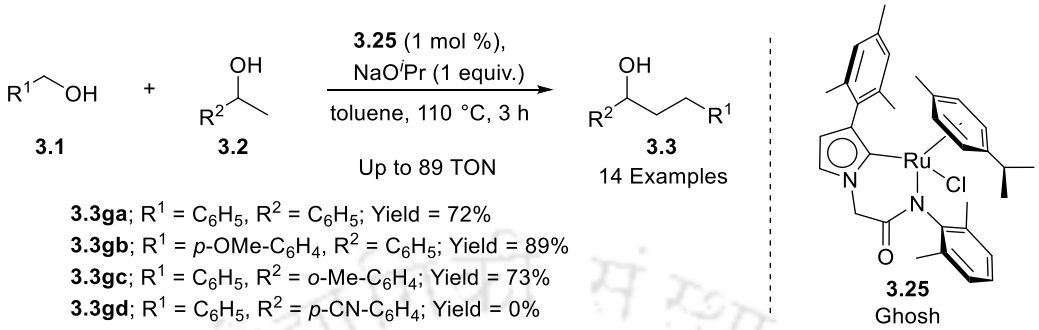

Scheme 3.13: Ruthenium-carbene catalyzed *C*-alkylation reaction.[50]

Cycloalkanes are omnipresent in natural and pharmaceutical products. The building block of these products could be synthesized through various pathways, like Diels-Alder[51] cycloaddition, Wurtz reaction[52] or Michael reaction.[53] Generally, all these approaches have some drawbacks, involve multistep procedures, and suffer from regio- or stereoselectivity.[54] However, Quadrelli and co-workers introduced an earth-abundant PNP based pincer-manganese **3.26** that catalyzed the synthesis of alcohol-containing cyclohexyl compounds through *C*-alkylation methodology (Scheme **3.14**).[55] Initially, 1,5-pentanediol derivative dehydrogenates to the corresponding aldehyde, which takes part in the intermolecular aldol condensation reaction with the dehydrogenated secondary alcohol (ketone). This is followed by an intramolecular aldol condensation resulting in cyclohexyl containing secondary alcohol *via* a re-hydrogenation. Notably, this concept is widely applicable for various substrates on aromatic groups as well as aliphatic parts. Basically, this molecular design is an engineering approach to synthesize direct consecutive C–C bond formation *via* hydrogen-borrowing strategy.

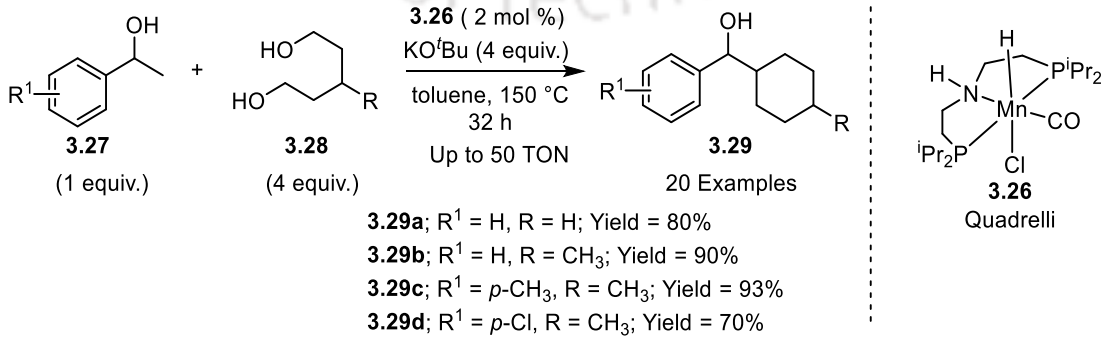

Scheme 3.14: *C*-alkylation reaction leading to the formation of cyclohexane derivatives starting from primary diols.[55]

3.2 Objectives

A comprehensive literature survey reveals that pincer complexes are more effective than others in catalyzing the *β*-alkylation of secondary alcohols with primary alcohols. To the best of our knowledge, there are no reports of either using *bis*(imino) pincer-ruthenium complexes or phosphine-free pincer complexes in the *β*-alkylation of secondary alcohols with primary alcohols. The previous chapter demonstrated the utility of NNN pincer-ruthenium complexes for *N*-alkylation of amines.[56-57] On the basis of these facts, the current chapter attempts to address the following questions

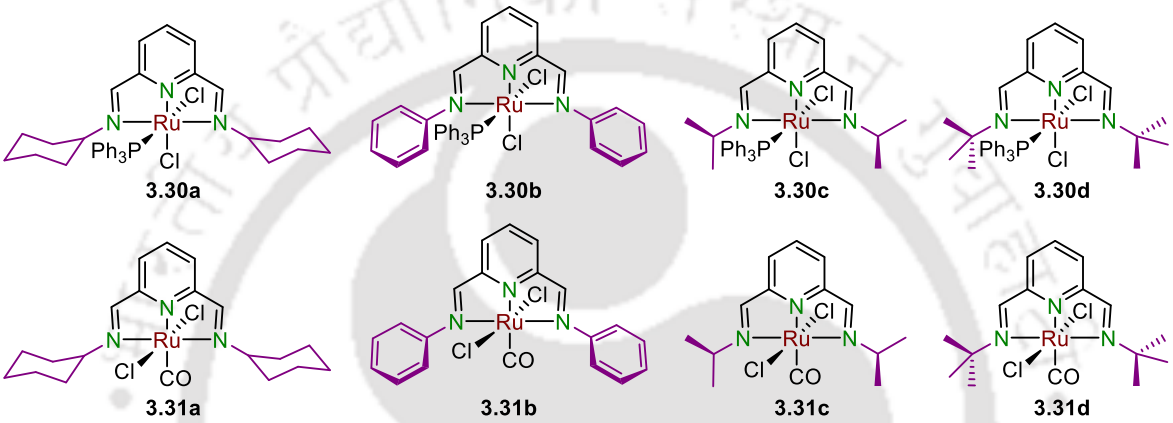

Figure 3.2: Pincer-Ru complexes that are used for *β*-alkylation of secondary alcohols in the current chapter.

- Can one utilize pincer-Ru complexes based on *bis*(imino) pyridine ligand for the *C*-alkylation?
- Can one extrapolate the *N*-alkylation activity to *β*-alkylation of secondary alcohols?
- What is the effect of catalyst and base loading on *β*-alkylation reaction?
- Are various functional groups tolerated?
- How does the *β*-alkylation activity of NNN *bis*(imino) pyridine ruthenium-PPh_3 complex compare with corresponding ruthenium-carbonyl complexes (Figure **3.2**)?
- The first step in the catalytic N-alkylation transformation being generation of 5-coordinate 16-electron species, it would be interesting to probe if for a similar *β*-alkylation reactivity, can a better control be obtained by a carbonyl to phosphine switch?".

3.3 Result and Discussion

3.3.1 Synthesis of complexes of the type (^{R2}NNN)RuCl$_2$CO: (3.31a; R = Cy, 3.31b; R = Ph, 3.31c; R = ^{i}Pr and 3.31d; R = ^{t}Bu)

The complexes were synthesized by heating to reflux ^{R2}NNN ligands (**3.32a**; R = Cy, **3.32b**; R = Ph, **3.32c**; R = ^{i}Pr and **3.32d**; R = ^{t}Bu; see Chapter II)[56] and [Ru(*p*-cymene)Cl$_2$]$_2$ in dry THF for about 2 h. This was followed by another 10 h of heating to reflux in the presence of an atmosphere of CO which resulted in the corresponding carbonyl complexes (^{R2}NNN)RuCl$_2$(CO) (**3.31a**; R = Cy, **3.31b**; R = Ph, **3.31c**; R = ^{i}Pr and **3.31d**; R = ^{t}Bu) with good yield (Scheme **3.15**). The complexes **3.31a**, **3.31c** and **3.31d** were fully characterized by HRMS, IR, ^{1}H and ^{13}C NMR spectroscopy studies. Also, complex **3.31b** was analyzed through HRMS and IR studies. The ^{1}H NMR spectra was taken in CDCl$_3$ and spectra for all complexes are well assigned except complex **3.31b**, as it has poor solubility. For both the complexes **3.31a** and **3.31c**, in the ^{1}H NMR spectra, the imine proton resonates as a singlet at 8.09 and 8.18 ppm respectively, while for **3.31d** the corresponding imine protons resonate as two different singlets at 8.07 and 8.02 ppm. In the ^{13}C NMR spectra, the carbonyl carbon appears at 205.21, 205.10 and 207.24 for **3.31a**, **3.31c** and **3.31d** respectively. The IR studies of **3.31a**, **3.31b**, **3.31c** and **3.31d** revealed the presence of the carbonyl group and showed prominent C–O stretching frequency at 1944 cm^{-1},1954 cm^{-1}, 1952 cm^{-1} and 1934 cm^{-1} respectively (Table **3.1**).

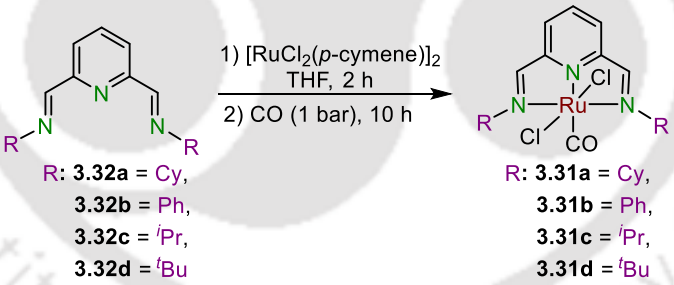

Scheme 3.15: Synthesis of pincer-ruthenium carbonyl complexes based on *bis*(imino) pyridine.

Table 3.1: IR data of complexes **3.31a-d**

3.31a	3.31b	3.31c	3.31d
1944 (s) cm^{-1}	1954 (s) cm^{-1}	1952 (s) cm^{-1}	1934 (s) cm^{-1}

Good quality single crystals were obtained by slow evaporation of dichloromethane (1 mL) solution of **3.31a** and **3.31c** (10 mg each). The crystal structure of **3.31a** and **3.31c** were determined by single-crystal X–ray diffraction analysis as in Figure **3.3**. In the complexes **3.31a** and **3.31c**, the Ru center adopted a distorted octahedral geometry. The pincer ligand is coordinated to Ru center in a meridional fashion, where other three coordination sites are satisfied by the two chlorides (*trans* to each other) and one carbon monoxide (CO) (*trans* to

pyridyl nitrogen atom). The complex **3.31a** crystallizes in the monoclinic $P2_1/n–1$ space group with two symmetry non-equivalent molecules in the asymmetric unit.

Table 3.2: Bond distances (Å) and angles (°) for the complexes **3.31a** and **3.31c**

	3.31a	**3.31c**
Ru–N(pyridine)	2.087 (8) (unit I)	2.099 (5)
	2.096 (3) (unit I)	2.116 (5)
	2.103 (7) (unit II)	
	2.103 (8) (unit II)	
Ru–N(imine)	2.018 (7) (unit I)	1.998 (6)
	2.020 (6) (unit II)	
Ru–Cl	2.396 (3) (unit I)	2.3937 (17)
	2.400 (3) (unit I)	2.3940 (17)
	2.390 (3) (unit II)	
	2.401 (3) (unit II)	
Ru–C(carbonyl)	1.872 (10) (unit I)	1.849 (10)
	1.871 (10) (unit II)	
C=N(imine)	1.296 (12) (unit I)	1.276 (8)
	1.280 (12) (unit I)	1.293 (8)
	1.276 (11) (unit II)	
	1.278 (12) (unit II)	
C≡O	1.135 (11) (unit I)	1.140 (8)
	1.123 (11) (unit II)	
(imine)N–Ru–N(imine)	154.7 (3) (unit I)	154.50 (3)
	154.0 (3) (unit II)	
(py)N–Ru–C	179.8 (4) (unit I)	178.00 (2)
	179.0 (4) (unit II)	
Ru–C–O	179.10 (11) (unit I)	178.90 (7)
	178.9 (10) (unit II)	

The complex **3.31a** consists of one molecule of acetone and two molecules of water in the crystal lattice. In complex **3.31a** the carbonyl C=O bond distances in both non-equivalent units was 1.135 (11) Å and 1.123 (11) Å respectively. In the solid-state, the complexes **3.31a** and **3.31c** were stabilized mainly by C–H···Cl–Ru and C–H···O–C–Ru interactions. In one of the non-equivalent units of the complex **3.31a**, both the chlorides exhibited C–H···Cl–Ru

interaction with C–H of both the cyclohexyl groups at 3.192 Å, 3.235 Å, 3.334 Å & 3.340 Å and 3.315 Å & 3.365 Å respectively. In addition, CO group of this non-equivalent unit in complex **3.31a** exhibited C–H···O–C–Ru interactions with C–H of cyclohexyl group (2.918 Å, 2.972 Å, 3.069 Å and 3.070 Å).[58] In the second non-equivalent unit of complex **3.31a**, the chloride shows C–H···Cl–Ru interaction with C–H of the both cyclohexyl groups at 3.244 Å, 3.354 Å, 3.305 Å & 3.256 Å and 3.251 Å, 3.489 Å, 3.301 Å & 3.368 Å respectively. The CO group of this non-equivalent unit in complex **3.31a** exhibited C–H···O–C–Ru interactions with C–H of cyclohexyl group (2.850 Å, 2.901 Å, 3.046 Å and 3.092 Å). The solvent (H_2O) in the crystal does not show any interaction, which is likely to act as a space-filler. While, the acetone molecule shows C–H···Cl–Ru interaction to chloride in one of the units of **3.31a,** with C–H bond distances of both methyl groups in acetone being 2.867 and 3.034 Å.[58] The complex **3.31c** crystallizes in the monoclinic *P2₁/c* space group. It consists of one molecule of water in the crystal lattice. Similar to complex **3.31a**, in complex **3.31c** both the chlorides exhibited C–H···Cl–Ru interaction with the C–H of the methyl groups at 3.229 Å, 3.362 Å, 3.331 Å & 3.371 Å and 3.232 Å, 3.245 Å, 3.305 Å & 3.287 Å respectively. The CO group in complex **3.31c** shows C–H···O–C–Ru interaction with C–H of the methyl group (2.850 Å, 2.950 Å, 2.935 Å and 3.058 Å). Interestingly, the solvent molecule (H_2O) in complex **3.31c** shows strong Ru–Cl···H–O interaction with one of the chloride atoms (2.375 Å). The selected bond lengths and bond angles around the metal center are illustrated in Table **3.2** for both **3.31a** and **3.31c**. The crystallographic data are provided in Table **3.6**.[58]

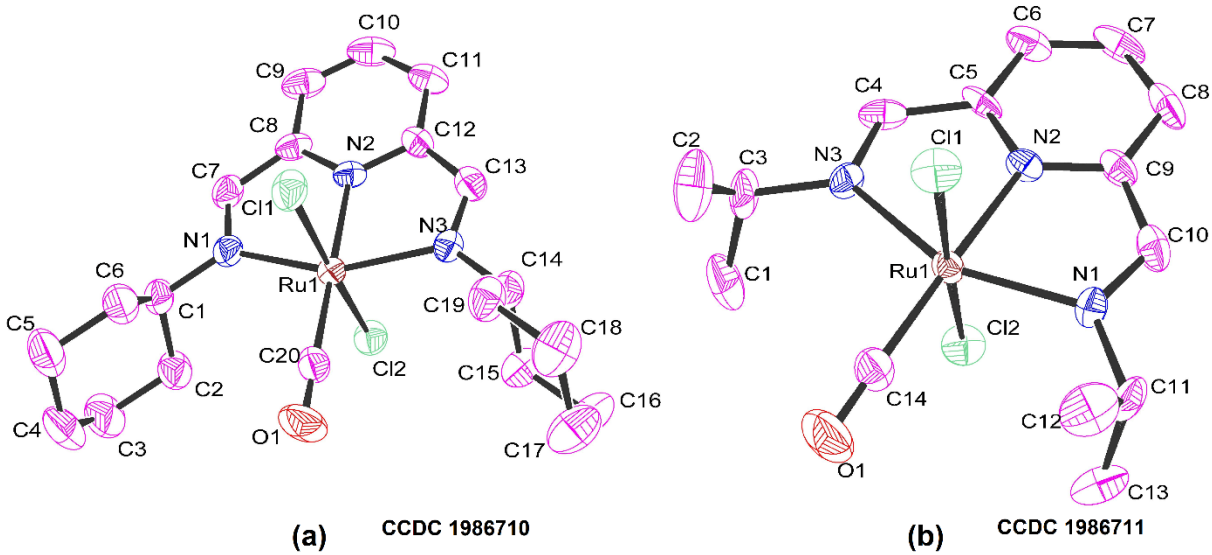

Figure 3.3: ORTEP diagram of **(a)** (^{Cy2}NNN)RuCl$_2$(CO) **3.31a** and **(b)** (^{iPr2}NNN)RuCl$_2$(CO) **3.31c** with ellipsoids drawn at 50% probability. The hydrogen atoms are omitted for the sake of clarity.

3.3.2 *β*-alkylation of secondary alcohols with primary alcohols catalyzed by (^{R2}NNN)RuCl$_2$CO: (3.31a; R = Cy, 3.31b; R = Ph, 3.31c; R = ^{i}Pr and 3.31d; R = ^{t}Bu)

Table 3.3: Optimization of *β*-alkylation of 1-phenyl ethanol with benzyl alcohol catalyzed by **3.31a**[a]

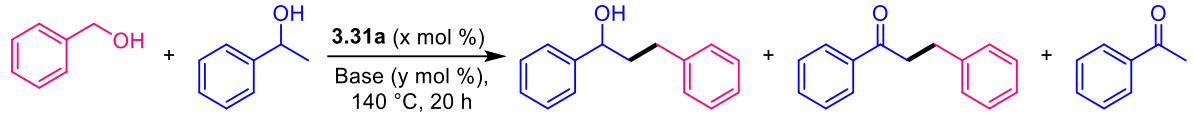

Entry	**3.31a** (x mol %)	Base (y mol %)	Yield[b] (%)				Total TON	Selectivity of **3.35**[c] (%)
			3.34′	**3.35**	**3.36**	Total		
1	0.05	NaO^{t}Bu, 5	13	57	12	82	1640	83
2	0.05	KO^{t}Bu, 5	8	65	6	79	1580	91
3	0.05	NaOH, 5	10	63	12	85	1700	84
4	0.05	KOH, 5	6	63	8	77	1540	89
5[d]	0.05	Na, 5	13	65	11	89	1780	85
6	0.05	K_2CO_3, 5	10	15	11	36	720	57
7	0.05	Na_2CO_3, 5	10	--	trace	10	200	--
8[e]	0.05	KO^{t}Bu, 2.5	10	65	8	83	1660	89
9	0.05	KO^{t}Bu, 10	5	69	5	79	1580	93
10	0.05	NaOH, 2.5	7	79	7	93	1860	91
11	0.05	NaOH, 10	10	65	10	85	1700	88
12	0.025	NaOH, 2.5	14	70	13	97	3880	84
13	0.025	KO^{t}Bu, 2.5	14	68	15	97	3880	82
14	0.0025	NaOH, 2.5	16	63	16	93	39600	79
15	0.00025	NaOH, 2.5	1	73	19	93	372000	79
16	0.025	--	5	4	2	6	--	--
17	--	KO^{t}Bu, 2.5	trace	6	1	4	440	--

[a]Reaction Condition: Benzyl alcohol (4.25 mmol), 1-phenyl ethanol (4.25 mmol), **3.31a** (0.05 mol %) and base (2.5-10 mol %) heated at 140 °C for 20 h. [b]Yield was determined from ^{1}H NMR spectroscopy by using toluene as an internal standard. [c]Selectivity of **3.35** was calculated as: (Yield of **3.35**/Total yield) x 100. [d]Sodium was used to generate base *in situ* in the reaction medium. [e]Toluene (0.5 mL) was used as a solvent.

The initial optimization of the catalytic conditions for the *β*-alkylation of secondary alcohols was performed with **3.31a** (0.05 mol %), 1-phenyl ethanol **3.34** and benzyl alcohol **3.33** in the presence of various bases (Tables **3.3**) at 140 °C under solvent-free conditions. In the **3.31a**

(0.05 mol %) catalyzed *β*-alkylation of **3.34** with **3.33**, bases (5 mol %) such as NaO^{t}Bu, KO^{t}Bu, NaOH and KOH provided good yields with good selectivity towards the *β*-alkylated alcohol **3.35** (entries 1-4, Table **3.3**). Interestingly, the use of sodium (5 mol %) to generate the base *in-situ*[57] (prior to addition of **3.31a**) also resulted in good yields of **3.35** (entry 5, Table **3.3**). Relatively poor reactivity was observed upon using K_2CO_3 and Na_2CO_3 (entries 6 and 7, Table **3.3**). The total yield of products obtained with 2.5 mol % base loading was better than the yield obtained with a base loading of either 5 mol % or 10 mol % (compare entry 9 with entries 2 & 10 and compare entry 10 vs. entries 3 & 11, Table **3.3**). The total yield of products increased upon lowering the loading of **3.31a** to 0.025 mol % (entries 10 and 12, Table **3.3**). Notably, the *β*-alkylation did not proceed either in the absence of a catalyst or in the absence of a base (entries 16 and 17, Table **3.3**). The rest of the catalytic reactions were performed with 2.5 mol % NaOH as the total yield of products was better with selectivity towards **3.35** comparable to that obtained with KO^{t}Bu. Upon further lowering the **3.31a** loading, the total yields were comparable (entries 14 and 15, Table **3.3**).

Table 3.4: *β*-alkylation of 1-phenyl ethanol with benzyl alcohol using various complexes of the type (^{R2}NNN)RuCl$_2$L (L = CO or PPh$_3$; R = Cy, Ph, ^{i}Pr and ^{t}Bu) (**3.30** and **3.31**).[a]

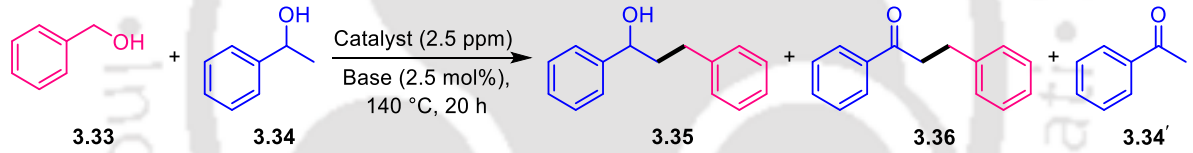

3.33 3.34 3.35 3.36 3.34′

Entry	Catalyst	Yield[b] (%)				Total TON	Selectivity of **3.35**[c] (%)
		3.34′	**3.35**	**3.36**	**Total**		
1	**3.30a**	1	81	7	89	356000	92
2	**3.30b**	2	65	15	80	320000	81
3	**3.30c**	2	75	9	86	344000	89
4	**3.30d**	2	78	7	87	348000	92
5	**3.31a**	1	73	19	93	372000	79
6	**3.31b**	2	57	3	62	248000	95
7	**3.31c**	1	78	10	89	356000	88
8	**3.31d**	1	78	10	89	356000	98

[a]Reaction Condition: Benzyl alcohol (4.25 mmol), 1-phenyl ethanol (4.25 mmol), catalyst (0.00025 mol %) and NaOH (2.5 mol %) heated at 140 °C for 20 h. [b]Yield was determined from ^{1}H NMR spectroscopy by using toluene as an internal standard. [c]Selectivity of **3.35** was calculated as: (Yield of **3.35**/Total yield) x 100.

The apparent decrease in selectivity towards **3.35** at lower catalyst loadings (entries 10, 12, 14 and 15, Table **3.3**) is attributable to secondary dehydrogenation of **3.35** to **3.36** (*vide infra*).

Gratifyingly, the turnover (ca. 372000) observed with 0.00025 mol % of **3.31a** is the highest reported yet in comparison with other ruthenium based catalytic systems.

Among the other variants of the carbonyl complexes, while **3.31c** (entry 7, Table **3.4**) and **3.31d** (entry 8, Table **3.4**) gave slightly lower yields in comparison to **3.31a** (entry 5, Table **3.4**), the activity of **3.31b** (entry 6, Table **3.4**) was considerably lower. Similarly, among the corresponding PPh_3 analogues (**3.30a-d**), the complex **3.30b** (entry 2, Table **3.4**) performed poorly in comparison with **3.30a, 3.30c** and **3.30d** (entries 1, 3 and 4, Table **3.4**).

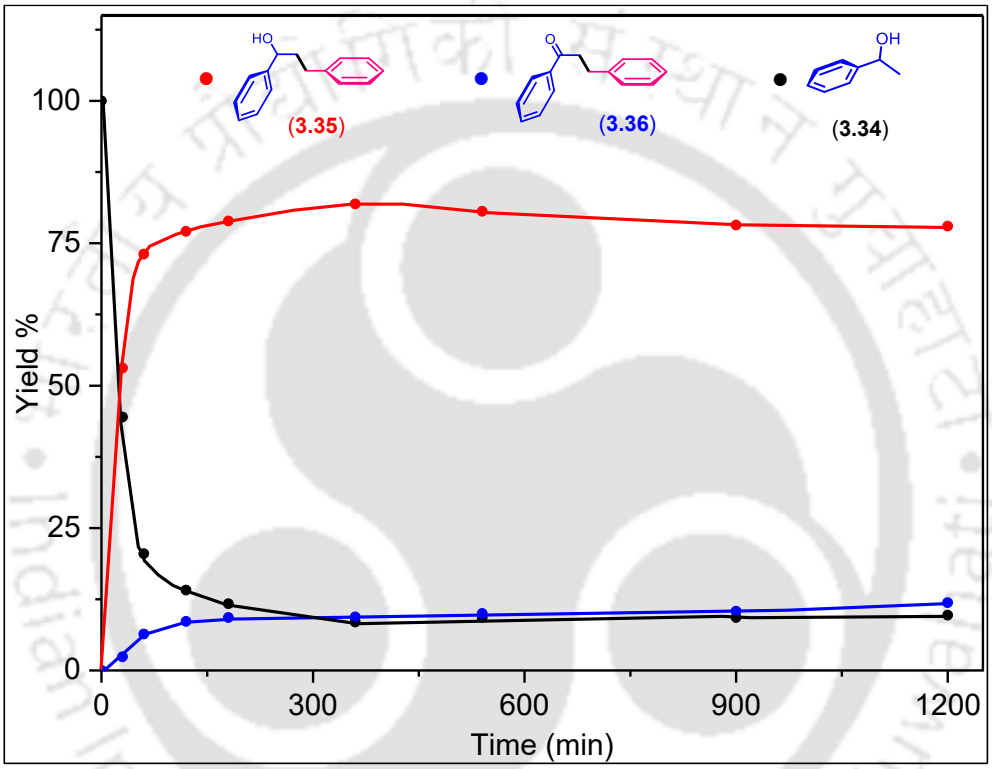

Figure 3.4: Time-course plot of *β*-alkylation of 1-phenyl ethanol **3.34** with benzyl alcohol **3.33** at 0.025 mol % loading of **3.31a** at 140 °C.

Figures **3.4-3.8** depicts the time course of the *β*-alkylation of **3.34** with **3.33** at different loadings of **3.31a**. At a higher loading (0.025 mol %) of **3.31a**, the absence of an initial build-up of **3.36** (Figure **3.4**) indicates that the formation of **3.35** *via* **3.36** is very rapid (Scheme **3.16-17** and mechanistic studies *vide-infra*). The observed growth of **3.36** in minor amounts actually occurs through secondary dehydrogenation of **3.35** catalyzed by **3.31a** at a stage when its activity eventually levels off (Figure **3.4**). Evidence to this understanding could be obtained by slowing down the *β*-alkylation (Figure **3.7** and **3.8**). Accordingly, in the reaction carried out with 0.00025 mol % of **3.31a** and 0.0025 mol % of **3.31a**, the formation of **3.36** was observed only after 3 h (Figure **4.7**) and 6 h (Figure **4.8**) of reaction respectively. Similar results were observed by Güelcemal in the Ir(I) **3.13** catalyzed reactions.[40]

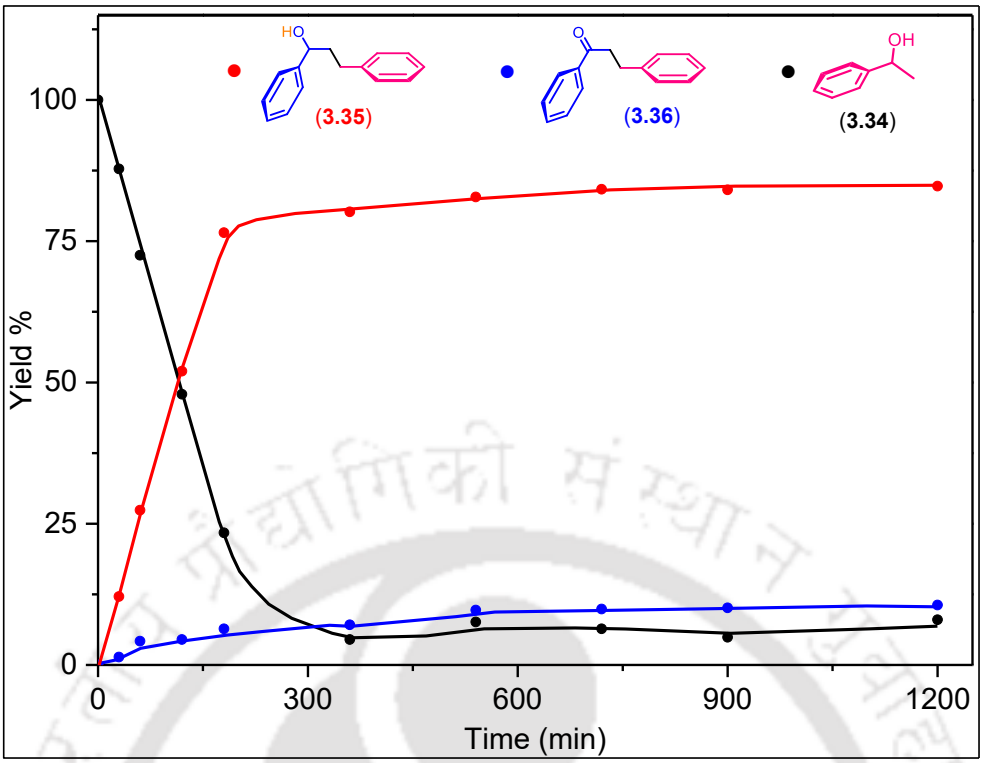

Figure 3.5: Time-course plot of *β*-alkylation of 1-phenyl ethanol **3.34** with benzyl alcohol **3.33** at 0.0175 mol % loading of **3.31a** at 140 °C.

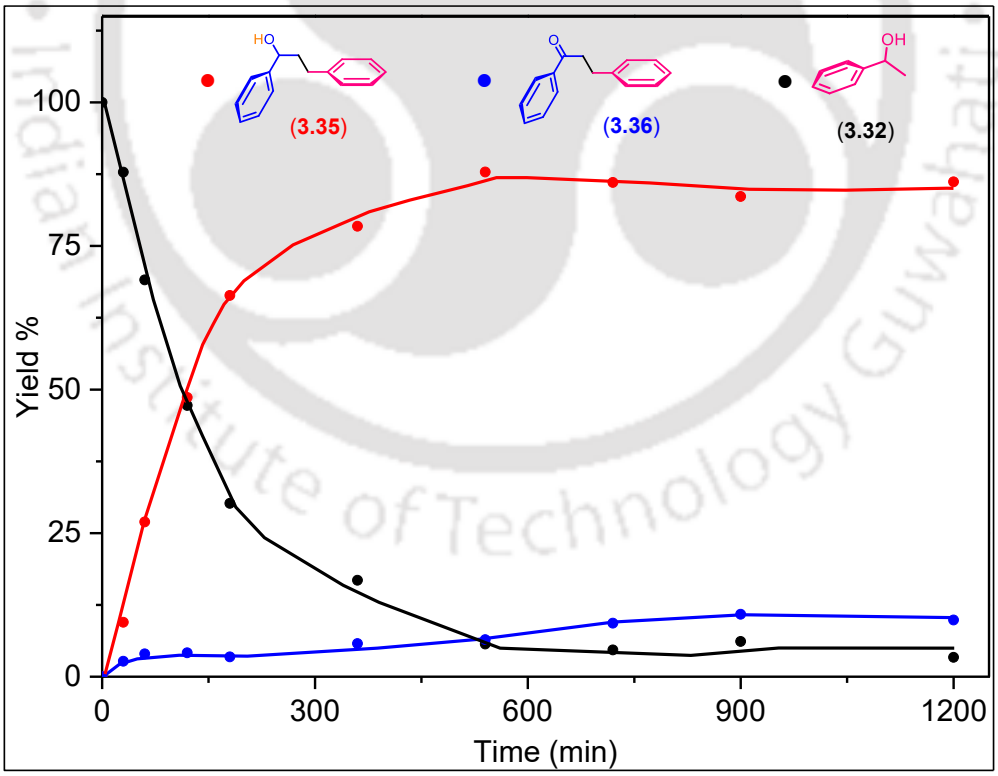

Figure 3.6: Time-course plot of *β*-alkylation of 1-phenyl ethanol **3.34** with benzyl alcohol **3.33** at 0.01 mol % loading of **3.31a** at 140 °C.

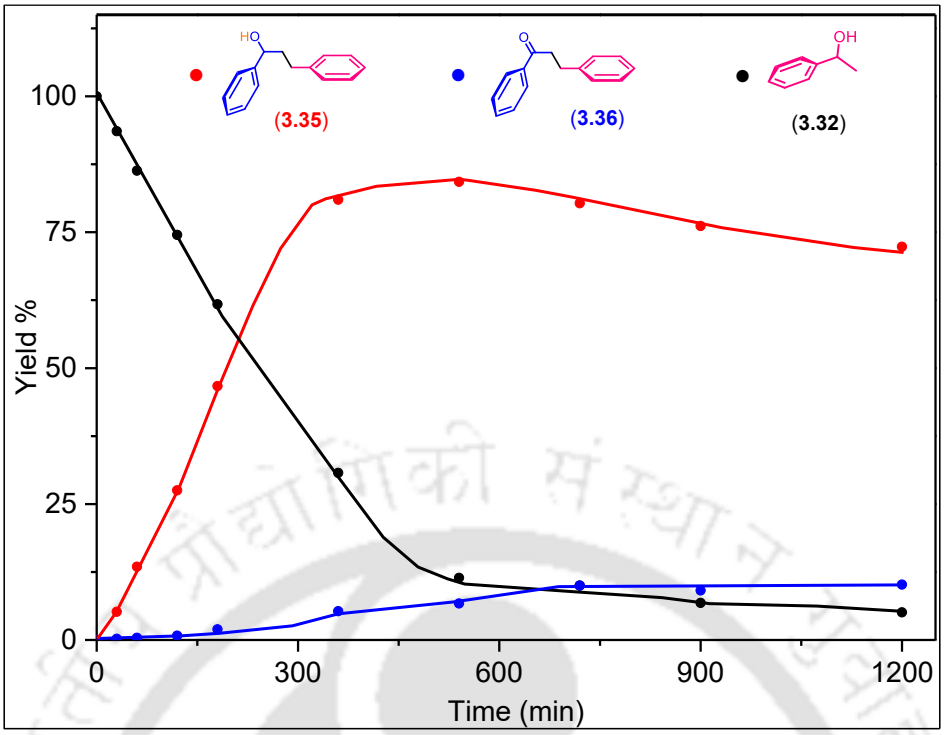

Figure 3.7: Time-course plot of *β*-alkylation of 1-phenyl ethanol **3.34** with benzyl alcohol **3.33** at 0.0025 mol % loading of **3.31a** at 140 °C.

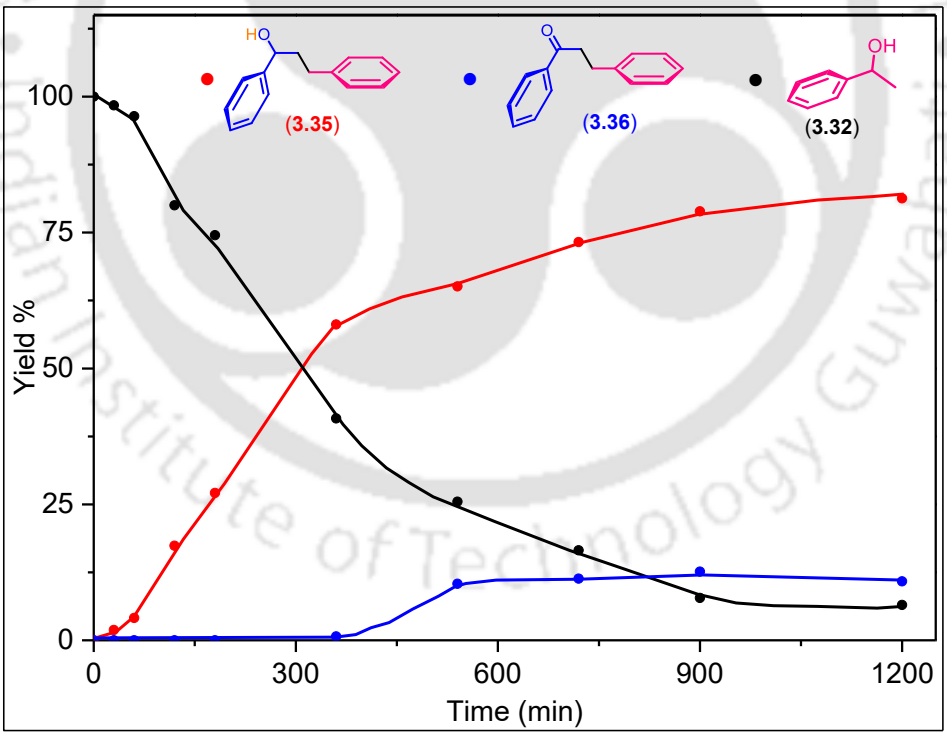

Figure 3.8: Time-course plot of *β*-alkylation of 1-phenyl ethanol **3.34** with benzyl alcohol **3.33** at 0.00025 mol % loading of **3.31a** at 140 °C.

This points to the fact that in the **3.31a** catalyzed *β*-alkylation of **3.34** with **3.33**, the hydrogenation and/or alcoholysis steps leading to both **3.35** and **3.36** are fast compared to dehydrogenation of **3.33** and **3.34** (Scheme **3.16-17** and mechanistic studies *vide-infra*).

This implies that the overall rate-determining step (RDS) is in the dehydrogenation segment (Scheme **3.16**, Figure **3.4-3.8** and mechanistic studies *vide-infra*). Nevertheless, the initial rate of catalysis was very high (12000 TO/h and 10972 TO/h) at 0.00025 mol % and 0.0025 mol % loading of **3.31a**, respectively (Figure **3.7** and **3.8**). Interestingly, according to the initial rate method, the plot of initial rate vs. [**3.31a**] was found to be linear indicative of the first-order dependence of the rate of the reaction on the catalyst concentration (Figure **3.9**).

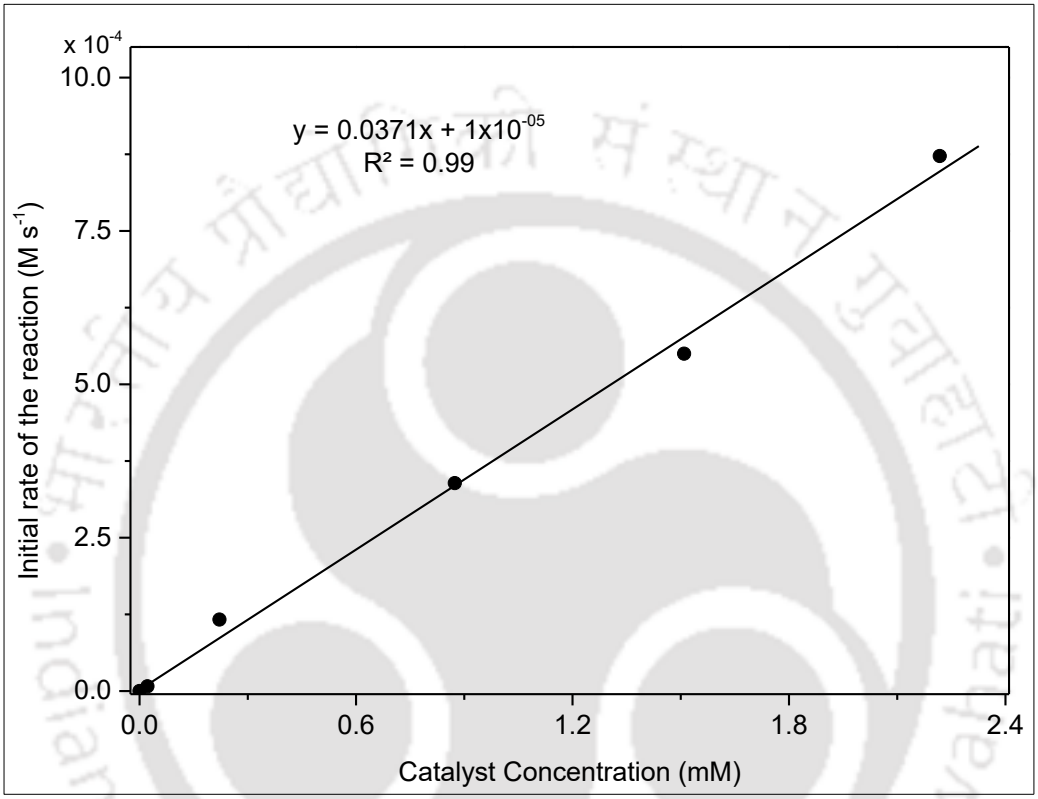

Figure 3.9: Plot of initial rate of the reaction *vs* catalyst concentration **3.31a** (0.022 to 2.2 mM) in the *β*-alkylation of 1-phenyl ethanol **3.34** with benzyl alcohol **3.33**.

The most efficient catalyst **3.31a** was selected for *β*-alkylation of substituted 1-phenyl ethanol with various benzyl alcohols using 2.5 mol % NaOH at 140 °C (Table **3.5**). Electron-donating groups such as methyl and methoxy either on benzyl alcohol or on 1-phenyl ethanol provided better yields of **3.35** (**3.35e**, **3.35f**, **3.35g**, **3.35h** and **3.35t**, Table **3.5**). On the other hand, substrates with electron-withdrawing groups gave poor results (**3.35b**, **3.35c**, **3.35d** and **3.35s**, Table **3.5**). These observations indicate that the C–H bond-breaking step (*β*-hydride elimination) is hampered by electron-withdrawing groups while being accelerated by electron-donating groups. This fortifies the fact that the overall RDS is present in the dehydrogenation segment (Scheme **3.16-17** and mechanistic studies *vide-infra*). The *β*-alkylation of 1-phenyl ethanol with aliphatic alcohols (**3.35p**, **3.35q**, **3.35r** and **3.35v**, Table **3.5**) and primary alcohols

containing heterocyclic groups (**3.35i**, **3.35j**, **3.35k**, **3.35l** and **3.35m**, Table **3.5**) proceeded with lower efficiency.

Table 3.5: *β*-Alkylation of Substituted 1-Phenyl Ethanol with Various Benzyl Alcohols Catalyzed by 0.00025 mol % of **3.31a**[a]

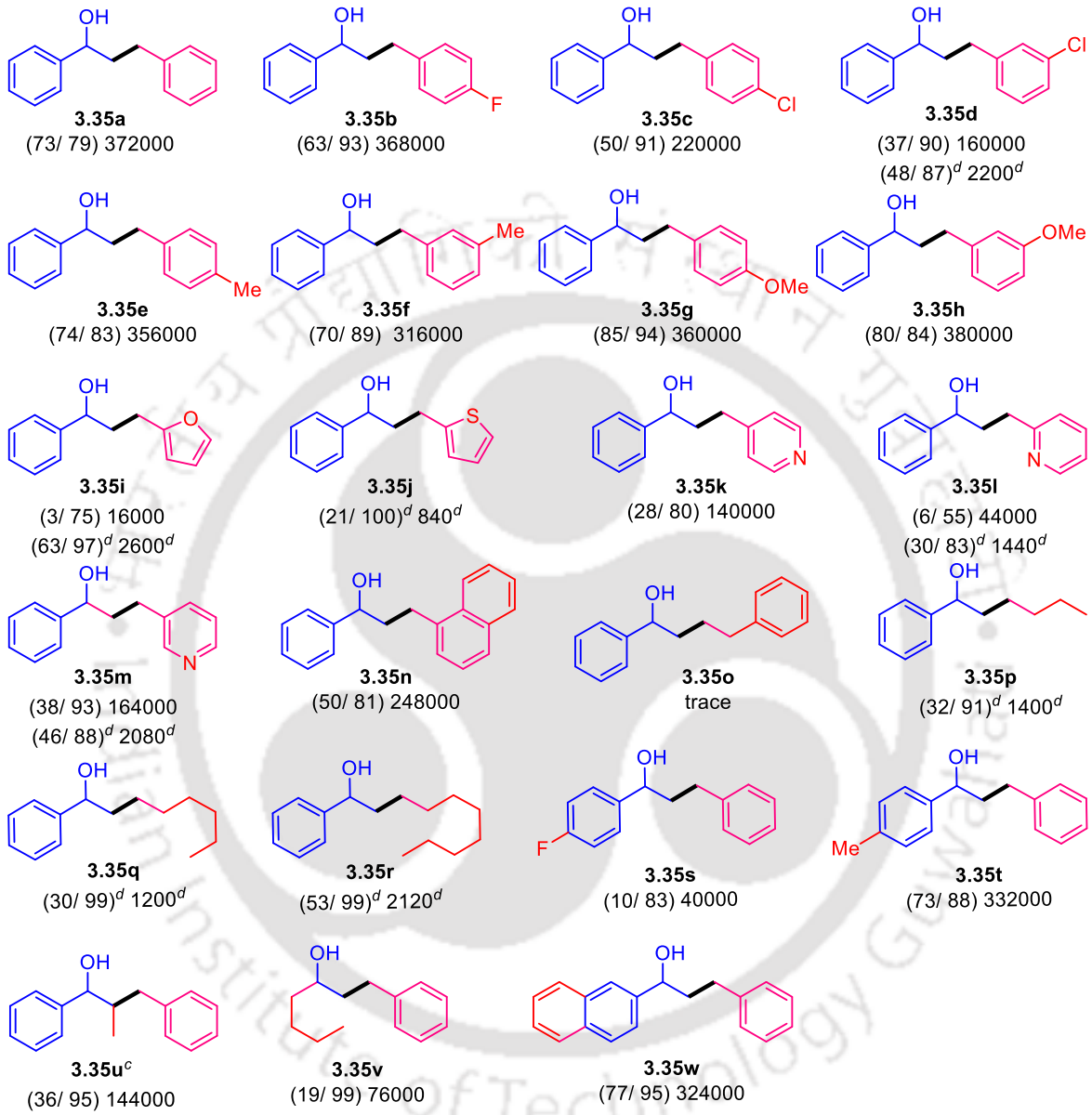

[a]Reaction Condition: Benzyl alcohol (4.25 mmol), 1-phenyl ethanol (4.25 mmol), **3.31a** (0.00025 mol %) and NaOH (5 mol %) heated at 140 °C for 20 h. [b]Yield was determined from ^{1}H NMR spectroscopy by using toluene as an internal standard [(% yield/ % selectivity) of **3.35**, total TON]. [c]Selectivity of **3.35** was calculated as: (Yield of **3.35**/Total yield) x 100. [c]Two diastereomer (52:48). [d]Reaction performed with 0.025 mol % of **3.31a**.

3.3.3 Mechanism of *β*-alkylation of Alcohols Catalyzed by 3.30 and 3.31.

In chapter **II** it has been shown that, benzaldehyde (**3.31′**) is formed in the **3.30d** catalyzed dehydrogenation of benzyl alcohol (**3.33**) along with the liberation of hydrogen (equation 1).[57] The catalytic intermediates were also identified (Scheme **3.16**). Similarly, one could expect the

formation of acetophenone (**3.34′**) starting from 1-phenyl ethanol (**3.34**). Several studies including those of Kundu[29, 31] and Ding[59] have shown that benzaldehyde (**3.33′**) reacts with acetophenone (**3.34′**) in the presence of a base to give the α,β-unsaturated ketone (**3.36′**) (equation 2).

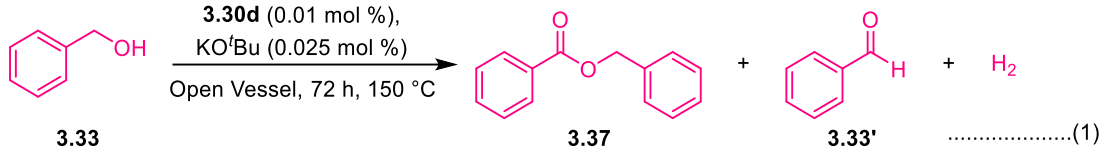

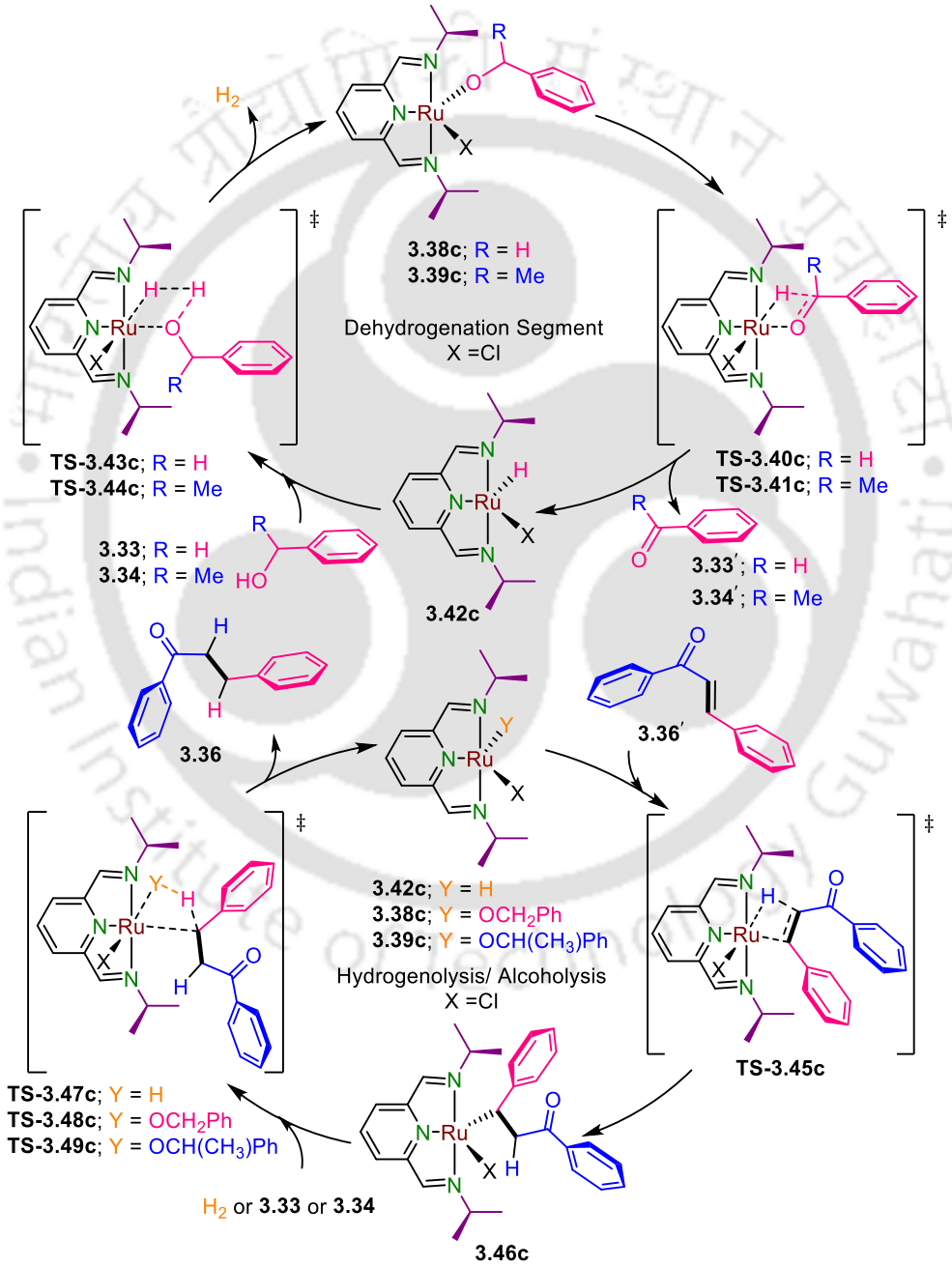

Scheme 3.16: Plausible mechanism involved catalytic dehydrogenation of alcohols and the formation of α-alkylated ketone.

The fact that we do not observe **3.36′** indicates its fast transformation to product **3.35** *via* **3.36** which is catalyzed by the NNN pincer-ruthenium catalysts (**3.30a-d** and **3.31a-d**). These observations form the basis of our proposed mechanism (Scheme **3.16-3.17**) using **3.30c/3.31c** as a model catalyst.

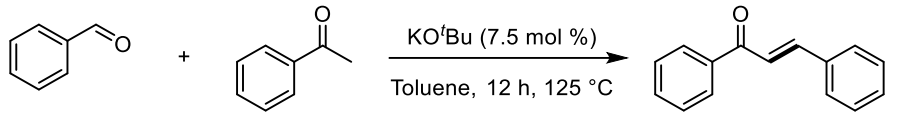

3.33' **3.34'** **3.36'** ..... (2)

The first step of the *β*-alkylation involves dissociation of either PPh_3[57] from **3.30c** or CO[60-64] from **3.31c** to generate the 16-electron five-coordinate dichloride species. In the presence of benzyl alcohol (**3.33**) and 1-phenyl ethanol (**3.34**), salt-metathesis of 16-electron five-coordinate dichloride species with KO^{t}Bu results in the formation of **3.38c** and **3.39c**, respectively.[57] A *β*-hydride elimination to give either benzaldehyde (**3.33′**) from **3.38c** or acetophenone (**3.34′**) from **3.39c** results in the formation of Ru–H species **3.42c** *via* **TS-3.40c** or **TS-3.41c**. This is followed by *σ*-bond metathesis between Ru–H of **3.42c** and O–H of **3.33/3.34** as in **TS-3.43c/3.44c** that results in the liberation of H_2 along with the regeneration of the active species **3.38c/3.39c** (Scheme **3.16**). The formation of **3.33′** and H_2 in these reactions has been recently reported by Kumar and co-workers.[57]

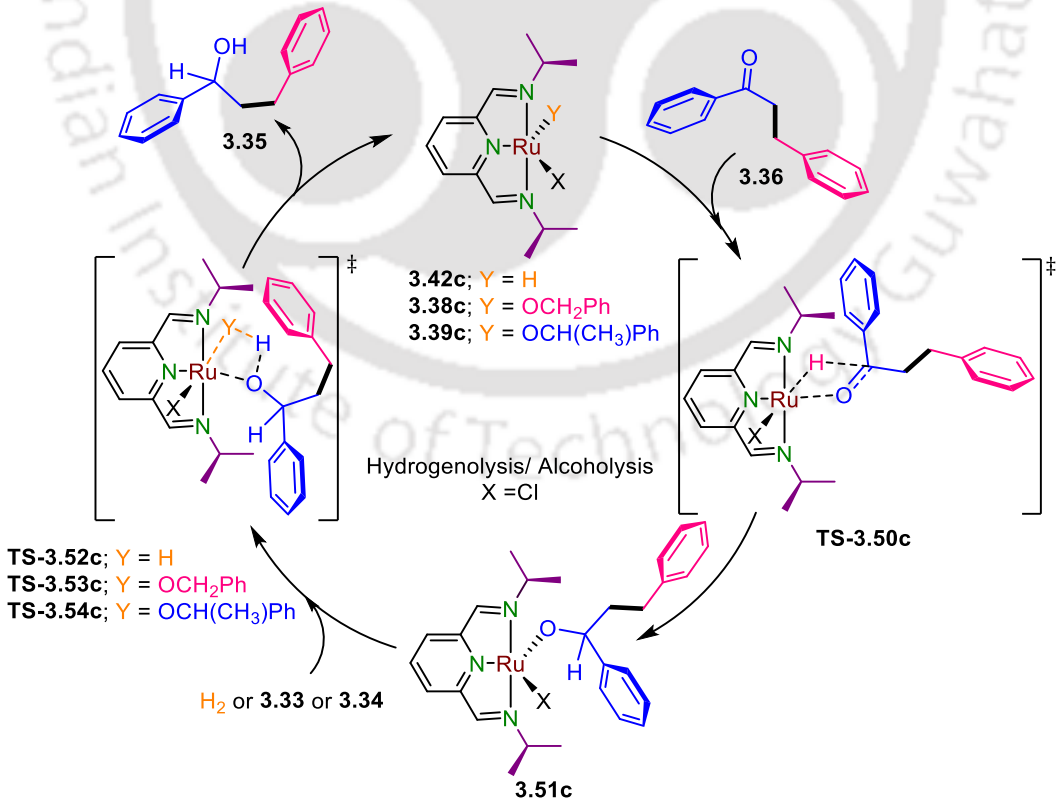

Scheme 3.17: Plausible mechanism involved in transformation of *α*-alkylated ketone to *β*-alkylated alcohol.

The benzaldehyde (**3.33′**) and acetophenone (**3.34′**) formed in the dehydrogenation segment, react with each other in the presence of a base to form the *α,β*-unsaturated ketone (**3.36′**) (equation 2). The C–C double bond in molecule **3.36′** undergoes insertion into the Ru–H bond in **3.42c** to generate the species **3.46c** *via* **TS-3.45c** (Scheme **3.16**).

Only the H^- transfer to the *α* carbon is considered owing to steric reasons. The product **3.36′** formation step along with the generation of catalytically active species **3.42c/3.38c/3.39c** could occur either by *σ*–bond metathesis between Ru–C of **3.46c** and O–H of **3.33/3.34** *via* **TS-3.48c/3.49c** (alcoholysis) or by *σ*-bond metathesis between Ru–C of **3.46c** and H–H while going through **TS-3.47c** (hydrogenolysis) (Scheme **3.16**). Similar hydrogenolysis and/or alcoholysis pathway can account for the transformation of **3.36** to **3.35** (Scheme **3.17**). Kinetic studies (Figure **3.4** to Figure **3.9**, *vide-supra*) indicate facile transformation of **3.36** to **3.35**.

3.3.4 Quantum Mechanical Calculations on the NNN Pincer-Ruthenium (3.30/3.31) Catalyzed *β*-Alkylation of Alcohols.

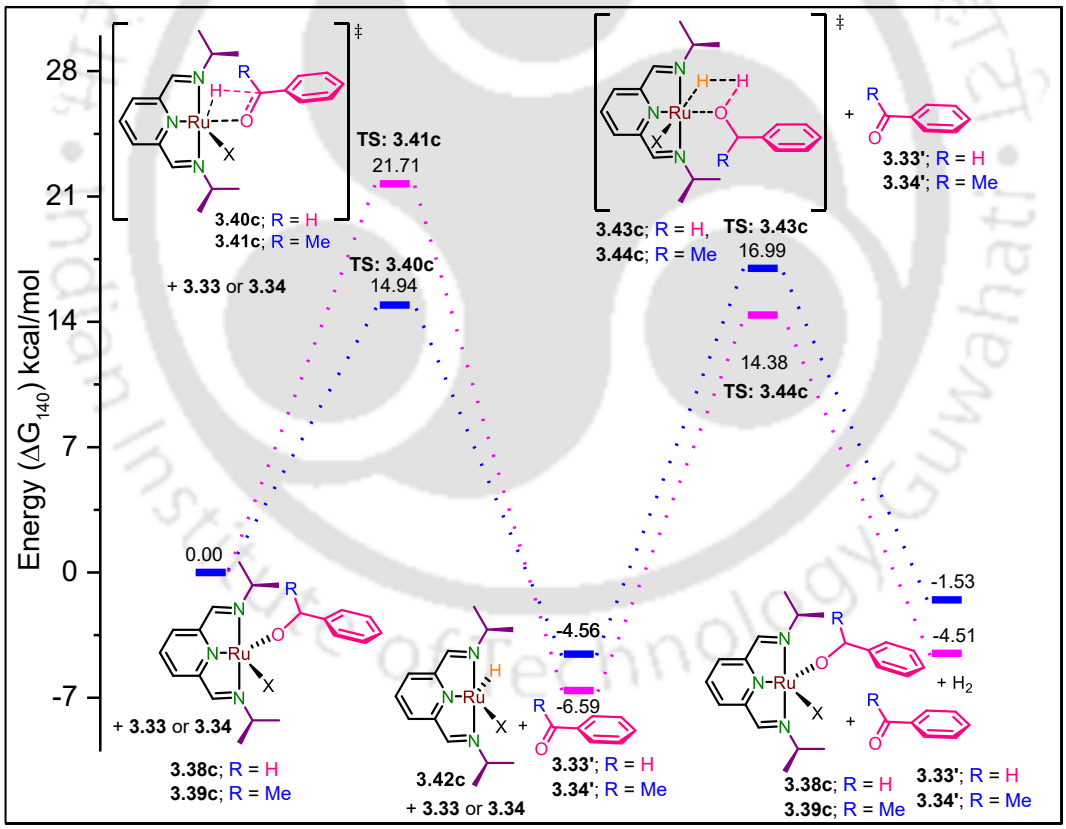

Figure 3.10: Relative free energies (140 °C) of intermediates involved in pincer-ruthenium **3.31a** catalyzed dehydrogenation of **3.33**/**3.34**.

Additional mechanistic information was obtained from DFT studies by modeling the various transition states (TSs) and intermediates involved in the pincer-ruthenium (**3.30c** and **3.31c**) catalyzed *β*-alkylation of **3.34** with **3.33** (Figure **3.10-3.12**). The formation of benzaldehyde

(**3.33′**) and the Ru–H species **3.42c** *via* *β*–hydride elimination from **3.38c** through **TS-3.40c** ($\Delta G^{\ddagger}_{140}$ = 14.94 kcal/mol) is a thermodynamically downhill process (ΔG_{140} = -4.56 kcal/mol) (blue lines, Figure. **3.10**). Interestingly the corresponding formation of acetophenone (**3.34′**) is also downhill (ΔG_{140} = -6.59 kcal/mol) but with a higher barrier (**TS-3.41c**, $\Delta G^{\ddagger}_{140}$ = 21.71 kcal/mol) (magenta lines, Figure **3.10**). The steps involving the *σ*-bond metathesis of Ru–H in **3.42c** with the O–H of **3.33** (blue dotted lines, Figure **3.10**) and with the O–H of **3.34** (magenta dotted lines, Figure **3.10**) are uphill (ΔG_{140} = 3.03 and 2.08 kcal/mol respectively) with almost similar barriers (**TS-3.43c**, $\Delta G^{\ddagger}_{140}$ = 21.55 kcal/mol and **TS-3.44c**, $\Delta G^{\ddagger}_{140}$ = 20.97 kcal/mol). For the dehydrogenation segment, the *β*-hydride elimination step involving the extrusion of acetophenone (**3.34′**) is the rate-determining step (RDS).

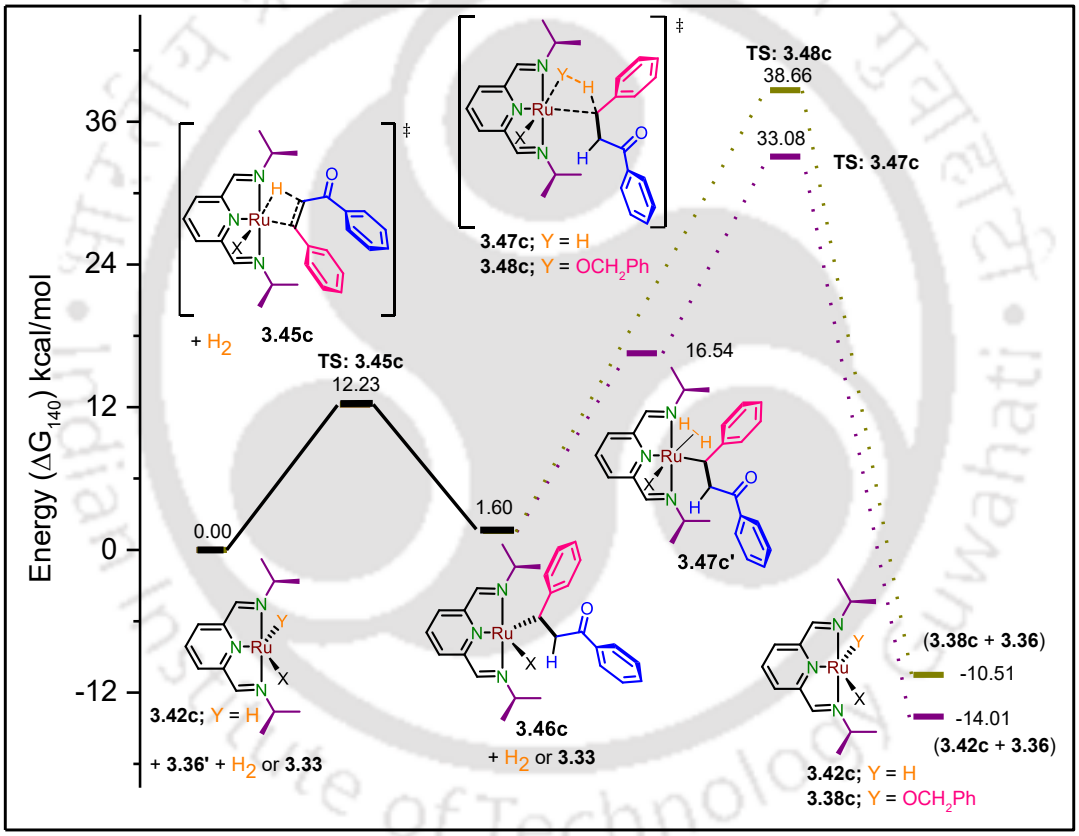

Figure 3.11: Relative free energies (140 °C) of intermediates involved in pincer-ruthenium **3.31a** catalyzed transformation of **3.36′** to **3.36**.

The insertion of the double bond in the *α*,*β*-unsaturated ketone (**3.36′**) into the Ru–H in **3.42c** to give species **3.46c** *via* **TS-3.45c** is slightly uphill (ΔG_{140} = 1.60 kcal/mol) with a barrier of 12.23 kcal/mol. In comparison to the alcoholysis step (olive dotted lines, Figure **3.11**), the hydrogenolysis step (purple dotted lines, Figure **3.11**) is more favorable as it is not only more downhill by 3.5 kcal/mol but also has a lower barrier (**TS-3.47c**, $\Delta G^{\ddagger}_{140}$ = 16.54 kcal/mol).

Thus, in the transformation of **3.36′** to **3.36**, the hydrogenolysis step is the preferred pathway and it is the RDS.

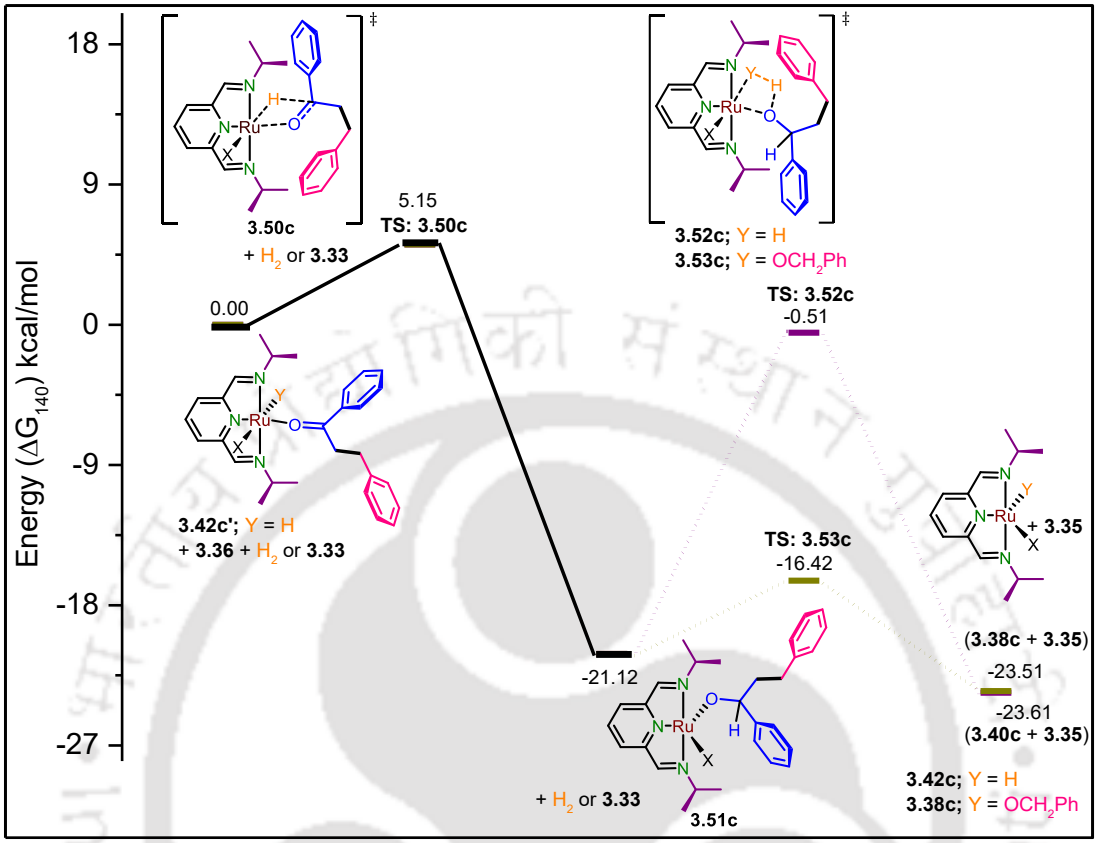

Figure 3.12: Relative free energies (140 °C) of intermediates involved in pincer-ruthenium **3.31a** catalyzed transformation of **3.36** to **3.35**.

The first step in the conversion of **3.36** to **3.35** that involves the insertion of the carbonyl group of **3.36** into Ru–H in **3.42c′** (Figure **3.12**) is a thermodynamically downhill process (ΔG_{140} = -21.12 kcal/mol) and proceeds with a low barrier (**TS-3.50c**, $\Delta G^{\ddagger}_{140}$ = 5.15 kcal/mol). The alcoholysis step (olive dotted lines, Figure **3.12**) is more favored than the hydrogenolysis step (purple dotted lines, Figure **3.12**) owing to its lower barrier (**TS-3.53c**, $\Delta G^{\ddagger}_{140}$ = 4.70 kcal/mol). The insertion of **3.36** into the Ru–H bond in **3.42c′** is the RDS for the conversion of **3.36** to **3.35**. For the **3.30c** and **3.31c** catalyzed *β*-alkylation, the *β*-hydride elimination step involving the extrusion of **3.36′** is the overall RDS ($\Delta G^{\ddagger}_{140}$ = 21.71 kcal/mol). This satisfactorily explains the absence of **3.36** during initial times in the *β*-alkylation (Figure **3.4** - **3.8**).

3.4 Conclusion

This chapter describes the synthesis and characterization of a series of phosphine-free NNN pincer-ruthenium carbonyl complexes based on *bis*(imino)pyridine ligands. These complexes have been utilized with great success to execute the catalytic alkylation of alcohols under

solvent-free conditions. For the *β*-alkylation of 1-phenyl ethanol with benzyl alcohol at 140 °C, (^{Cy2}NNN)RuCl$_2$(CO) (0.00025 mol %) in combination with NaOH (2.5 mol %) was found to be the most efficient among the considered catalysts. Gratifyingly, at such a low loading of the catalyst and the base, the *β*-alkylated product was obtained in high yield (ca. 93%, 372000 TON at 12000 TO/h) after 20 h. A variety of alcohol combinations could be *β*-alkylated by employing this catalytic system. Unprecedented activities (380000 TON at 19000 TO/h) were observed for the *β*-alkylation of 1-phenyl ethanol with 3-methoxy benzyl alcohol. Hitherto, this is the highest reported rate and turnover for a ruthenium-based catalyst. Mechanistic studies provide key information about the presence of the overall rate-determining step (RDS) in the dehydrogenation segment. Complementary evidence was obtained from DFT studies that indicate the *β*-hydride elimination step involving the extrusion of acetophenone is the overall RDS. While the hydrogenolysis is favored for the formation of *α*-alkylated ketone, the alcoholysis step is preferred for the formation of the *β*-alkylated product.

3.5 Experimental Section

3.5.1 General methods and materials

All optimizations were carried out under purified argon using a standard double manifold or a glove box. The solvents such as tetrahydrofuran (THF), hexane and toluene were dried *via* double distillation over Na/Benzophenone prior to the experiment.[65-66] All other compounds including pryidine-2,6-dicarboxylic acid, [RuCl$_2$(*p*-cymene)]$_2$, and CDCl$_3$ were purchased either from MERCK or Sigma-Aldrich and were used as such. The complexes (**3.30a–d**) were prepared according to the protocol reported in Chapter **II**.[56, 67]

^{1}H, ^{13}C NMR spectra were recorded either on Bruker ASCEND 600 operating at 600 MHz for ^{1}H, 150 MHz for ^{13}C or on Bruker AVANCE 400 operating at 400 MHz for ^{1}H, 100 MHz for ^{13}C. The mass analysis was done using an Agilent Accurate-Mass Q-Toff ESI-MS 6520. Fourier Transform Infrared (FT-IR) were recorded on Perkin Elmer Spectrum Two FT-IR spectrometer at room temperature within the region 400-4000 cm^{-1}. X–ray crystallographic data were collected on Bruker Nonius Smart Apex III X–ray single crystal diffractometer (CCD) with graphite -monochromatized Mo–Kα radiation. The data refinements and cell reduction were carried out using Bruker Apex III program. Structures were solved and further refined by full matrix least-squares method using SHELXS–14.[68]

3.5.2 Synthesis of complexes of the type (^{R2}NNN)RuCl$_2$(CO) (3.31a; R = Cy, 3.31b; R = Ph, 3.31c; R = ^{i}Pr, and 3.31d; R = ^{t}Bu).

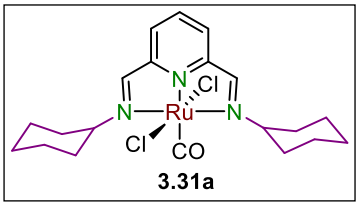

3.31a

Synthesis of (^{Cy2}NNN)RuCl$_2$(CO) (3.31a): In a two-neck round bottom flask (25 mL), the ligand **3.32a** (0.030 g 0.100 mmol) and [RuCl$_2$(*p*-Cymene)]$_2$ (0.031 g, 0.050 mmol) were taken in dry THF (5 mL) under argon atmosphere. The reaction mixture was heated at 60 °C for 2 h under argon atmosphere. Subsequently, the reaction mixture was further heated for another 10 h under an atmosphere of CO. The color of the reaction mixture changed from brown to dark greenish brown. This was followed by solvent evaporation to yield a dark green color solid which was washed by dry diethyl ether (3 x 5 mL) followed by hexane (2 x 5 mL) to yield 0.042 g of **3.31a** as a green color solid in 85% yield. ^{1}H NMR (600 MHz, CDCl$_3$): δ = 8.09 (s, 2H, N=C*H*), 7.88 (t, *J* = 7.7 Hz, 1H, Ar), 7.67 (d, *J* = 7.8 Hz, 2H, Ar), 3.62 (t, *J* = 11.2 Hz, 2H, NC*H*(CH$_2$)$_5$), 2.07 – 1.23 (m, 20H, NCH(C*H*$_2$)$_5$). ^{13}C NMR (151 MHz, CDCl$_3$): δ = 205.21 (*C*≡O), 161.03 (N=*C*H), 155.99, 138.84, 123.97 (Ar), 75.94 (N*C*H(CH$_2$)$_5$), 33.44, 25.37, 25.02 (NCH(*C*H$_2$)$_5$). HRMS (ESI): *m/z* calculated for [C$_{20}$H$_{27}$ClN$_3$ORu]$^+$; = 462.0918, Found = 462.0907; *m/z* calculated for [C$_{22}$H$_{31}$ClN$_4$ORu]$^+$; = 503.1184, Found = 503.1164. IR (cm^{-1}): ν = 2924, 2853, 2056, 1944 (s), 1936 (s), 1739, 1606, 1542, 1461, 1449, 1425, 1345, 1261, 1161, 1149, 1085, 1075, 1056, 1025, 972, 891, 856, 803, 753, 699, 686, 559, 523, 517, 488, 471, 435.

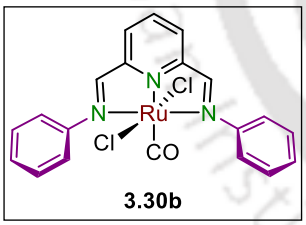

3.30b

Synthesis of (^{Ph2}NNN)RuCl$_2$(CO) (3.31b) complex: In a two-neck round bottom flask (25 mL), the ligand **3.32b** (0.030 g 0.10 mmol) and [RuCl$_2$(*p*-Cymene)]$_2$ (0.032 g, 0.05 mmol) were taken in dry THF (5 mL) under argon atmosphere. The reaction mixture was heated at 60 °C for 2 h under argon atmosphere. Subsequently, the reaction mixture was further heated for another 10 h under an atmosphere of CO. The color of the reaction mixture changed from light brown to dark brown. This was followed by solvent evaporation to yield a dark brown color solid which was washed by dry diethyl ether (3 x 5 mL) followed by hexane (2 x 5 mL) to yield 0.041 g of **3.31b** as a brown color solid in 81% yield. Low solubility posed challenges in NMR characterization. HRMS (ESI): *m/z* calculated for [C$_{20}$H$_{15}$ClN$_3$ORu]$^+$; = 449.9947, Found = 449.9998. IR (cm^{-1}): ν = 3060, 2866, 2977, 2062, 1954 (s), 1604, 1584, 1523, 1485, 1453, 1417, 1348, 1315, 1271, 1191, 1163, 1075, 1064, 1053, 1027, 1001, 938, 917, 904, 800, 763, 748, 697, 597, 579, 564, 542, 506, 461, 432.

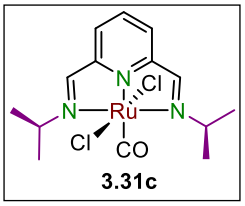

3.31c

Synthesis of (^{iPr2}NNN)RuCl$_2$(CO) (3.31c) complex: In a two-neck round bottom flask (25 mL), the ligand **3.32c** (0.030 g 0.13 mmol) and [RuCl$_2$(*p*-Cymene)]$_2$ (0.043 g, 0.07 mmol) were taken in dry THF (5 mL) under argon atmosphere. The reaction mixture was heated at 60 °C for 2 h under argon atmosphere. Subsequently, the reaction mixture was further heated for another 10 h under an atmosphere of CO. The color of the reaction mixture changed from brown to dark greenish brown. This was followed by solvent evaporation to yield a dark brown color solid which was washed by dry diethyl ether (3 x 5 mL) followed by hexane (2 x 5 mL) to yield 0.047 g of **3.31c** as a greenish color solid in 80% yield. ^{1}H NMR (400 MHz, CDCl$_3$): δ = 8.14 (s, 2H, N=C*H*), 7.93 (t, *J* = 7.9 Hz, 1H, Ar), 7.70 (d, *J* = 7.9 Hz, 2H, Ar), 4.03 (septet, *J* = 6.4 Hz, 2H, NC*H*(CH$_3$)$_2$), 1.51 (d, *J* = 6.4 Hz, 12H, NCH(C*H*$_3$)$_2$). ^{13}C NMR (101 MHz, CDCl$_3$): δ = 205.10 (*C*≡O), 161.05 (N=*C*H), 156.03, 138.94, 124.10 (Ar), 68.26 (N*C*H(CH$_3$)$_2$), 23.17 (NCH(*C*H$_3$)$_2$). HRMS (ESI): *m/z* calculated for [C$_{14}$H$_{19}$ClN$_3$ORu]$^+$; = 382.0292, Found = 382.0283; *m/z* calculated for [C$_{16}$H$_{22}$ClN$_4$ORu]$^+$; = 423.0558, Found = 423.0556. IR (cm^{-1}): ν = 2987, 2987, 2973, 2931, 2895, 2059, 1995, 1952 (s), 1604, 1469, 1447, 1423, 1398, 1382, 1367, 1327, 1273, 1163, 1144, 1121, 934, 913, 810, 797, 751, 606, 570, 482, 446.

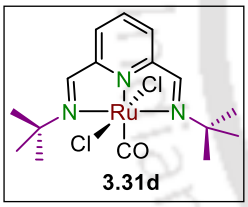

3.31d

Synthesis of (^{tBu2}NNN)RuCl$_2$(CO) (3.31d) complex: In a two-neck round bottom flask (25 mL), the ligand **3.32d** (0.025 g 0.10 mmol) and [RuCl$_2$(*p*-Cymene)]$_2$ (0.031 g, 0.05 mmol) were taken in dry THF (5 mL) under argon atmosphere. The reaction mixture was heated at 60 °C for 2 h under argon atmosphere. Subsequently, the reaction mixture was further heated for another 10 h under an atmosphere of CO. The color of the reaction mixture changed from brown to dark greenish brown. This was followed by solvent evaporation to yield a dark brown color solid which was washed by dry diethyl ether (3 x 5 mL) followed by hexane (2 x 5 mL) to yield 0.036 g of **3.31d** as a yellowish-brown color solid in 80% yield. ^{1}H NMR (400 MHz, CDCl$_3$): δ = 8.07 (s, 1H, N=C*H*), 8.02 (s, 1H, N=C*H*), 7.97 – 7.87 (m, 1H, Ar), 7.74 (dd, *J* = 16.4, 7.9 Hz, 2H, Ar), 1.61 (s, 9H, NC(C*H*$_3$)$_3$), 1.52 (s, 9H, NC(C*H*$_3$)$_3$). ^{13}C NMR (101 MHz, CDCl$_3$): δ = 207.24 (*C*≡O), 161.20, 160.27 (N=*C*H), 159.13, 156.36, 138.99, 136.28, 126.25, 124.89 (Ar), 68.27, 68.13 (N*C*(CH$_3$)$_3$), 29.91, 29.58 (NC(*C*H$_3$)$_3$). HRMS (ESI): *m/z* calculated for [C$_{16}$H$_{23}$ClN$_3$ORu]$^+$ Calculated = 410.0605, Found = 410.0610; *m/z* calculated for [C$_{18}$H$_{26}$ClN$_4$ORu]$^+$ Calculated = 451.0871, Found = 451.0877. IR (cm^{-1}): ν = 2974, 2930, 2869, 2057, 1995, 1934 (s), 1602, 1584, 1462, 1424, 1395, 1372, 1237, 1191, 1157, 1072, 1039, 1026, 928, 808, 774, 753, 610, 585, 574, 507, 484, 407.

3.5.3 General procedure of β-alkylation of secondary alcohol with primary alcohol

In a 25 mL two neck round bottom flask, 1-phenyl ethanol or benzyl alcohol were taken under argon atmosphere. This was followed by addition of 2.5 mol % of NaOH and 0.00025 mol % of **3.31a** (from a stock solution either in 1-phenyl ethanol or benzyl alcohol). After the addition, the reaction mixture contained 0.5 mL (4.14 mmol) of 1-phenyl ethanol, 0.43 mL (4.14 mmol) of benzyl alcohol, 8 mg (0.21 mmol) of NaOH and 1 mg (20 μmol) of **3.31a**. The mixture was heated at 140 °C for 20 h under Argon. The reaction mixture was then cooled to room temperature followed by addition of toluene as an internal standard. The yield of products were determined from ^{1}H NMR spectroscopy by using toluene as an internal standard.

3.5.4 Computational details

The geometries of all the considered complexes were fully optimized using the DFT (PBEPBE)[69] method on the Gaussian-16 program package.[70] The LANL2DZ[71-73] and 6-311G(d,p) basis set with a polarization function were used respectively for the metal (Ru) and non-metal atoms. The empirical dispersion-GD3 was used in all molecular geometry optimization and energy computations. The transition states were located using the synchronous transit-guided quasi-Newton (QST2) Genecp (gen keyword with the effective core potential) was included to define the basis set. Method and basis set was selected on the basis of previous reports on pincer complexes. Frequency calculations characterize the obtained stationary points as minima structures or transition states based on the number of imaginary frequencies. Single point calculations were performed to calculate the relative free energy values at 110 °C.

Table 3.6: Crystallographic data of complexes **3.31a** and **3.31c**

Name	(^{Cy}NNN)Ru(CO) **3.31a**	(^{iPr}NNN)Ru(CO) **3.31c**
CCDC	1986710	1986711
Empirical formula	$C_{43}H_{60}Cl_4N_6O_5Ru_2$	$C_{28}H_{42}Cl_4N_6O_4Ru_2$
Formula weight	1084.91	870.62
Crystal size (mm^3)	0.30 x 0.27 x 0.24	0.29 x 0.27 x 0.22
Crystal system	Monoclinic	Monoclinic
Space group	$P2_1/n$	$P2_1/c$
a (Å)	12.5516 (9)	9.2306 (5)
b (Å)	23.6644 (17)	10.8103 (6)
c (Å)	16.9746 (12)	18.2416 (10)
α (deg)	90.00	90.00
β (deg)	94.021 (2)	96.278 (2)
γ (deg)	90.00	90.00
V ($Å^3$)	5029.5 (6)	1809.33 (17)
Z	4	2
ρ_{calc} (g cm^{-3})	1.433	1.598
μ (M_0 Kα) (mm^{-1})	0.859	1.170
F (000)	2178.0	880.0
T(K)	296(2)	296(2)
Range of indices (h; k; l)	-13, 13; -25, 25; -18, 18	-7, 7; -9, 9; -15, 15
Number of reflections collected	137658	30846
Unique reflection	6967	1135
Completeness to 2θ	99.9	99.6
R_{int}	0.1274	0.2104
Data / restraints / parameters	6967/0/544	1135/0/206
goodness-of-fit	1.286	0.547
$R_1[I \geq 2\sigma(I)]$	0.0580	0.0312
$wR_2[I \geq 2\sigma(I)]$	0.0977	0.0745
R_1 (all data)	0.0796	0.0335
wR_2 (all data)	0.1087	0.0811
Δ_r (max, min) e $Å^{-3}$	0.71/-0.54	0.32/-0.59

Supporting information (containing the NMR spectra of various compounds, IR, HRMS, kinetic data and Cartesian coordinates of the computed complexes) for chapter **III** is available as appendix **II** and can be found at

https://drive.google.com/file/d/1X7JRlSmfIlof5NVGMfEf2g-zNxTkNJsc/view?usp=sharing

3.6 References

1. DeJong, W.; Wallack, L., *Health Educ. Q.* **1992**, *19*, 429-442.
2. Casswell, S.; Thamarangsi, T., *Lancet* **2009**, *373*, 2247-2257.
3. Xu, Q.; Chen, J.; Liu, Q., *Adv. Synth. Catal.* **2013**, *355*, 697-704.
4. Xu, Q.; Chen, J.; Tian, H.; Yuan, X.; Li, S.; Zhou, C.; Liu, J., *Angew. Chem., Int. Ed.* **2014**, *53*, 225-229.
5. Allen, L. J.; Crabtree, R. H., *Green Chem.* **2010**, *12*, 1362.
6. Wang, Q.; Wu, K.; Yu, Z., *Organometallics* **2016**, *35*, 1251-1256.
7. Makarov, I. S.; Madsen, R., *J. Org. Chem.* **2013**, *78*, 6593-6598.
8. Liao, S.; Yu, K.; Li, Q.; Tian, H.; Zhang, Z.; Yu, X.; Xu, Q., *Org. Biomol. Chem.* **2012**, *10*, 2973-2978.
9. Li, Q.; Fan, S.; Sun, Q.; Tian, H.; Yu, X.; Xu, Q., *Org. Biomol. Chem.* **2012**, *10*, 2966-2972.
10. Feng, S. L.; Liu, C. Z.; Li, Q.; Yu, X. C.; Xu, Q., *Chin. Chem. Lett.* **2011**, *22*, 1021-1024.
11. Liu, C.; Liao, S.; Li, Q.; Feng, S.; Sun, Q.; Yu, X.; Xu, Q., *J. Org. Chem.* **2011**, *76*, 5759-5773.
12. Sahoo, A. R.; Lalitha, G.; Murugesh, V.; Bruneau, C.; Sharma, G. V. M.; Suresh, S.; Achard, M., *J. Org. Chem.* **2017**, *82*, 10727-10731.
13. Zhang, C.; Zhao, J.-P.; Hu, B.; Shi, J.; Chen, D., *Organometallics* **2019**, *38*, 654-664.
14. Shi, J.; Hu, B.; Ren, P.; Shang, S.; Yang, X.; Chen, D., *Organometallics* **2018**, *37*, 2795.
15. Deng, D.; Hu, B.; Yang, M.; Chen, D., *Organometallics* **2018**, *37*, 2386.
16. Cho, C. S.; Kim, B. T.; Kim, H.-S.; Kim, T.-J.; Shim, S. C., *Organometallics* **2003**, *22*, 3608-3610.
17. Ruiz-Botella, S.; Peris, E., *Chem. Eur. J.* **2015**, *21*, 15263-15271.
18. Jiménez, M. V.; Fernández-Tornos, J.; Modrego, F. J.; Pérez-Torrente, J. J.; Oro, L. A., *Chem. Eur. J.* **2015**, *21*, 17877-17889.
19. Xu, C.; Goh, L. Y.; Pullarkat, S. A., *Organometallics* **2011**, *30*, 6499-6502.
20. Segarra, C.; Mas-Marzá, E.; Mata, J. A.; Peris, E., *Adv. Synth. Catal.* **2011**, *353*, 2078-2084.
21. Gong, X.; Zhang, H.; Li, X., *Tetrahedron Lett.* **2011**, *52*, 5596-5600.
22. Gnanamgari, D.; Sauer, E. L. O.; Schley, N. D.; Butler, C.; Incarvito, C. D.; Crabtree, R. H., *Organometallics* **2009**, *28*, 321-325.
23. da Costa, A. P.; Sanaú, M.; Peris, E.; Royo, B., *Dalton Trans.* **2009**, 6960-6966.
24. Pontes da Costa, A.; Viciano, M.; Sanaú, M.; Merino, S.; Tejeda, J.; Peris, E.; Royo, B., *Organometallics* **2008**, *27*, 1305-1309.
25. Gnanamgari, D.; Leung, C. H.; Schley, N. D.; Hilton, S. T.; Crabtree, R. H., *Org. Biomol. Chem.* **2008**, *6*, 4442-4445.
26. Fujita, K.-i.; Asai, C.; Yamaguchi, T.; Hanasaka, F.; Yamaguchi, R., *Org. Lett.* **2005**, *7*, 4017-4019.
27. Satyanarayana, P.; Reddy, G. M.; Maheswaran, H.; Kantam, M. L., *Adv. Synth. Catal.* **2013**, *355*, 1859-1867.
28. Roy, B. C.; Debnath, S.; Chakrabarti, K.; Paul, B.; Maji, M.; Kundu, S., *Org. Chem. Front.* **2018**, *5*, 1008-1018.
29. Roy, B. C.; Chakrabarti, K.; Shee, S.; Paul, S.; Kundu, S., *Chem. Eur. J.* **2016**, *22*, 18147-18155.
30. Shee, S.; Paul, B.; Panja, D.; Roy, B. C.; Chakrabarti, K.; Ganguli, K.; Das, A.; Das, G. K.; Kundu, S., *Adv. Synth. Catal.* **2017**, *359*, 3888-3893.

31. Chakrabarti, K.; Paul, B.; Maji, M.; Roy, B. C.; Shee, S.; Kundu, S., *Org. Biomol. Chem.* **2016**, *14*, 10988-10997.
32. Prades, A.; Viciano, M.; Sanaú, M.; Peris, E., *Organometallics* **2008**, *27*, 4254-4259.
33. Kose, O.; Saito, S., *Org. Biomol. Chem.* **2010**, *8*, 896-900.
34. Liu, T.; Wang, L.; Wu, K.; Yu, Z., *ACS Catal.* **2018**, *8*, 7201-7207.
35. El-Sepelgy, O.; Matador, E.; Brzozowska, A.; Rueping, M., *ChemSusChem* **2019**, *12*, 3099-3102.
36. Freitag, F.; Irrgang, T.; Kempe, R., *Chem. Eur. J.* **2017**, *23*, 12110-12113.
37. Yang, J.; Liu, X.; Meng, D. L.; Chen, H. Y.; Zong, Z. H.; Feng, T. T.; Sun, K., *Adv. Synth. Catal.* **2012**, *354*, 328.
38. Zhang, M.-J.; Li, H.-X.; Young, D. J.; Li, H.-Y.; Lang, J.-P., *Org. Biomol. Chem.* **2019**, *17*, 3567-3574.
39. Gladiali, S.; Alberico, E., *Chem. Soc.Rev.* **2006**, *35*, 226-236.
40. Genç, S.; Arslan, B.; Gülcemal, S.; Günnaz, S.; Çetinkaya, B.; Gülcemal, D., *J. Org. Chem.* **2019**, *84*, 6286-6297.
41. Kaur, M.; U Din Reshi, N.; Patra, K.; Bhattacherya, A.; Kunnikuruvan, S.; Bera, J. K., *Chem. Eur. J.* **2021**, *27*, 10737-10748.
42. Musa, S.; Ackermann, L.; Gelman, D., *Adv. Synth. Catal.* **2013**, *355*, 3077-3080.
43. Czap, A.; Heinemann, F. W.; van Eldik, R., *Inorg. Chem.* **2004**, *43*, 7832-7843.
44. Che, C.-M.; Ho, C.; Lau, T.-C., *J. Chem. Soc. Dalton Trans.* **1991**, 1901-1907.
45. Wei, C.; He, Y.; Shi, X.; Song, Z., *Coord. Chem. Rev.* **2019**, *385*, 1-19.
46. Busschaert, N.; Wenzel, M.; Light, M. E.; Iglesias-Hernández, P.; Pérez-Tomás, R.; Gale, P. A., *J. Am. Chem. Soc.* **2011**, *133*, 14136-14148.
47. Du, W.; Wang, Q.; Wang, L.; Yu, Z., *Organometallics* **2014**, *33*, 974-982.
48. Friedman, L.; Shechter, H., *J. Org. Chem.* **1960**, *25*, 877-879.
49. Cook, F. L.; Bowers, C. W.; Liotta, C. L., *J. Org. Chem.* **1974**, *39*, 3416-3418.
50. Prakasham, A. P.; Ta, S.; Dey, S.; Ghosh, P., *Dalton Trans.* **2021**, *50*, 15640-15654.
51. Ding, X.; Wang, H.; Wang, J.; Wang, S.; Lin, D.; Lv, L.; Zhou, Y.; Luo, X.; Jiang, H.; Aceña, J. L.; Soloshonok, V. A.; Liu, H., *Amino Acids* **2013**, *44*, 791-6.
52. Smith, M. B., *March's advanced organic chemistry: reactions, mechanisms, and structure*. John Wiley & Sons: **2020**.
53. Jung, M. E., in *Comprehensive Organic Synthesis*; Trost, B. M.; Fleming, I. Eds.; Pergamon: Oxford, **1991**, 1.
54. Haraguchi, R.; Takada, Y.; Matsubara, S., *Org. Biomol. Chem.* **2015**, *13*, 241-247.
55. Kaithal, A.; Gracia, L.-L.; Camp, C.; Quadrelli, E. A.; Leitner, W., *J. Am. Chem. Soc.* **2019**, *141*, 17487-17492.
56. Das, K.; Dutta, M.; Das, B.; Srivastava, H. K.; Kumar, A., *Adv. Synth. Catal.* **2019**, *361*, 2965-2980.
57. Das, K.; Nandi, P. G.; Islam, K.; Srivastava, H. K.; Kumar, A., *Eur. J. Org. Chem.* **2019**, *2019*, 6855-6866.
58. Pansuriya, P. B.; Maguire, G. E. M.; Friedrich, H. B., *J. Therm. Anal. Calorim.* **2016**, *124*, 269-278.
59. Pandey, B.; Xu, S.; Ding, K., *Org. Lett.* **2019**, *21*, 7420-7423.
60. Heinemann, S. H.; Hoshi, T.; Westerhausen, M.; Schiller, A., *Chem. Commun.* **2014**, *50*, 3644-3660.
61. Kautz, A. C.; Kunz, P. C.; Janiak, C., *Dalton Trans.* **2016**, *45*, 18045-18063.
62. Meyer, H.; Brenner, M.; Höfert, S.-P.; Knedel, T.-O.; Kunz, P. C.; Schmidt, A. M.; Hamacher, A.; Kassack, M. U.; Janiak, C., *Dalton Trans.* **2016**, *45*, 7605-7615.
63. Xiao, Z.; Jiang, R.; Jin, J.; Yang, X.; Xu, B.; Liu, X.; He, Y.; He, Y., *Dalton Trans.* **2019**, *48*, 468-477.

64. Warner, M. C.; Verho, O.; Bäckvall, J.-E., *J. Am. Chem. Soc.* **2011**, *133*, 2820-2823.
65. Armarego, W. L. F.; Chai, C., Chapter 4 - Purification of Organic Chemicals. In *Purification of Laboratory Chemicals (Seventh Edition)*, Armarego, W. L. F.; Chai, C., Eds. Butterworth-Heinemann: Boston, **2013**; pp 103-554.
66. Armarego, W. L. F.; Chai, C., Chapter 5 - Purification of Inorganic and Metal-Organic Chemicals. In *Purification of Laboratory Chemicals (Seventh Edition)*, Armarego, W. L. F.; Chai, C., Eds. Butterworth-Heinemann: Boston, **2013**; pp 555-661.
67. Mishra, D.; Naskar, S.; Chattopadhyay, S. K.; Maji, M.; Sengupta, P.; Dinda, R.; Ghosh, S.; Mak, T. C. W., *Transition Met. Chem.* **2005**, *30*, 352-356.
68. Sheldrick, G. M., *Acta Cryst.* **2015**, *71*, 3-8.
69. Perdew, J. P.; Burke, K.; Ernzerhof, M., *Phys. Rev. Lett.* **1996**, *77*, 3865-3868.
70. Gaussian 16, R. C., M. J. Frisch, G. W. Trucks, H. B. Schlegel, G. E. Scuseria, M. A. Robb, J. R. Cheeseman, G. Scalmani, V. Barone, G. A. Petersson, H. Nakatsuji, X. Li, M. Caricato, A. V. Marenich, J. Bloino, B. G. Janesko, R. Gomperts, B. Mennucci, H. P. Hratchian, J. V. Ortiz, A. F. Izmaylov, J. L. Sonnenberg, D. Williams-Young, F. Ding, F. Lipparini, F. Egidi, J. Goings, B. Peng, A. Petrone, T. Henderson, D. Ranasinghe, V. G. Zakrzewski, J. Gao, N. Rega, G. Zheng, W. Liang, M. Hada, M. Ehara, K. Toyota, R. Fukuda, J. Hasegawa, M. Ishida, T. Nakajima, Y. Honda, O. Kitao, H. Nakai, T. Vreven, K. Throssell, J. A. Montgomery, Jr., J. E. Peralta, F. Ogliaro, M. J. Bearpark, J. J. Heyd, E. N. Brothers, K. N. Kudin, V. N. Staroverov, T. A. Keith, R. Kobayashi, J. Normand, K. Raghavachari, A. P. Rendell, J. C. Burant, S. S. Iyengar, J. Tomasi, M. Cossi, J. M. Millam, M. Klene, C. Adamo, R. Cammi, J. W. Ochterski, R. L. Martin, K. Morokuma, O. Farkas, J. B. Foresman, and D. J. Fox,, *Gaussian inc., Wallingford CT 2016* **2016**, *2*, 4.
71. Hay, P. J.; Wadt, W. R., *J. Chem. Phys.* **1985**, *82*, 270-283.
72. Hay, P. J.; Wadt, W. R., *J. Chem. Phys.* **1985**, *82*, 299-310.
73. Wadt, W. R.; Hay, P. J., *J. Chem. Phys.* **1985**, *82*, 284-298.

Chapter IV

Biofuel Production via Pincer–Ruthenium Catalyzed Upgradation of Ethanol

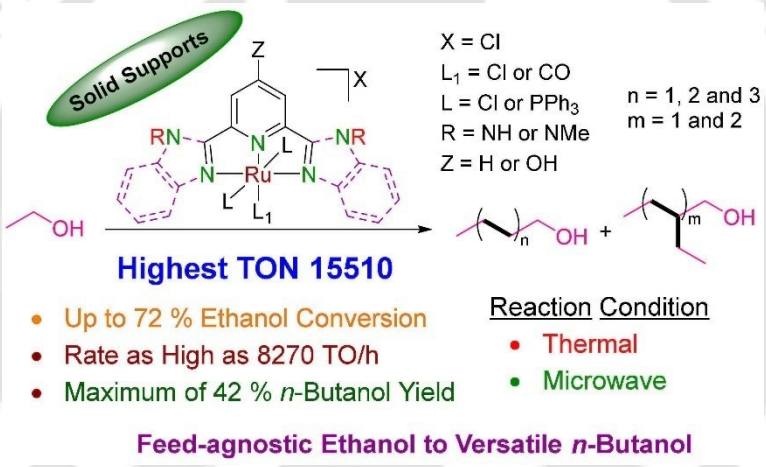

- **K. Das**, M. Dutta, B. Das, H. K. Srivastava, A. Kumar, *Adv. Synth. Catal*. **2019**, *361*, 2965.
- M. Dutta, **K. Das**, S. J. Prathapa, H. K. Srivastava, A. Kumar, *Chem. Commun*. **2020**, *56*, 9886.
- **K. Das**, E. Yasmin, B. Das, H. K. Srivastava, A. Kumar, *Catal. Sci. Technol*. **2020**, *10*, 8347.
- **K. Das**, L. Kathuria, R. V. Jasra, S. Dhole, A. Kumar, *Catal. Sci. Technol*., **2023**, *13*, 1763.

4.1 Introduction

The fast depleting fossil fuels in combination with the ever-increasing energy demand have triggered an intense search for the alternative energy resources.[1] In addition to energy security, alternative energy sources are pivotal to the protection of the environment.[2] In comparison to conventional gasoline, ethanol is widely accepted to be a sustainable fuel considering its easy accessibility through the crops fermentation process (ABE: Acetone-Butanol-Ethanol; process, Scheme **4.1**).[3-4]

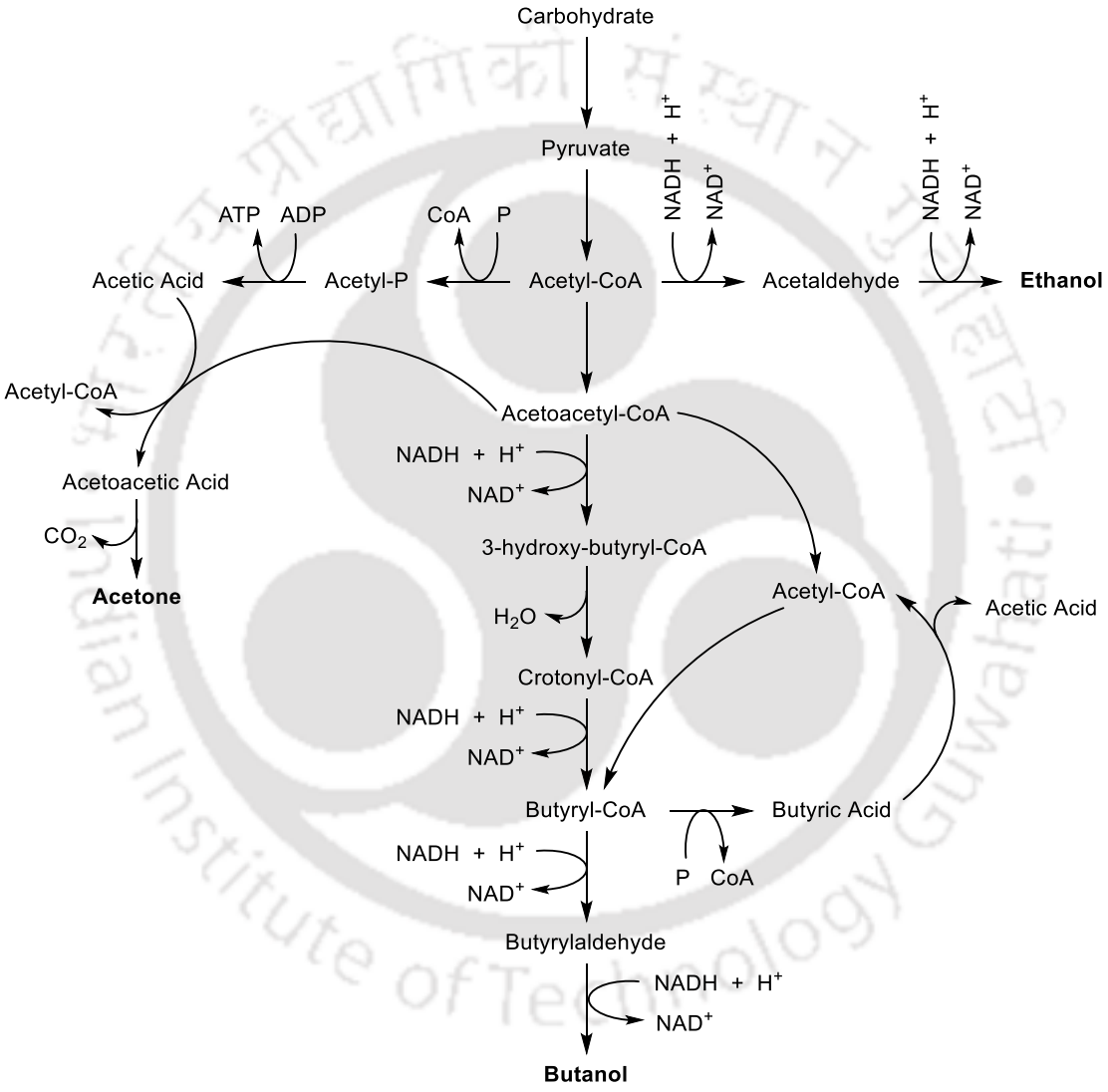

Scheme 4.1: Fermentation performed by enzyme in the ABE process

Chemically, *n*-butanol can be produced from common methods like crotonaldehyde hydrogenation.[5] On an industrial scale, conversion of C_2 or C_3 containing hydrocarbons to C_4 alcohols proves to be an efficient alternative *via* hydroformylation or hydrocarbonylation.[6-7] In this context, oxo synthesis using propylene gas has been reported in presence of carbon monoxide and hydrogen that is catalyzed by cobalt or rhodium catalyst resulting in

isobutyraldehyde and butyraldehyde.[8] Further hydrogenation of butyraldehyde affords *n*-butanol (oxo-synthesis; Scheme **4.2**).[8] Similarly, under low pressure and temperature, propylene has been converted to *n*-butanol using carbon monoxide and water. (Reppe synthesis; Scheme **4.2**).[9]

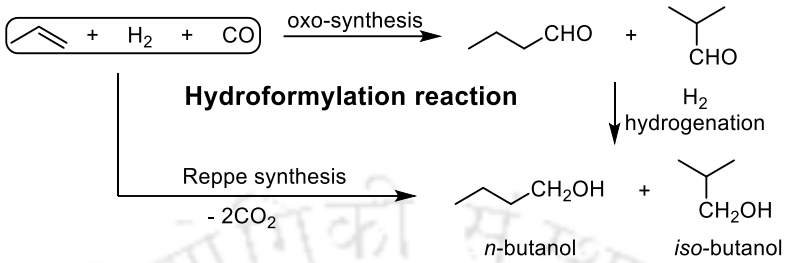

Scheme 4.2: Butanol synthesis from propylene

The steady rise in fuel consumption to meet the ever increasing energy demand has caused high emission of greenhouse gases.[10] The combustion of 1 kg of butanol emits lesser amount of CO_2 as well as generates equivalent amount of energy in comparison to gasoline as shown in Figure **4.1**.[11] On the other hand, to obtain equivalent amount of energy, more amount of ethanol is required, which again leads to a higher amount of CO_2 emission (Figure **4.1**).[12] In fact, the market of butanol globally is estimated to be 2.8 million tons annually, which is around 5 billion USD as of 2023.[13-14]

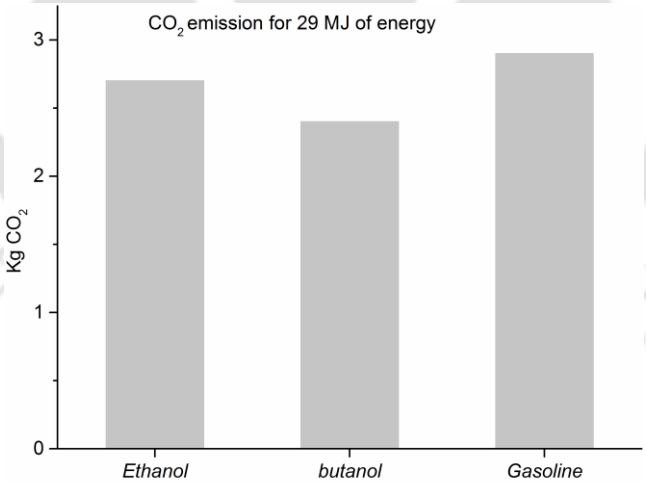

Figure 4.1: Comparison of CO_2 emission from different fuels (gasoline, butanol, and ethanol) for an energy generation of 29 MJ.[12]

The main energy requirement globally comes from fossil fuels (around 78.4%), which is a major concern for the predicted energy misbalance in near future (Figure **4.2**).[11, 15] The release of CO_2 from burning of fossil fuels contribute to the growing climate change which needs to be addressed by implementation of a new strategy.[16] By using modern technology, people are shifting significantly towards alternative and renewable energy source. Use of biofuel as an

energy source has gained considerable attention to researchers, apart from the focus on batteries, solar and wind energies.[17]

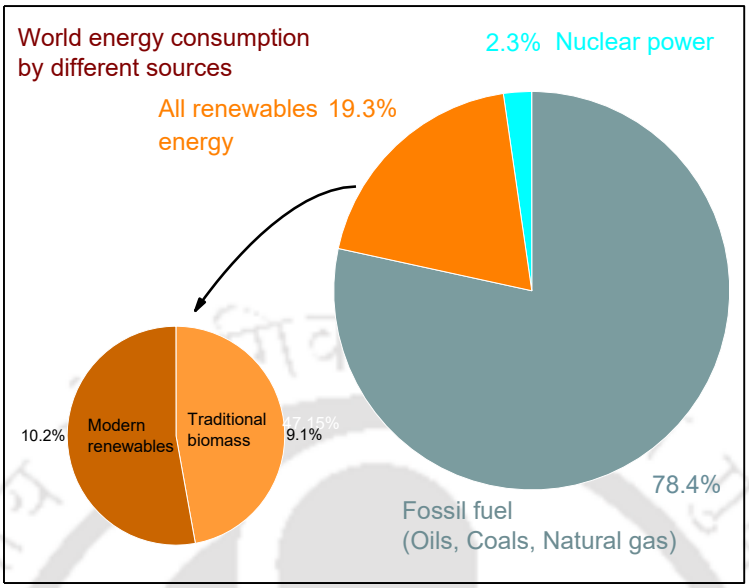

Figure 4.2: World energy consumption by different sources.[12]

4.1.1 History

The use of biofuel is an alternative strategy for energy source. In1912, Rudolf Diesel introduced the use of peanut oils as a fuel source to an engine.[14-15, 18] Henry Ford and Nikolaus August Otto proved that the pure ethanol is able to run an engine with their respective motors. However, in 2005, David Ramey drove a car using biofuel (butanol) instead of gasoline across the United States. Though it consumed about 9% higher butanol than gasoline, there was a reduction in CO, hydrocarbons and NOx (x = 0.5, 1 & 2) emission (http://www.butanol.com/, as of 31 August 2022).[14-15]

Recently, the Navigant research predicted an increase in demand of energy (biofuel) worldwide from *n*-butanol in comparison to that from other valuable alcohols Figure **4.3**.[12] Bio-butanol is also a valuable precursor to synthesis of numerous industrial scale products.[19] In addition, use of bio-butanol reduces the emission of CO_2 in comparison with the corresponding use of fossil fuel.[20]

4.1.2 Ethanol vs butanol

The Biofuel can be easily produced from biomass which is biodegradable and has properties such as renewable and reproductive, unlike gasoline. There are large number of biofuels available such as ethanol, butanol and biodiesel.[21] The biofuels exist in three states as solid, liquid and gas and among them those derived from solids (*e.g.* bio-coal, wood and charcoal)

constitute as the primary fuels for producing energy (table **4.2**). The secondary fuels (*i.e.* liquid and gas) are mainly used for transportation. The four-carbon containing *n*-butanol is largely produced (at a cost of 7.0–8.4 billion dollars per year) in industry as chemical, solvent and as supplement to biofuel.[22]

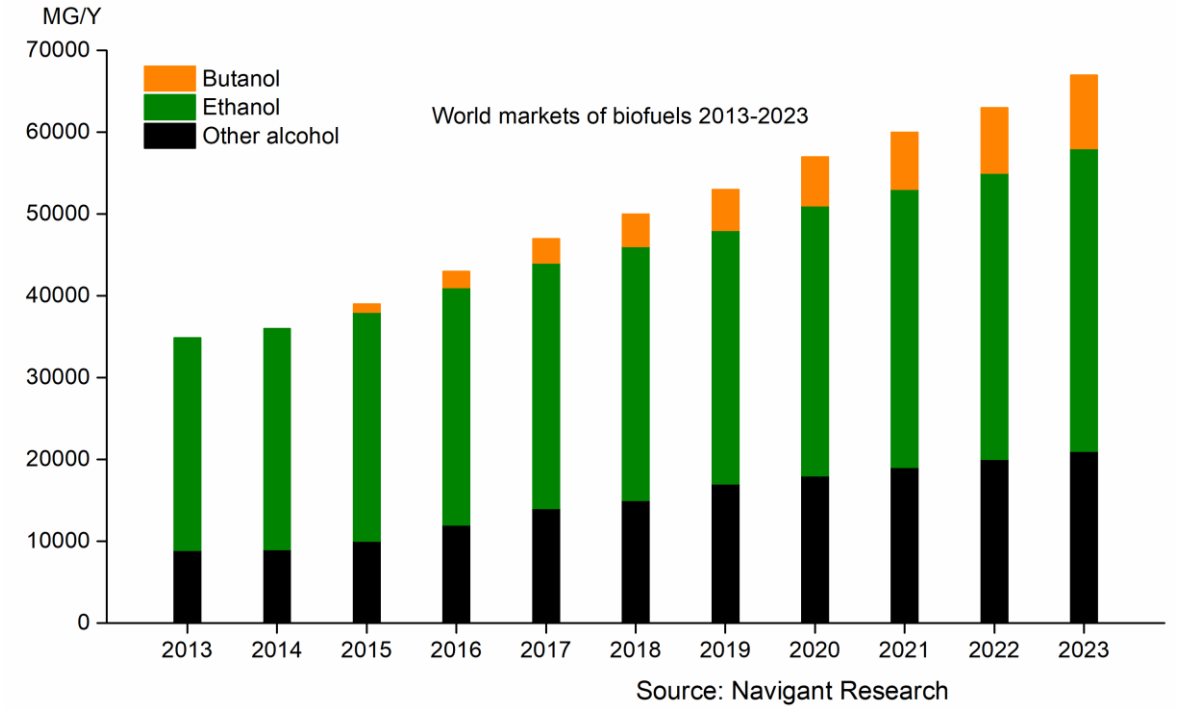

Figure 4.3: Total biofuels production around the globe.[12]

Table 4.1: Comparison of physical and chemical properties of butanol, ethanol, and gasoline

Properties	***Ethanol***	***Butanol***	***Gasoline***
Energy Density (MJ/L)	21.2	29.2	32.5
Fusion point (°C)	-114	-89.3	-40
Boiling point(°C)	78	117	27-225
Auto ignition temperature (°C)	423	385	257
Density (g/mL)	0.79	0.81	0.75
Water solubility (mL 100 mL^{-1})	miscible	9.1	<.0.01
Oxygen content (% vol)	34.7	21.6	<2.7
Vapour pressure (kPa)	16.5	18.6	75

n-Butanol has more advantages over other biofuels due to a higher energy density and relatively low self-ignition temperature. The other advantage is its low flammable nature, less volatility and low vapor pressure. Butanol can blend up to 85% with gasoline in an unmodified petrol engine compared to ethanol which reaches only up to 10%. Though ethanol has been

considered as a biofuel, it has several limitations like poor energy density (70% with respect to gasoline),[2-3, 23-24] corrosive nature[25] and higher water absorptivity[23, 26-27] and possesses challenges in its handling under state-of-art technologies. These limitations can be circumvented by the use of *n*-butanol, which not only has a higher energy density (86%), but also is non-corrosive while being immiscible in water (Table **4.1**).[15, 25]

Table 4.2: Comparison of various fuel in terms of energy production[28]

Entry	Fuel	Specific energy (M J/kg)	Energy density (M J/L)
1	Methanol	-22.70	-17.80
2	Ethanol	-29.70	-23.30
3	1-butanol	-36.10	-29.10
4	1-hexanol	-39.00	-31.70
5	1-octanol	-40.70	-33.50
6	Gasoline	-47.30	-33.80
7	Kerosene	-46.20	-38.30
8	Diesel	-44.80	-37.10
9	Coal (Anthracite)	-27.00	-36.40
10	Coal (Lignite)	-15.00	-12.00
11	Wood	-15.00	-9.00

n-Butanol can be synthesized *via* two major pathways; i) aldol condensation of acetaldehyde to form crotonaldehyde followed by hydrogenation to form *n*-butanol,[29] ii) hydroformylation of propylene followed by hydrogenation of butyraldehyde to *n*-butanol.[30-33] However, acetaldehyde also has to be synthesized *via* Waker process, where similar type of hydroformylation reaction involves reaction of ethylene with CO.[33] While, acetaldehyde or propylene productions requires the use of fossil fuels along with a huge energy consumption for the cracking of hydrocarbons, CO formation involves a partial thermal oxidation of alkanes (from fossil fuel and coal) which again leads to an overall high energy process.[34] Hence, conventional methodology has limitations for the industrial production of *n*-butanol synthesis.

Various heterogeneous catalytic systems are known to upgrade ethanol to *n*-butanol. Majorly, two features of the catalyst are required for the alcohol coupling reactions. One feature is related to the acidity/basicity of the catalyst.[35] The other involves the ability of the catalyst to facilitate dehydrogenation of the alcohol at the considered reaction temperature.[36] It is believed that a catalyst is active only when the main active sites on the catalyst are basic sites.[37] Therefore, to generate an efficient catalyst and to obtain *n*-butanol in high yields, the

composition of the catalyst and the associated basic sites density and strength are very important. Metal promoted zeolites,[38-41] hydroxyapatites,[42-46] and the metal oxide[47-51] systems are usually employed as catalytic materials for the reaction, yielding different activities and selectivities. The heterogeneous reaction mainly requires harsh conditions (>200 °C) and often suffers from lack of selectivity.[36]

4.1.3 Homogenous organometallic catalysts towards biofuel production

In this context, methods that upgrade ethanol to either *n*-butanol or higher analogues with higher energy density[24] are a subject of great interest. Not surprisingly, the Guerbet reaction[52-54] that involves the transformation of bio-ethanol to bio-butanol with water as the sole byproduct has been widely explored.[55-58] Based on the hydrogen-borrowing (HB) strategy (Scheme **4.3**), this reaction involves alcohol dehydrogenation into aldehyde, followed by aldol condensation and hydrogenation of the resulting higher α,β-unsaturated aldehyde into the higher molecular weight alcohol product.

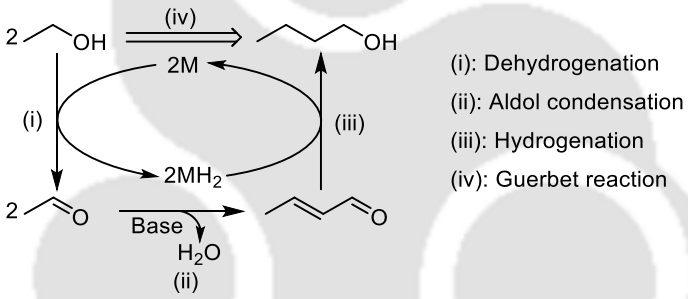

Scheme 4.3: Hydrogen-borrowing strategy for the upgradation of ethanol to *n*-butanol.

In 2009, Ishii and co-workers reported [Ir(COD)(acac)] (**4.7**)/dppp (**4.8a**) catalyzed Guerbet reaction in presence of 1,5-cyclooctadiene (1 mol %) which resulted in 1220 TON (turnover numbers) with 51% selectivity towards *n*-butanol.[59] The highest selectivity for *n*-butanol was obtained from [Ir(COD)(acac)] (**4.7**)/dppb (**4.8a**) complex with up to 67% in the presence of 5 mol % sodium ethoxide (Scheme **4.4**).[59]

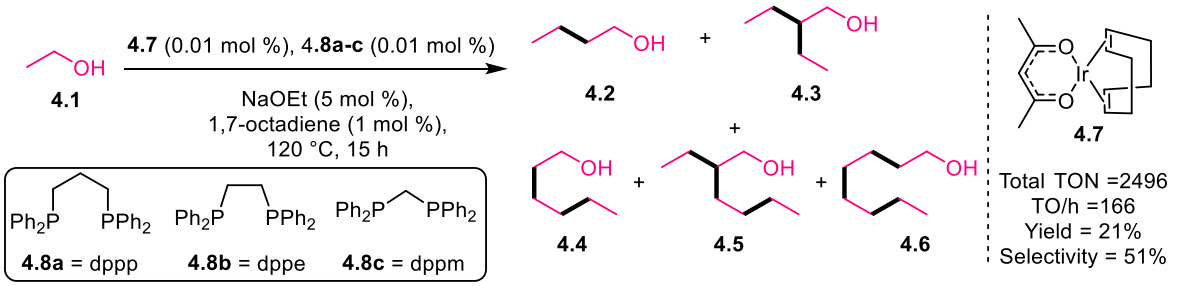

Scheme 4.4: Ethanol to *n*-butanol upgradation by an iridium catalyst.[59]

Wass and co-workers introduced ruthenium-based complexes for catalyzing ethanol upgradation reaction. Initially, they reported $[RuCl_2(\eta^6\text{-}p\text{-cymene})]_2$ (**4.9**) (0.1 mol %) as a catalyst towards upgradation of ethanol. The catalyst provided 7% ethanol conversion with 86% *n*-butanol selectivity at 150 °C. The authors then introduced ligands (**4.8a-c**) with the $[RuCl_2(\eta^6\text{-}p\text{-cymene})]_2$ (**4.9**) precursor and employed them as modified catalytic system (Scheme **4.5**, Table **4.3**). [56] The ethanol conversion raised up to 20.4% (18% *n*-butanol yield) in the absence of any hydrogen acceptor (Scheme **4.5**; entry 1, Table **4.3**). The complex, $RuCl_2(dppm)_2$ (**4.10**) resulted in 1300 TON and 13% ethanol conversion after 20 h (Scheme **4.5**; entry 5, Table **4.3**).[56]

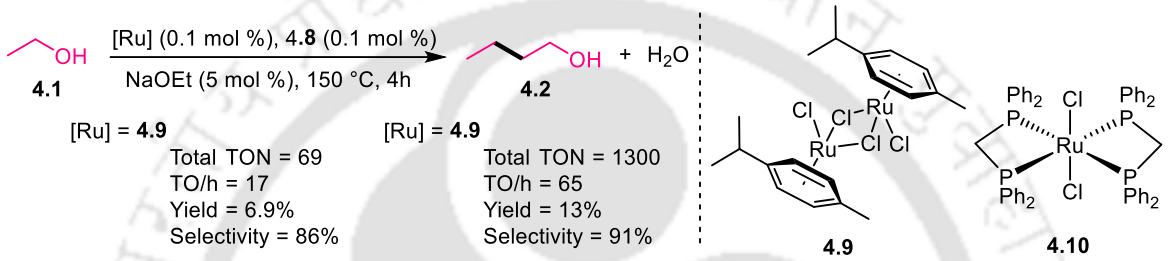

Scheme 4.5: Ethanol to *n*-butanol upgradation catalyzed by ruthenium complexes.[56]

Table 4.3: Ethanol to *n*-butanol upgradation catalyzed by ruthenium complexes.[56]

Entry	[Ru]	Ligand (0.1 mol %)	Conversion (%)	Selectivity (%)	TON
1	**4.9** (0.1 mol %)	**4.8a**	20.4	90.0	204
2	**4.9** (0.1 mol %)	**4.8b**	11.8	90.6	118
3	**4.9** (0.1 mol %)	**4.8c**	10.2	88.0	102
4	**4.9** (0.1 mol %)	--	6.9	86.1	69
5	**4.10** (0.01 mol %)	--	13.0	90.6	1300
6	**4.10** (0.1 mol %)	--	45.8	84.6	458

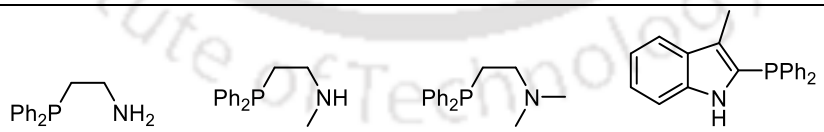

Figure 4.4: Various phosphine-amine based ligands used along with the ruthenium complex (**4.9**) for ethanol upgradation.[57]

Later, Wass and co-workers reported the use of ruthenium η^6-complex **4.9** along with various bidentate ligands (**4.11a-d**) towards ethanol upgradation. They obtained *n*-butanol with very high selectivity (up to 99%) and up to 98 TON. Among all the phosphine-amine ligand systems,

0.1 mol % of **4.11d** along with complex **4.9** (0.1 mol %) gave 93% *n*-butanol selectivity along with a total of 314 TON for the ethanol upgradation (Figure **4.4**).[57]

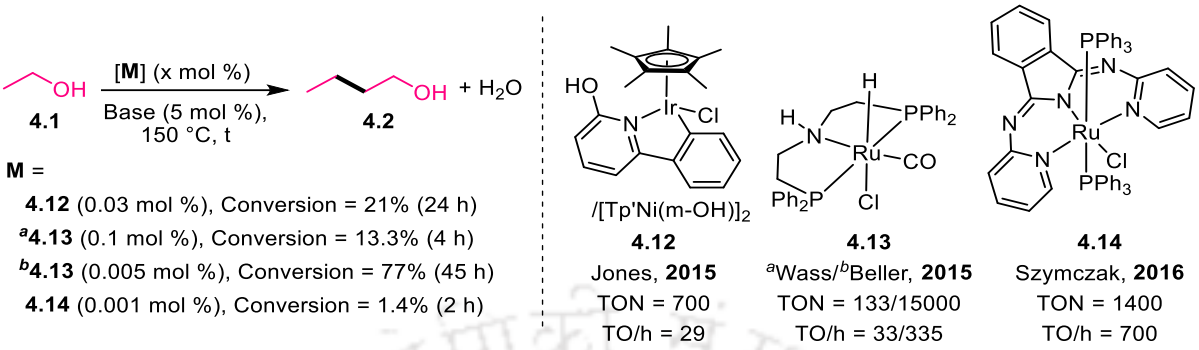

Scheme 4.6: Homogenous catalysts based on Ir and Ru for the upgradation of ethanol to *n*-butanol.[55, 60]

Szymczak and co-workers reported a NNN pincer-ruthenium catalyst **4.14** for *n*-butanol formation with 53% ethanol conversion and 78% selectivity (TON 530).[55] The highest turnover numbers obtained by them was 1400 TON with 1.4% ethanol conversion and 100% selectivity towards *n*-butanol. The highest yield obtained was 22.7 % of *n*-butanol (TON 286), and the highest selectivity reached up to 100% (TON 170) for the ethanol to *n*-butanol conversion (1.7%) (Scheme **4.6**).[55] Jones and co-workers initially reported a bifunctional iridium catalyst **4.12** with nickel-copper based complex for the ethanol upgradation. The bifunctional catalyst resulted in very high selectivity up to 99% at a very good conversion (700 TON), while 78% selectivity was observed towards *n*-butanol.[60] Further, Beller and co-workers reported dehydrogenation of ethanol to ethyl acetate with high TON (up to 15000) resulting in 77% yield after 46 h (Scheme **4.6**).[61]

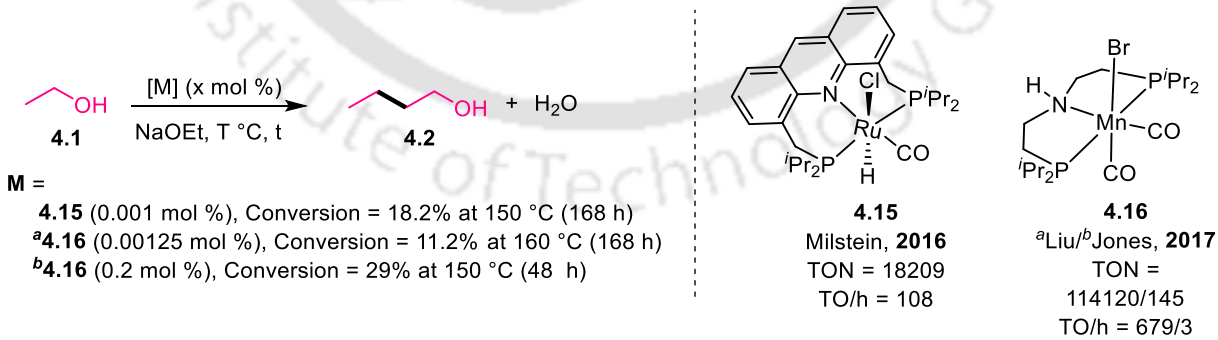

Scheme 4.7: Pincer-Ru and pincer-Mn catalysts reported for the upgradation of ethanol to *n*-butanol.

Milstein and co-workers investigated the PNP pincer-ruthenium complex (**4.15**) for the Guerbet reaction, and they obtained 73.4% ethanol conversion (Scheme **4.7**).[62] The highest *n*-butanol yield obtained was 38.4% (TON 3345) with 68.3% selectivity. Up to 73.4% ethanol

conversion was observed with 35.8% *n*-butanol yield (TON 3671) by using complex **4.15** (Scheme **4.7**). Recently, Q. Liu reported PNP pincer-manganese complex (**4.16**) for the upgradation of ethanol to higher alcohols, reaching up to 114120 TON with 11.2% ethanol conversion after 7 days (Scheme **4.7**) in the presence of NaOEt (12 mol %).[63] On the other hand, Jones and co-workers employed the same PNP pincer-manganese complex **4.16** that resulted in 145 TON in the presence of 25 mol % NaOEt for the Guerbet reaction. They also demonstrated that, external addition of water to the reaction mixture led to deactivation of the catalyst (Scheme **4.7**).[64]

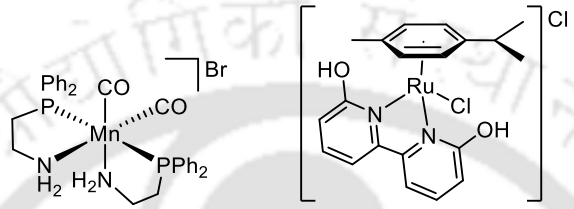

4.17
Wass (**2020**)
100 TON

4.18
Jones (**2021**)
31 TON

Figure 4.5: Homogenous catalysts reported for the upgradation of ethanol to *n*-butanol.[65-68]

Recently, Wass and co-workers have reported the use of manganese diphosphine and phosphinoamine catalysts **4.17** for accomplishing the Guerbet reaction with moderate selectivity (74%) and turnovers (> 100 over 90 h) (Figure **4.5**).[65] Very recently, Wass also reported a series of rhenium complexes supported by bidentate and tridentate phosphinoamine ligands which were used to catalyze isobutanol (35% yield, with 97% selectivity) formation from methanol and ethanol over 16 h.[66] Jones and co-workers reported a ruthenium catalyst **4.18** for upgrading ethanol to *n*-butanol at 80 °C in up to a 28% yield and 57% selectivity (Figure **4.5**).[68] However, the polymerization of acetaldehyde leads to C_{6+} species and the low activation barrier of ethyl acetate formation from ethanol, results in lower yield and selectivity toward *n*-butanol. Therefore, Liauw has explained why Ru-MACHO-BH (**4.13**) performance is poor in stitching two ethanol to *n*-butanol (Scheme **4.6**).[67]

4.2 Objective

In chapter **II** and **III**, a series of NNN pincer-ruthenium complexes have been described that show very good reactivity towards *N*-alkylation and *C*-alkylation reactions.[69-70] In this regard, this chapter aims to examine the applicability of these complexes towards a more useful alkylation, *viz.* the transformation of ethanol to *n*-butanol. Considering the fact that the reports with homogeneous ruthenium systems for the ethanol upgradation are very scarce, it would be interesting to address this issue with the following questions in mind,

- Can the NNN based pincer-Ru catalyst that demonstrated good activity towards alkylation of aromatic amines and aromatic alcohols act as good catalysts for the ethanol upgradation as well Figure (**4.6**)?
- Can one accomplish better reactivity towards alcohols with phosphine free pincer catalysts?
- Is it possible to obtain a through kinetic and mechanistic understanding?
- Do microwave conditions enhance the reactivity?
- Would heterogeniation of these complexes on solid support be feasible? Will there be any recyclability?

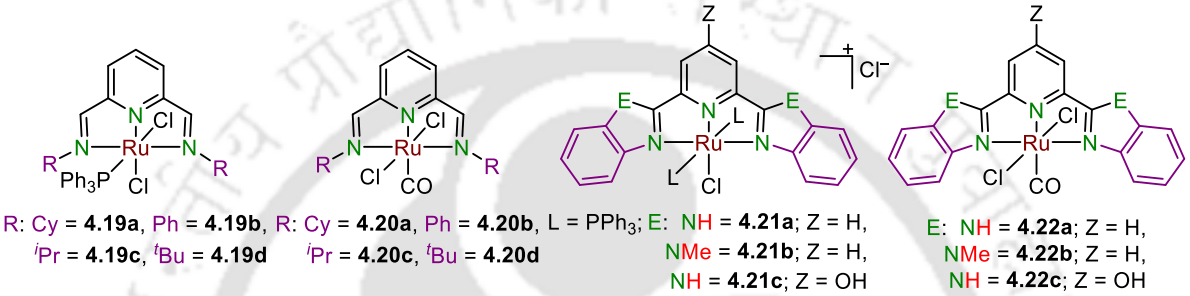

Figure 4.6: Complexes that were used for the Guerbet reaction in current study.

4.3 Result and discussion

4.3.1 Synthesis of *bis*(benzimidazole) ligands and their complexes

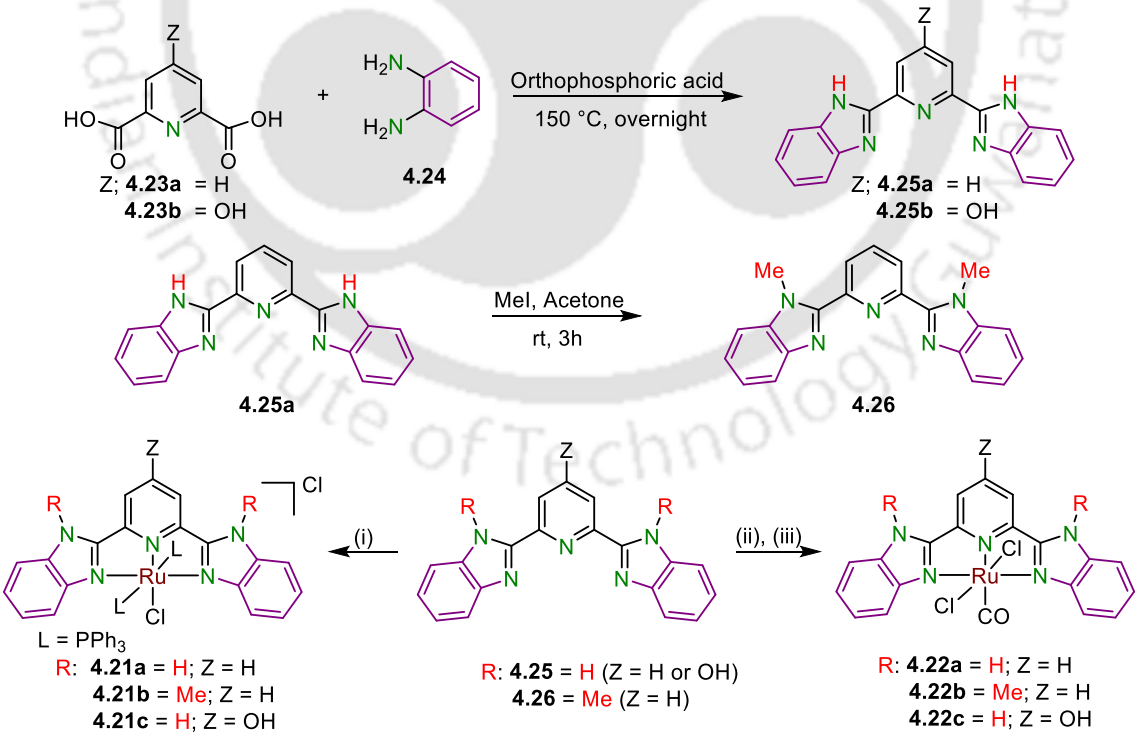

Scheme 4.8: General route for synthesis of complex (^{RBim}NNN)RuCl$_2$(CO) and [(^{RBim}NNN)RuClL$_2$]Cl (R = H or Me; L = PPh$_3$, Z = H or OH).

The NNN 2,6-*bis*(benzimidazol-2-yl)pyridine ligand was synthesized by refluxing 4-hydroxypyridine/pyridine-2,6-dicarboxylic acid (**4.23**) with *o*-phenylenediamine (**4.24**) in the presence of orthophosphoric acid. The complex (**4.21/22a-c**) based on ligand (*p*-z^{RBim}NNN) (**4.25a**: R = Z = H; **4.25b**: R = Me, Z = H; **4.26**: R = H, Z = OH) were synthesized by slight modifications to the literature procedure[71-72] and the previous chapter. Notably Zhang and Peng have reported similar complexes but with acetonitrile as ancillary ligands which were shown to be active for transformation of benzyl alcohols to corresponding acids (Scheme **4.8**).[73] The pincer-ruthenium complexes (**4.21a-c** and **4.22a-c**) were characterized by NMR, HRMS and IR analysis. The IR studies of **4.22a**, **4.22b** and **4.22c** also revealed the presence of the carbonyl group and the prominent C≡O stretching frequency was observed at 1965 cm^{-1}, 1939 cm^{-1} and 1958 cm^{-1} respectively. Treatment of **4.21a** with $NaPF_6$ in methanol resulted in **4.21a″** which was characterized by single-crystal X-ray analysis (Figure **4.7**). The ^{31}P NMR revealed that the major isomer in complex **4.21a-c** had the two PPh_3 groups *trans* to each other (Figure **4.7**).

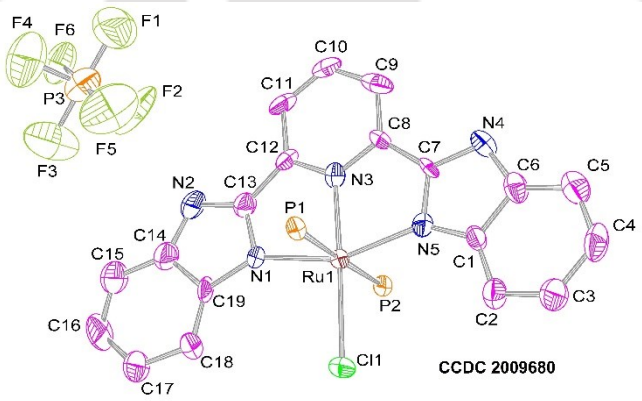

Figure 4.7: ORTEP diagram of [(^{Bim2}NNN)RuCl(PPh_3)$_2$]PF_6 (**4.21a″**) with the ellipsoids drawn at the 50% probability level. The Ph groups on P and all the H atoms were omitted for the sake of clarity.

4.3.2 Catalytic transformation of ethanol to bio-butanol under thermal condition

In the Chapter III it has been described that, the reactivity (Table **3.3**) of aliphatic alcohols towards *β*-Alkylation is very poor. Therefore, the optimization conditions were revisited for the upgradation of ethanol using (^{Cy2}NNN)RuCl$_2$(CO) (**4.20a**) (Table **4.4**) at 140 °C in the presence of various base. For variations with NaO^{t}Bu as a base, the productivity was higher (195 TON) with 0.05 mol % **4.20a** in the presence of 10 mol % NaO^{t}Bu (entry 1, Table **4.4**). Use of KOH resulted in slightly lower reactivity and *n*-butanol selectivity (entry 3, Table **4.4**). The reactivity was very low with the use of KO^{t}Bu as base (entry 4, Table **4.4**). No reactions were observed when Et_3N, K_2CO_3 and Mg were used (entries 5, 6 and 7, Table **4.4**). Upon employing NaH, the productivity (260 TON) improved with comparable selectivity (90%)

towards *n*-butanol (entry 8, Table **4.4**). In the presence of NaOH (10 mol %), the **4.20a** (0.05 mol %) catalyzed reaction provided higher turnovers (310) at a selectivity of 85% towards *n*-butanol (entry 9, Table **4.4**). These productivity and selectivity values hardly changed with increase in temperature and at prolonged reaction times (entries 12 and 13, Table **4.4**). On increasing the base loading to 20 mol %, while the selectivity dropped to 70%, the turnovers slightly increased (entry 11, Table **4.4**).

Table 4.4: Optimization of Guerbet reaction catalyzed by **4.20a**.[a]

Entry	Base (X mol %)	*n*-Butanol[b] yield (%)	Selectivity of *n*-butanol[g]	Total TON[c]
1	NaO^{t}Bu (10)	8.4	90	195
2	NaO^{t}Bu (20)	6.9	95	145
3	KOH (10)	6.1	85	155
4	KO^{t}Bu (10)	2.2	85	65
5	Et_3N (10)	0	0	0
6	K_2CO_3 (10)	0	0	0
7	Mg (10)	0	0	0
8	NaH (10)	10.8	90	260
9	NaOH (10)	12.5	85	310
10	NaOH (5)	5.9	85	150
11	NaOH (20)	11.6	80	330
12[d]	NaOH (10)	12.6	90	290
13[d,e]	NaOH (10)	13.9	90	320
14[f]	NaOEt (10)	13.9	90	335
15[e,f]	NaOEt (10)	17.1	90	410

[a]Reaction conditions: 8.56 mmol of ethanol, X mol % of base and 4.28 µmol of **4.20a**. [b]Selectivity and TON were calculated by GC analysis using toluene as an internal standard. [c]Total ethanol converted to products. [d]The reaction was carried out at 150 °C. [e]Reaction was carried out for 48 h. [f]NaOEt was generated *in-situ* using ethanol (110 mol %) and Na(10 mol %) prior to addition of **4.20a**. [g]Selectivity = Yield of *n*-butanol/Conversion of **4.1**.

Following up on our recent approach of generating the base *in situ*, when 10 mol % Na was used to generate 10 mol % NaOEt very high turnovers (ca. 335) were obtained with 90% selectivity towards *n*-butanol after 24 h (entry 14, Table **4.4**). Upon continuing the reaction to 48 h, the productivity was further enhanced with no loss of selectivity (entry 15, Table **4.4**). This condition was used for further optimization with various catalysts (Table **4.5** and Table **4.6**).

Table 4.5: Guerbet reaction catalyzed by phosphine based pincer-ruthenium complexes.[a]

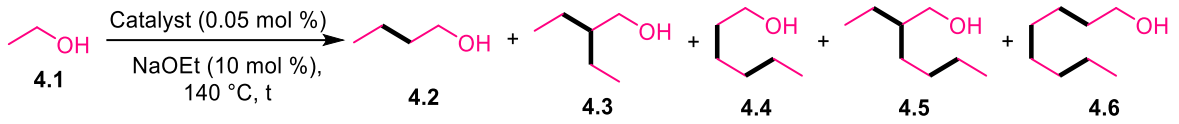

Entry	Catalyst	Time (h)	*n*-Butanol (TON)	*n*-Butanol selectivity (%)[c]	Total (TON)[b]
1	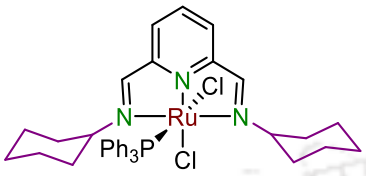 **4.19a**	0.5	85	90	90
		3.0	185	80	225
		9.0	240	80	300
		72	340	75	450
2	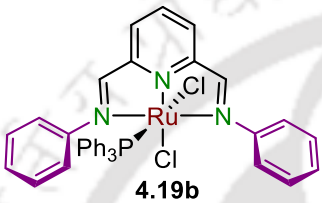 **4.19b**	0.5	160	95	170
		3.0	310	80	385
		9.0	370	80	475
		72	375	75	495
3	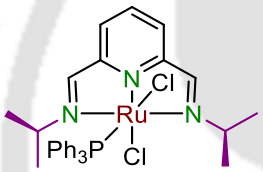 **4.19c**	0.5	145	90	160
		3.0	250	80	320
		9.0	260	75	340
		72	300	75	395
4	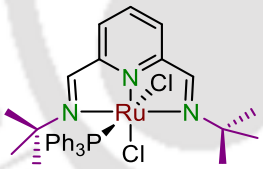 **4.19d**	0.5	45	80	60
		3.0	200	75	270
		9.0	240	70	335
		72	250	70	355
5	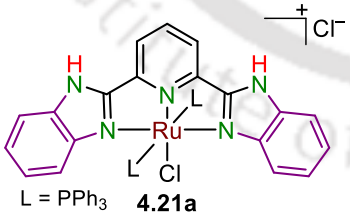 L = PPh_3 **4.21a**	0.5	50	80	60
		3.0	550	85	660
		9.0	800	75	1090
		72	780	70	1115
6	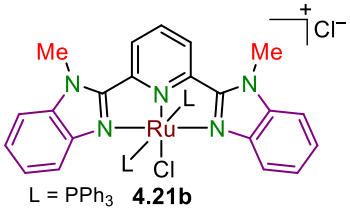 L = PPh_3 **4.21b**	0.5	270	65	420
		3.0	285	65	430
		9.0	305	65	450
		72	375	60	620

[a]Reaction conditions: 8.56 mmol of ethanol, 0.86 mmol of NaOEt and 0.05 mol % of catalyst. [b]Calculated by GC analysis using toluene as an internal standard. [c]Selectivity = Yield of *n*-butanol/Conversion of **4.1**.

Table 4.6: Guerbet reaction catalyzed by carbonyl based pincer-ruthenium complexes.[a]

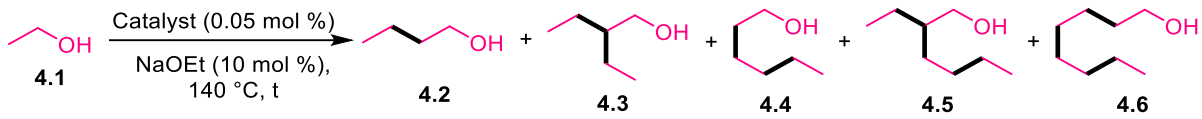

Entry	Catalyst	Time (h)	*n*-Butanol (TON)[b]	*n*-Butanol selectivity (%)[c]	Total (TON)[b]
1	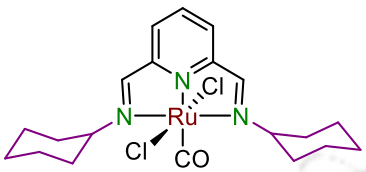 **4.20a**	0.5	125	90	135
		3.0	200	85	235
		9.0	235	75	310
		72	260	80	335
2	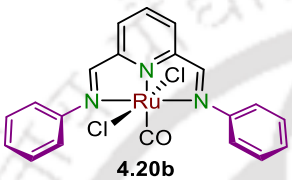 **4.20b**	0.5	100	95	105
		3.0	225	90	250
		9.0	235	80	300
		72	255	75	340
3	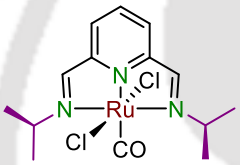 **4.20c**	0.5	85	90	90
		3.0	175	90	190
		9.0	310	80	385
		72	385	75	520
4	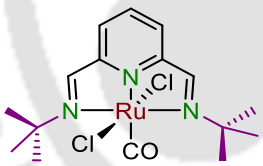 **4.20d**	0.5	115	75	150
		3.0	125	75	165
		9.0	140	60	238
		72	135	65	215
5	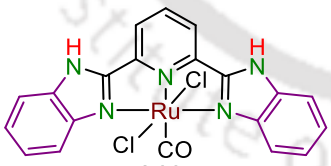 **4.22a**	0.5	295	85	355
		3.0	710	80	880
		9.0	720	80	920
		72	765	80	975
6	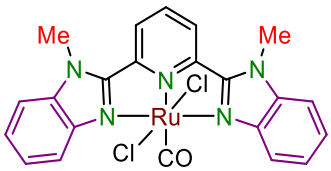 **4.22b**	0.5	135	75	180
		3.0	165	75	230
		9.0	205	75	275
		72	280	75	385

[a]Reaction conditions: 8.56 mmol of ethanol, 0.86 mmol of NaOEt and 0.05 mol % of catalyst. [b]Calculated by GC analysis using toluene as an internal standard. [c]Selectivity = Yield of *n*-butanol/Conversion of **4.1**.

Table 4.7: Ethanol upgradation catalyzed by varying amount of **4.22a**.[a]

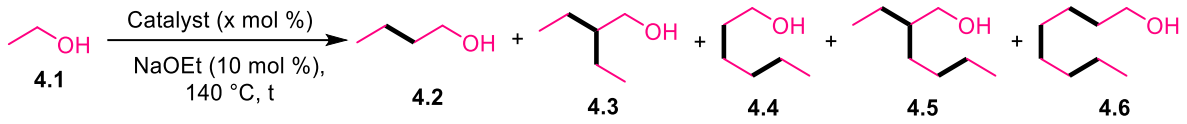

Entry	Catalyst (x mol %)	Time (h)	*n*-butanol (**4.2**)[b]		TON[b]	
			Yield (%)	Selectivity (%)[c]	**4.2**	Total
1	0.025	0.5	5.23	95	330	335
		3.0	19.80	80	795	1015
		9.0	32.02	85	1280	1495
		72	37.73	70	1510	2100
2	0.035	0.5	8.44	90	155	267
		3.0	26.73	80	740	970
		9.0	33.28	80	925	1155
		72	36.58	65	1045	1670
3	0.055	0.5	14.82	85	300	355
		3.0	35.44	80	710	880
		9.0	35.81	80	715	920
		72	38.21	80	765	975
4	0.075	0.5	18.84	95	250	255
		3.0	35.44	80	475	580
		9.0	32.88	75	440	585
		72	36.07	65	480	740
5	0.099	0.5	21.26	95	215	225
		3.0	36.94	80	370	475
		9.0	38.52	75	385	500
		72	43.32	75	435	585

[a]Reaction conditions: 8.56 mmol of ethanol, 0.86 mmol of base and x mol % of **4.22a**. [b]Calculated by GC analysis using toluene as an internal standard. [c]Selectivity = Yield of *n*-butanol/Conversion of **4.1**.

The ethanol upgradation was first tested for a series of NNN pincer-ruthenium complexes containing PPh_3 ancillary ligands (Table **4.5**). With catalyst **4.19d**, the rate of the reaction was low and the productivity levelled off after 9 hours (entry 4, Table **4.5**). The rate of **4.19a** catalyzed ethanol upgradation was about 1.5 times that of rate obtained with **4.19d** (entry 1, Table **4.5**). Both the catalysts **4.19b** and **4.19c** demonstrated rates that were about 1.75 folds higher than the corresponding rate observed with **4.19a** (entry 2 and 3, Table **4.5**). Kumar and co-workers have recently reported that complex **4.21a** that has less steric crowding around the Ru center efficiently catalyzes the dehydrogenation of glycerol.[74] When **4.21a** was explored for the Guerbet reaction of ethanol, it exhibited a rate similar to that observed with **4.19d** but with a much higher (3.1 folds) productivity (1115 TON after 72 h) (entry 5, Table **4.5**). On the

other hand, complex **4.21b** demonstrated a rate (ca. 840 TO/h) about 7 folds higher than its *N*-H analogue **4.21a** before levelling off almost quickly.

Table 4.8: Ethanol upgradation catalyzed by **4.22a** with varying amount ethanol concentration.[a]

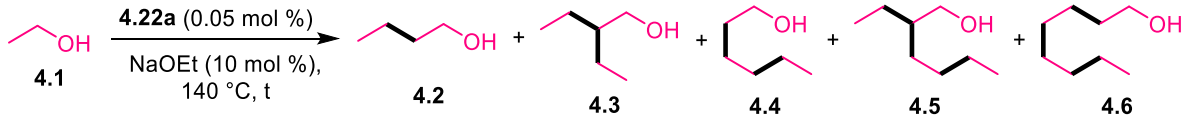

Entry	Ethanol (M)	Time (h)	*n*-butanol (**4.2**)[b]		TON[b]	
			Yield (%)	Selectivity (%)[c]	**4.2**	Total
1	6.11	0.5	10.7	95	215	225
		3.0	23.6	80	470	585
		9.0	23.6	75	470	610
		72	23.3	70	465	680
2	8.56	0.5	11.8	95	235	240
		3.0	21.6	85	430	500
		9.0	28.3	80	565	690
		72	27.8	75	555	710
3	12.23	0.5	14.82	85	300	355
		3.0	35.44	80	710	880
		9.0	35.81	80	715	920
		72	38.21	80	765	975
4	13.46	0.5	15.4	65	305	480
		3.0	32.1	65	640	1015
		9.0	35.5	65	710	1100
		72	39.6	60	795	1380

[a]Reaction conditions: X mmol of ethanol, 0.86 mmol of base and 0.05 mol % of **4.22a**. [b]Calculated by GC analysis using toluene as an internal standard. [c]Selectivity = Yield of *n*-butanol/Conversion of **4.1**.

The phosphine-free complexes (**4.20a-d** and **4.22a-b**) were also tested as catalysts for the Guerbet reaction (Table **4.6**). In comparison to **4.19a** and **4.19d**, their phosphine-free counterparts **4.20a** and **4.20d** exhibited a better rate towards the ethanol upgradation reaction (entries 1 and 4, Table **4.6**). The rate of ethanol upgradation catalyzed by **4.20b** and **4.20c** were comparable (entries 2 and 3, Table **4.6**) and about 1.3-1.5 times slower than **4.20a** and **4.20d**. The rate of **4.22b** catalyzed (entry 6, Table **4.6**) Guerbet reaction was two folds faster than that catalyzed by **4.20b** and **4.20c**. Among all the catalysts screened, the catalyst **4.22a** demonstrated not only very good rate (ca. 710 TO/h) but also high productivity (975 TONs at 49% ethanol conversion) (entry 5, Table **4.6**). Hence, further exploration involving the variation of catalyst loading for Guerbet reaction was carried out using the phosphine-free catalyst **4.22a** (Table **4.6**).

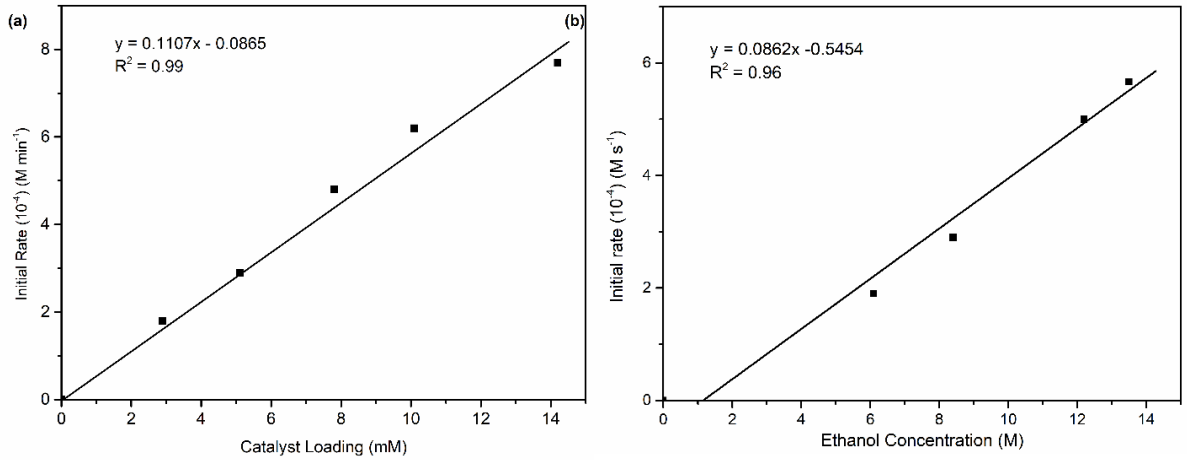

Figure 4.8: Plot depicting the (a) initial rate vs. [**4.22a**] and (b) initial rate vs. [Ethanol] in the ethanol upgradation catalyzed by **4.22a**.

Dehydrogenation and Alcoholysis ..... (1)

$(^{iPr2}NNN)RuCl(OEt) \xrightleftharpoons{K_1} (^{iPr2}NNN)RuClH + CH_3CHO$

$(^{iPr2}NNN)RuClH + EtOH \xrightleftharpoons{K_2} (^{iPr2}NNN)RuCl(OEt) + H_2$

$2CH_3CHO \xrightarrow{k_3} CH_3CHCHCHO + H_2O$

$(^{iPr2}NNN)RuClH + CH_3CHCHCHO \xrightleftharpoons{K_4} (^{iPr2}NNN)RuCl(CH_3CH_2CHCHO)$

$(^{iPr2}NNN)RuCl(CH_3CH_2CHCHO) + EtOH \xrightleftharpoons{K_5} (^{iPr2}NNN)RuCl(OEt) + CH_3CH_2CH_2CHO$

$(^{iPr2}NNN)RuClH + CH_3CH_2CH_2CHO \xrightleftharpoons{K_6} (^{iPr2}NNN)RuCl(OCH_2CH_2CH_2CH_3)$

$(^{iPr2}NNN)RuCl(OCH_2CH_2CH_2CH_3) + EtOH \xrightleftharpoons{K_7} (^{iPr2}NNN)RuCl(OEt) + CH_3CH_2CH_2CH_2OH$

Dehydrogenation and Hydrogenolysis ..... (2)

$(^{iPr2}NNN)RuCl(OEt) \xrightleftharpoons{K_1} (^{iPr2}NNN)RuClH + CH_3CHO$

$(^{iPr2}NNN)RuClH + EtOH \xrightleftharpoons{K_2} (^{iPr2}NNN)RuCl(OEt) + H_2$

$2CH_3CHO \xrightarrow{k_3} CH_3CHCHCHO + H_2O$

$(^{iPr2}NNN)RuClH + CH_3CHCHCHO \xrightleftharpoons{K_4} (^{iPr2}NNN)RuCl(CH_3CH_2CHCHO)$

$(^{iPr2}NNN)RuCl(CH_3CH_2CHCHO) + H_2 \xrightleftharpoons{K_5} (^{iPr2}NNN)RuClH + CH_3CH_2CH_2CHO$

$(^{iPr2}NNN)RuClH + CH_3CH_2CH_2CHO \xrightleftharpoons{K_6} (^{iPr2}NNN)RuCl(OCH_2CH_2CH_2CH_3)$

$(^{iPr2}NNN)RuCl(OCH_2CH_2CH_2CH_3) + H_2 \xrightleftharpoons{K_7} (^{iPr2}NNN)RuClH + CH_3CH_2CH_2CH_2OH$

In both path alcoholysis and hydrogenation, $k_2 > k_{-2}$, under low steady state concentration of $CH_3CHCHCHO$

$$Rate = (k_2)[(^{iPr2}NNN)RuClH][EtOH]$$

Scheme 4.9: Rate equation for the **4.22a** catalyzed ethanol upgradations to *n*-butanol.

The catalyst loading was varied from 0.25 to 0.1 mol % for ethanol upgradation. The highest rate (ca. 710 TO/h) was obtained for 0.05 mol % **4.22a** catalyzed reaction (entry 3, Table **4.7**). While the highest turnovers (ca. 2100) were obtained at 0.025 mol % loading of **4.22a** (entry

1, Table **4.7**), the highest conversion (ca. 58%) of ethanol to products was obtained upon use of either 0.035 mol % (entry 2, Table **4.7**) or 0.1 mol % (entry 5, Table **4.7**) of **4.22a**.

Similarly, on variation of ethanol concentration, highest rate (ca. 960 TO/h) was obtained in 0.05 mol % of **4.22a** catalyzed reaction (entry 4, Table **4.8**) at 13.46 M of ethanol (up to 1380 TON). The highest ethanol conversion was obtained (up to 66%) in the above reaction conditions (entry 4, Table **4.8**).

Kinetic experiments were carried as above on the Guerbet reaction catalyzed by **4.22a** at 140 °C at varying catalyst loading (Table **4.7**) and varying ethanol concentration (Table **4.8**). With the aid of initial rate method, it was observed that the plot of initial rate vs. [**4.22a**] (Figure **4.8a**) and initial rate vs. [ethanol] (Figure **4.8b**) was linear. This points to the first order dependence of rate on concentration of both **4.22a** and ethanol. Not surprisingly these observations indicate the involvement of a mechanistic path as depicted in Scheme **4.9** with a rate as given in either equation (1) or equation (2) in Scheme **4.9**.

4.3.3 Catalytic transformation of ethanol to biobutanol under microwave condition

The studies were initiated by repeating the best results reported in the above discussion, where, in the presence of 10 mol % NaOEt, **4.22a** (0.025 mol %) catalyzed the Guerbet reaction under conventional heating at 140 °C to yield an ethanol conversion of 58% (ca. 2100) at an initial rate of 710 TO/h (entry 1, Table **4.7** and **4.9**). Lowering the temperature of conventional heating reactions gave poorer results (entry 2-4, Table **4.9**). Considering the good microwave absorptivity of ethanol, it would be interesting to probe the reactivity of **4.22a** towards Guerbet reaction under microwave heating at 110 °C where conventional heating was ineffective. Under microwave conditions (75 W) at 110 °C in the presence of 10 mol % of NaOEt, the **4.22a** catalyzed Guerbet reaction proceeded at an initial rate of 1160 TO/h and resulted in about 50% ethanol conversion in 2 h of which about 28% is *n*-butanol with a selectivity of 56% (entry 5, Table **4.9**). At 110 °C, the results obtained with microwave reactions are far superior (11-fold increase in the initial rate of *n*-butanol production) than the corresponding results obtained under conventional heating (compare entries 4 and 5, Table **4.9**). Notably, while the productivity of microwave reaction after 2 h is comparable (entry 5 vs. entry l, Table **4.9**) to the above results under conventional heating albeit at a much lower temperature (110 °C), the initial rates obtained in the current microwave condition is about 1.6 folds higher. Poor results were obtained under microwave heating (75 W) at a lower temperature (100 °C, entry 6, Table **4.9**).

Table 4.9: Upgradation of ethanol catalyzed by **4.22a** under conventional and microwave heating.[a]

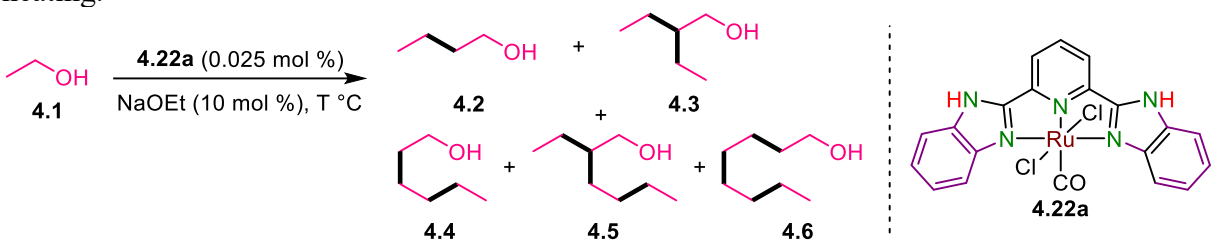

Entry	T (°C)	Time (min)	Yield of **4.2** (%)[b]	Conversion of **4.1** (%)[c]	Selectivity of **4.2** (%)[d]	Total TON[e]
1	140	30	8	8.4	98	336
		60	13	15	84	600
		120	26	33	78	1320
		4320	36	52	69	2099
2	130	30	3	3	99	120
		60	4	4	99	176
		120	6	6	99	260
		4320	30	40	73	1614
3	120	30	2	2	99	80
		60	2	2	99	88
		120	6	6	99	240
		4320	30	35	84	1416
4	110	30	1	1	99	37
		60	1	1	99	45
		120	3.7	3.8	99	152
		4320	22	25	85	1014
5[f]	110	30	11	14	79	580
		60	18	26	69	1045
		120	28	50	56	2000
6[f]	100	30	0.7	0.7	100	30
		60	0.9	0.9	100	40
		120	2.0	2.0	100	80
7[g]	110	30	1	1	100	55
		60	2	3	67	115
		120	7	8	88	330
8[h]	110	30	6	8	75	335
		60	13	17	76	675
		120	20	30	67	1215
9[i]	110	30	12	14	86	580
		60	18	24	75	945
		120	29	40	73	1600

[a]Reaction condition: ethanol (1 mL, 17.12 mmol), NaOEt (10 mol %) and **4.22a** (0.025 mol %) at T °C. [b]Yield was determined by GC analysis using toluene as an internal standard. [c]Conversion was determined by GC analysis using toluene as an internal standard. [d]Selectivity = Yield of *n*-butanol/Conversion of **4.1**. [e]Total TON = Total yield of upgraded products/**4.22a** loading. [f]Under 75 W microwave. [g]Under 50 W microwave. [h]Under 65 W microwave. [i]Under 90 W microwave.

The initial rate and productivity of the *n*-butanol formation improved upon increasing the power of microwave irradiation and followed the trend 50 W < 65 W < 75 W (entry 5 vs. entries 7 and 8, Table **4.9**). However, upon the further increase in the power to 90 W, there was hardly any improvement in the formation or *n*-butanol (entry 5 vs. entry 9, Table **4.9**).

Further optimization was hence carried out using a microwave irradiation of 75 W at 110 °C to arrive at the most efficient catalytic system. Various inorganic and organic bases were screened for the Guerbet reaction in the presence of (^{Bim2}NNN)RuCl$_2$(CO) (**4.22a**) (Table **4.10**). In comparison to NaOEt, under otherwise identical conditions, the productivity and initial rate in the presence of NaO^{t}Bu (10 mol %) was 3.6 folds and 72 folds lower respectively (entry 2 vs. l, Table **4.10**).

The **4.22a** catalyzed Guerbet reaction in the presence of KO^{t}Bu (10 mol %) proceeded about 1.65 times slower than the corresponding reaction with NaOEt but with comparable productivity (entry 3 vs. 1, Table **4.10**). While both NEt$_3$ and Na$_2$CO$_3$ were not reactive (entry 4 and 5, Table **4.10**), poor activity (160 TON at an initial rate of 40 TO/h) were obtained upon the use of K$_2$CO$_3$ (entry 6, Table **4.10**). The initial rate of the **4.22a** catalyzed Guerbet reaction in the presence of NaOH was comparable to that performed in the presence of NaOEt albeit with 50% of the productivity (entry 7 vs. l, Table **4.10**). In comparison, the results obtained from the corresponding reactions with KOH were modest (800 TON at an initial rate of 880 TO/h, entry 8, Table **4.10**). Thus, the catalytic system containing NaOEt performed exceedingly well in comparison to other bases. Further optimization revealed that the best results were obtained at a loading of 10 mol % of NaOEt (entry 1 vs. entries 9-12, Table **4.10**).

With the increase in **4.22a** loading from 0.025 mol % to 1 mol % the initial-rate and productivity of *n*-butanol formation increased only up to about 1.5 times with an associated drastic decrease (28 folds) in turnovers (entry 1 vs. entries 2-6, Table **4.11**). Hence, further optimization of various catalysts was carried out at a catalyst loading of 0.025 mol % (Table **4.12**). However, it should be noted that with 1 mol % loading of **4.22a**, 42% yield of *n*-butanol was obtained at an ethanol conversion of 72%. These unprecedented results eclipse the previous best obtained with these catalysts under conventional heating that too at considerably lower temperature (entry l, Table **4.9** vs. entry 6, Table **4.11**). The performance of pincer-Ru catalysts based on *bis*(imino)pyridine ligands was not on-par in comparison with the corresponding catalysts based on 2,6-*bis*(benzimidazole-2yl) pyridine ligands (entries 1-4 and 7-10 vs. entries 5-6 and 11-12, Table **4.12**). Furthermore, the pincer-Ru carbonyl complexes **4.22a** and **4.22c**

were more productive towards *n*-butanol formation than their corresponding phosphine counterparts **4.21a** and **4.21c** (entries 5-6 vs. 11-12, Table **4.12**).

Table 4.10: Upgradation of ethanol catalyzed by **4.22a** in the presence of various bases.[a]

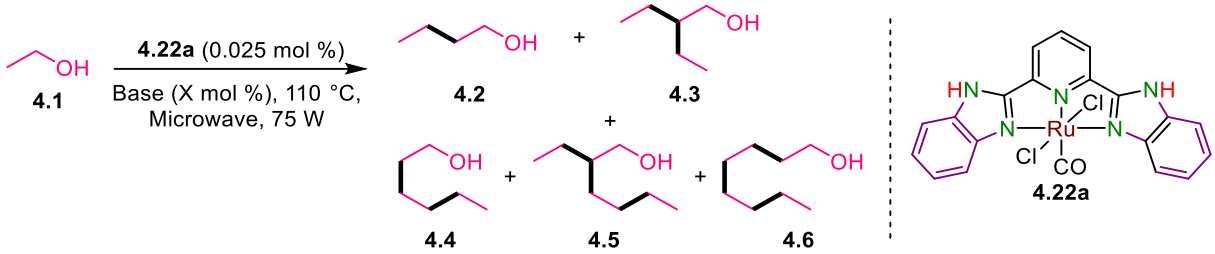

Entry	Base (X mol %)	Time (min)	Yield of **4.2** (%)[b]	Conversion of **4.1** (%)[c]	Selectivity of **4.2** (%)[d]	Total TON[e]
1	NaOEt	30	11	14	79	580
	10.0	120	28	50	56	2000
2	NaO^{t}Bu	30	2	2	100	80
	10.0	120	10	14	71	560
3	KO^{t}Bu	30	8	8	100	350
	10.0	120	34	46	74	1845
4	NEt_3	30	0	0	--	--
	10.0	120	0	0	--	--
5	Na_2CO_3	30	0	0	--	--
	10.0	120	0	0	--	--
6	K_2CO_3	30	0.5	0.5	100	20
	10.0	120	4	4	100	160
7	NaOH	30	10	13	77	520
	10.0	120	22	29	76	1160
8	KOH	30	12	12	100	480
	10.0	120	18	20	90	800
9	NaOEt	30	5	5	100	215
	2.5	120	19	23	83	930
10	NaOEt	30	2	2	100	80
	5.0	120	20	24	83	970
11	NaOEt	30	4	5	80	210
	7.5	120	29	36	81	1455
12	NaOEt	30	2	3	67	120
	20	120	8	9	89	380

[a]Reaction condition: ethanol (1 mL, 17.12 mmol), base (X mol %) and **4.22a** (0.025 mol %) at 110 °C under 75 W microwave. [b]Yield was determined by GC analysis using toluene as an internal standard. [c]Conversion was determined by GC analysis using toluene as an internal standard. [d]Selectivity = Yield of *n*-butanol/Conversion of **4.1**. [e]Total TON = Total yield of upgraded products/**4.22a** loading.

Table 4.11: Upgradation of ethanol at various loading of **4.22a**.[a]

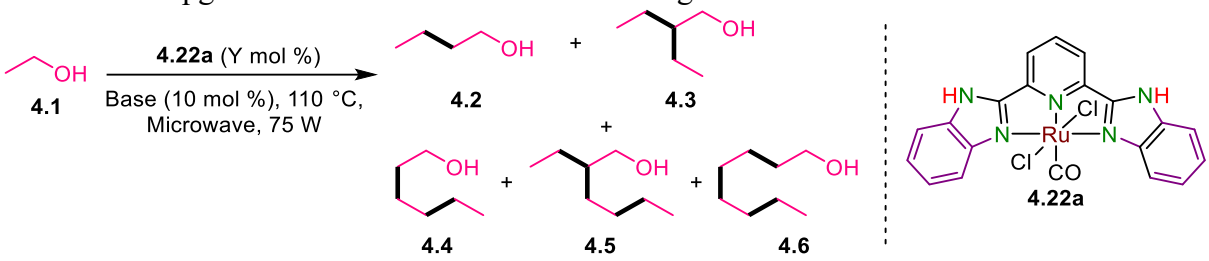

Entry	**4.22a** (Y mol %)	Time (min)	Yield of **4.2** (%)[b]	Conversion of **4.1** (%)[c]	Selectivity of **4.2** (%)[d]	Total TON[e]
1	0.025	30	11	14	79	580
		60	18	26	69	1045
		120	28	50	56	2000
2	0.050	30	14	16	88	320
		60	25	32	78	640
		120	34	51	67	1020
3	0.075	30	15	17	88	230
		60	29	40	73	540
		120	40	61	66	815
4	0.100	30	13	15	87	150
		60	32	44	73	445
		120	41	69	59	690
5	0.500	30	15	18	86	35
		60	30	47	64	94
		120	41	71	58	142
6	1.000	30	18	21	87	21
		60	35	50	69	50
		120	42	72	57	72

[a]Reaction condition: ethanol (1 mL, 17.12 mmol), NaOEt (10 mol %) and **4.22a** (Y mol %) at 110 °C under 75 W microwave. [b]Yield was determined by GC analysis using toluene as an internal standard. [c]Conversion was determined by GC analysis using toluene as an internal standard. [d]Selectivity = Yield of *n*-butanol/Conversion of **4.1**. [e]Total TON = Total yield of upgraded products/**4.22a** loading.

Among the pincer-Ru carbonyl complexes based on 2,6-*bis*(benzimidazole-2-yl) pyridine ligands, while **4.22a** demonstrated a better initial rate in ethanol to *n*-butanol upgradation, the catalyst **4.22c** was not only more selective towards *n*-butanol formation but also more sustainable and hence more productive (entry 5 vs. 6, Table **4.12**). The better *n*-butanol selectivity and productivity obtained with **4.22c** offers great promise as its hydroxyl group could potentially be heterogenized on various solid supports to achieve recyclability.

Table 4.12: Pincer-ruthenium catalyzed ethanol upgradation.[a]

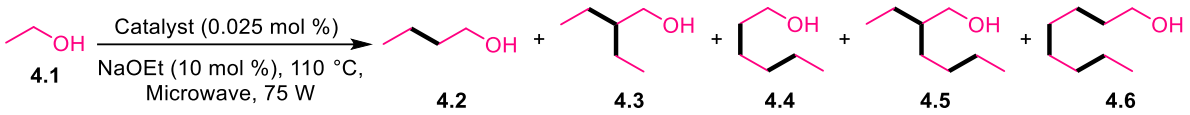

Entry	Catalyst	Time (min)	Yield of **4.2** (%)[b]	Conversion of **4.1** (%)[c]	Selectivity of **4.2** (%)[d]	Total TON[e]
1	**4.20a**	30	4	4	100	160
		120	4	4	100	180
2	**4.20b**	30	3	3	100	120
		120	6	6	100	230
3	**4.20c**	30	3	3	100	105
		120	4	4	100	180
4	**4.20d**	30	2	2	100	80
		120	5	6	83	250
5	**4.22a**	30	11	14	79	580
		120	28	50	56	2000
6	**4.22c**	30	8	8	100	310
		120	45	61	74	2440
7	**4.19a**	30	3	3	100	125
		120	5	5	100	205
8	**4.19b**	30	5	5	100	205
		120	10	12	83	490
9	**4.19c**	30	5	5	100	190
		120	6	6	100	250
10	**4.19d**	30	2	2	100	90
		120	4	4	100	160
11	**4.21a**	30	8	9	89	375
		120	27	36	75	1430
12	**4.21c**	30	7	9	78	380
		120	27	31	87	1255

[a]Reaction conditions: ethanol (1 mL, 17.12 mmol), NaOEt (10 mol %) **4.19a-d**, **4.20a-d**, **4.21a**, **4.21c**, **4.22a** and **4.22c** (0.025 mol %) at 110 °C under 75 W microwave. [b]Yield was determined by GC analysis using toluene as an internal standard. [c]Conversion was determined by GC analysis using toluene as an internal standard. [d]Selectivity = Yield of *n*-butanol/Conversion of **4.1**. [e]Total TON = Total yield of upgraded products/catalyst loading.

4.3.4 Mechanistic studies on the upgradation of ethanol catalyzed by pincer-ruthenium catalysts.

Magnetic moments were calculated using the Evan's NMR spectroscopy method.[75] The magnetic moment of the reaction mixture was recorded in $CDCl_3$ containing **3.22a** (0.025 mol %) in the presence of 10 mol % NaOEt. No shift was observed of the toluene peak for the samples in the inner and outer tubes, which indicates the absence of Ru(III) species (Figure **4.9**). Similar result was observed by EPR study of the reaction mixture (Appendix III). On the

other hand, in presence of TEMPO (10 mol %) the rate of reaction was not hampered (44% ethanol conversion at 25% *n*-butanol yield with 57% selectivity).

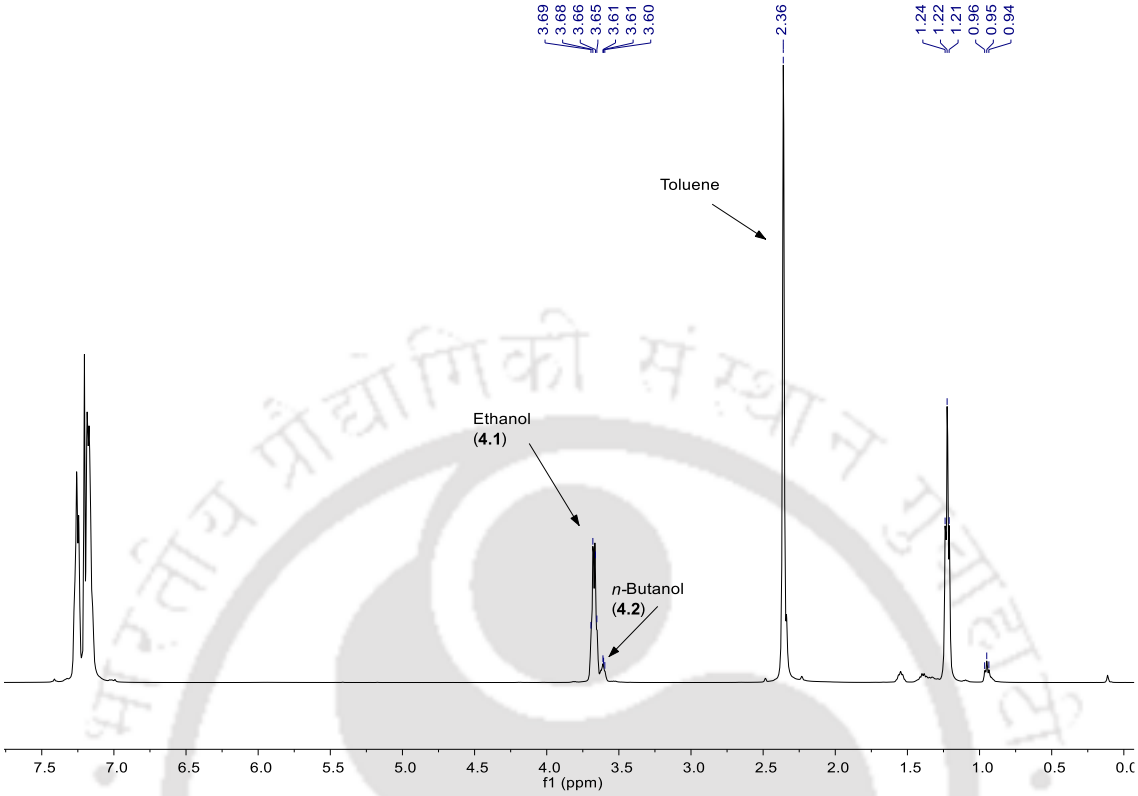

Figure 4.9: ^{1}H NMR spectra of the reaction mixture in $CDCl_3$ of **4.22a** catalyzed ethanol upgradation with NaOEt (10 mol %) after 30 minutes heating at 110 °C under microwave radiation.

The 16-electron five coordinate dichloride species **4.27** (Scheme **4.10**) is likely to be the active species that is generated in the first step of the Guerbet *via* the dissociation of the ancillary ligand (PPh_3 from **4.21a** Scheme **4.10**). The loss of PPh_3 was detected as Ph_3PO in the reaction catalyzed by **4.21a** (Figure **4.10**). The salt metathesis of 16-electron five-coordinate dichloride species **4.27′** with NaOEt results in the formation of the active Ru-ethoxide species **4.27**.[70]

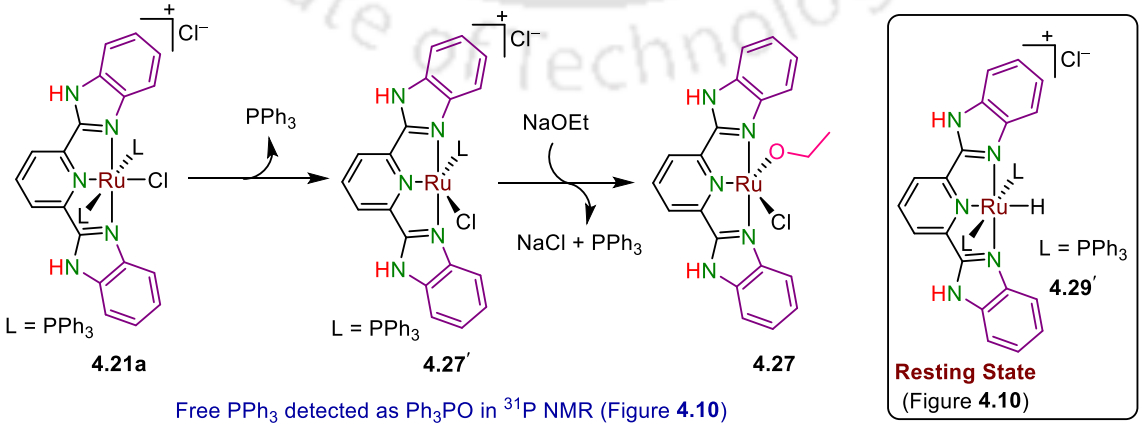

Scheme 4.10: Mechanistic studies on the upgradation of ethanol catalyzed by pincer-ruthenium catalysts

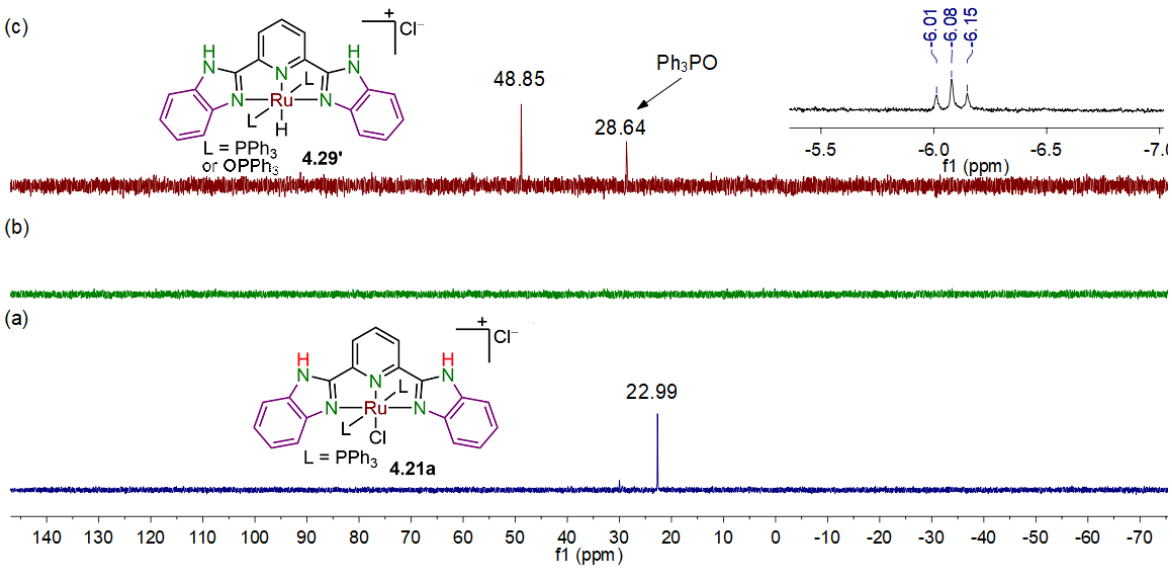

Figure 4.10: (a) The ^{31}P NMR spectra of **4.21a** in $CDCl_3$. (b) The ^{31}P NMR spectra of **4.21a** (10 mol %) in C_6D_6. (c) The ^{31}P NMR spectra of **4.21a** (10 mol %) in C_6D_6 containing ethanol (6 μL, 0.10 mmol), NaOEt (25 mol %) after subjecting to conventional heating (140 °C) for 10 minutes. The region of the corresponding ^{1}H NMR spectra that depicts the hydride signal is given in the inset.

Subsequent β-hydride elimination (Path **A**, Scheme **4.11**) gives acetaldehyde (**4.1a**) while leading to the formation of Ru–H species **4.29** *via* **TS-4.28.** This step is downhill (ΔG_{110} = -6.84 kcal/mol) with a barrier of 10.47 kcal/mol. A follow-up σ-bond metathesis between the O–H of **4.1** and the Ru–H of **4.29** results in release of H_2 apart from the regeneration of the active species **4.27** (Path **A**, Scheme **4.11**). The evolution of H_2 in these reactions have been confirmed by GC analysis of the head space (Figure **4.11**).[70]

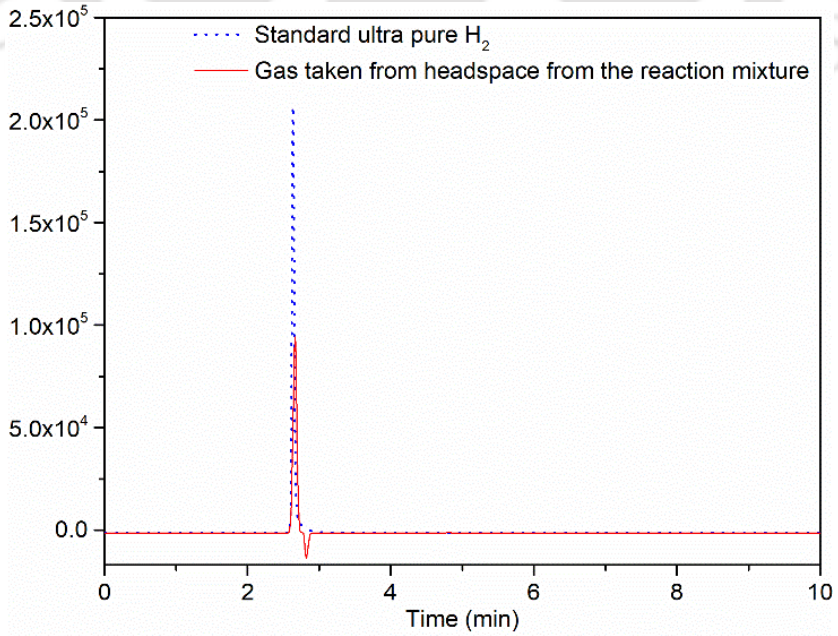

Figure 4.11: H_2 analyzed *via* GC analysis of the head-space of the reaction vessel during the ethanol upgradation reaction catalyzed by **4.22a** at 110 °C under 75 W microwave.

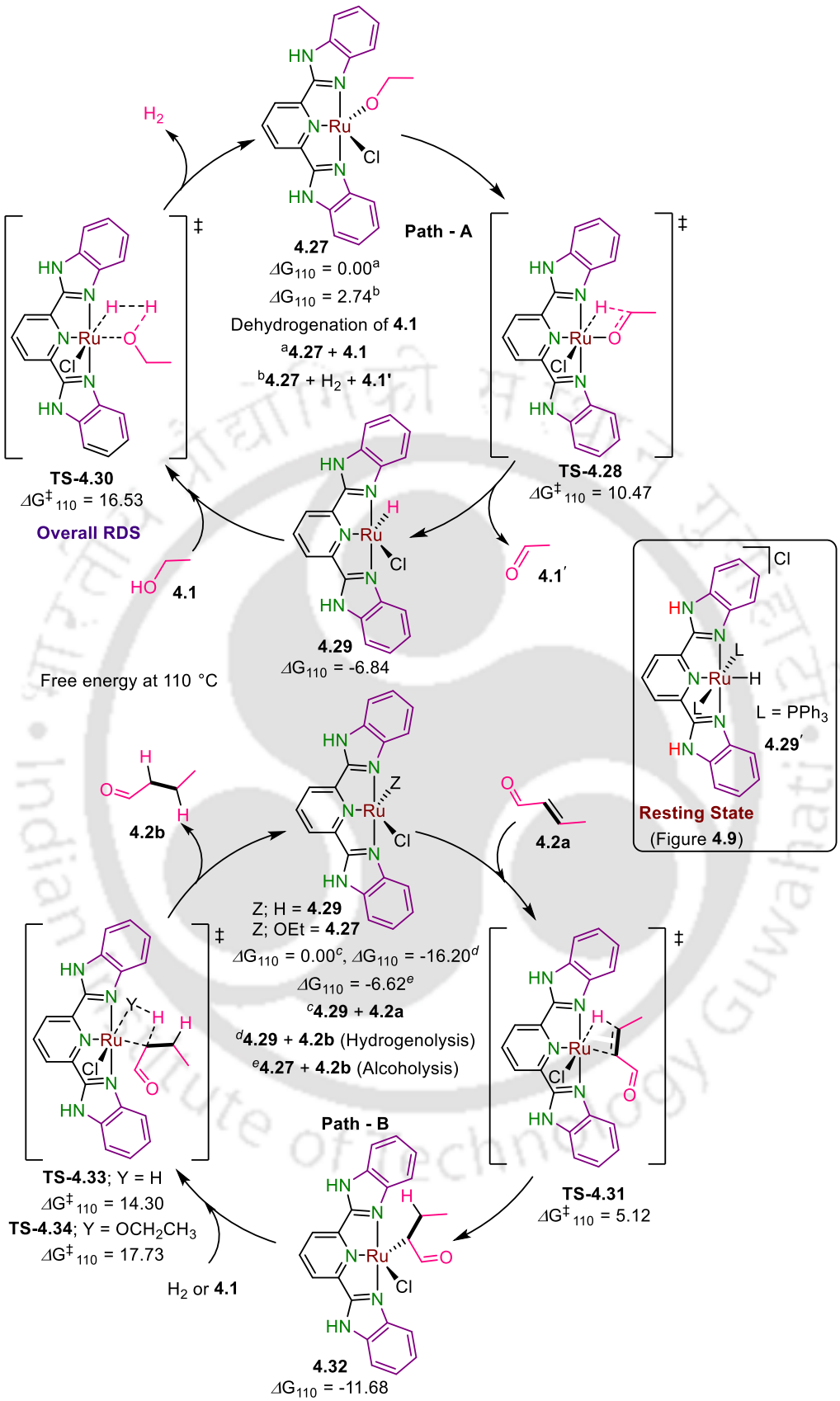

Scheme 4.11: Plausible mechanism involved in **4.21**/**4.22** catalyzed dehydrogenation of **4.1** and hydrogenolysis/alcoholysis of **4.2a**. Free energy are given in kcal/mol and calculated at 110 °C.

Furthermore, this rate-determining step (RDS) which goes through **TS-4.30** ($\Delta G^{\ddagger}_{110}$ = 23.37 kcal/mol) is computed to be an uphill process (ΔG_{110} = 9.58 kcal/mol). Gratifyingly, the lower energy intermediate **4.29**, of this RDS **4.29→4.27** is detected as its phosphine adduct **4.29'** (Figure **4.10**). This is not surprising as further computational analysis of other segments (*vide-infra*) reveals that **4.29→4.27** is the overall RDS and hence **4.29'** is the resting state of the reaction. The overall dehydrogenation is uphill by 2.74 kcal/mol.

An aldol condensation of acetaldehyde (**4.1a**) in the presence of NaOEt gives rise to the α,β-unsaturated aldehyde (**4.2a**) (equation 1) The next step involving the insertion of the C–C double bond in molecule **4.2a** into the Ru–H bond in **4.27** can occur either *via* the H^- transfer to the β-carbon of **4.2a** (Path **B**, Scheme **4.11**) or to the α-carbon of **4.2a** (Path **C**, Scheme **4.12**). The hydride transfer to the β-carbon would generate the species **4.32** *via* **TS-4.31** ($\Delta G^{\ddagger}_{110}$ = 5.12 kcal/mol) in a downhill reaction (ΔG_{110} = -11.68 kcal/mol) (Path **B**, Scheme **4.11**). The hydrogenolysis step **4.32→TS-4.33→4.29** is downhill (ΔG_{110} = -4.52 kcal/mol) with a barrier of 25.98 kcal/mol. On the other hand, the alcoholysis step **4.32→TS-4.34→4.29** is uphill (ΔG_{110} = 5.06 kcal/mol) with a high barrier ($\Delta G^{\ddagger}_{110}$ = 29.41 kcal/mol) (Path **B**, Scheme **4.11**). If Path **B** is involved it is likely to proceed *via* hydrogenolysis owing to its lower barrier in comparison to alcoholysis. Moreover, hydrogenolysis is the RDS of this segment involving Path **B**.

On the other hand, the hydride transfer to the α-carbon **4.2a** (Path **C**, Scheme **4.12**) would generate the species **4.36** *via* **TS-4.35** ($\Delta G^{\ddagger}_{110}$ = 12.10 kcal/mol) in a downhill reaction (ΔG_{110} = -3.85 kcal/mol) (Path **C**, Scheme **4.12**). This is followed by the product **4.2b** formation step *via* a σ-bond metathesis between Ru–C of **4.36** and H–H *via* **TS-4.37** ($\Delta G^{\ddagger}_{110}$ = 22.54 kcal/mol, hydrogenolysis) while regenerating **4.29** in a downhill process (ΔG_{110} = -12.35 kcal/mol). Alternatively, the σ-bond metathesis between Ru–C of **4.36** and the O–H of **4.1** while going through **TS-4.38** ($\Delta G^{\ddagger}_{110}$ = 24.53 kcal/mol) would also lead to **4.2b** in addition to the formation of **4.27** which is also downhill (ΔG_{110} = -2.77 kcal/mol) (Path **C**, Scheme **4.12**).

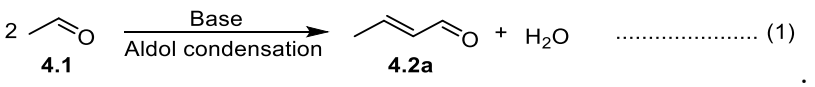

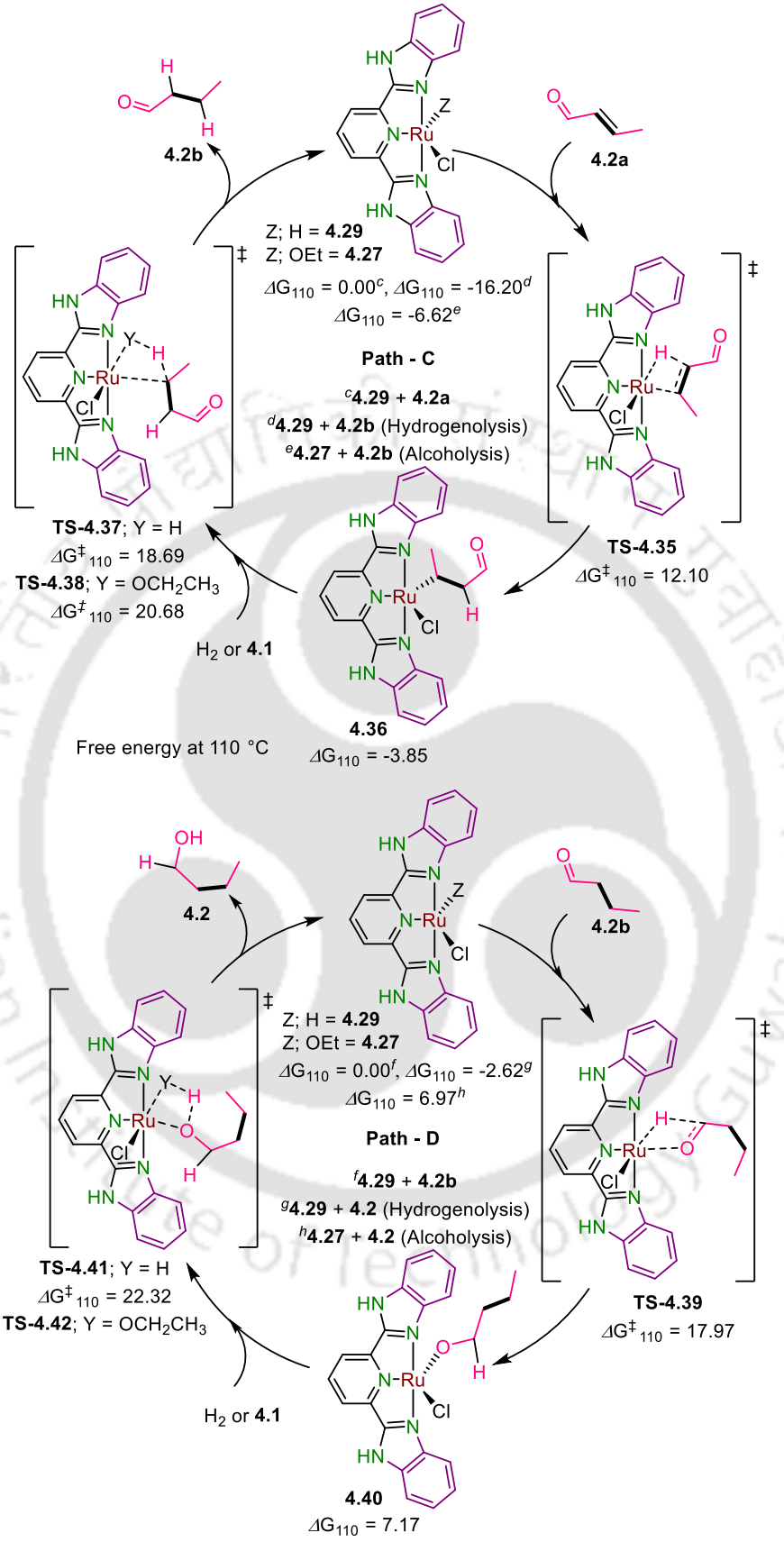

Scheme 4.12: Plausible mechanism involved in **4.21**/**4.22** catalyzed hydrogenolysis/alcoholysis of **4.2a** & **4.2b**. Free energy are given in kcal/mol and calculated at 110 °C.

Very similar to Path **B**, even in the case of Path **C**, hydrogenolysis is more favored in comparison with alcoholysis and is the RDS. However, the RDS ($\Delta G^{\ddagger}_{110}$ = 22.54 kcal/mol) of Path **C** has a lower barrier than the corresponding RDS ($\Delta G^{\ddagger}_{110}$ = 25.98 kcal/mol) of Path **B** which is indicative of the fact that the step involving the insertion of the C–C double bond in molecule **4.2a** into the Ru–H bond in **4.29** actually occurs *via* the H^- transfer to the α-carbon of **4.2a** (Path **C**, Scheme **4.12**).

The first step in the transformation of **4.2b** to **4.2** involves the insertion of **4.2b** into the Ru–H bond of **4.29** giving rise to **4.40** while going through **TS-4.39** $\Delta G^{\ddagger}_{110}$ = 17.97 kcal/mol) in an uphill reaction $\Delta G^{\ddagger}_{110}$ = 7.17 kcal/mol) (Path **D**, Scheme **4.12**). While the hydrogenolysis step **4.40→TS-4.41→4.29** is downhill $\Delta G^{\ddagger}_{110}$ = -9.79 kcal/mol) with a barrier of 15.15 kcal/mol, the corresponding alcoholysis step **4.40→TS-4.42→4.27** is almost thermodynamically neutral the barrier of which could not be determined. However, taking a cue from Path **B** and Path **C**, one can deduce that in Path **D**, hydrogenolysis would be kinetically more favorable in addition to the fact that it is thermodynamically preferred in comparison to alcoholysis by 9.59 kcal/mol. Insertion of **4.2b** into the Ru–H bond in **4.27** thus appear to be the RDS even in the case of Path **D** (Scheme **4.12**).

Upon comparison of the individual RDS of Path **A** ($\Delta G^{\ddagger}_{110}$ = 23.37 kcal/mol), Path **B** ($\Delta G^{\ddagger}_{110}$ = 22.54 kcal/mol) and Path **D** $\Delta G^{\ddagger}_{110}$ = 17.97 kcal/mol) that contribute to the overall upgradation of ethanol (**4.1**) to *n*-butanol (**4.2**), one can infer that the generation of hydrogen *via* the alcoholysis step **4.29→4.27** is the overall RDS. This sort of bodes well with the detection of lower energy intermediate **4.29** in the form of its phosphine adduct **4.29'** as the resting state of the catalyst **4.21a** (Figure **4.10**).

4.3.5 Upgradation of ethanol catalyzed by pincer-ruthenium catalysts immobilized on solid supports.

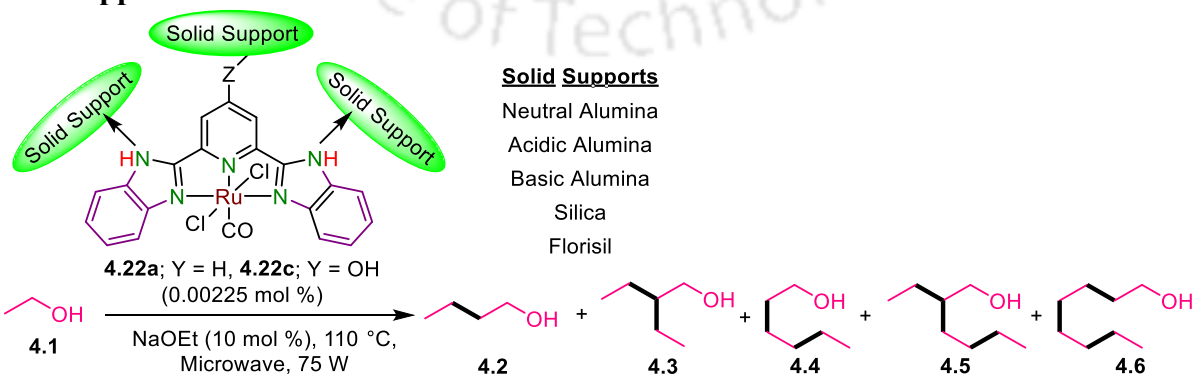

Scheme 4.13: Upgradation of ethanol catalyzed by carbonyl pincer-ruthenium catalysts immobilized on solid supports.

Table 4.13. Upgradation of ethanol by **4.22a** and **4.22c** heterogenized on various solid supports (See Scheme **4.13**).[a]

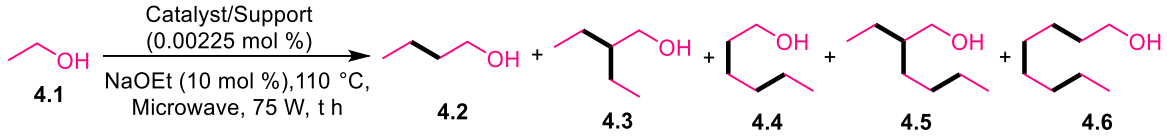

Entry	Catalyst /Support	Time (min)	Yield of **4.2** (%)[b]	Conversion of **4.1** (%)[c]	Selectivity of **4.2** (%)[d]	Total TON[e]
1	**4.22a**	30	2.8	2.8	100	1245
		60	5.2	5.4	96	2400
		120	22.8	29.3	78	13022
2	**4.22a**/Neutral Alumina	30	4.3	4.3	100	1867
		60	5.5	5.6	98	2193
		120	6.9	9.2	75	4090
3	**4.22a**/Acidic Alumina	30	2.7	2.7	100	1080
		60	3.2	3.2	100	1285
		120	5.2	5.8	90	2580
4	**4.22a**/Basic Alumina	30	1.2	1.2	100	535
		60	1.4	1.4	100	550
		120	4.6	5.1	92	2265
5	**4.22a**/Silica	30	2.2	2.2	100	975
		60	3.9	4.2	94	1865
		120	9.1	9.9	92	4400
6	**4.22a**/Florisil	30	2.1	2.2	95	980
		60	4.1	4.4	93	1955
		120	9.1	9.7	93	4310
7	**4.22c**	30	5.2	5.2	99	2310
		60	19.6	20.6	95	9155
		120	25.4	28.6	89	12710
8	**4.22c**/Neutral Alumina	30	6.2	9.3	67	4135
		60	11.5	15.9	72	7065
		120	13.0	19.6	66	8710
9	**4.22c**/Acidic Alumina	30	5.6	5.6	100	2489
		60	12.1	12.6	96	5620
		120	26.8	34.9	77	15510
10	**4.22c**/Basic Alumina	30	2.6	2.7	96	1200
		60	3.1	3.3	94	1465
		120	5.8	6.4	90	2845
11	**4.22c**/Silica	30	6.2	6.5	95	2890
		60	12.0	12.8	93	5690
		120	21.2	27.7	76	12310
12	**4.22c**/Florisil	30	2.9	2.9	100	1290
		60	6.0	6.8	88	3020
		120	9.6	10.9	88	4845

[a]Reaction conditions: ethanol (1 mL, 17.12 mmol), NaOEt (10 mol %) **4.22a** or **4.22c** (0.00225 mol %) at 110 °C under 75 W microwave. [b]Yield was determined by GC analysis using toluene as an internal standard. [c]Conversion was determined by GC analysis using toluene as an internal standard. [d]Selectivity = Yield of *n*-butanol/Conversion of **4.1**. [e]Total TON = Total yield of upgraded products/**4.22a** or **4.22c** loading.

With an objective to obtain better turnovers, the loading of the pincer-Ru carbonyl complexes **4.22a** and **4.22b** which demonstrated the best efficiency was further lowered to 0.00225 mol % (entries 1 and 7, Table **4.13**). Gratifyingly, even at such low loadings good selectivity, high rate (2490 TO/h) and turnovers (13022 TON) were obtained in the **4.22a** catalyzed ethanol upgradation to *n*-butanol (entry l, Table **4.13**, Scheme **4.13**). Notably there was hardly any drop (0.82 times) in the *n*-butanol yield when the **4.22a** loading was decreased 11 folds from 0.025 mol % to 0.00225 mol % (entry 5, Table **4.9** vs. entry 1, Table **4.13**).

Even at lower loadings **4.22c** out-performed **4.22a** in terms of rate, productivity and selectivity towards *n*-butanol formation (entry 7 vs. entry l, Table **4.13**). The catalyst **4.22a** with polar NH groups could be anchored on various solid supports and it was observed that in all cases the productivity was lost by 3 folds (neutral alumina, silica and florisil, entries 2, 5 and 6, Table **4.13**) to 6 folds (acidic alumina, and basic, entries 3 and 4, Table **4.13**). The initial rate obtained with **4.22a** anchored on to neutral alumina was however better than **4.22a** alone by 1.37 folds (entry 1 vs. entry 2, Table **4.13**). The catalytic systems comprising of **4.22a** on various supports were however not recyclable.

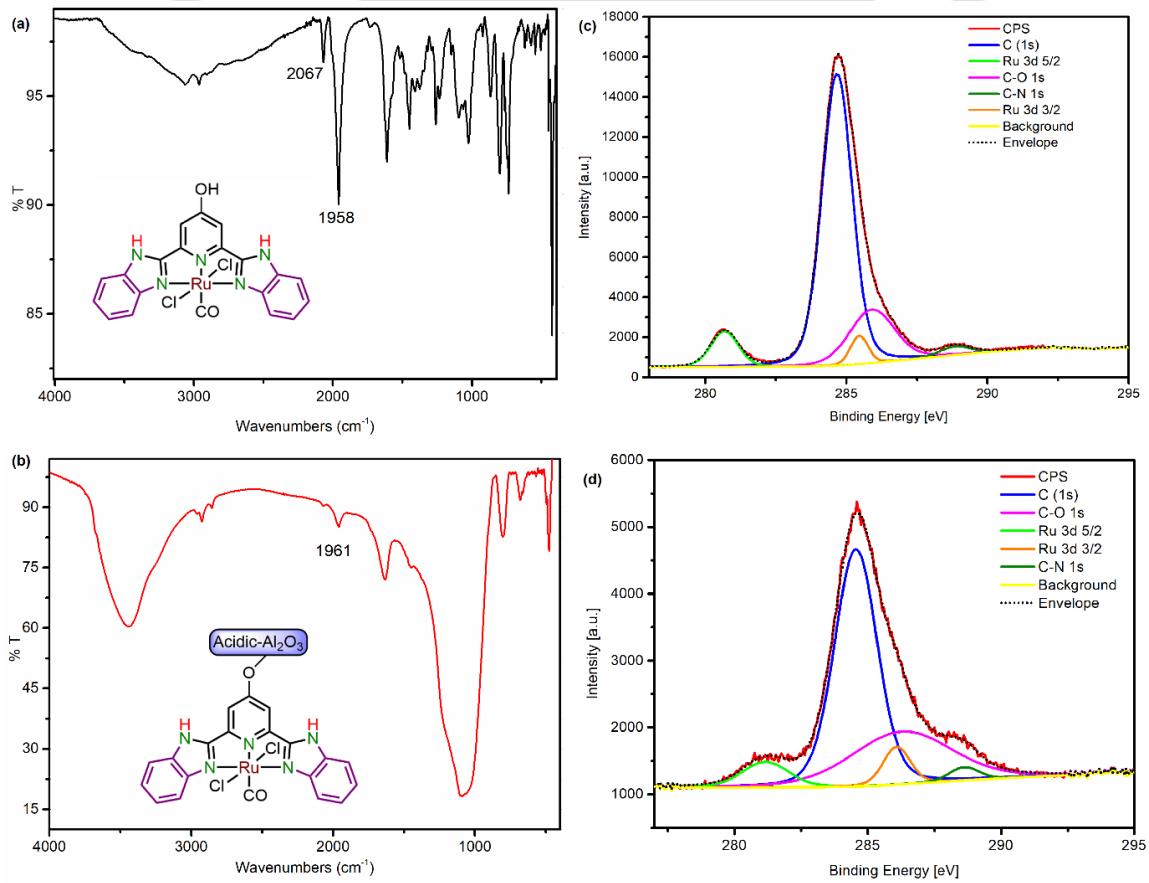

Figure 4.12: (a) IR spectra of **4.22c**. (b) IR spectra of **4.22c** immobilized on acidic alumina. (c) XPS analysis of **4.22c**. (d) XPS analysis of **4.22c** immobilized on acidic alumina.

Better results were obtained when **4.22c** with a polar OH group in the *para*-position of the arene ring was heterogenized. Figure **4.12** depicts the IR and XPS analysis of **4.22c** before and after immobilization on acidic alumina. After anchoring **4.22c** on to acidic alumna, while IR studies indicate that the carbonyl group is intact thereby providing an indirect evidence for the presence of immobilized molecular Ru complex as well, XPS analysis demonstrate that the central Ru retains its +2-oxidation state.[76] The collective inference drawn from IR and XPS analysis clearly suggests that the integrity of the molecular complex is not hampered upon immobilization. The catalytic system comprising of **4.22c** on neutral alumina resulted in a 1.79-fold increase in the rate of the reaction whereas the productivity dropped by 1.46 folds (entries 7 vs. 8, Table **4.13**). On the other hand, upon using **4.22c**/acidic alumina, higher productivity was observed with comparable initial rates (entries 7 vs. 9, Table **4.13**). Use of basic alumina and florisil had a detrimental effect on both the initial rates and the productivity of ethanol upgradation (entries 10 and 12, Table **4.13**).

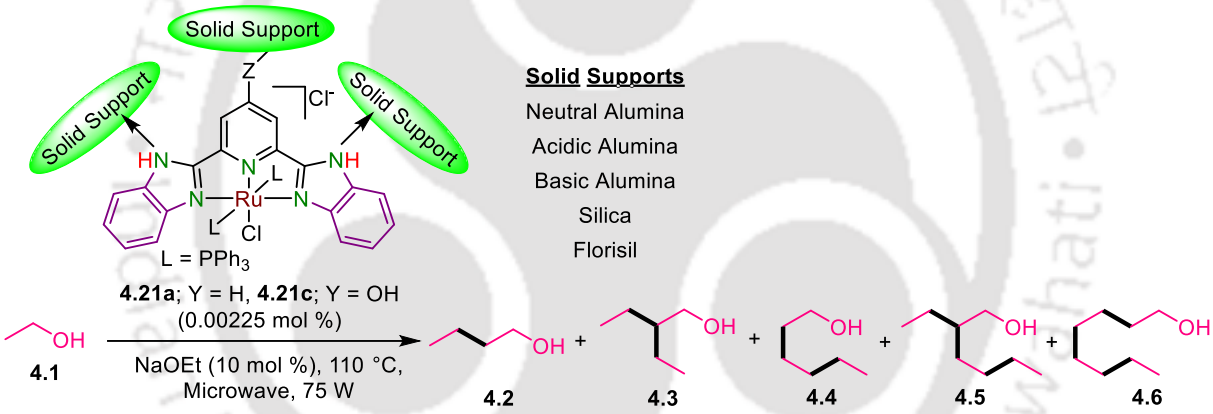

Scheme 4.14: Upgradation of ethanol catalyzed by phosphine based pincer-ruthenium catalysts immobilized on solid supports.

The catalytic system based on **4.22c**/silica performed at rates comparable to **4.22c** and resulted in similar productivity as that of **4.22c**. However, similar to the results obtained with catalytic systems containing **4.22a** over various supports, analogous systems comprising of **4.22c** on various supports were also not recyclable. The catalytic systems containing **4.21a** and **4.21c** over various supports (Table **4.14**, Scheme **4.14**) were also not recyclable and their reactivity were not on-par when compared to analogous systems comparing of **4.22a** and **4.22c** on various support (Table **4.13**).

Table 4.14. Upgradation of ethanol by **4.21a** and **4.21c** heterogenized on various solid supports (See Scheme **4.14**).[a]

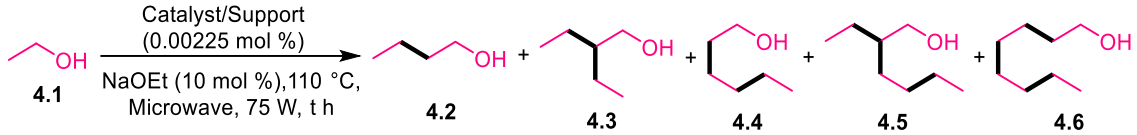

Entry	Catalyst /Support	Time (min)	Yield of **4.2** (%)[b]	Conversion of **4.1** (%)[c]	Selectivity of **4.2** (%)[d]	Total TON[e]
1	**4.21a**	30	9.0	9.6	94	4489
		60	13.3	16.3	81	7266
		120	19.1	26.8	71	11955
2	**4.21a**/Neutral Alumina	30	7.6	7.6	100	3380
		60	14.4	14.7	98	6535
		120	23.5	24.3	97	10800
3	**4.21a**/Acidic Alumina	30	trace	trace	--	--
		60	trace	trace	--	--
		120	3.0	3.1	98	1375
4	**4.21a**/Basic Alumina	30	2.5	2.5	100	1110
		60	4.1	4.7	87	2090
		120	9.2	11.7	78	5200
5	**4.21a**/Silica	30	6.7	6.7	100	2978
		60	10.6	12.2	87	5430
		120	17.8	23.5	76	10445
6	**4.21a**/Florisil	30	5.2	6.0	86	2660
		60	10.1	18.9	77	8400
		120	15.2	20.7	73	9200
7	**4.21c**	30	5.8	6.5	89	2889
		60	11.3	12.7	89	5644
		120	19.7	24.1	82	10711
8	**4.21c**/Neutral Alumina	30	1.8	1.9	94	845
		60	3.6	4.1	88	1820
		120	6.2	7.1	87	3155
9	**4.21c**/Acidic Alumina	30	0.52	0.52	100	230
		60	0.85	0.85	100	380
		120	0.97	0.97	100	444
10	**4.21c**/Basic Alumina	30	3.6	4.2	86	1865
		60	6.8	9.8	78	4355
		120	12.1	17.2	70	7645
11	**4.21c**/Silica	30	0.6	0.6	100	266
		60	1.1	1.1	100	420
		120	2.2	2.2	100	978
12	**4.21c**/Florisil	30	0.61	0.61	100	270
		60	0.87	0.87	100	385
		120	1.31	1.31	100	580
13	Alumina Silica, Florisil	120	No reaction	No reaction	--	--

[a]Reaction conditions: ethanol (1 mL, 17.12 mmol), NaOEt (10 mol %) **4.21a** or **4.21c** (0.00225 mol %) at 110 °C under 75 W microwave. [b]Yield was determined by GC analysis using toluene as an internal standard. [c]Conversion was determined by GC analysis using toluene as an internal standard. [d]Selectivity = Yield of *n*-butanol/Conversion of **4.1**. [e]Total TON = Total yield of upgraded products/**4.21a** or **4.21c** loading.

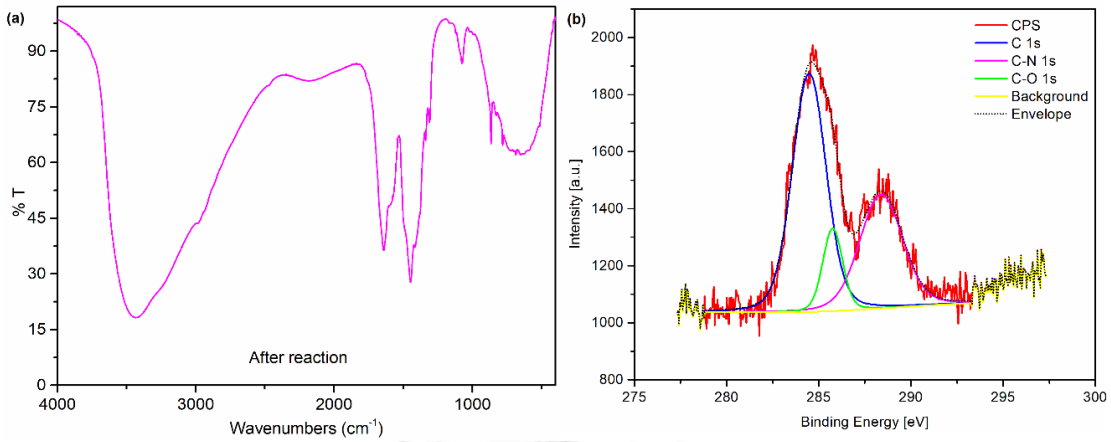

Figure 4.13. (a) IR spectra of spent catalyst (**4.22c** immobilized on acidic alumina). (b) XPS analysis of spent catalyst (**4.22c** immobilized on acidic alumina).

Notably, there was no reaction when the Guerbet reaction was attempted only with each of the solid-support under identical reaction conditions however in the absence of any catalyst (entry 13, Table **4.14**). In order to obtain insight into the lack of recyclability, the IR and XPS analysis (Figure **4.13**) were performed on the spent catalyst obtained from entry 9, Table **4.13**. While IR spectra demonstrates a complete lack of the carbonyl band, the XPS analysis indicates the lack of Ru in any form on the support. These studies provide clear evidence for the complete leaching of Ru from the solid-support upon subjecting it to the reaction conditions.

3.4 Conclusion

The catalytic *β*-alkylation protocol was applied to investigate the upgradation of ethanol to biofuels such as *n*-butanol and higher alcohols. Use of (^{Cy2}NNNRu)Cl_2(CO) resulted in high productivity (335 TONs at 170 TO/h) among the pincer-ruthenium carbonyl complexes based on *bis*(imino)pyridine ligands. By employing sterically more open pincer-ruthenium carbonyl complexes such as (^{Bim2}NNNRu)Cl_2(CO) and (^{MeBim2}NNNRu)Cl_2(CO) based on 2,6-*bis*(benzimidazole-2yl) pyridine ligands, the catalytic activity was greatly enhanced. It is gratifying to note that not only good ethanol conversion (ca. 58 %) but also high turnovers (ca. 2100) with a good rate (ca. 710 TO/h) in the (^{Bim2}NNNRu)Cl_2(CO) catalyzed upgradation of ethanol were observed. Kinetic studies on the ethanol upgradation catalyzed by (^{Bim2}NNNRu)Cl_2(CO) exhibit linear dependence of rate on the concentration of both catalyst and ethanol.

The good microwave absorptivity of ethanol was instrumental in improving the reactivity of the pincer-Ru catalysts towards Guerbet reaction under microwave heating at 110 °C where conventional heating was ineffective. Among the considered carbonyl and phosphine pincer-

ruthenium complexes, ruthenium carbonyl complexes based on 2,6-*bis*(benzimidazole-2-yl)pyridine ligands showed higher activity towards the Guerbet reaction. The corresponding pincer-ruthenium complexes based on *bis*(imino) pyridine ligands demonstrated poor activity. The highest rate (8534 TO/h, ca. 18% yield of *n*-butanol at 90% selectivity) was obtained for the ethanol upgradation catalyzed by 0.00225 mol % [^{Bim2}NNN)RuCl(PPh$_3$)$_2$]Cl in the presence of 10 mol % NaOEt at 110 °C under microwave irradiation at 75 W. However, the best productivity (72% ethanol conversion and 42% yield of *n*-butanol at 57% selectivity) and turnover (ca. 13022 TON with 22.8% yield of *n*-butanol at 73% selectivity) was obtained in the (^{Bim2}NNN)RuCl$_2$(CO) (0.025 mol % and 0.00225 mol % respectively) catalyzed reactions. While DFT calculations indicate the generation of hydrogen to be the rate-determining step (RDS), the corresponding hydride species involved in the RDS has been detected as its phosphine adduct by NMR spectroscopy studies. The hydroxy group on (*p*-OH^{Bim2}NNN)RuCl$_2$(CO) could successfully be anchored on various solid supports and used as a heterogeneous catalyst for the Guerbet reaction albeit with no recyclability. While the catalytic system comprising of (*p*-OH^{Bim2}NNN)RuCl$_2$(CO) immobilized over neutral alumina resulted in the highest rate (8270 TO/h), the corresponding system heterogenized over acidic alumina gave the best productivity of 15510 TON. The current study on use of pincer-Ru catalysts and their immobilized versions at very low loadings under microwave conditions to upgrade feed agnostic ethanol to versatile *n*-butanol at a very high rate along with good yields and unprecedented turnovers offers ample opportunities for future improvisations of related catalytic systems for this reaction of high synthetic utility.

3.5 Experimental section

3.5.1 General methods and materials

All optimizations were carried out under purified Ar using a standard double manifold or a glove box. The solvents such as tetrahydrofuran (THF), hexane and toluene were dried *via* double distillation over Na/Benzophenone prior to the experiment.[77-78] Ethanol was dried and distilled under argon condition according to the literature procedure.[77-78] All other compounds including pryidine-2,6-dicarboxylic acid, 4-hydroxypryidine-2,6-dicarboxylic acid, *o*-penylenediamnine, [RuCl$_2$(*p*-cymene)]$_2$, Al$_2$O$_3$, SiO$_2$, MgSiO$_3$, DMSO-d$_6$ and CDCl$_3$ were purchased either from MERCK or Sigma-Aldrich and were used as such. The complexes (**4.19a-d** and **4.20a-d**) were prepared according to the procedure reported in Chapter **II** and **III**.[69, 71]

^{1}H, ^{13}C, ^{31}P NMR spectra were recorded either on Bruker ASCEND 600 operating at 600 MHz for ^{1}H, 150 MHz for ^{13}C & 243 MHz for ^{31}P or on Bruker AVANCE 400 operating at 400 MHz for ^{1}H, 100 MHz for ^{13}C & 162 MHz for ^{31}P. The mass analysis was done using an Agilent Accurate-Mass Q-Toff ESI-MS 6520. Fourier Transform Infrared (FT-IR) were recorded on Perkin Elmer Spectrum Two FT-IR spectrometer at room temperature with the region 400-4000 cm^{-1}. All microwave reactions were performed using a CEM Discover microwave system unit (operating at 110 V, microwave irradiation of 2.45 GHz, maximum microwave output of 300 W) in a 10 mL microwave tube. GC analyses (FID detection) were performed on a Agilent 8860-GC instrument fitted with Agilent Front SSL inlet N2 HP-5 column (30 m length ´ 0.32 mm ID) using the following method: Agilent 8860-GC Detector, Oven temperature 60-300 °C, Time at starting temp: 0 min, Final time = 10 min, Flow rate (carrier): 1 mL/min (N2), Split ration: 250, Inlet temperature: 250 °C, Detector temperature: 300 °C. H_2 gas analysis (TCD detection) was performed on a Agilent 7820-GC instrument fitted with Agilent Front SSZ Inlet N2 HP-PLOT Q column (30 m length ´ 0.53 mm ID) using the following method: Agilent 7820-GC Detector, Oven temperature 40 °C, Time at starting temp: 0 min, Hold time = 10 min, Flow rate (carrier): 1 mL/min (N2), Split ration: 50, Inlet temperature: 40 °C, Detector temperature: 250 °C. XPS analysis was carried out in ULVAC-PHI measurement in PHI 5000 Versa Prob III scanning XPS microprobe.

4.5.2 Synthesis of complexes of the type [(*p*-z^{R2}NNN)RuCl(PPh$_3$)$_2$]Cl (4.21a; R = Bim, z = H, 4.21b; R = Bim, z = OH, 4.21c and R = MeBim, z = H) and (*p*-z^{R2}NNN)RuCl$_2$(CO) (4.22a; R = Bim, z = H, 4.22b; R = Bim, z = OH, 4.22c and R = MeBim, z = H).

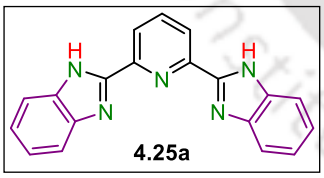

Synthesis of 2,6-*bis*(1H-benzimidazol-2-yl)pyridine (4.25a): To a two-necked round bottom flask (100 mL) containing pyridine-2,6-dicarboxylic acid (**4.23a**) (0.050 g, 0.6 mmol) and *o*-phenylenediamine (**4.24**) (0.260 g, 1.2 mmol), orthophosphoric acid (10 mL) was added. The reaction mixture was heated overnight at 150 °C. A bluish green precipitate was obtained to which sodium bicarbonate solution (10 mL) was added. The residue was filtered and washed with water. The product was crystallized in methanol to obtain 0.135 g of an off-white solid in 74% yield. ^{1}H NMR (400 MHz, DMSO-d_6) δ = 12.99 (s, 2H, N*H*), 8.34 (d, J = 7.8 Hz, 2H, Ar), 8.17 (t, J = 9.0 Hz, 1H, Ar), 7.78 (d, J = 8.0 Hz, 2H, Ar), 7.73 (d, J = 7.9 Hz, 2H, Ar), 7.35 (t, J = 7.5 Hz, 2H, Ar), 7.28 (t, J = 7.6 Hz, 2H, Ar). ^{13}C NMR (101 MHz, DMSO-d_6) δ = 149.98, 147.23, 143.67, 138.70, 133.87, 123.24, 121.71, 120.88, 119.23, 111.27 (Ar). HRMS (ESI): *m/z* calculated for $[C_{19}H_{13}N_5+H]^+$; = 312.1243, Found = 312.1413.

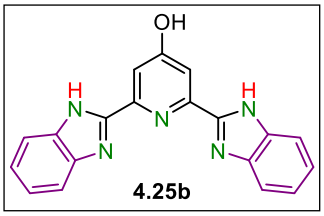

Synthesis of 2,6-*bis*(1H-benzo[d]imidazol-2-yl)pyridin-4-ol (4.25b): To a two-necked round bottom flask (100 mL) containing 4-Hydroxypyridine-2,6-dicarboxylic acid (**4.23b**) (0.2 g, 1.09 mmol) and *o*-phenylenediamine (**4.24**) (0.236 g, 2.18 mmol), orthophosphoric acid (20 mL) was added. The reaction mixture was heated overnight at 150 °C. A bluish green precipitate was obtained to which sodium bicarbonate solution (10 mL) was added. The residue was filtered and washed with water (10 mL). The product was crystallized in methanol to obtain 0.195 g of an off-white solid in 55% yield. ^{1}H NMR (600 MHz, DMSO-d_6) δ = 13.10 (s, 2H, N*H*), 7.70-7.64 (m, Hz, 4H, Ar), 7.43 (d, J = 19.7 Hz, 2H, Ar), 7.22 (d, J = 14.1 Hz, 4H, Ar). ^{13}C NMR (151 MHz, DMSO-d$_6$) δ = 169.74, 166.40, 166.05, 165.21, 150.64, 149.91, 149.23, 148.80, 122.94, 112.49, 111.16, 108.76 (Ar). HRMS (ESI): *m/z* calculated for $[C_{19}H_{13}N_5O+H]^+$; = 328.1198, Found = 328.1187

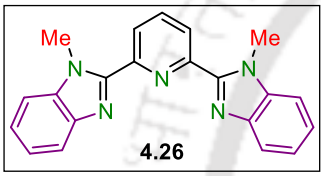

Synthesis of 2,6-*bis*(1-methyl-1H-benzo[d]imidazol-2-yl)pyridine (4.26): To a round bottom flask (50 mL) containing **4.25a** (0.100 g, 0.32 mmol) and KOH (0.090, 1.60 mmol), acetone (10 mL) was added and stirred for 15 minutes. Subsequently, methyl iodide (0.2 mL, 3.2 mmol) was added in dropwise fashion. The reaction was stirred at room temperature for additional 3 hours. The reaction mixture was poured into water (50 mL) and the resulting white precipitate was filtered. The residue was dried and recrystallized in methanol (off white solid, 0.098 g, 90% yield). ^{1}H NMR (400 MHz, DMSO-d_6) δ = 8.40 (d, J = 7.7 Hz, 2H, Ar), 8.22 (t, J = 7.6 Hz, 1H, Ar), 7.77 (d, J = 8.0 Hz, 2H, Ar), 7.70 (d, J = 8.0 Hz, 2H, Ar), 7.34 (dt, J = 24.4, 7.3 Hz, 4H, Ar), 4.27 (s, 6H, NCH_3) ^{13}C NMR (101 MHz, DMSO-d_6) δ = 149.73, 149.30, 142.10, 138.54, 137.10, 125.05, 123.32, 122.51, 119.52, 110.92 (Ar), 32.56 (NCH_3). HRMS (ESI): *m/z* calculated for $[C_{21}H_{17}N_5+H]^+$; = 340.1556, Found = 340.1585.

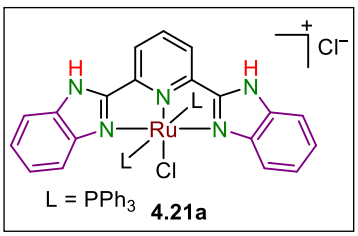

Synthesis of [(^{Bim2}NNN)RuCl(PPh$_3$)$_2$]Cl (4.21a): To a two neck round bottom flask (25 mL) 2,6-*bis*(1H-benzimidazol-2-yl)pyridine (**4.25a**) (0.07 g, 0.224 mmol) and $RuCl_2(PPh_3)_3$ (0.215 g, 0.224 mmol) were taken in dry THF (5 mL) under argon atmosphere. Then the reaction mixture was reflux for 12 h under argon. The color of the reaction mixture changed from brown to orange turbid. After that the solvent was evaporated under vacuum and the residue was washed with dry ether (3 x 5 mL) followed by hexane (3 x 5 mL). A yellowish reddish orange color solid (0.181 g) was obtained

in 81% yield. ^{1}H NMR (400 MHz, $CDCl_3$) δ = 14.30 (s, 2H, N*H*), 8.49 (d, *J* = 8.1 Hz, 2H, Ar), 8.05 (br, 2H, Ar), 7.68 (dd, *J* = 12.0, 7.0 Hz, 1H, Ar), 7.55 (dd, *J* = 26.3, 5.3 Hz, 4H, Ar), 7.26 – 6.80 (m, 32H, Ar). ^{31}P NMR (162 MHz, $CDCl_3$) δ = 29.99 (minor, cis), 22.67(major, trans). HRMS(SEI): Calculated for $[C_{55}H_{43}ClN_5P_2Ru]^+$; = 972.1758, found 972.2608.

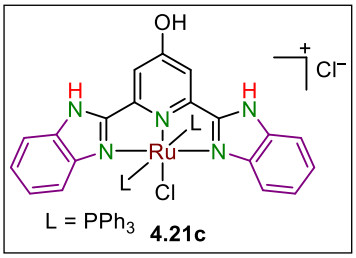

Synthesis of [(*p*-OH^{Bim2}NNN)RuCl](PPh$_3$)$_2$]Cl (4.21c): To a two-necked round bottom flask (25 mL) containing 2,6-*bis*(1H-benzo[d]imidazol-2-yl)pyridin-4-ol (**4.25b**) (0.093 g, 0.28 mmol) and $RuCl_2(PPh_3)_3$ (0.270 g, 0.28 mmol), dry THF (5mL) was added under argon atmosphere. The reaction mixture was then refluxed for 12 h under argon. During the reaction, the color of the reaction mixture changed from brown to light pink. Subsequently, the solvent was evaporated under reduced pressure to obtain a dark green colored gel. The residue was washed with dry diethyl ether (3 x 5 mL) followed by hexane (3 x 5 mL). A green color solid (0.23 g) was obtained in 79% yield. ^{1}H NMR (600 MHz, $CDCl_3$) δ = 7.68 (dd, *J* = 12.0, 7.4 Hz, 4H, Ar), 7.55 (t, *J* = 7.4 Hz, 2H, Ar), 7.47 (dt, *J* = 8.0, 4.0 Hz, 4H, Ar), 7.38 – 6.17 (m, 24H, Ar). ^{31}P NMR (243 MHz, $CDCl_3$) δ = 29.81. HRMS (ESI): *m/z* calculated for $[C_{57}H_{45}N_6P_2ORu]^+$; = 993.2205, Found = 993.2131.

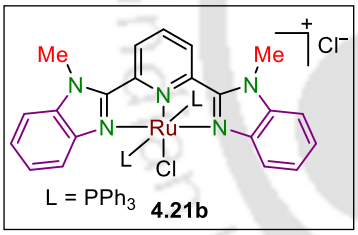

Synthesis of [(^{MeBim2}**NNN)RuCl(PPh$_3$)$_2$]Cl (4.21b):** To a two-necked round bottom flask (25 mL) containing 2,6-*bis*(1-methyl-1H-benzo[d]imidazol-2-yl)pyridine (**4.26**) (0.07 g, 0.206 mmol) and $RuCl_2(PPh_3)_3$ (0.215 g, 0.207 mmol), dry THF (5mL) was added under argon atmosphere. The reaction mixture was then refluxed for 12 h under argon. During the reaction, the color of the reaction mixture changed from brown to light pink. Subsequently, the solvent was evaporated under reduced pressure to obtain a dark pink colored gel. The residue was washed with dry diethyl ether (3 x 5 mL) followed by hexane (3 x 5 mL). A purple color solid (0.135 g) was obtained in 63% yield. ^{1}H NMR (600 MHz, $CDCl_3$) δ = 8.76 (bs, 2H, Ar), 8.40 (bs, 1H, Ar), 8.27 (bs, 1H, Ar), 8.00 (bs, 1H, Ar), 7.84 (bs, 1H, Ar), 7.67 (dd, *J* = 11.7, 7.8 Hz, 5H, Ar), 7.57 – 7.52 (m, 4H, Ar), 7.47 (t, *J* = 6.3 Hz, 5H, Ar), 7.39 (bs, 3H, Ar), 7.08 (d, *J* = 44.4 Hz, 15H, Ar), 6.84 (bs, 9H, Ar), 3.72 (bs, 6H, NC*H*$_3$). ^{13}C NMR (151 MHz, $CDCl_3$) δ = 158.80, 151.70, 150.38, 141.93, 136.02, 133.27, 133.24, 133.21, 132.86, 132.19, 132.12, 132.05, 132.03, 131.03, 130.90, 130.78, 129.65, 128.63, 128.55, 128.24, 128.22, 125.75, 125.41, 124.50, 123.75, 122.58, 122.37, 122.16, 122.05, 119.70, 119.12, 110.42 (Ar), 29.75 (N*C*H$_3$). ^{31}P NMR (243 MHz, $CDCl_3$) δ =

29.29(1P), 23.27 (1P). HRMS (ESI): *m/z* calculated for $[C_{57}H_{47}ClN_5P_2Ru]^+$; = 1000.2039, Found = 1000.2236.

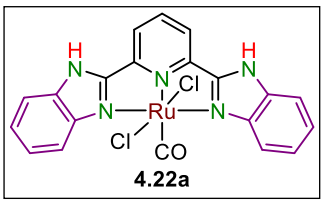

4.22a

Synthesis of (^{Bim2}NNN)RuCl$_2$(CO) (4.22a): To a two-necked round bottom flask (25 mL) containing ligand **4.25a** (0.025 g 0.08 mmol) and $[RuCl_2(p\text{-Cymene})]_2$ (0.025 g, 0.04 mmol), dry THF (5 mL) was added under argon atmosphere. The reaction mixture was heated at 60 °C for 2 h under argon atmosphere. Subsequently an atmosphere of CO was introduced and the reaction mixture was further heated for another 10 h. During the course of the reaction, the color of the reaction mixture changed from brown to straw color. Solvent evaporation yielded a dark brown solid which upon washing with dry diethyl ether (3 x 5 mL) followed by hexane (2 x 5 mL) and the solid was dried under vacuum. An orange yellowish solid 0.031 g of **4.22a** in 74% yield. Low solubility posed challenges in NMR characterization. IR (cm^{-1}): ν = 3448 (br), 3053 (br), 2062, 1965 (s),1605, 1591, 1494, 1487, 1458, 1379, 1346, 1320, 1278, 1233, 1174, 1118, 1022, 996, 912, 849, 809, 761, 746, 674, 634, 596, 583, 572, 492, 434, 415. HRMS (ESI): *m/z* calculated for [**4.22a**–Cl]$^+$ $[C_{20}H_{13}ClN_5ORu]^+$ = 475.9884, Found = 476.0372.

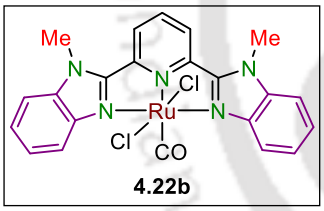

4.22b

Synthesis of (^{MeBim2}NNN)RuCl$_2$(CO) (4.22b): To a two-necked round bottom flask (25 mL) containing ligand **4.25a** (0.03 g 0.08 mmol) and $[RuCl_2(p\text{-Cymene})]_2$ (0.025 g, 0.04 mmol), dry THF (5 mL) was added under argon atmosphere. The reaction mixture was heated at 60 °C for 2 h under argon atmosphere. Subsequently an atmosphere of CO was introduced and the reaction mixture was further heated for another 10 h. During the course of the reaction, the color of the reaction mixture changed from brown to straw color. Solvent evaporation yielded a dark brown solid which upon washing with dry diethyl ether (3 x 5 mL) followed by hexane (2 x 5 mL) and the solid was dried under vacuum. A brown yellowish solid 0.035 g of **4.22b** in 71% yield. Low solubility posed challenges in NMR characterization. IR (cm^{-1}): ν = 1939, 1598, 1508, 1473, 1420, 1337, 1255, 1162, 1009, 866, 813, 801, 772, 758, 739, 602, 492, 435. HRMS (ESI): *m/z* calculated for $[C_{22}H_{17}ClN_5ORu]^+$; = 504.0197, Found = 504.0289; *m/z* calculated for $[C_{24}H_{20}ClN_6ORu]^+$; = 545.0463, Found = 545.0539.

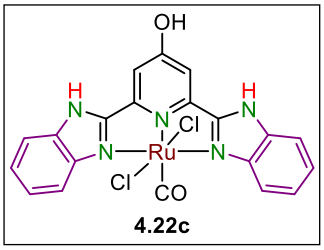

4.22c

Synthesis of (*p*-OH^{Bim2}NNN)RuCl$_2$(CO) (4.22c): To a two-necked round bottom flask (25 mL) containing 2,6-*bis*(1H-benzo[d]imidazol-2-yl)pyridin-4-ol (**4.25b**) (0.07g, 0.206 mmol) and $RuCl_2(PPh_3)_3$ (0.200g, 0.207 mmol), dry THF (5mL) was added under argon atmosphere. The reaction mixture was then refluxed for 12 h under argon. During the reaction, the color of the reaction mixture changed from pink to brown color. Then the solvent was evaporated under reduced pressure to obtain a dark brown colored gel. The residue was washed with dry diethyl ether (3 x 5 mL) followed by hexane (3 x 5 mL). A yellowish-brown color solid (0.07g) was obtained in 86% yield. IR (cm^{-1}): ν = 3049. 2068, 1958, 1611, 1450, 1409, 1372, 1257, 1228, 1096, 1022, 866, 800, 734, 619, 543, 449, 422. HRMS (ESI): *m/z* calculated for $[C_{20}H_{13}N_5ClO_2Ru]^+$; = 491.9833, Found = 491.9790

4.5.3 General procedure for Guerbet reaction under thermal condition. A 5 mL Schlenk flask was charged with **4.22a** (1.8 mg, 4.28 μmol), ethanol (0.5 mL, 8.56 mmol) and NaOEt (58 mg, 0.86 mmol). The volume was made up to 0.7 mL by using toluene which is used as an internal standard. The vessel was sealed and the reaction mixture was heated at 140 °C for 72 h. At regular intervals, an aliquot was taken out and the products were analyzed by GC.

4.5.4 General procedure for the Guerbet reaction under microwave. A 10 mL microwave vial was charged with NaOEt (10 mol %) (0.116 g, 1.71 mmol) and **4.22a** (0.0013 g, 2.5 μmol) inside the glove box. This was followed by addition of dry ethanol (1 mL, 17.12 mmol) and dry toluene (50 μL) as an internal standard. The reaction mixture was heated at 110 °C under microwave conditions at an operating power of 75 W. At regular intervals about 20 μL of the sample was collected and analyzed by GC. The product was analyzed by GC analysis.

4.5.5 General synthesis procedure for heterogenization. A 10 mL Schlenk flask was charged with solid support (Al_2O_3, SiO_2 and $MgSiO_3$) (300 mg) and the catalyst (15 mg, 5% wt./wt.) inside the glovebox. Then KOH (4 mg) was introduced followed by addition of dry toluene (5 mL). The reaction mixture was then stirred for two days under argon. The immobilization of the complex onto the solid was confirmed by its coloration and the concomitant decoloration of the solution. The excess solvent was decanted and the solid was washed by toluene (5mL). The solid was then dried under vacuum prior to its use in catalysis.

4.5.6 Computational details

The geometries of all the considered complexes were fully optimized using the DFT (PBEPBE)[79] method on the Gaussian-16 program package.[80] The LANL2DZ[81-83] and 6-

311G(d,p) basis set were used respectively for the metal (Ru) and non-metal atoms. Genecp (gen keyword with the effective core potential) was included to define the basis set. Method and basis set was selected on the basis of previous reports on pincer complexes.[68-69, 73] Frequency calculations characterize the obtained stationary points as minima structures or transition states based on the number of imaginary frequencies. Single point calculations were performed to calculate the relative free energy values at 110 °C.

Table 4.15. Crystallographic data of complex [(^{Bim2}NNN)RuCl(PPh$_3$)$_2$]PF$_6$ (**4.21a″**)

Name	[(^{Bim2}NNN)RuCl(PPh$_3$)$_2$]PF$_6$ (**4.21a″**)
CCDC	2009680
Empirical formula	$C_{55}H_{43}ClF_6N_5P_3Ru$
Formula weight	1117.37
Crystal size (mm^3)	0.32 x 0.28 x 0.24
Crystal system	monoclinic
Space group	$P2_1/n$
a (Å)	9.9974(5)
b (Å)	38.806(4)
c (Å)	13.9459(7)
α (deg)	90.00
β (deg)	92.722(5)
γ (deg)	90.00
V (Å^3)	5404.4(7)
Z	4
ρ_{calc} (g cm^{-3})	1.373
μ (M_0 Kα) (mm^{-1})	0.494
F (000)	2272.0
T(K)	296
Range of indices (h; k; l)	-11, 11; -39, 46; -16, 16
Number of reflection collected	20714
Unique reflection	8995
Completeness to 2θ	99.9
R_{int}	0.0848
Data / restraints / parameters	9501/448/704
goodness-of-fit	1.148
$R_1[I \geq 2\sigma(I)]$	0.1203
$wR_2[I \geq 2\sigma(I)]$	0.2244
R_1 (all data)	0.1516
wR_2 (all data)	0.2418
Δ_r (max, min) e Å^{-3}	0.93/-2.14

Table 4.16. Selected Bond lengths (Å) and angles (°) around metal center in [(^{Bim2}NNN)RuCl(PPh$_3$)$_2$](PF$_6$) (**4.21a″**)

[(^{Bim2}NNN)RuCl(PPh$_3$)$_2$]PF$_6$ (**4.21a″**)			
Ru1–N1	2.089 (7)	Ru1–P1	2.418 (3)
Ru1–N3	2.010 (8)	Ru1–P2	2.417 (3)
Ru1–N5	2.092 (8)	Ru1–Cl1	2.459 (2)
N1–Ru1–N3	79.2 (3)	N3–Ru1–Cl1	174.1 (2)
N1–Ru1–N5	157.7 (3)	N5–Ru1–P1	87.6 (2)
N1–Ru1–P1	89.1 (2)	N5–Ru1–P2	90.2 (2)
N1–Ru1–P2	93.1 (2)	N5–Ru1–Cl1	105.2 (2)
N1–Ru1–Cl1	97.1 (2)	Cl1–Ru1–P1	94.44 (9)
N3–Ru1–N5	78.8 (3)	Cl1–Ru1–P2	85.84 (9)
N3–Ru1–P1	90.0 (2)	P1–Ru1–P2	177.79 (9)
N3–Ru1–P2	89.8 (2)		

Supporting information (containing NMR spectra of various compound, IR, HRMS, EDX, Kinetics data and Cartesian coordinates of the computed complexes) for chapter **IV** is available as appendix **III** and can be found at

https://drive.google.com/file/d/1X7JRlSmfIlof5NVGMfEf2g-zNxTkNJsc/view?usp=sharing

4.6 References

1. Ragauskas, A. J.; Williams, C. K.; Davison, B. H.; Britovsek, G.; Cairney, J.; Eckert, C. A.; Frederick, W. J.; Hallett, J. P.; Leak, D. J.; Liotta, C. L.; Mielenz, J. R.; Murphy, R.; Templer, R.; Tschaplinski, T., *Science* **2006**, *311*, 484.
2. Sheehan, J.; Aden, A.; Paustian, K.; Killian, K.; Brenner, J.; Walsh, M.; Nelson, R., *J. Ind. Ecol.* **2003**, *7*, 117-146.
3. Jin, C.; Yao, M.; Liu, H.; Lee, C.-f. F.; Ji, J., *Renew. Sust. Energy Rev.* **2011**, *15*, 4080-4106.
4. Weizmann, C., *British patent* **1915**, *4845*.
5. Tamura, M.; Tokonami, K.; Nakagawa, Y.; Tomishige, K., *ACS Catal.* **2016**, *6*, 3600-3609.
6. Kohlpaintner, C. W.; Fischer, R. W.; Cornils, B., *Appl. Catal., A* **2001**, *221*, 219-225.
7. Liu, H.; Wang, G.; Zhang, J., *Liquid, Gaseous and Solid Biofuels-Conversion Techniques* **2013**, 175-198.
8. García, V.; Päkkilä, J.; Ojamo, H.; Muurinen, E.; Keiski, R. L., *Renew. Sustain. Energy Rev.* **2011**, *15*, 964-980.
9. Lee, S. Y.; Park, J. H.; Jang, S. H.; Nielsen, L. K.; Kim, J.; Jung, K. S., *Biotechnol. Bioeng.* **2008**, *101*, 209-228.
10. Shaheen, S. A.; Lipman, T. E., *IATSS Research* **2007**, *31*, 6-20.
11. Azad, A. K., *Advances in Eco-fuels for a Sustainable Environment*. Woodhead Publishing: **2018**.

12. Nawab, S.; Wang, N.; Ma, X.; Huo, Y.-X., *Microb. Cell Fact.* **2020**, *19*, 79.
13. Bharathiraja, B.; Jayamuthunagai, J.; Sudharsanaa, T.; Bharghavi, A.; Praveenkumar, R.; Chakravarthy, M.; Yuvaraj, D., *Renew. Sust. Energy Rev.* **2017**, *68*, 788-807.
14. Dürre, P., *Biotechnology Journal: Healthcare Nutrition Technology* **2007**, *2*, 1525-1534.
15. Dürre, P., *Biotechnol. J.* **2007**, *2*, 1525-1534.
16. DeCicco, J. M., *Sustainability* **2018**, *10*, 1581.
17. Xin, F.; Dong, W.; Zhang, W.; Ma, J.; Jiang, M., *Trends Biotechnol.* **2019**, *37*, 167-180.
18. Rutz, D.; Janssen, R., *WIP Renewable energies* **2007**, *95*.
19. Ndaba, B.; Chiyanzu, I.; Marx, S., *Biotechnol. Rep.* **2015**, *8*, 1-9.
20. Gurney, K. R.; Razlivanov, I.; Song, Y.; Zhou, Y.; Benes, B.; Abdul-Massih, M., *Environ. Sci. Technol.* **2012**, *46*, 12194-12202.
21. Bertsch, J.; Müller, V., *Biotechnol. Biofuels* **2015**, *8*, 210.
22. Kolesinska, B.; Fraczyk, J.; Binczarski, M.; Modelska, M.; Berlowska, J.; Dziugan, P.; Antolak, H.; Kaminski, Z. J.; Witonska, I. A.; Kregiel, D., *Materials* **2019**, *12*, 350.
23. Harvey, B. G.; Meylemans, H. A., *J. Chem. Technol. Biotechnol.* **2011**, *86*, 2.
24. Hileman, J. I.; Stratton, R. W.; Donohoo, P. E., *J. Propul. Power* **2010**, *26*, 1184-1196.
25. Harvey, B. G.; Meylemans, H. A., *J. Chem. Technol. Biotechnol.* **2011**, *86*, 2-9.
26. Dürre, P., *Biotechnol. J.* **2007**, *2*, 1525.
27. Jin, C.; Yao, M.; Liu, H.; Lee, C. f. F.; Ji, J., *Renew. Sustain. Energy Rev.* **2011**, *15*, 4080.
28. https://neutrium.net/properties/specific-energy-and-energy-density-of-fuels/.
29. Cornils, B.; Herrmann, W. A., *Applied Homogeneous Catalysis with Organometallic Compounds: Applications; Volume 2. Developments; Volume 3. Developments*. Wiley-VCH: **2002**.
30. Spargo, P., Industrial Organic Chemistry, Completely Revised 4th ed By K. Weissermel and H.-J. Arpe. Wiley-VCH: Weinheim. **2003**. 491 pp.£ 119. ISBN 3-527-30578-5. ACS Publications: 2003.
31. Di Cosimo, J. I.; Apesteguı; a, C. R.; Ginés, M. J. L.; Iglesia, E., *J. Catal.* **2000**, *190*, 261-275.
32. Hilmen, A.-M.; Xu, M.; Gines, M. J. L.; Iglesia, E., *Appl. Catal., A* **1998**, *169*, 355-372.
33. Maitlis, P.; Haynes, A., Chapter 4 Syntheses Based on Carbon Monoxide. In *Metal-catalysis in Industrial Organic Processes*, The Royal Society of Chemistry: **2006**; pp 114-162.
34. Falbe, J.; Bahrmann, H., *New syntheses with carbon monoxide*. Springer: **1980**; Vol. 11.
35. Wang, Y.; Chen, B.-b.; Crocker, M.; Zhang, Y.-j.; Zhu, X.-b.; Shi, C., *Catal. Commun.* **2015**, *59*, 195-200.
36. Galadima, A.; Muraza, O., *Ind. Eng. Chem. Res.* **2015**, *54*, 7181-7194.
37. Jaumain, D.; Su, B.-L., *J. Mol. Catal. A: Chem.* **2003**, *197*, 263-273.
38. Madeira, F. F.; Gnep, N. S.; Magnoux, P.; Maury, S.; Cadran, N., *Appl. Catal., A* **2009**, *367*, 39-46.
39. Kubo, K.; Iida, H.; Namba, S.; Igarashi, A., *Appl. Catal., A* **2015**, *489*, 272-279.
40. Chiang, H.; Bhan, A., *J. Catal.* **2010**, *271*, 251-261.
41. Wu, X.; Fang, G.; Tong, Y.; Jiang, D.; Liang, Z.; Leng, W.; Liu, L.; Tu, P.; Wang, H.; Ni, J.; Li, X., *ChemSusChem* **2018**, *11*, 71-85.
42. Kiani, D.; Baltrusaitis, J., *Chem. Catal.* **2021**, *1*, 782-801.
43. Tsuchida, T.; Sakuma, S.; Takeguchi, T.; Ueda, W., *Ind. Eng. Chem. Res.* **2006**, *45*, 8634-8642.

44. Hanspal, S.; Young, Z. D.; Shou, H.; Davis, R. J., *ACS Catal.* **2015**, *5*, 1737-1746.
45. Ho, C. R.; Shylesh, S.; Bell, A. T., *ACS Catal.* **2016**, *6*, 939-948.
46. Kiani, D.; Baltrusaitis, J., *Chem Catalysis* **2021**, *1*, 782-801.
47. Jang, W.-J.; Jeong, D.-W.; Shim, J.-O.; Kim, H.-M.; Han, W.-B.; Bae, J. W.; Roh, H.-S., *Renew. Energy* **2015**, *79*, 91-95.
48. Ueda, W.; Kuwabara, T.; Ohshida, T.; Morikawa, Y., *J. Chem. Soc., Chem. Commun.* **1990**, 1558-1559.
49. Marcu, I.-C.; Tichit, D.; Fajula, F.; Tanchoux, N., *Catal. Today* **2009**, *147*, 231-238.
50. Nair, H.; Gatt, J. E.; Miller, J. T.; Baertsch, C. D., *J. Catal.* **2011**, *279*, 144-154.
51. Rechi Siqueira, M.; Micali Perrone, O.; Metzker, G.; de Oliveira Lisboa, D. C.; Thoméo, J. C.; Boscolo, M., *Mol. Catal.* **2019**, *476*, 110516.
52. Veibel, S.; Nielsen, J. I., *Tetrahedron* **1967**, *23*, 1723.
53. Guerbet, M. C. R., *Acad. Sci. Paris* **1899**, *128*, 1002-1004.
54. Guerbet, M. C. R., *Acad. Sci. Paris* **1909**, *149*, 129-132.
55. Tseng, K. N. T.; Lin, S.; Kampf, J. W.; Szymczak, N. K., *Chem. Commun.* **2016**, *52*, 2901-2904.
56. Dowson, G. R. M.; Haddow, M. F.; Lee, J.; Wingad, R. L.; Wass, D. F., *Angew. Chem., Int. Ed.* **2013**, *52*, 9005-9008.
57. Wingad, R. L.; Gates, P. J.; Street, S. T. G.; Wass, D. F., *ACS Catal.* **2015**, *5*, 5822-5826.
58. Xu, G.; Lammens, T.; Liu, Q.; Wang, X.; Dong, L.; Caiazzo, A.; Ashraf, N.; Guan, J.; Mu, X., Direct self-condensation of bio-alcohols in the aqueous phase. In *Green Chem.*, **2014**; Vol. 16, pp 3971-3977.
59. Koda, K.; Matsu-ura, T.; Obora, Y.; Ishii, Y., *Chem. Lett.* **2009**, *38*, 838-839.
60. Chakraborty, S.; Piszel, P. E.; Hayes, C. E.; Baker, R. T.; Jones, W. D., *J. Am. Chem. Soc.* **2015**, *137*, 14264-14267.
61. Nielsen, M.; Junge, H.; Kammer, A.; Beller, M., *Angew. Chem., Int. Ed.* **2012**, *51*, 5711-5713.
62. Xie, Y.; Ben-David, Y.; Shimon, L. J. W.; Milstein, D., *J. Am. Chem. Soc.* **2016**, *138*, 9077-9080.
63. Fu, S.; Shao, Z.; Wang, Y.; Liu, Q., *J. Am. Chem. Soc.* **2017**, *139*, 11941-11948.
64. Kulkarni, N. V.; Brennessel, W. W.; Jones, W. D., *ACS Catal.* **2018**, *8*, 997–1002.
65. King, A. M.; Sparkes, H. A.; Wingad, R. L.; Wass, D. F., *Organometallics* **2020**, *39*, 3873–3878.
66. King, A. M.; Wingad, R. L.; Pridmore, N. E.; Pringle, P. G.; Wass, D. F., *Organometallics* **2021**, *40*, 2844-2851.
67. Ohligschläger, A.; van Staalduinen, N.; Cormann, C.; Mühlhans, J.; Wurm, J.; Liauw, M. A., *Chemistry–Methods* **2021**, *1*, 181-191.
68. DiBenedetto, T. A.; Jones, W. D., *Organometallics* **2021**, *40*, 1884-1888.
69. Das, K.; Dutta, M.; Das, B.; Srivastava, H. K.; Kumar, A., *Adv. Synth. Catal.* **2019**, *361*, 2965-2980.
70. Das, K.; Nandi, P. G.; Islam, K.; Srivastava, H. K.; Kumar, A., *Eur. J. Org. Chem.* **2019,** *2019*, 6855-6866.
71. Mishra, D.; Naskar, S.; Chattopadhyay, S. K.; Maji, M.; Sengupta, P.; Dinda, R.; Ghosh, S.; Mak, T. C. W., *Transition Met. Chem.* **2005**, *30*, 352-356.
72. Braden, D. J.; Cariou, R.; Shabaker, J. W.; Taylor, R. A., *Appl. Catal., A* **2019**, *570*, 367-375.
73. Dai, Z.; Luo, Q.; Meng, X.; Li, R.; Zhang, J.; Peng, T., *J. Organomet. Chem.* **2017**, *830*, 11-18.

74. Dutta, M.; Das, K.; Prathapa, S. J.; Srivastava, H. K.; Kumar, A., *Chem. Commun.* **2020**, *56*, 9886-9889.
75. Huheey, J. E.; Keiter, E. A.; Keiter, R. L.; Medhi, O. K., *Inorganic chemistry: principles of structure and reactivity*. Pearson Education India: 2006.
76. Morgan, D. J., *Surf. Interface Anal.* **2015**, *47*, 1072-1079.
77. Armarego, W. L. F.; Chai, C., Chapter 4 - Purification of Organic Chemicals. In *Purification of Laboratory Chemicals (Seventh Edition)*, Armarego, W. L. F.; Chai, C., Eds. Butterworth-Heinemann: Boston, **2013**; pp 103-554.
78. Armarego, W. L. F.; Chai, C., Chapter 5 - Purification of Inorganic and Metal-Organic Chemicals. In *Purification of Laboratory Chemicals (Seventh Edition)*, Armarego, W. L. F.; Chai, C., Eds. Butterworth-Heinemann: Boston, **2013**; pp 555-661.
79. Perdew, J. P.; Burke, K.; Ernzerhof, M., *Phys. Rev. Lett.* **1996**, *77*, 3865-3868.
80. Gaussian 16, R. C., M. J. Frisch, G. W. Trucks, H. B. Schlegel, G. E. Scuseria, M. A. Robb, J. R. Cheeseman, G. Scalmani, V. Barone, G. A. Petersson, H. Nakatsuji, X. Li, M. Caricato, A. V. Marenich, J. Bloino, B. G. Janesko, R. Gomperts, B. Mennucci, H. P. Hratchian, J. V. Ortiz, A. F. Izmaylov, J. L. Sonnenberg, D. Williams-Young, F. Ding, F. Lipparini, F. Egidi, J. Goings, B. Peng, A. Petrone, T. Henderson, D. Ranasinghe, V. G. Zakrzewski, J. Gao, N. Rega, G. Zheng, W. Liang, M. Hada, M. Ehara, K. Toyota, R. Fukuda, J. Hasegawa, M. Ishida, T. Nakajima, Y. Honda, O. Kitao, H. Nakai, T. Vreven, K. Throssell, J. A. Montgomery, Jr., J. E. Peralta, F. Ogliaro, M. J. Bearpark, J. J. Heyd, E. N. Brothers, K. N. Kudin, V. N. Staroverov, T. A. Keith, R. Kobayashi, J. Normand, K. Raghavachari, A. P. Rendell, J. C. Burant, S. S. Iyengar, J. Tomasi, M. Cossi, J. M. Millam, M. Klene, C. Adamo, R. Cammi, J. W. Ochterski, R. L. Martin, K. Morokuma, O. Farkas, J. B. Foresman, and D. J. Fox,, *Gaussian inc., Wallingford CT 2016* **2016**, *2*, 4.
81. Hay, P. J.; Wadt, W. R., *J. Chem. Phys.* **1985**, *82*, 270-283.
82. Hay, P. J.; Wadt, W. R., *J. Chem. Phys.* **1985**, *82*, 299-310.
83. Wadt, W. R.; Hay, P. J., *J. Chem. Phys.* **1985**, *82*, 284-298.

Chapter V

Pincer-Ruthenium Catalyzed Oxygen Mediated Etherification of Alcohols and Ortho-Alkylation of Phenols

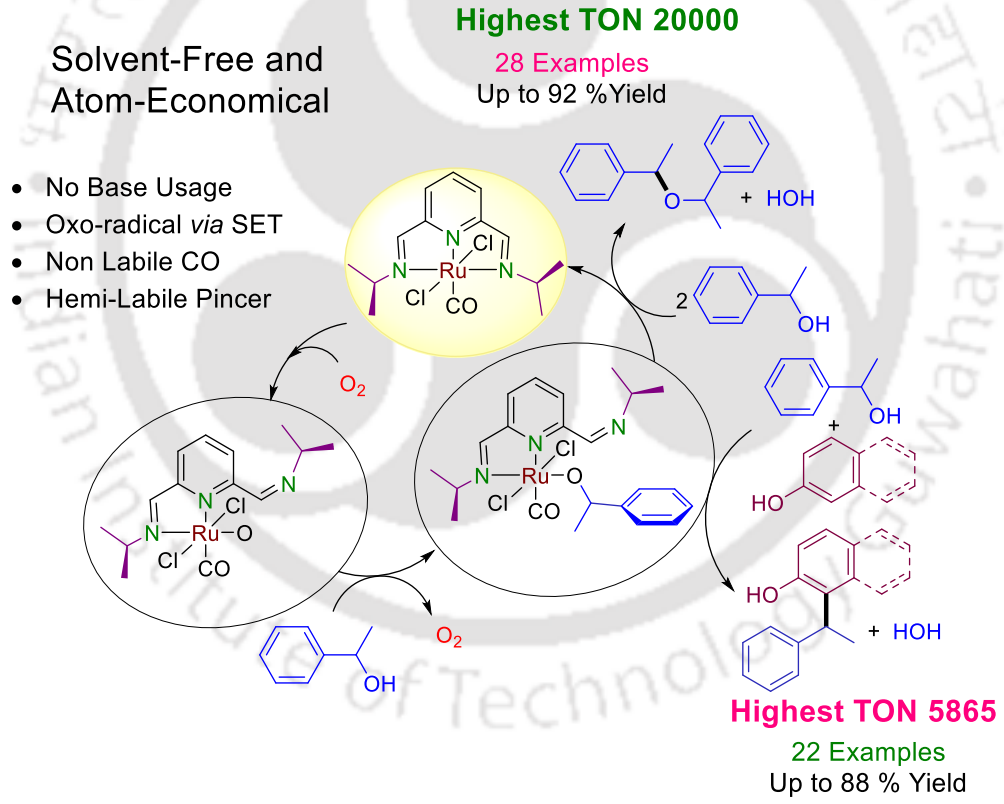

- **K. Das**, M. Dutta, B. Das, H. K. Srivastava, A. Kumar, *Adv. Synth. Catal*. **2019**, *361*, 2965.
- **K. Das**, E. Yasmin, B. Das, H. K. Srivastava, A. Kumar, *Catal. Sci. Technol*. **2020**, *10*, 8347.
- **K. Das**, E. Yasmin, A. Kumar, *Adv. Synth. Catal*. **2022**, *364*, 3895.

5.1 Introduction

Ethers[1-2] are commercially invaluable chemicals with a wide range of applications in fragrances, herbicides, plasticizers, disinfectants and intermediates in pharmaceuticals products apart from their use as solvents.[3-5] Typical industrial approach to ethers involves the Williamson synthesis[6] where an alkali metal phenoxide is treated with an appropriate alkyl/aryl halide. Generation of stoichiometric amounts of inorganic waste and harsh reaction conditions are the drawbacks of this process (Scheme **5.1**).[3-4, 7]

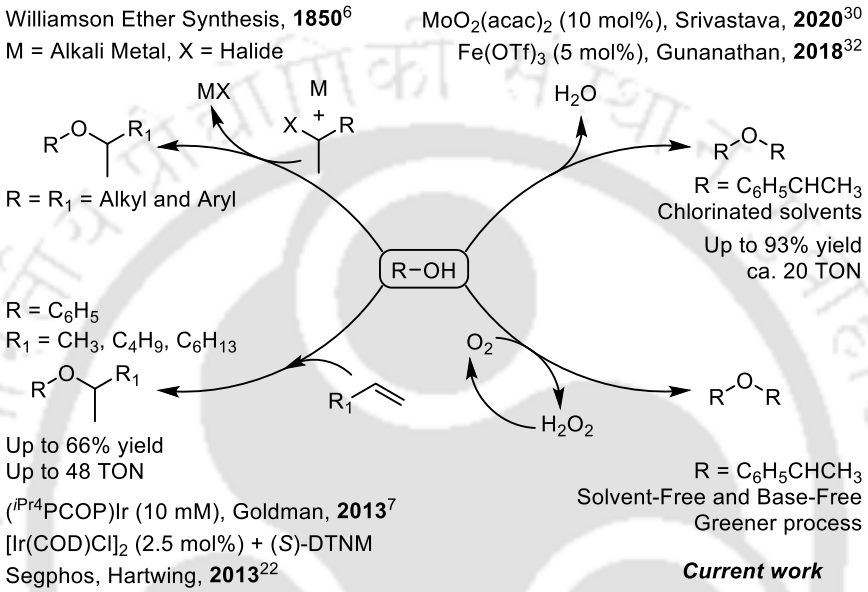

Scheme 5.1: Various synthetic pathways reported for etherification of alcohols.

On the other hand, Brønsted acid and Lewis acid catalyzed synthesis of ethers suffers from competing Friedel-Crafts alkylations and very poor chemoselectivity.[8-9] He and co-workers have demonstrated that the well-studied transition-metal precatalysts[2, 10-17] for the etherification are actually Brønsted acid delivery systems[18] with triflic acid[19] as the catalytically active species (Scheme **5.2**).

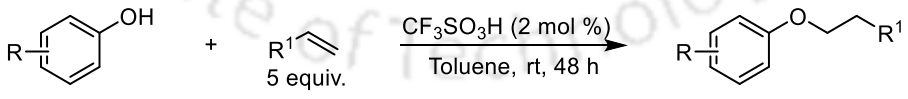

5.3a; R = *p*-NO_2, R^1 = $C_6H_5CH_2$; Yield = 93%
5.3b; R = *p*-NO_2, R^1 = $C_6H_5C_2H_4$; Yield = 40%
5.3c; R = *p*-OMe, R^1 = $C_6H_5CH_2$; Yield = 62%
5.3d; R = *p*-OMe, R^1 = $C_6H_5C_2H_4$; Yield = 57%

Scheme 5.2: Brønsted acid caytalyzed etherification of alcohols and olefin.

Generation of C–O bonds *via* greener and atom economical routes *via* purely organometallic pathways[7,10, 20-25] has thus been a field of immense interest. While Marks has reported several

examples of intramolecular O–H addition to multiple bonds,[23-25] pioneering independent work by Goldman[7] and Hartwig[22] have led to several recent reports[21, 26] on transition metal catalyzed intermolecular addition of O–H bonds across the double bond (Scheme **5.1** and **5.3**).

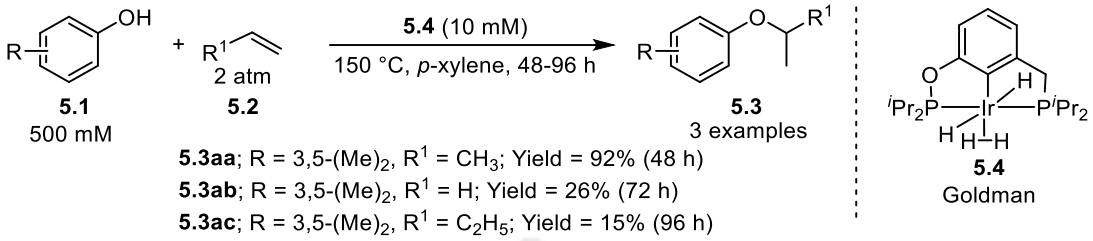

Scheme 5.3: Pincer–iridium catalyzed hydroaryloxylation of olefin.[7]

Notably, there are only a few studies on ether synthesis *via* either the reductive coupling[27-28] (see in Scheme **5.8**) of carbonyl compounds with alcohols or the direct catalytic dehydrative intramolecular[29] and intermolecular[16,27, 30-35] coupling of alcohols. The intermolecular coupling of alcohols is dominated by transition-metal catalyzed reactions.[16, 27, 30-33, 35] However, current studies are trying to push the synthesis of ether through a milder, greener pathway *via* O-H bond activation[12-14] and dehydration reaction (Scheme **5.1**).[10-11, 15-16, 36] Gebbink reported minor amounts of ethers in the Re_2O_7 catalyzed dehydration of benzylic alcohols to corresponding styrene at 100 °C using toluene as solvent (Scheme **5.4**).[33]

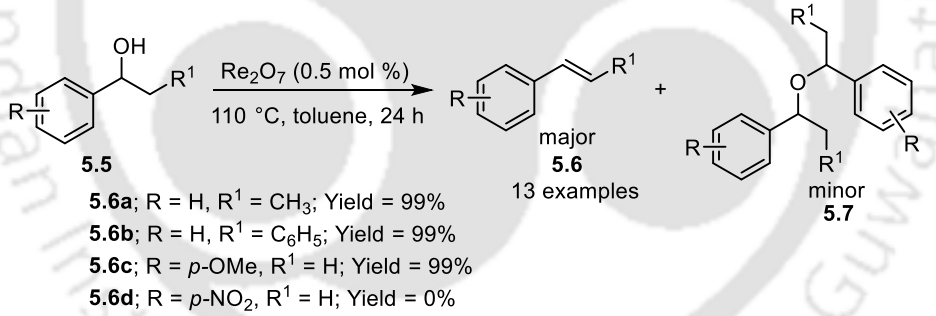

Scheme 5.4: Rhenium catalyzed dehydration of alcohols to olefin.[33]

Srivastava reported up to 82% yield of the corresponding ether in the $MoO_2(acac)_2$ (10 mol%) catalyzed dehydrative coupling of 1-phenyl ethanol at 60 °C in the presence of 1,2-dicholoroethane as solvent.[30] The selective (up to 95%) synthesis of unsymmetrical ethers (up to 94% yield) *via* dehydrative etherification was also reported by Yi in the presence of $[(C_6H_6)(PCy)_3(CO)RuH]^+BF_4^-$ (0.1-1 mol%) at 50-110 °C using chlorobenzene as solvent (Scheme **5.5**).[35] The cationic ruthenium-hydride complex **5.11** provides high chemo- and stereoselectivity towards ether formation. This catalytic system is also applicable for unsymmetrical substrates and formation of functionalized α-chiral ethers.

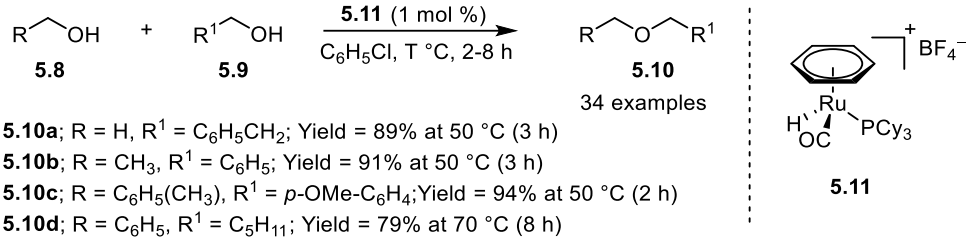

5.10a; R = H, R^1 = $C_6H_5CH_2$; Yield = 89% at 50 °C (3 h)
5.10b; R = CH_3, R^1 = C_6H_5; Yield = 91% at 50 °C (3 h)
5.10c; R = $C_6H_5(CH_3)$, R^1 = *p*-OMe-C_6H_4;Yield = 94% at 50 °C (2 h)
5.10d; R = C_6H_5, R^1 = C_5H_{11}; Yield = 79% at 70 °C (8 h)

Scheme 5.5: Ruthenium catalyzed dehydration of alcohols to ethers.[35]

Readily available, environmentally benign iron(III) triflate turned out to be a cheap and efficient catalyst for the direct etherification of alcohols. The Gunanathan group used ammonium chloride (5 mol %) as an additive to tune the selectivity towards ethers in the $Fe(OTf)_3$ (5 mol %) catalyzed dehydrative coupling of 1-phenyl ethanol at 0 °C in dichloromethane (Scheme **5.6**).[32] The use of ammonium chloride suppressed the other side reactions and selectively afforded ether as one of the major product. A large number of functional groups are well tolerated for this etherification reaction under mild reactions conditions in air.

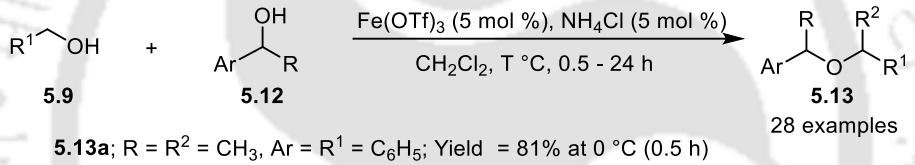

5.13a; R = R^2 = CH_3, Ar = R^1 = C_6H_5; Yield = 81% at 0 °C (0.5 h)
5.13b; R = R^2 = C_6H_5, Ar = R^1 = C_6H_5; Yield = 82% at 0 °C (1 h)
5.13c; R = CH_3, R^1 = C_2H_5, R^2 = H, Ar = C_6H_5; Yield = 88% at 45 °C (12 h)
5.13d; R = CH_3, R^1 = p-F-C_6H_4, R^2 = H, Ar = *p*-Me-C_6H_4; Yield = 82% at 45 °C (24 h)

Scheme 5.6: Iron(III) catalyzed etherification of substituted benzyl alcohol.[32]

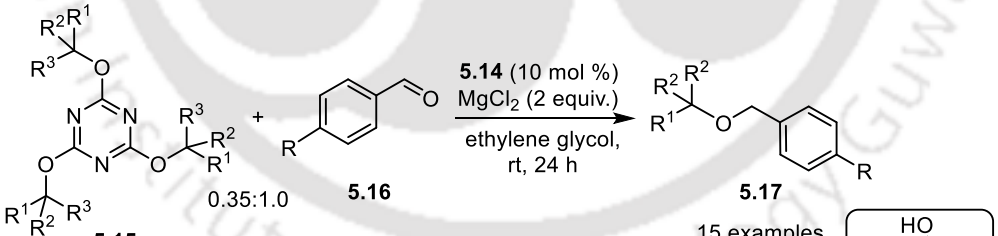

5.17a; R^1 = C_6H_5, R^2 = H, R^3 = CH_3, R = H; Yield = 73%
5.17b; R^1 = C_6H_5, R^2 = H, R^3 = CH_3, R = NO_2; Yield = 70%
5.17c; R^1 = R^2 = R^3 = C_6H_5, R = H; Yield = 68%
5.17d; R^1 = C_6H_5, R^2 = R^3 = *o*-OMe-C_6H_4, R = H; Yield = 63%

Scheme 5.7: Nickel catalyzed reductive coupling of secondary and tertiary benzylic C–O electrophiles with aldehyde.[37]

In comparison, Williamson[6] methodology employing alkali metal mediated etherification often suffer because of substrate scope, sensitivity and expensive materials required for the reaction. The other way for unsymmetrical[38] etherification through coupling of an alcohol precursor with an aldehyde is one of the most promising approach. In this context, Iranpoor and co-workers

reported an alternative method by using nickel catalyzed etherification of tertiary alkyl C-O of 2,4,6-trichloro-1,3,5-triazine (TCT) electrophiles with aldehydes (Scheme **5.7**).[37] Here, ethylene glycol acts as a reducing agent as well as a solvent, thereby achieving a more environmental friendly approach.

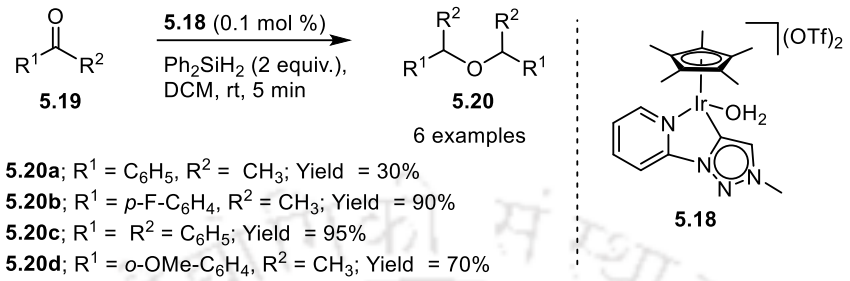

Scheme 5.8: Iridium catalyzed reductive ether formation from aldehyde and ketone.[27]

Methodological catalytic etherification under the mild reaction conditions have been a main focus in recent days. Etherification reaction generally requires alcohols or carbonyl substrates. The Lewis acids such as silyltriflate,[39] zinc(II),[40] or indium[41] play an important role in the transformation of alcohols or carbonyl substrates to ether along with quenching the water formed during the reaction. Though several challenges are resolved by the use of Lewis acid, any improvement in the reaction time or the catalyst loading makes it an efficient pathway for etherification. In one such examples, an iridium complex has been used to reduce the reaction time along with an additional reduction in the temperature and catalyst loading. The use of triazole ligand based Ir((III)Cp* complex leads to wide scope and functional group tolerance towards etherification reaction as shown by Albrecht and co-workers (Scheme **5.8**).[27]

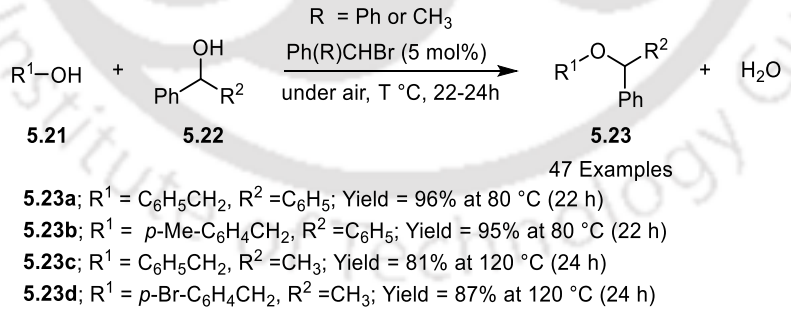

Scheme 5.9: Dehydrative cross etherification of alcohols.[34]

Synthesis of symmetrical and unsymmetrical ethers *via* traditional Williamson ether synthesis often requires toxic reagents and/or equivalent amounts of base along with hazardous organohalides.[6] The disadvantage due to the competing potential *β*-hydride elimination leads to lowering in the yield especially in case of secondary and tertiary organohalide.[42] However, this requires the synthesis of catalyst in an inert and standard glovebox reaction conditions. Therefore, simple and efficient methodology for etherification of alcohols are gaining more

attraction. With a practical and greener approach, Hu and co-workers reported an alternative pathway for etherification of alcohols,[34] using organohalides which can catalyze *O*-selective alkylation of activated alcohols to ether. (Scheme **5.9**).[34]

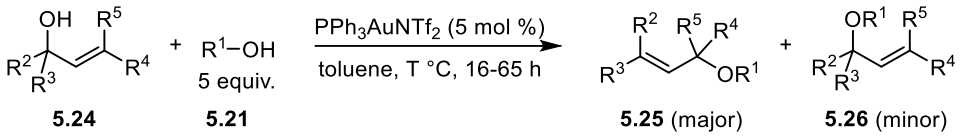

5.25a; $R^1 = C_{16}H_{33}$, $R^2 = {}^tC_4H_9$, R^3 = Me, $R^4 = R^5$ = H; Yield = 83% at 50 °C (16 h)
5.25b; $R^1 = p$-MeO_2C-C_6H_4, $R^2 = {}^tC_4H_9$, R^3 = Me, $R^4 = R^5$ = H; Yield = 74% at 50 °C (32 h)
5.25c; $R^2 = R^1 = {}^nC_4H_9$, $C_{10}H_{21}$, $R^3 = R^4 = R^5$ = H; Yield = 91% at 50 °C (26 h)
5.25d; $R^1 = C_6H_5C_2H_4$, $R^2 = C_6H_5$, $R^3 = R^5$ = H, $R^4 = CH_3$; Yield = 68% at 50 °C (65 h)

Scheme 5.10: Gold catalyzed allylic etherification.[43]

Similarly, allylic etherification requires an activated leaving group of an allylic alcohol or alkyne as a substrate. This generally requires highly inert atmosphere and therefore holds limited scope. A recent development was demonstrated by Carreire and co-workers where they reported the Ir-catalyzed allylic etherification of alcohols without using any activator.[16] Though this complementary methodology had a wide scope in case of primary alcohols but lacks efficiency for the secondary alcohols. Whereas, utilization of an air stable gold(I)-catalyst for direct allylic etherification of unactivated alcohols under mild conditions, provides good regio- and stereoselectivity (*E*) without the use of any allylic-electrophile or nucleophile. Compared to other etherification reactions, gold(I) catalyzed reactions can tolerate direct allylic etherification of primary, secondary and tertiary allylic alcohols along with various functional groups (Scheme **5.10**).[43]

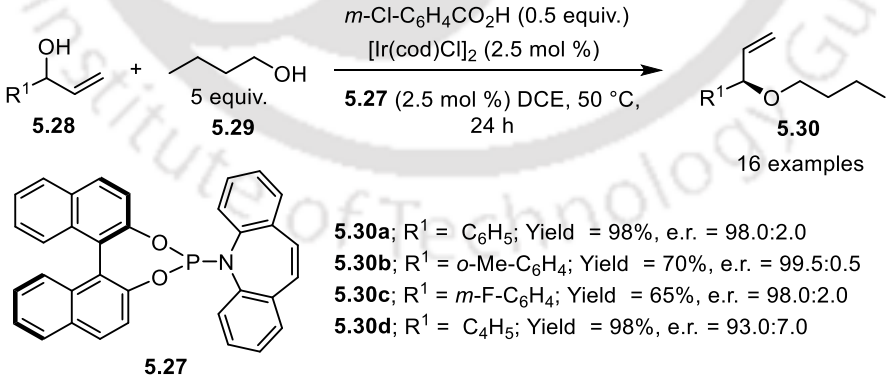

5.30a; $R^1 = C_6H_5$; Yield = 98%, e.r. = 98.0:2.0
5.30b; $R^1 = o$-Me-C_6H_4; Yield = 70%, e.r. = 99.5:0.5
5.30c; $R^1 = m$-F-C_6H_4; Yield = 65%, e.r. = 98.0:2.0
5.30d; $R^1 = C_4H_5$; Yield = 98%, e.r. = 93.0:7.0

Scheme 5.11: Iridium catalyzed enantioselective allylic etherification of allylic alcohols.[16]

Along with ether synthesis, allylic enantioselective ether formation starting from alcohols has great synthetic utility in organic transformations.[44] Iridium catalyzed ether formation reactions utilizing an alkoxide have provided promising results. Alexakis,[45] Hartwig,[10] and Helmchen[46] independently have reported iridium catalyzed insertion of alcohols into olefin to yield

enantioselective allylic ethers. Later, Evans and co-workers reported the usage of rhodium catalyst to obtain optically active ether allylic carbonates.[47] Similarly, Carreira and co-workers reported optically active allylic ether synthesis *via* dehydrative coupling of allylic alcohols with aliphatic alcohols using iridium catalyst (Scheme **5.11**).[16] They also described the kinetic resolution of the enantioselective isomer with time. Furthermore, the use of Brønsted acid (such as H_2SO_4, H_3PO_4 and CF_3SO_2H) plays a crucial role thus enhancing the activity of the Ir-precatalyst.

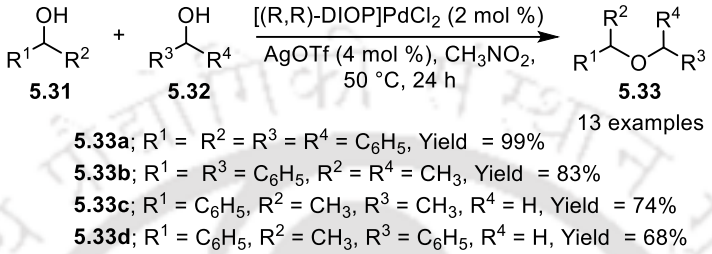

Scheme 5.12: Palladium catalyzed symmetrical and unsymmetrical etherification reactions.[48]

A wide range of synthetic methods reported for the ether synthesis often requires high temperature along with several other limitations (excessive generation of waste salt and requirement of acid catalyst). Abu-Omar and co-workers investigated a palladium catalyzed etherification of various benzylic and alkyl alcohols with phenylethyl alcohol to provide excellent yields.[48] They demonstrated that expensive palladium catalyst is more advantageous over earth abundant metal complexes as it provides higher selectivity towards etherification. They also extended the versatile activity of this palladium catalyst towards amination and thioetherification reactions (Scheme **5.12**).[48]

However, the designing of an efficient catalyst which can generate valuable products with the use of cheap and abundant starting materials would prove to be useful.[49] Albrecht group demonstrated the use of pyridyl triazolylidene ligand system based iridium complex **5.34** towards ether formation. The stronger donor property of the ligand influences the catalytic activity in dehydrative etherification of alcohols. (Figure **5.13**).[50]

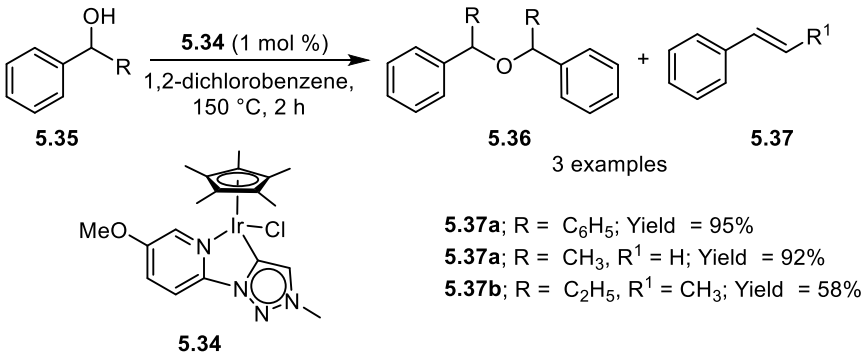

Scheme 5.13: Iridium catalyzed dehydrative transformations of 1-phenylethanol.[50]

The example of protection and deprotection has been employed in various natural and bio-active compounds in organic synthesis.[51] One such example is use of diphenylmethanol (DPM) for protection of alcohols under mild conditions in presence of catalyst.[52-53] Harper and co-workers demonstrated acid catalyzed etherification of DPM with alcohols.[54] Similarly, Kim and co-workers developed a $FeCl_3$ catalyzed synthetic, efficient and novel method for diphenylmethyl etherification with various alcohols (Scheme **5.14**).[55] In contrast, Martin reported that pyridyl-triazolylidene-Ir chloride catalyzed 1-phenylethanol dehydration gave styrene as a major product.[56]

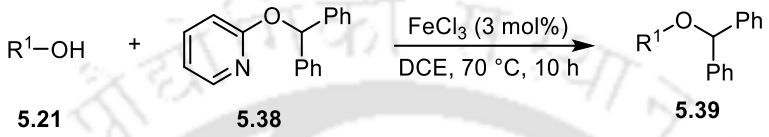

5.21 **5.38** **5.39**

31 Examples

5.39a; $R^1 = C_6H_5CH_2$, Yield = 94%
5.39b; $R^1 = C_4H_9$, Yield = 94%
5.39c; $R^1 = C_6H_{11}$, Yield = 87%
5.39d; $R^1 = C_6H_5$, Yield = 90%

Scheme 5.14: Catalytic etherification of alcohols with 2-diphenylmethoxypyridine.[55]

The common methods used for etherification of alcohols involves the usage of catalysts such as $FeCl_3$,[57] $ZnCl_2$,[58] $BiBr_3$[59] and $GaCl_3$.[58] However, drawbacks like the use of stoichiometric amount of catalyst, high temperature, low yields and expensive reagents makes them less effective in etherification reaction. Therefore, a mild and efficient method for (un)symmetrical etherification of alcohols using zirconium tetrachloride as catalyst in shorter reaction time has been reported by Das and co-workers (Scheme **5.15**).[60] This reaction ensures that the readily available catalyst precursor provides good yields and high selectivity towards a variety of ethers.

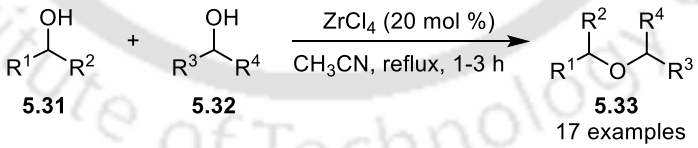

5.31 **5.32** **5.33**

17 examples

5.33a; $R^1 = R^4 =$ *p*-OMe-C_6H_4, $R^2 = R^3 = CH_3$; Yield = 85% (1 h)
5.33b; $R^1 = R^4 =$ *p*-NO_2-C_6H_4, $R^2 = R^3 = CH_3$; Yield = 55% (3 h)
5.33c; $R^1 = R^2 = C_6H_5$, $R^3 = CH_3$, $R^4 =$ *p*-Me-C_6H_4; Yield = 70% (2.5 h)
5.33d; $R^1 = C_6H_5$, $R^2 = CH_3$, $R^3 = H$, $R^4 = C_6H_5$; Yield = 64% (3 h)

Scheme 5.15: $ZrCl_4$ catalyzed ether formation from alcohols.[60]

Dehydrative etherification of alcohols in a more atom economical and less hazardous reaction conditions with the use of an iron catalyst has recently gained attention. By the development of various iron catalysts, Xu recently reported, NNN ligand based iron(II)/(III) catalyzed oxygenation of ethers[61] or olefin[62] to carbonyl compounds under mild reaction condition with

excellent chemo-selectivity. Similarly, the cross unsymmetrical etherification by iron complex generated *in-situ* from $Fe(OTf)_2$ and *bis*-imidazoline pyridine ligand was reported by the same group. They achieved high yield and selectivity under mild conditions for the synthesis of aliphatic ethers (Scheme **5.16**).[31]

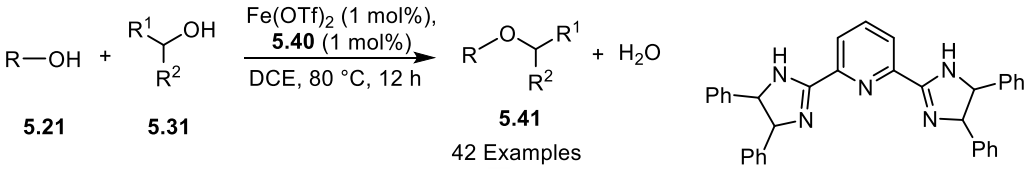

5.41a; R = *p*-OMe-C_6H_4, R^1 = H, R^2 = *p*-Me-C_6H_4; Yield = 78%
5.41b; R = *p*-OMe-C_6H_4, R^1 = H, R^2 = *p*-F-$C_6H_4C_2H_4$; Yield = 66%
5.41c; R = CH_3, R^1 = CH_3, R^2 = *p*-Me-C_6H_4; Yield = 71%
5.41d; R = CH_3, R^1 = H, R^2 = *p*-^{i}Pr-C_6H_4; Yield = 71%

Scheme 5.16: Iron catalyzed cross etherification of alcohols.[31]

In the earlier chapters, the use of NNN-ruthenium pincer complexes for alkylation leading to C–C and C–N bond formation have been probed using alcohols as alkylation agents.[63-64] Base was required to promote these reactions. It would be interesting to know what happens in the absence of a base. Interestingly, Kumar and co-workers demonstrated the use of the same NNN pincer-ruthenium systems towards ATRA (atom transfer radical addition) reaction of CCl_4 to styrene without the need of a cocatalyst or any radical initiator.[65] A 16e^- species (after release of PPh_3) was key to this reaction that involved a SET (single electron transfer) mechanistic pathway.[65]

5.2 Objectives

The aim is to use a less hazardous catalytic system and a more effective method for the etherification of alcohols that has a significant atom-economy. The methods reported so far for the dehydrative etherification of alcohols have obvious limitations that prevent them from being useful for synthetic purposes (including controlling the selectivity towards ethers and using chlorinated solvents).[7h, 13b, 15a-d, 15f] The vast literature survey indicates that the transition metal catalyzed direct etherification through greener process is a very attractive alternate. There are no reports where direct etherification of alcohols are catalyzed using pincer metal complexes under solvent free conditions. In this context, in the current chapter, the following questions have been addressed,

- Will there be any reactivity towards etherification when NNN pincer-Ru catalyst are used with alcohols in the absence of any base (Scheme **5.17**)?
- Can the reaction be promoted by oxygen?

- What will be the operative pathway for etherification?
- Would the protocol be generic and will various functional groups be tolerated?

R: Cy = **5.42a**, Ph = **5.42b**, ^{i}Pr = **5.42c**, ^{t}Bu = **5.42d**

R: Cy = **5.43a**, Ph = **5.43b**, ^{i}Pr = **5.43c**, ^{t}Bu = **5.43d**

Figure 5.1: Pincer-ruthenium complexes screened for etherification reaction in this chapter

5.3 Result and Discussion

5.3.1 Optimization of the conditions for the pincer-ruthenium (5.42a-d and 5.43a-d) catalyzed etherification of 1-phenyl ethanol (5.44).

The pincer-ruthenium complexes (**5.42a-d** and **5.43a-d**) were synthesized following the protocol reported in chapter II and III.[63-67] The etherification studies on 1-phenyl ethanol (**5.44**) were initiated by using **5.42a** as a model catalyst (Table **5.1**). A solution of **5.44** containing 0.015 mol % of **5.42a** was heated at 140 °C under argon atmosphere for 72 h. A ^{1}H NMR spectra of the reaction mixture indicated the formation of acetophenone (**5.45**) and (oxy*bis*(ethane-1,1-diyl))dibenzene (**5.46**) in 4% and 18% yield respectively (entry l, Table **5.1**).

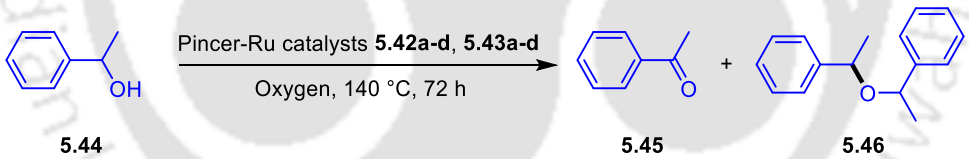

5.44 **5.45** **5.46**

Scheme 5.17: Ruthenium catalyzed etherification reaction under oxygen.

Repeating the experiment with degassed **5.44** resulted in no reaction (entry 2, Table **5.1**). This points to the involvement of oxygen in the **5.42a** catalyzed formation of **5.46**. Indeed, performing the reaction in the presence of oxygen atmosphere gave the ether **5.46** in 20% yield (entry 3, Table **5.l**). Under an oxygen atmosphere, use of solvents resulted in poor yields of **5.46** (entries 4 and 5, Table **5.1**). Radical scavenger like TEMPO resulted in complete inhibition of formation of **5.46** despite carrying out the reaction in an oxygen atmosphere (entries 6 and 7, Table **5.l**). On the other hand, presence of TBHP which is a radical initiator resulted in a 2.3-fold increase (46%) in the yield of **5.46** (entry 3 vs. entry 8, Table **5.1**). One can thus infer the participation of radical species in the reaction. A systematic increase in the yield of **5.46** was observed upon increasing the **5.42a** loading (entries 9-13, Table **5.l**). A maximum of 47% yield of **5.46** was obtained upon use of 1 mol % **5.42a** (entry 13, Table **5.l**). To attain a clear idea on

the comparative catalytic activity, the etherification reaction was repeated with 0.015 mol % of the other considered catalysts (Figure **5.1**).

Table 5.1: Pincer-Ru Catalyzed Etherification of 1-Phenyl Ethanol.[a]

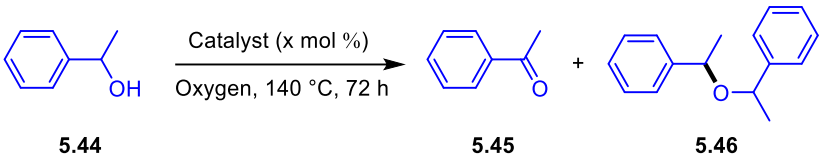

5.44 **5.45** **5.46**

entry	Catalyst (x mol %)	Reaction condition	**5.45**[b]	**5.46**[b]	TON
1	**5.42a** (0.015)	argon	4	18	1200
2[c]	**5.42a** (0.015)	argon	--	--	--
3	**5.42a** (0.015)	oxygen	3	20	1335
4[d]	**5.42a** (0.015)	oxygen	3	0	--
5[e]	**5.42a** (0.015)	oxygen	2	7	465
6[f]	**5.42a** (0.015)	oxygen	--	--	--
7[g]	**5.42a** (0.015)	oxygen	--	--	--
8[h]	**5.42a** (0.015)	oxygen	2	46	3065
9	**5.42a** (0.030)	oxygen	2	32	1065
10	**5.42a** (0.060)	oxygen	5	34	565
11	**5.42a** (0.100)	oxygen	4	38	380
12	**5.42a** (0.500)	oxygen	5	45	90
13	**5.42a** (1.000)	oxygen	5	47	45
14	**5.42b** (0.015)	oxygen	4	12	800
15	**5.42c** (0.015)	oxygen	5	11	735
16	**5.42d** (0.015)	oxygen	7	16	1065
17	**5.43a** (0.015)	oxygen	3	7	465
18	**5.43b** (0.015)	oxygen	9	92	6135
19	**5.43c** (0.015)	oxygen	3	47	3135
20	**5.43d** (0.015)	oxygen	7	16	1065
21	**5.43b** (0.0015)	oxygen	7	30	20000
22	**5.43b** (0.150)	oxygen	1	91	605
23	**5.43b** (0.500)	oxygen	2	90	180
24	**5.43b** (1.500)	oxygen	2	90	60
25	--	oxygen	--	--	--
26	--	argon	--	--	--
27	$RuCl_3.3H_2O$ (0.015)	oxygen	13	12	800
28	H_2O_2 (10)	oxygen	--	--	--
29	Tempo (10)	oxygen	--	--	--
30	TBHP (10)	oxygen	--	--	--

[a]Reaction conditions: 1-phenylethanol (0.5 mL,4.1 mmol), catalyst X mol % at 140 °C, [b]Yield was calculated from ^{1}H NMR spectroscopy by using toluene as an internal standard. [c]Degassed 1-phenylethanol was used. [d]Toluene (1 mL) was used as solvent. [e]1,4-dioxane (1 mL) was used as solvent. [f]Tempo (10 mol %) was used, [g]Tempo (20 mol %) was used. [h]TBHP (10 mol %) was used.

The activity of **5.42b** and **5.42c** towards formation of **5.46** was half of that demonstrated by **5.42a** (entries 14 and 15 vs. entry 3, Table **5.l**). On the other hand, the productivity of **5.42d** and **5.43d** were comparable and was 0.75 times as efficient as **5.42a** (entries 16 and 20 vs. entry 3, Table **5.l**). The catalyst **5.43c** was 2.35 times more productive than **5.42a** (entry 19 vs. entry 3, Table **5.l**). While the catalyst **5.43a** was one-third as active as **5.42a** (entry 17 vs. entry 3, Table **5.l**), the catalyst **5.43b** demonstrated an activity 4.6-folds higher (92% yield, ca. 6133 TON) than that of **5.42a** towards formation of **5.46** (entry 18 vs. entry 3, Table **5.l**). Upon lowering the loading of **5.43b** to 0.0015 mol %, the yield of **5.46** decreased (30%) but very high turnovers were obtained (20000 TON) (entry 21 vs. entry 18, Table **5.l**). However, the yield of **5.46** was comparable at higher loadings of **5.43b** (entries 22-24 vs. entry 18, Table **5.l**). There was no reactivity in the absence of a pincer-ruthenium catalyst either under an argon atmosphere or under an oxygen atmosphere (entries 25 and 26, Table **5.1**). In general, the better reactivity of pincer-Ru complexes containing carbonyl groups in comparison to their phosphine counterparts is attributable to the efficient stabilization of active species **5.53c** (see mechanistic insights, *vide-infra*) owing to the better π-accepting ability of the former.

5.3.2 Mechanistic insights into the pincer-ruthenium (5.42a-d and 5.43a-d) catalyzed etherification of 1-phenyl ethanol (5.44).

In the pincer-ruthenium (**5.42a-d** and **5.43a-d**) catalyzed etherification of 1-phenyl ethanol (**5.44**), oxygen has been found to be pivotal for the productivity of the reaction which involves the formation of radical species (*vide-supra*, entries 2, 6, 7 and 8, Table **5.1**). The volatiles obtained from a cold-trap of a typical reaction indicated that 4.1 mmol of alcohol in presence of 0.015 mol % **5.43b** gave 1.85 mmol (90% yield) each of ether and water along with hydrogen peroxide which was quantitatively confirmed to be 1 mol % by an iodometric titration.[68-71] So, in the considered reaction, hydrogen peroxide formation is catalytic along with stoichiometric generation of water.

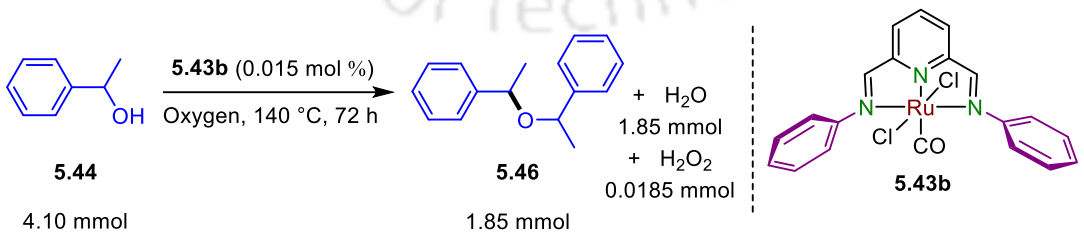

Scheme 5.18. Experiment performed to determine the mass-balance of the **5.43b** catalyzed etherification reaction.

The role of oxygen is hence likely to be catalytic (Scheme **5.18** and Scheme **5.20**) in this dehydrative etherification reaction. This bodes well with the overall energetics of the

dehydration reaction (ΔG_{140} = 1.12 kcal/mol) which is downhill by 29.38 kcal/mol in comparison with the oxidative dehydration (release of stoichiometric amounts of H_2O_2, ΔG_{140} = 30.50 kcal/mol). The latter is hence unfavorable when compared to the former.

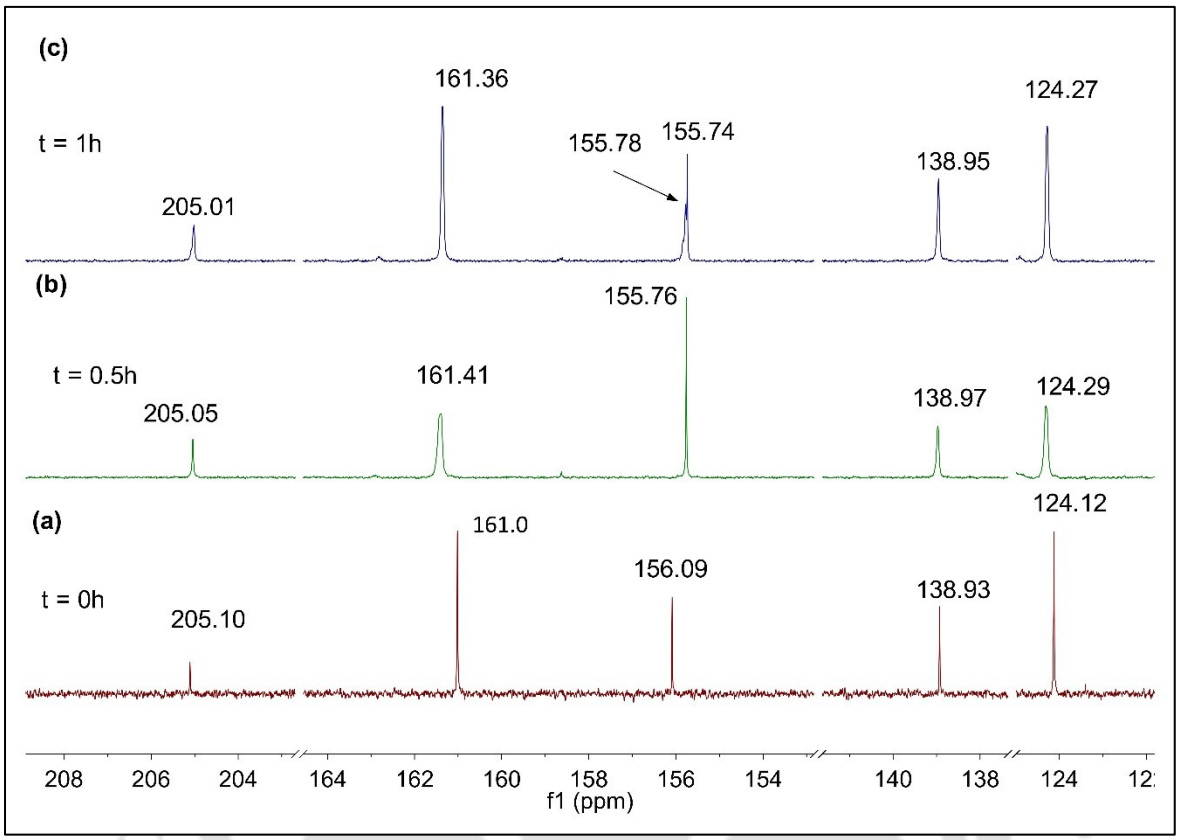

Figure 5.2. The carbonyl region of the ^{13}C NMR spectra of the reaction mixture containing 10 mol % **5.43c** in **5.44** in the presence of oxygen at (a) t = 0 h at room temperature, (b) t = 0.5 h after heating at 140 °C and (c) t = 1 h after heating at 140 °C

The ^{13}C NMR spectra analysis of a reaction mixture containing **5.43c** and **5.44** in 1:1 ratio indicated the presence of CO ligand even after heating for 1 h at 140 °C under an atmosphere of oxygen (Figure **5.2**). It is noteworthy that after heating, while the signals (around 161 ppm) corresponding to the aza-carbonyl carbons are broad and slightly down-field shifted (Figure **5.2b** and **5.2c**), the peak around 158 ppm corresponding to the aromatic carbon α to the aza-carbonyl carbon is also broad having multiple signals with an overall up-field shift. The broadening of the ^{13}C signals (Figure **5.2**) are attributable to the fluxional nature of the hemi-labile imine groups (Figure **5.4**). Similar observations were made in the ^{1}H NMR spectra of the reaction mixture that was heated at 140 °C for 1 h which indicated that the two imine protons of **5.43c** are chemically different but are readily interchangeable owing to their fluxional behavior (Figure **5.2** and **5.4**). The fast interchange relative to the NMR time-scale results in

broadening of the imine protons which apparently points to the hemi-labile nature of the imine groups (Path **B**, Scheme **5.15**).

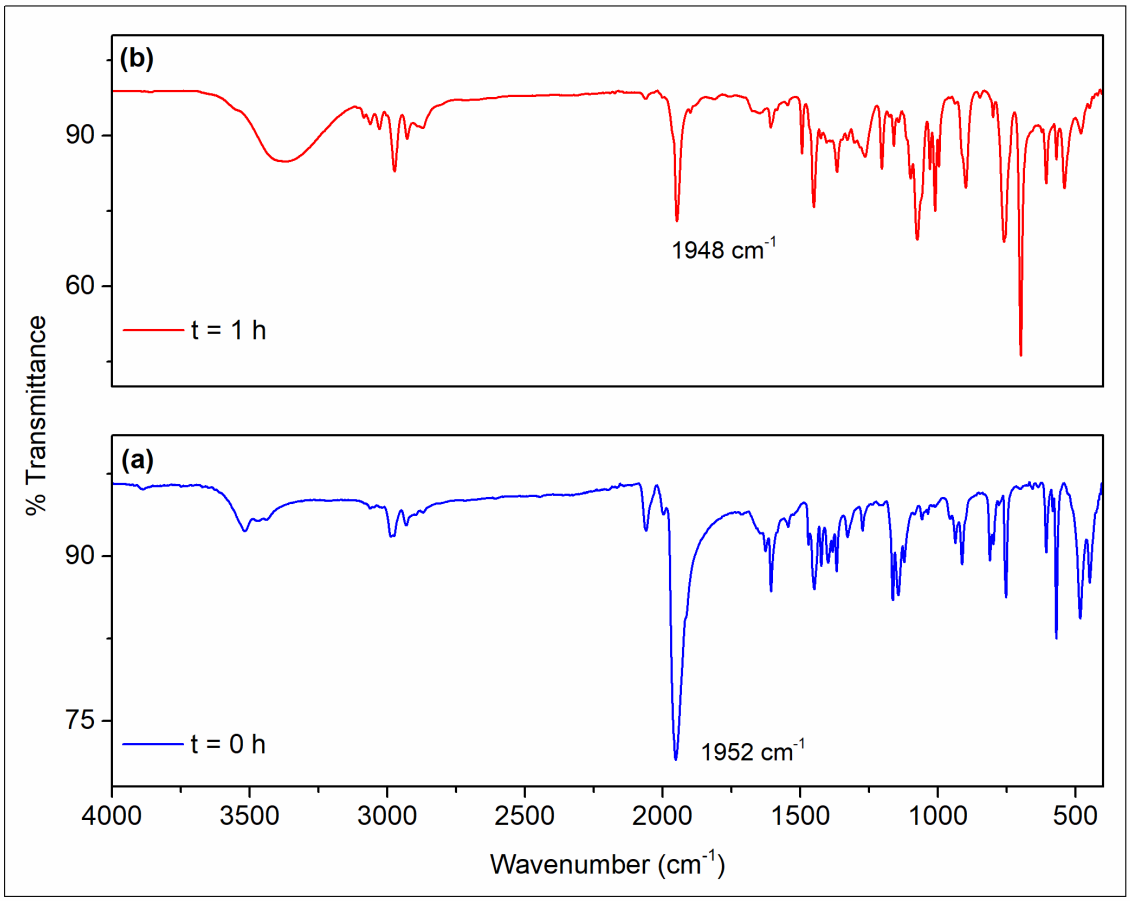

Figure 5.3. IR spectra of the reaction mixture containing 10 mol % **5.43c** in **5.44** in the presence of oxygen at (a) t = 0 h at room temperature, (b) t = 1 h after heating at 140 °C.

Similar to the NMR spectroscopy studies, IR spectroscopy (Figure **5.3**) measurements with **5.43c** and HRMS spectroscopy (Figure **5.5**) analysis with **5.43b** also indicate that the CO ligand is not labile and remains coordinated to the Ru. Notably, all the peaks observed in the HRMS could be assigned to various pincer-ruthenium carbonyl derivatives (Figure **5.5**) whose significance from a mechanistic point of view is discussed in detail (*vide-infra*). While immediately after addition (t = 0 h), the reaction mixture containing 10 mol % **5.43b** in **5.44** in the presence of oxygen at room temperature was EPR silent, a signal was observed after heating at 140 °C for one hour (Figure **5.6**). EPR experiments thus reveal that a Ru(III) species is involved in the reaction at 140 °C in the presence of oxygen (Figure **5.6**). These forms the basis of the mechanism proposed (Scheme **5.18** and **5.19**) that employs **5.43c** as a model catalyst. As experimental evidence rules out Path **A** (Scheme **5.19**), quantum mechanical calculations were carried to determine the most favorable route among Path **B** and Path **C** (Scheme **5.19**).

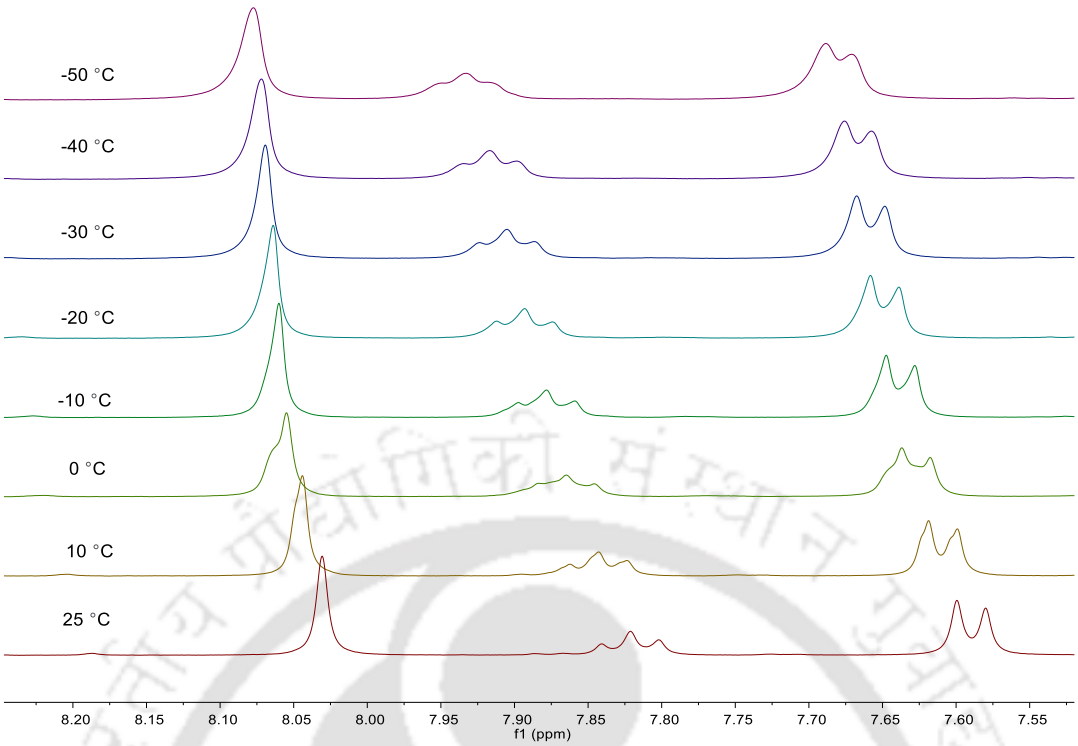

Figure 5.4: Variable temperature ^{1}H NMR spectra of the reaction mixture containing 10 mol % **5.43c** in **5.44** in the presence of oxygen after heating at 140 °C in $CDCl_3$ for 1 h.

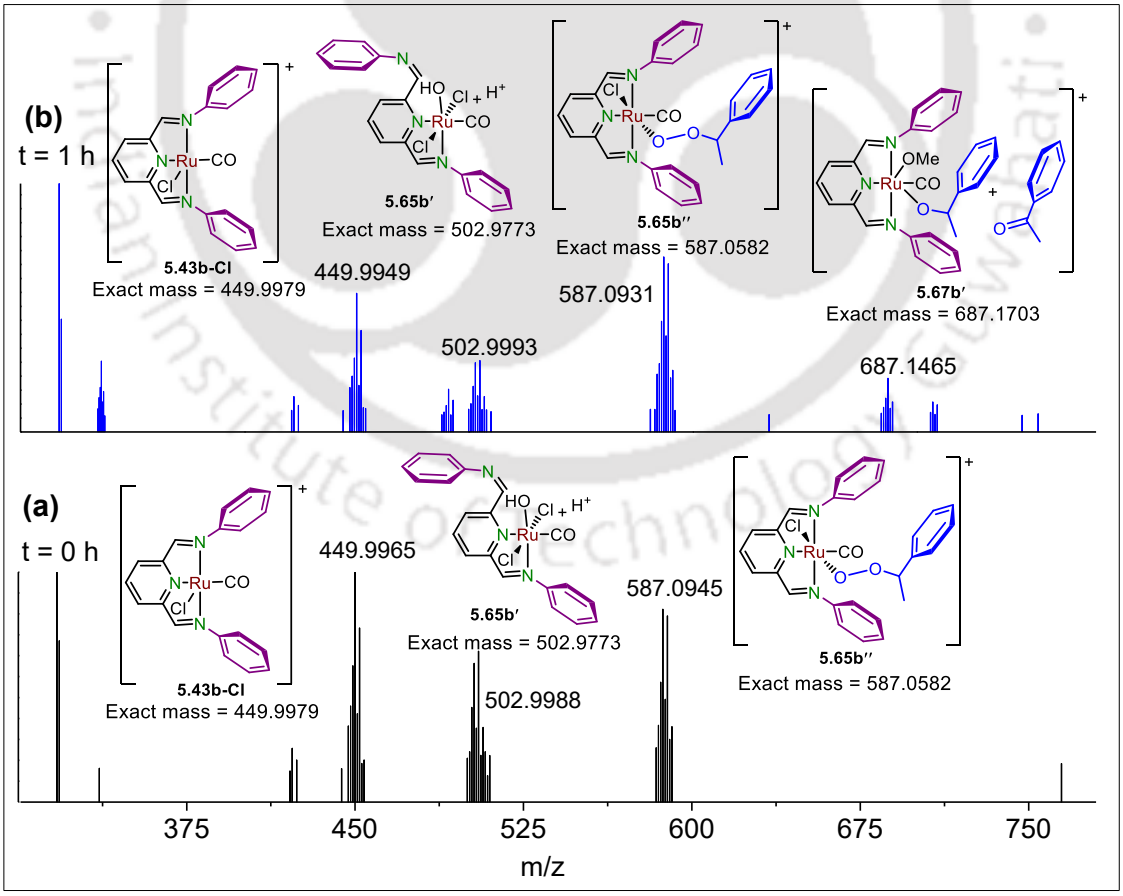

Figure 5.5. HRMS(ESI) analysis of the reaction mixture containing 10 mol % **5.43b** in **5.44** in the presence of oxygen at (a) t = 0 h at room temperature, (b) t = 1 h after heating at 140 °C.

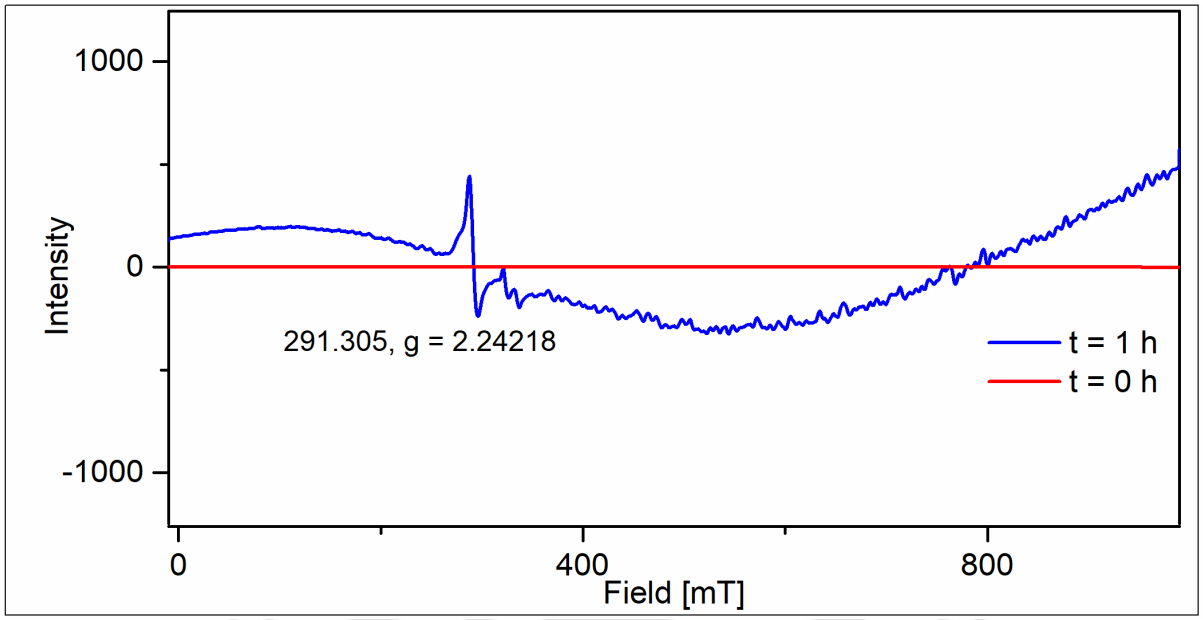

Figure 5.6. EPR spectra recorded at 77 K of the reaction mixture containing 10 mol % **5.43c** in 1-phenyl ethanol (**5.44**) in the presence of oxygen at (a) t = 0 h at room temperature, (b) t = 1 h after heating at 140 °C.

The geometries were optimized using the PBEPBE functional[72-73] and empirical dispersion GD3[74] as implemented in the Gaussian 09 package[75] in conjunction with 6-31G(d,p) basis sets[76] for the non-metallic elements. For Ru, effective core pseudopotentials (LANL2DZ)[77-79] and the associated basis sets with a polarization function was used. The empirical dispersion-GD3 was used in all molecular geometry optimization and energy computations. The transition states were located using the synchronous transit-guided quasi-Newton (QST2) approach. An analytical frequency calculation verified all the stationary points. The Gibbs free energies were computed at 413.15° K and at atmospheric pressure (unless specified otherwise), assuming an ideal gas behaviour using unscaled harmonic vibrational frequencies obtained within the rigid rotor approximation. Free energies (ΔG) were obtained by adding the gas phase's thermal corrections to the internal energies. The oxygen molecule was considered in its triplet state.

The release of CO from **5.43c** to form the 16-electron five coordinate species **5.48c** is an uphill process (ΔG_{140} = 26.24 kcal/mol) with a high energy barrier (**TS-5.47c**, $\Delta G^{\ddagger}_{140}$ = 35.77 kcal/mol) (Path **A**, Scheme **5.19**). The subsequent association of **5.48c** with an oxygen molecule is slightly uphill (ca. ΔG_{140}= 2.72 kcal/mol) with a much lower barrier (**TS-5.49c**, $\Delta G^{\ddagger}_{140}$ = 9.81 kcal/mol). The overall transformation **5.43c→5.50c** is uphill (ΔG_{140} = 28.96 kcal/mol). As the activation energy for the concerted step *via* **TS-5.51c** is 8.64 kcal/mol higher than the highest barrier involved in the sequential step, the latter is the more preferred if Path **A** (Scheme **5.19**) is involved. The dissociation of one of the pincer *N* arms from **5.43c** to

generate the 16-electron five coordinate species **5.53c** *via* **TS-5.52c** ($\Delta G^{\ddagger}_{140}$ = 28.44 kcal/mol) is uphill by 18.61 kcal/mol (Path **B**, Scheme **5.19**). The coordination of oxygen to **5.53c** is also uphill (ΔG_{140} = 6.45 kcal/mol) albeit with a lower barrier (**TS-5.54c**, $\Delta G^{\ddagger}_{140}$ = 8.17 kcal/mol). The barrier (**TS-5.56c**, $\Delta G^{\ddagger}_{140}$ = 34.61 kcal/mol) for the concerted path **5.43c→5.55c** is unfavorable in comparison to the highest barrier **TS-5.52c** ($\Delta G^{\ddagger}_{140}$ = 28.44 kcal/mol) *via* the sequential path **5.43c→5.53c→5.55c**. Similarly, for the Path **C** (Scheme **5.19**) involving the formation of cationic active species **5.60c**, the overall transformation **5.43c→5.60c** is uphill (ΔG_{140} = 31.92 kcal/mol) (Path **C**, Scheme **5.19**). Notably, the concerted step is again kinetically unfavorable in comparison to the sequential step by 4.6 kcal/mol. Furthermore, among all the considered paths, Path **B** (Scheme **5.19**) has the lowest overall barrier for the formation of the catalytically active oxygen-adduct species. This indicates that **5.55c** is formed upon reaction of **5.43c** with oxygen which is in line with the observations from NMR, HRMS and IR spectroscopy studies which not only demonstrate that the carbonyl group is intact but also show that the imine groups are labile and hence chemically different but yet fluxional.

In the catalytic cycle, one could envisage the reaction of Ru(II) species **5.55c** with another Ru(II) species **5.43c** leading to a 17-electron Ru(III) species **5.63c** *via* **TS-5.62c** (Scheme **5.20**). Involvement of Ru(III) species in the reaction has been confirmed by EPR studies (Figure **5.6**). Subsequent homolytic cleavage of the O–O bond in **5.63c** would give rise to **5.64c**. Under the reaction conditions, the alcohol **5.44** could easily generate the corresponding radical **5.44′** and H$^{\bullet}$. While the former could lose another H$^{\bullet}$ resulting in the formation of **5.43** (detected in trace amounts in the ^{1}H NMR spectra, Figure **5.2** and **5.4**), the latter when picked up by **5.65b** is being detected as **5.65b′** in HRMS spectra analysis (*m/z* = 502.9993, Figure **5.5**). Notably, the adduct of **5.44′** with **5.64b** has been detected as **5.65b″** in the HRMS analysis (Figure **5.5**).

Further reaction of **5.64c** with **5.44** leads to the formation of a hydroxyl radical bound within the coordination sphere[65] of the 17-electron Ru(III) species **5.67c** *via* **TS-5.66c**. Two hydroxyl radicals could combine to yield H_2O_2 which has been quantitatively determined by iodometric titration (Scheme **5.18**).[68-71] In the **5.43b** catalyzed etherification reaction, **5.67b′** (*m/z* = 687.1465, Figure **5.5**) has been detected in the HRMS studies.

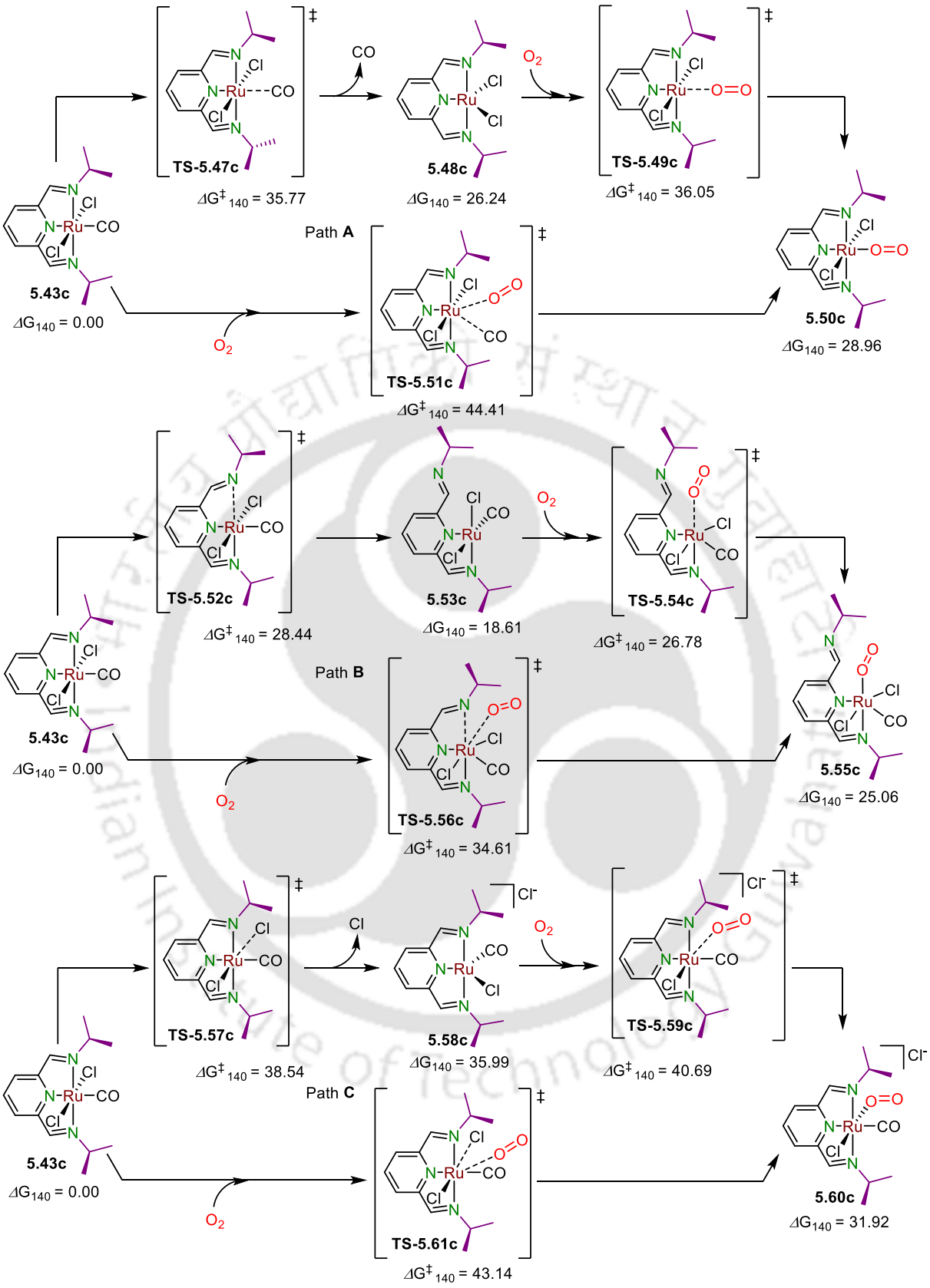

Scheme 5.19. Generation of active species **5.50c/5.55c /5.60c** from the reaction of **5.43c** with oxygen. Free energy are given in kcal/mol and calculated at 140 °C.

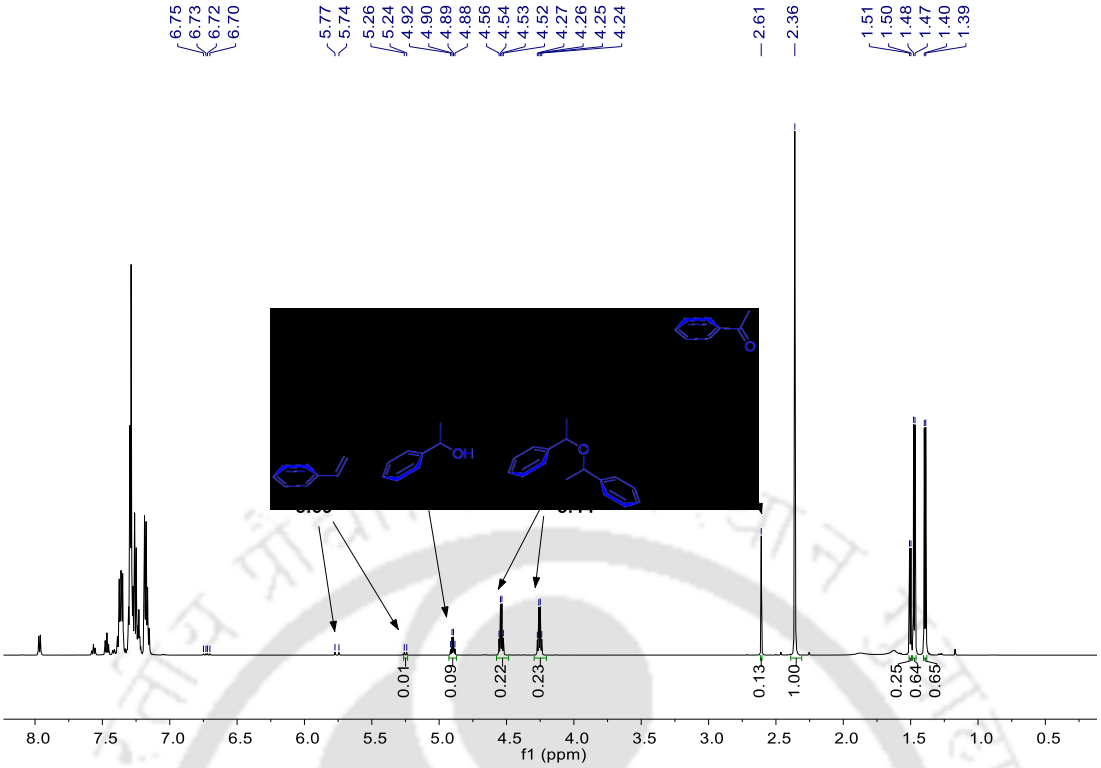

Figure 5.7. ^{1}H NMR spectra of the reaction mixture obtained from the **5.43b** catalyzed etherification of 1-phenylethanol in $CDCl_3$ (entry 24, Table **5.1**).

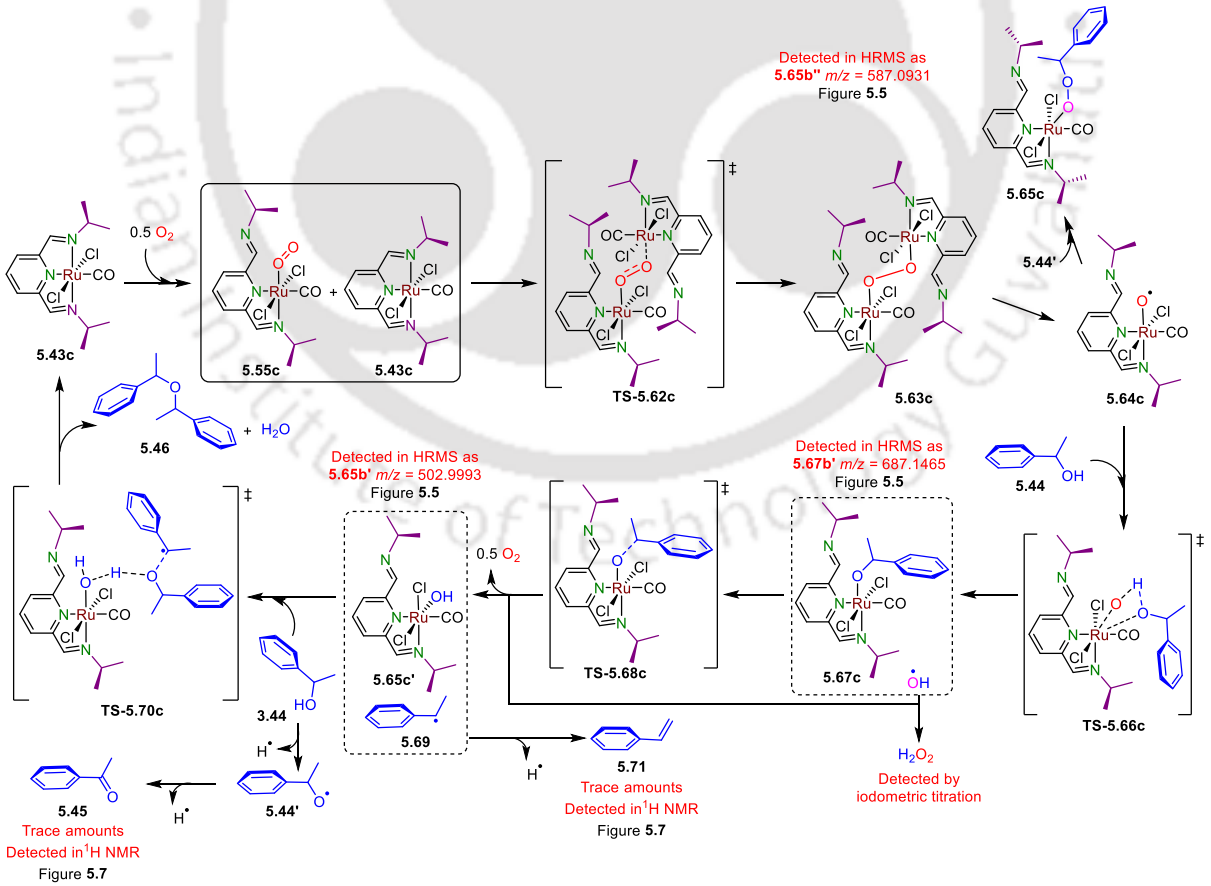

Scheme 5.20. A plausible mechanism involved in the **5.43c** catalyzed etherification of **5.44**.

Further reaction of the 17-electron Ru(III) species **5.67c** in the presence of the hydroxyl radical leads to the generation of the secondary radical **5.69** bound within the coordination sphere[65] of the 17-electron Ru(III) species **5.65c′** along with evolution of oxygen. The half a mole of oxygen consumed in the first step is regenerated here which explains the catalytic role of oxygen in the reaction. The loss of H$^{\bullet}$ from the secondary radical **5.69** would result in the formation of styrene (**5.71**) which has been detected in trace amounts in the ^{1}H NMR spectra of the reaction mixture (Figure **5.7**). The lower stability of the corresponding primary radical arising from benzyl alcohol explains its poor reactivity and lack of product formation (**5.46w**, Table **5.2**). Additional evidence for the formation of **5.67** was obtained by trapping it with the radicals generated from phenols that resulted in their selective *ortho*-alkylation (**5.75a-v**, Table **5.3**). Furthermore, **5.65b′** is detected in the HRMS analysis (Figure **5.5**). The fact that the fragments **5.71**, **5.67b′**, **5.65b′** and **5.65b″** that have been detected could be mapped to the step **5.67c→5.65c′** points to its possible involvement in the rate-determining step (RDS). Subsequent reaction of 17-electron Ru(III) species **5.65c′** with another molecule of **5.44** while going through **TS-5.70c** yields the product **5.46** and water along with the regeneration of 18-electron Ru(II) precursor **5.43c**.

5.3.3 The (^{Ph2}NNN)RuCl$_2$(CO) (5.43b) catalyzed etherification of various 1-phenyl ethanols.

The catalyst (^{Ph2}NNN)RuCl$_2$(CO) (**5.43b**) which demonstrated the best activity (Entries 18, 23 and 24, Table **5.1**) towards the etherification of 1-phenyl ethanol (**5.44**), was then employed to accomplish the corresponding etherification of various 1-phenyl ethanol derivatives (Table **5.2**). In general, regardless of the electron-donating and/or electron-withdrawing nature of the group present in the derivative of **5.44**, the yield of the ether products **5.46ab** & **5.46b-5.46o** were slightly lower (60-70%) in comparison to that of **5.46a** (90%).

The poor yield of **5.46g** is attributed to the fact that the reaction was done in a sealed vessel with measured amounts of oxygen owing to the volatile nature (b.p = 91 °C) of precursor 1-(4-fluorophenyl)ethanol. Secondary alcohols based on 1-(2-naphthyl)ethanol and diphenylmethanol gave good yields of the corresponding ethers **5.46q** and **5.46ab** in the **5.43b** catalyzed reaction at 140 °C. On the other hand, benzyl alcohol and aliphatic secondary alcohols were either unreactive (**5.46w** and **5.46x**) or gave poor yields (**5.46y**) of the ether product. Barring 1-(pyridine-4-yl)ethanol, secondary alcohols containing heterocyclic groups gave moderate yields of ethers (**5.46r-5.46v**) in the **5.43b** catalyzed reaction at 140 °C. Thus,

the current protocol provides a convenient route to ethers starting from a wide range of secondary alcohols and only requires the presence of highly abundant molecular oxygen and small amounts (0.015 mol %) of pincer-ruthenium catalyst at 140 °C without the need of either a chlorinated solvent or a base.

Table 5.2. The **5.43b** catalyzed dehydrative etherification of various 1-phenyl ethanol derivatives.[a]

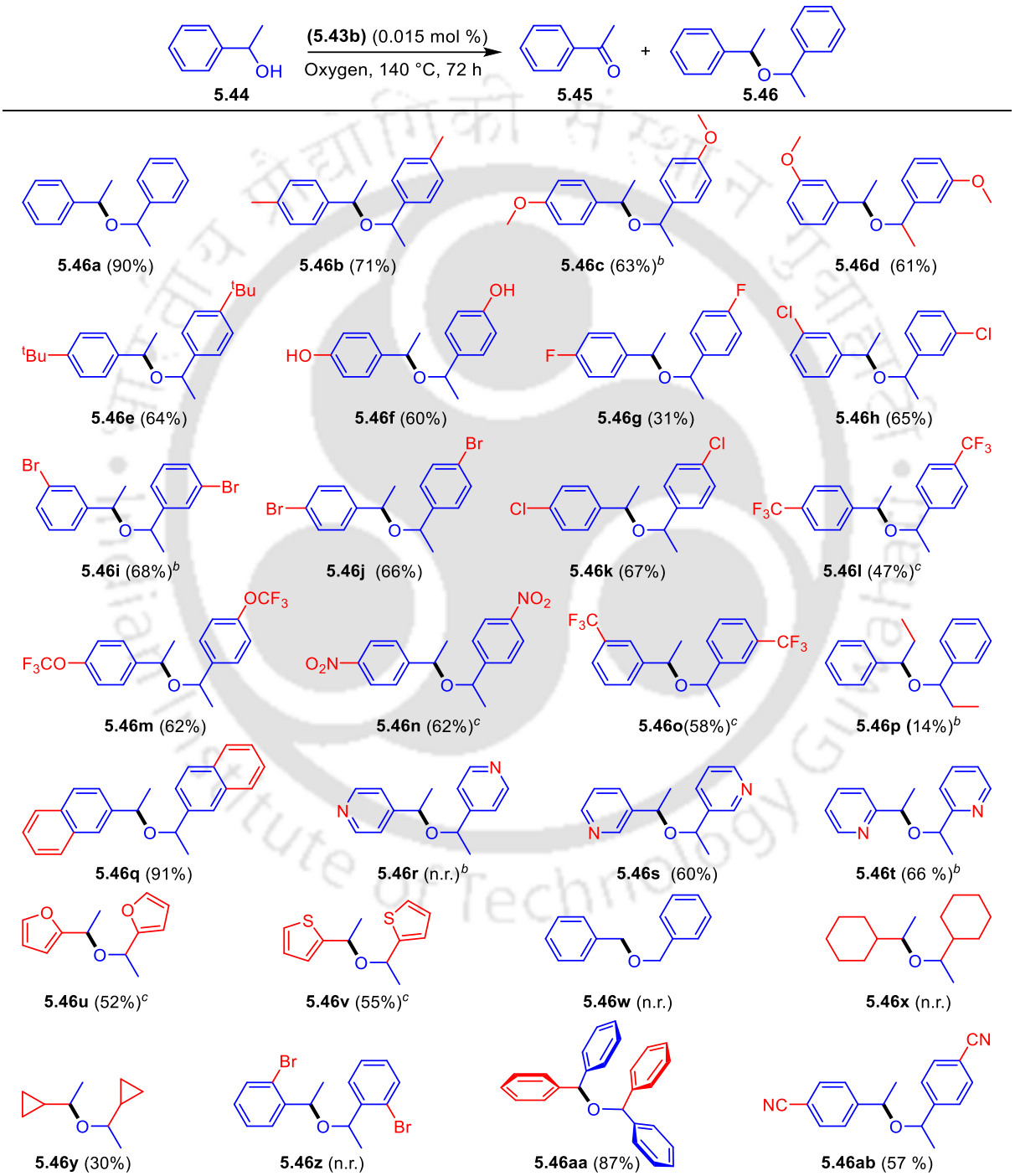

[a]Reaction conditions: 1-phenylethanol derivative (4.1 mmol), **5.43b** 0.015 mol % at 140 °C for 72h under an atmosphere of oxygen. Yield determined from ^{1}H NMR spectroscopy by using toluene as an internal standard. [b]0.5 mol % of **5.43b** was used. [c]Isolated yield.

5.3.4 The (^{Ph2}NNN)RuCl$_2$(CO) (5.43b) catalyzed cross-etherification and *ortho*-alkylation of phenols with various 1-phenyl ethanols.

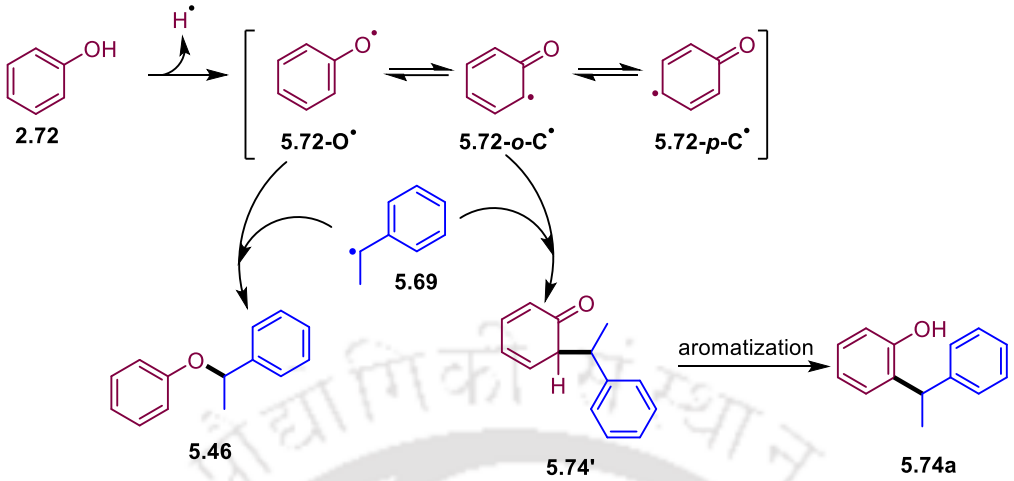

Scheme 5.21. Resonance stabilized phenoxyl radicals as potential coupling partners for the secondary radical **5.67**.

It would be interesting to see if the secondary radical **5.69** that is generated under the reaction conditions could be trapped by other radicals thereby leading to new reactivity. In this regard, resonance-stabilized phenoxyl radicals (Scheme **5.21**) offer great promise as potential coupling partners and could result in the formation of cross-etherification product **5.75a**[80] (Table **5.3**). Considering the greater stability[81-83] of the **5.72-*o*-C•**, one can also envisage the formation of C–C bonds *via* *o*-alkylation as in **5.74a** upon reaction with **5.69** (Scheme **5.21**).[84-85] Thus, apart from the formation of **5.46** and water, the reaction of 1-phenyl ethanol (**5.44**) with phenol (**5.72a**) catalyzed by **5.43b** in the presence of molecular oxygen could lead to cross-etherification (**5.75a**) and *o*-alkylation (**5.74a**) along with the extrusion of hydrogen peroxide in catalytic amounts (Scheme **5.20**, Scheme **5.21** and Table **5.3**). The pincer-ruthenium catalyzed reactions were then extended to the cross-etherification and/or *ortho*-alkylation of phenols with various 1-phenyl ethanols (Table **5.3**). The yield of the cross-ether **5.75** was found to be better when two equivalents of **5.72a** was used (footnote a, Table **5.3**) rather than one or three equivalents (footnotes b and c, Table **5.3**). Furthermore, while pincer-ruthenium catalyzed reaction of various phenols with 1-phenyl ethanol gave mixture of ethers and *o*-alkylated products (**5.75a-d**), the corresponding reactions of either *β*-naphthol with 1-phenyl ethanol derivatives or phenol with diphenylmethanol were selective towards the formation of *o*-alkylated products (**5.74e-v**). In fact, it was observed that the reaction of *β*-naphthol with 1-phenyl ethanol derivatives is nearly complete within two hours (footnote g, Table **5.3**).

Table 5.3. The **5.43b** catalyzed dehydrative etherification of various 1-phenyl ethanol derivatives.[a]

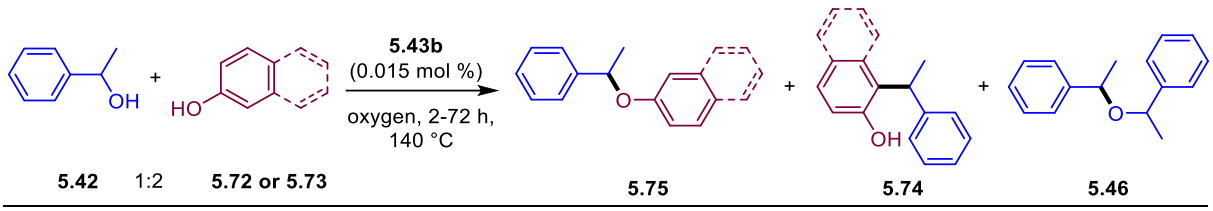

5.42 1:2 **5.72 or 5.73** **5.75** **5.74** **5.46**

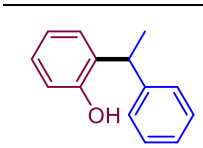

5.74a
(34%,[d] 26%,[e] 18%[f])[b]
(42%,[d] 24%,[e] 12%[f])
(38%,[d] 28%,e 10%[f])[c]

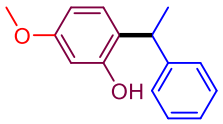

5.74b
(41%,[d] 15%,[e] 15%[f])

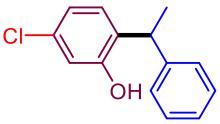

5.74c
(32%,[d] 20%,[e] 0%[f])

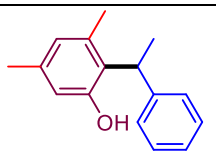

5.74d
(22%,[d] 47%,[e] 0%[f])

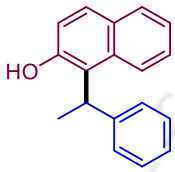

5.74e
(0%,[d] 88%,[e] 0%[f])
(0%,[d] 65%,[e] 0%[f])[g]

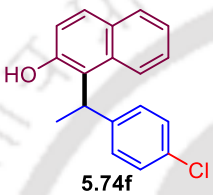

5.74f
(0%,[d] 76%,[e] 0%[f])
(9%,[d] 67%,[e] 0%[f])[g]

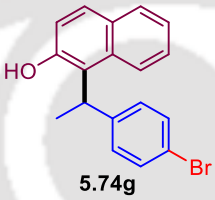

5.74g
(0%,[d] 43%,[e] 0%[f])
(0%,[d] 61%,[e] 0%[f])[g]

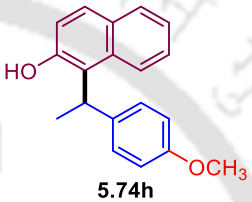

5.74h
(0%,[d] 71%,[e] 0%[f])
(0%,[d] 70%,[e] 0%[f])[g]

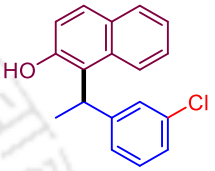

5.74i
(0%,[d] 42 %,[e] 0%[f])
(0%,[d] 3%,[e] 0%[f])[g]

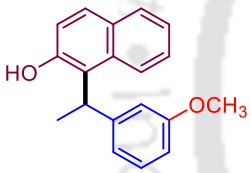

5.74j
(0%,d 59%,e 0%f)
(0%,d 9%,e 0%f)g

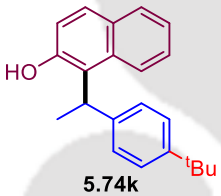

5.74k
(0%,[d] 78%,[e] 0%[f])
(0%,[d] 69%,[e] 0%[f])[g]

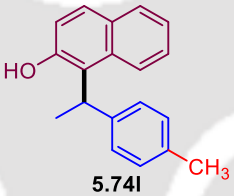

5.74l
(0%,[d] 56%,[e] 0%[f])
(0%,[d] 76%,[e] 0%[f])[g]

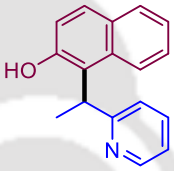

5.74m
(n.r.)

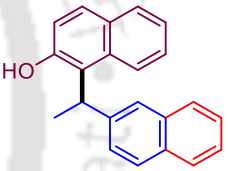

5.74n
(0%,[d] 78%,[e] 0%[f])
(0%,[d] 85%,[e] 0%[f])[g]

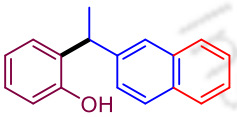

5.74o
(0%,[d] 56%,[e] 0%[f])
(22%,[d] 47%,[e] 0%[f])[g]

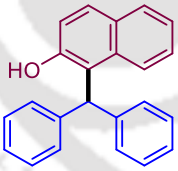

5.74p
(0%,[d] 76%,[e] 0%[f])
(0%,[d] 51%,[e] 0%f)[g]

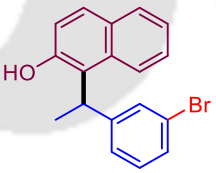

5.74q
(20%,[d] 46%,[e] 0%[f])
(10%,[d] 18%,[e] 0%[f])[g]

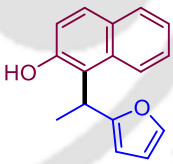

5.74r
(n.r.)

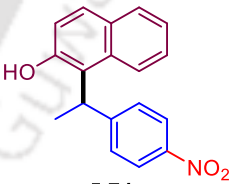

5.74s
(n.r.)

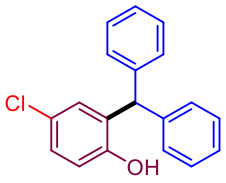

5.74t
(0%,[d] 45%,[e] 0%[f])

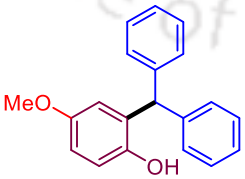

5.74u
(0%,[d] 33%,[e] 0%[f])

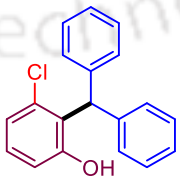

5.74v
(0%,[d] 39%,[e] 0%[f])

[a]Reaction conditions: 1-phenylethanol derivative (4.1 mmol), phenol derivative (8.2 mmol), **5.43b** 0.015 mol % at 140 °C for 72 h under an atmosphere of oxygen. Yield determined from ^{1}H NMR spectroscopy by using toluene as an internal standard. [b]4.1 mmol of phenol was used. [c]12.3 mmol of phenol was used. [d]Yield of the corresponding derivative of **5.74**, [e]Yield of the corresponding derivative of **5.75**, [f]Yield of the corresponding derivative of **5.46**. [g]Yield of the corresponding derivative of **5.75** after 2 h.

5.4 Conclusions

In the current report, a dehydration strategy has been formulated for the selective etherification of secondary alcohols catalyzed by NNN pincer-ruthenium(II) carbonyl complexes based on *bis*(imino)pyridine ligands in the presence of molecular oxygen under solvent-free and base-free conditions at 140 °C. Under these conditions, very high yields (up to 92%, ca. 6133 TON) of the corresponding ethers are obtained at a very low catalyst loading (ca. 0.015 mol %). Mechanistic studies provide key evidence for the various events that occur during the catalytic cycle. While iodometric titration gives quantitative proof for the liberation of hydrogen peroxide in catalytic amounts and hence confirms the role of oxygen as a co-catalyst, DFT, HRMS, IR and ^{13}C NMR spectra analysis are indicative of the non-labile nature of the ancillary CO ligand. On the other hand, DFT, NMR and HRMS spectroscopies studies reveal the hemi-labile nature of the pincer-ligand in the presence of oxygen.

EPR analysis provide conclusive evidence for generation of Ru(III) species *via* single electron transfer (SET) from O_2. Apparently the Ru(III) species (^{Ph2}NN)$RuCl_2$(CO)(OH) is the resting-state of the etherification reaction and several of its derivatives have been detected by HRMS analysis. The pincer-ruthenium catalyzed etherification of 1-phenyl ethanol has been successfully extended not only to various aromatic secondary alcohols but also to the cross etherification and/or *o*-alkylation of 1-phenyl ethanols with a variety of phenols. Readily available oxygen and tiny amounts (0.015 mol %) of pincer-Ru catalyst are the only requirement for this atom-economical and environmentally benign dehydrative etherification reaction which apparently has not been reported thus far.

5.5 Experimental Section

5.5.1 General Methods and Materials.

All manipulations were carried out under purified argon using a standard double manifold or a glove box. The solvents such as tetrahydrofuran (THF), hexane and toluene were dried *via* double distillation over Na/Benzophenone prior to experiments.[86-87] All other compounds including pryidine-2,6-dicarboxylic acid, $[RuCl_2(p\text{-cymene})]_2$, and $CDCl_3$ were purchased either from MERCK or Sigma-Aldrich and used as such. The complexes (**5.42a-d** and **5.43a-d**) were prepared according to the procedure followed in the previous chapters (chapter II and chapter III).[64-65]

^1H, ^{13}C & ^{19}F NMR spectra were recorded either on Bruker ASCEND 600 operating at 600 MHz for ^1H, 150 MHz for ^{13}C & 564 MHz for ^{19}F or on Bruker AVANCE 500 operating at

500 MHz for ^{1}H, 125 MHz for ^{13}C & 469 MHz for ^{19}F or on Bruker AVANCE 400 operating at 400 MHz for ^{1}H, 100 MHz for ^{13}C & 376 MHz for ^{19}F. The mass analysis was done using an Agilent Accurate-Mass Q-Toff ESI-MS 6520. Fourier Transform Infrared (FT-IR) were recorded on Perkin Elmer Spectrum Two FT-IR spectrometer at room temperature within the region 400-4000 cm^{-1}. The X-band EPR spectra were recorded on a JES-FA200 ESR spectrometer, at 298 K and 77 K with microwave power of 0.998 mW and microwave frequency of 9.14 GHz.

5.5.2 General procedure for the 5.43b catalyzed etherification reaction

In a two-necked round bottom flask (25 mL), 1-phenylethanol (0.5 mL, 4.1 mmol) and **5.43b** (0.3 mg, 0.6 μmol) were taken. Subsequently, the reaction mixture was heated at 140 °C for about 72 h under an atmosphere of oxygen. The reaction mixture was then cooled down to room temperature and toluene (typically 100 μL) as added as an internal standard. An aliquot (typically 10 mg) of the reaction mixture was withdrawn into an NMR tube containing $CDCl_3$ (0.5 mL) and the yield of **5.46** was determined from ^{1}H NMR spectra. Silica gel (60-120 mesh) column chromatography was performed on the rest of the reaction mixture using 0–20% ethyl acetate in hexane as eluent to yield the product **5.46** (mixture of two diastereomers) in a pure form.

5.5.3 General procedure for the 5.43b catalyzed reaction of phenol with 1-phenylethanol

In a two-necked round bottom flask (25 mL), 1-phenylethanol (0.5 mL, 4.1 mmol), phenol (0.7 mL, 8.2 mmol) and **5.43b** (0.3 mg, 0.6 μmol) were taken. Subsequently, the reaction mixture was heated at 140 °C for about 72h under an atmosphere of oxygen. The reaction mixture was then cooled down to room temperature and toluene (typically 100 μL) as added as an internal standard. An aliquot (typically 10 mg) of the reaction mixture was withdrawn into an NMR tube containing $CDCl_3$ (0.5 mL) and the yield of **5.75**, **5.74** and **5.46** were determined from ^{1}H NMR spectra. Silica gel (60-120 mesh) column chromatography was performed on the rest of the reaction mixture using 0–20% ethyl acetate in hexane as eluent to yield the products **5.74** and **5.75** in the pure form.

5.5.4 General procedure for the H_2O_2 detection

In a two-necked round bottom flask (25 mL), 1-phenylethanol (0.5 mL, 4.1 mmol) and **5.43b** (0.3 mg, 0.6 μmol) were taken. The reaction mixture was heated at 140 °C for 72 h under an atmosphere of oxygen. Subsequently, the reaction mixture was extracted using a 1:2 mixture

(20 mL) of dichloromethane and water. The aqueous part was then collected followed by addition of H_2SO_4 and KI. The straw yellow color solution was qualitatively titrated against a $Na_2S_2O_3$ solution.

5.5.5 Experimental procedure for the EPR analysis

The X-band EPR spectra of the reaction mixture containing 1-phenylethanol (50 μL, 0.4 mmol) and **5.43b** (0.021 g, 41 μmol) in an EPR tube under oxygen was recorded at 77 K immediately after mixing the contents at room temperature (t = 0 h) and after heating at 140 °C (t = 1 h).

5.5.6 Experimental procedure for the IR and mass analysis

The IR and Mass spectra of the reaction mixture containing 1-phenylethanol (50 μL, 0.4 mmol) and **5.43b** (0.021 g, 41 μmol) under oxygen were recorded immediately after mixing the contents at room temperature (t = 0 h) and after heating at 140 °C (t = 1 h).

5.5.7 Computational methodology

The geometries of all the considered complexes were fully optimized using the DFT (PBEPBE)[72-73] method on the Gaussian-09 program package.[75] The LANL2DZ[77-79] and 6-311G(d,p)[76] basis set was used respectively for the metal (Ru) and non-metal atoms. Genecp (gen keyword with the effective core potential) was included to define the basis set. The empirical dispersion-GD3[74] was used for all molecular geometry optimization. The transition states were located using the synchronous transit-guided quasi-Newton (QST2) approach. An analytical frequency calculation verified all the stationary points. The Gibbs free energies were computed at 140 °C and at atmospheric pressure (unless specified otherwise), assuming an ideal gas behavior using unscaled harmonic vibrational frequencies obtained within the rigid rotor approximation. Free energies (ΔG) were obtained by adding the gas phase's thermal corrections to the internal energies. The oxygen molecule was considered in its triplet state.

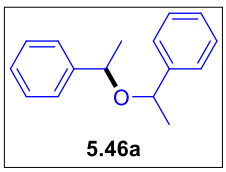

5.46a

(oxy*bis*(ethane-1,1-diyl))dibenzene (5.46a).[29] ^{1}H NMR (600 MHz, $CDCl_3$): δ = 7.36 (t, J = 7.5 Hz, 4H, Ar), 7.32 – 7.20 (m, 16H, Ar), 4.54 (q, J = 6.4 Hz, 2H, OC*H*(Ar)CH$_3$), 4.25 (q, J = 6.5 Hz, 2H, OC*H*(Ar)CH$_3$), 1.47 (d, J = 6.4 Hz, 6H, OCH(Ar)C*H*$_3$), 1.39 (d, J = 6.5 Hz, 6H, OCH(Ar)C*H*$_3$). ^{13}C NMR (151 MHz, $CDCl_3$): δ = 144.36, 144.27, 128.59, 128.38, 127.52, 127.28, 126.45, 126.36 (Ar), 74.76, 74.54 (O*C*H(Ar)CH$_3$), 24.84, 23.11 (OCH(Ar)*C*H$_3$). Colorless liquid, isolated yield 0.40 g (90%).

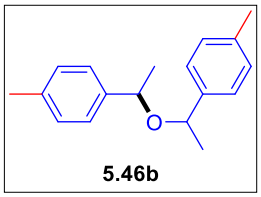

4,4'-(oxy*bis*(ethane-1,1-diyl))*bis*(methylbenzene) (5.46b).[29] ^{1}H NMR (600 MHz, $CDCl_3$): δ = 7.20-7.11 (m, 15.6H, Ar), 4.51 (q, J = 6.4 Hz, 1.9H, OC*H*(Ar)CH_3), 4.23 (q, J = 6.6 Hz, 2H, OC*H*(Ar)CH_3), 2.38 (s, 6H, ArC*H*$_3$), 2.34 (s, 5.7H, ArC*H*$_3$), 1.45 (d, J = 6.4 Hz, 5.7H, OCH(Ar)C*H*$_3$), 1.37 (d, J = 6.5 Hz, 6H, OCH(Ar)C*H*$_3$). ^{13}C NMR (151 MHz, $CDCl_3$): δ = 141.44, 141.29, 137.10, 136.83, 129.26, 129.06, 126.43, 126.32 (Ar), 74.37, 74.05 (O*C*H(Ar)CH_3), 24.85, 23.01 (OCH(Ar)*C*H$_3$), 21.30, 21.24 (Ar*C*H$_3$). Colorless liquid, isolated yield 0.36 g (70%).

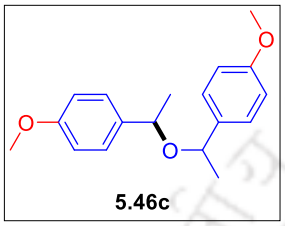

4,4'-(oxy*bis*(ethane-1,1-diyl))*bis*(methoxybenzene) (5.46c).[29] ^{1}H NMR (500 MHz, $CDCl_3$): δ = 7.20 (dd, J = 8.7, 2.2 Hz, 7H, Ar), 6.89 (d, J = 8.7 Hz, 4H, Ar), 6.83 (d, J = 8.7 Hz, 4H, Ar), 4.47 (q, J = 6.4 Hz, 2H, OC*H*(Ar)CH_3), 4.20 (d, J = 6.5 Hz, 2H, OC*H*(Ar)CH_3), 3.82 (s, 6H, ArOC*H*$_3$), 3.79 (s, 5.7H, ArOC*H*$_3$), 1.43 (d, J = 6.3 Hz, 6H, OCH(Ar)C*H*$_3$), 1.35 (d, J = 6.4 Hz, 5.7H, OCH(Ar)C*H*$_3$).^{13}C NMR (126 MHz, $CDCl_3$): δ = 159.05, 158.86, 136.57, 136.31, 127.65, 127.60, 113.93, 113.75 (Ar), 73.90, 73.85 (O*C*H(Ar)CH_3), 55.39 (ArO*C*H$_3$), 24.80, 22.91 (OCH(Ar)*C*H$_3$). Colorless liquid, isolated yield 0.35 g (59%).

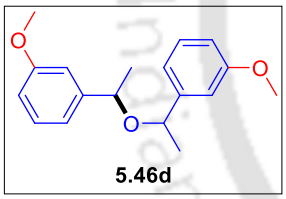

3,3'-(oxy*bis*(ethane-1,1-diyl))*bis*(methoxybenzene) (5.46d).[29] ^{1}H NMR (500 MHz, $CDCl_3$): δ = 7.20 – 6.68 (m, 13.7H, Ar), 4.43 (q, J = 6.4 Hz, 1.4H, OC*H*(Ar)CH_3), 4.18 (q, J = 6.5 Hz, 2H, OC*H*(Ar)CH_3), 3.75 (s, 6H, ArOC*H*$_3$), 3.67 (s, 4H, ArOC*H*$_3$), 1.38 (d, J = 6.4 Hz, 4.2H, OCH(Ar)C*H*$_3$), 1.31 (d, J = 6.5 Hz, 6H, OCH(Ar)C*H*$_3$). ^{13}C NMR (126 MHz, $CDCl_3$): δ = 159.96, 146.09, 129.59, 129.35, 118.88, 118.77, 112.92, 112.89, 111.78 (Ar), 74.81, 74.74 (O*C*H(Ar)CH_3), 55.34, 55.26 (ArO*C*H$_3$), 24.81, 23.13 (OCH(Ar)*C*H$_3$). Colorless liquid, isolated yield 0.36 g (61%).

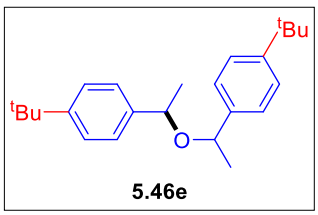

4,4'-(oxy*bis*(ethane-1,1-diyl))*bis*(tert-butylbenzene) (5.46e).[29] ^{1}H NMR (600 MHz, $CDCl_3$): δ = 7.37 – 7.21 (m, 14.4H, Ar), 4.52 (q, J = 6.4 Hz, 1.6H, OC*H*(Ar)CH_3), 4.25 (q, J = 6.5 Hz, 2H, OC*H*(Ar)CH_3), 1.45 (d, J = 6.4 Hz, 4.8H, OCH(Ar)C*H*$_3$), 1.37 (d, J = 6.5 Hz, 6H, OCH(Ar)C*H*$_3$), 1.34 (s, 18H, ArC(C*H*$_3$)$_3$), 1.30 (s, 14.4H, ArC(C*H*$_3$)$_3$). ^{13}C NMR (151 MHz, $CDCl_3$): δ = 150.23, 150.04, 141.29, 141.27, 126.11, 125.38, 125.24 (Ar), 74.36, 73.95 (O*C*H(Ar)CH_3), 34.66, 31.57, 31.54 (Ar*C*(*C*H$_3$)$_3$), 24.87, 22.81 (OCH(Ar)*C*H$_3$). White solid, isolated yield 0.44 g (63%).

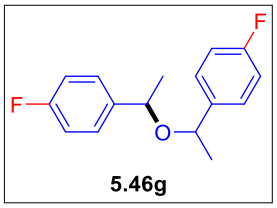

4,4'-(oxy*bis*(ethane-1,1-diyl))*bis*(fluorobenzene) (5.46g).[29] ^{1}H NMR (500 MHz, $CDCl_3$): δ = 7.25 – 6.94 (m, 14.8H, Ar), 4.47 (q, J = 6.4 Hz, 1.7H, OC*H*(Ar)CH_3), 4.19 (q, J = 6.5 Hz, 2H, OC*H*(Ar)CH_3), 1.44 (d, J = 6.4 Hz, 5.5H, OCH(Ar)C*H*$_3$), 1.35 (d, J = 6.5 Hz, 6H, OCH(Ar)C*H*$_3$). ^{13}C NMR (126 MHz, $CDCl_3$): δ = 163.32, 163.14, 161.37, 161.19, 140.04, 140.01, 139.80, 139.78, 128.01, 127.95, 127.88, 115.56, 115.40, 115.26, 115.09 (Ar), 74.29, 74.12 (O*C*H(Ar)CH_3), 24.80, 23.25 (OCH(Ar)*C*H$_3$). ^{19}F NMR (471 MHz, $CDCl_3$): δ = -115.31, -115.68. Colorless liquid, isolated yield 0.16 g (30%).

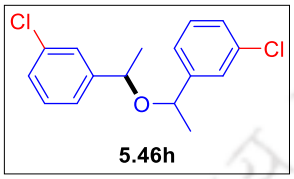

3,3'-(oxy*bis*(ethane-1,1-diyl))*bis*(chlorobenzene) (5.46h). ^{1}H NMR (400 MHz, $CDCl_3$): δ = 7.31 – 7.09 (m, 14H, Ar), 4.46 (q, J = 6.4 Hz, 1.5H, OC*H*(Ar)CH_3), 4.20 (q, J = 6.5 Hz, 2H, OC*H*(Ar)CH_3), 1.44 (d, J = 6.4 Hz, 4.5H, OCH(Ar)C*H*$_3$), 1.37 (d, J = 6.5 Hz, 6H, OCH(Ar)C*H*$_3$).^{13}C NMR (101 MHz, $CDCl_3$): δ = 146.29, 146.25, 134.66, 134.33, 130.02, 129.73, 127.83, 127.55, 126.58, 126.48, 124.56, 124.43 (Ar), 74.64, 74.61 (O*C*H(Ar)CH_3), 24.73, 23.23 (OCH(Ar)*C*H$_3$). Colorless liquid, isolated yield 0.38 g (68%).

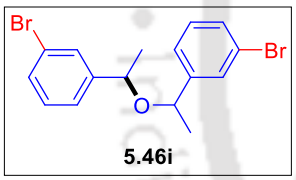

3,3'-(oxy*bis*(ethane-1,1-diyl))*bis*(bromobenzene) (5.46i).[29] ^{1}H NMR (600 MHz, $CDCl_3$): δ = 7.45 – 7.32 (m, 8H, Ar), 7.25 – 7.12 (m, 8H, Ar), 4.45 (q, J = 6.4 Hz, 2H, OC*H*(Ar)CH_3), 4.20 (q, J = 6.6 Hz, 2H, OC*H*(Ar)CH_3), 1.44 (d, J = 6.4 Hz, 6H, OCH(Ar)C*H*$_3$), 1.37 (d, J = 6.6 Hz, 6H, OCH(Ar)C*H*$_3$). ^{13}C NMR (151 MHz, $CDCl_3$): δ = 146.51, 146.45, 130.76, 130.49, 130.34, 130.05, 129.51, 129.40, 125.01, 124.89, 122.88, 122.55 (Ar), 74.63, 74.57 (O*C*H(Ar)CH_3), 24.77, 23.25 (OCH(Ar)*C*H$_3$). Colorless liquid, isolated yield 0.56 g (65%).

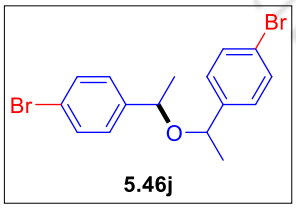

4,4'-(oxy*bis*(ethane-1,1-diyl))*bis*(bromobenzene) (5.46j).[29] ^{1}H NMR (500 MHz, $CDCl_3$): δ = 7.48 (d, J = 8.3 Hz, 4H, Ar), 7.40 (d, J = 8.4 Hz, 4H, Ar), 7.13 (dd, J = 10.6, 8.3 Hz, 8H, Ar), 4.45 (q, J = 6.4 Hz, 2H, OC*H*(Ar)CH_3), 4.17 (q, J = 6.5 Hz, 2H, OC*H*(Ar)CH_3), 1.42 (d, J = 6.4 Hz, 6H, OCH(Ar)C*H*$_3$), 1.34 (d, J = 6.5 Hz, 6H, OCH(Ar)C*H*$_3$). ^{13}C NMR (126 MHz, $CDCl_3$): δ = 143.22, 143.02, 131.83, 131.54, 128.16, 128.02, 121.38, 121.15, 74.35, 74.32 (O*C*H(Ar)CH_3), 24.67, 23.18 (OCH(Ar)*C*H$_3$). Colorless liquid, isolated yield 0.57 g (66%).

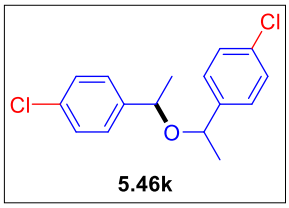

5.46k

4,4'-(oxy*bis*(ethane-1,1-diyl))*bis*(chlorobenzene) (5.46k).[29] ^{1}H NMR (500 MHz, $CDCl_3$): δ = 7.34-7.17 (m, 15.8H, Ar), 4.47 (q, J = 6.4 Hz, 2H, OC*H*(Ar)CH_3), 4.18 (q, J = 6.5 Hz, 2H, OC*H*(Ar)CH_3), 1.43 (d, J = 6.4 Hz, 6H, OCH(Ar)C*H*$_3$), 1.35 (d, J = 6.5 Hz, 5.7H, OCH(Ar)C*H*$_3$). ^{13}C NMR (126 MHz, $CDCl_3$): δ = 142.75, 142.55, 133.31, 133.07, 128.87, 128.59, 127.80, 127.68 (Ar), 74.33 (O*C*H(Ar)CH_3), 24.69, 23.21 (OCH(Ar)*C*H$_3$). Colorless liquid, isolated yield 0.44 g (67%).

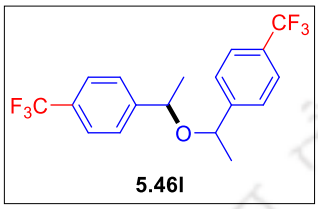

5.46l

4,4'-(oxy*bis*(ethane-1,1-diyl))*bis*((trifluoromethyl)benzene) (5.46l).[29] ^{1}H NMR (500 MHz, $CDCl_3$): δ = 7.63 - 7.34 (m, 14.4H, Ar), 4.56 (q, J = 6.4 Hz, 1.6H, OC*H*(Ar)CH_3), 4.27 (q, J = 6.5 Hz, 2H, OC*H*(Ar)CH_3), 1.48 (d, J = 6.4 Hz, 4.8H, OCH(Ar)C*H*$_3$), 1.39 (d, J = 6.5 Hz, 6H, OCH(Ar)C*H*$_3$). ^{13}C NMR (151 MHz, $CDCl_3$): δ = 148.10, 148.05, 130.33, 130.11, 129.90, 129.80, 129.69, 129.59, 129.37, 127.01, 126.98, 126.64, 126.52, 125.80, 125.77, 125.75, 125.72, 125.53, 125.48, 125.45, 125.42, 125.40, 125.20, 125.18, 123.40, 123.38, 121.60 (Ar), 74.80, 74.78 (O*C*H(Ar)CH_3), 25.31, 24.71, 23.36 (OCH(Ar)*C*H$_3$). ^{19}F NMR (471 MHz, $CDCl_3$): δ = -62.49, -62.49, -62.54, -62.55. Colorless liquid, isolated yield 0.34 g (46%).

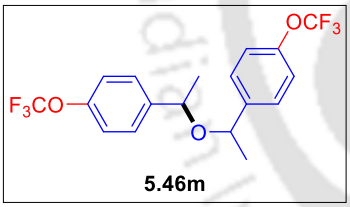

5.46m

4,4'-(oxy*bis*(ethane-1,1-diyl))*bis*((trifluoromethoxy)benzene) (5.46m).[29] ^{1}H NMR (600 MHz, $CDCl_3$): δ = 7.63 – 7.35 (m, 14.3H, Ar), 4.60 – 4.52 (m, 2H, OC*H*(Ar)CH_3), 4.32 – 4.24 (m, 1.8H, OC*H*(Ar)CH_3), 1.48 (d, J = 5.1 Hz, 6H, OCH(Ar)C*H*$_3$), 1.40 (d, J = 5.3 Hz, 5.3H, OCH(Ar)C*H*$_3$). ^{13}C NMR (151 MHz, $CDCl_3$): δ = 148.10, 148.05, 130.33, 130.11, 130.01, 129.90, 129.80, 129.69, 129.59, 129.37, 127.01, 126.98, 126.64, 126.51, 125.79, 125.77, 125.75, 125.72, 125.47, 125.45, 125.42, 125.40, 125.20, 125.18, 123.40, 123.38, 121.60, 121.58 (Ar), 74.80, 74.78 (O*C*H(Ar)CH_3), 24.71, 23.36 (OCH(Ar)*C*H$_3$). ^{19}F NMR (471 MHz, $CDCl_3$): δ = -62.49, -62.55. Colorless liquid, isolated yield 0.58 g (62%).

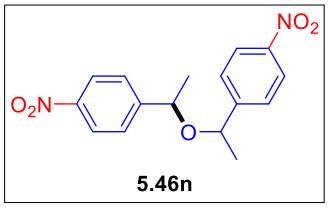

5.46n

4,4'-(oxy*bis*(ethane-1,1-diyl))*bis*(nitrobenzene) (5.46n).[29] ^{1}H NMR (500 MHz, $CDCl_3$): δ = 8.25 - 7.41 (m, 14.9H, Ar), 4.60 (q, J = 6.4 Hz, 2H, OC*H*(Ar)CH_3), 4.32 (q, J = 6.5 Hz, 1.7H, OC*H*(Ar)CH_3), 1.50 (d, J = 6.4 Hz, 6H, OCH(Ar)C*H*$_3$), 1.42 (d, J = 6.5 Hz, 5.2H, OCH(Ar)C*H*$_3$). ^{13}C NMR (126 MHz, $CDCl_3$): δ =151.28, 151.26, 147.80, 147.53,

127.06, 126.88, 124.19, 123.91 (Ar), 75.04, 74.75 (O*C*H(Ar)CH$_3$), 24.60, 23.44 (OCH(Ar)*C*H$_3$). White solid, isolated yield 0.66 g (62%).

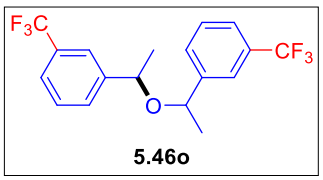

5.46o

3,3'-(oxy*bis*(ethane-1,1-diyl))*bis*((trifluoromethyl)benzene) (5.46o).[29] ^{1}H NMR (600 MHz, CDCl$_3$): δ = 7.57 – 7.35 (m, 15.5H, Ar), 4.54 (q, J = 6.5 Hz, 2H, O*C*H(Ar)CH$_3$), 4.27 (q, J = 6.5 Hz, 1.9H, O*C*H(Ar)CH$_3$), 1.49 (d, J = 6.5 Hz, 6H, OCH(Ar)C*H*$_3$), 1.40 (d, J = 6.5 Hz, 5.6H, OCH(Ar)C*H*$_3$). ^{13}C NMR (151 MHz, CDCl$_3$): δ = 145.04, 145.00, 131.47, 131.26, 131.04, 130.84, 130.63, 130.42, 129.70, 129.63, 129.25, 128.90, 126.98, 126.93, 125.17, 125.12, 124.64, 124.61, 124.59, 124.56, 124.33, 124.31, 124.28, 124.26, 123.37, 123.32, 123.21, 123.19, 123.16, 123.14, 123.11, 123.09, 123.06, 123.04 (Ar), 75.36, 74.83 (O*C*H(Ar)CH$_3$), 24.73, 23.42 (OCH(Ar)*C*H$_3$). ^{19}F NMR (471 MHz, CDCl$_3$): δ = -62.66, -62.72. Colorless liquid, isolated yield 0.43 g (58%).

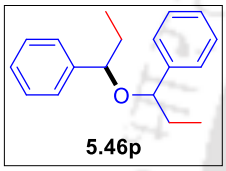

5.46p

(oxy*bis*(propane-1,1-diyl))dibenzene (5.46p).[29] ^{1}H NMR (600 MHz, CDCl$_3$): δ = 7.34 – 7.17 (m, 16.9H, Ar), 4.28 (t, J = 6.2 Hz, 2H, O*C*H(Ar)CH$_2$CH$_3$), 3.94 (t, J = 6.8 Hz, 1.4H, O*C*H(Ar)CH$_2$CH$_3$), 1.80 (m, 6.7H, OCH(Ar)C*H*$_2$CH$_3$), 0.86 (t, J = 7.4 Hz, 6H, OCH(Ar)CH$_2$C*H*$_3$), 0.78 (t, J = 7.4 Hz, 4.1H, O*C*H(Ar)CH$_2$C*H*$_3$).^{13}C NMR (151 MHz, CDCl$_3$): δ = 128.36, 128.05, 127.49, 127.31, 127.04, 126.92 (Ar), 80.69, 80.11 (O*C*H(Ar)CH$_2$CH$_3$), 31.46, 29.85 (OCH(Ar)*C*H$_2$CH$_3$), 10.59, 9.89 (OCH(Ar)CH$_2$*C*H$_3$). Colorless liquid, isolated yield 0.07 g (14%).

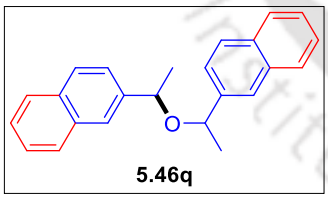

5.46q

2,2'-(oxy*bis*(ethane-1,1-diyl))dinaphthalene (5.46q).[29] ^{1}H NMR (600 MHz, CDCl$_3$): δ = 7.91 – 7.65 (m, 15H, Ar), 7.54 – 7.42 (m, 11H, Ar), 4.75 (q, J = 6.4 Hz, 1.7H, O*C*H(Ar)CH$_3$), 4.46 (q, J = 6.5 Hz, 2H, O*C*H(Ar)CH$_3$), 1.59 (d, J = 6.4 Hz, 5.1H, OCH(Ar)C*H*$_3$), 1.49 (d, J = 6.6 Hz, 6H, OCH(Ar)C*H*$_3$). ^{13}C NMR (151 MHz, CDCl$_3$): δ = 141.75, 141.60, 133.46, 133.40, 133.21, 133.01, 128.60, 128.22, 128.02, 127.98, 127.89, 127.77, 126.25, 126.07, 125.89, 125.74, 125.41, 125.04, 124.71, 124.46 (Ar), 74.95, 74.77 (O*C*H(Ar)CH$_3$), 24.74, 23.07 (OCH(Ar)*C*H$_3$). Colorless gel, isolated yield 0.60 g (90%).

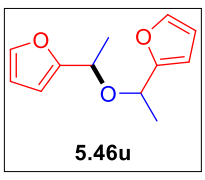

5.46u

2,2'-(oxy*bis*(ethane-1,1-diyl))difuran (5.46u).[29] ^{1}H NMR (600 MHz, CDCl$_3$): δ = 7.28-6.93 (m, 10H, Ar), 4.84 (q, J = 6.4 Hz, 2H, O*C*H(Ar)CH$_3$), 4.67 (q, J = 6.5 Hz, 1.3H, O*C*H(Ar)CH$_3$), 1.58 (d, J = 6.4 Hz, 6H, OCH(Ar)C*H*$_3$), 1.48 (d, J = 6.5 Hz,4.1H, OCH(Ar)C*H*$_3$). ^{13}C NMR (151

MHz, $CDCl_3$): δ = 148.11, 147.93, 126.52, 126.45, 124.81, 124.78, 124.77, 124.14 (Ar), 70.43, 70.34 (O*C*H(Ar)CH_3), 25.21, 23.02 (OCH(Ar)*C*H_3). Colorless liquid, isolated yield 0.26 g (52%).

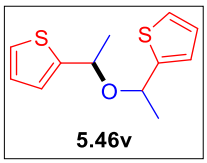

5.46v

2,2'-(oxy*bis*(ethane-1,1-diyl))dithiophene (5.46v). ^{1}H NMR (500 MHz, $CDCl_3$): δ = 7.28 – 6.92 (m, 8.3H, Ar), 4.84 (q, *J* = 6.4 Hz, 0.7H, OC*H*(Ar)CH_3), 4.68 (q, *J* = 6.5 Hz, 2H, OC*H*(Ar)CH_3), 1.58 (d, *J* = 6.2 Hz, 2.3H, CH(Ar)C*H*$_3$), 1.49 (d, *J* = 6.5 Hz, 6H, CH(Ar)C*H*$_3$). ^{13}C NMR (126 MHz, $CDCl_3$): δ = 148.13, 147.94, 126.52, 126.44, 124.79, 124.76, 124.13 (Ar), 70.46, 70.37 (O*C*H(Ar)CH_3), 25.19, 23.03 (OCH(Ar)*C*H_3). Colorless liquid, isolated yield 0.31 g (55%).

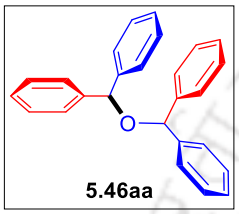

5.46aa

(oxy*bis*(methanetriyl))tetrabenzene (5.46aa).[29] ^{1}H NMR (500 MHz, $CDCl_3$): δ = 7.37-7.25 (m, 20H, Ar), 5.39 (s, 2H, OC*H*(Ar)$_2$). ^{13}C NMR (126 MHz, $CDCl_3$): δ = 142.36, 128.52, 127.57, 127.41 (Ar), 80.16 (O*C*H(Ar)$_2$). White solid, isolated yield 0.59 g (82%).

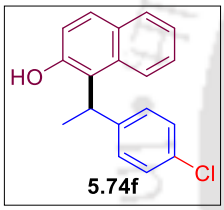

5.74f

1-(1-(4-chlorophenyl)ethyl)naphthalen-2-ol (5.74f).[30] ^{1}H NMR (400 MHz, $CDCl_3$): δ = 7.95 (d, *J* = 8.6 Hz, 1H, Ar), 7.80 (dd, *J* = 7.7, 1.4 Hz, 1H, Ar), 7.68 (d, *J* = 8.8 Hz, 1H, Ar), 7.44 (ddd, *J* = 8.6, 6.7, 1.5 Hz, 1H, Ar), 7.34 (t, J = 7.4 Hz, 1H, Ar), 7.2-7.26 (m, 4H, Ar), 7.01 (d, *J* = 8.8 Hz, 1H, Ar), 5.14 (q, *J* = 7.2 Hz, 1H, C*H*(Ar)$_2$CH$_3$), 4.82 (bs, 1H, O*H*), 1.80 (d, *J* = 7.3 Hz, 3H, CH(Ar)$_2$C*H*$_3$). ^{13}C NMR (101 MHz, $CDCl_3$): δ = 151.35, 142.90, 132.87, 132.32, 129.93, 129.05, 129.00, 128.96, 128.68, 126.73, 123.55, 123.32, 123.03, 119.13 (Ar), 34.47 (*C*H(Ar)$_2$CH$_3$), 17.47 (CH(Ar)$_2$*C*H$_3$). Colorless gel, isolated yield 0.81 g (70%). HRMS (ESI): *m/z* calculated for $[M+H]^+$: 283.0884, found 283.0897.

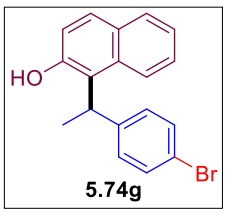

5.74g

1-(1-(4-bromophenyl)ethyl)naphthalen-2-ol (5.74g).[30] ^{1}H NMR (400 MHz, $CDCl_3$): δ = 7.94 (d, *J* = 8.6 Hz, 1H, Ar), 7.79 (d, *J* = 8.0 Hz, 1H, Ar), 7.68 (d, *J* = 8.8 Hz, 1H, Ar), 7.46 – 7.39 (m, 3H,Ar), 7.33 (t, *J* = 7.4 Hz, 1H, Ar), 7.23 (d, *J* = 8.4 Hz, 2H, Ar), 7.01 (d, *J* = 8.7 Hz, 1H, Ar), 5.11 (q, *J* = 7.3 Hz, 1H, C*H*(Ar)$_2$CH$_3$), 4.81 (bs, 1H, O*H*), 1.79 (d, *J* = 7.2 Hz, 3H, CH(Ar)$_2$C*H*$_3$). ^{13}C NMR (101 MHz, $CDCl_3$): δ = 151.33, 143.49, 132.86, 131.89, 129.93, 129.08, 129.05, 129.01, 126.74, 123.50, 123.33, 123.05, 119.10 (Ar), 34.53 (*C*H(Ar)$_2$CH$_3$), 17.42 (CH(Ar)$_2$*C*H$_3$). Colorless gel, isolated yield 0.49 g (37%). HRMS (ESI): *m/z* Calculated for $[M+H]^+$: calculated:327.0379; found 328.0362.

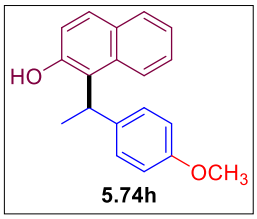

5.74h

1-(1-(4-methoxyphenyl)ethyl)naphthalen-2-ol (5.74h).[30] ^{1}H NMR (500 MHz, $CDCl_3$): δ = 8.07 (d, J = 8.6 Hz, 1H, Ar), 7.81 (dd, J = 8.2, 1.4 Hz, 1H, Ar), 7.68 (d, J = 8.8 Hz, 1H, Ar), 7.49 (ddd, J = 8.5, 6.7, 1.4 Hz, 1H, Ar), 7.38 – 7.29 (m, 3H, Ar), 7.02 (d, J = 8.7 Hz, 1H, Ar), 6.89 (d, J = 8.7 Hz, 2H, Ar), 5.12 (d, J = 7.3 Hz, 1H, C*H*(Ar)$_2$CH$_3$), 3.80 (s, 3H, ArOC*H*$_3$), 1.76 (d, J = 7.3 Hz, 3H, CH(Ar)$_2$C*H*$_3$). ^{13}C NMR (126 MHz, $CDCl_3$): δ = 158.64, 151.83, 135.31, 132.98, 129.78, 129.00, 128.78, 128.38, 126.70, 123.91, 123.20, 122.62, 119.62, 114.68 (Ar), 55.43 (ArO*C*H$_3$), 34.24 (*C*H(Ar)$_2$CH$_3$), 17.45 (CH(Ar)$_2$*C*H$_3$). Colorless gel, isolated yield 0.75 g (60%).

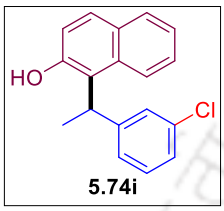

5.74i

1-(1-(3-chlorophenyl)ethyl)naphthalen-2-ol (5.74i).[30] ^{1}H NMR (400 MHz, $CDCl_3$): δ = 7.94 (d, J = 8.6 Hz, 1H, Ar), 7.81 (d, J = 8.2 Hz, 1H, Ar), 7.69 (d, J = 8.8 Hz, 1H, Ar), 7.44 (d, J = 14.8 Hz, 1H, Ar), 7.37 – 7.32 (m, 2H, Ar), 7.25 – 7.17 (m, 3H, Ar), 7.02 (d, J = 8.8 Hz, 1H, Ar), 5.15 (q, J = 7.2 Hz, 1H, C*H*(Ar)$_2$CH$_3$), 4.85 (bs, 1H, O*H*), 1.80 (d, J = 7.3 Hz, 3H, CH(Ar)$_2$C*H*$_3$). ^{13}C NMR (101 MHz, $CDCl_3$): δ = 151.32, 146.78, 134.84, 132.86, 130.02, 129.94, 129.05, 127.50, 126.76, 126.66, 125.47, 123.38, 123.33, 123.05, 119.08 (Ar), 34.79 (*C*H(Ar)$_2$CH$_3$), 17.39 (CH(Ar)$_2$*C*H$_3$). Colorless gel, isolated yield 0.40 g (35%). HRMS (ESI): *m/z* calculated for $[M+H]^+$: 283.0884; found 283.0880.

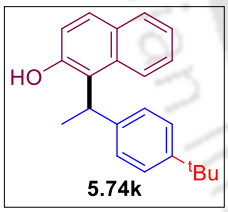

5.74k

1-(1-(3-(tert-butyl)phenyl)ethyl)naphthalen-2-ol (5.74k).[30] ^{1}H NMR (500 MHz, $CDCl_3$): δ = 8.09 (d, J = 8.6 Hz, 1H, Ar), 7.82 (d, J = 8.1 Hz, 1H, Ar), 7.69 (d, J = 8.8 Hz, 1H, Ar), 7.50 (t, J = 7.7 Hz, 1H, Ar), 7.41 – 7.31 (m, 5H, Ar), 7.02 (d, J = 8.8 Hz, 1H, Ar), 5.14 (q, J = 7.4 Hz, 1H, C*H*(Ar)$_2$CH$_3$), 4.96 (bs, 1H, O*H*), 1.77 (dd, J = 7.4, 1.6 Hz, 3H, CH(Ar)$_2$C*H*$_3$), 1.31 (s, 9H, C(C*H*$_3$)$_3$). ^{13}C NMR (126 MHz, $CDCl_3$): δ = 151.84, 150.09, 140.23, 133.04, 129.80, 129.02, 128.81, 127.02, 126.74, 126.27, 123.91, 123.22, 122.60, 119.70 (Ar), 34.60 (*C*H(Ar)$_2$CH$_3$), 31.47 (*C*(CH$_3$)$_3$), 17.26 (CH(Ar)$_2$*C*H$_3$ and C(*C*H$_3$)$_3$). Colorless gel, isolated yield 0.88 g (71%). HRMS (ESI): *m/z* calculated for $[M+H]^+$: 305.1900; found 305.1870.

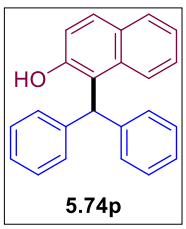

5.74p

1-benzhydrylnaphthalen-2-ol (5.74p).[30] ^{1}H NMR (600 MHz, $CDCl_3$): δ =7.94 (d, J = 8.5 Hz, 1H, Ar), 7.80 (dd, J = 8.3, 3.5 Hz, 2H, Ar), 7.46 – 7.28 (m, 7H, Ar), 7.22 – 7.17 (m, 4H, Ar), 7.10 – 7.03 (m, 2H, Ar), 5.83 (s, 1H, C*H*(Ar)$_3$). ^{13}C NMR (151 MHz, $CDCl_3$): δ = 150.32, 149.56, 146.53, 131.83, 130.96, 129.46, 129.22, 128.95, 128.71, 127.82, 127.52, 126.88, 126.64,

125.02, 124.23, 123.80, 123.23, 118.14, 116.83, 115.91 (Ar), 42.15 (*C*H(Ar)$_3$). Colorless gel, isolated yield 0.87 g (69%). HRMS (ESI): *m/z* calculated for $[M+NH_4]^+$: 328.1701; found 328.1696.

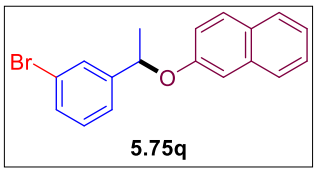

5.75q

2-(1-(3-bromophenyl)ethoxy)naphthalene (5.75q).[30] ^{1}H NMR (500 MHz, $CDCl_3$): δ = 7.73 (dd, J = 8.5, 3.6 Hz, 2H, Ar), 7.64 – 7.57 (m, 2H, Ar), 7.41 – 7.34 (m, 3H, Ar), 7.32 – 7.28 (m, 1H, Ar), 7.23 – 7.17 (m, 2H, Ar), 7.01 (d, J = 2.3 Hz, 1H, Ar), 5.42 (q, J = 6.4 Hz, 1H, OC*H*(Ar)CH_3), 1.68 (d, J = 6.4 Hz, 3H, OCH(Ar)C*H*$_3$). ^{13}C NMR (126 MHz, $CDCl_3$): δ =155.61, 145.69, 134.48, 130.79, 130.45, 129.61, 129.14, 128.82, 127.71, 126.94, 126.42, 124.35, 123.89, 122.94, 119.46, 109.21 (Ar), 75.42 (O*C*H(Ar)CH_3), 24.50 (OCH(Ar)*C*H$_3$). Colorless oil, isolated yield 0.26 g (20%). HRMS (ESI): *m/z* calculated for $[M+H]^+$: 327.0379; found 327.0414.

Supporting information (containing NMR spectra of various compounds and Cartesian coordinates of the computed complexes) for chapter **V** is available as appendix **IV** and can be found at https://drive.google.com/file/d/1X7JRlSmfIlof5NVGMfEf2g-zNxTkNJsc/view?usp=sharing

5.6 References

1. Mandal, S.; Mandal, S.; Ghosh, S. K.; Sar, P.; Ghosh, A.; Saha, R.; Saha, B., *RSC Adv.* **2016**, *6*, 69605-69614.
2. Hartwig, J. F., *Angew. Chem. Int. Ed.* **1998**, *37*, 2046-2067.
3. Ley, S. V.; Thomas, A. W., *Angew. Chem. Int. Ed.* **2003**, *42*, 5400-5449.
4. Dermer, O. C., *Chem. Rev.* **1934**, *14*, 385-430.
5. Pagliaro, M.; Ciriminna, R.; Kimura, H.; Rossi, M.; Della Pina, C., *Angew. Chem. Int. Ed.* **2007**, *46*, 4434-4440.
6. Williamson, A., *Lond. Edinb. Dublin philos. mag. j. sci.* **1850**, *37*, 350-356.
7. Haibach, M. C.; Guan, C.; Wang, D. Y.; Li, B.; Lease, N.; Steffens, A. M.; Krogh-Jespersen, K.; Goldman, A. S., *J. Am. Chem. Soc.* **2013**, *135*, 15062-15070.
8. Shrigadi, N. B.; Shinde, A. B.; Samant, S. D., *Appl. Catal., A* **2003**, *252*, 23-35.
9. Sun, B.; Khan, F.-A.; Süss-Fink, G.; Therrien, B., Chapter 12 - Metal Catalysts Intercalated in Smectite Clays. In *Encapsulated Catalysts*, Sadjadi, S., Ed. Academic Press: **2017**; pp 387-441.
10. Ueno, S.; Hartwig, J. F., *Angew. Chem. Int. Ed.* **2008**, *47*, 1928-1931.
11. Faustino, H.; Varela, I.; Mascareñas, J. L.; López, F., *Chem. Sci.* **2015**, *6*, 2903-2908.
12. Neufeldt, S. R.; Sanford, M. S., *Acc. Chem. Res.* **2012**, *45*, 936-946.
13. Enthaler, S.; Company, A., *Chem. Soc. Rev.* **2011**, *40*, 4912-4924.
14. Desai, L. V.; Hull, K. L.; Sanford, M. S., *J. Am. Chem. Soc.* **2004**, *126*, 9542-9543.
15. Hartwig, J. F., *Acc. Chem. Res.* **1998**, *31*, 852-860.
16. Roggen, M.; Carreira, E. M., *Angew. Chem. Int. Ed.* **2011**, *50*, 5568-5571.
17. Yang, C.-G.; He, C., *J. Am. Chem. Soc.* **2005**, *127*, 6966-6967.
18. Li, Z.; Zhang, J.; Brouwer, C.; Yang, C.-G.; Reich, N. W.; He, C., *Org. Lett.* **2006**, *8*, 4175-4178.

19. Rosenfeld, D. C.; Shekhar, S.; Takemiya, A.; Utsunomiya, M.; Hartwig, J. F., *Org. Lett.* **2006**, *8*, 4179-4182.
20. Hintermann, L., Recent Developments in Metal-Catalyzed Additions of Oxygen Nucleophiles to Alkenes and Alkynes. **2010**; Vol. 31, p 123.
21. Zhou, Y.; Xu, X.; Sun, H.; Tao, G.; Chang, X.-Y.; Xing, X.; Chen, B.; Xu, C., *Nat. Commun.* **2021**, *12*, 1953.
22. Sevov, C. S.; Hartwig, J. F., *J. Am. Chem. Soc.* **2013**, *135*, 9303-9306.
23. Dzudza, A.; Marks, T. J., *Chem. Eur. J.* **2010**, *16*, 3403-3422.
24. Seo, S.; Yu, X.; Marks, T. J., *J. Am. Chem. Soc.* **2009**, *131*, 263-276.
25. Dzudza, A.; Marks, T. J., *Org. Lett.* **2009**, *11*, 1523-1526.
26. Yadav, I. S.; Alsaleh, A. Z.; Misra, R.; D'Souza, F., *Chem. Sci.* **2021**, *12*, 1109-1120.
27. Petronilho, A.; Vivancos, A.; Albrecht, M., *Catal. Sci. Technol.* **2017**, *7*, 5766-5774.
28. Kalutharage, N.; Yi, C. S., *Org. Lett.* **2015**, *17*, 1778-1781.
29. Bunrit, A.; Srifa, P.; Rukkijakan, T.; Dahlstrand, C.; Huang, G.; Biswas, S.; Watile, R. A.; Samec, J. S. M., *ACS Catal.* **2020**, *10*, 1344-1352.
30. Singh, R. R.; Whittington, A.; Srivastava, R. S., *Mol. Catal.* **2020**, *492*, 110954.
31. Zhang, L.; Gonzalez-de-Castro, A.; Chen, C.; Li, F.; Xi, S.; Xu, L.; Xiao, J., *Mol. Catal.* **2017**, *433*, 62-67.
32. Sahoo, P. K.; Gawali, S. S.; Gunanathan, C., *ACS Omega* **2018**, *3*, 124-136.
33. Korstanje, T. J.; Jastrzebski, J. T. B. H.; Klein Gebbink, R. J. M., *ChemSusChem* **2010**, *3*, 695-697.
34. Xu, Q.; Xie, H.; Chen, P.; Yu, L.; Chen, J.; Hu, X., *Green Chem.* **2015**, *17*, 2774-2779.
35. Kim, J.; Lee, D.-H.; Kalutharage, N.; Yi, C. S., *ACS Catal.* **2014**, 3881-3885.
36. Hartwig, J. F., *Angew. Chem. Int. Ed.* **1998**, *37*, 2046-2067.
37. Rahimi, S.; Panahi, F.; Bahmani, M.; Iranpoor, N., *J. Org. Chem.* **2018**, *83*, 973-979.
38. Cuenca, A. B.; Mancha, G.; Asensio, G.; Medio-Simón, M., *Chem. Eur. J.* **2008**, *14*, 1518-1523.
39. Sassaman, M. B.; Kotian, K. D.; Prakash, G. K. S.; Olah, G. A., *J. Org. Chem.* **1987**, *52*, 4314-4319.
40. Kim, S.; Chung, K. N.; Yang, S., *J. Org. Chem.* **1987**, *52*, 3917-3919.
41. Mineno, T.; Tsukagoshi, R.; Iijima, T.; Watanabe, K.; Miyashita, H.; Yoshimitsu, H., *Tetrahedron Lett.* **2014**, *55*, 3765-3767.
42. March, J., **1992**, *Advanced organic chemistryReaction, Mechanisms, And Structure*.
43. Young, P. C.; Schopf, N. A.; Lee, A.-L., *Chem. Commun.* **2013**, *49*, 4262-4264.
44. Hartwig, J. F., *Organotransition metal chemistry : from bonding to catalysis*. 2010.
45. Polet, D.; Alexakis, A.; Tissot-Croset, K.; Corminboeuf, C.; Ditrich, K., *Chem. Eur. J.* **2006**, *12*, 3596-3609.
46. Welter, C.; Dahnz, A.; Brunner, B.; Streiff, S.; Dübon, P.; Helmchen, G., *Org. Lett.* **2005**, *7*, 1239-1242.
47. Evans, P. A.; Leahy, D. K.; Andrews, W. J.; Uraguchi, D., *Angew. Chem.* **2004**, *116*, 4892-4895.
48. Miller, Kimberly J.; Abu-Omar, Mahdi M., *Eur. J. Org. Chem.* **2003**, *2003*, 1294-1299.
49. Blanco, V.; Leigh, D. A.; Marcos, V., *Chem. Soc. Rev.* **2015**, *44*, 5341-5370.
50. Olivares, M.; Albrecht, M., *J. Organomet. Chem.* **2020**, *920*, 121290.
51. Prakash, G. S.; Narang, S. C., *Synthesis* **1978**, *1978*, 825-825.
52. Martín, R.; Murruzzu, C.; Pericàs, M. A.; Riera, A., *J. Org. Chem.* **2005**, *70*, 2325-2328.
53. Mairanovsky, V. G., *Angew. Chem. Int. Ed. Engl.* **1976**, *15*, 281-292.
54. George, S. R. D.; Frith, T. D. H.; Thomas, D. S.; Harper, J. B., *Org. Biomol. Chem.* **2015**, *13*, 9035-9041.

55. Tran, V. H.; La, M. T.; Kim, H.-K., *Org. Biomol. Chem.* **2019**, *17*, 6221-6228.
56. Olivares, M.; Albrecht, M., *J. Org. Chem.* **2020**, *920*, 121290.
57. Salehi, P.; Iranpoor, N.; Kargar Behbahani, F., *Tetrahedron* **1998**, *54*, 943-948.
58. Choi, J.-W.; Kang, Y.-H., *Bull. Korean Chem. Soc.* **2005**, *26*, 343-344.
59. Boyer, B.; Keramane, E.-M.; Roque, J.-P.; Pavia, A. A., *Tetrahedron Lett.* **2000**, *41*, 2891-2894.
60. Das, B.; Krishnaiah, M.; Veeranjaneyulu, B.; Srinivas, Y.; Rao, Y. K., *J. Chem. Res.* **2007**, *2007*, 717-719.
61. Gonzalez-de-Castro, A.; Robertson, C. M.; Xiao, J., *J. Am. Chem. Soc.* **2014**, *136*, 8350-8360.
62. Gonzalez-de-Castro, A.; Xiao, J., *J. Am. Chem. Soc.* **2015**, *137*, 8206-8218.
63. Das, K.; Nandi, P. G.; Islam, K.; Srivastava, H. K.; Kumar, A., *Eur. J. Org. Chem.* **2019**, *2019*, 6855-6866.
64. Das, K.; Yasmin, E.; Das, B.; Srivastava, H. K.; Kumar, A., *Catal. Sci. Technol.* **2020**, *10*, 8347-8358.
65. Das, K.; Dutta, M.; Das, B.; Srivastava, H. K.; Kumar, A., *Adv. Synth. Catal.* **2019**, *361*, 2965-2980.
66. Nandi, P. G.; Jadi, P. K.; Das, K.; Prathapa, S. J.; Mandal, B. B.; Kumar, A., *Inorg. Chem.* **2021**, *60*, 7422-7432.
67. Dutta, M.; Das, K.; Prathapa, S. J.; Srivastava, H. K.; Kumar, A., *Chem. Commun.* **2020**, *56*, 9886-9889.
68. Monzani, E.; Quinti, L.; Perotti, A.; Casella, L.; Gullotti, M.; Randaccio, L.; Geremia, S.; Nardin, G.; Faleschini, P.; Tabbì, G., *Inorg. Chem.* **1998**, *37*, 553-562.
69. Monzani, E.; Battaini, G.; Perotti, A.; Casella, L.; Gullotti, M.; Santagostini, L.; Nardin, G.; Randaccio, L.; Geremia, S.; Zanello, P.; Opromolla, G., *Inorg. Chem.* **1999**, *38*, 5359-5369.
70. Adhikary, J.; Chakraborty, P.; Das, S.; Chattopadhyay, T.; Bauzá, A.; Chattopadhyay, S. K.; Ghosh, B.; Mautner, F. A.; Frontera, A.; Das, D., *Inorg. Chem.* **2013**, *52*, 13442-13452.
71. Sengupta, D.; Bhattacharjee, R.; Pramanick, R.; Rath, S. P.; Saha Chowdhury, N.; Datta, A.; Goswami, S., *Inorg. Chem.* **2016**, *55*, 9602-9610.
72. Perdew, J. P.; Burke, K.; Ernzerhof, M., *Phys. Rev. Lett* **1997**, *78*, 1396-1396.
73. Perdew, J. P.; Burke, K.; Ernzerhof, M., *Phys. Rev. Lett.* **1996**, *77*, 3865-3868.
74. Grimme, S.; Antony, J.; Ehrlich, S.; Krieg, H., *J. Chem. Phys.* **2010**, *132*, 154104.
75. M. J. Frisch, G. W. T., H. B. Schlegel, G. E. Scuseria, M. A. Robb, J. R. Cheeseman, G. Scalmani, V. Barone, B. Mennucci, G. A. Petersson, H. Nakatsuji, M. Caricato, X. Li, H. P. Hratchian, A. F. Izmaylov, J. Bloino, G. Zheng, J. L. Sonnenberg, M. Hada, M. Ehara, K. Toyota, R. Fukuda, J. Hasegawa, M. Ishida, T. Nakajima, Y. Honda, O. Kitao, H. Nakai, T. Vreven, J. A. Montgomery, Jr., J. E. Peralta, F. Ogliaro, M. Bearpark, J. J. Heyd, E. Brothers, K. N. Kudin, V. N. Staroverov, R. Kobayashi, J. Normand, K. Raghavachari, A. Rendell, J. C. Burant, S. S. Iyengar, J. Tomasi, M. Cossi, N. Rega, J. M. Millam, M. Klene, J. E. Knox, J. B. Cross, V. Bakken, C. Adamo, J. Jaramillo, R. Gomperts, R. E. Stratmann, O. Yazyev, A. J. Austin, R. Cammi, C. Pomelli, J. W. Ochterski, R. L. Martin, K. Morokuma, V. G. Zakrzewski, G. A. Voth, P. Salvador, J. J. Dannenberg, S. Dapprich, A. D. Daniels, Ö. Farkas, J. B. Foresman, J. V. Ortiz, J. Cioslowski, and D. J. Fox, Gaussian 09 (Gaussian, Inc., Wallingford CT, 2009). *Gaussian-09* **2009**, *78*.
76. Kendall, R. A.; Dunning, T. H.; Harrison, R. J., *J. Chem. Phys.* **1992**, *96*, 6796-6806.
77. Hay, P. J.; Wadt, W. R., *J. Chem. Phys.* **1985**, *82*, 270-283.
78. Wadt, W. R.; Hay, P. J., *J. Chem. Phys.* **1985**, *82*, 284-298.

79. Hay, P. J.; Wadt, W. R., *J. Chem. Phys.* **1985**, *82*, 299-310.
80. Veenboer, R. M. P.; Nolan, S. P., *Green Chem.* **2015**, *17*, 3819-3825.
81. Lucarini, M.; Pedrielli, P.; Pedulli, G. F.; Cabiddu, S.; Fattuoni, C., *J. Org. Chem.* **1996**, *61*, 9259-9263.
82. Lundqvist, M. J.; Eriksson, L. A., *J. Phys. Chem. B* **2000**, *104*, 848-855.
83. Jähnert, T.; Hager, M. D.; Schubert, U. S., *J. Mater. Chem. A* **2014**, *2*, 15234-15251.
84. Yang, G.-P.; Dilixiati, D.; Yang, T.; Liu, D.; Yu, B.; Hu, C.-W., *Appl Organometal Chem.* **2018**, *32*, e4450.
85. Lee, D.-H.; Kwon, K.-H.; Yi, C. S., *J. Am. Chem. Soc.* **2012**, *134*, 7325-7328.
86. Armarego, W. L. F.; Chai, C., Chapter 4 - Purification of Organic Chemicals. In *Purification of Laboratory Chemicals (Seventh Edition)*, Armarego, W. L. F.; Chai, C., Eds. Butterworth-Heinemann: Boston, **2013**; pp 103-554.
87. Armarego, W. L. F.; Chai, C., Chapter 5 - Purification of Inorganic and Metal-Organic Chemicals. In *Purification of Laboratory Chemicals (Seventh Edition)*, Armarego, W. L. F.; Chai, C., Eds. Butterworth-Heinemann: Boston, 2**013**; pp 555-661.

Summary and Outlook

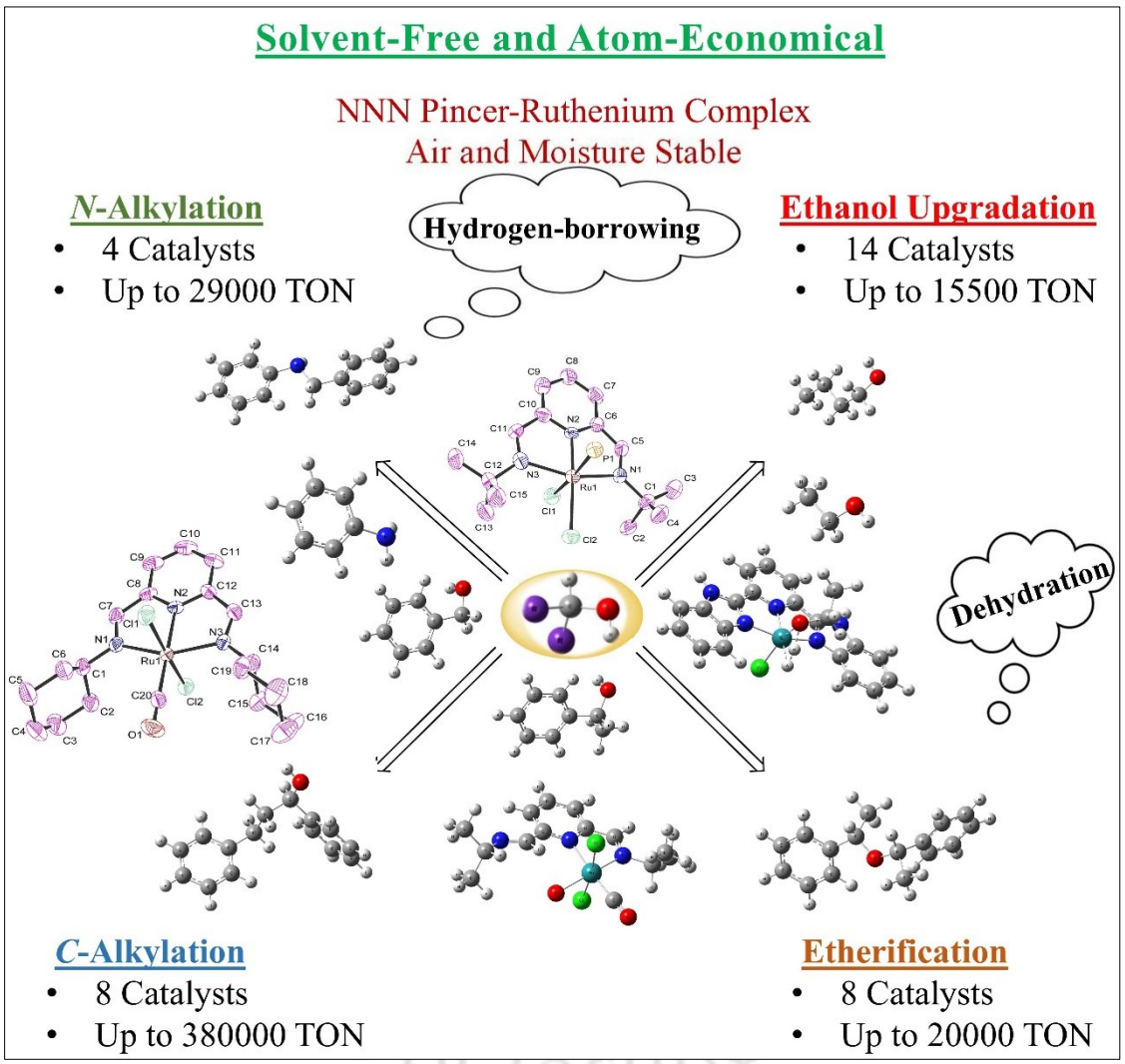

The current thesis describes the synthesis and characterization of a new series of NNN pincer-ruthenium complexes (Figure 1). These pincer-ruthenium complexes have been employed towards various (de)hydrofunctionalization of alcohols and their derivatives leading to value-added chemicals. All the probed reactions have been studied from a detailed synthetic and mechanistic point of view.

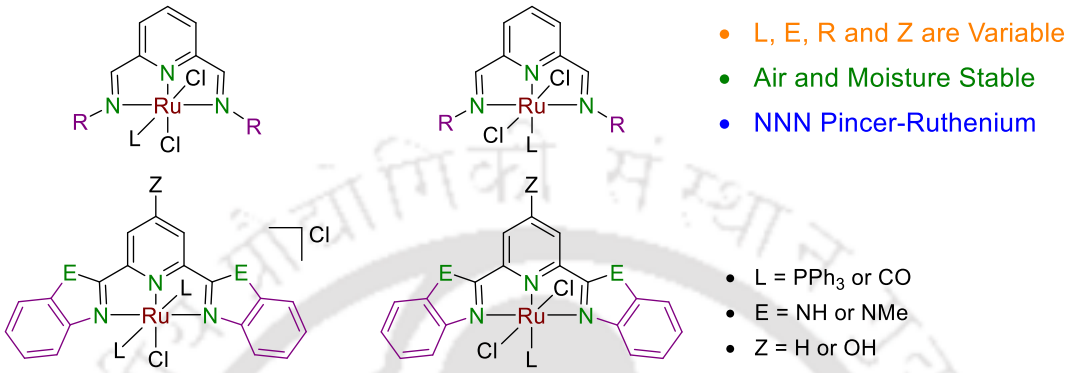

Figure 1: *Bis*(imino) and *bis*benzimidazole ligand based NNN pincer-ruthenium complexes.

Chapter I provides an overview of organometallic complexes in catalysis. Among a huge library of transition metal-based complexes known in literature, the pincer-metal complexes have been found to play a pivotal role while enjoying great success in organometallic catalysis. With particular focus on their use in catalytic transformations for organic synthesis, the emergence and development of pincer-metal chemistry has been systematically documented. The chapter ends with a discussion on the scope of the current thesis.

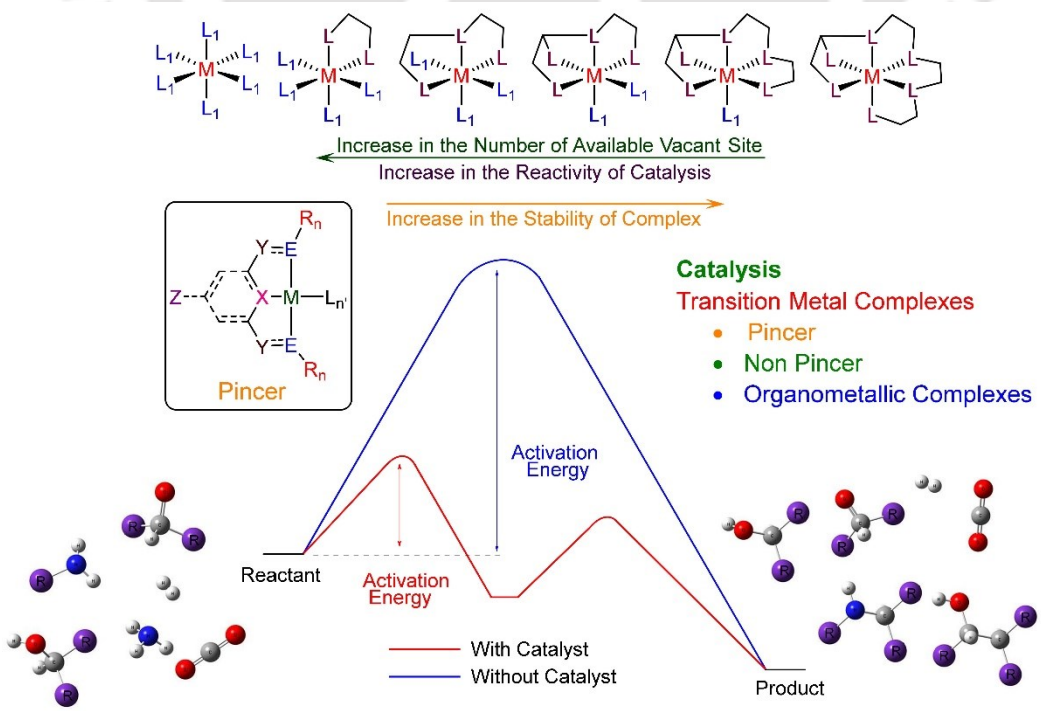

Figure 2: Pincer catalytic systems in organic transformations.

Chapter II deals with the synthesis of NNN-pincer–ruthenium complexes of the type (^{R2}NNN)RuCl$_2$(PPh$_3$) (R = Cy, Ph, ^{i}Pr, and ^{t}Bu) and their reactivity towards *N*-alkylation of primary amines under solvent-free conditions. For the first time, the base that is required to promote these reactions is generated *in-situ* from the alcohol by the use of sodium. The resulting sodium alkoxide regenerates the alcohol substrate while also acting as the water scavenger. Among the catalysts screened, (^{t}Bu^{2}NNN)RuCl$_2$(PPh$_3$) gives very high turnovers and good yields. Excellent turnovers (ca. 29000) were obtained for the (^{t}Bu^{2}NNN)RuCl$_2$(PPh$_3$) (0.002 mol %) catalyzed *N*-alkylation of aniline with cyclohexyl methanol. The turnovers obtained in the corresponding catalytic methylation of *p*-anisidine were also very high (ca. 12000) at 140 °C. The (^{t}Bu^{2}NNN)RuCl$_2$(PPh$_3$) catalyzed reactions have also been accomplished under open-vessel conditions for the transformation of benzene-1,2-diamines to benzimidazoles with high productivity (ca. 12000 turnovers). DFT studies indicate that while *β*-hydride elimination is rate-determining for the alcohol dehydrogenation segment which is endothermic, the insertion of the imine is rate-determining for its hydrogenation that is exothermic.

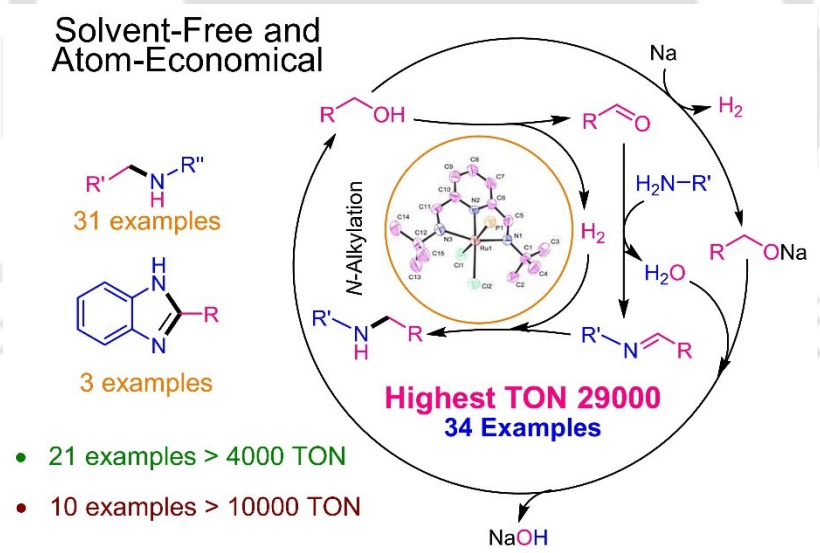

Figure 3: Pincer-ruthenium catalyzed *N*–alkylation of amines using alcohols.

In Chapter III, the phosphine-free pincer-ruthenium carbonyl complexes based on *bis*(imino)pyridine ligands have been synthesized. For the *β*-alkylation of 1-phenyl ethanol with benzyl alcohol at 140 °C under solvent-free conditions, (^{Cy2}NNN)RuCl$_2$(CO) (0.00025 mol %) in combination with NaOH (2.5 mol %) was highly efficient (ca. 93% yield, 372000 TONs at 12000 TO/h). These are the highest reported values hitherto for a ruthenium-based catalyst. The *β*-alkylation of various alcohol combinations were accomplished with ease which

culminated to give 380000 TONs at 19000 TO/h for the *β*-alkylation of 1-phenyl ethanol with 3-methoxy benzyl alcohol. DFT studies were complementary to mechanistic studies and indicate the insertion of *α*-alkylated ketone into the Ru-H bond to be the overall RDS. From kinetic studies, it can be concluded that the rate of the reaction has first-order dependence on the catalyst concentration.

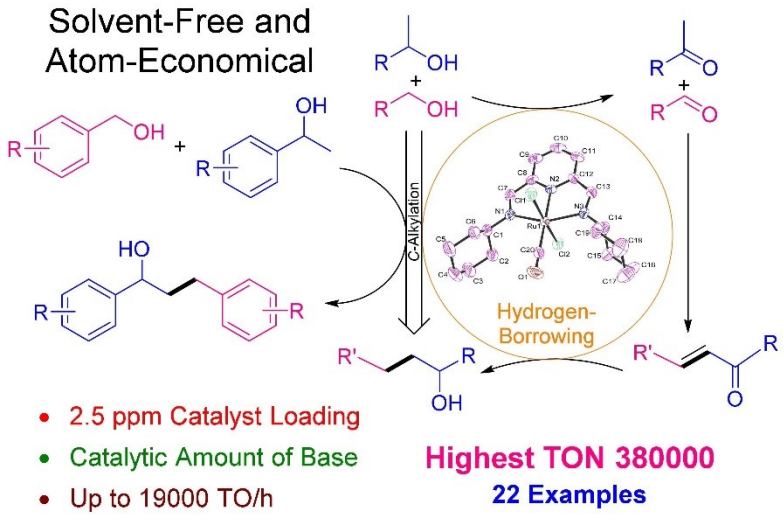

Figure 4: Pincer-ruthenium catalyzed *β*-alkylation of secondary alcohols with primary alcohols.

In chapter IV, the catalytic *β*-alkylation protocol was extended to investigate the upgradation of bio-ethanol to bio-*n*-butanol and higher alcohols. By employing sterically more open pincer-ruthenium carbonyl complex (^{Bim2}NNNRu)Cl$_2$(CO) based on 2,6-*bis*(benzimidazole-2yl) pyridine ligands, better catalytic activity was obtained in comparison to the corresponding catalytic activity of the *bis*(imino)pyridine ligand based (^{Cy2}NNNRu)Cl$_2$(CO) complexes at 140 °C. It is gratifying to note that one could arrive at conditions that give not only good ethanol conversion (ca. 58%) but also high turnovers (ca. 2100) with a good rate (ca. 710 TO/h) in the (^{Bim2}NNNRu)Cl$_2$(CO) catalyzed upgradation of ethanol in the presence of 10 mol % NaOEt under conventional heating (140 °C). Kinetic studies on the ethanol upgradation catalyzed by (^{Bim2}NNNRu)Cl$_2$(CO) exhibit linear dependence of rate on the concentration of both catalyst and ethanol. The good microwave absorptivity of ethanol was instrumental in improving the reactivity of the pincer-Ru catalysts towards Guerbet reaction under microwave heating at 110 °C where conventional heating was ineffective. In particular, under microwave condition ruthenium carbonyl complexes based on 2,6-*bis*(benzimidazole-2-yl)pyridine ligands showed higher activity towards the Guerbet reaction in stark contrast to their pincer-Ru counterparts based on *bis*(imino) pyridine ligands. Up to 42 % yield of *n*-butanol at 57 % selectivity and

turnover as high as 13022 TON with 22.8% yield of *n*-butanol at 78% selectivity was obtained in the (^{Bim2}NNN)$RuCl_2$(CO) catalyzed reactions at loadings of 0.025 mol% and 0.00225 mol% respectively in very short reaction times (ca. 2 h). Quantum mechanical calculations point to the step involving the evolution of hydrogen as the rate-determining step (RDS). Success was also achieved in heterogenizing the (*p*-OH^{Bim2}NNN)$RuCl_2$(CO) on to various solid supports apart from using the resulting system to fairly accomplish the Guerbet reaction albeit with no recyclability. The best productivity (15510 TON) was obtained with a combination of (*p*-OH^{Bim2}NNN)$RuCl_2$(CO) over acidic alumina.

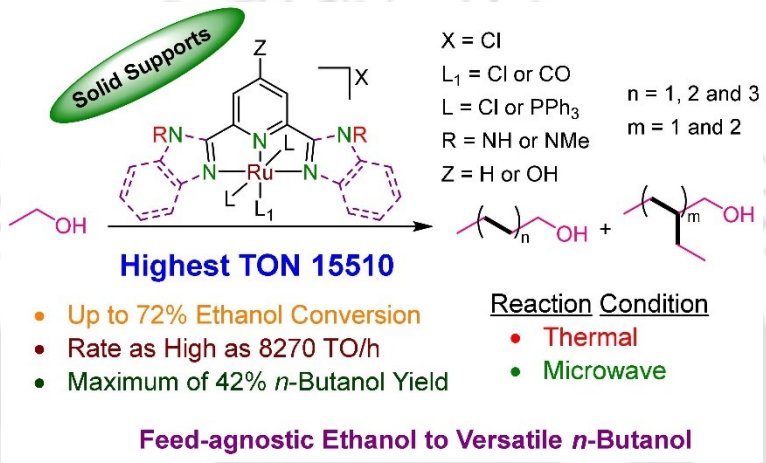

Figure 5: Biofuel production *via* pincer-ruthenium catalyzed upgradation of ethanol

Chapter V describes, the catalytic transformation of secondary alcohols to ethers that has been formulated for the first time *via* an oxygen-assisted dehydration strategy. The NNN pincer-ruthenium(II) carbonyl complexes based on *bis*(imino)pyridine ligands in the presence of molecular oxygen accomplishes the etherification of secondary alcohols under solvent-free conditions at 140 °C in high yields (up to 92%, ca. 6133 TON). Mechanistic studies have provided vital insights into the various events that occur during the catalytic cycle. The liberation of hydrogen peroxide in catalytic amounts during the oxygen assisted pincer-ruthenium catalyzed etherification was confirmed by iodometric titration. This points to the role of oxygen as a co-catalyst and not as a substrate. In the presence of oxygen, key evidence to the non-labile nature of the ancillary CO ligand and the hemi-labile nature of the NNN pincer fragment were obtained from HRMS, IR, ^{13}C NMR and DFT analysis. The generation of Ru(III) *via* single electron transfer (SET) from O_2 was confirmed by EPR analysis. The reaction is hypothesized to proceed *via* the intermediacy of a Ru(III) oxo-radical (^{Ph2}NN)$RuCl_2$(CO)(O$^{\bullet}$) which subsequently leads to 17-electron 1-phenyl ethoxide Ru(III) species (^{Ph2}NN)$RuCl_2$(CO)(OCH(CH$_3$)Ph). The generation of the secondary radical (CH$_3$)$^{\bullet}$CH(Ph)

bound within the coordination sphere to the 17-electron (^{Ph2}NN)RuCl$_2$(CO)(OH) is the overall RDS. A few derivatives of this 17-electron Ru(III) resting-state species (^{Ph2}NN)RuCl$_2$(CO)(OH) have been detected by HRMS analysis. The pincer-ruthenium catalyzed etherification exhibits wide substrate scope and has been successfully implemented not only to the dehydrative etherification of various aromatic secondary alcohols but also to the cross-etherification and/or *o*-alkylation of 1-phenyl ethanols with a variety of phenols. The ubiquitous nature of oxygen and the very low loading (0.015 mol%) of the pincer-Ru catalyst makes this atom-economical and environmentally benign oxygen assisted dehydrative etherification more exciting and offers ample possibilities.

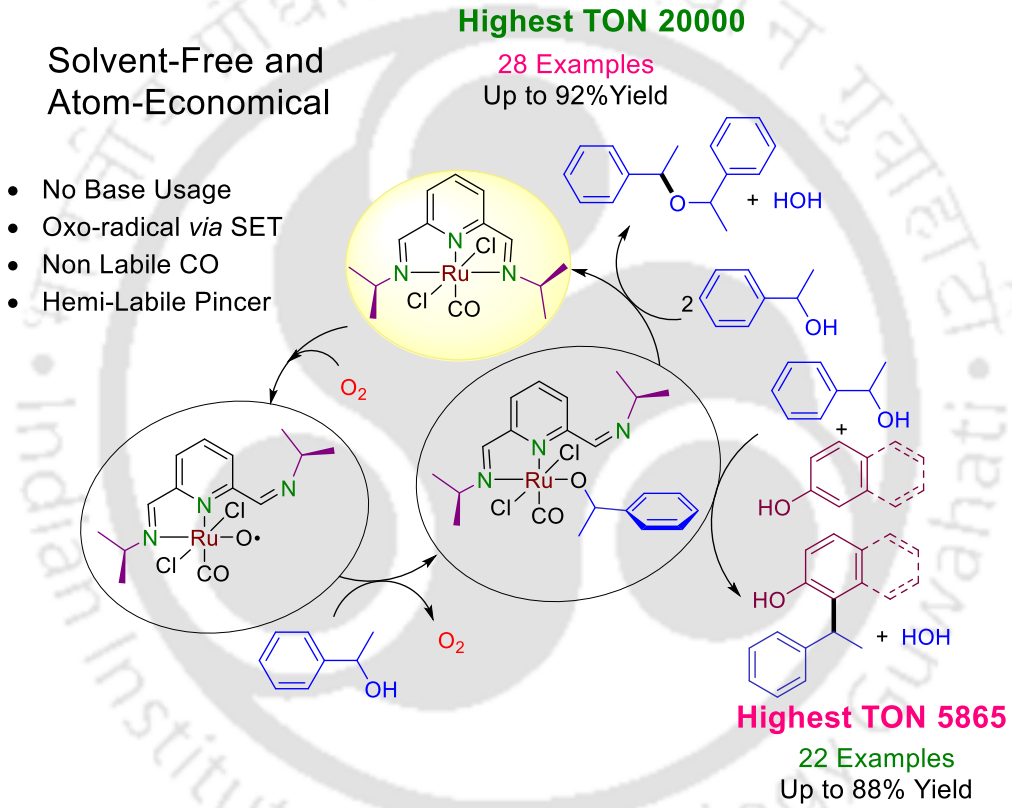

Figure 6: Pincer-ruthenium catalyzed oxygen mediated etherification of alcohols and *ortho*-alkylation of phenols.

The current thesis has demonstrated a synthetic protocol for a new series of pincer complexes based on ruthenium. These pincer-ruthenium complexes have been utilized for various organic transformations with a systematic understanding of the reaction mechanism. The reactivity demonstrated by these pincer-ruthenium complexes is reflective of their versatility in catalytic organic transformations. Among many other exciting possibilities, the current thesis could open new avenues in asymmetric catalysis and recyclable molecular catalytic systems for synthesizing fuel, fine and value-added chemicals.

Catalytic reactions are widely used in industrial processes because they result in increased reaction rates, selectivity, and high efficiency. However, after optimizing the performance of catalytic reactions throughout the chapters, following challenges still remain such as,

(i) Do the most efficient and effective pincer ruthenium based on either *bis*(imino) or *bis*(imidazole) pyridine based ligands bring about the challenging activation of small molecules such as methane, CO_2 and N_2?

(ii) Can one design catalytic systems based on *bis*(imino)pyridine pincers that employ 3d-metals rather than Ru?

(iii) Can the reactions probed in this thesis be catalytically accomplished under milder reaction conditions (say < 100 °C), thereby ensuring safe and efficient catalytic operation?

Overall there is a need for a multidisciplinary approach that combines fundamental research, catalyst design, computational modeling, and process optimization for efficient catalytic transformations under mild reaction conditions. These will have a significant impact on future research.

Curriculum Vitae

Kanu Das

Ph.D. Student

Department of Chemistry

Indian Institute of Technology Guwahati

Guwahati – 781039, Assam, India

Email – kanudaskd@gmail.com

kanudaskd@iitg.ac.in

Academic Qualifications

B.Sc. Chemistry (Honours), Physics and Mathematics (Subsidiary)
Department of Chemistry — 2014
University of Burdwan, West Bengal, India

M.Sc. in Chemistry
Department of Chemistry
Indian Institute of Technology Guwahati, — 2016
Guwahati – 781039, Assam, India

Ph.D. in Organometallic Chemistry — 2023

Department of Chemistry
Indian Institute of Technology Guwahati,
Guwahati – 781039, Assam, India
Thesis Supervisor: Dr. Akshai Kumar A S
Thesis Tittle: "*Pincer-Ruthenium Catalyzed (De)Hydrofunctionalization of Alcohols and Related Value-Added Transformations*"

Area of Research

- Organometallics Chemistry
- Inorganic Synthesis
- Catalysis
- Mechanistic Studies
- Computational Chemistry (DFT)

List of Publications

1 **Das**, **K**.; Dutta, M.; Das, B.; Srivastava, H. K.; Kumar, A. Efficient PincerRuthenium Catalysts for Kharasch Addition of Carbon Tetrachloride to Styrene. *Adv. Synth. Catal*. **2019**, *361*, 2965-2980.

2 **Das**, **K**.; Nandi, P. G.; Islam, K.; Srivastava, H. K.; Kumar, A. Solvent-Free and Efficient Pincer-Ruthenium Catalytic Systems for N-Alkylation of Amines Promoted by a Base Generated In-Situ from Alcohols. *Eur. J. Org. Chem*. **2019**, *2019*, 68556866.

3 Arora, V.; Dutta, M.; **Das**, **K**.; Das, B.; Srivastava, H. K.; Kumar, A. Solvent-Free N-Alkylation and Dehydrogenative Coupling Catalyzed by a Highly Active PincerNickel Complex. *Organometallics* **2020**, *39*, 2162–2176.

4 Dutta, M.; **Das**, **K**.; Prathapa, S. J.; Srivastava, H. K.; Kumar, A. Selective and High Yield Transformation of Glycerol to Lactic Acid Using NNN Pincer Ruthenium Catalysts. *Chem. Commun*. **2020**, *56*, 9886.

5 **Das**, **K**.; Yasmin, E.; Das, B.; Srivastava, H. K.; Kumar, A. Phosphine-Free PincerRuthenium for Biofuel Production High Rate and Turnovers of Solventless Alcohol Alkylation. *Catal. Sci. Technol*., **2020**, *10*, 8347.

6 Nandi, P. G.; Jadi, K. P.; **Das**, **K**.; Prathapa, S. J.; Mandal, B.;* Kumar, A.* Synthesis of NNN Chiral Ruthenium Complexes and their Cytotoxicity Studies. *Inorg. Chem*., **2021**, *60*, 7422–7432.

7 **Das**, **K**.; Yasmin, E.; Pasha, F.; Kumar, A. Pincer-Ruthenium Catalyzed Oxygen Mediated Dehydrative Etherification of Alcohols and Ortho-Alkylation of Phenols. *Adv. Synth. Catal*. **2022**, *364*, 3895-3909.

8 **Das**, **K**.; Kathuria, L.; Jasra, R. V.; Dhole, S.; Kumar, A. Microwave Assisted PincerRuthenium Catalyzed Guerbet Reaction for the Upgradation of Bio-Ethanol Selectively to Bio-Butanol in High Yields. *Catal. Sci. Technol*., **2023**, *13*, 1763.

9 **Das**, **K**.;† Kathuria, L.;† Yasmin, E.; Dhole, S.; Jasra, R. V.; Kumar, A. Catalytic systems for upgradation of ethanol *via* Guerbet reaction. Manuscript under preparations.

10 **Das**, **K**.; Srivastava, H. K.; Pasha, F.; Kumar, A. A thermotical approaches reduction of CO_2 to methanol by pincer iron and ruthenium complexes. Manuscript under preparations

List of Patents

1 Kumar, **K. Das**, A PROCESS FOR UPGRADATION OF ETHANOL OR ALKYLATION OF ALCOHOLS, IN Patent Application; 202031022124, May 27, **2020**

2 A. Kumar, M. Dutta, **K. Das**, H. K. Srivastava, A PROCESS FOR PRODUCTION OF LACTIC ACID FROM GLYCEROL, IN Patent Application; 202031021709, May 23, **2020**

Book Chapter

1 **Das**, **K.**; Kumar, A. Alkane dehydrogenation reactions catalyzed by pincer-metal complexes. *Adv. Organomet. Chem*., **2019**, Vol 72, 1-57.

Conferences Attended

1 **Das**, **K.**; Dutta, M.; Das, B.; Srivastava, H. K.; Kumar, A. Oral presentation during International Conference on Frontiers in Chemical Sciences (FICS - **2018**) from 6- 8th December, IIT Guwahati "Highly Efficient Pincer-Ruthenium Catalysts for Atom Transfer Radical Additions."

2 **Das**, **K.**; Dutta, M.; Das, B.; Srivastava, H. K.; Kumar, A.National Conference on Research Conclave-**2019** from 6-8th March, IIT Guwahati, (Poster presentation) "Highly Efficient Pincer-Ruthenium Catalysts for Atom Transfer Radical Additions."

3 **Das**, **K.**; Kelkar, A.; Srivastava, H. K.; Kumar, A. Poster presentation during 19th National Workshop on Catalysis for Clean Energy and Sustainable Future2019, 6-8th June, IIT Delhi, May **2019**. "Rational Design of Pincer-Metal Complexes for Catalytic Functionalization of Carbon Dioxide."

4 **Das**, **K.**; Nandi, P. G.; Islam, K. I.; Srivastava, H. K.; Kumar, A. Poster presentation during Modern Trends in Inorganic Chemistry MTIC-XVIII, 14-18th December, IIT Guwahati, Guwahati. December **2019**. "Solvent-Free and Efficient Pincer-Ruthenium Catalytic Systems for N-Alkylation of Amines Promoted by a Base Generated In-Situ from Alcohol."

5 **Das**, **K.**; Yasmin, E.; Das, B.; Srivastava, H.K.; Kumar, A. Poster presentation during **2021** #RSCPoster Twitter Conference 2 March 2021 12:00 - 3 March 2021 12:00,

United Kingdom. “Experimental and Computational Studies on Pincer-Ruthenium Catalysed C-Alkylation Reactions for Bio-Fuel Production.”

6 **Das**, **K**.; Kumar, A. Oral presentation in ACS National Meeting & Exposition, ACS Spring 2022, March 20-24, **2022** “Pincer-Ruthenium Catalyzed Production of Biofuels and Value-Added Chemicals *via* Alkylation of Amines and Alcohols.”

7 **Das**, **K**.; Kumar, A. Poster presentation in Chemical Research Society of India 28th National Symposium in Chemistry (CRSI NSC-28), March 25-27, **2022** “Biofuels and Value-Added Chemicals Production Catalyzed by Ru−Pincer Based Complexes *via* Alkylation of Amines and Alcohols.”